

EVALUATION OF CAMBER AND DEFLECTIONS FOR BRIDGE GIRDERS

OR19-002

Final Report

03/31/2021

Prepared For:

Michigan Department of Transportation
Research Administration
8885 Ricks Rd.
P.O. Box 30049
Lansing MI 48909

Prepared By:

Furkan Cakmak (Graduate Research Assistant)
Fatmir Menkulasi (PI)
Christopher Eamon (Co-PI)
Anthony Victor (Graduate Research Assistant)

Wayne State University
5050 Anthony Wayne Drive
Detroit, MI 48202

Ihab Darwish (Industry Partner)

Alfred Benesch & Company
4660 S. Hagadorn Road
Suite 315
East Lansing, MI 48823



TECHNICAL REPORT DOCUMENTATION PAGE

1. Report No. SPR-1697	2. Government Accession No. N/A	3. Recipient's Catalog No.	
4. Title and Subtitle Evaluation of Camber and Deflections for Bridge Girders		5. Report Date March 31, 2021	
		6. Performing Organization Code N/A	
7. Author(s) Furkan Cakmak, Fatmir Menkulasi, Christopher Eamon, Anthony Victor, Ihab Darwish		8. Performing Organization Report No. N/A	
9. Performing Organization Name and Address Wayne State University 5057 Woodward Ave., Suite 13001 Detroit, MI 48202		10. Work Unit No. N/A	
		11. Contract or Grant No. Contract 2016-0070 Z7	
12. Sponsoring Agency Name and Address Michigan Department of Transportation (MDOT) Research Administration 8885 Ricks Road P.O. Box 33049 Lansing, Michigan 48909		13. Type of Report and Period Covered Final Report, 3/1/2019 to 3/31/2021	
		14. Sponsoring Agency Code N/A	
15. Supplementary Notes Conducted in cooperation with the U.S. Department of Transportation, Federal Highway Administration. MDOT research reports are available at www.michigan.gov/mdotresearch .			
16. Abstract A methodology to predict each stage of camber and displacements in composite prestressed concrete and steel bridge superstructures from inception to end of service life including a prediction of rebound in deck replacement projects is presented. The methodology invokes the use of multiple creep curves and allows the proper simulation of various construction activities each of which feature unique loading events. The proposed method captures the influence of several factors, such as creep and shrinkage of beam and deck concrete as well as prestresses losses induced because of these phenomena. Additionally, the prediction methodology offers the capability to quantify the influence of temperature gradients on beam camber and displacements at any point in time. The proposed method can be used to predict beam rebound during a deck replacement activity by considering the removal of the deck as well as the removal of the locked-in time dependent internal forces. The overall framework for the prediction methodology is based on principles of engineering mechanics, although components of the methodology are based on empirical models such as the estimation of the modulus of elasticity at prestress release and 28 days, its variation with time, prediction of creep and shrinkage properties, and relaxation of prestressing strands. The proposed methodology has been evaluated using measured pre-erection camber data for a total of fourteen projects, which feature a total of 90 beams. An alternative simplified method suitable for preliminary design and based on time dependent multipliers is presented. Pre-erection camber predictions based on the proposed methodology and the Time Dependent Multiplier Method are more accurate than those based on the PCI Multiplier Method and the MDOT multiplier method. A computer program called MDOT Camber was developed to facilitate data input and summarize essential output.			
17. Key Words Prestressed concrete beam; steel beam; camber; deflection; rebound; creep; shrinkage; prestress loss; time-dependent behavior		18. Distribution Statement No restrictions. This document is also available to the public through the Michigan Department of Transportation.	
19. Security Classif. (of this report) Unclassified	20. Security Classif. (of this page) Unclassified	21. No. of Pages 399	22. Price N/A

ACKNOWLEDGEMENTS

The authors would like to express their gratitude to the Michigan Department of Transportation (MDOT) for sponsoring this research and for providing them the opportunity to work on this project. The authors are especially grateful to Mr. Kyle Kooper (project manager) who was instrumental in the completion of this project and helped with supplying short term and long-term camber data, bridge drawings, quality assurance and quality control reports, and with many other tasks. Special thanks also go to Mr. Michael Townley, and Mr. Bradley Wagner for their valuable comments during the progress meetings, which helped enhance the quality and clarity of this report. The authors are also thankful to Mr. Juan Alcantar and Ms. Melissa Donoso for evaluating the MDOT Camber program and for providing valuable feedback. The authors would also like to thank Mr. Fernando Roldan at Peninsula Prestress for allowing access to their precast facility to obtain camber measurements throughout the duration of this project. Special thanks also go to Ms. Deanna Papanek who helped with the coordination of activities to collect concrete cylinders for laboratory testing. The authors would also like to thank Mr. Anil Mehta at The Prestressed Group who allowed the research team to collect additional camber measurements at the Windsor, Ontario plant.

DISCLAIMER

This publication is disseminated in the interest of information exchange. The Michigan Department of Transportation (hereinafter referred to as MDOT) expressly disclaims any liability, of any kind, or for any reason, that might otherwise arise out of any use of this publication or the information or data provided in the publication. MDOT further disclaims any responsibility for typographical errors or accuracy of the information provided or contained within this information. MDOT makes no warranties or representations whatsoever regarding the quality, content, completeness, suitability, adequacy, sequence, accuracy or timeliness of the information and data provided, or that the contents represent standards, specifications, or regulations.

TABLE OF CONTENTS

Chapter 1 : Introduction	5
1.1 Research Objectives	7
1.2 Significance of Work.....	7
1.3 Organization of the Report.....	7
Chapter 2 : Literature Review.....	10
2.0 Introduction	10
2.1 Factors that Affect Camber at Release and Long-term Camber, Deflections, and Rebound	11
2.2 Methods to Measure Camber at Release and Long-term Camber.....	12
2.3 Methods to Predict Camber at Release and Long-term Camber and Deflections.....	13
2.3.1 Multiplier Method (Martin 1977).....	13
2.3.2 Incremental Time-Steps Method (Nilson 1987).....	14
2.3.3 Approximate Time-Steps Method (Branson and Ozell 1961)	17
2.3.4 Axial Strain and Curvature Method (Ghali and Favre 1986).....	17
2.3.5 Prestress Loss Method (Tadros et al. 1985).....	17
2.3.6 CEB-FIB Model Code Method (CEB-FIP 1990)	17
2.3.7 Section Curvature Method (ACI 435R-95).....	18
2.4 Previous Studies.....	18
2.5 Summary of Literature Review	18
2.6 Prestressed Concrete Beam Camber Questionnaire	19
Chapter 3 : Prediction Methodology	24
3.1 Time Dependent Cross-sectional Curvature Method	24
3.1.1 Iteration No. 1.....	25
3.1.2 Iteration No. 2.....	31
3.1.3 Iteration No. 3.....	39
3.1.4 Iteration No. 4.....	43
3.1.5 Iteration No. 5.....	44
3.1.6 Iteration No. 6.....	47

3.1.7 Modulus of Elasticity Prediction.....	56
3.1.8 Creep and Shrinkage Models.....	61
3.1.9 Strand Relaxation Loss.....	65
3.1.10 Temperature Gradients.....	66
3.1.11 Limitations of the Proposed Prediction Methodology.....	68
3.2 Time Dependent Multiplier Method.....	69
Chapter 4 : Beam camber and displacement data sets.....	71
4.1 Introduction	71
4.2 Camber and Displacement Data Sets Provided by MDOT.....	73
4.3 Camber and Displacement Data Sets collected from the Windsor Plant	76
4.4 Relationship between Specified and Measured f'_c	79
4.5 Relationship between Calculated and Measured E_{ci}	80
4.6 Relationship between Specified and Measured Concrete Unit Weight	84
4.7 Relationship between Specified and Measured Prestressing Force.....	84
4.8 Relationship between Specified and Measured Beam Length.....	85
4.9 Summary of Relationships between Measured and Specified/Calculated Properties	86
4.10 Solar Radiation Study	86
4.11 Data Collection Guidelines	87
Chapter 5 : Evaluate factors that affect prestressed concrete beam camber	90
5.1 Introduction	90
5.2 Sensitivity Analysis.....	90
5.2.1 Influence of Creep and Shrinkage Model on Pre-erection Camber.....	94
5.2.2 Influence of Model to Predict Modulus of Elasticity at Prestress Release and 28 Days	95
5.2.3 Influence of the Model for Capturing the Variation of Modulus with Time.....	96
5.2.4 Influence of Overstrength Factors.....	97
5.2.5 Influence of Time when Camber at Release is Measured	98
5.2.6 Slab and Screed Guidance	99
5.3 Summary and Conclusions.....	100

Chapter 6 : Evaluate Factors that Affect Camber and Displacements in the Composite

System.....	103
6.1 Introduction	103
6.2 Sensitivity Analysis.....	103
6.2.1 Influence of Creep and Shrinkage Model on Service Camber.....	108
6.2.2 Influence of Model to Predict Modulus of Elasticity at Prestress Release and 28 Days	109
6.2.3 Influence of the Model for Capturing the Variation of Modulus with Time.....	110
6.2.4 Influence of Overstrength Factors.....	111
6.2.5 Influence of the Time when the Deck is Placed	111
6.2.6 Influence of the Temperature Gradient.....	112
6.3 Summary and Conclusions.....	114

Chapter 7 : Evaluate Factors that Affect Beam Rebound and Behavior after Deck

Replacement	117
7.1 Introduction	117
7.2 Comparison of Rebound and Net Camber after Deck Removal	117
7.3 Influence of Deck Replacement Time.....	119
7.4 Summary and Conclusions.....	120

Chapter 8 : Evaluation of Various Prediction Methodologies for Time Dependent Flexural

Deformations	122
8.1 Introduction	122
8.2 Evaluation of Predictions for Camber at Release.....	122
8.3 Evaluation of Predictions for Pre-erection Camber.....	124
8.4 Evaluation of Predicted Camber Growth Curve	125
8.5 Comparison of Incremental Time Step Method (Nilson 1987) and Proposed Prediction Methodology	128
8.5.1 Variation of Prestress and Prestress Losses with Time.....	128
8.6 Comparison of Various Approaches within the Proposed Prediction Methodology.....	134

8.6.1 Comparison of Iterations No. 1 through No. 6 for Pre-erection Camber.....	134
8.6.2 Comparison of Iterations No. 2 to No. 6 for Service camber without Deck Replacement.....	135
8.6.3 Comparison of Iterations No. 4 to No. 6 for Service Camber with Deck Replacement.	136
8.6.4 Impact of Method to Generate Time Steps within Iteration No. 6.....	137
8.6.5 Influence of Number of Beam Sections Specified in Iteration No. 6.....	138
8.7 Derivation of Time Dependent Multiplier Method.....	140
8.8 Comparison of Proposed Prediction Methodology and Time Dependent Multiplier Method	140
8.9 Summary and Conclusions.....	144
Chapter 9 : Summary and Conclusions.....	147
9.1 Chapter 3 - General:	147
9.2 Chapter 5 - Factors that Affect Prestressed Concrete Beam Camber	148
9.3 Chapter 6 - Factors that Affect Camber and Displacements in the Composite System ...	148
9.4 Chapter 7 - Factors that Affect Beam Rebound and Behavior after Deck Replacement..	149
9.5 Chapter 8 - Evaluation of Various Design Procedures.....	150
References.....	152
APPENDIX A : PREVIOUS STUDIES.....	159
A.1 Buettner and Libby (1979).....	160
A.2 Tadros et al. (1985).....	160
A.3 Kelly et al. (1987).....	161
A.4 Brown (1998).....	161
A.5 Yazdani et al. (1999).....	162
A.6 Wyffels et al. (2000).....	162
A.7 Jáuregui et al. (2002)	162
A.8 Stallings, Barnes, and Eskildsen (2003).....	163
A.9 Waldron (2004).....	163
A.10 Cook and Bloomquist (2005)	164
A.11 Barr et al. (2005)	164

A.12 Hinkle (2006).....	165
A.13 Rosa et al. (2007).....	165
A.14 Jayaseelan and Russell (2007).....	166
A.15 Omar et al. (2008).....	166
A.16 Barr and Angomas (2010).....	166
A.17 Lee (2010).....	167
A.18 Tadros et al. (2011).....	167
A.19 French and O'Neill (2012).....	167
A.20 Schrantz (2012).....	168
A.21 Johnson (2012).....	168
A.22 Precast/Prestressed Concrete Institute Committee on Bridges (2012).....	169
A.23 Bažant et al. (2012).....	169
A.24 Storm et al. (2013).....	170
A.25 Mahmood (2013).....	170
A.26 He (2013).....	171
A.27 Nervig (2014).....	171
A.28 Hofrichter (2014).....	172
A.29 Isbilibiroglu (2014).....	172
A.30 Nguyen (2014).....	172
A.31 Honarvar et al. (2015).....	173
A.32 Keraga (2016).....	173
A.33 Menkulasi et al. (2018).....	173
A.34 Mante et al. (2019).....	174
APPENDIX B : CAMBER SURVEY	175
APPENDIX C : COMPUTATIONAL INFRASTRUCTURE FRAMEWORK AND IMPLEMENTATION	203
C.1 Tab 1: Introduction	208
C.2 Tab 2: Girder Properties.....	210
C.3 Tab 3: Girder Concrete Properties	214
C.4 Tab 4: Deck Properties.....	217

C.5 Tab 5: Prestressing Steel Properties	219
C.6 Tab 6: Creep and Shrinkage Model Selection.....	221
C.7 Tab 7: Time, Environment and Measured Camber Properties	222
C.8 Tab 8: Results.....	225
APPENDIX D : PRESTRESSED CONCRETE BEAM EXAMPLE	232
D.1 Definition of the Problem.....	240
D.2 Definition of Parameters	244
D.3 Camber at Release	273
D.4 Pre-erection Camber	278
D.5 Camber just after Placement of 1 st Deck	284
D.6 Camber just before Application of Barrier and Overlay Loads on 1 st Superstructure.....	286
D.7 Camber just after Application of Barrier and Overlay Loads on 1 st Superstructure	291
D.8 Camber just before Deck Removal Process.....	292
D.9 Camber just after Deck Removal Process	295
D.10 Camber just before 2 nd Deck Placement.....	299
D.11 Camber just after 2 nd Deck Placement.....	300
D.12 Camber just before Application of Barrier and Overlay Loads on 2 nd Super-structure.	301
D.13 Camber just after Application of Barrier and Overlay Loads on 2 nd Super-structure ...	303
D.14 Camber at Final Time	305
D.15 Nomenclature	309
APPENDIX E : STEEL BEAM EXAMPLE	316
E.1 Definition of the Problem.....	322
E.2 Definition of Parameters.....	325
E.3 Pre-erection Camber	338
E.4 Camber just after Placement of 1 st Deck.....	340
E.5 Camber just before Application of Barrier and Overlay Loads on 1 st Superstructure	341
E.6 Camber just after Application of Barrier and Overlay Loads on 1 st Superstructure.....	344
E.7 Camber just before Deck Removal Process	346
E.8 Camber just after Deck Removal Process.....	348
E.9 Camber just before 2 nd Deck Placement.....	351

E.10 Camber just after 2 nd Deck Placement.....	351
E.11 Camber just before Application of Barrier and Overlay Loads on 2 nd Superstructure ..	352
E.12 Camber just after Application of Barrier and Overlay Loads on 2 nd Superstructure	353
E.13 Camber at Final Time.....	355
E.14 Nomenclature	358
APPENDIX F : RECOMMENDED REVISIONS, UPDATES AND GUIDELINES.....	362

List of Figures

Fig. 2.1. Illustration of creep induced strain due to prestress and prestress loss	16
Fig. 3.1. Distribution of forces in a prestressed concrete girder.....	27
Fig. 3.2. Illustration of Approach No. 1 for predicting time-dependent flexural deformations; a) assumed stress history, b) discretized stress history, and c) elastic and creep induced strains using Effective Modulus (EM) and Age-adjusted Effective Modulus (AAEM) approaches and based on discretized stress history	28
Fig. 3.3. Illustration of Age Adjusted Effective Modulus (AAEM) concept to capture creep effects.....	29
Fig. 3.4. Distribution of internal forces in: a) composite prestressed concrete beam, and b) composite steel beam.....	34
Fig. 3.5. Illustration of Approach No. 2 for predicting time-dependent flexural deformations; a) assumed stress history, b) discretized stress history, and c) elastic and creep induced strains due to discretized stress history	34
Fig. 3.6. Curvature diagrams for composite and non-composite sections.....	38
Fig. 3.7. Illustration of Approach No. 3-5 for predicting time-dependent flexural deformations for Approach No. 3-5; a) assumed stress history, b) discretized stress history, and c) elastic and creep induced strains due to discretized stress history	40
Fig. 3.8. Flowchart for approach used in Iteration 5	46
Fig. 3.9. Empirical model selection in the proposed prediction methodology	47
Fig. 3.10. Flowchart for iteration No. 6	48
Fig. 3.11. a) Illustration of effective modulus (EM) and age adjusted effective modulus (AAEM) concept, b) effect of loading age on creep coefficient according to AASHTO LRFD model for an interior prestressed concrete beam used in the S-11 project, c) assumed stress history, idealized stress history, and creep induced strain due to a varying stress history (multiple time steps with multiple creep curves).....	49
Fig. 3.12. Modulus of elasticity as a function of time based on the ACI 209R-92 Model.....	59
Fig. 3.13. Modulus of Elasticity as a function of time based on the fib MC 2010 Model.....	61
Fig. 3.14. Variation in creep coefficient and shrinkage strain based on different shrinkage and creep models for: a) PCBT 54 used in S11 project (Flange width 49 in., t_c =one day steam curing, t_{load} = one day, Cement Type I); b) Deck used in S11 project (t_c =one day steam curing, t_{load} =	

one day, Type I cement, mixture proportions are based on a typical deck mix featuring normal weight concrete and fly ash).....	63
Fig. 3.15. Test setup for creep test.....	64
Fig. 3.16. Comparison of measured and predicted creep coefficient.....	64
Fig. 3.17. Comparison of measured and predicted shrinkage strain.....	65
Fig. 3.18. Positive temperature gradients for solar radiation zone 3	67
Fig. 4.1. Nominal Dimensions (in mm) for the CPCI-1600 prestressed concrete beams ($A = 515 \text{ mm}^2 \times 10^3$, $Y_b = 793 \text{ mm}$, $I_x = 1.78 \times 10^{11} \text{ mm}^4$).....	78
Fig. 4.2. a) Illustration of methodology for measuring camber in four CPCI-1600 prestressed concrete beams, b) photograph showing measurement setup and device made for taking consistent measurements across beam bottom flange, c) photograph showing device used to match the bottom flange of the beam and to receive the measuring rod.	79
Fig. 4.3. Ratio of measured over specified: a) initial concrete compressive strength, b) 28 day concrete compressive strength.....	80
Fig. 4.4. Development of modulus of elasticity with time using specified (left) and measured (right) properties for: a) R04 (CG1); b) R04 (CG2); c) S02 (CG3); d) B02 (CG4) projects	83
Fig. 4.5. Variation in camber due to radiation induced thermal gradient for: a) Girder G2-6, b) Girder G2-7, c) Girder G2-8, d) Girder G2-9	87
Fig. 5.1. Variation of pre-erection camber for S-11 project using different creep and shrinkage models	95
Fig. 5.2. a) Comparison of calculated modulus of elasticity at prestress release and 28 days; b) influence of model to predict modulus of elasticity at prestress release and 28 days on camber for S-11 project.....	96
Fig. 5.3. a) Comparison of functions for predicting the development of modulus of elasticity with respect to time, b) influence of considered time dependent modulus functions on camber for S-11 project.....	97
Fig. 5.4. Influence of inclusion of overstrength factors for S-11 project.....	98
Fig. 5.5. Variation of predicted camber during the first 10 days after beam fabrication.....	99
Fig. 5.6. Illustration of various stages of deflection during beam erection and deck placement for the S-11 project.....	100

Fig. 6.1. Influence of creep and shrinkage problems on the full displacement history of: a) prestressed concrete beams used in the S-11 project, and b) steel beams used in the M-20 project	108
Fig. 6.2. a) Comparison of calculated modulus of elasticity at prestress release and 28 days based on different models; b) influence of model to predict modulus of elasticity at prestress release and 28 Days on camber history for S-11 project.....	110
Fig. 6.3. a) Comparison of predictions for development of modulus of elasticity with respect to time based on different models; b) influence of time dependent modulus model on camber for S-11 project.....	110
Fig. 6.4. Influence of inclusion of overstrength factors for S-11 project.....	111
Fig. 6.5. Influence of the time when the deck is placed on beam camber and displacements at service for: a) S10-2 project; b) S11 project.....	112
Fig. 6.6. Influence of temperature gradients on beam camber and displacements at service: ...	113
Fig. 8.1. Comparison of measured, predicted, and design camber at prestress release	123
Fig. 8.2. Comparison of measured and predicted pre-erection camber.....	125
Fig. 8.3. Variation of measured and predicted camber for the prestressed concrete beams fabricated in PSI Windsor for the Tiffin Street Overpass Project: a) full scale, b) reduced scale	126
Fig. 8.4. Influence of beam creep coefficient and beam shrinkage strain on beam camber considering the beams used in the Tiffin Street Overpass project.....	127
Fig. 8.5. Variation of prestress as a function of time in a composite bridge system at mid-span (S-11 project).....	129
Fig. 8.6. Variation of prestress losses with time in a composite bridge system at midspan (S-11 project)	130
Fig. 8.7. Comparison of calculated separate and total prestress losses for S-11 project using proposed prediction methodology and AASHTO (2020) Body provisions	132
Fig. 8.8. Comparison of proposed method with the Incremental Time Step Method (Nilson 1987) for the: a) M5 project; b) S10-2 project; c) S11 project and d) S12-1 project.....	133
Fig. 8.9. Comparison of various iterations for pre-erection camber for: a) S10-2 project, b) S-11 project.....	134

Fig. 8.10. Comparison of various approaches for service camber without deck replacement for: a) S10-2 project, b) S-11 Project, c) M-20 project.....	136
Fig. 8.11 Comparison of predicted displacement history based on Iterations No. 4, 5, and 6 including a deck replacement activity after 50 years of service for: a) S10-2 project, b) S11 project, c) M-20 project	137
Fig. 8.12. Impact of method to generate the number of time steps on full camber and displacement history for: a) S10-2 project, b) S-11 project.....	138
Fig. 8.13. Sensitivity of camber predictions at midspan for the beams used in S-11 project to the number of sections considered: a) number of odd sections, b) number of even sections, c) number of sections (odd or even)	139
Fig. 8.14. Variation of multipliers as a function of time (prediction curves for each project are based on specified properties)	142
Fig. 8.15. Camber growth prediction for Tiffin Street Overpass Project using proposed time- dependent multiplier for: a) G2-6 beam; b) G2-7 beam; c) G2-8 beam; and d) G2-9 beam.....	144

List of Tables

Table 3.1. Description of iterations used to develop the proposed prediction methodology	25
Table 3.2. Approach used for creation of time array	51
Table 3.3. Determination of aggregate type dependent parameter.....	57
Table 3.4. Comparison of modulus of elasticity prediction models.....	58
Table 3.5 Parameters for ACI 209R-92 time dependent modulus of elasticity model	58
Table 3.6. Coefficients for strength class of cement based on fib MC 2010 model.....	60
Table 4.1. Curing techniques used by precast beam fabricators that supply prestressed concrete bridge beams for MDOT.....	74
Table 4.2. Camber and Displacement Data Sets	75
Table 4.3. Relationship between calculated and measured modulus of elasticity at release (calculated modulus is based on specified compressive strength).....	82
Table 4.4. Relationship between calculated and measured modulus of elasticity at release (calculated modulus is based on measured compressive strength)	82
Table 4.5. Comparison of specified and measured concrete unit weight	84
Table 4.6. Comparison of specified and measured prestressing force at release	84
Table 4.7. Comparison of specified and measured beam length.....	85
Table 4.8. Summarized results for the relationship between measured and specified parameters	86
Table 5.1. Influence of various parameters on camber at release	93
Table 5.2. Influence of various parameters on pre-erection camber.....	94
Table 6.1. Influence of various parameters on camber and displacements at service	107
Table 7.1. Comparison of rebound, net camber after deck removal, and net camber before new deck placement.....	118
Table 7.2. Comparison of net camber prior to placement of deck to net camber after removal of deck.....	119
Table 7.3. Influence of deck replacement time on beam rebound, net camber after deck removal, and net camber before new deck placement based on Iteration No. 6 (S-11 project)	120
Table 8.1. Summary of camber at prestress release predictions.....	124
Table 8.2. Summary of pre-erection camber predictions on a beam-by-beam basis.....	125

Table 8.3. Comparison of separate and total prestress losses computed using the proposed prediction methodology and AASHTO LRFD Specifications (2020) for the S-11 project.....	132
Table 8.4. Beam based comparison of several approaches for pre-erection camber	142
Table 8.5. Comparison of proposed multiplier with different initial camber values	142
Table 8.6. Camber growth prediction for Tiffin Street Overpass Project using proposed time-dependent multiplier.....	143

Executive Summary

A methodology to predict each stage of camber and displacements in composite prestressed concrete and steel bridge superstructures from inception to end of service life including a prediction of rebound in deck replacement projects is presented. For prestressed concrete beams the prediction methodology can be used to predict camber and displacements at any point in time during the life of the beam. For steel beams, the prediction methodology can be used to predict camber and displacements in the composite bridge system. The proposed methodology was based on six iterations each of which represents a theoretical improvement in prediction accuracy compared to the previous iteration. The last iteration (i.e. Iteration No. 6) is presented as an algorithm written in Matlab that features a graphical user interface. In addition to the proposed prediction methodology, two alternative methods for predicting pre-erection camber were evaluated. These include the Incremental Time Step method (Nilson 1987) and the Time Dependent Multiplier Method. The Time Dependent Multiplier Method was derived from the proposed prediction methodology using curve-fitting techniques.

The proposed method invokes the use of multiple creep curves and allows the proper simulation of various construction activities each of which feature unique loading events. The proposed method captures the influence of several factors, such as creep and shrinkage of beam and deck concrete as well as prestresses losses induced because of these phenomena. Additionally, the prediction methodology offers the capability to quantify the influence of temperature gradients on beam camber and displacements at any point in time thus providing lower and upper bounds for anticipated camber and displacements. The proposed method can be used to predict beam rebound during a deck replacement activity by considering the removal of the deck as well as the removal of the locked in time dependent internal forces in the deck. In the proposed methodology the lifespan of the bridge is broken down into time steps that represent certain construction activities. These time steps are further broken down into time sub-steps the length of which varies in a logarithmic fashion. Separate creep curves are used for forces applied at a given time sub-step as opposed to a single creep curve with an age adjusted effective modulus. The overall framework for the prediction methodology is based on principles of engineering mechanics. However, components of the methodology are based on empirical models such as the estimation of the modulus of elasticity at prestress release and at 28 days and its variation with time, prediction of creep and shrinkage properties, and relaxation of prestressing strands.

The proposed methodology has been evaluated using measured pre-erection camber data for a total of fourteen projects, which feature a total of 90 beams. Camber and displacement predictions obtained from the proposed prediction methodology are blind predictions, in the sense that no calibration was conducted to match measured camber values. An alternative simplified method suitable for preliminary design and based on time dependent multipliers is presented. This method was empirically derived based on data produced by the proposed prediction methodology for the beams used in the projects considered in this study. Pre-erection camber predictions based on the proposed methodology and the Time Dependent Multiplier Method are more accurate than those based on the PCI Multiplier Method and the MDOT multiplier method. Additionally, camber at prestress release predictions based on the proposed methodology were also more accurate and consistent than the current MDOT procedure. While the use of measured properties resulted in comparable predictions with specified properties it is believed that if the database of specimens were to be expanded the use measured properties would result overall in more accurate predictions. Therefore, an overstrength factor of 1.2 is recommended for compressive strength at release and 28 days to adjust specified values.

While it is determined that the unit weight of concrete, w , the magnitude of the prestressing force at jacking, $P_{jacking}$, and beam length, L , all have a significant influence on camber at release and pre-erection beam camber, it is determined that these parameters do not vary significantly from specified values and therefore do not represent a significant source of uncertainty. Modulus of elasticity at release, E_{ci} , had a proportional influence on camber at release and pre-erection beam camber. Similarly, beam compressive strength at release, f'_{ci} , also had a close to proportional influence on camber at release and pre-erection camber, although this influence was quantified through the use of compressive strength dependent equation for modulus of elasticity. Transfer length, $L_{transfer}$, debonded length, $L_{debonded}$, support conditions during storage, $L_{overhang}$, and location of harping point, $L_{harping}$, influence camber at release and pre-erection camber at a degree that in some cases is worth considering. The selection of the creep and shrinkage model has a marked influence on the prediction of pre-erection camber development. The time when initial camber is measured appears to be an important parameter since marked differences were found between predicted camber at release and predicted camber during the first 10 days. The proposed prediction methodology (Iteration No. 6) provides the user the flexibility of accounting for the influence of all the above-mentioned factors.

Factors that led to a single digit average % change in net camber and displacement in the composite system due to the induced 10% change include: beam overhang length at precast facility (i.e. storage conditions), transfer length, debonded length, deck modulus, and beam overhang length at the bridge site. Factors that led to a double-digit average % change in net camber and displacement in the composite system due to the induced 10% change include: beam concrete compressive strength at release and 28 days, beam concrete unit weight, beam concrete modulus of elasticity at release and 28 days, location of harping point, beam spacing, compressive strength of deck at 28 days, and unit weight of deck. Factors that led to a triple digit average % change in net camber and displacement in the composite system due to the induced 10% change include: beam length, and prestressing force. The influence of the selected creep and shrinkage model on the full displacement history of a prestressed concrete beam bridge was investigated and it was concluded that this selection has a marked influence on the beam displacement history. Some models result in rather similar displacements after 75 years despite initial differences in pre-erection camber and net displacements after deck placement. Influence of deck placement time on the full beam displacement history was investigated and it was concluded that while pre-erection camber is highly influenced by it, camber and displacements after 75 years were rather similar. The influence of temperature gradients was rather uniform throughout the displacement history of the beam with positive temperature gradients having a higher influence on camber and displacements compared to negative temperature gradients.

Deck replacement time had no influence on the magnitude of beam rebound and net camber after deck removal provided that the deck is replaced at least after 40 years. Deck replacement time had a minor influence on the net camber before new deck placement with greater deck replacement times resulting in slightly lower net cambers before new deck placement. The influence of solution method (Iteration No. 5 vs. Iteration No. 6) on beam rebound, net camber after deck removal, and net camber before new deck placement was investigated. It was determined that Iteration No. 6 leads to smaller rebounds compared to Iteration No. 5. Additionally, predictions based on Iteration No. 5 showed that there is no change between net camber after deck removal, and net camber before new deck placement whereas Iteration No. 6 suggests that there is a slight camber growth.

Chapter 1: Introduction

Chapter 1: Introduction

The ride quality of bridges in Michigan has been the subject of increased focus in recent years. Two factors that can significantly impact ride quality are beam camber and deflection. Flexural deformations in composite bridge superstructures that feature prestressed concrete or steel beams with a cast in place concrete deck are time dependent. Excessive camber growth due to concrete creep may result in an unpleasant transition from the roadway to the bridge and from bridge to the roadway. A similar problem may be caused by excessive downward deflections due to differential shrinkage between the deck and the girder. Time dependent flexural deformations in such composite bridge superstructures combined with live load deflections may also affect the vertical under clearance, which may lead to traffic restrictions for the roadway underneath.

Camber and deflection different than those estimated during design can also lead to the need for changes during construction, which can result in increased cost and longer construction duration. Differences between calculated and actual camber could result in either excessive or negative haunches. Excessive haunches may affect the embedment depth of extended stirrups in prestressed concrete beams or shear studs in steel beams. Negative haunches may impact deck thickness over beam flanges. Similarly, any deviations from the specified deck surface elevations may result in grinding of the deck to ensure that the finished deck surface matches the vertical roadway geometry as close as possible.

A related concern is accurately predicting beam rebound and subsequent deflections when decks are removed for replacement. For this assessment, the “rule of thumb” procedure used by MDOT designers has, in some cases, produced unreliable estimates of beam rebound and resultant camber. The consequences of inaccurate rebound prediction are similar to those of inaccurate pre-erection camber predictions (i.e. excessive or negative haunches). Steel beams should be able to rebound to their original position, assuming that the deterioration that has prompted the replacement of the deck has not affected the beams and that pin and roller supports behave as intended. Conversely, rebound in prestressed concrete beams is a function of the loading history and the competing effects of prestress and self-weight induced creep as well as differential shrinkage.

MDOT currently relies on multiplier based empirical equations to determine camber and long-term deflection for prestressed concrete beams. However, these expressions may not be suitable when concrete mixtures featuring high strength concrete or formulations different than

those for which the multiplier method may be appropriate are specified for prestressed concrete beams. Therefore, there is a desire to re-evaluate existing MDOT procedures for estimating beam camber and deflection. Ideally, revised procedures should be validated by actual values for camber and deflection measured during Michigan bridge construction projects, as well as account for current fabrication practices.

The multiplier method used by many state DOTs to predict long-term camber was originally developed by Martin (1977) for precast double tees used in buildings with a 2 in. concrete topping and normal strength concrete. However, the typical strength of concrete at prestress release has increased from about 4500 psi in the past to 6500 psi and even 12000 psi, as shown in recent work by FHWA and Nebraska Department of Roads (Morcous and Tadros 2009). This increase in concrete strength has led to complications when using the multiplier method, resulting in inaccurate camber predictions. For example, higher strength concretes are often used with more slender beams, which require a corresponding increase in prestress, and result in an expected level of camber greater than that associated with traditional mixes. While, this increase in camber is somewhat counterbalanced by the greater modulus and lower creep associated with high strength concrete, it is uncertain what the extent of this counterbalancing effect is. Additionally, in higher strength concrete, the majority of creep and shrinkage take place in the first few months rather than throughout longer periods of time, as is the case for lower strength mixes, altering the assumption of gradual development of camber and deflection inherent in the multiplier method. The interaction of these factors is not only complex, but also consequential as they represent significant changes in the assumptions used to develop the multiplier method, causing it to produce inaccurate estimates of camber.

Another inherent problem associated with the multiplier approach is that the multipliers provide a single lump sum value to predict behavior, while camber and deflections are affected by many factors that vary with time such as creep, differential shrinkage, temperature gradients, age of concrete, loading history, etc. As a result, the use of a single numerical multiplier for predicting beam camber or deflections at a specific time is not an adequate approach to accurately capture the influence of the multiple factors that affect long-term beam response.

The research presented in this report aims to address the problem above, by providing a procedure in which the effects of all significant factors that influence camber and deflections are

quantified individually and appropriately combined to produce an accurate model for predicting camber, deflections, and rebound of MDOT beams as a function of time.

1.1 Research Objectives

The specific objectives of this research are to:

1. Synthesize relevant research and current practices of other DOTs.
2. Develop a procedure that can accurately predict the camber of prestressed concrete beams.
3. Develop a procedure that can accurately predict deflection at all stages of construction for prestressed concrete and steel beams used in new and existing bridges.
4. Develop a procedure that can accurately predict beam rebound after the removal of existing deck in deck replacement projects.
5. Develop guidelines for calculating slab and screed elevations on the bridge.

1.2 Significance of Work

The final product of this research is a computational framework (Matlab based algorithm) that can be used to estimate beam camber, deflections, and rebound, at any point in time during the service life of the bridge. This is done by individually quantifying the influence of significant factors that affect camber and deflections at: 1) the material level through the use of appropriate models for predicting the free creep and shrinkage of concrete; 2) the cross-sectional level by determining how the distribution of strain, stress, and curvature is affected while maintaining strain compatibility, and; 3) the element and structure level by considering how changes in curvature at the cross-sectional level alter beam camber and deflection as a function of time. The developed guidelines will allow MDOT to improve slab and screed elevation calculations for future projects. Additional benefits include improved ride quality, more precise camber and deflection predictions, and fewer adjustments in the field. Those impacted by this research include MDOT bridge designers, construction staff and consultants performing bridge work, as well as motorists.

1.3 Organization of the Report

Chapter 2 provides a review of the literature in the subject matter including the results of a nationwide survey. Chapter 3 presents the details of the proposed prediction methodology. Chapter 4 presents details about the beam camber and displacement dataset that was used to

validate the proposed prediction methodology. Chapter 5 presents an evaluation of factors that affect prestressed concrete beam camber through a sensitivity analysis, which was conducted using the proposed prediction methodology. Chapter 6 presents an evaluation of factors that affect camber and displacements in composite bridge superstructures that feature prestressed concrete and steel beams through a sensitivity analysis that includes deck related parameters in addition to those considered for the beam. Chapter 7 presents an evaluation of factors that affect beam rebound and behavior after deck replacement. Chapter 8 presents an evaluation of various prediction methodologies for time dependent flexural deformations. This includes various versions of the proposed prediction methodology, a new time dependent multiplier method, MDOT's fixed multiplier method, and PCI's fixed multiplier method. Chapter 9 provides a summary and conclusions. Appendix A provides additional details on previous studies conducted on the subject matter. Appendix B presents the details of the nationwide survey on the topic of beam camber and displacements. Appendix C illustrates the implementation of the proposed prediction methodology through a Matlab based computer program called MDOTCamber. Appendix D and E provide details of how the proposed prediction methodology computes camber and deflections in a prestressed concrete beam and steel beam superstructure, respectively. Appendix F includes recommended revisions, updates, and guidelines for several MDOT documents that were reviewed as part of this research project.

Chapter 2: Literature Review

Chapter 2: Literature Review

2.0 Introduction

Prestressed concrete beam camber and deflections is a topic that has been investigated in detail by various Department of Transportation (DOT)-sponsored research projects. Some of these include:

- North Carolina (Storm et al. 2013),
- Alabama (Stallings et al. 2003; Schrantz 2012; Johnson 2012; Isbilioğlu 2014; Mante 2016),
- Nebraska (Tadros et al. 2011),
- Washington (Rosa et al. 2007; Davidson 2014; Barr and Angomas 2010),
- Iowa (Nervig 2014; Honarvar et al. 2015; He 2013), Kentucky (Mahmood 2013),
- Texas (Kelly et al. 1987),
- Oklahoma (Jayaseelan and Russell 2007),
- Minnesota (French and O'Neill 2012; Wyffels et al. (2000)),
- Florida (Cook and Bloomquist 2005), and
- Idaho (Brown 1998).

Other studies include those conducted by Buettner and Libby (1979); Tadros et al. (1985); Hinkle (2006); Omar et al. (2008); Lee (2010); the PCI Committee on Bridges (2012); Keske (2014); and Hofrichter (2014).

Most of these studies have dealt with improving the accuracy of pre-erection camber. The subject of predicting long-term beam deflections in the composite system, and beam rebound once the deck is removed, has not received similar attention. A common conclusion found in the majority of these studies is that the main reasons for the difference between predicted and measured camber are: 1) a disparity exists between the assumed and observed concrete properties (modulus, creep, shrinkage), and; 2) local fabrication practices are often not properly considered within the prediction method such as type of curing, storage time and conditions, ambient relative humidity, temperature gradients, etc.

In past decades, NCHRP has sponsored related work such as NCHRP 496, in which guidelines were presented to obtain realistic estimates of concrete elastic modulus, shrinkage, and creep, and how these properties could affect prestress losses, camber, and deflections (Tadros et al. 2003). Much earlier, NCHRP Projects 12-1 and 12-6 addressed deflection and loss of camber

in steel girders, considering shrinkage and creep in the concrete slab among other factors (Baldwin and Guell 1975), while the effect of thermal changes in concrete bridges was investigated by Imbsen et al. (1985) in NCHRP 276.

2.1 Factors that Affect Camber at Release and Long-term Camber, Deflections, and Rebound

One of the reasons why camber, deflections, and rebound are difficult to predict accurately is the uncertainty in quantifying the various factors that affect beam behavior. Consider, for instance, the simple case of a simply supported PC beam with a harped tendon profile loaded with self-weight only. Deflection at mid-span due to self-weight is given by Eq. 2.1, while camber due to prestressing force is given by Eq. 2.2:

$$\Delta_w = \frac{5wl^4}{384EI} \quad (2.1)$$

$$\Delta_p = \frac{P_i l^2}{8EI} \left[(e_m + (e_e - e_m) \frac{4b^2}{3l^2}) \right] \quad (2.2)$$

Although both are theoretically ‘exact’ models, none of the input parameters are usually precisely known. For example, the modulus of elasticity (E) at the time of prestress release, a key factor for determining camber at release and long-term camber, deflections, and prestress losses, is typically calculated using approximate formulas as a function of compressive strength (f'_c), that are known to have a large amount of scatter (Pauw 1960; Raphael 1985). Although perhaps known with less uncertainty, beam self-weight (w), the initial prestressing force (P_i), beam length (l), location of harping points (b), cross-sectional geometry (moment of inertia (I)), and prestress eccentricities at the ends (e_e) and mid-span (e_m), are all estimates of actual conditions. Other factors that affect camber at release are unintended cracking, inaccurate estimates of transfer length, and any debonding between the strands and concrete. Storm et al. (2013) investigated the effects of fabrication practices on prestressed concrete beams and concluded that the actual compressive strength at release, the deformation of internal void forms in box beams during casting, and curing method all significantly affect camber.

The effect of these uncertainties is further compounded when long-term behavior accounting for creep and shrinkage is considered. When a beam is cast using typical fabrication methods and placed within an actual structure, a multitude of factors may significantly affect the magnitude of beam camber and deflections. For example, downward deflections are not only

caused by beam and deck self-weight and associated creep, but also by other factors such as: differential shrinkage between the beam and strands in the initial non-composite section; differential shrinkage between the deck and beam in the final composite section; and negative temperature gradients. Conversely, camber is primarily caused by the prestressing force and associated creep as well as positive temperature gradients. In both cases, concrete creep and shrinkage will vary depending on the initial concrete properties; the member size effect (volume to surface ratio); the method and length of curing; age at loading; level and variation of prestressing force and other sustained loads; as well as environmental conditions.

Additional factors will affect the rebound of all beam types, such as the weight of the removed deck, unintended support stiffness, connectivity to other components such as diaphragms and end walls, as well as member deterioration.

2.2 Methods to Measure Camber at Release and Long-term Camber

While most state DOTs have guidelines to measure camber, a consistent standard does not exist (Honarvar et al. 2015). Common methods of measurement in the precast industry include the use of simple, inexpensive tools such as a tape measure and a stretched string along the length of the beam, a rotary laser, and occasionally, survey equipment such as a theodolite or total station. Different approaches also exist for where (top flange, bottom flange, or web) and when camber is measured (immediately after release of prestress, or up to three hours after prestress transfer (Honarvar et al. 2015)). MDOT allows camber at release to be reported within seven days of detensioning the strands (MDOT 2018).

Typically, the industry practice for quantifying camber involves measuring from the prestressing bed to the bottom of the beam at mid-span using a conventional tape measure recorded to the nearest 1/8 in. This method requires that the beam rests free on the prestressing bed at the time of camber measurement. Variations in industry practice include differences in benchmark points for locating mid-span (where camber is measured); the refinement of the value read from the tape measure; and the time at which camber is measured. Potential sources of error in camber measurement include bed defects, friction between the precasting bed and beam ends, and inconsistently flat top or bottom flange surfaces locally or along the beam length.

The string method was used by Storm et al. (2013) and Menkulasi et al. (2014a; 2014b). However, this approach may lead to inaccurate measurements due to string elongation and

anchorage slippage unless strict precautions are followed. Honarvar et al. (2015) used a rotary laser to accurately measure camber, and developed adjustment procedures for measuring camber using more traditional methods. Regardless of the method used, camber can be measured accurately if appropriate procedures are followed and possible errors are properly accounted for.

2.3 Methods to Predict Camber at Release and Long-term Camber and Deflections

Typical methods used to predict camber at release include tabulated equations, moment area theorems, and energy methods. The computation of long-term camber is more complex because of the number of parameters involved and the time-dependent and interrelated nature of these parameters. Although AASHTO (2020) provides limited guidance for long-term camber calculation, ACI 435R-95 (1963; 2003) summarizes seven methods for computing long-term deflections in prestressed concrete one-way flexural members, which include the:

- 1) Multiplier Method (Martin 1977);
- 2) Incremental Time-Steps Method (Nilson 1987);
- 3) Approximate Time-Steps Method (Branson and Ozell 1961);
- 4) Axial Strain and Curvature Method (Ghali and Favre 1986);
- 5) Prestress Loss Method (Tadros et al. 1985);
- 6) CEB-FIB Model Code Method (CEB-FIP 1990); and
- 7) Section Curvature Method (ACI 435R-95)

2.3.1 Multiplier Method (Martin 1977)

The multiplier method was originally developed by Martin (1977) for building double tees with a 2 in. concrete topping and normal strength concrete, and does not provide reliable estimates for bridge girders with high strength concrete subject to a variety of environmental conditions. The multiplier method was later refined by Zia (1979) and Tadros (1985), and was ultimately adopted in the PCI Design Handbook (2010) and the PCI Bridge Design Manual (2011). However, Stallings et al. (2003) concluded that the PCI Design Handbook (2010) multiplier method significantly overestimated camber at the time of girder erection. In 2011, Tadros et al. (2011) revisited the topic of precast girder camber variability and concluded that designs should allow for up to a 50% variation in results unless future research offers a refined procedure.

2.3.2 Incremental Time-Steps Method (Nilson 1987)

The incremental time-steps method (Nilson 1987) is based on the idea that correctly capturing the variation of the prestressing force with time leads to a more accurate estimation of time dependent camber and displacement. The design life of the structure is divided into several increasingly larger time intervals (ACI 435R-95). PCI recommends that at least four time steps are used when implementing this method and requires the adoption of creep, shrinkage and relaxation time dependent functions. The strain distributions, curvatures, and prestressing forces are calculated for each interval together with the incremental shrinkage, creep, and relaxation losses during the particular time interval. (ACI 435R-95). The procedure is repeated for all subsequent incremental intervals, and an integration or summation of the incremental curvatures is made to give the total time dependent curvature at the particular section along the span (ACI 435R-95). These calculations should be made for a sufficient number of points along the span to allow the construction of a curvature diagram with reasonable accuracy. This diagram can then be used to calculate deflections using numerical integration and the second moment area theorem. Eq. 2.3 can be used to determine curvature at a given section in a prestressed concrete beam at any given point in time.

$$\phi_{pt} = -\frac{P_i e_x}{E_c I_c} + \sum_0^t (P_{n-1} - P_n) \frac{e_x}{E_c I_c} - \sum_0^t (C_n - C_{n-1}) P_{n-1} \frac{e_x}{E_c I_c} \quad 2.3$$

where P_i is the prestressing force at prestress transfer; e_x is the eccentricity of the strand group with respect to the beam centroid; E_c is the modulus of elasticity of beam concrete at prestress transfer; I_c is the moment of inertia of the beam; P_{n-1} and P_n are the prestressing force at time $n-1$ and n , respectively; and C_n and C_{n-1} are the creep coefficients at time n at time $n-1$, respectively.

The first term in Eq. 2.3 represents the curvature due to prestressing force, the second term represents the reduction in curvature due to prestress loss, and the third term represents the increase in curvature due to the average prestress force induced creep. As can be seen, a creep model needs to be adopted to implement this method and a number of time steps. It is implied in this method that the user is going to adopt a methodology to estimate prestress losses at every considered time step. Detailed guidance for how to estimate prestress losses is provided in ACI 423.10R-16. The method also allows for the use of various moduli of elasticity at every time step considered provided that a time dependent function for modulus is employed. One possible approach to

implement the incremental time-steps method (Nilson 1987) considering four time steps is as follows:

Step 1 (t_0): Prestress Transfer – Determine all immediate losses. Determine force in the tendon immediately after transfer. $P_1 = P_j - (E.S. + RE + AS)$ where P_j is the prestressing force at step 1; P_j is the prestressing force at jacking; ES, RE, and AS are prestress losses due to elastic shortening, relaxation of strands, and anchorage seating.

Step 2 ($t_0 - t_1$): Prestress Transfer to 30 Days – Calculate losses during this period using P_1 and calculate $P_2 = P_1 - CR_{1-2} - RE_{1-2} - SH_{1-2}$ where P_2 is the prestressing force at step 2 and CR_{1-2} , RE_{1-2} , and SH_{1-2} are creep, relaxation, and shrinkage losses between step 1 and 2. This can be done as follows:

- Calculate strain in concrete at the centroid of tendons, ϵ_o .
- Calculate creep coefficient $\phi(t_1, t_0)$
- Calculate creep strain $\epsilon_o \phi(t_1, t_0)$
- Calculate shrinkage strain $\epsilon_{SH}(t_1, t_0)$
- Calculate creep and shrinkage prestress loss $E[\epsilon_o \phi(t_1, t_0) + \epsilon_{SH}(t_1, t_0)]$
- Calculate relaxation loss (select a function)
- Calculate $P_2 = P_1 - CR_{1-2} - RE_{1-2} - SH_{1-2}$

Step 3 ($t_1 - t_2$): 30 days to one year – Calculate losses during this period of time using P_2 and calculate $P_3 = P_2 - CR_{2-3} - RE_{2-3} - SH_{2-3}$

- ❖ First, considering the loads applied at t_0 (P_1):
 - Calculate creep coefficient $\phi(t_2, t_0)$ and subtract $\phi(t_1, t_0)$
 - Calculate creep strain for loads applied at t_0 , $\epsilon_o [\phi(t_2, t_0) - \phi(t_1, t_0)]$ (Fig. 2.1.)
- ❖ Second, considering the loads applied at t_1 (P_2):
 - Calculate strain at the centroid of tendons due to loads applied at t_1 , ϵ_1
 - Calculate creep coefficient $\phi(t_2, t_1)$
 - Calculate creep strain $\epsilon_1 \phi(t_2, t_1)$
 - Calculate shrinkage strain $\epsilon_{SH}(t_2, t_1)$
- ❖ Third,
 - Calculate creep and shrinkage prestress loss over interval:

$$E(\varepsilon_0 [\phi(t_2, t_0) - \phi(t_1, t_0)] - \varepsilon_1 \phi(t_2, t_1) + \varepsilon_{SH}(t_1, t_0))$$

- Calculate relaxation loss over interval
- Calculate force in tendon at the end of time step

$$P_3 = P_2 - CR_{2-3} - RE_{2-3} - SH_{2-3}$$

Step 4: One year to end of service life. Repeat.

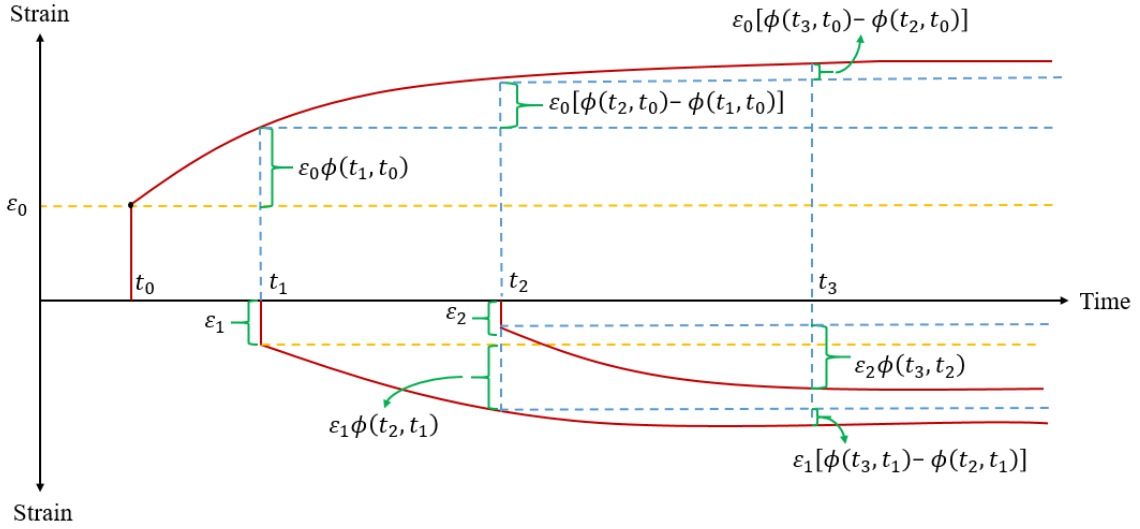


Fig. 2.1. Illustration of creep induced strain due to prestress and prestress loss

Once the prestress losses for every time step are calculated, they can be implemented in Eq. 2.3 to calculate curvature at various sections along the beam and then calculate camber using the second moment area theorem. Pre-erection camber predictions based on the incremental time-steps method (Nilson 1987) are compared to predictions based on the proposed methodology later in this report. The incremental time-steps method (Nilson 1987) is intended to capture the variation of prestressing force with time and how that force affects camber and displacements. However, this method cannot capture flexural deformations caused by differential shrinkage between the deck and the girder concrete or shrinkage induced creep. Therefore, the comparison with the methodology proposed in this report is conducted only for pre-erection camber and not after the deck is cast because the downward displacement caused by differential shrinkage is significant and cannot be captured by the incremental time-steps method (Nilson 1987).

2.3.3 Approximate Time-Steps Method (Branson and Ozell 1961)

The approximate time-step method, also known as the creep coefficient and average prestress force method (Nilson 1987), is a simplified version of the incremental time steps method (Nilson 1987) and it includes an initial and a final time step. The approximate time-steps method originally presented by Branson and Ozell (1961), and ACI 435R-95 (1963), tends to yield in most cases comparable results to the PCI multiplier method (ACI 435R-95).

2.3.4 Axial Strain and Curvature Method (Ghali and Favre 1986)

This method originally developed by Ghali and Favre (1986) and further discussed in Ghali (1986) and Elbadry and Ghali (1989) is based on a strain compatibility based cross-sectional analysis, which is used to calculate curvatures and deflections. The method can be used for uncracked and cracked sections and does not require the determination of prestress losses. Transformed section properties are used to conduct the cross-sectional analysis and the modulus of elasticity of concrete is calculated using the Age Adjusted Effective Modulus (AAEM) (Trost 1967; Bazant 1972) concept to account for concrete creep and aging effects (ACI 435R-95).

2.3.5 Prestress Loss Method (Tadros et al. 1985)

This method is outlined in Tadros et al. (1985) and uses a set of time dependent multipliers for predicting camber and displacements at discrete points in time similar to the method proposed by Martin (1977). However, unlike Martin (1977), this method provides a time dependent coefficient for prestress losses due to creep, shrinkage, and relaxation. It should be noted that the time dependent multipliers in question are provided at discrete times namely at erection, final time, and long term, which is defined as the difference between final time and erection time.

2.3.6 CEB-FIB Model Code Method (CEB-FIP 1990)

This method provides detailed and simplified approaches for evaluating deflection and camber in prestressed concrete elements, cracked or uncracked (ACI 435R-95). Details of this approach are given in CEB-FIB (1990). The simplified method includes the use of multipliers that account for long terms effects including creep, cracking, and percentage of reinforcement.

2.3.7 Section Curvature Method (ACI 435R-95)

This method is provided in Appendix B of ACI 435R-95 and is a comprehensive method for the computation of deformations in plane frames. The method is based on a strain compatibility based cross-sectional analysis, which is used to obtain axial strains and curvatures along the length of the members with the purpose of calculating frame deflections, translations and rotations. The method requires the use of creep and shrinkage models to account for time dependent effects and employs the AAEM method (Trost 1967; Bazant 1972).

2.4 Previous Studies

A detailed summary of previous studies is provided in Appendix A.

2.5 Summary of Literature Review

The topic of accurately estimating time-dependent deflections in prestressed concrete bridge girders has received rigorous attention over the last 50 years. Most studies reviewed concluded that the first step towards an accurate estimation of camber is the accurate estimate of the parameters that affect camber. For example, modulus of elasticity is a key factor that affects camber at release and long-term camber and is typically estimated using formulas that are a function of compressive strength, unit weight, and aggregate factors. Some previous studies (Mante 2016; Rizkalla et al. 2013; Rosa et al. 2007) investigated the modification of such formulas to account for regional practices, such as providing a calibration factor to account for local aggregates. Similarly, a relationship between the specified and measured f_c was investigated to develop equations that relate the two. The establishment of such a relationship was conducted under the hypothesis that a more accurate input for the compressive strength would lead to a more accurate estimation of the modulus of elasticity. Also, many investigations on camber predictions were followed up with additional investigations for how to accurately predict, modulus, creep, and shrinkage properties of regionally used concrete mixes used in prestressed concrete beam fabrication. The accurate estimation of such properties is paramount because they serve as input values in the prediction framework. Although, currently, there is no consensus as to which model best predicts creep and shrinkage in concrete. In many studies, it was emphasized that support conditions during storage also play a role in camber growth. Therefore, such storage conditions should be recorded including the type of support and should be taken into account when estimating

pre-erection camber. The multiplier method has resulted many times in inaccurate camber predictions due to its inability to account for a variety of conditions. Refinements of this method have been somewhat successful in improving time-dependent camber predictions, especially when the effects of creep and shrinkage are considered. However, the incremental time step method was identified as one of the most accurate methods to predict camber.

2.6 Prestressed Concrete Beam Camber Questionnaire

A prestressed concrete beam camber questionnaire consisting of 31 questions was distributed nationwide with the purpose of gaining a better understanding of the current practice for estimating the camber and deflection of bridge superstructures. The questions that were included in the survey as well as the answers received are provided in Appendix B.

Almost 70% of the 40 respondents reported that they have experienced camber related problems with prestressed concrete bridge beams that are often beyond normal construction tolerances.

As stated at the beginning of this chapter and as corroborated by the results of the survey, at least 13 states have sponsored camber related research with the purpose of improving methods for predicting camber.

When asked what method the respondents use to predict prestressed concrete beam camber; 45.95% of the 37 respondents indicated that they used the multiplier method; 27.03% indicated that they used the prestress loss method; 2.70 % indicated that they used the approximate time step method; another 2.70% indicated that they used the incremental time step method; and 21.62 % indicated that they use other methods. These results suggest that the number of states that currently use the relatively more accurate incremental time step method is rather small (1 out of 37 respondents).

When asked whether the method that the respondents use considers explicitly the effects of creep and shrinkage only nine out of 43 respondents provided answers. Out of these nine respondents 56% responded “yes” and 44% responded “no”.

When asked which model the respondents used to predict the effects of creep and shrinkage, 25 out of 32 respondents (78%) indicated that they used the AASHTO LRFD Specification (2020) method, one respondent indicated that they used the ACI 209R-92 model, and six respondents indicated that they used other methods. However, out of the six respondents

who chose other methods, one referred to the recommendations in the NCHRP Report 496, one mentioned the name of the software used to calculate camber, one indicated that only creep effects are accounted for, and rest indicated that creep and shrinkage are not explicitly accounted for.

When asked whether the respondents had a tool that they used to predict camber and displacement at a given time after the erection of the deck and after the opening of the bridge to traffic, the majority of the respondents responded “no”. A few referenced the “Leap Concrete Bridge Software”, some referenced the multiplier method, some responded that camber and displacement after the deck is cast is not of interest, and some referenced in house programs and procedures.

When asked what the range of concrete compressive strength at release and 28 days that the respondents typically specified was, the response most of the time included a range between 4-8 ksi. Lower and upper bounds included 4 ksi and 12 ksi.

When asked how the respondents determined the modulus of elasticity in camber predictions, 24 out of the 30 respondents (80%) indicated that they used the equation in the AASHTO LRFD Specifications (2020), and nine out of 30 indicated that they used other methods. However, many of the nine respondents indicated that they used a version of the AASHTO LRFD Specification (2020) equation with various values for coefficient K . For example, one respondent indicated that they use $K=0.9$ because of old Nebraska aggregate. Other respondents indicated that they use $K=0.85$, and another indicated that they use $K=1.0$. As can be seen some type of regional calibration is provided to account for local conditions. TxDOT policy is to set all concrete moduli to 5000 ksi for stress and deflection calculations. One respondent indicated that they used the equation in ACI 363R-92 and another indicated that they had derived their own equation based on curve fitting techniques using historical data.

When asked whether the respondents used the specified value for compressive strength or some other value when calculating modulus using the equation provided in AASHTO LRFD Specifications (2020), most respondents stated that they used specified values. One respondent stated that the specified release strength is increased by 25% and specified 28-day strength is increased by 45%. Another responded that they have adopted a procedure to adjust based on expected strengths since they are typically higher. One respondent stated that specified rather than expected values are used since the variability in compressive strength is believed to be included in the multipliers.

When asked whether a specific curing technique was required, 17 out of 32 responded indicated “yes” and the rest indicated “no”. Out of the 17 respondents who indicated that a specific curing technique was required, four indicated that they specified steam curing, three moist curing, and the rest chose “other”. Other techniques identified included radiant heat and steam and moist curing depending on the season during fabrication. When asked which curing technique was most prevalent in the state, the answers primarily included steam or moist curing.

When asked which method the respondents used to measure camber, most answers included either the string line or surveying methods. Similar results were reported when asked which tools the respondents used when measuring camber.

When asked how frequently camber was measured, answers included once, twice, three times, weekly, monthly, rarely, and as needed. The policies for when camber was measured varied.

When asked what time of the day camber was measured, most responded that there was not a specific time required and any time during daylight hours was acceptable.

When asked what procedure or approach (such as pre-loading) was used to minimize or control camber overgrowth most responded that either they did not resort to such techniques or used either rarely or occasionally.

When asked how inaccurate camber predictions were typically dealt with, respondents reported various techniques such as adjustments in haunch height, seat elevations, screed elevations, stirrup extensions, and asphalt overlay.

When asked whether box beams were prone to inaccurate camber predictions, 13 out of 27 respondents stated “yes”, six “no”, and eight indicated that this beam type was not used in their state. It is interesting to note how the box beams are not used in eight states. In general, no specific box beam size was indicated to be more prone to inaccurate camber predictions.

When asked whether cored slabs were prone to inaccurate camber predictions, four out of 28 respondents stated “yes”, five “no”, and 19 indicated that this beam type was not used in their state.

When asked whether AASHTO I-beams were prone to inaccurate camber predictions, seven out of 30 respondents stated “yes”, 11 “no”, and 12 indicated that this beam type is not used in their state.

When asked whether bulb T beams were more prone to inaccurate camber predictions, 14 out of 29 respondents stated “yes”, 11 “no”, and four stated that this beam type was not used in their state.

When asked whether other beam types were prone to inaccurate camber predictions, seven out of 30 respondents indicated “yes”, 15 “no”, and interestingly eight respondents indicated that this beam type was not used in their state.

When asked whether the respondent had a procedure or tool to predict beam rebound in deck replacement projects, most respondents indicated “no”.

When asked whether the respondents had measured beam rebound in existing beams after deck weight is removed and the deflection of the beams after the new deck has been placed, 10 out of 28 respondents indicated “yes”, and 18 “no”. When asked whether a correlation existed between rebound and deflection, the answers among the 10 respondents varied between “no” and “yes”.

In summary, the results of the national survey were useful in revealing the practices of various states related to camber prediction and provided context for the various tasks discussed as part of this research project.

Chapter 3: Prediction Methodology

Chapter 3: Prediction Methodology

3.1 Time Dependent Cross-sectional Curvature Method

In this chapter, the proposed prediction methodology is discussed and the approach for its development is presented. The proposed prediction methodology is general and is able to predict camber and displacements at any point during the life of a prestressed concrete beam or composite bridge superstructure featuring prestressed concrete or steel beams and a concrete deck. The overall framework for the prediction methodology is based on principles of engineering mechanics, although components of the methodology are based on empirical models, such as: the estimation of the modulus of elasticity for beam and deck concrete, relaxation of steel strands, and prediction of concrete creep and shrinkage properties. The proposed prediction methodology was developed based on several iterations/approaches (Table 3.1). Iteration No. 6 represents the final version of the proposed prediction methodology. The details of the other iterations are presented with the purpose of discussing their advantages and limitations and to provide some context for comparisons presented later in this report between camber predictions obtained using various approaches. The implementation of Iteration No. 6 is presented in Appendix C through the use of a Matlab based algorithm that features a graphical user interface. Examples of how the algorithm used in Iteration No. 6 works are provided in Appendix D and E for composite prestressed concrete and steel beams, respectively.

All iterations are based on the principle of superposition. The principle of superposition was first applied by McHenry (1943) who stated that the strain produced by a stress increment applied at any time τ_i is not affected by any stress applied either earlier or later. Gilbert and Ranzi (2011) report that for increasing stress histories, the principle of superposition agrees well with experimental observations, whereas for decreasing stress histories it overestimates creep recovery. In the case of composite systems, increasing stress histories include the placement of deck and superimposed dead loads, whereas decreasing stress histories include time dependent prestress losses and deck removal. In general, it has been reported (Gilbert and Ranzi 2011) that the principle of superposition provides a good approximation of the time dependent strains in concrete caused by a time-varying stress history.

Some of the initial iterations are similar to the sectional curvature method (Ghali et al. 2002) presented in Appendix B of ACI 435R-95 (ACI Committee 1995). All iterations are based on the assumption that tensile and flexural creep are equal to compressive creep due to a lack of

consensus for how tensile and flexural creep relate to compressive creep, with some researchers (Chu and Carreira 1986; Bazant and Oh 1984) multiplying creep coefficients obtained for compressive creep by factors that range from one to three to characterize tensile creep behavior (Gilbert and Ranzi 2011). Iteration No. 6 provides an opportunity to enter tensile creep and flexural creep magnification factors if a consensus on the subject matter were to be reached. The default value for these magnification factors is 1.0.

Table 3.1. Description of iterations used to develop the proposed prediction methodology

Camber predicted at	Iteration/Approach No.						
	1		2	3	4	5	6
	Analysis Level		Analysis Level	Analysis Level	Analysis Level	Analysis Level	Analysis Level
	Basic	Advanced	Advanced	Advanced	Advanced	Advanced	Advanced
Release	A	B	B	B	B	B	B
Pre-erection	A C	B C	B C	B D	B D	B E	B F
Any time (no deck replacement)			B C	B D	B D	B E	B F
At any time (with deck replacement)					B D	B E	B F
A: Ignore debonding, transfer length, and variation in support location. B: Consider debonding, transfer length, and variation in support location. C: Creep effects = AAEM, $\mu=0.7/1.0$, discrete time steps, number of sections = end and mid-span, single creep curve D: Creep effects = EM, multiple time steps, Mod. = $f(t)$, number of sections = end and mid-span, single creep curve E: Creep effects = EM, multiple time steps, Mod. = $f(t)$, number of sections = multiple, single creep curve F: Creep effects = EM, multiple time steps, Mod. = $f(t)$, number of sections = multiple, multiple creep curves							

3.1.1 Iteration No. 1

This approach is concerned with the estimation of pre-erection camber and is similar to the axial strain and curvature method proposed by Ghali and Favre (1986) and section curvature method provided in ACI 435R-95. The method features two levels of analyses: 1) basic and 2) advanced. Both levels of analyses were used to predict camber at release and pre-erection. In the basic approach strand debonding, transfer length, and variation of support location was not considered. Strands were assumed to be harped at $0.4L$, where L is the overall length of the beam and support locations were assumed to be at the ends of the beam. Elastic shortening losses were calculated using gross-section properties and the closed form equation provided in the commentary of AASHTO LRFD Bridge Design Specifications (2020) (Eq. C5.9.3.2.3a-1). Pre-erection camber was calculated using the Age Adjusted Effective Modulus (AAEM) method (Trost 1967; Bazant 1972) to account for creep and concrete aging effects. Pre-erection camber can be calculated at

any time before the deck is placed on the beam. Initial stress conditions are calculated when the strands are detensioned. Only one time step is considered between camber at release and pre-erection camber. Cross-sectional analysis based on strain compatibility is conducted to estimate curvatures at mid-span and end of the beam, construct curvature diagrams, and estimate camber using the second moment area theorem. Camber predictions are conducted in Mathcad.

In the advanced approach, the algorithm takes into account the location of supports, transfer length, debonding, multiple strand patterns, and uses transformed cross-sectional properties. In lieu of deducting elastic shortening losses from the jacking force, transformed section properties are used together with the jacking force to calculate camber at release. This resulted in similar estimations for camber at prestress release with those obtained using the basic approach. The estimation of pre-erection camber was conducted using the same approach. Camber is calculated as the difference in beam elevation at mid-span and supports. The supports can be temporary supports during storage at the precast facility or permanent supports at the bridge site. Prestress losses due to creep and shrinkage are considered using a time dependent sectional analysis and are calculated at pre-erection. Similarly, prestresses losses due to the relaxation of steel are calculated at pre-erection using the formula (C5.9.3.4.2c-1) provided in the commentary of AASHTO LRFD Specifications (2020), which provides a time dependent function for the calculation of relaxation losses. In this formula, one of the required inputs is the elastic shortening loss, which was calculated using the gross section properties and the closed form formula (Eq. C5.9.3.2.3a-1) provided in the commentary of AASHTO (2020). Elastic shortening losses were calculated solely to compute the variation of strand stress with time and to calculate relaxation losses. Elastic shortening losses were not included when calculating cross-sectional curvatures and beam displacements since transformed section properties were utilized. All calculated long-term losses are used to adjust the magnitude of the prestressing force at the beginning of the subsequent time step so that camber and displacements at service can be calculated accordingly.

In this approach, the time dependent effects of prestress and self-weight induced creep, and differential shrinkage between the beam and the strands are considered simultaneously, despite the fact that the curvature diagrams for each phenomenon are different. This is done to avoid conducting several strain compatibility based cross-sectional analysis as mid-span and beam ends for each phenomenon. Pre-erection camber is calculated using a curvature diagram that is most appropriate for the combined effects of these phenomena. This approximation is addressed in

Iteration No. 2 in which the effects of these phenomena are treated separately so that the appropriate curvature diagram can be used in each case.

Fig. 3.1 shows the distribution of forces in a prestressed concrete girder. The time dependent strain at any fiber in the precast girder can be calculated by summing the elastic and creep strains due to initial stresses, elastic and creep strains due to changes in stress, shrinkage strain, and strains due to thermal gradients (Eq. 3.1).

$$\varepsilon_t = \frac{\sigma_0}{E_0}(1 + \varphi_{t,t_0}) + \int_{t_0}^t \left[\frac{1}{E(\tau)} \frac{d\sigma(\tau)}{d\tau} (1 + \varphi(t, \tau)) \right] d\tau + \varepsilon_{sh,t} + \varepsilon_{TG} \quad (3.1)$$

ε_t is the total strain at time t ; $\sigma_0, \sigma(\tau)$ is the stress at time t_0 and τ , respectively; $E_0, E(\tau)$ is the modulus of elasticity at times t_0 and τ , respectively; $\varphi_{t,t_0}, \varphi(t, \tau)$ is the creep coefficient at time t due to load applied at time t_0 and τ , respectively; $\varepsilon_{sh,t}$ is the shrinkage strain at time t ; and ε_{TG} is the strain due to temperature gradient. Term 1 represents the elastic and creep strains due to a stress applied at time t_0 . Term 2 represents the elastic and creep strains due to changes in stress in the time interval t_0 to t . Term 3 represents the shrinkage strain at time t and Term 4 represents the strain caused by temperature gradients.

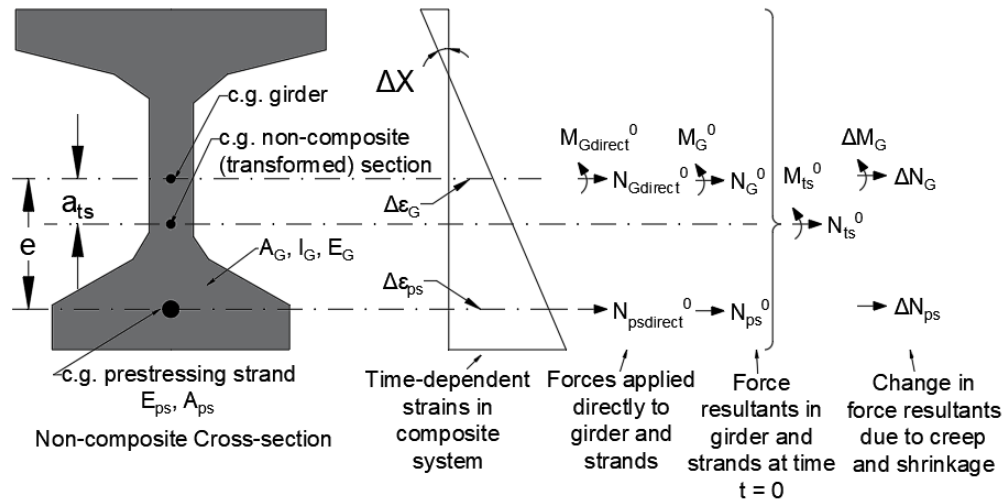


Fig. 3.1. Distribution of forces in a prestressed concrete girder

Eq. 3.1 uses an integral type creep law and uses the principle of superposition of stepwise prescribed stress histories. The integral term can be replaced by an algebraic expression if an aging coefficient μ is introduced. Eq. 3.1 can then be reformulated as shown in Eq. 3.2. The assumed

stress history shown in Fig. 3.2a is idealized such that the initial stress and the change in stress are applied simultaneously over the considered time step (Fig. 3.2b). The initial and creep induced strains due initial stresses and changes in stress are illustrated in Fig. 3.2c.

$$\varepsilon_t = \frac{\sigma_0}{E_0}(1 + \varphi_{t,t_0}) + \frac{\Delta\sigma}{E_0}(1 + \mu_{t,t_0}\varphi_{t,t_0}) + \varepsilon_{sh,t} + \varepsilon_{TG} \quad (3.2)$$

The first two terms can also be expressed as:

$$\varepsilon_{(t,t_0)} = [\varepsilon_0 + \varepsilon_0\varphi_o(t, t_o)] + [\Delta\varepsilon_0 + \Delta\varepsilon_0\mu(t, t_o)\varphi_o(t, t_o)]$$

$$\varepsilon_t = \frac{\sigma_0}{E_{EM}} + \frac{\Delta\sigma}{E_{AAEM}} + \varepsilon_{sh,t} + \varepsilon_{TG} \quad (3.3)$$

$$E_{EM} = \frac{E_0}{(1 + \varphi_{t,t_0})} \quad (3.4)$$

$$E_{AAEM} = \frac{E_0}{(1 + \mu_{t,t_0}\varphi_{t,t_0})} \quad (3.5)$$

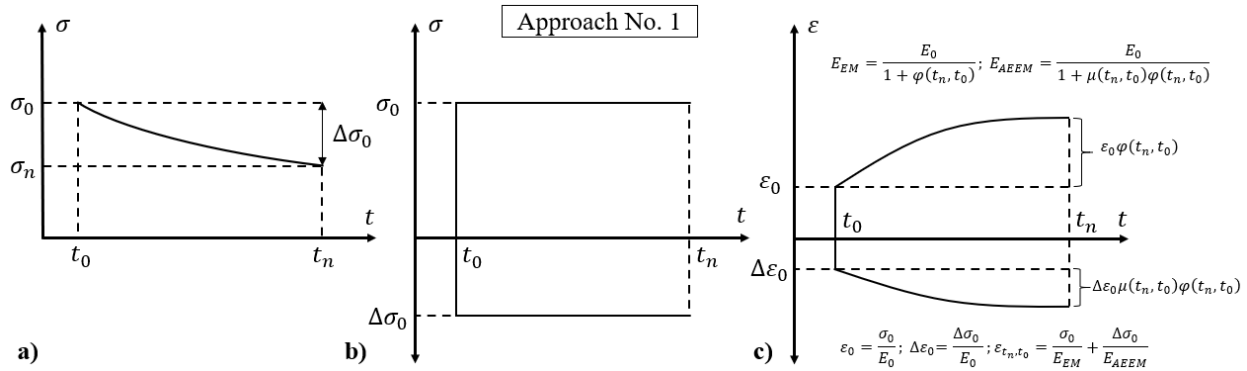


Fig. 3.2. Illustration of Approach No. 1 for predicting time-dependent flexural deformations; a) assumed stress history, b) discretized stress history, and c) elastic and creep induced strains using Effective Modulus (EM) and Age-adjusted Effective Modulus (AAEM) approaches and based on discretized stress history

Creep effects can be estimated by either using the AAEM method developed by Trost (1967), Dilger and Neville (1971), and Bazant (1972), or Effective Modulus (EM) method. The AAEM method is used in cases when only a limited number of time steps are considered and an adjustment for the concrete age is made to account for: 1) the stiffening of the material with time, and 2) the change in concrete's viscoelastic behavior as a function of various ages of loading. If the EM method is used, a sufficient number of time steps should be considered together with a

time dependent function for the modulus to partially account for the effect of aging. This is the approach used in Iterations No. 3, 4, and 5 which ignore the effect of loading age on concrete viscoelastic behavior, as well as in Iteration No. 6, which takes into account the loading age by invoking separate creep curves in every time step.

In the AAEM method, creep effects are modeled by varying the modulus of elasticity with time as a function of the creep coefficient and an aging coefficient. For example, consider a concrete cylinder subject to a sustained load as in a typical creep test (Fig. 3.3). Strain will initially increase proportionally with load until the load is kept constant at a certain magnitude (typically $0.4f'_c$). After the load is held constant, the cylinder will continue to deform (strain) due to creep. This increase in strain at constant stress can be captured by using a reduced modulus, which will vary with time. This time-varying modulus can be conveniently used to capture the effects of creep. However, as the cylinder is loaded over time, creep effects are slightly counterbalanced by an increase in modulus due to the maturing concrete. As a result, to properly capture creep effects, the initial modulus is reduced with a creep coefficient, ϕ , but modified with an aging coefficient, μ , representing the AAEM approach. As a result, Eq. 3.2 can be re-written as shown in Eq. 3.3 using the effective and age adjusted effective modulus, respectively (E_{EM} , E_{AAEM}), which are defined in Eqs. 3.4 and 3.5. The creep coefficient (ϕ) and the shrinkage coefficient can be based on various existing models. A typical recommended value for the aging coefficient is 0.7, and this is the value adopted in this study.

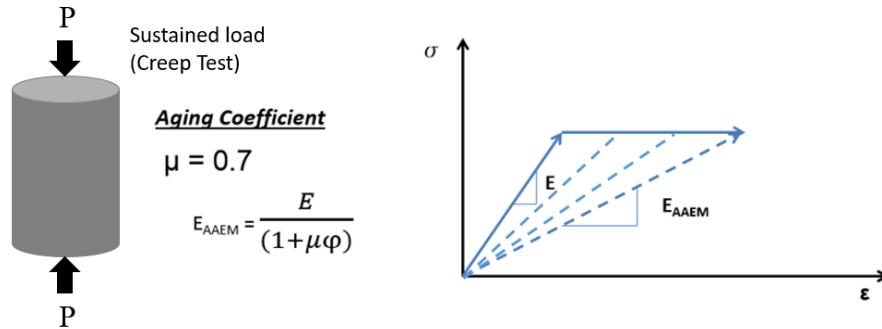


Fig. 3.3. Illustration of Age Adjusted Effective Modulus (AAEM) concept to capture creep effects

As defined earlier σ_0 represent initial stresses in the member. These stresses can be created by forces and moments that are initially directly applied to the precast girder or by forces and moments that are initially applied to the heterogeneous system (girder concrete+strands). It is assumed that the girder self weight and prestressing force are applied to the heterogeneous system.

To utilize the free shrinkage and creep properties of the precast beam, it is useful to decouple the internal forces acting on the heterogenous section, into forces acting separately on the beam and strands.

The term $\Delta\sigma$ in Eq. 3.2 represents the change in stress due to changes in axial forces and bending moments in the girder or prestressing strands. The changes in strains and stresses due to time dependent effects can be calculated by using equations of material constitutive relationships, equilibrium and compatibility (Eq. 3.6-3.11). For example, the change in axial strain at the centroid of the girder can be expressed by summing the creep strain due to initial axial forces, the elastic and creep strain due to the change in axial force over time and the free shrinkage strain (Eq. 3.6). The change in curvature in the girder can be expressed by summing the creep curvature due to initial moments and the elastic and creep curvatures due to changes in these moments over time (Eq. 3.7). The change in prestressing strand strain over time can be calculated by dividing the change in stress in the strand by the modulus of elasticity of the strand (Eq. 3.8). The change in stress in the strand over time represents either a prestress loss or prestress gain due to differential shrinkage and creep. Prestresses losses due to relaxation can be added to losses caused by creep and shrinkage to calculate the magnitude of the prestressing force at the end of the considered time step and at the beginning of the next time step.

In a statically determinate system, because there are no externally applied axial forces over time, the sum of changes in the axial forces in each component must equal zero (Eq. 3.9). In addition, in such a determinate system because there are no externally applied bending moments over time, the sum of moment about the centroid of the girder must equal zero (Eq. 3.10). Finally, assuming perfect bond between girder concrete and prestressing strands the axial strains at the centroid of each of these components can be inter-related by using the change in curvature and the distances between the centroids (Eq. 3.11).

Equations 3.6 to 3.11 form a set of linear equations, which can be solved simultaneously to determine the six unknowns caused by the time dependent effects ($\Delta\varepsilon_G, \Delta\varepsilon_{ps}, \Delta X, \Delta N_G, \Delta N_{ps}, \Delta M_G$).

Material Constitutive Relationships

$$\varepsilon_{G(t_n t_o)} = \frac{(N_{Gdirect}^0 + N_G^0)[\varphi_{G_o}(t_n t_o)]}{E_{G_o} A_G} + \frac{\Delta N_G [1 + \mu_G(t_n t_o) \varphi_{G_o}(t_n t_o)]}{E_{G_o} A_G} + \varepsilon_{ShG}(t_n); \quad (3.6)$$

where: $N_{Gdirect}^0 = 0$, $N_G^0 = \frac{A_G N_{ts}^0}{A_{ts0}} - \frac{M_{ts}^0 a_{ts0} A_G}{I_{ts0}}$; $N_{ts}^0 = -P_e$ and $M_{ts}^0 = M_{Gsw} - P_e e_{tr}$

$$\Delta X_{(t_n t_o)} = \frac{(M_{Gdirect}^0 + M_G^0)[1 + \phi_{G_o}(t_n t_o)]}{E_{G_o} I_G} + \frac{\Delta M_G [1 + \mu_G(t_n t_o) \phi_{G_o}(t_n t_o)]}{E_{G_o} I_G}; \quad (3.7)$$

where: $M_{Gdirect}^0 = 0$, $M_G^0 = \frac{M_{ts}^0 I_G}{I_{ts0}}$

$$\Delta \varepsilon_{ps(t_n t_o)} = \frac{\Delta N_{ps}}{E_{ps} A_{ps}} \quad (3.8)$$

Equilibrium

$$\Delta N_G + \Delta N_{ps} = 0 \quad (3.9)$$

$$\Delta M_G + \Delta N_{ps} e = 0 \quad (3.10)$$

Compatibility

$$\Delta \varepsilon_{ps(t_n t_o)} = \Delta \varepsilon_{G(t_n t_o)} + \Delta X_{(t_n t_o)} e \quad (3.11)$$

3.1.2 Iteration No. 2

In this approach, the basic level of analysis was removed and only the advanced analysis was further developed since all calculations were conducted in Mathcad 15 and there was no convenience to implement simplifying assumptions. Additionally, the approach used in the advanced analysis in Iteration No. 1 was extended to predict camber and displacements in a composite bridge superstructure featuring prestressed concrete or steel beams. Changes in beam camber and displacements due to deck replacement were not considered and were within the scope of Iteration No. 4. In this approach, the effects of prestress, self-weight, beam shrinkage, prestress induced creep, self-weight induced creep, and differential shrinkage are considered as separate phenomena to utilize the curvature diagram appropriate for each. This creates the inconvenience of conducting several strain compatibility based cross-sectional analysis at the ends and mid-span for each phenomenon to obtain the corresponding curvatures. This inconvenience is addressed in Iterations No. 5 and 6 when the effects of these phenomena are treated simultaneously, and numerical integration is used to compute camber and displacements. An algorithm written in Mathcad 15 was developed in which the user provides certain inputs and the algorithm calculates

camber and displacements at the desired time. Two Mathcad files were prepared. The first was used to calculate camber and displacements in a prestressed concrete beam or a bridge that features such beams, and the second was used to predict service camber and displacements in a bridge that features steel girders. The algorithm considers the following five key time steps to compute time dependent beam camber and displacements:

- 1) detensioning of the strands,
- 2) time from detensioning of the strands to deck placement,
- 3) placement of the deck,
- 4) placement of any superimposed dead loads (such as overlay and barriers) and opening of the bridge to traffic, and
- 5) time from opening of the bridge to traffic to the end of service life.

The approach is similar to that presented in Iteration No. 1 except that there is a new component (i.e. the deck). Fig. 3.4 shows the distribution of forces in a composite system consisting of a precast prestressed concrete girder and a cast-in-place deck or a steel girder and a cast-in-place concrete deck. Since the analysis consists of a total of five time steps, three of which are discrete (strand detensioning, deck placement, and placement of superimposed loads) while the other two vary in length, the aging coefficient was taken equal to 0.7 for the time step between strand detensioning and deck placement, and 1.0 for the time step from deck placement to end of service life. This was done due to the fact that most of the maturing of concrete will take place during the time step from strand detensioning to deck placement. This of course does not take into account the effect of loading age on concrete creep behavior. When considering creep effects in the deck, the only time step that applies is the one from placement of superimposed loads to end of bridge service life. Therefore, the aging coefficient for the deck concrete was taken equal to 0.7 in this time step. The modulus of elasticity used in the time step from strand detensioning to deck placement is the initial modulus (i.e. the modulus when the strands are detensioned), whereas the one used for the time step from deck placement to end of service life is the 28 day modulus.

In this approach, the actual stress history shown in Fig. 3.5a is discretized using two timesteps (unlike in Approach No. 1, in which one-time step was used). The incurred changes in stress are separated between changes that occur during step 1 and those that occur during step 2. The discretized stress history is shown in Fig. 3.5b. The initial and creep induced strains due to initial stresses and changes in stress is illustrated in Fig. 3.5c.

As defined earlier σ_0 represent initial stresses in the member. These stresses can be created by forces and moments that are initially directly applied to the precast girder or the cast-in-place deck ($M_{Ddirect}^0, N_{Ddirect}^0, M_{Gdirect}^0, N_{Gdirect}^0, N_{psdirect}^0$) or by forces and moments that are initially applied to the composite system (M^0, N^0). For example, an eccentric prestressing force in a pre-tensioned girder creates axial forces and bending moments that are applied directly to the girder in addition to the axial force applied directly to the prestressing strand. To utilize the free shrinkage and creep properties of the precast concrete beam and cast-in-place concrete deck, it is useful to decompose the internal forces and moments acting on the composite section, into forces and moments acting separately on the girder and deck ($M_D^0, N_D^0, M_G^0, N_G^0, N_{ps}^0$). Examples of axial forces and bending moment that are applied initially to the composite system include post-tensioning forces applied after the system is made composite and bending moments created due to superimposed dead loads.

The term $\Delta\sigma$ in Eq. 3.2 represents the change in stress due to changes in axial forces and bending moments in the deck, girder or prestressing strands. These are denoted as $\Delta M_D, \Delta N_D, \Delta M_G, \Delta N_G$ and ΔN_{ps} in (Fig. 3.4). The changes in strains and stresses due to time dependent effects can be calculated by using equations of material constitutive relationships, equilibrium and compatibility (Eq. 3.12-3.28). For example, the change in axial strain at the centroid of the deck and girder can be expressed by summing the creep strain due to initial axial forces, the elastic and creep strain due to the change in axial force over time and the free shrinkage strain (Eq. 3.12 and 3.13). The change in curvature in the deck and girder can be expressed by summing the creep curvature due to initial moments and the elastic and creep curvatures due to changes in these moments over time (Eq. 3.14 and 3.15). The change in prestressing strand strain over time can be calculated by dividing the change in stress in the strand by the modulus of elasticity of the strand (Eq. 3.16). The change in stress in the strand over time represents either a prestress loss or prestress gain due to differential shrinkage and creep. Prestresses losses due to relaxation can be added to losses caused by creep and shrinkage to calculate the magnitude of the prestressing force at the end of the considered time step and at the beginning of the next time step.

In a statically determinate system, because there are no externally applied axial forces over time, the sum of changes in the axial forces in each component must equal zero (Eq. 3.17). In addition, in such a determinate system because there are no externally applied bending moments over time, the sum of moment about the centroid of the girder must equal zero (Eq. 3.18). Finally,

assuming perfect bond between deck concrete, girder concrete and prestressing strands the axial strains at the centroid of each of these components can be inter-related by using the change in curvature and the distances between the centroids (Eq. 3.19 and 3.20).

Equations 3.12 to 3.20 for composite prestressed concrete beams and Eq. 3.21-3.28 for composite steel beams form sets of linear equations, which can be solved simultaneously to determine the nine unknowns caused by the time dependent effects in a composite prestressed concrete beam system ($\Delta\epsilon_D, \Delta\epsilon_G, \Delta\epsilon_{ps}, \Delta X, \Delta N_D, \Delta N_G, \Delta N_{ps}, \Delta M_D, \Delta M_G$) and seven unknowns in a composite steel girder system ($\Delta\epsilon_D, \Delta\epsilon_G, \Delta X, \Delta N_D, \Delta N_G, \Delta M_D, \Delta M_G$).

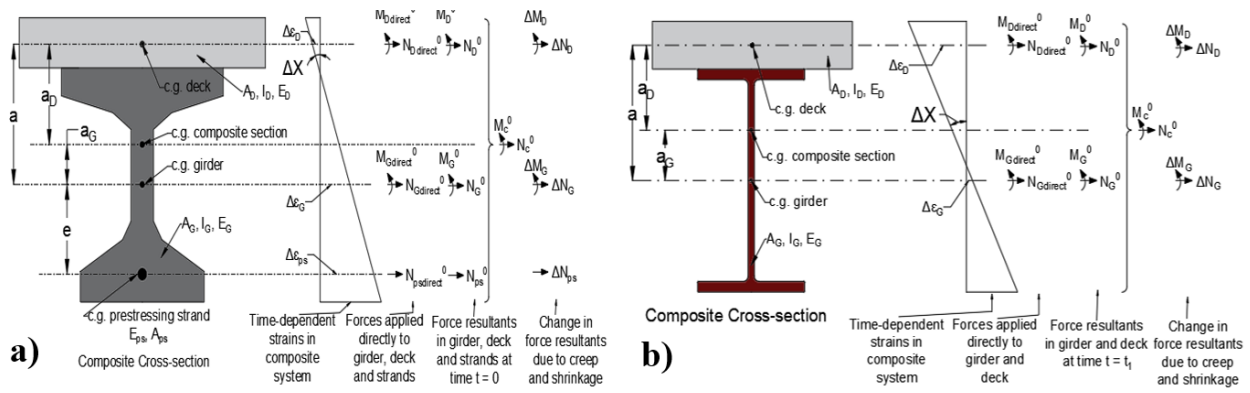


Fig. 3.4. Distribution of internal forces in: a) composite prestressed concrete beam, and b) composite steel beam

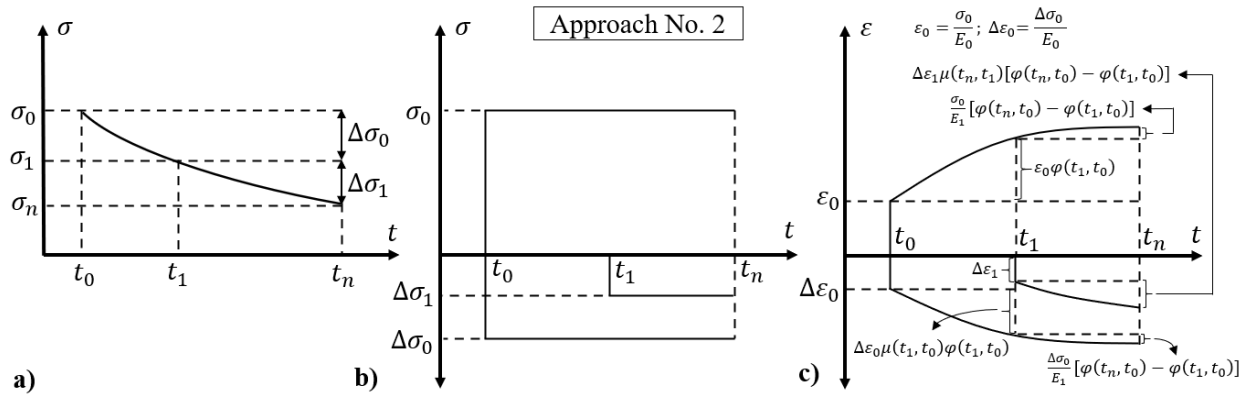


Fig. 3.5. Illustration of Approach No. 2 for predicting time-dependent flexural deformations; a) assumed stress history, b) discretized stress history, and c) elastic and creep induced strains due to discretized stress history

Cross-sectional Analysis for Composite Prestressed Concrete Beams

$$\Delta \varepsilon_{G(t_n t_d)} = \frac{N_{Gd} [\varphi_{G_o}(t_n t_o) - \varphi_{G_o}(t_d t_o)]}{E_{Gd} A_G} + \frac{\Delta N_{Gd} [1 + \mu_G(t_n t_d) [\varphi_{G_o}(t_n t_o) - \varphi_{G_o}(t_d t_o)]]}{E_{Gd} A_G} + [\varepsilon_{ShG}(t_n) - \varepsilon_{ShG}(t_d)]; \quad (3.12)$$

$$\text{where: } N_{G_0} = N_{Gdirect}^0 + N_G^0, N_{Gdirect}^0 = 0, N_G^0 = \frac{A_G N_{ts}^0}{A_{ts_0}} - \frac{M_{ts}^0 a_{ts_0} A_G}{I_{ts_0}} + \frac{A_G N_c^0}{A_{c_0}} + \frac{M_c^0 a_{G_0} A_G}{I_{c_0}},$$

$$N_{Gd} = N_{G_0} + \Delta N_{G_0}$$

$$\Delta \varepsilon_{D(t_n t_d)} = \frac{(N_{Ddirect}^0 + N_D^0) \varphi_{D_o}(t_n t_d)}{E_{D_o} A_D} + \frac{\Delta N_D [1 + \mu_D(t_n t_d) \varphi_{D_o}(t_n t_d)]}{E_{D_o} A_D} + \varepsilon_{ShD}(t_n); \quad (3.13)$$

$$\text{where: } N_{Ddirect}^0 = 0, N_D^0 = \frac{n_o A_D N_c^0}{A_{c_0}} - \frac{M_c^0 a_{D_o} n_o A_D}{I_{c_0}}$$

$$\Delta X_{(t_n t_d)} = \frac{M_{Gd} [\varphi_{G_o}(t_n t_o) - \varphi_{G_o}(t_d t_o)]}{E_{Gd} I_G} + \frac{\Delta M_{Gd} [1 + \mu_G(t_n t_d) [\varphi_{G_o}(t_n t_o) - \varphi_{G_o}(t_d t_o)]]}{E_{Gd} I_G}; \quad (3.14)$$

$$\text{where: } M_{G_0} = M_{Gdirect}^0 + M_G^0, M_{Gdirect}^0 = 0, M_G^0 = \frac{M_{ts}^0 I_G}{I_{ts_0}} + \frac{I_G M_c^0}{I_{c_0}}, M_{Gd} = M_{G_0} + \Delta M_{G_0}$$

$$\Delta X_{(t_n t_d)} = \frac{(M_{Ddirect}^0 + M_D^0) \varphi_{D_o}(t_n t_d)}{E_{D_o} I_D} + \frac{\Delta M_D [1 + \mu_D(t_n t_d) \varphi_{D_o}(t_n t_d)]}{E_{D_o} I_D}; \quad (3.15)$$

$$\text{where: } M_{Ddirect}^0 = 0, M_D^0 = \frac{M_c^0 n_o I_D}{I_{c_0}};$$

$$\text{Note: } N_{ts}^0 = -P_e, M_{ts}^0 = M_{Gsw} + M_{dsw} - P_e e_{tr}, N_c^0 = 0, M_c^0 = M_{bsw} + M_{osw}$$

$$\Delta \varepsilon_{ps(t_n t_d)} = \frac{\Delta N_{ps}}{E_{ps} A_{ps}} \quad (3.16)$$

$$\Delta N_{Gd} + \Delta N_D + \Delta N_{ps} = 0 \quad (3.17)$$

$$\Delta M_{Gd} + \Delta M_D - \Delta N_D a + \Delta N_{ps} e = 0 \quad (3.18)$$

$$\Delta \varepsilon_{D(t_n t_d)} = \Delta \varepsilon_{G(t_n t_d)} - \Delta X_{(t_n t_d)} a \quad (3.19)$$

$$\Delta \varepsilon_{ps(t_n t_d)} = \Delta \varepsilon_{G(t_n t_d)} + \Delta X_{(t_n t_d)} e \quad (3.20)$$

Cross-sectional Analysis for Composite Steel Beams

$$\Delta \varepsilon_{D(t_n, t_d)} = \frac{(N_{Ddirect}^0 + N_D^0) \varphi_{D_o}(t_n, t_d)}{E_{D_o} A_D} + \frac{\Delta N_D [1 + \mu_D(t_n, t_d) \varphi_{D_o}(t_n, t_d)]}{E_{D_o} A_D} + \varepsilon_{ShD}(t_n); \quad (3.21)$$

$$\text{where: } N_{Ddirect}^0 = 0, N_D^0 = \frac{n_o A_D N_c^0}{A_{c_o}} - \frac{M_c^0 a_{D_o} n_o A_D}{I_{c_o}}$$

$$\Delta X_{(t_n, t_d)} = \frac{(M_{Ddirect}^0 + M_D^0) \varphi_{D_o}(t_n, t_d)}{E_{D_o} I_D} + \frac{\Delta M_D [1 + \mu_D(t_n, t_d) \varphi_{D_o}(t_n, t_d)]}{E_{D_o} I_D}; \quad (3.22)$$

$$\text{where: } M_{Ddirect}^0 = 0, M_D^0 = \frac{M_c^0 n_o I_D}{I_{c_o}}$$

$$\text{Note: } N_c^0 = 0, M_c^0 = M_{bsw} + M_{osw}$$

$$\Delta X_{(t_n, t_d)} = \frac{\Delta M_G}{E_G I_G} \quad (3.23)$$

$$\Delta \varepsilon_{G(t_n, t_d)} = \frac{\Delta N_G}{E_G A_G} \quad (3.24)$$

$$\Delta \varepsilon_{ps(t_n, t_d)} = \frac{\Delta N_{ps}}{E_{ps} A_{ps}} \quad (3.25)$$

$$\Delta N_D + \Delta N_G = 0 \quad (3.26)$$

$$\Delta M_G + \Delta M_D - \Delta N_D a = 0 \quad (3.27)$$

$$\Delta \varepsilon_{D(t_n, t_d)} = \Delta \varepsilon_{G(t_n, t_d)} - \Delta X_{(t_n, t_d)} a \quad (3.28)$$

The initial curvatures and the change in curvature obtained using Eq. 3.14 and 3.22 can be used to obtain camber and displacements at the beginning of the time step as well as at the end of it using the moment area method and the applicable curvature diagrams. Fig. 3.6 shows the curvature diagrams in a typical prestressed concrete beam. While this approach allows the use of various harping points, in Fig. 3.6 the prestressing strands are assumed to be harped at $0.4L$, where L is the length of the beam. Curvatures are calculated based on the transformed section properties for both the non-composite and composite sections. Prestress and prestress creep create negative curvatures. Beam shrinkage in the non-composite section and deck shrinkage in the composite section create positive curvatures, whereas beam shrinkage in the composite section creates negative curvatures. The self-weight of beam and deck and the creep due to self-weight create positive curvatures. These curvature diagrams can be used to calculate camber and displacements

at any point in time using the moment area method. The proposed method can be summarized as follows:

- Perform time dependent analysis at the cross-sectional level for each time step assuming the beam is simply supported.
 - Calculate curvatures for each time step at mid-span and ends of beam
 - Time Step 1: Calculate curvatures due to the effects of the prestressing force and self-weight using transformed section properties.
 - Time Step 2: Calculate time dependent effects (such as changes in forces and curvatures) at the cross-sectional level using transformed section properties (beam+steel) due to forces computed in Time Step 1.
 - Time Step 3: Calculate instantaneous curvatures due to deck weight and superimposed dead loads.
 - Time Step 4: Calculate time dependent effects at a sectional level using transformed section properties (beam+deck+steel) due to forces computed in the previous time steps.
 - Draw curvature diagram for the beam/superstructure at each time step
 - Calculate camber and displacements using the second moment area theorem at each time step



3.1.3 Iteration No. 3

This approach uses the Effective Modulus (EM) method as opposed to the AAEM method used in the previous approach. In the EM method, additional time substeps are considered between major construction activities that constitute the major time steps used in the AAEM method. Additionally, a time dependent function for the modulus is adopted so that the appropriate modulus can be used for each time step. This approach partially removes the necessity to use an aging coefficient since the modulus of elasticity is updated continuously throughout the analysis using the adopted time depend function. The need for an aging coefficient is not entirely removed since a single creep curve is used for the beam and another for the deck concrete. Therefore, the effect of loading age on creep behavior is ignored. Additionally, the utilization of additional time substeps theoretically improves camber and displacement predictions for the next time step since initial stress conditions are continuously updated. However, the impact of this improvement was not clear and this iteration provided an opportunity to quantify the difference between predictions using this approach and that used in Iteration No. 2. The strain compatibility based cross-sectional analysis is conducted in an identical manner with that presented in the previous approach with the exception that the aging coefficient is set equal to 1.0. This iteration is also implemented in Mathcad and the user is asked to provide input related to girder properties, deck properties, prestressing steel properties, and environmental conditions at the precast facility or bridge site. Then the user is asked to select the desired creep and shrinkage model to be used in the time dependent analysis. Finally, the algorithm also has the ability to calculate camber and displacements caused by temperature gradients for beams featuring certain geometries.

The strain at any given fiber in composite or non-composite cross-sections can be calculated using Eq. 3.29. This is illustrated in Fig. 3.7. The set of equations that can be used to conduct time dependent cross-sectional analysis for non-composite (but heterogenous) cross-sections, composite cross-sections featuring a prestressed concrete beam, and composite cross-sections featuring a steel beam are provided in Eq. 3.30-3.35, Eq. 3.36-3.44, and Eq. 3.45-3.51, respectively. These sets of equations apply also to Iterations No. 4 and No. 5, although there are differences in the way that they are implemented. These differences are explained in the subsequent sections.

Fundamental Equation

$$\varepsilon_{(t_n, t_o)} = \varepsilon_o + \sum_{j=0}^m \left[\frac{\sigma_o}{E_j} [\varphi_o(t_{j+1}, t_o) - \varphi_o(t_j, t_o)] + \left[\Delta\varepsilon_j + \sum_{i=j}^m \frac{\Delta\sigma_j}{E_i} [\varphi_o(t_{i+1}, t_o) - \varphi_o(t_i, t_o)] \right] \right] \quad (3.29)$$

$$\varepsilon_i = \frac{\sigma_i}{E_i}; \Delta\varepsilon_i = \frac{\Delta\sigma_i}{E_i}; n = \text{number of time steps}; m = \text{number of loading events}; n = m + 1$$

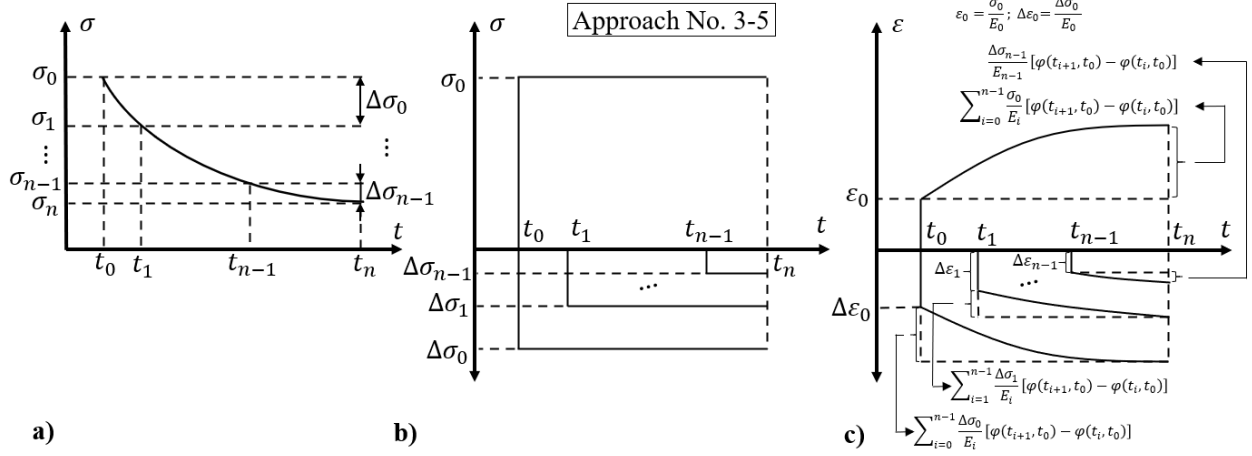


Fig. 3.7. Illustration of Approach No. 3-5 for predicting time-dependent flexural deformations for Approach No. 3-5; a) assumed stress history, b) discretized stress history, and c) elastic and creep induced strains due to discretized stress history

Cross-sectional Analysis for Non-composite Prestressed Concrete Beams

$$\Delta\varepsilon_{G(t_n, t_o)} = \sum_{i=0}^m \left[\frac{N_{G_i} [\varphi_{G_o}(t_{i+1}, t_o) - \varphi_{G_o}(t_i, t_o)]}{E_{G_i} A_G} + \frac{\Delta N_{G_i} [1 + [\varphi_{G_o}(t_{i+1}, t_o) - \varphi_{G_o}(t_i, t_o)]]}{E_{G_i} A_G} + [\varepsilon_{ShG}(t_{i+1}) - \varepsilon_{ShG}(t_i)] \right]; \quad (3.30)$$

$$\text{where: } N_{G_0} = N_{G_{direct}}^0 + N_G^0, N_{G_{direct}}^0 = 0, N_G^0 = \frac{N_{ts}^0 A_G}{A_{ts_0}} - \frac{M_{ts}^0 a_{ts_0} A_G}{I_{ts_0}}, N_{G_{i+1}} = N_{G_i} + \Delta N_{G_i}$$

$$\Delta X_{(t_n, t_o)} = \sum_{i=0}^m \left[\frac{M_{G_i} [\varphi_{G_o}(t_{i+1}, t_o) - \varphi_{G_o}(t_i, t_o)]}{E_{G_i} I_G} + \frac{\Delta M_{G_i} [1 + [\varphi_{G_o}(t_{i+1}, t_o) - \varphi_{G_o}(t_i, t_o)]]}{E_{G_i} I_G} \right]; \quad (3.31)$$

$$\text{where: } M_{G_0} = M_{G_{direct}}^0 + M_G^0, M_{G_{direct}}^0 = 0, M_G^0 = \frac{M_{ts}^0 I_G}{I_{ts_0}}, M_{G_{i+1}} = M_{G_i} + \Delta M_{G_i}$$

$$\text{Note: } N_{ts}^0 = -P_e \text{ and } M_{ts}^0 = M_{G_{sw}} - P_e e_{tr}$$

$$\Delta \varepsilon_{ps(t_n t_o)} = \frac{\sum_{i=0}^m \Delta N_{ps_i}}{E_{ps} A_{ps}} \quad (3.32)$$

$$\Delta N_{G_i} + \Delta N_{ps_i} = 0 \quad (3.33)$$

$$\Delta M_{G_i} + \Delta N_{ps_i} e = 0 \quad (3.34)$$

$$\Delta \varepsilon_{ps(t_n t_o)} = \Delta \varepsilon_{G(t_n t_o)} + \Delta X_{(t_n t_o)} e \quad (3.35)$$

Cross-sectional Analysis for Composite Prestressed Concrete Beams

$$\Delta \varepsilon_{G(t_n t_d)} = \sum_{i=r}^m \left[\frac{N_{G_i} [\varphi_{G_o}(t_{i+1}, t_o) - \varphi_{G_o}(t_i t_o)]}{E_{G_i} A_G} + \frac{\Delta N_{G_i} [1 + [\varphi_{G_o}(t_{i+1}, t_o) - \varphi_{G_o}(t_i t_o)]]}{E_{G_i} A_G} + [\varepsilon_{ShG}(t_{i+1}) - \varepsilon_{ShG}(t_i)] \right]; \quad (3.36)$$

$$where: N_{G_0} = N_{G_{direct}}^0 + N_G^0, N_{G_{direct}}^0 = 0, N_G^0 = \frac{N_{ts}^0 A_G}{A_{ts_0}} - \frac{M_{ts}^0 a_{ts_0} A_G}{I_{ts_0}},$$

$$N_{G_r} = N_{G_0} + \frac{N_c^0 A_G}{A_{c_0}} + \frac{M_c^0 a_{G_0} A_G}{I_{c_0}} + \left[\sum_{i=0}^{(r-1)} \Delta N_{G_i} \right], N_{G_{i+1}} = N_{G_i} + \Delta N_{G_i}$$

$$\Delta \varepsilon_{D(t_n t_d)} = \sum_{i=r}^m \left[\frac{N_{D_i} [\varphi_{D_o}(t_{i+1}, t_d) - \varphi_{D_o}(t_i t_d)]}{E_{D_i} A_D} + \frac{\Delta N_{D_i} [1 + [\varphi_{D_o}(t_{i+1}, t_d) - \varphi_{D_o}(t_i t_d)]]}{E_{D_i} A_D} + [\varepsilon_{ShD}(t_{i+1}) - \varepsilon_{ShD}(t_i)] \right]; \quad (3.37)$$

$$where: N_{D_0} = N_{D_{direct}}^0 + N_D^0, N_{D_{direct}}^0 = 0, N_D^0 = \frac{N_c^0 n_0 A_D}{A_{c_0}} - \frac{M_c^0 a_{D_0} n_0 A_D}{I_{c_0}},$$

$$N_{D_r} = N_{D_0}, N_{D_{i+1}} = N_{D_i} + \Delta N_{D_i}$$

$$\Delta X_{(t_n t_d)} = \sum_{i=r}^m \left[\frac{M_{G_i} [\varphi_{G_o}(t_{i+1}, t_o) - \varphi_{G_o}(t_i t_o)]}{E_{G_i} I_G} + \frac{\Delta M_{G_i} [1 + [\varphi_{G_o}(t_{i+1}, t_o) - \varphi_{G_o}(t_i t_o)]]}{E_{G_i} I_G} \right]; \quad (3.38)$$

$$where: M_{G_0} = M_{G_{direct}}^0 + M_G^0, M_{G_{direct}}^0 = 0, M_G^0 = \frac{M_{ts}^0 I_G}{I_{ts_0}},$$

$$M_{G_r} = M_{G_0} + \frac{M_c^0 I_G}{I_{c_0}} + \left[\sum_{i=0}^{(r-1)} \Delta M_{G_i} \right], M_{G_{i+1}} = M_{G_i} + \Delta M_{G_i}$$

$$\Delta X_{(t_n, t_d)} = \sum_{i=r}^m \left[\frac{M_{D_i} [\varphi_{D_o}(t_{i+1}, t_d) - \varphi_{D_o}(t_i, t_d)]}{E_{D_i} I_D} + \frac{\Delta M_{D_i} [1 + [\varphi_{D_o}(t_{i+1}, t_d) - \varphi_{D_o}(t_i, t_d)]]}{E_{D_i} I_D} \right]; \quad (3.39)$$

where: $M_{D_0} = M_{D_{direct}}^0 + M_D^0, M_{D_{direct}}^0 = 0, M_D^0 = \frac{M_c^0 n_o I_D}{I_{c_0}}, M_{D_r} = M_{D_0}, M_{D_{i+1}} = M_{D_i} + \Delta M_{D_i}$

Note: $N_{ts}^0 = -P_e, M_{ts}^0 = M_{Gsw} + M_{dsw} - P_e e_{tr}, N_c^0 = 0, M_c^0 = M_{bsw} + M_{osw}$

$$\Delta \varepsilon_{ps(t_n, t_d)} = \frac{\sum_{i=r}^m \Delta N_{ps_i}}{E_{ps} A_{ps}} \quad (3.40)$$

$$\Delta N_{D_i} + \Delta N_{G_i} + \Delta N_{ps_i} = 0 \quad (3.41)$$

$$\Delta M_{G_i} + \Delta M_{D_i} - \Delta N_{D_i} a + \Delta N_{ps_i} e = 0 \quad (3.42)$$

$$\Delta \varepsilon_{D(t_n, t_d)} = \Delta \varepsilon_{G(t_n, t_d)} - \Delta X_{(t_n, t_d)} a \quad (3.43)$$

$$\Delta \varepsilon_{ps(t_n, t_d)} = \Delta \varepsilon_{G(t_n, t_d)} + \Delta X_{(t_n, t_d)} e \quad (3.44)$$

Cross-sectional Analysis for Composite Steel Beams

$$\Delta \varepsilon_{D(t_n, t_d)} = \sum_{i=r}^m \left[\frac{N_{D_i} [\varphi_{D_o}(t_{i+1}, t_d) - \varphi_{D_o}(t_i, t_d)]}{E_{D_i} A_D} + \frac{\Delta N_{D_i} [1 + [\varphi_{D_o}(t_{i+1}, t_d) - \varphi_{D_o}(t_i, t_d)]]}{E_{D_i} A_G} + \right. \\ \left. [\varepsilon_{ShD}(t_{i+1}) - \varepsilon_{ShD}(t_i)] \right]; \quad (3.45)$$

where: $N_{D_0} = N_{D_{direct}}^0 + N_D^0, N_{D_{direct}}^0 = 0, N_D^0 = \frac{N_c^0 n_o A_D}{A_{c_0}} - \frac{M_c^0 a_{D_0} n_o A_D}{I_{c_0}}, N_{D_r} =$

$$N_{D_0}, N_{D_{i+1}} = N_{D_i} + \Delta N_{D_i}$$

$$\Delta X_{(t_n, t_d)} = \sum_{i=r}^m \left[\frac{M_{D_i} [\varphi_{D_o}(t_{i+1}, t_d) - \varphi_{D_o}(t_i, t_d)]}{E_{D_i} I_D} + \frac{\Delta M_{D_i} [1 + [\varphi_{D_o}(t_{i+1}, t_d) - \varphi_{D_o}(t_i, t_d)]]}{E_{D_i} I_D} \right]; \quad (3.46)$$

where: $M_{D_0} = M_{D_{direct}}^0 + M_D^0, M_{D_{direct}}^0 = 0, M_D^0 = \frac{M_c^0 n_o I_D}{I_{c_0}}, M_{D_r} = M_{D_0}, M_{D_{i+1}} = M_{D_i} + \Delta M_{D_i}$

Note: $N_c^0 = 0, M_c^0 = M_{bsw} + M_{osw}$

$$\Delta X_{(t_n, t_d)} = \frac{\Delta M_G}{E_G I_G} \quad (3.47)$$

$$\Delta \varepsilon_{G(t_n, t_d)} = \frac{\Delta N_G}{E_G A_G} \quad (3.48)$$

$$\Delta N_{D_i} + \Delta N_{G_i} = 0 \quad (3.49)$$

$$\Delta M_{G_i} + \Delta M_{D_i} - \Delta N_{D_i} a = 0 \quad (3.50)$$

$$\Delta \varepsilon_{D(t_n, t_d)} = \Delta \varepsilon_{G(t_n, t_d)} - \Delta X_{(t_n, t_d)} (y_{D_{bottom}} - y_{G_{bottom}}) \quad (3.51)$$

3.1.4 Iteration No. 4

In this approach, the EM method used in Iteration No. 3 was extended to capture the effects of deck replacement on beam camber and displacement. To model the effect of deck removal and the corresponding beam rebound, the loading history was modified to include unloading steps for the self-weight of existing barrier, existing overlay, existing deck, and locked in forces in the deck, as well as new loading steps for the weight of the new deck, weight of new overlay, and weight of new barrier. The removal of the self-weight of the deck and the removal of internal forces present in the deck were treated as new forces applied at the time of deck removal to the non-composite beam section. The removal of barrier and overlay were considered as new forces applied to the composite system. The calculation of the immediate rebound involves calculating the upward displacement (camber) caused by the removal of existing barrier, overlay, and deck weight, as well as the removal of internal axial forces and moments in the existing deck. The calculation of longer-term rebound requires a time dependent analysis. Time dependent effects due to these newly applied forces were calculated using the remaining creep coefficient for the beam concrete based on a creep curve with a loading time of one day (i.e. the application of prestressing force when the beams are fabricated). This approach, similar to the approaches presented so far, relies on the use of a single creep curve for beam and deck concrete. In this approach, each phenomenon that causes time dependent camber and displacements is treated separately and the strain compatibility based cross-sectional analysis is based on two sections: beam end and midspan. For each phenomenon the corresponding curvature diagrams are used to predict camber and displacements at midspan.

A total of eight key time steps were considered to compute time dependent camber and displacements. These time steps include the:

- 1) detensioning of the strands;
- 2) time from detensioning of the strands to deck placement;

- 3) time at which the deck is placed;
- 4) time from deck placement to placement of barriers, overlay and the opening of bridge to traffic;
- 5) time from the opening of the bridge to traffic to deck removal for projects that features a deck replacement;
- 6) time from deck removal to new deck placement;
- 7) time from new deck placement to placement of new barrier, overlay, and reopening of bridge to traffic; and
- 8) time from reopening of bridge to traffic to the end of service life, which is currently considered to be 75 years.

In this iteration, the user has the ability to enter time in days for all these eight key time steps such that camber and displacements are calculated at the desired times. Additionally, because camber and displacements at a given time step depend on the conditions in the previous time step, such as the predicted camber and forces in the previous time step, the user has the ability to enter the camber in the previous time step if such information is available. In this case, the algorithm overrides the predicted camber in the previous time step with that specified by the user. When camber and displacements in a steel bridge are desired, pre-erection camber must be provided as an input. Then the effect of differential shrinkage between the deck and the steel girder is considered to calculate service camber and displacements.

3.1.5 Iteration No. 5

In this approach, the algorithm prepared in Mathcad was translated into Matlab, was improved to develop a graphical user interface, and was further enhanced to improve the accuracy of camber and displacement predictions. Unlike the previous iterations, in this approach the strain compatibility based cross-sectional analysis is conducted for several sections along the length of the beam rather than only at mid-span and beam ends. The calculated cross-sectional curvatures are then used to construct a curvature diagram and numerical integration together with the second moment area theorem is used to compute camber and displacements at mid-span. In this approach, the effects of creep and shrinkage (element based as well as differential), as well as steel relaxation are considered simultaneously during the strain compatibility based cross-sectional analysis. This is different from the approach used in the previous iterations in which the effects of these

phenomena were considered separately to utilize the curvature diagrams appropriate for each phenomenon. The utilization of numerical integration removes the need to rely on curvature diagrams for which existing deflection formulations can be employed to predict camber and displacements. The flowchart used to create the code for this approach is provided in Fig. 3.8.

The algorithm starts with the creation of arrays for the number of time steps and number of sections. Then time dependent material properties such as the modulus of elasticity, creep, and shrinkage are calculated. Similarly, time dependent section properties are calculated since the calculation of composite section properties depends on the modular ratio (E_c/E_s or E_{deck}/E_{beam}). Then, initial curvatures, axial forces, bending moments, and deflections caused by self-weight and the prestressing force are calculated. The algorithm operates based on two loops. The first represents the number of time steps at which camber and displacements are desired to be calculated. The second, which runs within the first loop, represents the number of sections along the beam. For a given time step, a strain compatibility based cross-sectional analysis is conducted for multiple sections along the length of the beam with the purpose of constructing a curvature diagram and computing deflections by using numerical integration and second moment area theorem. The change in axial force, bending moment, and strand strain is recorded and this information is used to update initial conditions for next time step. This procedure is repeated until all desired time steps are considered. The computed camber and displacement can then be plotted as a function of time.

Another improvement offered by Iteration No. 5, is the ability to calculate the deflected shape of the beam as a function of time. The graphical user interface offers the user the ability to plot camber/displacements as a function of time and location along the beam span from beam end to midspan. In this iteration, just like in the previous iterations, axial forces and moments are summed at the end of each time step so that time dependent effects can be calculated for the next time step based on a single creep curve for beam and deck concrete with loading times that correspond with prestress release and deck placement, respectively.

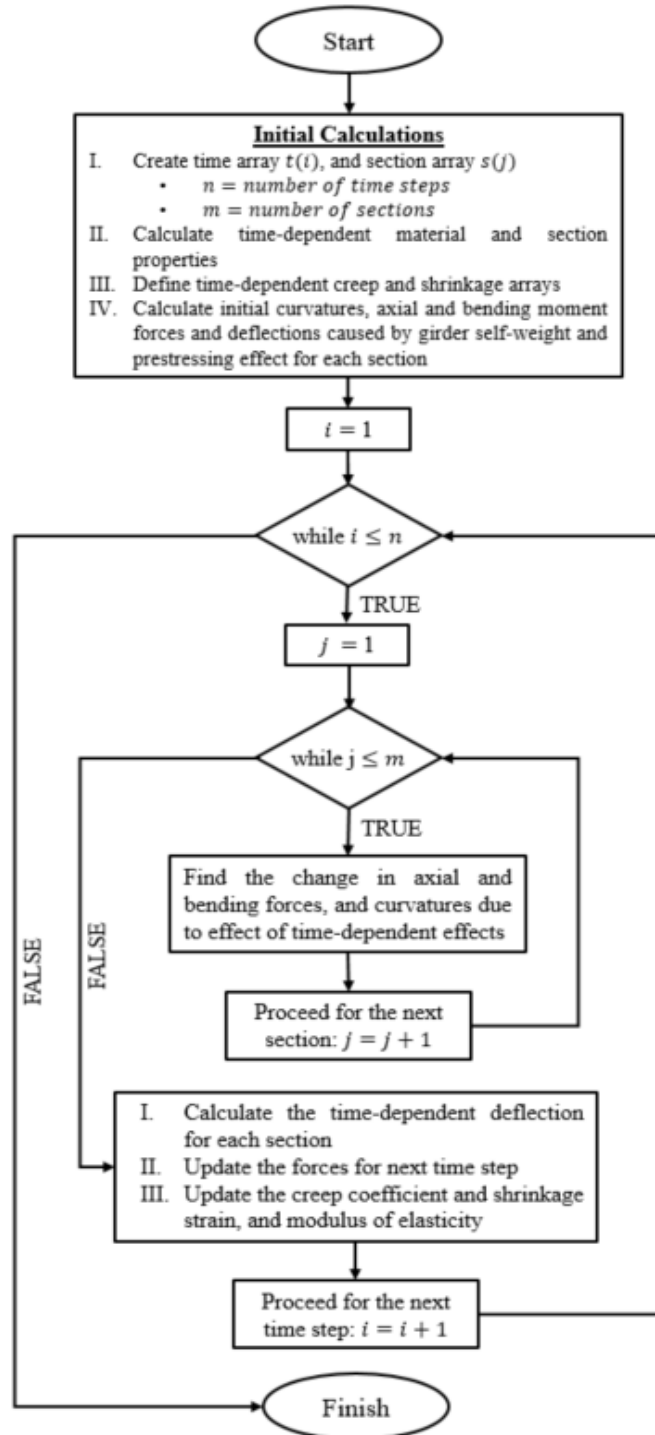


Fig. 3.8. Flowchart for approach used in Iteration 5

3.1.6 Iteration No. 6

In Iteration No. 6, the algorithm used in Iteration No. 5 was further improved to allow the use of multiple creep curves rather than a single creep curve. This iteration is based on the principle of superposition, multiple creep curves, a time dependent function for the modulus of elasticity, and multiple time substeps. The method included in this iteration removes some of the limitations included in the previous iterations and provides the user the ability to obtain the complete deformation history of the beam including non-composite and composite states as well as deck replacement activities. The proposed prediction methodology relies on the selection of several empirical models which are summarized in Fig. 3.9 and discussed in the subsequent sections.

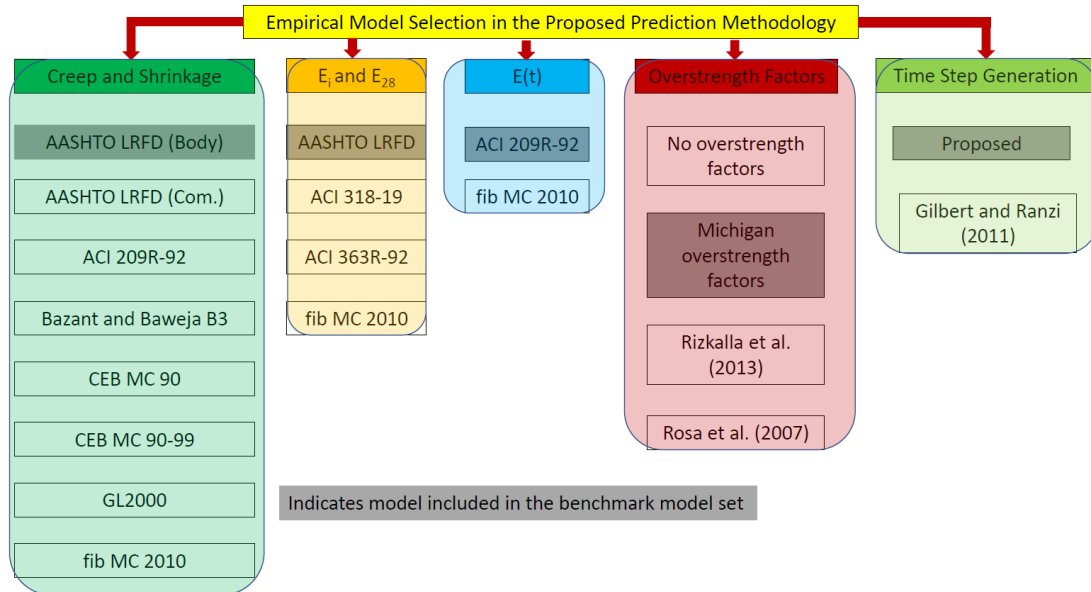


Fig. 3.9. Empirical model selection in the proposed prediction methodology

The approach used in Iteration No. 6 is summarized in the flowchart shown in Fig. 3.10. In previous iterations, only one creep curve was used for beam and deck concrete to predict time dependent camber and displacements. The creep curve for beam concrete was developed based on a loading time of one day (prestress release). The time dependent effects of any changes in forces in the beam were accounted for by calculating the remaining creep coefficient obtained from this curve based on the time that each new force was applied. The same approach was used for deck concrete. A single creep curve was used assuming that the loading time was the time that corresponded with the placement of the deck. Remaining creep coefficients were calculated for any changes in deck forces after the placement of deck.

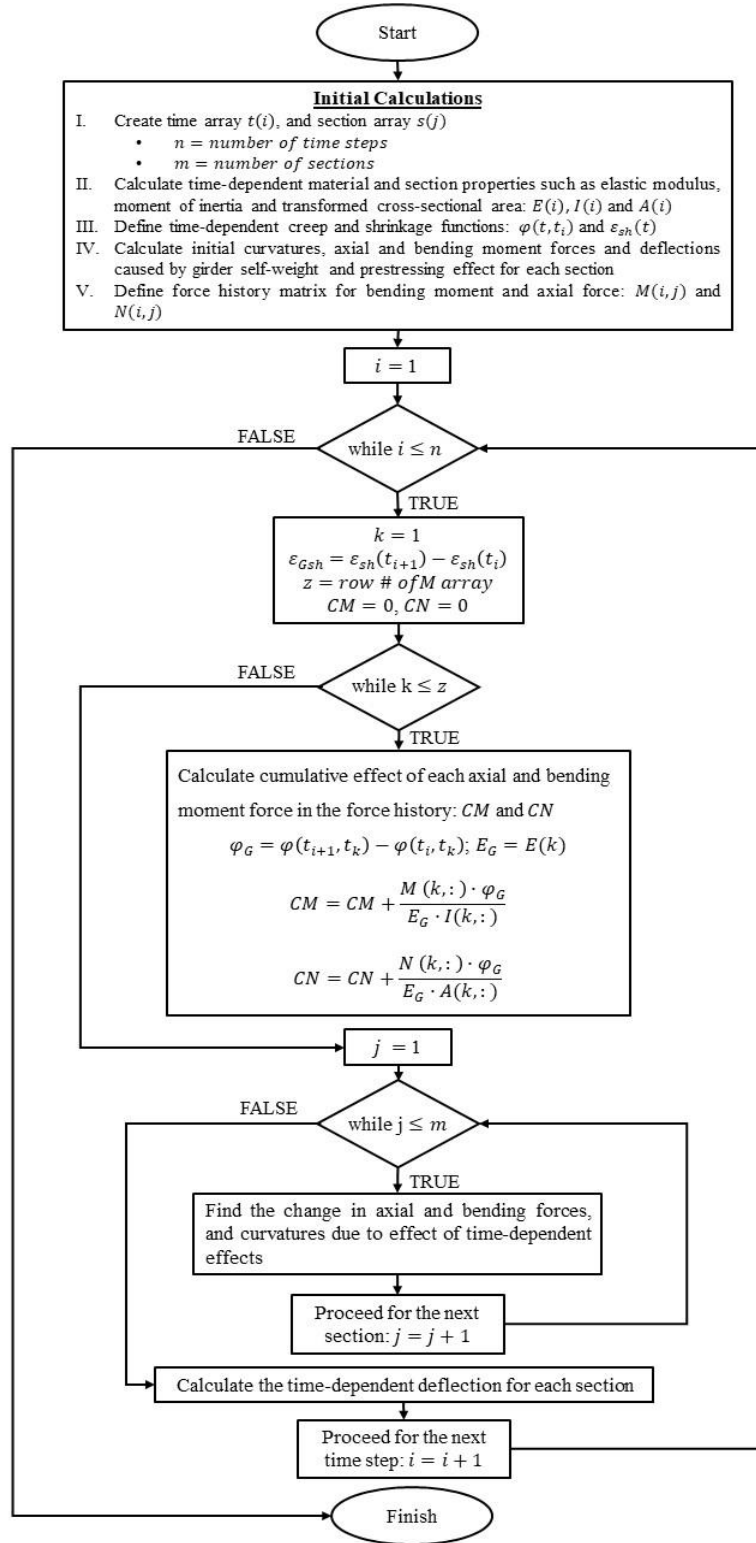


Fig. 3.10. Flowchart for iteration No. 6

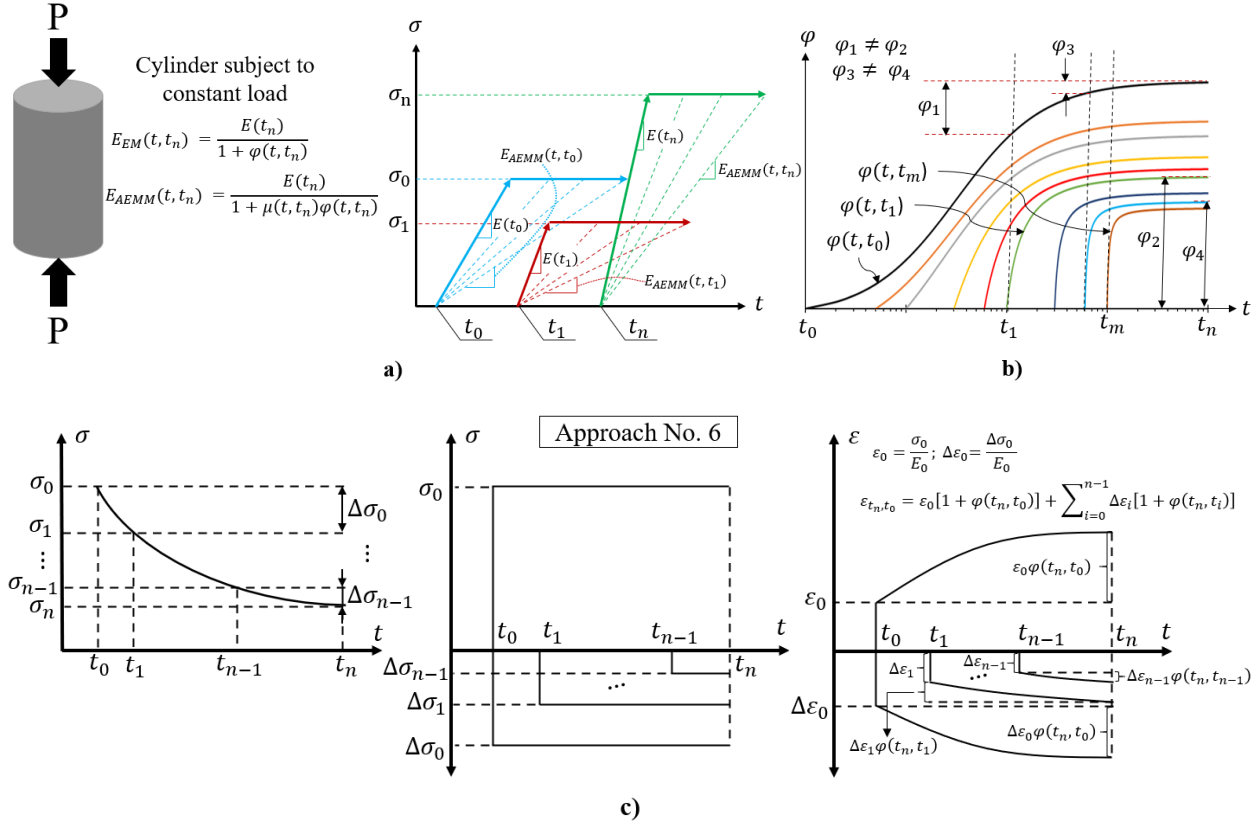


Fig. 3.11. a) Illustration of effective modulus (EM) and age adjusted effective modulus (AAEM) concept, b) effect of loading age on creep coefficient according to AASHTO LRFD model for an interior prestressed concrete beam used in the S-11 project, c) assumed stress history, idealized stress history, and creep induced strain due to a varying stress history (multiple time steps with multiple creep curves)

This approach (i.e. the one used in previous iterations) does not fully take into account the aging effect of concrete, which requires the utilization of a separate creep curves. For example, consider a concrete cylinder that was initially loaded at time t_0 (Fig. 3.11 a) and a new additional force was applied at time t_{n-1} . If a single creep curve is used (i.e. the one with a loading time of t_0) the remaining creep coefficient between time t_{n-1} and t_n would be small (φ_3). However, if a new creep curve is developed based on a loading time of t_{n-1} then the creep coefficient at time t_n would be greater than the remaining creep coefficient calculated using the single creep curve ($\varphi_4 \gg \varphi_3$). This constitutes a fundamental difference between Iteration No. 5 and Iteration No. 6.

Additionally, in Iteration No. 6 since each newly created force is associated with its own creep curve, forces at the end of each time step are not updated so that a single axial force and bending moment can be used for the next time step to calculate the corresponding time dependent effects. Rather, each existing and newly developed force is considered independently, and the

principle of superposition is used to calculate total curvatures and axial strain at a given time. The curvature diagram is then numerically integrated to obtain camber and displacements. The only exception is for a deck replacement event, during which all internal axial forces and bending moments present in the deck are summed and are applied as equal and opposite forces when the deck is removed. After this point, any newly created axial forces and bending moment in the beam or in the new deck are associated with separate creep curves. The consideration of multiple sets of axial forces and bending moment in the beam and deck concrete rather than a single set for each component, constitutes another fundamental difference between Iteration No. 5 and 6. In Iteration No. 5 axial forces and bending moments in the beam and deck were summed at the end of each time step so that time dependent effects for the next time step could be calculated based on single creep curves for beam and deck concrete. In Iteration No. 6 this summation is not conducted intentionally to distinguish between the loading time of various events and to facilitate the use of different creep curves.

The general mechanism for the flowchart provided in Fig. 3.10 is provided below:

1. Create a time and section array.

The time array is created such that the number of time steps increases in a logarithmic fashion to account for the fact that the majority of creep takes place during the early stages of a loading event. The approach used for the creation of time array is presented in Table 3.2. An alternative approach is proposed by Gilbert and Ranzi (2011), which is based on a geometric series. The proposed algorithm allows the user to select either approach. The impact of this decision is presented later. The section array is created by dividing half of the beam length in an equal number of sections. The user has the option to select how many sections are considered. To obtain a smooth deflected shape for the beam a minimum of 51 sections are recommended. The influence of the number of sections in the accuracy of camber and displacement predictions is discussed later.

Table 3.2. Approach used for creation of time array

Activity	Time steps between activities	Time step length (days)
Release	Discrete	-
Time between Release and Deck Placement	1 days to 10 days	1
	11 days to 30 days	2
	30 days to time at deck placement	3
Deck Placement	Discrete	-
Time between Deck Placement and Application of Superimposed Dead Loads (Typically short – around seven days)	1 days to 10 days	1
	11 days to 30 days	2
	31 days to 100 days	3
	101 days to 1,000 days	100
	1,001 days to 10,000 days	1,000
Application of Superimposed Dead Loads	Discrete	-
Time between Application of Superimposed Dead Loads and Final Time (75 years)	1 days to 10 days	1
	11 days to 30 days	2
	31 days to 100 days	3
	101 days to 1,000 days	100
	1,001 days to 10,000 days	1,000
	10,001 days to final time (75 years)	10,000

2. Generate time-dependent arrays for material and section properties.

A time dependent function is used to account for the variation of modulus of elasticity with time. Since a prestressed concrete beam and a composite bridge superstructure are heterogeneous members, the variation in modulus affects the calculation of modular ratio, centroid of transformed section, and moment of inertia. Therefore, these parameters are calculated for every time step considered and include modulus of elasticity, modular ratio, transformed moment of inertia, transformed cross-sectional area, composite moment of inertia, composite cross-sectional area, prestressing strand area, and eccentricity for each time and section, if applicable. It should be noted that some of the parameters are only time-dependent (ex: E_{G_i} , E_{D_i}), some of them are only section-dependent (ex: e_q , A_{ps_q}), and some of them are both time and section-dependent (ex: $I_{ts_{i,q}}$, $A_{ts_{i,q}}$, $I_{c_{i,q}}$, $A_{c_{i,q}}$).

3. Create functions for creep coefficients and shrinkage strains

The number of time steps considered determines the number of creep curves that need to be calculated since at every time step internal forces in the beam and deck change due to time dependent effects. Unlike the creep curves only two shrinkage curves are developed for the beam and deck concrete since shrinkage does not depend on the time at which the load is applied. The user can select one of out eight creep and shrinkage models.

4. Calculate initial strains, curvatures, axial forces, bending moments and deflections caused by girder self-weight and prestressing effect for each section.
5. Define matrix for history of axial forces, bending moments, and curvatures.
6. For every time step and beam section considered:
 1. Conduct a time dependent strain compatibility-based cross-section analysis (see Eq. 3.53-3.74). Calculate changes in strains, curvatures, axial forces, bending moments. Calculate the time dependent deflection for each time step and for each section the obtain the complete history of flexural deformations as a function of time and distance along the span. The flowchart operates based on two main loops. The first considers the number of time steps in the time frame of interest, and the second considers the number of beams sections along the span.
7. After each beam section is considered, net camber/displacement at each section $\Delta_{i+1,q}$ is calculated using net curvature values along the span (Σ_X) and second moment-area theorem together with numerical integration.
8. The procedure is repeated until all time steps are considered. Camber and displacement history can be obtained using the calculated camber/displacement values.

The mathematical framework for Iteration No. 6 is provided by Eq. 3.52-3.74.

Fundamental Equation

$$\varepsilon_{(t_n, t_o)} = \varepsilon_o[1 + \varphi_o(t_n, t_o)] + \sum_{i=0}^m \Delta \varepsilon_i [1 + \varphi_i(t_n, t_i)] \quad (3.52)$$

$$\varepsilon_i = \frac{\sigma_i}{E_i}; \Delta \varepsilon_i = \frac{\Delta \sigma_i}{E_i}; n = \text{number of time steps}; m = \text{number of loading events};$$

$$n = m + 1$$

Cross-sectional Analysis for Non-composite Prestressed Concrete Beams

$$\Delta \varepsilon_{G(t_n, t_o)} = \sum_{i=0}^m \left[\left[\sum_{j=0}^{i-1} \frac{N_{Gj} \alpha_1 [\varphi_{Gj}(t_{i+1}, t_j) - \varphi_{Gj}(t_i, t_j)]}{E_{Gj} A_G} \right] + \frac{\Delta N_{Gi} [1 + \alpha_2 \varphi_{Gi}(t_{i+1}, t_i)]}{E_{Gi} A_G} + [\varepsilon_{ShG}(t_{i+1}) - \varepsilon_{ShG}(t_i)] \right]; \quad (3.53)$$

$$where: N_{G_0} = N_{Gdirect}^0 + N_G^0, N_{Gdirect}^0 = 0, N_G^0 = \frac{N_{ts}^0 A_G}{A_{ts_0}} - \frac{M_{ts}^0 a_{ts_0} A_G}{I_{ts_0}};$$

$$i > 0 \rightarrow N_{G_i} = \Delta N_{G_i} \& N_{G_0} = N_{G_0} + \Delta N_{G_0}; \text{ if } N_{G_i} > 0 \rightarrow \alpha_1 = \text{Tensile creep factor},$$

$$\text{otherwise} \rightarrow \alpha_1 = 1; \text{ if } \Delta N_{G_i} > 0 \rightarrow \alpha_2 = \text{Tensile creep factor}, \text{ otherwise} \rightarrow \alpha_2 = 1;$$

$$\Delta X_{(t_n t_o)} = \sum_{i=0}^m \left[\left[\sum_{j=0}^{i-1} \frac{M_{Gj} \beta [\varphi_{Gj}(t_{i+1} t_j) - \varphi_{Gj}(t_i t_j)]}{E_{Gj} I_G} \right] + \frac{\Delta M_{G_i} [1 + \beta \varphi_{G_i}(t_{i+1} t_i)]}{E_{G_i} I_G} \right]; \quad (3.54)$$

$$where: M_{G_0} = M_{Gdirect}^0 + M_G^0, M_{Gdirect}^0 = 0, M_G^0 = \frac{M_{ts}^0 I_G}{I_{ts_0}};$$

$$i > 0 \rightarrow M_{G_i} = \Delta M_{G_i} \& M_{G_0} = M_{G_0} + \Delta M_{G_0}$$

$$\Delta \varepsilon_{ps(t_n t_o)} = \frac{\sum_{i=0}^m \Delta N_{ps_i}}{E_{ps} A_{ps}} \quad (3.55)$$

$$\Delta N_{G_i} + \Delta N_{ps_i} = 0 \quad (3.56)$$

$$\Delta M_{G_i} + \Delta N_{ps_i} e = 0 \quad (3.57)$$

$$\Delta \varepsilon_{ps(t_n t_o)} = \Delta \varepsilon_{G(t_n t_o)} + \Delta X_{(t_n t_o)} e \quad (3.58)$$

Cross-sectional Analysis for Composite Prestressed Concrete Beams

$$\Delta \varepsilon_{G(t_n t_d)} = \sum_{i=r}^m \left[\left[\sum_{j=0}^{i-1} \frac{N_{Gj} \alpha_1 [\varphi_{Gj}(t_{i+1} t_j) - \varphi_{Gj}(t_i t_j)]}{E_{Gj} A_G} \right] + \frac{\Delta N_{G_i} [1 + \alpha_2 \varphi_{G_i}(t_{i+1} t_i)]}{E_{G_i} A_G} + [\varepsilon_{ShG}(t_{i+1}) - \varepsilon_{ShG}(t_i)] \right]; \quad (3.59)$$

$$where: N_{G_0} = N_{Gdirect}^0 + N_G^0, N_{Gdirect}^0 = 0, N_G^0 = \frac{N_{ts}^0 A_G}{A_{ts_0}} - \frac{M_{ts}^0 a_{ts_0} A_G}{I_{ts_0}},$$

$$N_{G_i} = \Delta N_{G_i} \text{ if } 0 < i < (r - 1), N_{G_{r-1}} = \Delta N_{G_{r-1}} + \frac{N_c^0 A_G}{A_{c_0}} + \frac{M_c^0 a_{G_0} A_G}{I_{c_0}}, N_{G_i} = \Delta N_{G_i} \text{ if } i \geq r,$$

$$\text{if } N_{G_i} > 0 \rightarrow \alpha_1 = \text{Tensile creep factor}, \text{ otherwise} \rightarrow \alpha_1 = 1; \text{ if } \Delta N_{G_i} > 0 \rightarrow \alpha_2 = \text{Tensile creep}$$

$$\text{factor}, \text{ otherwise} \rightarrow \alpha_2 = 1;$$

$$\Delta \varepsilon_{D(t_n, t_d)} = \sum_{i=r}^m \left[\left[\sum_{j=r}^{i-1} \frac{N_{Dj} \alpha_1 [\varphi_{Dj}(t_{i+1}, t_j) - \varphi_{Dj}(t_i, t_j)]}{E_{Dj} A_D} \right] + \frac{\Delta N_{Di} [1 + \alpha_2 \varphi_{Di}(t_{i+1}, t_i)]}{E_{Di} A_D} + [\varepsilon_{ShD}(t_{i+1}) - \varepsilon_{ShD}(t_i)] \right]; \quad (3.60)$$

$$here: N_{Dr} = N_{Ddirect}^0 + N_D^0, N_{Ddirect}^0 = 0, N_D^0 = \frac{N_c^0 n_0 A_D}{A_{c0}} - \frac{M_c^0 a_{D0} n_0 A_D}{I_{c0}};$$

$$i > r \rightarrow N_{Di} = \Delta N_{Di} \text{ \& } N_{Dr} = N_{Dr} + \Delta N_{Dr};$$

if $N_{Di} > 0 \rightarrow \alpha_1 = \text{Tensile creep factor}$, otherwise $\rightarrow \alpha_1 = 1$; if $\Delta N_{Di} > 0 \rightarrow \alpha_2 = \text{Tensile creep factor}$, otherwise $\rightarrow \alpha_2 = 1$

$$\Delta X_{(t_n, t_d)} = \sum_{i=r}^m \left[\left[\sum_{j=0}^{i-1} \frac{M_{Gj} \beta [\varphi_{Gj}(t_{i+1}, t_j) - \varphi_{Gj}(t_i, t_j)]}{E_{Gj} I_G} \right] + \frac{\Delta M_{Gi} [1 + \beta \varphi_{Gi}(t_{i+1}, t_i)]}{E_{Gi} I_G} \right]; \quad (3.61)$$

$$where: M_{G0} = M_{Gdirect}^0 + M_G^0, M_{Gdirect}^0 = 0, M_G^0 = \frac{M_{ts}^0 I_G}{I_{ts0}},$$

$$M_{Gi} = \Delta M_{Gi} \text{ when } 0 < i < (r - 1), M_{Gr-1} = \Delta M_{Gr-1} + \frac{M_c^0 I_G}{I_{c0}}, M_{Gi} = \Delta M_{Gi} \text{ when } i \geq r,$$

$$\Delta X_{(t_n, t_d)} = \sum_{i=r}^m \left[\left[\sum_{j=r}^{i-1} \frac{M_{Dj} \beta [\varphi_{Dj}(t_{i+1}, t_j) - \varphi_{Dj}(t_i, t_j)]}{E_{Dj} I_D} \right] + \frac{\Delta M_{Di} [1 + \beta \varphi_{Di}(t_{i+1}, t_i)]}{E_{Di} I_D} \right]; \quad (3.62)$$

$$where: M_{Dr} = M_{Ddirect}^0 + M_D^0, M_{Ddirect}^0 = 0, M_D^0 = \frac{M_c^0 n_0 I_D}{I_{c0}},$$

$$i > r \rightarrow M_{Di} = \Delta M_{Di} \text{ \& } M_{Dr} = M_{Dr} + \Delta M_{Dr}$$

$$\underline{\text{Note:}} N_{ts}^0 = -P_e, M_{ts}^0 = M_{Gsw} + M_{dsw} - P_e e_{tr}, N_c^0 = 0, M_c^0 = M_{bsw} + M_{osw},$$

$\beta = \text{flexural creep factor}$

$$\Delta \varepsilon_{ps(t_n, t_d)} = \frac{\sum_{i=r}^n \Delta N_{psi}}{E_{ps} A_{ps}} \quad (3.63)$$

$$N_{Di} + \Delta N_{Gi} + \Delta N_{psi} = 0 \quad (3.64)$$

$$\Delta M_{Gi} + \Delta M_{Di} - \Delta N_{Di} a + \Delta N_{psi} e = 0 \quad (3.65)$$

$$\Delta \varepsilon_{D(t_n, t_d)} = \Delta \varepsilon_{G(t_n, t_d)} - \Delta X_{(t_n, t_d)} a \quad (3.66)$$

$$\Delta \varepsilon_{ps(t_n, t_d)} = \Delta \varepsilon_{G(t_n, t_d)} + \Delta X_{(t_n, t_d)} e \quad (3.67)$$

Cross-sectional Analysis for Composite Steel Beams

$$\Delta \varepsilon_{D(t_n, t_d)} = \sum_{i=r}^m \left[\left[\sum_{j=r}^{i-1} \frac{N_{Dj} \alpha_1 [\varphi_{Dj}(t_{i+1}, t_j) - \varphi_{Dj}(t_i, t_j)]}{E_{Dj} A_D} \right] + \frac{\Delta N_{Di} [1 + \alpha_2 \varphi_{Di}(t_{i+1}, t_i)]}{E_{Di} A_D} + [\varepsilon_{ShD}(t_{i+1}) - \varepsilon_{ShD}(t_i)] \right]; \quad (3.68)$$

$$\text{where: } N_{Dr} = N_{Ddirect}^0 + N_D^0, N_{Ddirect}^0 = 0, N_D^0 = \frac{N_c^0 n_o A_D}{A_{c_0}} - \frac{M_c^0 a_{D_0} n_o A_D}{I_{c_0}};$$

$$i > r \rightarrow N_{Di} = \Delta N_{Di} \text{ \& } N_{Dr} = N_{Dr} + \Delta N_{Dr}$$

if $N_{Di} > 0 \rightarrow \alpha_1 = \text{Tensile creep factor}$, otherwise $\rightarrow \alpha_1 = 1$; if $\Delta N_{Di} > 0 \rightarrow \alpha_2 = \text{Tensile creep factor}$, otherwise $\rightarrow \alpha_2 = 1$;

$$\Delta X_{(t_n, t_d)} = \sum_{i=r}^m \left[\left[\sum_{j=r}^{i-1} \frac{M_{Dj} \beta [\varphi_{Dj}(t_{i+1}, t_j) - \varphi_{Dj}(t_i, t_j)]}{E_{Dj} I_D} \right] + \frac{\Delta M_{Di} [1 + \beta \varphi_{Di}(t_{i+1}, t_i)]}{E_{Di} I_D} \right]; \quad (3.69)$$

$$\text{where: } M_{Dr} = M_{Ddirect}^0 + M_D^0, M_{Ddirect}^0 = 0, M_D^0 = \frac{M_c^0 n_o I_D}{I_{c_0}};$$

$$i > r \rightarrow M_{Di} = \Delta M_{Di} \text{ \& } M_{Dr} = M_{Dr} + \Delta M_{Dr}$$

Note: $N_c^0 = 0, M_c^0 = M_{bsw} + M_{osw}, \beta = \text{flexural creep factor}$

$$\Delta X_{(t_n, t_d)} = \frac{\Delta M_G}{E_G I_G} \quad (3.70)$$

$$\Delta \varepsilon_{G(t_n, t_d)} = \frac{\Delta N_G}{E_G A_G} \quad (3.71)$$

$$\Delta N_{Di} + \Delta N_{Gi} = 0 \quad (3.72)$$

$$\Delta M_{Gi} + \Delta M_{Di} - \Delta N_{Di} a = 0 \quad (3.73)$$

$$\Delta \varepsilon_{D(t_n, t_d)} = \Delta \varepsilon_{G(t_n, t_d)} - \Delta X_{(t_n, t_d)} a \quad (3.74)$$

3.1.7 Modulus of Elasticity Prediction

Modulus of elasticity is one of the most influential parameters on beam camber and displacement as it represents the stiffness of the material. Its development with time is also important when predicting time dependent camber and deflections. In this section, four models for predicting the modulus of elasticity at release and at 28 days are presented. Additionally, two models for predicting the development of modulus with time are discussed. The proposed prediction methodology allows the user to select the desired model.

Prediction of Modulus of Elasticity at release and 28 days

AASHTO LRFD (2020) Model

In this model, modulus of elasticity is expressed as function of aggregate type, K_1 , concrete unit weight, w_c , and compressive strength of concrete at release, f'_{ci} , or at 28 days, f'_c (Eq. 3.75 and 3.76). Eq. 3.75 and 3.76 are intended for normal weight concrete with design compressive strength up to 15.0 ksi and lightweight concrete up to 10.0 ksi, with unit weights between 0.090 and 0.155 kcf. The units for w_c are kcf and for f'_{ci} , or f'_c are ksi. The modulus of elasticity is computed in ksi.

$$E_{ci} = 120,000 K_1 w_c^{2.0} f'_{ci}{}^{0.33} \quad (3.75)$$

$$E_{c28} = 120,000 K_1 w_c^{2.0} f'_c{}^{0.33} \quad (3.76)$$

where for normal weight concrete, $w_c = 0.145$ kcf for $f'_c \leq 5$ ksi and $w_c = 0.140 + 0.001 f'_c$ kcf for $5.0 < f'_c \leq 15.0$ ksi

ACI 318-19 Model

This model is similar with the AASHTO LRFD (2020) model in format (Eq. 3.17 and 3.18). However, the powers to which the unit weight of concrete and compressive strength are raised are different. In addition, the ACI 318-19 model does not distinguish between various types of aggregates. The units for w are pcf and for f'_{ci} , or f'_c are psi. The modulus of elasticity is computed in psi.

$$E_{ci} = 33w^{1.5} \sqrt{f'_{ci}} \quad (3.77)$$

$$E_{c28} = 33w^{1.5} \sqrt{f'_c} \quad (3.78)$$

ACI 363R-92 Model

This model is similar to the ACI 318-19 model in terms the parameters that the modulus of elasticity is expressed as a function of (Eq. 3.79 and 3.80). The units for w_c are pcf and for f'_{ci} or f'_c are psi. The modulus of elasticity is computed in psi.

$$E_{ci} = \left(40,000 \sqrt{f'_{ci}} + 10^6 \right) \left(\frac{w_c}{145} \right)^{1.5} \quad (3.79)$$

$$E_{c28} = \left(40,000 \sqrt{f'_c} + 10^6 \right) \left(\frac{w_c}{145} \right)^{1.5} \quad (3.80)$$

fib MC 2010 Model

This model, similar to the AASHTO LRFD (2020) model expresses the modulus of elasticity as a function of concrete compressive strength and aggregate type (Eq. 3.81 and 3.82). However, unlike the other models it does not include the unit weight of concrete as a parameter. The aggregate type dependent parameter can be selected based on Table 3.3.

$$E_{ci} = 2760 \alpha_E \sqrt[3]{f'_{ci}} \quad (3.81)$$

$$E_{c28} = 2760 \alpha_E \sqrt[3]{f'_c} \quad (3.82)$$

Table 3.3. Determination of aggregate type dependent parameter

Aggregate type	α_E
Basalt, dense limestone	1.2
Quartzite	1.0
Limestone	0.9
Sandstone	0.7

Comparison of Various Models

Consider a normal weight concrete beam with aggregate factor 1.0 and initial and 28-day compressive strengths of 7 and 10 ksi, respectively. The unit weight of concrete for all models except for the AASHTO (2020) model is assumed as 145 pcf, whereas for the AASHTO (2020) model it is computed based on Table 3.5.1-1 in AASHTO LRFD Bridge Design Specifications (2020), which relates compressive strength to unit weight. The modulus of elasticity predictions at release and at 28-days using the four different models discussed above are presented in Table

3.4. The AASHTO LRFD (2020) and fib MC 2010 models produce the highest estimates followed by ACI 318-19 model and ACI 363R-92 model.

Table 3.4. Comparison of modulus of elasticity prediction models

Modulus of Elasticity	Prediction Models			
	AASHTO LRFD (2020)	ACI 318-19	ACI 363R-92	fib MC 2010
E_{ci} (ksi)	5165	4821	4347	5280
E_{c28} (ksi)	5817	5762	5000	5946

Prediction of Modulus of Elasticity as a Function of Time

ACI 209R-92 Model

In this model the development of modulus of elasticity with time is expressed as function of modulus at 28 days and two parameters which are selected based on the type of cement used and curing method (Eq. 3.83). The determination of α and β is based on Table 3.5. This model covers only concretes that features either cement type I or III. In the proposed prediction methodology, the user has two options to obtain the development of modulus with time. The first include the use of 28 days modulus and parameters α and β . However, in this approach, it is possible that the predicted modulus at release may not match the measured modulus if such information is available or if it can be obtained using one of the four models presented above that express modulus as a function of compressive strength.

$$E_c(t) = \left(\frac{t}{\alpha + \beta t} \right)^{0.5} E_{c28} \quad (3.83)$$

Table 3.5 Parameters for ACI 209R-92 time dependent modulus of elasticity model

Type of Cement	Moist-cured concrete		Steam-cured concrete	
	α	β	α	β
I	4	0.85	1	0.95
III	2.3	0.92	0.7	0.98

Alternatively, the development of modulus with time can be obtained by using the initial modulus and 28 day modulus as anchor points and back calculating the parameters α and β such

that predicted modulus at release and 28 day matches the measured or assumed one. This can be done using Eq. 3.84 and 3.85.

$$\beta = \frac{E_{c28}^2 \cdot t_1 - 28E_{ci}^2}{E_{ci}^2 \cdot (t_1 - 28)} \quad (3.84)$$

$$\alpha = 28(1 - \beta) \quad (3.85)$$

Fig. 3.5 shows the development of modulus of elasticity as a function of time by considering a concrete with an initial (1 day) and 28-day modulus of elasticity of 3000 ksi and 5000 ksi, respectively. Fig. 3.12 suggests that the modulus of elasticity reaches a stable value after 28 days with only minor differences between concretes featuring cement type I and III and those that are moist and steam cured. Additionally, even if the parameters α and β were back calculated based on the specified initial and 28 day modulus the modulus after 28 days is similar with the other approach. It is worth noting, however, that there are some differences between the predicted modulus up to 28 days depending on which approach, which type of cement and which method of curing is selected. According to this model, steam curing helps the stiffening of concrete during the first 28 days compared to moist curing. The back calculated curve is similar to that obtained for Type III cement and moist cured concrete.

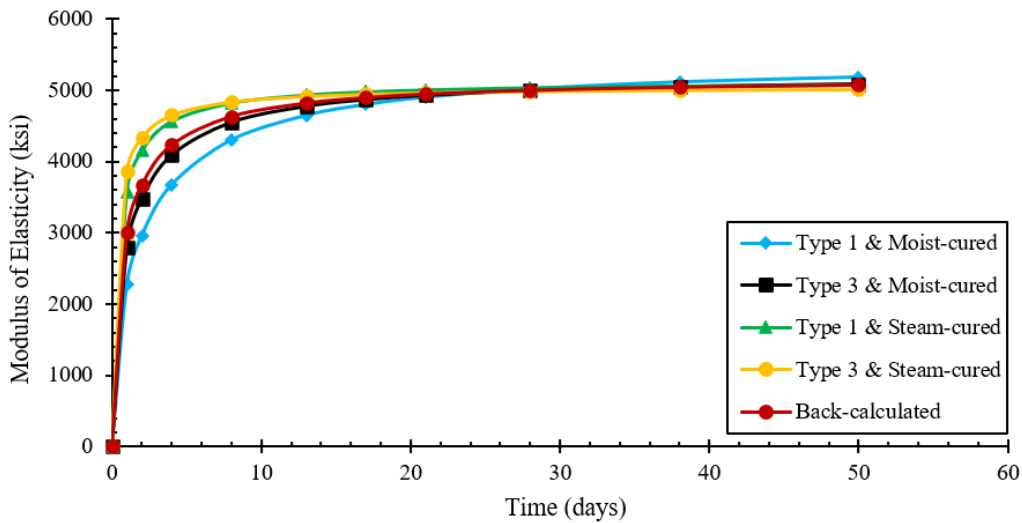


Fig. 3.12. Modulus of elasticity as a function of time based on the ACI 209R-92 Model

fib MC 2010 Model

In this model the development of modulus of elasticity with time is expressed as a function modulus of elasticity at 28 days as well as the strength class of cement used (Eq. 3.86 and 3.87). Unlike the previous model, the type of curing is not a parameter that influences the development

of modulus with time. The parameter s that reflects the strength class of cement used in the mix may be calculated based on Table 3.6. The mean compressive strength may be taken as 1.2 ksi more than specified strength. Additionally, if both initial and 28 day modulus values are known, the parameter “ s ” may be back-calculated using Eq. 3.88. The proposed prediction methodology allows the user to select either prediction model and either approach within each prediction model for estimating the development of modulus with time. Fig. 3.13 shows the development of modulus as a function of time using different classes for the strength of cement by considering a concrete with initial (1 day) and 28-day modulus of elasticity of 3000 psi and 5000 psi, respectively. The curve obtained by back calculating the coefficient s is also presented. Fig. 3.13 suggests that the development of modulus with time is generally similar for all cases with lower strength cements featuring a lower modulus. This is different from the previous model in which pronounced differences in the development of modulus with time up to 28 days were observed depending on the type of curing method.

$$E_c(t) = \beta_E(t)E_{c28} \quad (3.86)$$

$$\beta_E(t) = \sqrt{e^{s\left(1-\sqrt{\frac{28}{t}}\right)}} \quad (3.87)$$

Table 3.6. Coefficients for strength class of cement based on fib MC 2010 model

Mean compressive strength (ksi)	Strength class of cement	s
≤ 8.7	32.5 N	0.38
	32.5 R, 42.5 N	0.25
	42.5 R, 52.5 N, 52.5 R	0.20
> 8.7	all classes	0.20

$$s = \frac{\ln \left[\left(\frac{E_{ci}}{E_{c28}} \right)^2 \right]}{1 - \sqrt{\frac{28}{t_1}}} \quad (3.88)$$

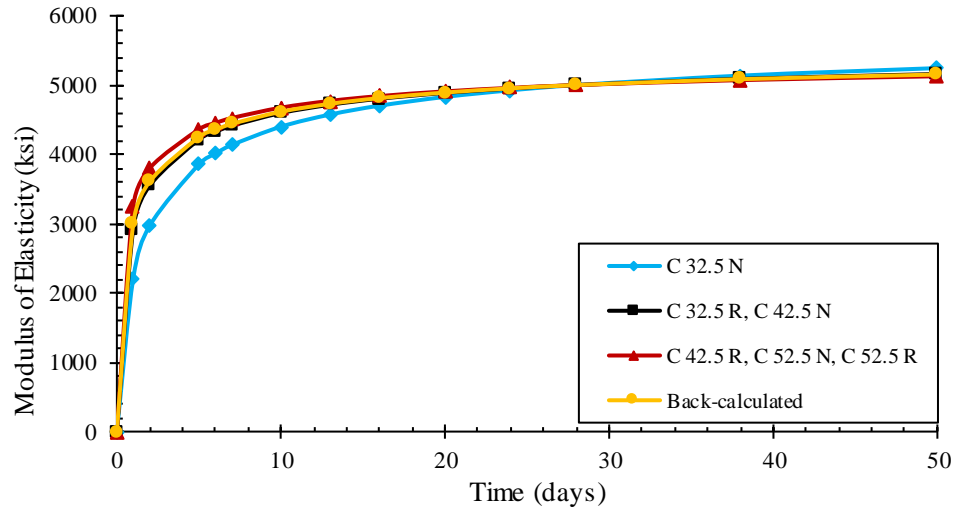


Fig. 3.13. Modulus of Elasticity as a function of time based on the fib MC 2010 Model

3.1.8 Creep and Shrinkage Models

The calculation of long-term camber and displacements is highly dependent on the creep and shrinkage models that are selected. ACI 209.2R-08 (2008) provides four models for calculating shrinkage and creep in hardened concrete, namely: ACI 209R-92 model, Bažant-Baweja B3 model, CEB MC90-99 model and GL2000 model. The Precast Prestressed Concrete Institute (PCI) bridge design manual (2016) recommends two methods for estimating the creep coefficient and shrinkage strain. The first is the same with the ACI 209.2R-08 (2008) model and the second is based on modifications suggested by Huo (1997). AASHTO LRFD Bridge Design Specifications (2020) also provide models for estimating shrinkage and creep in hardened concrete. LeRoy et al. (1996), Tadros et al. (2003), and Lopez and Khan (2004) developed models for estimating the creep behavior of high strength concrete. The proposed methodology allows the selection of the following creep and shrinkage models: 1) AASHTO Body (2020) (provisions in the main body), 2) AASHTO Commentary (2020) (provisions in the commentary), 3) ACI 209R-92, 4) Bažant-Baweja B3 model, 5) CEB MC90, 6) CEB MC90-99, 7) GL2000, and 8) fib MC 2010.

Fig. 3.14 illustrates how the free shrinkage strain and creep coefficient vary with time for a PCBT 54 beam used in the S-11 project and the corresponding deck based on different shrinkage and creep models. The variation is shown using a logarithmic timescale for fixed values of f'_{ci} , RH, and V/S. The variation of creep coefficient with time generally exhibits an asymptotic behavior. As can be seen, the creep coefficient at a given beam age can vary significantly

depending on which model is chosen. The same conclusion can be drawn for beam and deck shrinkage. The considered models include the AASHTO (2020) models using the provisions provided in the body as well as in the commentary, ACI 209R-92 model, B3 model, CEB MC90 model, CEB MC90-99 model, and GL 2000 model. The variation of the creep coefficient based on the B3 model and GL 2000 model was significantly higher than that predicted by the other models. As a result, these two models were excluded to show more clearly the variation between the other models. The variation of shrinkage strain and creep coefficient for beam and deck concrete as a function of the selected model highlights once again the challenge of obtaining accurate long-term camber and displacement predictions. It should be noted that ACI Committee 209 has refrained from endorsing a particular model due to a lack of consensus on the set of data that should be used to evaluate different models as well as the statistical indicators that should be used if an agreement on the data set was reached. The majority of the data presented in this report are based on the AASHTO (2020) provisions provided in the main body. While these provisions together with the selection of the other models for the prediction of modulus at prestress release and 28 days as well as its variation with time, have resulted in reasonably accurate predictions of pre-erection camber as will be demonstrated later, the user is encouraged to explore the use of different models to get a sense for the variation in camber results.

The research team conducted a creep test on a Michigan concrete mix used in one of the projects listed in Chapter 4. The creep test setup is shown in Fig. 3.15 and the test was conducted in accordance with ASTM C512. The cylinders were loaded when they were 15 days old due to logistics related to the sulfur capping of the cylinder ends. Companion cylinders were cast to measure the shrinkage strain so that this shrinkage strain could be deducted from the total strain measured in the creep test so that remaining strain could be attributed solely to creep. The measured data was used to calculate a creep coefficient, which was then compared with predictions based on different models. Predictions for the considered models were based on measured compressive strength of concrete at release and 28 days ($f'_{ci} = 8.3$ ksi and $f'_c = 10$ ksi). This information was used to calculate modulus of elasticity at prestress release and 28 days. Such input is required in either all or some prediction models. The initial concrete compressive strength f'_{ci} is also a required parameter in the AASHTO (2020) creep and shrinkage model. In addition, the mix design for cylinders in question was made available and used when calculating creep coefficients based on a specific model. The results of this comparison are shown in Fig. 3.16. The model based

on AASHTO (2020) main body provisions provided the most accurate prediction for the creep coefficient. However, it should be noted that this conclusion is based solely on the data collected for this one mix. The shrinkage data collected from the companion cylinders was compared with predicted shrinkage strains based on different models. The cylinders were steam cured for one day and then let to dry for 14 days prior to measuring shrinkage strain since the specimens were loaded in the creep frame after 15 days. The measured shrinkage strain after 15 days was compared with the predicted change in strain after 15 days based on different models. The results are shown in Fig. 3.17. The majority of the models provided reasonable predictions with the exception of Bazant-Baweja B3 model and ACI 209R-92 model, which provided lower and upper bounds. The impact of the aforementioned models on long-term prestressed concrete beam camber is investigated later by comparing predicted values with measured ones for the Tiffin Street Overpass project for which multiple camber data for several beams were measured by the research team.

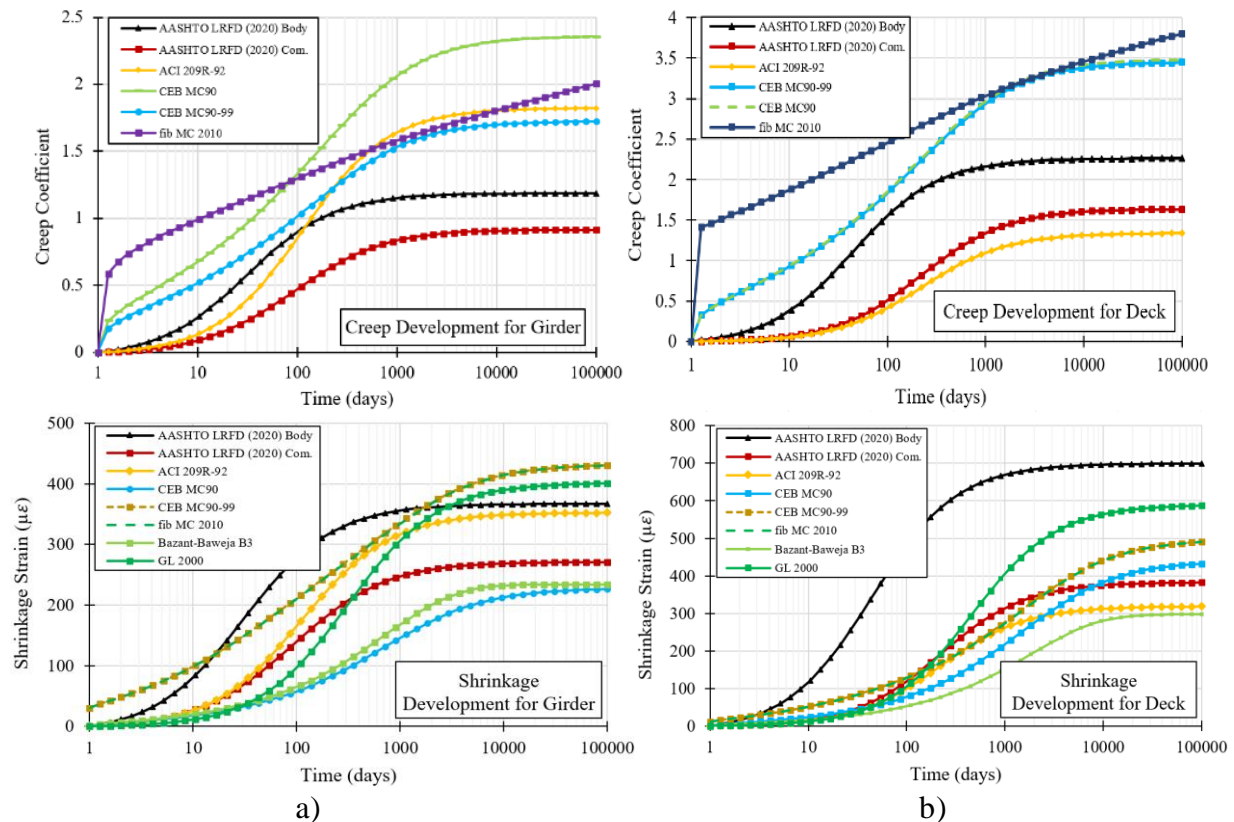


Fig. 3.14. Variation in creep coefficient and shrinkage strain based on different shrinkage and creep models for: a) PCBT 54 used in S11 project (Flange width 49 in., t_c = one day steam curing, t_{load} = one day, Cement Type I); b) Deck used in S11 project (t_c = one day steam curing, t_{load} = one day, Type I cement, mixture proportions are based on a typical deck mix featuring normal weight concrete and fly ash)

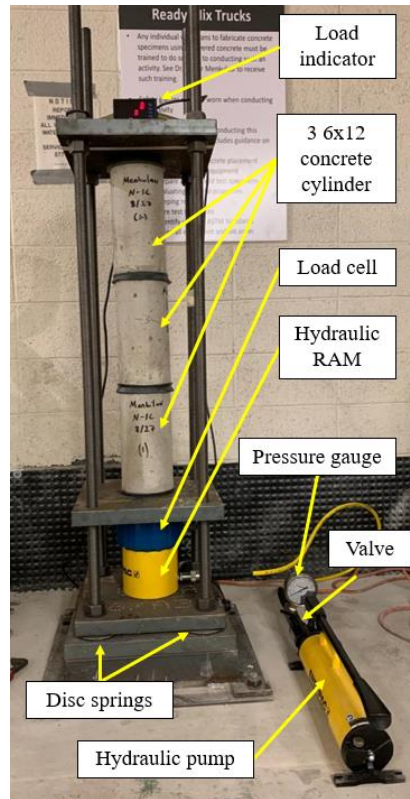


Fig. 3.15. Test setup for creep test

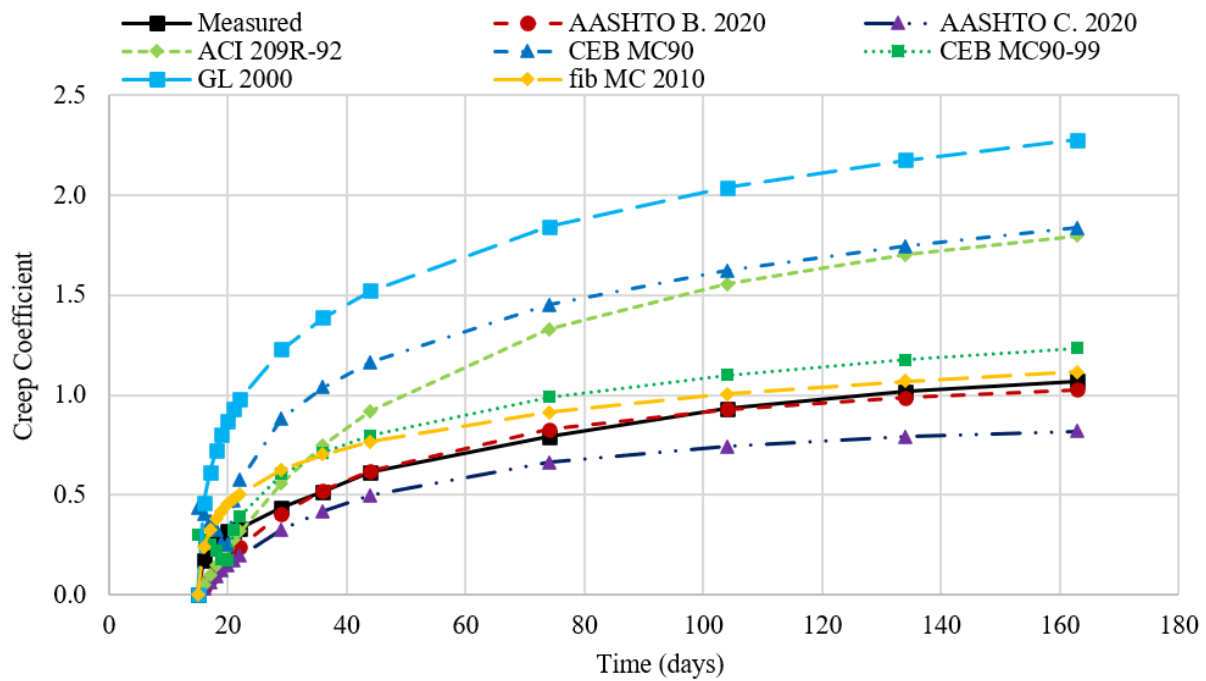


Fig. 3.16. Comparison of measured and predicted creep coefficient

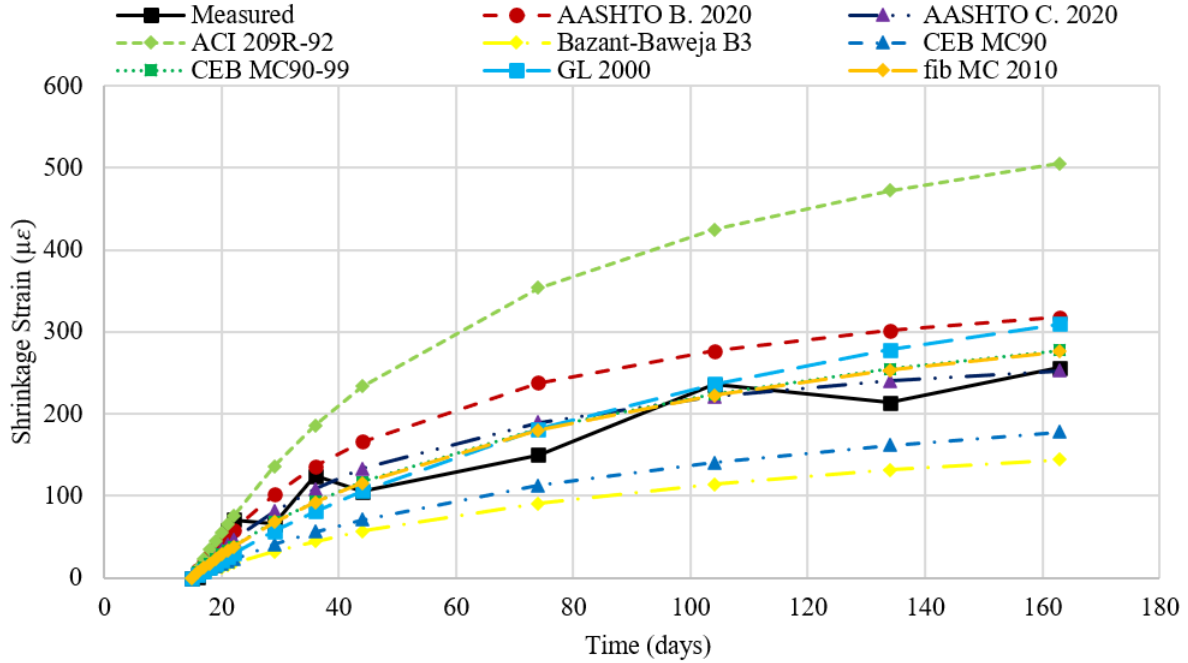


Fig. 3.17. Comparison of measured and predicted shrinkage strain

3.1.9 Strand Relaxation Loss

Strand relaxation losses are calculated based on the AASHTO LRFD (2020) model. According to this model, relaxation loss is a function of strand type, strand grade and level of stress on the strands. The relaxation loss between transfer of prestress and deck placement can be estimated using Eq. 3.89, which is provided in the body of AASHTO LRFD Specifications (2020). In this model any relaxation losses between the tensioning of the strands and prestress release are ignored. In Eq. 3.89, Δf_{pR1} is the relaxation loss between transfer and deck placement (ksi); f_{pt} is the stress in prestressing strand immediately after transfer, taken not less than $0.55 f_{py}$ (ksi); f_{py} is the yield strength of strands, typically taken as $0.9 f_{pu}$ (ksi); f_{pu} is the ultimate strength of the strands (ksi); and K_L is the factor accounting for type of steel taken as 30 for low-relaxation stands, and 7.0 for other prestressing strands.

$$\Delta f_{pR1} = \frac{f_{pt}}{K_L} \left(\frac{f_{pt}}{f_{py}} - 0.55 \right) \quad (3.89)$$

According to AASHTO LRFD Specifications (2020) a more accurate estimation of relaxation loss between prestress transfer and deck placement can be calculated using Eq. 3.90, which is provided in the commentary of AASHTO (2020)/NCHRP Report 496. In this equation,

K'_L can be taken as 45 for lox-relaxation steel and 10.5 for other strand types; t and t_i are the times at which relaxation loss is desired and at prestress transfer (hours), respectively; Δf_{pSR} is the loss in the strands caused by shrinkage of concrete (ksi); and Δf_{pCR} is the loss in the strands caused by creep of concrete (ksi). The second term in Eq. 3.90 accounts for the reduction in strand stress due to losses caused by shrinkage and creep.

$$\Delta f_{pR1} = \left[\frac{f_{pt}}{K'_L} \frac{\log(24t + 1)}{\log(24t_i + 1)} \left(\frac{f_{pt}}{f_{py}} - 0.55 \right) \right] \left[1 - \frac{3(\Delta f_{pSR} + \Delta f_{pCR})}{f_{pt}} \right] K_i \quad (3.90)$$

$$K_i = \frac{1}{1 + \frac{E_p}{E_{ci}} \frac{A_{ps}}{A} \left(1 + \frac{Ae^2}{I} \right) [1 + \varphi(t, t_i)]} \quad (3.91)$$

E_p = modulus of elasticity of strands (ksi); E_{ci} = modulus of elasticity of concrete at release (ksi); A_{ps} = total cross-sectional area of prestressing strands (in.²); A = cross-sectional area of: a) girder between transfer and deck placement, b) composite structure between deck placement and final time; e = eccentricity of prestressing strands with respect to: a) centroid of girder, b) centroid of composite section (in.); I = moment of inertia of: a) girder, b) composite structure (in.⁴); $\varphi(t, t_i)$ = creep coefficient at time t for the load applied at t_i ; t_i = loading time (days); t = time of interest (days)

Alternatively, AASHTO (2020) allows relaxation loss to be taken equal to 1.2 ksi for low-relaxation strands between prestress transfer and deck placement and between deck placement and final time. The proposed methodology uses the equation provided in the commentary of AASHTO (2020) for computing strand relaxation loss since it is claimed to provide more accurate estimates. While it is attempted to compute relaxation losses as accurately as possible it should be noted that relaxation losses are rather small compared to losses caused by other effects.

3.1.10 Temperature Gradients

Temperature gradients create similar effects to the ones created by differential shrinkage between the concrete and the strands or between the deck concrete and beam concrete. Because temperature can vary through the depth of the cross-section, some parts of the cross-section will tend to contract or expand more than the other parts. The temperature gradient used in this report for quantifying its effects on beam camber and displacements was obtained from AASHTO LRFD Bridge Design Specifications (2020) for solar radiation zone 3. The positive temperature gradient has a bi-linear shape and is shown in Fig. 3.18. When calculating the effects of temperature gradients on beam camber and displacements, creep effects were not considered because it was

assumed that the temperature gradient would develop over a period of eight hours. Accordingly, creep effects over such a short period of time would be negligible. Curvatures caused by positive temperature gradients can be calculated by dividing the moment due temperature gradient by the flexural stiffness of the composite section (Eq. 3.92). The moment due to the temperature gradients is calculated by integrating the stress over the depth of the composite section where the temperature gradient applies and by multiplying each infinitesimal stress block by the corresponding distance to the neutral axis of the composite section (Eq. 3.93).

$$\Phi_{TG} = \frac{-M_{TG}}{E_b I_t} \quad (3.92)$$

$$M_{TG} = \int_0^{h_{ctop}} \alpha T(y) E_b b(y) y dy \quad (3.93)$$

Φ_{TG} = curvature due to temperature gradient (1/mm)

M_{TG} = moment due to temperature gradient (N-mm)

α = coefficient of thermal expansion/contraction 6×10^{-6} (mm/mm/°F)

y = distance from the centroid of the composite section (mm)

b = width of the composite section (varies along the height) (mm)

T = temperature gradient defined in Fig. 3.18.

h_{ctop} = distance from centroid of composite section to top of deck

E_b = modulus of elasticity of beam at 28 days

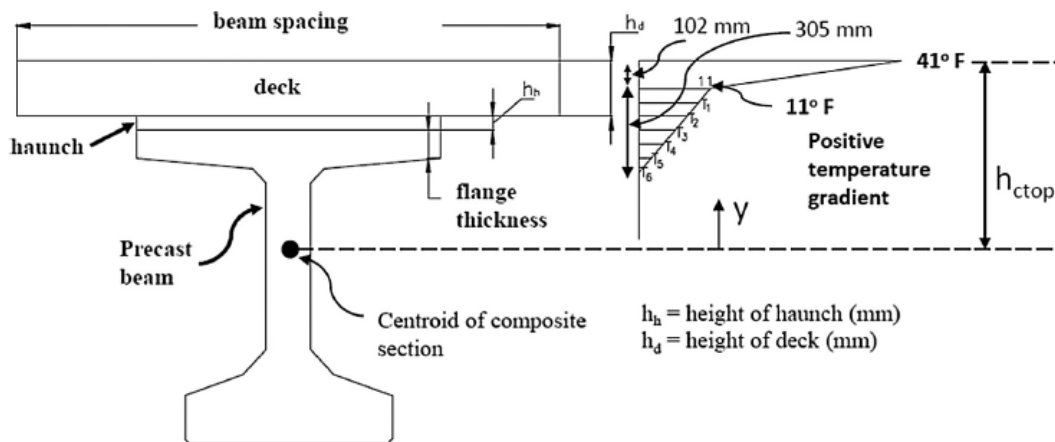


Fig. 3.18. Positive temperature gradients for solar radiation zone 3

3.1.11 Limitations of the Proposed Prediction Methodology

The previous sections presented the approach as well as the assumptions made during the development of the proposed prediction methodology. For fully prestressed concrete beams the prediction methodology can be used to predict camber and displacements at any point in time during the life of the beam. For steel beams, the prediction methodology can be used to predict camber and displacements in the composite system. In both cases the non-composite and composite beams are assumed to be prismatic and simply supported. The proposed prediction methodology does not address multi-span continuous bridges or non-prismatic members. It also does not address partially prestressed concrete beams (i.e. beams that are allowed to crack under service loads), although in Michigan such beams are rare due to the aggressive environment created by the cold climate and the treatment of bridge decks with deicing salts. The extension of the prediction methodology to continuous bridges could very well be the scope of a future project. If this is pursued the following would need to be considered:

- 1) Quantification of restraint moments and their impact on beam camber and displacements. This will depend on the detail adopted by MDOT to create continuity for live loads.
- 2) Unequal spans and different beams for each span. This will require the entry of the relevant information for each span. This is a significant research endeavor as it requires to extend the capabilities of the computational tool to include time dependent analysis in statically indeterminate structures.
- 3) Consideration of various construction sequences. For example, in multi-span continuous bridges, the deck is sometimes placed such that the portion over the interior supports is placed later than the rest of the deck to reduce the likelihood of any transverse deck cracking due to negative restraint moments or any continuity diaphragm cracking due to positive restraint moments. This sequence is different compared to the case where the entire deck is placed in one installation in terms of the history of beam camber and displacements.
- 4) Consideration of continuity in pin-hanger connections in terms of how it affects the variation of internal forces if the tool is anticipated to be used in these cases.
- 5) Consideration of any potential cracking in the deck or beams if partially prestressed beams were ever pursued or if it is found that existing prestressed concrete bridges crack under service loads.

3.2 Time Dependent Multiplier Method

While the algorithm developed based on the proposed methodology (Iteration No. 6) is relatively straightforward to use, it does require the input of several variables. When only pre-erection camber is of interest, an alternative method to predict it is to use time dependent multipliers. The benefit of this method is that it provides a multiplier that is time dependent and thus removes the limitation imposed by PCI and MDOT fixed value multipliers for any pre-erection time. The disadvantage of this approach is that these multipliers are empirically derived based on the dataset used as part of this research project. In this approach, time dependent multiplier curves were developed for the each bridge project based on results obtained from the proposed methodology. The ratio between long-term camber and camber at release was plotted as a function of time. The analysis was conducted up to 90 days. The multipliers are applied to the net camber at prestress release (i.e. the camber due to prestress plus beam self-weight).

Chapter 4: Beam Camber and Displacement Data Sets

Chapter 4: Beam camber and displacement data sets

4.1 Introduction

The research team was provided with a dataset of measured camber for various prestressed concrete and steel beams used in bridge projects in Michigan. The measured camber typically included measured camber at release and measured pre-erection camber. In addition, the dataset included bridge drawings, quality assurance (QA) and quality control (QC) reports. The QA/QC reports included measured concrete compressive strength, measured prestressing force at release, measured unit weight, and measured beam length. The camber and displacement dataset provided by MDOT were evaluated in terms of frequency, time, location, and instrumentation used to measure camber as well as other information provided as part of the dataset. This evaluation was done with the purpose that the provided dataset could later be used to assess the accuracy of the proposed long-term camber prediction method.

In terms of frequency, camber and displacement data sets provided by MDOT were supplied at two different times for each project; once after the detensioning of the strands (first set) and another time prior to the erection of the beams at the bridge site (second set). The first set of camber data was measured by the fabricator and was accompanied with information on the measured concrete strength when the strands were detensioned, measured length of beams, measured unit weight, and measured prestressing force. However, not all of this information was provided for each project discussed in this section. MDOT's policy in terms of the time frame for collecting this set of data is that camber be measured at mid-span for each beam no more than seven calendar days after releasing the prestressing force. The second set of data was measured by agencies hired by MDOT before the beam leaves the precaster's facility for erection (between 14 and 21 calendar days prior to setting the beam seat elevations at the abutments and piers). While these two sets of data taken at two discrete times were certainly helpful in evaluating the accuracy of the proposed methodology, the research team collected additional data at a higher frequency from a precast plant in Windsor, Canada to further validate the proposed prediction methodology and to develop the full camber growth curve for several beams. The precast fabricator in Windsor is Prestressed Systems Inc. (PSI).

In terms of time, ideally, daily measurements should be taken early in the morning to eliminate the effects of radiation-induced temperature gradients and allow collection of consistent data. However, given that the first set of camber data were prepared by the precast fabricator who

measured camber sometime after the detensioning of the strands, and that the second set was measured by other agencies employed by MDOT sometime prior to the erection of the beams at the bridge site, it may be difficult to ensure short term and long term collection of camber data at a specified period of time during the day. However, if possible, collection of such data at a consistent time during the day will help eliminate the effects of radiation-induced temperature gradients and allow collection of consistent data. To quantify the effects of radiation-induced temperature gradients the research team collected data on several beams at the PSI Windsor plant several times during a day including early in the morning, mid-morning, and noon.

In terms of location, the first set of camber data prepared by the fabricator were measured at mid-span of the beam. It was assumed that the beam was supported as shown in the drawings with supports located a distance L_t away from the ends of the beam. In cases when the support conditions were not shown in the drawings it was assumed that the beams were supported as indicated in MDOT's Standard Specifications for Prestressed Concrete Beams, which state: "Support stockpiled beams across the full width on two battens, each greater than 4 in. wide. Do not support beams at more than two points. Use battens to hold beams off the ground over the full length. Place battens in from the beam ends no greater than $1\frac{1}{2}$ times the depth of the beams, or 3 feet, whichever is less."

The second set of data were collected at multiple points along the span of the beam as outlined in the document titled "Special Provision for Structure Survey during Construction" prepared by MDOT. This document requires the reporting of the location of the supports during storage as this information affects the magnitude of displacements due to self-weight and consequently the magnitude of camber. However, such information was not provided. As a result, similar to camber at prestress release predictions, long term camber predictions used the support distance L_t discussed above.

In terms of instrumentation, information regarding instruments used by the fabricator to measure short-term camber and those used by the other agencies to measure long term camber was not provided.

The information provided by the precast fabricator contained information on actual beam length, magnitude of prestressing force, concrete unit weight, and measured concrete compressive strength at release. This information was used to quantify the variability between specified and

measured properties because such variation has been reported to be one of the main reasons for the disparity between predicted and measured camber.

The provided short term (first set) and long-term (second set) camber and displacement data were used to evaluate the accuracy of the proposed methodology. The following sections provide detailed information on the camber and displacement data sets provided by MDOT, and camber data collected by the research team at the PSI Windsor plant.

4.2 Camber and Displacement Data Sets Provided by MDOT

Camber and displacement data sets were provided by MDOT on 17 projects, which are summarized in Table 4.2. The prestressed concrete beams for these projects were fabricated by either Peninsula Prestress or PSI Decatur. Based on information supplied by MDOT the following procedures/policies are used during the fabrication of the prestressed concrete beams by various precast fabricators who supply prestressed concrete beams for bridge projects in Michigan.

1. **Casting of Concrete:** Concrete is prepared and mixed in the precast facility and transported to the forms. Several fresh concrete tests are conducted to ensure compliance with the specifications such as: concrete temperature, slump, and air content. Also, concrete cylinders are prepared for compressive strength testing at release and 28 days. If the results from fresh air concrete tests deviate from the specifications, then an attempt can be made to adjust concrete such that it complies with specification requirements within the time permitted in the MDOT Standard Specifications to avoid rejected concrete. For example, concrete can be adjusted in truck mixers by doing an additional 30 revolutions at mixing speed. During concrete placement, the steam is shut off and is turned back on after initial set to help with accelerated curing. At the end of the concrete placement, tarps are secured over the beams for moisture retention and insulating purposes. Whenever any type of external heat source is used, thermocouplers are used to record the concrete temperature (maximum concrete temp allowed is 150°F).
2. **Curing:** The curing techniques used by various precast fabricators that supply prestressed concrete beams for bridge projects in Michigan are summarized in the following table. The curing process is completed once the specified f_{ci} is reached. The MDOT specifications for beam curing are provided in section 708.3 of Standard Specifications for Construction.

3. Detensioning the strands: Prestressing force is transferred only after the specified concrete compressive strength at release is reached. Detensioning of the strands is done gradually according to a specified sequence to minimize eccentricities.
4. Beam Storage: Once the strands are detensioned, the beam is stored in the yard until the time comes to ship it.

Table 4.1. Curing techniques used by precast beam fabricators that supply prestressed concrete bridge beams for MDOT

Precast Fabricator	Curing Technique
Peninsula Prestress	Live steam. The steam lines run on the outside bottom of the beam beds
Mack, Zilwaukee	Boiler heating system (oil) run along outside bottom of beam beds ^a
Mack, Kalamazoo	Radiant heat or live steam is used along outside bottom of beam beds
PSI-Decatur	<i>Sure Cure System</i> (electrical curing system) programmable to ensure the concrete follows a consistent time/temp curve
Spancrete	Live steam
Kerkstra Precast	Indoor prestressing beds. Curing technique uncertain ^a
^a There were no active projects at this plant at the time of writing of this report	

Table 4.2. Camber and Displacement Data Sets

Project name	Girder type and depth (in.)	No. of beams/data ⁹	Span length (ft.)	Deck thickness (in.)	Center-to-center spacing (ft.)	Strand configuration? ¹	Available camber data ²	Fabricator ⁷	f'_{ci} (psi) ⁴	f'_c (psi) ⁴	f'_{deck} (psi) ⁴
M5 1-2	Bulb tee (42)	6/6	144.33	6	6.00	H@0.4L	R & P	PP	6100	8000	4000
M57	MI 1800 (71)	8/8	137.80	9	7.92	H@0.4L	R	PP	6000	6000	4000
M89	Spread Box (17)	6/6	28.25	9	8.00	D	R & P	PP	4300	5000	4000
M311	Bulb tee (60)	6/6	147.33	9	7.46	D	R & P	PSI - LLC	7000	8500	4000
TSO ⁸	Bulb tee (63)	4/4	98.33	8.85	8.20	H@(0.40-0.33)L	R & P	PSI	6100	7200	NA ¹⁰
Conc. A. 1	Bulb tee (48)	8/4	115.50	9	6.50	D	R	PP	7200	9000	4000
Conc. A. 2	Bulb tee (48)	8/8	91.50	9	6.50	D	R	PP	5200	9000	4000
I75-B05	AASHTO Type II (36)	9/9	39.50	9	5.83	-	R	PSI - LLC	6000	8000	4000
I75-S05	Bulb tee (60)	11/11	152.50	9	9.04	D & H@0.4L	R & P	PSI - LLC	7000	10000	4000
I75-S09-1	Bulb tee (48)	9/9	115.54	9	7.00	D	R	PSI - LLC	7000	10000	4000
I75-S09-2	Bulb tee (48)	9/9	112.79	9	7.00	D	R	PSI - LLC	7000	10000	4000
I75-S10-1	Bulb tee (42)	8/8	80.83	9	8.88	H@0.4L	R & P	PSI - LLC	7000	10000	4000
I75-S10-2	Bulb tee (42)	8/8	97.33	9	8.88	D & H@0.4L	R & P	PSI - LLC	7000	10000	4000
I75-S11	Bulb tee (54)	9/9	136.00	9	8.42	D & H@0.33L	R & P	PSI - LLC	7000	10000	4000
I75-S12-1	Bulb tee (42)	7/7	96.75	9	8.08	H@0.4L	R & P	PSI - LLC	7000	10000	4000
I75-S12-2	Bulb tee (42)	7/7	106.17	9	8.08	H@0.4L	R & P	PSI - LLC	7000	10000	4000
French Rd. over I94 1-2	Bulb tee (42)	18/14	99.04	9	7.00	H@0.4L	R & P ⁶	PP	6000	8000	4000
Shepherd Rd. 1-3	Spread Box (21)	10/4	55.92	NA ¹⁰	7.00	D	P ³	PP	6500	7000	NA ¹⁰
Shepherd Rd. 2	Spread Box (21)	5/5	62.17	NA ¹⁰	7.00	D	P ⁵	PP	6500	7000	NA ¹⁰
I75-Springwells-1	Bulb tee (48)	11/2	86.67	9	9.15	D & H@0.4L	R	PP	7000	8000	4000
I75-Springwells-2	Bulb tee (48)	11/2	74.67	9	9.15	D & H@0.4L	R	PP	7000	8000	4000
I75-Livernois-1	Bulb tee (48)	12/0	111.00	9	6.63	D & H@0.4L	NA ¹⁰	PP	7000	8000	4000
I75-Livernois-2	Bulb tee (48)	12/2	96.75	9	6.63	D & H@0.4L	R	PP	7000	8000	4000
Saginaw County	Bulb tee (42)	12/12	118.9	NA ¹⁰	6.17	D & H@0.4L	R & P	PP	7000	10000	NA ¹⁰
M20	I-shaped steel beam (70)	20/20	172-190 ¹¹	9	10.0-10.50 ¹²	Not applicable	PRC & PC ¹³	NA ¹⁰	Not applicable		4000

1. H: Harped, D: Debonded.

2. R: Camber at release, P: Camber at pre-erection.

3. Camber measurements were recorded at the precast facility nine days after beams were cast.

4. Specified concrete strength.

5. Camber measurements were recorded at the precast facility 1 to 3 days after beams were cast.

6. Provided measured pre-erection camber data could not be used due to insufficient information.

7. PP: Peninsula Prestress, PSI: Prestress Services Industries.

8. TSO: Tiffin Street Overpass, Canadian Project.

9. Represents number of beams for which camber and displacement data was available.

10. Not available.

11. There are four spans whose lengths vary.

12. There are five beams in the transverse direction whose spacings vary.

13. PRC: pre-construction camber (without beam self-weight), PC: post-construction camber

4.3 Camber and Displacement Data Sets collected from the Windsor Plant

In addition to the data provided by MDOT, the research team collected additional camber data from the PSI Windsor plant for four prestressed concrete beams used in the Tiffin Street Overpass project. This bridge has a span of 96 ft 9 in. and features a total of seven prestressed concrete beams. However, due to the tight casting and shipping schedule, camber data was collected only for four beams. PSI supplied partial bridge drawings and specifications so that the research team could predict short term and long-term camber. Camber data was collected twice a week for a period of four weeks, which was approximately the period of time that the girders stayed in the precast facility prior to being shipped to the bridge site. The number of camber data points collected per beam varied from four to eight depending on when the beam was cast. This increase in the number of camber data points compared to the two data points per beam supplied for the MDOT projects provided an opportunity to create a camber growth curve for the beams in question and to validate the long-term camber predictions at additional times. In addition, for all four beams several measurements were taken two days before the girders were shipped to the construction site at various times during the day such as morning, mid-morning, and noon to quantify the effects of radiation induced temperature gradient.

As stated earlier, the Tiffin Street Overpass project features a total of seven 98 foot long CPCI 1600 prestressed concrete beams whose properties and dimensions are illustrated in Fig. 4.1. The prestressed concrete beams did not feature any debonded strands, but did have three sets of harped strands. The following procedure/policy was used during fabrication:

1. *Casting of Concrete:* Concrete was prepared and mixed in the precast facility and transported to the forms. Several fresh concrete tests were conducted to ensure compliance with the specifications such as: concrete temperature, slump, and air content. Also, concrete cylinders were prepared for compressive strength testing at release and 28 days. If the results from fresh air concrete tests deviate from the specifications, concrete is rejected.
2. *Curing:* A minimum of four-day moist curing is typically used. During the moist curing and moisture retention period, the members may be exposed to ambient condition for no more than a total of three hours. The concrete temperature during production, moist curing and moisture retention period shall not fall below 10 °C before the concrete has reached

75% of the specified 28-day compressive strength. Once the concrete reaches 75% of specified 28-day compressive strength, then temperature control does not apply.

3. Detensioning the strands: Prestressing force is transferred only after the specified concrete compressive strength at release is reached. Detensioning of the strands is done gradually according to a specified sequence to minimize eccentricities.
4. Additional Curing: After the initial four-day moist curing and moisture retention period the girder can be moved outside without any additional curing if the ambient temperature is 5°C or higher. If the member is moved outside, and the outside ambient temperature is below 5 °C, the girder is protected via temperature control using an outside curing chamber for a minimum of three additional days. In this case, the total curing period becomes seven days.
5. Beam Storage: Once the curing process is completed, the beam is stored in the yard until the time comes to ship it. Deep I-beams are braced for stability.

The difference between the fabrication practices used in the PSI Windsor plant and those used by precast fabricators in Michigan is primarily in the initial curing and post curing process. The predominant curing technique in Michigan appears to be steam curing and the curing process is complete once the strands are detensioned. Whereas in the PSI Windsor plant, an initial minimum four day moist curing is used, which may be accompanied by an additional three day curing depending on the outside ambient temperature, when the beam is moved from the prestressing bed. While only the Michigan data was used to develop the time dependent multiplier method, the PSI Windsor measurements were used to further validate the robustness of the proposed prediction methodology by obtaining additional data points per beam. Additionally, the PSI Windsor data was used to quantify the influence of solar radiation induced temperature gradients on camber.

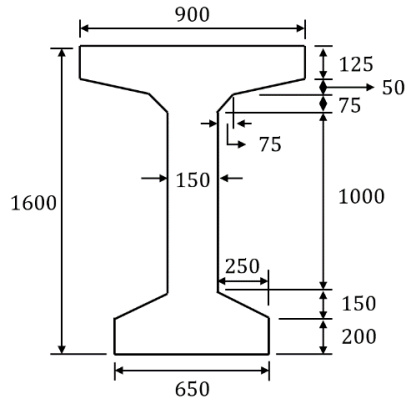
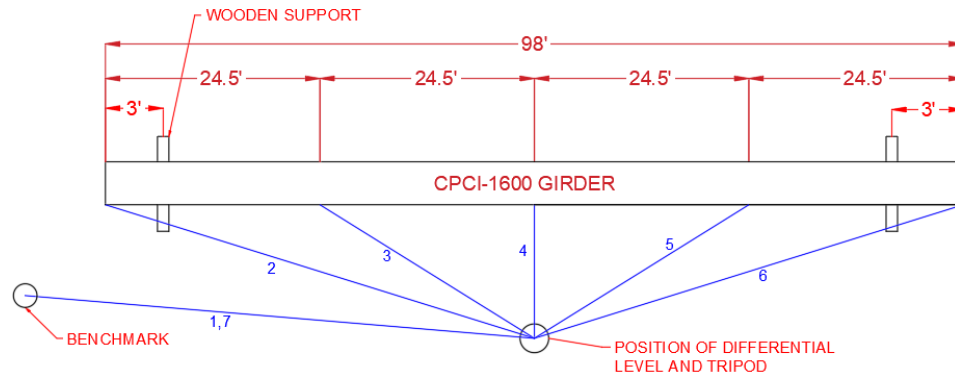
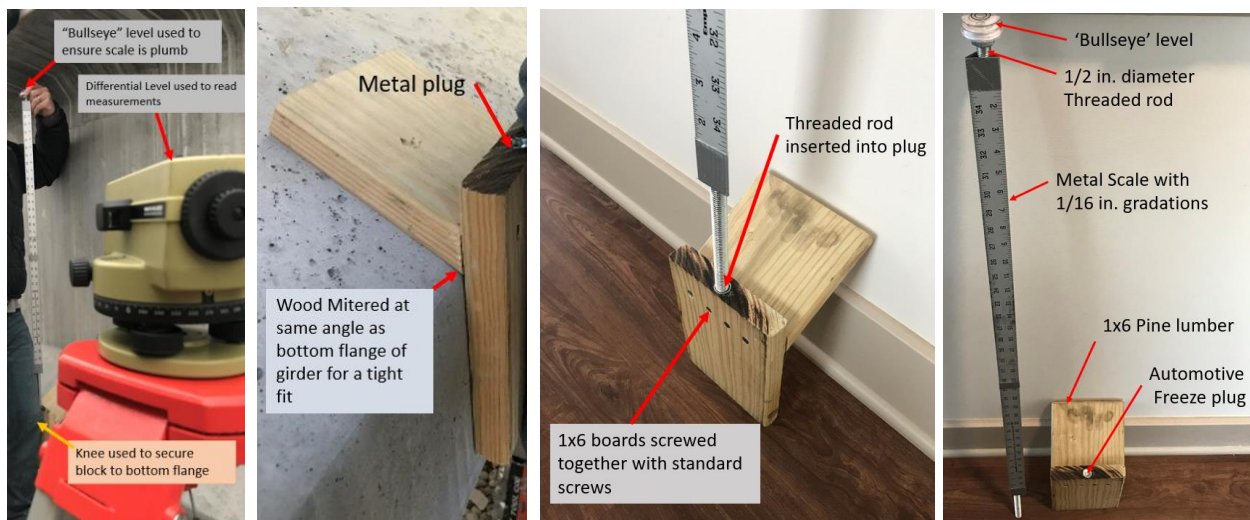


Fig. 4.1. Nominal Dimensions (in mm) for the CPCI-1600 prestressed concrete beams ($A = 515 \text{ mm}^2 \times 10^3$, $Y_b = 793 \text{ mm}$, $I_x = 1.78 \times 10^{11} \text{ mm}^4$)

The first camber measurement for each girder was taken a few days after the girder was removed from the moist-cure chamber and placed into storage. Camber was measured using surveying equipment, which featured a differential level, tripod, a custom made measuring rod, and a bearing block for the rod. The beams were placed on wooden blocks positioned approximately 3 feet from each end. The custom made measuring rod replaced the standard surveying rod, which was too tall to fit between the top and bottom flanges of the beam and featured divisions of up to 1/8 in. as opposed to the custom made rod, which provided divisions up to 1/16 in. The custom made rod was made using a threaded steel rod, which was fitted with a scale and bullseye level. The scale's precision was 1/16 in. The bearing block for the rod was made using dimensional lumber, which was saw cut to fit the bottom flange of the CPCI-1600 Girders being measured and is illustrated in Fig. 4.2. b. This provided a solid point to place the measuring rod and obtain consistent measurements across the length of the girder. Fig. 4.2 shows the basic layout of the girder and differential level used to take measurements. The sight was first leveled using the leveling bubble on the differential level. After leveling the sight, a benchmark reading was taken at position 1. Beam elevations were then recorded at the ends, quarter-points, and at mid-span (positions 2 through 6 in Fig. 4.2). Then a final benchmark reading was taken at position 7 (same as position 1) to ensure the level did not move during measurements. This procedure was repeated for each beam. Beam elevations were then used to calculate camber at quarter points and mid-span. Since for this project camber measured by the fabricator at release was not provided, the first set of measurements, which was taken typically two days after the release of the prestressing force, was used to indicate camber at release.



a)



b)

c)

Fig. 4.2. a) Illustration of methodology for measuring camber in four CPCI-1600 prestressed concrete beams, b) photograph showing measurement setup and device made for taking consistent measurements across beam bottom flange, c) photograph showing device used to match the bottom flange of the beam and to receive the measuring rod.

4.4 Relationship between Specified and Measured f'_c

Since the modulus of elasticity is typically calculated using empirical formulas that are a function of the compressive strength of concrete, it could be deduced that an accurate estimation of the actual concrete compressive strength helps improve the accuracy of the estimation for the modulus of elasticity and consequently camber predictions. Since measured compressive strength data was made available as part of the quality control and quality assurance reports, the relationship between the specified concrete compressive strength at release, $f'_{ci_specified}$, and the measured

concrete compressive strength at release, $f'_{ci_measured}$, was investigated (Fig. 4.3a). Additionally, measured concrete compressive strength data when beams were shipped from the precast facility to the bridge site were also available for some projects. When the beams were shipped to the bridge site, the age of beams was between 28-30 days old. Therefore, measured compressive strength data when the beams were shipped were used to establish a relationship between measured and specified compressive strength at 28 days (Fig. 4.3b). The average ratio between measured and specified compressive strength at prestress release was calculated for beams fabricated by three companies: Prestress Services Industries LLC, Peninsula Prestress, and PSI Windsor (Canadian Company). Since only Prestress Services Industries LLC and Peninsula Prestress fabricate beams for bridge projects constructed in Michigan, only data from these companies were used to calculate an average overstrength factor for the concrete compressive strength at release. This overstrength factor (i.e. average ratio of $f'_{ci_measured}/f'_{ci_specified}$) was 1.21 and the coefficient of variation (COV) was 14%. Similarly, the average ratio between measured and specified compressive strength at 28 days ($f'_{c_measured}/f'_{c_specified}$) for the beam fabricated by Prestress Services Industries LLC was 1.21 and the COV was 11%. These overstrength factors are included as an option in the algorithm (Iteration No. 6) so that the user can adjust specified compressive strengths accordingly for improved camber predictions.

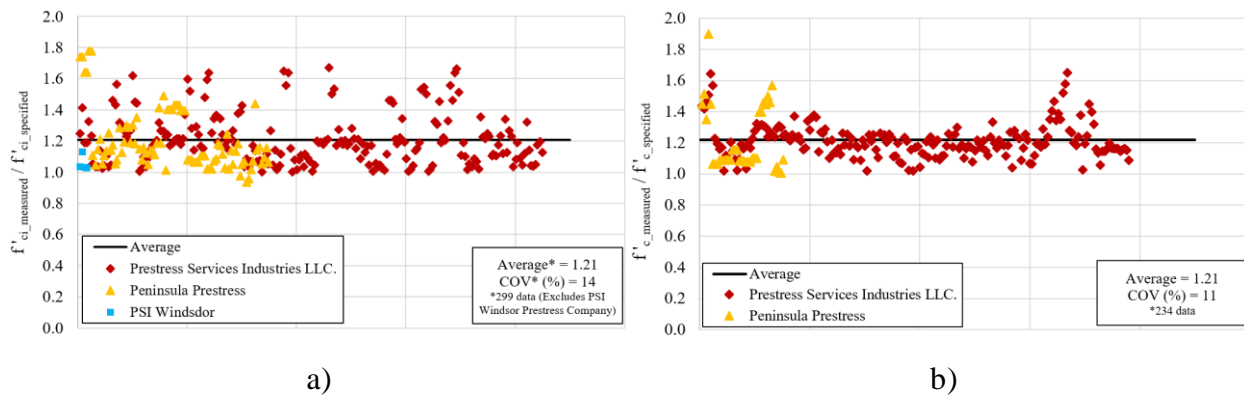


Fig. 4.3. Ratio of measured over specified: a) initial concrete compressive strength, b) 28 day concrete compressive strength

4.5 Relationship between Calculated and Measured E_{ci}

Since the modulus of elasticity of concrete at release is one of the key parameters for accurately estimating camber at release as well as long-term camber, the relationship between the calculated modulus at release and the measured modulus was investigated. The calculated modulus was obtained using Eqs. 3.75, 3.77, 3.79 and 3.81 provided in the AASHTO LRFD Bridge Design

Specifications (2020), ACI 318-19, ACI 363R-92 (1992), and fib MC 2010, respectively. Modulus of elasticity was calculated once using the specified concrete compressive strength, specified unit weight, and $K_f=1.0$ (Table 4.3) and another time using measured compressive strength (Table 4.4). The calculated modulus was compared to the measured modulus for several bridge projects. Modulus of elasticity tests were conducted in accordance with ASTM C469. The results are shown in Table 4.3 and 4.4. As can be seen, Eq. 3.75, 3.77, 3.79 and 3.81 underestimate modulus of elasticity at release of prestressing force. When specified compressive strengths are used average ratios of measured over predicted modulus for AASHTO (2020), ACI 318-19, ACI 363 (1992), and fib MC (2010) are 1.20, 1.24, 1.37, and 1.12 and COVs of 15% , 16%, 15%, and 15%, respectively. As can be seen, the fib MC 2010 model provides the most accurate and consistent estimations of modulus. When measured compressive strength are used, average ratios of measured over predicted modulus for AASHTO (2020), ACI 318-19, ACI 363 (1992), and fib MC (2010) are 1.13, 1.14, 1.30, and 1.09 and COVs of 5% , 5%, 4%, and 5%, respectively. As can be seen, the fib MC 2010 model still provides the most accurate and consistent estimations of modulus. It should be noted that this conclusion is based on only a limited set of data for Michigan concretes. The proposed prediction methodology allows the use of any of these models for predicting modulus. The user of the proposed prediction tool is encouraged to evaluate each model. As a starting point, it is recommended that the AASHTO (2020) model be used since it is provided in the main body of AASHTO LRFD Specifications (2020). In addition, this model together with other models that capture the variation of modulus of elasticity, creep, and shrinkage with time resulted in reasonable predictions of pre-erection camber when compared with measured values as will be demonstrated in the subsequent chapters. The use of measured compressive strength improved the accuracy and consistency of modulus of elasticity predictions. The specified overstrength factors for compressive strength can be used in the proposed prediction methodology to utilize this increase in modulus prediction accuracy.

$$E_{ci} = 120,000 K_1 w_c^{2.0} f_{ci}'^{0.33} \quad (3.75)$$

$$E_{ci} = 33 w^{1.5} \sqrt{f_{ci}'} \quad (3.77)$$

$$E_{ci} = (40,000 \sqrt{f_{ci}'} + 10^6) \left(\frac{w}{145} \right)^{1.5} \quad (3.79)$$

$$E_{ci} = 2760 \alpha_E \sqrt[3]{f_{ci}'} \quad (3.81)$$

Table 4.3. Relationship between calculated and measured modulus of elasticity at release (calculated modulus is based on specified compressive strength)

Fabricator	Project	Beam ID	$E'_{ci_calculated}^*$ (ksi)				$E'_{ci_measured}$ (ksi)	Ratio = $\frac{E'_{ci_measured}}{E'_{ci_calculated}}$			
			AASHTO (2020)	ACI 318-19	ACI 363R-92	fib MC 2010 ⁺		AASHTO (2020)	ACI 318-19	ACI 363R-92	fib MC 2010 ⁺
Peninsula Prestress	Concord Avenue	NA	4960	4821	4347	5280	4461	0.90	0.93	1.03	0.84
		NA	4960	4821	4347	5280	4682	0.94	0.97	1.08	0.89
	R04	NA	4960	4821	4347	5280	6533	1.32	1.36	1.50	1.24
		NA	4960	4821	4347	5280	6440	1.30	1.34	1.48	1.22
	R04	NA	4960	4821	4347	5280	6346	1.28	1.32	1.46	1.20
		N1	4960	4821	4347	5280	6272	1.26	1.30	1.44	1.19
	S02	O1	4484	4273	3967	4872	6443	1.44	1.51	1.62	1.32
	B02	P1	4960	4821	4347	5280	5320	1.07	1.10	1.22	1.01
	S07	NA	4960	4821	4347	5280	6377	1.29	1.32	1.47	1.21
	*Using specified properties; ⁺ Aggregate factor, α_E , was taken 1.0.						Avg.	1.20	1.24	1.37	1.12
							St. Dev	0.18	0.19	0.21	0.17
							COV (%)	15.3	15.7	15.1	15.0

Table 4.4. Relationship between calculated and measured modulus of elasticity at release (calculated modulus is based on measured compressive strength)

Fabricator	Project	Beam ID	$E'_{ci_calculated}^*$ (ksi)				$E'_{ci_measured}$ (ksi)	Ratio = $\frac{E'_{ci_measured}}{E'_{ci_calculated}}$			
			AASHTO (2020)	ACI 318-19	ACI 363R-92	fib MC 2010 ⁺		AASHTO (2020)	ACI 318-19	ACI 363R-92	fib MC 2010 ⁺
Peninsula Prestress	R04	NA	5790	5733	4980	5926	6533	1.13	1.14	1.31	1.10
		NA	5790	5733	4980	5926	6440	1.11	1.12	1.29	1.09
		NA	5790	5733	4980	5926	6346	1.10	1.11	1.27	1.07
	R04	N1	5343	5249	4644	5588	6272	1.17	1.19	1.35	1.12
	S02	O1	5315	5218	4622	5566	6443	1.21	1.23	1.39	1.16
	B02	P1	4991	4855	4371	5305	5320	1.07	1.10	1.22	1.00
	S07	NA	5844	5791	5020	5966	6377	1.09	1.10	1.27	1.07
	*Using measured properties; ⁺ Aggregate factor, α_E , was taken 1.0.						Avg.	1.13	1.14	1.30	1.09
							St. Dev	0.05	0.05	0.06	0.05
							COV (%)	4.5	4.6	4.4	4.5

The development of modulus of elasticity with time was also examined by conducting modulus of elasticity tests at various concrete ages and by comparing the measured modulus with the time dependent calculated modulus using specified as well as measured compressive strengths. Fig. 4.4 suggests that the use of measured compressive strengths resulted in closer agreements between measured and calculated time dependent modulus. Fig. 4.4. suggests that the use of the fib MC (2010) model and the combination of AASHTO LRFD (2020) and ACI 209R-92 model resulted in more accurate predictions compared with the combination of ACI 363R-92 and ACI 209R-92 model. As noted earlier, the amount of long-term modulus data is too limited to draw any firm conclusions about the superiority of a given model for Michigan concretes. Since the proposed

prediction methodology allows the use to select any combination of models the user is encouraged to explore this benefit to obtain a sense for the range of variability in the results for a given project. However, the combination of the AASHTO LRFD (2020) and ACI 209R-92 models can be used as the starting point for predicting the modulus of elasticity with time.

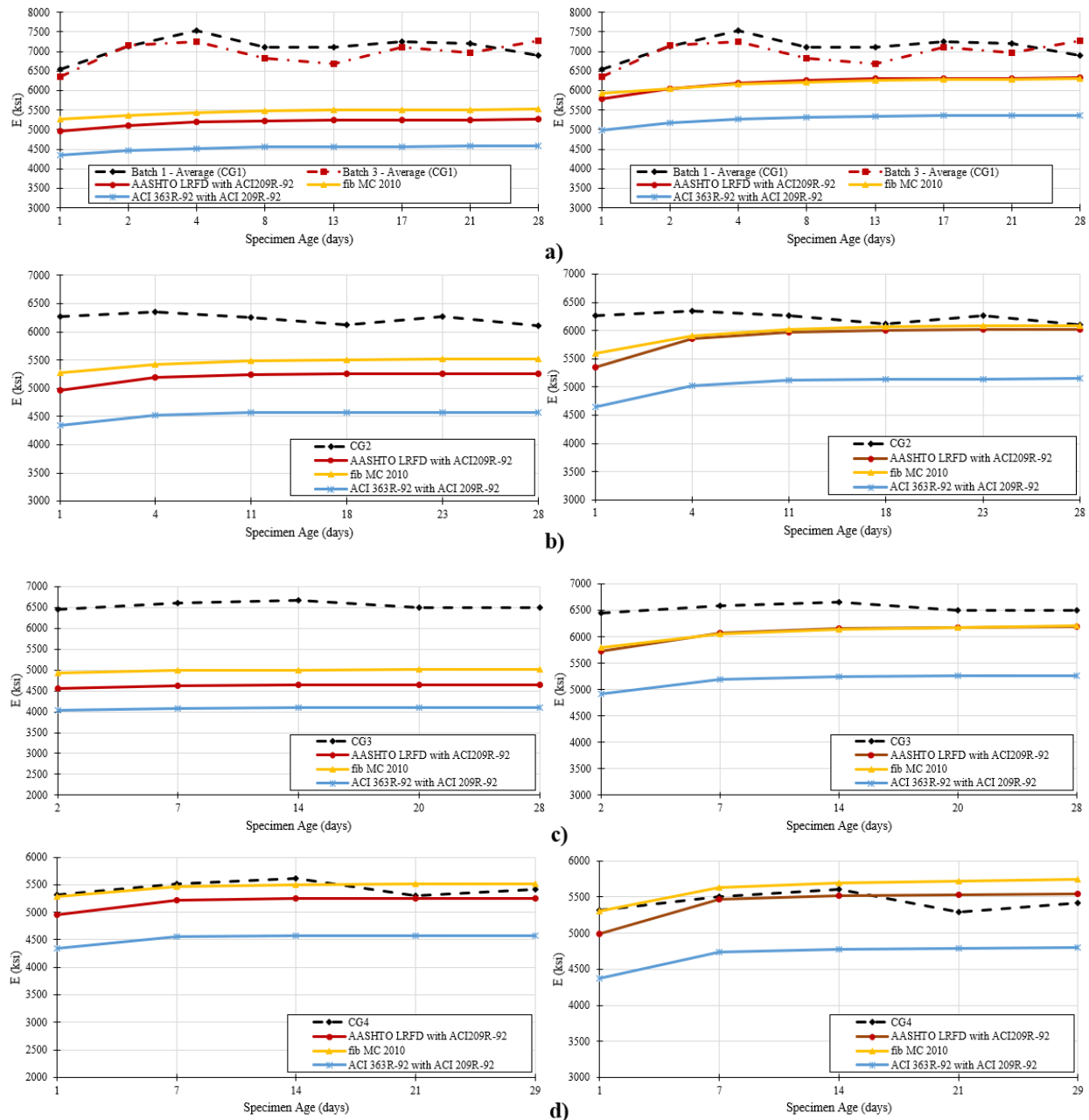


Fig. 4.4. Development of modulus of elasticity with time using specified (left) and measured (right) properties for: a) R04 (CG1); b) R04 (CG2); c) S02 (CG3); d) B02 (CG4) projects

4.6 Relationship between Specified and Measured Concrete Unit Weight

The relationship between the specified and measured unit weight was investigated for the beams fabricated by Peninsula Prestress. Since concrete unit weight is an important factor when estimating the self-weight of the beam and consequently the displacement due to self-weight, the quantification of any variation in this parameter is of interest. The results shown in Table 4.5 suggest that there is not much variation between the specified and measured unit weight. The average ratio between measured and specified unit weight is 1.0 and the COV is 1.0%.

Table 4.5. Comparison of specified and measured concrete unit weight

Fabricator	Project	Beam ID	$w_{specified}$ (pcf)	$w_{measured}$ (pcf)	Ratio = $\frac{w_{measured}}{w_{specified}}$
Peninsula Prestress	M-89	All	145	145.12	1.00
	M-5	All	145	145.42	1.00
	M-57	B-2, C-3	145	146.00	1.01
		D-4	145	146.32	1.01
		E-5	145	142.00	0.98
		H-7	145	144.56	1.00
	Avg.				1.00
	Std.				0.01
	COV				0.01

4.7 Relationship between Specified and Measured Prestressing Force

One of the parameters that affect the magnitude of camber is the magnitude of the prestressing force. Therefore, using the correct prestressing force when estimating camber at release or long term camber is paramount. The relationship between the measured and specified prestressing force was investigated to determine the degree of variability. The results shown in Table 4.6 suggest that there is no significant variation between the specified and measured prestressing force. The average ratio between measured and specified prestressing force is 1.03 and the COV is 1.0%.

Table 4.6. Comparison of specified and measured prestressing force at release

Fabricator	Project	Beam ID	$P_{i_specified}$ (kips)	$P_{i_measured}$ (kips)	Ratio = $\frac{P_{i_measured}}{P_{i_specified}}$
Peninsula Prestress	M-89	All	44	45.5	1.03
	M-57	All	44	45.0	1.03
Avg.					1.03
Std.					0.01
COV					0.01

4.8 Relationship between Specified and Measured Beam Length

Beam length is one of the key parameters when estimating displacements and camber because a small variation in it causes large changes in displacements and camber. For example, displacements due to beam self weight are a function of the beam length raised to the power of four. Similarly, camber due to prestress is a function of beam length raised to the power of two. The relationship between the specified beam length and supplied one was investigated for all three Michigan projects whose beams were fabricated by Peninsula Prestress. The results of such comparison are shown in Table 4.7. As can be seen, there is negligible variation between the specified and measured beam length. Therefore, beam length can be eliminated as a source of uncertainty.

Table 4.7. Comparison of specified and measured beam length

Fabricator	Project	Beam I.D.	$L_{specified}$ (in.)	$L_{measured}$ (in.)	$L_{measured}/L_{specified}$
Peninsula Prestress	M89	A1	355.00	355.00	1.00
		F5	355.00	355.13	1.00
		B2	355.00	355.00	1.00
		C3	355.00	355.13	1.00
		D4	355.00	355.00	1.00
		E2	355.00	355.13	1.00
	M5	1B	1381.00	1380.50	1.00
		1A	1381.00	1381.00	1.00
		1C	1381.00	1381.13	1.00
		2A	1381.00	1380.75	1.00
		2B	1381.00	1380.63	1.00
		2C	1381.00	1381.25	1.00
	M57	1A	1664.63	1665.38	1.00
		D4	1664.63	1664.50	1.00
		B2	1664.63	1665.38	1.00
		C3	1664.63	1664.50	1.00
		E5	1664.63	1665.00	1.00
		G6	1664.63	1665.38	1.00
		F2	1664.63	1665.13	1.00
		H7	1664.63	1664.75	1.00
	Avg.				1.00
	Std.				0.00
	COV.				0.00

4.9 Summary of Relationships between Measured and Specified/Calculated Properties

Table 4.7 provides a summary of the relationships between measured and specified/calculated properties using various statistical indicators. The average ratio and COV of measured over specified concrete compressive strength at prestress release and 28 days was 1.21 and 1.21, and 14% and 11%, respectively. Therefore, the algorithm based on Iteration No. 6 provides the user the option to use Michigan Overstrength Factor of 1.2 for both f'_{ci} and f'_c . The average ratio and COV of measured over calculated modulus of elasticity at prestress release based on AASHTO LRFD Specifications (2020) are 1.20 and 15%, respectively, when the specified compressive strength was used to calculate the modulus. When measured properties were used, the average ratio and COV. of measured over calculated modulus of elasticity at prestressed release based on AASHTO LRFD (2020) are 1.13 and 5%, respectively. Finally, as previously indicated there was negligible variation between measured and specified unit weight, prestressing force, and beam length.

Table 4.8. Summarized results for the relationship between measured and specified parameters

Statistical parameters	$\frac{f'_{ci, measured}}{f'_{ci, specified}}$	$\frac{f'_{c, measured}}{f'_{c, specified}}$	$\frac{E_{ci, measured}}{E_{ci, calculated}^*}$	$\frac{E_{ci, measured}}{E_{ci, calculated}^{**}}$	$\frac{w_{measured}}{w_{specified}}$	$\frac{P_{i, measured}}{P_{i, specified}}$	$\frac{L_{measured}}{L_{specified}}$
Min.	0.94	1.01	0.90	1.07	0.98	1.03	1.00
Max.	1.78	1.90	1.44	1.21	1.02	1.03	1.00
Avg.	1.21	1.21	1.20	1.13	1.00	1.03	1.00
COV. (%)	14	11	15	4.5	1	1	0
# of tests	299	234	9	7	8	2	20
*Based on AASHTO LRFD (2020) with specified concrete compressive strength.							
**Based on AASHTO LRFD (2020) with measured concrete compressive strength.							

4.10 Solar Radiation Study

To quantify the influence of solar radiation induced temperature gradient on beam camber, several measurements were taken for the beams fabricated by PSI Windsor on April 27, 2019 between 8:30 a.m. and 1:30 p.m. in Windsor, Canada. Three measurements were taken for each beam; the first at 8:30-9:00 a.m., the second at 11:00-11:30 a.m., and the third at 1:00-1:30 p.m. The weather during the day was mostly sunny and the temperature varied from 38°F to 51°F. All four girders were directly exposed to sunlight throughout the time measurements were taken. The measured data is illustrated graphically in Fig. 4.5. Camber varied as much as 0.22 in. due to the influence of daily temperature gradient. This was a smaller variation than that reported by Hinkle (2006) in Virginia who reported that camber varied as much as 0.5 in. due to solar radiation induced temperature gradient. However, Hinkle (2006) conducted his measurements in August 25, in

Virginia, between 7:30 a.m. and 1:30 p.m. The recorded temperatures varied from 82°F to 90°F. The differences between the camber variation that was measured in Windsor, Canada and that reported by Hinkle (2006) in Virginia are attributed to differences in climate and season although both Michigan and Virginia fall in solar radiation zone 3 (Windsor, Canada is assumed to be in the same solar radiation zone due to its proximity to Michigan).

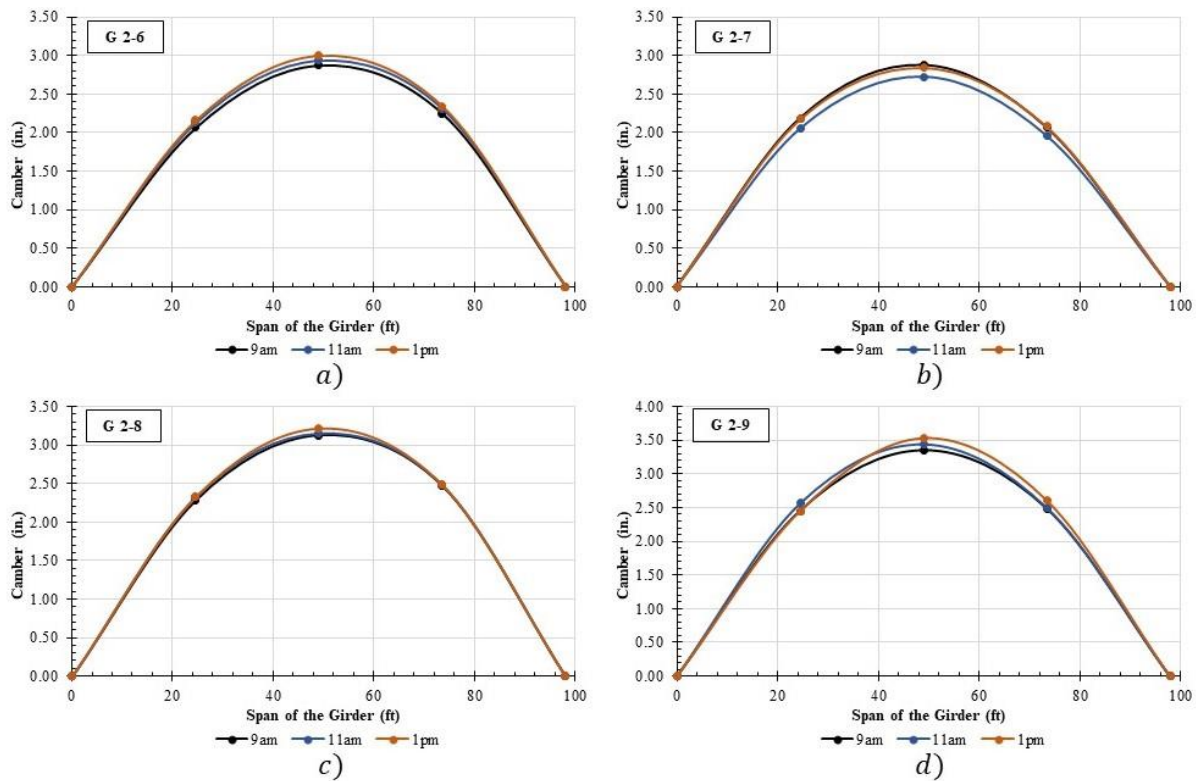


Fig. 4.5. Variation in camber due to radiation induced thermal gradient for: a) Girder G2-6, b) Girder G2-7, c) Girder G2-8, d) Girder G2-9

4.11 Data Collection Guidelines

There are many factors that affect camber at release and long-term camber and each factor is associated with some degree of uncertainty. To minimize uncertainties related to the influence of radiation induced temperature gradient it is recommended that camber measurements are collected at a specific time frame during the day, such as early in the morning and this time should be indicated in the survey report. Additionally, to further quantify the influence of solar radiation induced temperature gradient it would be useful to collect multiple readings during the same day at various times in the day such as early morning, mid-morning, noon, and afternoon. Additionally,

the storage and support conditions for the beams should be indicated in the survey report to properly quantify the influence of the self-weight of the beam on the reported beam elevations throughout the span. Such reporting is required in the document titled “Special Provision for Structure Survey during Construction” prepared by MDOT, however, this type of data was not provided as part of the data set. Furthermore, the instrument with which camber is measured should be indicated in the survey report to ensure that reliable techniques are used to measure camber.

Chapter 5: Evaluate Factors that Affect Prestressed Concrete Beam Camber

Chapter 5: Evaluate factors that affect prestressed concrete beam camber

5.1 Introduction

Factors known to affect camber at release of prestressing force are: unit weight of concrete, member geometry (cross-section and beam length), strand layout and magnitude of the prestressing force, modulus of elasticity at prestress release, transfer length, debonding, intended or unintended cracking, support conditions during storage, and temperature gradients. A sensitivity analysis was conducted to quantify the influence of several of these factors on camber at release and long-term camber. The parameters that were considered in the sensitivity analysis include the length of the beam, the unit weight of concrete, the magnitude of the prestressing force, modulus of elasticity at prestress release, and the time when initial camber is measured. For pre-erection camber, additional parameters such as the creep and shrinkage model, the model to predict modulus of elasticity at prestress release and 28 days as well as its variation with time, and overstrength factors were considered to quantify their influence on pre-erection camber.

5.2 Sensitivity Analysis

The results of the sensitivity analysis are shown in Table 5.1 and Table 5.2. The analysis was conducted using the approach presented in Iteration No. 6 for each project using specified properties and then the considered parameters were varied by +/- 10%. The results in Table 5.1 and Table 5.2 show the average as well as the lower and upper bounds in terms of % change in net deflection (i.e. camber) for all projects considered.

A +/- 10% change in the length of the beam resulted in a change in camber at release that varied from -18.6% to 17.1%. The average change in camber at release for a +/-10% change in beam length was 8.6% and -12.1%, respectively. A similar influence was observed for pre-erection camber. It is interesting to note the range of the percent change in net camber due a fixed percent change in the length of the beam. This range emphasized the need to conduct the sensitivity analysis for various projects rather than draw conclusions based on conducting a sensitivity analysis for a single project. While the results suggest that a 10% change in beam length can cause as high as a 17.1% change in camber, the results presented in Chapter 4 suggest that the variation in beam length is minimal and this parameter does not constitute a source of high uncertainty. Additionally, while beam length is expected to have an exponential effect on either prestressed induced camber or gravity induced downward displacement, the net effects is as shown by the

lower and upper bounds as well as the average change. This is due to the competing effects of prestressing force and gravity as well as other factors such as support conditions during storage.

A $\pm 10\%$ change in the specified compressive strength at release resulted in a change in camber at release that varied from -4.9% to 5.6% and a change in pre-erection camber that varied from -6.9% to 8.2% . The average change in camber at release for a $\pm 10\%$ change in f'_{ci} was -4.4% and 5% , respectively. While the compressive strength itself does not influence in service behavior during which stresses are within the linear elastic range of the stress strain curve for concrete, compressive strength is typically used as an indicator to characterize the class of concrete being used including its stiffness (modulus of elasticity). Because the compressive strength is used in the empirical equations used to calculate modulus, it has a marked influence on initial and pre-erection camber. Its higher influence on the pre-erection camber is explained by the fact that the compressive strength is a parameter in the creep model provided in the AASHTO LFRD Specifications (2020).

A $\pm 10\%$ change in the magnitude of the prestressing force at jacking resulted in a change in camber at release that varied from -20.7% to 20.7% . The average change in camber at release for a $\pm 10\%$ change in $P_{jacking}$ was 15.1% and -15.2% , respectively. A similar influence is observed for pre-erection camber. As can be seen, the influence of a change in the magnitude of the prestressing force, similar to that of a change in beam length, has a significant influence on the magnitude of calculated camber. The maximum influence of a change in the magnitude of the prestressing force is slightly higher than that of a change in beam length (20.7% versus 17.1%). However, the results presented in Chapter 4 indicate that precast fabricators have good control over the magnitude of the applied prestressing force, therefore, this parameter does not constitute a source of high uncertainty.

A $\pm 10\%$ change in the magnitude of the unit weight of concrete resulted in a change in camber at release that varied from -10.8% to 10.8% , suggesting this parameter also has a significant influence. The average change in camber at release for a $\pm 10\%$ change in w was -5.2% and 5.1% , respectively. A similar influence was observed for pre-erection camber. However, the results presented in Chapter 4 suggest that precast fabricators have good control over the supplied unit weight of concrete used for the prestressed concrete beams and that the measured unit weight matches well with the specified unit weight.

A +/- 10% change in the modulus of elasticity of beam concrete at release resulted in a change in camber at release that varied from -9.8% to 10.6%. The average change in camber at release for a +/-10% change in E_{ci} was -8.6% and 10.3%, respectively. A similar change was observed for pre-erection camber. This suggests that a certain percent change in the initial modulus results in a comparable change in camber at release. Although the influence of the modulus of elasticity of concrete does not appear to be as high as that of beam length or prestressing force, this parameter constitutes a high source of uncertainty compared to the other three parameters discussed above. This is due to the fact that the equation used to determine the modulus of elasticity was obtained using curve fitting techniques and the scatter in data is large. Naturally, the influence of the initial and 28 day modulus on beam camber and displacements was stronger than that of the initial beam concrete compressive strength. This is because the former has a direct influence on camber and displacements, whereas the latter only influences camber and displacements through the calculated modulus (which is a function of $\sqrt{f'_{ci}}$).

The influence of the support locations during beam storage in the precast facility on initial and pre-erection camber was investigated by varying the location of these supports by +/- 10%. A +/- 10% variation in support locations resulted in -1.4% to 0.8% change in camber at release and -1.0% to 0.9% change in pre-erection camber. The average change in camber at release for a +/- 10% change in $L_{overhang}$ was 0.4% and -0.6%, respectively. These results suggest that support location influences pre-erection camber to a degree that may be worth considering in the prediction methodology. As a result, the prediction framework provided as part of this report includes provisions for accounting for the support locations during storage.

A +/- 10% change in transfer length resulted in a +/-1.4% change in initial camber and +/- 0.9% change in pre-erection camber, suggesting that the influence transfer length may also be worth considering. The average change in camber at release for a +/-10% change in $L_{transfer}$ was -0.1% and 0.1%, respectively.

A similar observation was made for the influence of debonded length for beams that featured strands that were debonded from concrete for a certain length at the ends of the beams to control the magnitude of tensile stresses at the ends of the beam. A +/- 10% change in debonded length resulted in a +/-1.4% change in initial camber and a +/-1.8 change in and pre-erection camber, suggesting again that debonded length may be worth considering in the prediction

methodology. The average change in camber at release for a +/-10% change in $L_{debonded}$ was -0.4% and 0.3%, respectively.

A +/- 10% change in the location of the harping points resulted in -3.0% to 2.7% change in initial camber and -3.0% to 2.7% change in pre-erection camber suggesting that the location of the harping points has a marked influence on pre-erection camber and should be accounted for in the prediction methodology. The average change in camber at release for a +/-10% change in $L_{harping}$ was -1.9% and 1.7%, respectively.

The proposed prediction methodology (Iteration No. 6) accounts of support locations during storage, transfer length, debonded length, and location of harping point thus providing the user a tool with great flexibility and which accounts for a variety of scenarios and designs.

Table 5.1. Influence of various parameters on camber at release

Camber at Release Sensitivity Analysis			
Parameter varied	Lower bound % change for net camber	Upper bound % change for net camber	Average
Baseline (Iteration No. 6)	-	-	-
L +10 %	-4.8	17.1	8.6
L -10 %	-18.6	-4.1	-12.1
f'_{ci_beam} +10 %	-4.9	-4.0	-4.4
f'_{ci_beam} -10 %	4.3	5.6	5.0
$P_{jacking}$ +10 %	11.4	20.7	15.1
$P_{jacking}$ -10 %	-20.7	-12.2	-15.2
w +10 %	-10.8	-2.4	-5.2
w -10 %	1.4	10.8	5.1
E_{ci} +10 %	-9.8	-8.4	-8.6
E_{ci} -10 %	9.8	10.6	10.3
$L_{overhang}$ +10 %	0.0	0.8	0.4
$L_{overhang}$ -10 %	-1.4	-0.3	-0.6
$L_{transfer}$ +10 %	-1.4	0.0	-0.1
$L_{transfer}$ -10 %	0.0	1.4	0.1
$L_{debonded}$ +10 %	-1.4	0.0	-0.4
$L_{debonded}$ -10 %	0.0	1.4	0.3
$L_{harping}$ +10 %	-3.0	-0.8	-1.9
$L_{harping}$ -10 %	0.5	2.7	1.7

L = Beam length, f'_{ci_beam} = compressive strength of beam concrete at release, $P_{jacking}$ = prestressing force at jacking, w = unit weight, E_{ci} = modulus of elasticity at release, $L_{overhang}$ = beam overhang length, $L_{transfer}$ = transfer length, $L_{debonded}$ = debonded length, $L_{harping}$ = location of harping point measured from support location

Table 5.2. Influence of various parameters on pre-erection camber

Pre-erection Camber Sensitivity Analysis			
Parameter varied	Lower bound % change for net camber	Upper bound % change for net camber	Average
Baseline (Iteration No. 6)	-	-	-
L +10 %	-7.7	18.2	8.1
L -10 %	-17.3	-2.6	-11.5
f_{ci}^* +10 %	-6.9	-5.4	-5.8
f_{ci}^* -10 %	6.6	8.2	7.0
$P_{jacking}$ +10 %	12.7	21.8	15.4
$P_{jacking}$ -10 %	-22.0	-11.5	-15.3
w +10 %	-12.1	-1.8	-5.4
w -10 %	2.7	11.9	5.6
E_{ci} +10 %	-9.7	-7.7	-9.0
E_{ci} -10 %	10.7	11.8	11.0
$L_{overhang}$ +10 %	0.0	0.9	0.5
$L_{overhang}$ -10 %	-1.0	0.0	-0.5
$L_{transfer}$ +10 %	-0.9	0.0	-0.1
$L_{transfer}$ -10 %	0.0	0.9	0.1
$L_{debonded}$ +10 %	-1.8	0.0	-0.4
$L_{debonded}$ -10 %	0.0	1.8	0.4
$L_{harping}$ +10 %	-3.1	-0.6	-1.9
$L_{harping}$ -10 %	0.6	2.7	1.7

L = Beam length, $f_{ci_beam}^*$ = compressive strength of beam concrete at release, $P_{jacking}$ = prestressing force at jacking, w = unit weight, E_{ci} = modulus of elasticity at release, $L_{overhang}$ = beam overhang length, $L_{transfer}$ = transfer length, $L_{debonded}$ = debonded length, $L_{harping}$ = location of harping point measured from support location

5.2.1 Influence of Creep and Shrinkage Model on Pre-erection Camber

The influence of the selected creep and shrinkage model for beam concrete on pre-erection camber was investigated by computing pre-erection camber for the first 28 days for the prestressed concrete beams used in the S-11 project. The results are shown in Fig. 5.1. Predictions based on Bazant-Baweja B3 model and GL 2000 model were significantly higher than measured pre-erection camber values as well as predictions based on other models and are therefore not included in Fig. 5.1. Fig. 5.1 suggests that the selection of the creep and shrinkage model for beam concrete has a marked influence on the prediction of pre-erection camber development. The proposed prediction methodology (Iteration No. 6) provides the user the ability to choose one out of eight models. Since most predictions presented in this report were based on the AASHTO LRFD (2020) creep and shrinkage models provided in the body of AASHTO (2020), and since these predictions

matched well with measured pre-erection camber, it is recommended that these models be used as a starting point. Other models may be used to quantify the expected range of camber predictions.

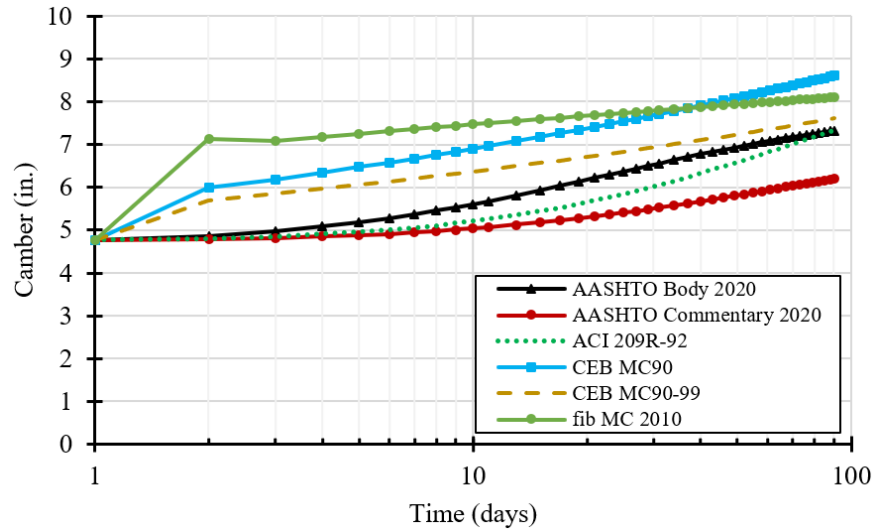


Fig. 5.1. Variation of pre-erection camber for S-11 project using different creep and shrinkage models

5.2.2 Influence of Model to Predict Modulus of Elasticity at Prestress Release and 28 Days

The influence of the model to predict modulus of elasticity at prestress release and 28 days on pre-erection camber was evaluated by running the proposed prediction methodology four times for the S-11 project; one time with the benchmark model (AASHTO LRFD (2020)) and three other times using ACI 318-19 model, ACI 363R-92 model, and fib MC 2010 model, respectively. When using the AASHTO LRFD (2020) model the aggregate factor, K_I , was taken equal to 1.0 and concrete unit weight, w_c , was calculated using the compressive strength dependent formula. Additionally, the ACI 209R-92 model was selected to capture the variation of modulus with time, no overstrength factors were used, and the AASHTO LRFD (2020) models for creep and shrinkage were used as part of the benchmark model. When using the fib MC 2010 model the aggregate type was assumed to be quartzite. The number of beam sections along half the span was selected as 51, and the proposed time step generation method was used. Fig. 5.2a show a comparison of predicted moduli of elasticity at prestress release and 28 days using each model and Fig. 5.2b shows the difference in pre-erection camber magnitude when each model is considered. Fig. 5.2b suggests that the selection of the model for modulus of elasticity at prestress release and 28 days has a

noteworthy influence on pre-erection camber with the ACI 363R-92 model resulting in differences up to 14% and ACI 318-19 resulting in differences up to 6%. Since the benchmark model used in the evaluations presented in this report resulted in reasonable predictions of pre-erection camber when compared to measured values, it is recommended that the AASHTO LRFD (2020) model is used. Investigation of other models may be used to determine the limits of variability for pre-erection camber.

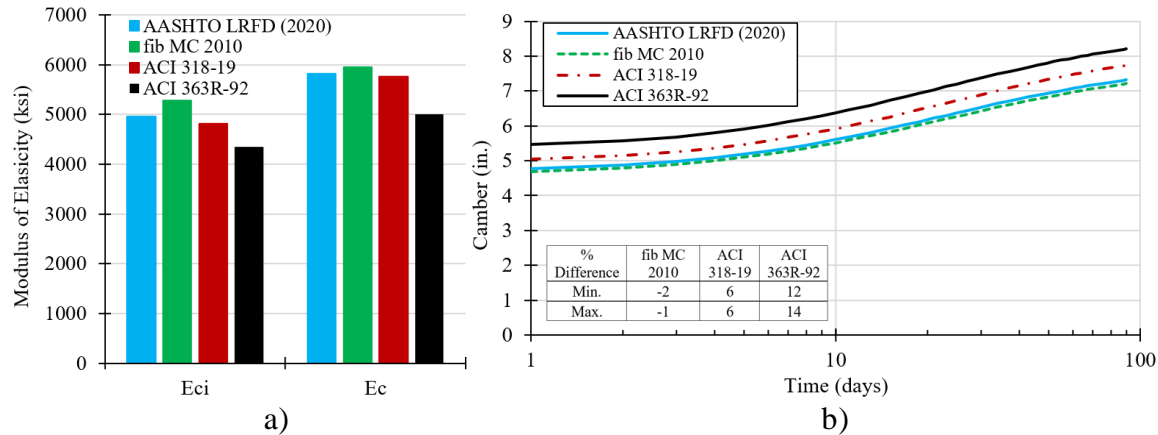


Fig. 5.2. a) Comparison of calculated modulus of elasticity at prestress release and 28 days; b) influence of model to predict modulus of elasticity at prestress release and 28 days on camber for S-11 project

5.2.3 Influence of the Model for Capturing the Variation of Modulus with Time

The influence of the model to capture the variation of modulus with time was selected by running the algorithm twice; once based on the benchmark model (i.e. ACI 209R-92), and another time using the fib MC 2010 model. When using the benchmark model, the AASHTO LRFD (2020) model for creep and shrinkage as well as prediction of modulus at prestress release and 28 days were used. The number of beam sections along half the span was selected as 51 and the proposed time step generation method was used. Fig. 5.3a shows the prediction of modulus as a function of time and suggests that there are some minor differences between the two models. Fig. 5.3b shows that camber predictions based on both models are almost identical, therefore the selection of one model or the other is inconsequential. The % difference in pre-erection camber predictions is less than 0.1%.

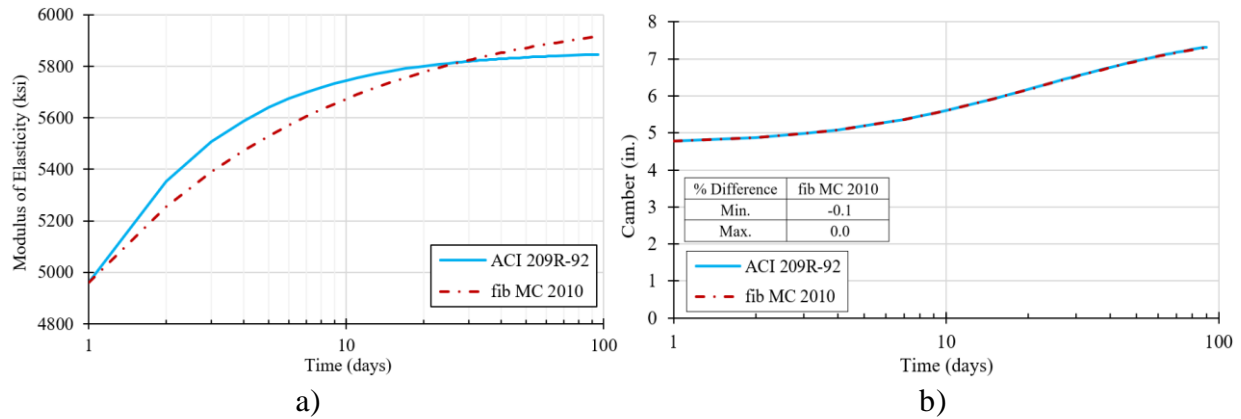


Fig. 5.3. a) Comparison of functions for predicting the development of modulus of elasticity with respect to time, b) influence of considered time dependent modulus functions on camber for S-11 project

5.2.4 Influence of Overstrength Factors

The influence of overstrength factors for beam concrete compressive strength at prestress release and 28 days was investigated by running the algorithm once without overstrength factors and another time with Michigan based overstrength factors. It should be noted that the use of overstrength factors for f_{ci} affects the calculation of modulus at prestress release, E_{ci} , which affects the calculation of pre-erection camber. Additionally, the use of overstrength factors affect both f_a and f'_c , which in turn affect moduli of elasticity at prestress release and 28 days. These moduli of elasticity at these two times serve as anchor points for the model that predicts the development of modulus with time. The benchmark model was based on no overstrength factors, AASHTO LRFD (2020) model for modulus at release and 28 days as well as creep and shrinkage, and the ACI 209R-92 model for capturing the variation of modulus with time. The only change in the second analysis was the inclusion of the overstrength factors for f_{ci} and f'_c . The number of beam sections along half the span was selected as 51 and the proposed time step generation method was used. The results are shown in Fig. 5.4. The inclusion of overstrength factors does have a noteworthy effect on pre-erection camber predictions with differences between the two models being up to 10%. As expected, the inclusion of overstrength factors results in lower camber predictions.

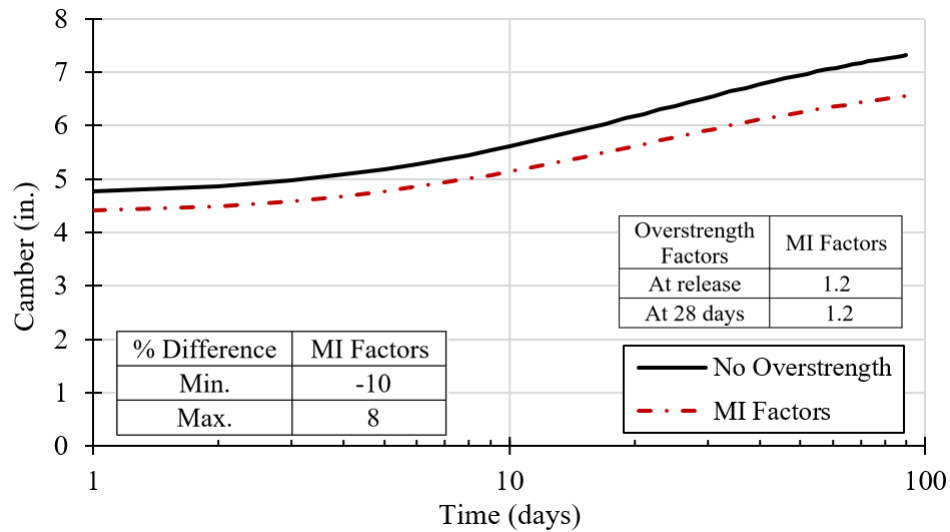


Fig. 5.4. Influence of inclusion of overstrength factors for S-11 project

5.2.5 Influence of Time when Camber at Release is Measured

When camber at release is calculated, time dependent effects are typically ignored because by definition the term camber at release means the camber induced in the prestressed concrete beam immediately after the detensioning of the strands. According to MDOT's Special Provision for Structure Survey during Construction, for projects with new prestressed concrete beam superstructures, the release date of the prestressing force and the observed camber at midspan for each beam should be provided to the engineer no more than seven calendar days after releasing the prestressing force. The effect of time on camber at release was investigated by predicting camber for up to 10 days after the release of the prestressing force for four projects: M-5, M-89, Tiffin Street Overpass, and S-11. This investigation was conducted by using the benchmark model set described in Chapter 3. The results are shown in Fig. 5.5. Detensioning time was assumed to be one day after placement of concrete. The change in percentage between the predicted initial camber at one day and 10 days varies from 17% to 26% introducing yet another source of uncertainty when comparing predicted and measured camber at release values. This is not an issue when the proposed prediction methodology is used because it offers the ability to predict camber at any time, however, traditional techniques such as classical equations for prediction camber at release and the multiplier method for predicting long term camber cannot capture these nuances in camber variation. In any case, this topic was investigated to quantify the variation in camber during the first seven days so that the engineer can have a sense for the degree of this variation.

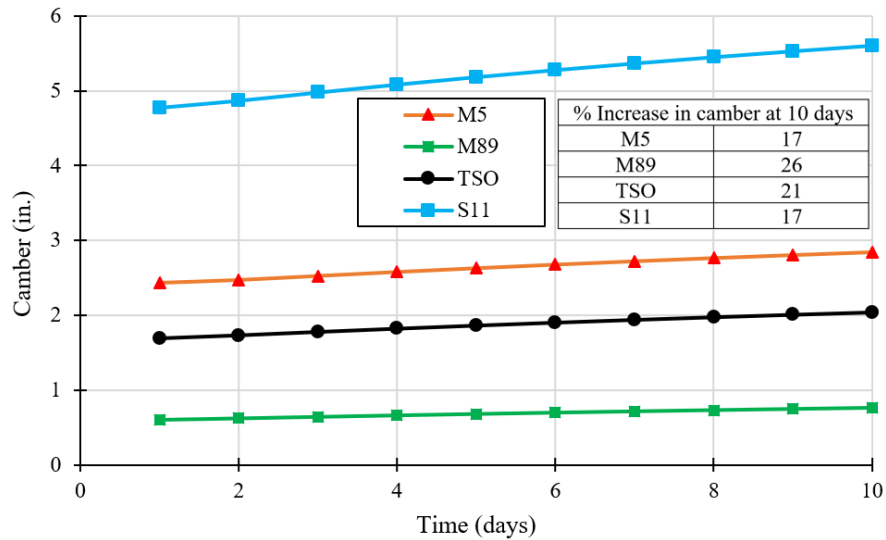


Fig. 5.5. Variation of predicted camber during the first 10 days after beam fabrication

5.2.6 Slab and Screed Guidance

The proposed methodology provides camber data at various points along the span of the beam so that this information can be used to plot the full camber profile for the beam. The cambered beam profile can then be used to determine slab and screed elevations in accordance with MDOT Slab and Screed Guidance document. The proposed methodology may be cited as the tool to obtain beam deflection at various stages. Currently, in the MDOT Slab and Screed Guidance document the following stages of deflection are referenced: 1) Deflection of the beam due to self-weight (pre-erection camber), 2) Deflection of the beam due to the weight of forms and rebar, 3) Deflection of the beam due to the weight of deck concrete, and 4) Deflection of the beam due to the weight of sidewalk or barrier. The proposed methodology provides beam camber data for each stage. This data can be downloaded so that beam profiles for each stage can be plotted and slab and screed elevations can be set accordingly. An example is provided in Fig. 5.6, which shows the deflected shape of the beam at various stages. In this example, the following loads were used: 10 psf for formwork, 10 psf for reinforcement, 145 pcf for plain concrete, and 150 pcf for reinforced concrete. This is consistent with Michigan Design Manual Bridge Design - Chapter 7: LRFD Section 7.02.22.

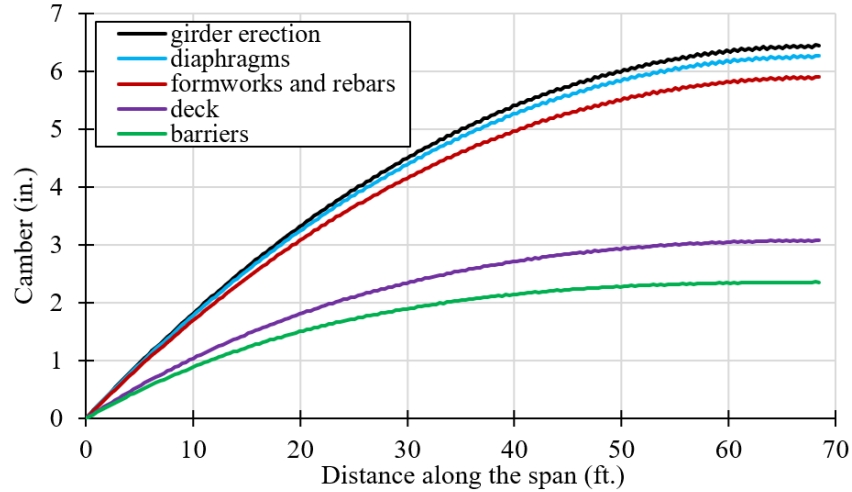


Fig. 5.6. Illustration of various stages of deflection during beam erection and deck placement for the S-11 project

5.3 Summary and Conclusions

While it is determined that the unit weight of concrete, w , the magnitude of the prestressing force at jacking, $P_{jacking}$, and beam length, L , all have a significant influence on pre-erection beam camber, it is determined that these parameters do not vary significantly from specified values and therefore do not represent a significant source of uncertainty. Modulus of elasticity at release, E_{ci} , had a proportional influence on pre-erection beam camber. Similarly, beam compressive strength at release, f'_{ci} , also had a close to proportional influence on pre-erection camber, although this influence was quantified through the use of compressive strength dependent equation for modulus of elasticity. Transfer length, $L_{transfer}$, debonded length, $L_{debonded}$, support conditions during storage, $L_{overhang}$, and location of harping point, $L_{harping}$, influence pre-erection camber at a degree that in some cases is worth considering. The selection of the creep and shrinkage model has a marked influence on the prediction of pre-erection camber development. The time when initial camber is measured appears to be an important parameter since marked differences were found between predicted camber at release and predicted camber during the first 10 days. The influence of the model for calculating modulus at prestress release and 28 days has a marked effect on pre-erection camber predictions, whereas the model to predict the variation of modulus with time had negligible effect. The inclusion of overstrength factors also had a marked effect on pre-erection camber predictions. The default set of models used in most predictions presented in this report is shown in Fig. 3.9. This selection resulted in reasonable predictions of pre-erection camber as will be

demonstrated later and is therefore recommended for design. The other models may be investigated to quantify the variability of pre-erection camber predictions. The proposed prediction methodology (Iteration No. 6) provides the user the flexibility of accounting for the influence of all the abovementioned factors. In addition, the proposed prediction methodology provides the necessary beam camber data such that the profile of the beam can be plotted for various stages of deflection and slab and screed elevations can be determined accordingly.

Chapter 6: Evaluate Factors that Affect Camber and Displacements in the Composite System

Chapter 6: Evaluate Factors that Affect Camber and Displacements in the Composite System

6.1 Introduction

Various factors affect displacements in a composite bridge superstructure that features prestressed concrete or steel beams and a cast in place concrete deck. Beam creep as a result of the prestressing force (for PC beams), and positive temperature gradients cause negative curvature (i.e. upward deflection). Conversely, the self-weight of deck and beam and associated creep, differential shrinkage between the deck and beam, and negative temperature gradients cause positive curvature (i.e. downward deflection). Even for PC beams, differential shrinkage between the deck and beam occurs since the majority of the shrinkage in the beam has already taken place when the deck is cast, while the shrinkage of deck begins after the moist curing of the deck ends. A similar effect applies to composite steel beams with the exception that differential shrinkage in this case is more pronounced since steel beams do not shrink.

When PC beams are considered, differential shrinkage and creep between the deck and beam strongly depend on the age of the beam at deck placement. This age is perhaps the most critical and influential factor in determining beam deflections in the composite bridge superstructure. The type of bridge superstructure also affects the magnitude of beam deflections in the composite system and must be considered. For example, beam deflections in a two span continuous bridge differ from those in a simply supported bridge. When composite steel beams are considered, the deflection components involving the prestressing effect, beam creep and beam shrinkage can be ignored, and the same methodology can be used to compute deflections at any point in time while accounting for deck shrinkage and creep. The prediction methodology presented in this report allows the calculation of deflections at any point in time and the inclusion of appropriate shrinkage and creep coefficients for each component.

6.2 Sensitivity Analysis

Overview: The influence of various factors that affect camber and displacements in the composite system was evaluated using Iteration No. 6 of the proposed prediction methodology. The influence of some factors was expressed in % change in net camber as a function of a given % change in the factor under consideration. This influence was expressed in terms of the average, minimum, and maximum change for all projects considered. The considered final service time for this evaluation

was 75 years. The results of this analysis are shown in Table 6.1. It should be noted that minimum and maximum changes were sometimes driven by the net camber for the baseline case. For example, if the net camber for the baseline is close to zero, even a small change in camber or displacement would result in a high % change and can therefore be misleading. The provision of the average change addresses this to a certain degree. The induced change was +/-10%. Factors that led to a single digit average % change in net camber and displacement due to the induced 10% change include: beam overhang length at precast facility (i.e. storage conditions), transfer length, debonded length, deck modulus, and beam overhang length at the bridge site. Factors that led to a double digit average % change in net camber and displacement due to the induced 10% change include: beam concrete compressive strength at release and 28 days, beam concrete unit weight, beam concrete modulus of elasticity at release and 28 days, location of harping point, beam spacing, compressive strength of deck at 28 days, and unit weight of deck. Factors that led to a triple digit average % change in net camber and displacement due to the induced 10% change include: beam length, and prestressing force.

Additional Information: The parameter with the strongest influence was beam length. For example, a +/-10 % change in beam length resulted in a change in camber and displacements that varied from -3155.6% to 1866.7%, suggesting that long-term camber and displacements are very sensitive to beam length. The average change in net camber or displacement at service at 75 years for a +/-10% change in beam length was -199% and 110%, respectively. The beams used in project M-5 dominated the lower bound for this analysis. The net predicted camber at 75 years for these beams is 0.06 in. (i.e. nearly zero). Therefore, a 1 in. change in net camber due to a change in beam length or other factors causes a $(1-0.06)/0.06 \times 100 = 1566\%$ in net camber. Therefore, when the net camber value that serves as the baseline for comparison is small, any deviation from that value results in a large % change.

A +/-10 % in the initial compressive strength led to a change in camber and displacements that varied from -455.6% to 566.7%. Although, the average change in net camber or displacement at service at 75 years for a +/-10% change in f'_{ci} was -47.1% and 57.9%, respectively.

Similarly, a +/-10 % change in the 28 days design compressive strength led to a change in camber and displacement that varied from -655.6% to 566.7%. Although, the average change in

net camber or displacement at service at 75 years for a $\pm 10\%$ change in f'_c was -23.3% and 18.4% , respectively.

The magnitude of the prestressing force also had a strong influence on long-term camber and displacements at service. For example, a $\pm 10\%$ change in P_{jacking} led to -1411% to 1400% change in camber and displacements at service. Although, the average change in net camber or displacement at service at 75 years for a $\pm 10\%$ change in P_{jacking} was 118.1% and -119% , respectively.

Beam concrete unit weight also had a strong influence on camber and displacements at service featuring a variation $\pm 778\%$ due to a $\pm 10\%$ change in unit weight. The average change in net camber or displacement at service at 75 years for a $\pm 10\%$ change in w was $\pm 56.9\%$.

The influence of the initial modulus of elasticity of beam concrete on camber and displacements at service was also significant but not as strong as that of the aforementioned parameters with the exception of concrete compressive strength. A $\pm 10\%$ change in E_{ci} led to a change in camber and displacements at service that varied from -667% to 811% . The average change in net camber or displacement at service at 75 years for a $\pm 10\%$ change in E_{ci} was $+62.6\%$ and -76.5% , respectively.

Beam concrete modulus at 28 days also had a strong influence but not as strong as that of the initial modulus. A $\pm 10\%$ change in E_c led to a change in camber and displacements at service that varied from -656% to 566.7% . The average change in net camber or displacement at service at 75 years for a $\pm 10\%$ change in E_c was 45.8% and -53.2% , respectively.

Beam overhang length during storage at the precast facility as well as beam overhang past the bearing points at the bridge site had a lower influence than that of all parameters considered so far. A $\pm 10\%$ change in the beam overhang length led to a $\pm 22\%$ change in beam camber and displacements at service.

The influence of transfer length and strand debonded length on beam camber and displacements at service was also lower than that of all aforementioned parameters, with a $\pm 10\%$ change in transfer length and strand debonded length leading to a $\pm 3-7\%$ change in beam camber and displacements at service.

A $\pm 10\%$ change in the location of harping points led to -178% to 156% change in beam camber and displacements at service.

Finally, a $\pm 10\%$ change in beam spacing led to -333% to 356% change in beam camber and displacements at service concluding the sensitivity analysis conducted for concrete beam related parameters on beam camber and displacements. The sensitivity analysis continued by investigating the influence of several deck related parameters on beam camber and displacements at service.

A $\pm 10\%$ change in the 28 day deck concrete compressive strength led to -167% to 156% change in beam camber and displacements at service. Naturally, the influence of deck concrete compressive strength on beam camber and displacements is not as strong as that of the beam concrete compressive strength since the beam comprises the majority of the composite section.

Similarly, a $\pm 10\%$ change in the 28 day deck concrete modulus led to a $\pm 33\%$ change in beam camber and displacements at service. The influence of deck concrete modulus on beam camber and displacements is also not as strong as that of the beam concrete modulus since the beam comprises the majority of the composite section.

Table 6.1. Influence of various parameters on camber and displacements at service

Parameter varied	Service Camber Sensitivity Analysis		
	% Change in net camber/displacement		
	Min.	Max.	Average
Baseline (Iteration No. 6)	-	-	-
$L +10\%$	-3155.6	141.1	-198.7
$L -10\%$	-257.6	1866.7	109.7
$f'_{ci_beam} +10\%$	-455.6	-14.5	-47.1
$f'_{ci_beam} -10\%$	17.8	566.7	57.9
$f'_{c_beam} +10\%$	3.4	288.9	23.3
$f'_{c_beam} -10\%$	-38.3	522.2	18.4
$P_{jacking} +10\%$	21.7	1400.0	118.1
$P_{jacking} -10\%$	-1411.1	-21.7	-119.0
$w_{beam} +10\%$	-777.8	-2.9	-56.9
$w_{beam} -10\%$	4.3	777.8	56.9
$E_{ci_beam} +10\%$	-666.7	-15.9	-62.6
$E_{ci_beam} -10\%$	19.7	811.1	76.5
$E_{c_beam} +10\%$	6.8	566.7	45.8
$E_{c_beam} -10\%$	-655.6	-5.8	-53.2
$L_{overhang} +10\%$	0.0	22.2	1.7
$L_{overhang} -10\%$	-22.2	0.0	-1.6
$L_{transfer} +10\%$	-1.4	0.0	-0.3
$L_{transfer} -10\%$	0.0	2.9	0.3
$L_{debonded} +10\%$	-7.1	0.0	-1.3
$L_{debonded} -10\%$	0.0	7.1	1.4
$L_{harping} +10\%$	-177.8	-2.3	-22.7
$L_{harping} -10\%$	2.0	155.6	19.9
$S +10\%$	-333.3	-4.3	-30.0
$S -10\%$	5.8	355.6	32.3
$f'_{c_deck} +10\%$	2.8	155.6	14.9
$f'_{c_deck} -10\%$	-166.7	-1.9	-16.0
$w_{deck} +10\%$	-233.3	-2.9	-27.5
$w_{deck} -10\%$	-100.0	233.3	17.2
$E_{deck} +10\%$	0.0	33.3	4.2
$E_{deck} -10\%$	-33.3	0.0	-4.0
$L_{overhang_bridge} +10\%$	0.0	11.1	1.5
$L_{overhang_bridge} -10\%$	-11.1	3.2	-1.0

L = Beam length, f'_{ci_beam} = compressive strength of beam concrete at release, f'_{c_beam} = 28 day beam concrete compressive strength, $P_{jacking}$ = prestressing force at jacking, w_{beam} = beam concrete unit weight, E_{ci_beam} = modulus of elasticity at release, E_{c_beam} = 28 day modulus of elasticity of beam concrete, $L_{overhang}$ = beam overhang length, $L_{transfer}$ = transfer length, $L_{debonded}$ = debonded length, $L_{harping}$ = location of harping point measured from support location, S = beam spacing, f'_{c_deck} = 28 day deck concrete compressive strength, w_{deck} = Deck concrete unit weight, E_{deck} = Deck Modulus of Elasticity, $L_{overhang_bridge}$ = Beam overhang length at bridge

6.2.1 Influence of Creep and Shrinkage Model on Service Camber

The influence of creep and shrinkage models for beam and deck concrete on camber and displacements at service was investigated by predicting the full displacement history for the prestressed concrete girders used in the S-11 project from the time they were fabricated to the assumed end of service life for this bridge (75 years). This comparison is shown in Fig. 6.1a. Predictions based on Bazant and Baweja B3 model and those based on GL 2000 model provided much higher estimates of pre-erection camber than measured values and were therefore removed from this comparison. Fig. 6.1a suggests that the selection of creep and shrinkage models has a marked influence on the full displacement history of the prestressed concrete beams. It is worth noting how the AASHTO LRFD (2020) model based on specifications provided in the body of AASHTO (2020) and fib MC 2010 model predict an increase in downward displacements after placement of deck whereas the rest of the models, including the one based on specifications provided in the commentary of AASHTO (2020) predict an increase in camber. Similarly, the predicted camber after 75 years is generally similar between the fib MC 2010 model, AASHTO (2020) commentary and CEB MC90-99 model. Although, this value is much different than that predicted by the AASHTO (2020) body model. The CEB MC90 and ACI 209R-92 models also provide similar predictions of camber after 75 years, although different from the rest of the models. Finally, all models show that there is generally some stability in net camber after one year.

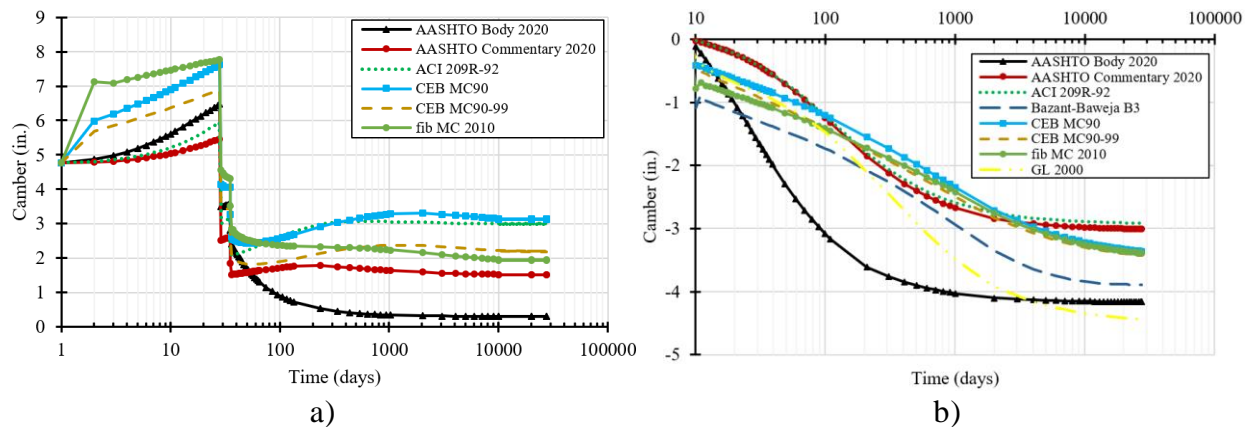


Fig. 6.1. Influence of creep and shrinkage problems on the full displacement history of: a) prestressed concrete beams used in the S-11 project, and b) steel beams used in the M-20 project

A similar comparison was conducted for the steel beams used in the M-20 project (Fig. 6.1b). In this comparison it was assumed that the net camber after the placement of deck and superimposed dead loads was zero. This was done due to the fact that there was some ambiguity as to what the pre-erection camber in the steel beams was and whether this pre-erection camber included the effects of beam self-weight. Therefore, the displacement history starts after the placements of superimposed dead loads (barrier+overlay) (i.e. after the opening of the bridge to service). Predictions based on Bazant and Baweja B3 model and those based on GL 2000 model are included in this comparison. As can be seen, the selection of creep and shrinkage model influences the entire displacement history leading to different predictions. The cause of these differences is primarily due to differences in the predicted shrinkage in the deck, which leads to differential shrinkage between the concrete deck and the steel beam. Differential shrinkage induced creep is a second reason for the differences in predicted displacements, although its influence is not as strong as that of deck shrinkage.

6.2.2 Influence of Model to Predict Modulus of Elasticity at Prestress Release and 28 Days

The influence of the model to predict modulus of elasticity at prestress release and 28 days on camber history was evaluated by running the proposed prediction methodology four times for the S-11 project; one time with the benchmark model (AASHTO LRFD (2020)) and three other times using the ACI 318-19 model, ACI 363R-92 model, and fib MC 2010 model, respectively. When using the AASHTO LRFD (2020) model the aggregate factor, K_I , was taken equal to 1.0 and concrete unit weight, w_c , was calculated using the compressive strength dependent function. Additionally, the ACI 209R-92 model was selected to capture the variation of modulus with time, no overstrength factors were used, and the AASHTO LRFD (2020) models for creep and shrinkage were used as part of the benchmark model. When using the fib MC 2010 model the aggregate type was assumed to be quartzite. The number of beam sections along half the span was selected as 51 and the proposed time step generation method was used. Fig. 6.2a shows the comparison between moduli of elasticity at prestress release and 28 days using various models. Fig. 6.2b shows the difference in camber magnitude when each model is considered. Fig. 6.2b suggest that the selection of the model for modulus of elasticity at prestress release and 28 days has a noteworthy influence on camber history with the ACI 318-19 model resulting in differences up to 148% and ACI 363R-92 resulting in differences up to 74%.

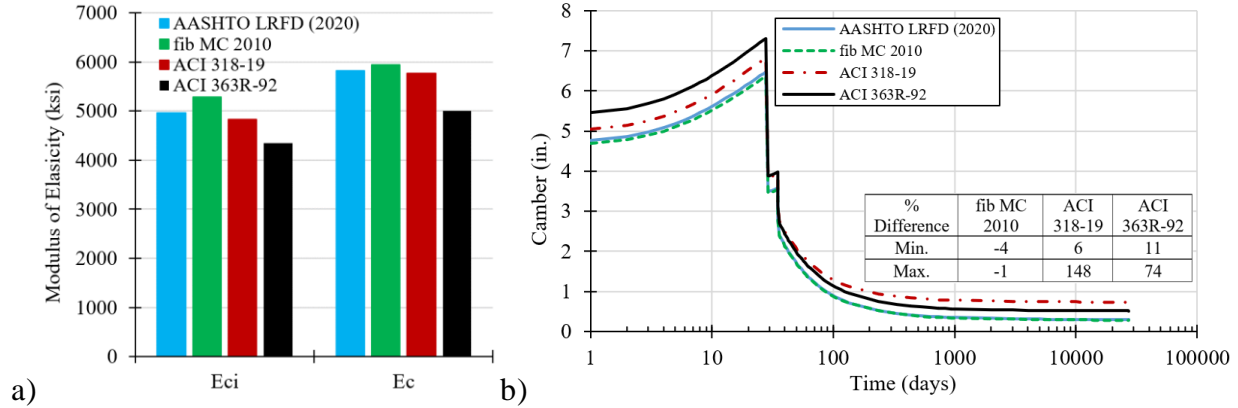


Fig. 6.2. a) Comparison of calculated modulus of elasticity at prestress release and 28 days based on different models; b) influence of model to predict modulus of elasticity at prestress release and 28 Days on camber history for S-11 project.

6.2.3 Influence of the Model for Capturing the Variation of Modulus with Time

The influence of the model to capture the variation of modulus with time on camber history was investigated by running the algorithm twice; once based on the benchmark model (i.e. ACI 209R-92), and another time using the fib MC 2010 model. When using the benchmark model, the AASHTO LRFD (2020) model for creep and shrinkage as well as prediction of modulus at prestress release and 28 days were used. The number of beam sections along half the span was selected as 51 and the proposed time step generation method was used. The results are shown in Fig. 6.3, which shows that predictions based on both models are almost identical, therefore the selection of one model or the other is inconsequential. The % difference in camber history predictions is less than 0.5%.

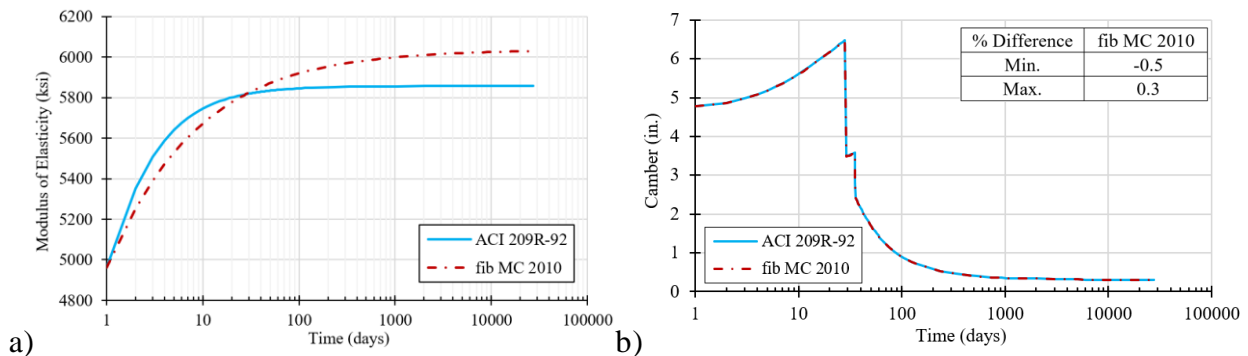


Fig. 6.3. a) Comparison of predictions for development of modulus of elasticity with respect to time based on different models; b) influence of time dependent modulus model on camber for S-11 project.

6.2.4 Influence of Overstrength Factors

The influence of overstrength factors for beam concrete compressive strength at prestress release and 28 days was investigated by running the algorithm once without overstrength factors and another time with Michigan based overstrength factors. It should be noted that the use of overstrength factors for f_{ci} affects the calculation of modulus at prestress release, E_{ci} , which affects the calculation camber history. Additionally, the use of overstrength factors affects both f_{ci} and f'_{cs} , which in turn affect moduli of elasticity at prestress release and 28 days. These moduli of elasticity at these two times serve as anchor points for the model that predicts the development of modulus with time. The benchmark model was based on no overstrength factors, AASHTO LRFD (2020) model for modulus at release and 28 days as well as creep and shrinkage, and the ACI 209R-92 model for capturing the variation of modulus with time. The only change in the second analysis was the inclusion of the overstrength factors for f_{ci} and f'_{cs} . The number of beam sections along half the span was selected as 51 and the proposed time step generation method was used. The results are shown in Fig. 6.4. The inclusion of overstrength factors does have a marked effect on camber history predictions with differences between the two models being up to 160%. As expected, the inclusion of overstrength factors results in lower camber predictions.

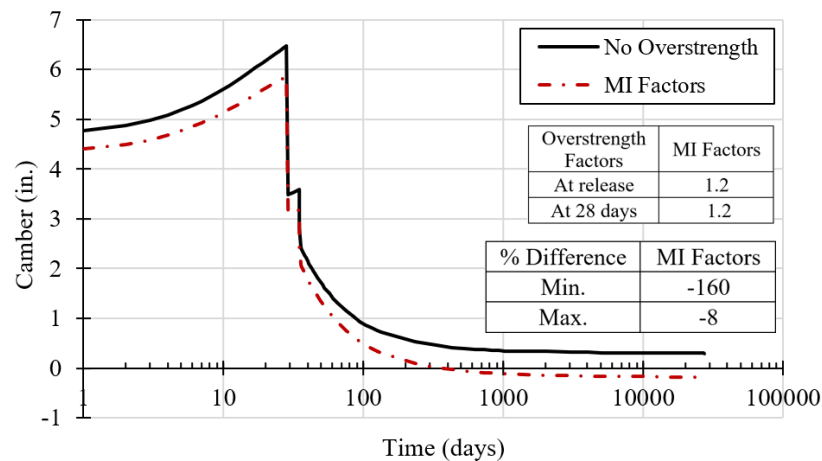


Fig. 6.4. Influence of inclusion of overstrength factors for S-11 project

6.2.5 Influence of the Time when the Deck is Placed

The influence of the time when the deck is placed on beam camber and displacements was investigated by varying the time when the deck was placed from 20 days to 55 days and to 90 days. This exercise was conducted for two projects, S10-2, and S11. Fig. 6.5 shows the full displacement

history for the three considered deck placement times. As can be seen, the longer the time when the deck is placed the higher the pre-erection camber. While this is intuitive, interestingly, a delay in the time when the deck is placed causes the final camber to be lower. This seemingly counterintuitive finding is due to the fact that differential shrinkage between the deck and the girder dominates the prestressing force induced camber growth at a greater extent when the placement of the deck is delayed. It is also interesting to note how camber and displacements after 75 years appear to be rather similar regardless of when the deck is placed.

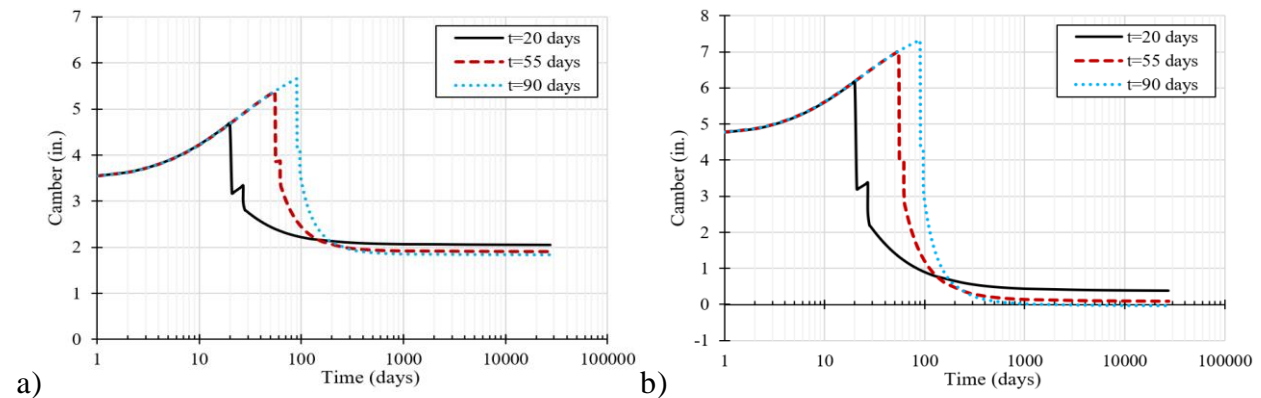


Fig. 6.5. Influence of the time when the deck is placed on beam camber and displacements at service for: a) S10-2 project; b) S11 project

6.2.6 Influence of the Temperature Gradient

The influence of temperature gradients on beam camber and displacements was investigated by considering the S10-2, S11, and M20 projects and by using Iteration No. 6 of the proposed prediction methodology. Camber and displacements were first calculated at various points in time by ignoring the influence of temperature gradients to establish a baseline, and then were recalculated by considering both positive and negative temperature gradients based on solar radiation zone 3 described in AASHTO LRFD Bridge Design Specifications (2020). The results of this analysis are shown in Fig. 6.6. The evolution of camber in both S10-2 and S11 projects is characterized by the traditional growth between the detensioning of the strands and the placement of the deck, followed by a sudden decrease in camber due to the placement of the deck, and a further decrease due to time dependent effects. The influence of both negative and positive temperature gradients is rather consistent throughout the life of the beams with the positive temperature gradients having a stronger influence on camber and displacements. Therefore, if construction activities are conducted during the summer months, the contractor should be mindful

of the impact that temperature gradients can have on pre-erection camber and orchestrate activities accordingly. Fig. 6.6c suggests that the influence of temperature gradients on the M20 project, which features steel beams was similar to that observed in the prestressed concrete beam projects (S10-2 and S11). The camber and displacement history for the steel beams in the M-20 project start at deck placement since it is assumed that the beams come with a certain fabricated pre-erection camber. For S10-2, S-11, and M-20 projects, the absolute maximum % difference values in camber caused by positive temperature gradients are 20% , 217% , and 600% and those caused by negative temperature gradients are 6% , 65% , and 180% respectively.

The influence of temperature gradient appears to be large in terms of % change with the baseline value. However, this is because in some cases the deflection of the beams is either small or switches from an upward displacement (camber) to a downward displacement. This results in the baseline value used for comparison to be small and yields large % differences in camber predictions when in fact the difference in camber or displacement magnitudes is smaller. The proposed prediction methodology has the ability to quantify camber and displacements due to temperature gradients and this information can be used to plan for certain construction operations such as the placement of the deck.

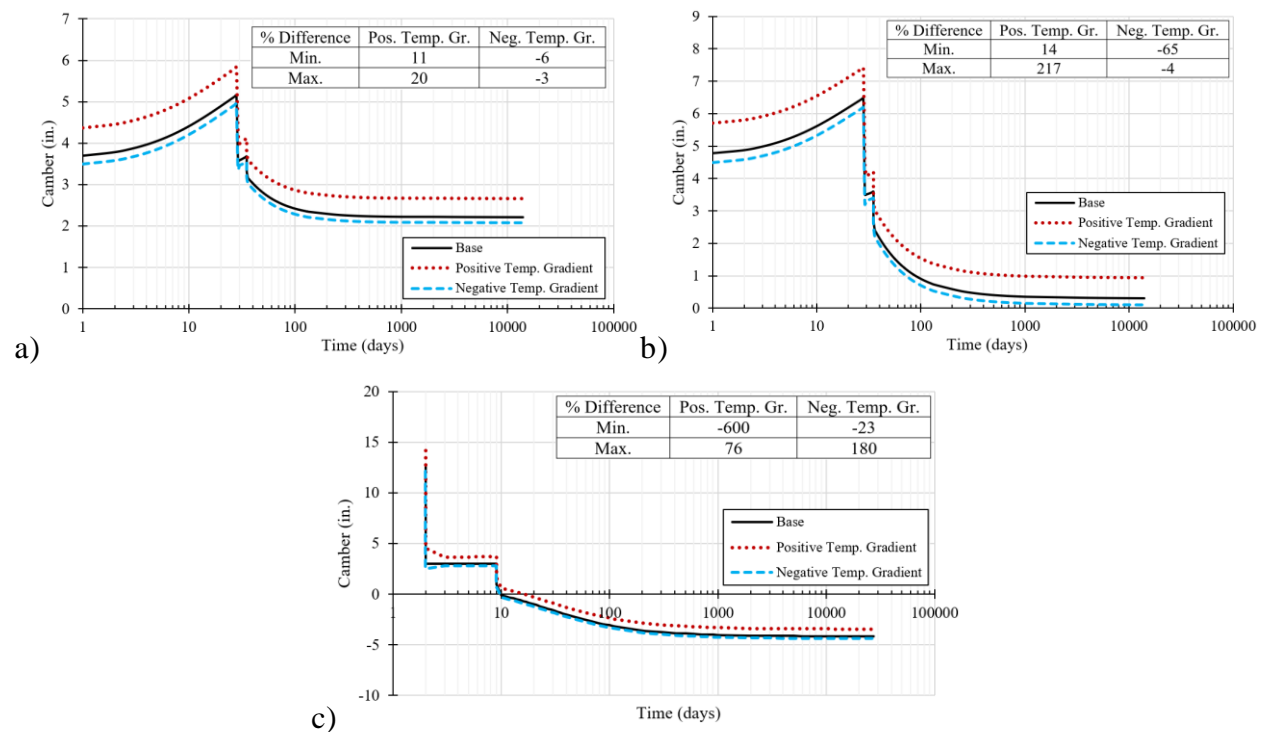


Fig. 6.6. Influence of temperature gradients on beam camber and displacements at service:
a) S10-2 project; b) S11 project, c) M20 project

6.3 Summary and Conclusions

The influence of various factors that affect camber and displacements in the composite system was evaluated using Iteration No. 6 of the proposed prediction methodology. The influence of some factors was expressed in % change in net camber as a function of a given % change in the factor under consideration. This influence was expressed in terms of the average, minimum, and maximum change for all projects considered. It should be noted that minimum and maximum changes were sometimes driven by the net camber for the baseline case. For example, if the net camber for the baseline is close to zero, even a small change in camber or displacement would result in a high % change and can therefore be misleading. The provision of the average change addresses this to a certain degree. The induced change was $\pm 10\%$.

Factors that led to a single digit average % change in net camber and displacement due to the induced 10% change include: beam overhang length at precast facility (i.e. storage conditions), transfer length, debonded length, deck modulus, and beam overhang length at the bridge site.

Factors that led to a double-digit average % change in net camber and displacement due to the induced 10% change include: beam concrete compressive strength at release and 28 days, beam concrete unit weight, beam concrete modulus of elasticity at release and 28 days, location of harping point, beam spacing, compressive strength of deck at 28 days, and unit weight of deck.

Factors that led to a triple digit average % change in net camber and displacement due to the induced 10% change include: beam length, and prestressing force.

The influence of the selected creep and shrinkage model on the full displacement history of a prestressed concrete beam bridge was investigated and it was concluded that this selection has a marked influence on the beam displacement history. Some models result in rather similar displacements after 75 years despite initial differences in pre-erection camber and net displacements after deck placement.

The selection of the model to predict modulus of elasticity at prestress release and 28 days had a marked effect on camber history with differences from the baseline being as high as 148%. The influence of the model to predict the variation of modulus with time was inconsequential.

The inclusion of overstrength factors also had a marked effect on camber history with differences with the case when they are not included being as high as 160%.

Influence of deck placement time on the full beam displacement history was investigated and it was concluded that while pre-erection camber is highly influenced by it, camber and

displacements after 75 years were rather similar. The influence of temperature gradients was rather uniform throughout the displacement history of the beam with positive temperature gradients having a higher influence on camber and displacements compared to negative temperature gradients.

Chapter 7: Evaluate Factors that Affect Beam Rebound and Behavior after Deck Replacement

Chapter 7: Evaluate Factors that Affect Beam Rebound and Behavior after Deck Replacement

7.1 Introduction

Intuitively, factors affecting existing steel and concrete beam rebound, net camber after deck removal, and net camber before new deck placement include: the weight of the existing deck; the age of beam concrete when the deck is removed; the time between the removal of exiting deck and the placement of the new deck; conditions of the beam and deck concrete at the time of deck removal, including any changes in geometry or material properties such as those caused by deterioration; and the type of structure (simply supported or continuous).

The proposed prediction methodology provides the means to estimate beam rebound, net camber after deck removal, and net camber before new deck placement for simply supported bridges that feature prestressed concrete and steel beams. The estimation was done using Iteration No. 5 and No. 6 to see the difference in results. In the majority of the analysis conducted it was assumed that the old deck would be replaced after 50 years and that the time between the old deck removal and new deck placement is 10 days, although the user can enter different values to investigate various scenarios. The influence of deck replacement time was investigated by varying it from 40 years to 60 years in increments of five years. It was further assumed that for the first seven days after the placement of the new deck, the new deck will be moist cured such that no deck shrinkage is taking place. The bridge structures were assumed to be simply supported and that no significant beam deterioration has taken place in terms of section loss and material degradation. The only consequential deterioration is assumed to have taken place in the deck thus prompting a deck replacement.

7.2 Comparison of Rebound and Net Camber after Deck Removal

Table 7.1 provides a comparison between beam rebound, net camber after deck removal, and net camber before new deck placement. This exercise was conducted for four projects using Iterations No. 5 and No. 6 of the proposed prediction methodology. There are some differences between the predicted elastic change in camber (rebound) when Iterations No. 5 and No. 6 are used. Iteration No. 6 leads to smaller rebounds compared to Iteration No. 5. This difference is due the different effective moduli of elasticity used in Iteration No. 5 and 6, respectively. Recall that the effective modulus is a function of the creep coefficient, and Iteration No. 5 and No. 6 use

different creep coefficients because the former is based on a single creep curve whereas the latter is based on multiple creep curves. Another reason why the elastic change in displacement (rebound) is different in Iterations No. 5 and No. 6 is due to the fact that the internal axial forces and bending moments in the deck, which are considered as newly applied forces on the non-composite beam section, are different. Since they are different, the rebound caused by their removal will be different.

In the light of this discussion, it is natural to expect differences in the net camber after deck removal since the history of forces in the beam and deck is different. Additionally, predictions based on Iteration No. 5 suggest that there is no change between net camber after deck removal, and net camber before new deck placement whereas Iteration No. 6 suggests that there is a slight camber growth. This comparison highlights the fundamental differences between the approaches used in Iterations No. 5 and No. 6. The reason why the net camber after deck removal and net camber before new deck placement is identical in Iteration No. 5 is due to the fact that the remaining creep coefficient calculated based on a single creep curve for beam concrete is nearly zero. Iteration No. 6 on the other hand uses a different creep curve for the unloading of the beam due to the removal of the deck, and this different creep curve suggests that concrete can still creep after 50 years.

Table 7.1. Comparison of rebound, net camber after deck removal, and net camber before new deck placement

Project Name	Approach No. 5			Approach No. 6		
	Elastic change (rebound) in camber* (in.)	Net camber after deck removal ⁺ (in.)	Net camber before new deck placement ⁺ (in.)	Elastic change (rebound) in camber* (in.)	Net camber after deck removal ⁺ (in.)	Net camber before new deck placement ⁺ (in.)
M5	3.67	2.80	2.80	3.39	1.51	1.81
TSO	1.52	2.33	2.33	1.43	2.00	2.13
S10-2	2.60	4.84	4.84	2.43	4.44	4.64
S11	4.65	5.53	5.53	4.44	4.74	5.10

*Old deck is assumed to be removed at 50 years.

⁺Elapsed time between after deck removal and before new deck placement is assumed to be 10 days.

Net camber prior to placement of the first deck was compared to the net camber after the removal of the deck to determine whether the beam would rebound to its original position. Five prestressed concrete beam and one steel beam project were considered. The results are shown in Table 7.2. The penultimate column shows the ratio (f/a) of net camber after removal of deck (and consequently locked in forces in the deck) to the net camber prior to the placement of the first

deck. For the steel beam project this ratio is equal to 1.00. This is logical because steel beams do not creep or shrink, and after the concrete deck is removed, there are no obstacles for the beam to rebound to its original position. In reality, this may not be the case due to a change in the boundary conditions (i.e. pin supports may not behave as pin supports), and possible plate action due to the presence of diaphragms which may restrain the movement of some beams relative to adjacent beams. For the prestressed concrete beams the ratio f/a varies from 0.47 to 0.92 (i.e. <1.0), which is an indication that after the deck is placed the beam continues to deflect downwards due to differential shrinkage and differential shrinkage induced creep. This additional downward deflection, combined with the smaller immediate rebound when the deck is removed due to the increased modulus of the beam results in f/a ratios that are lower than 1.0.

Table 7.2. Comparison of net camber prior to placement of deck to net camber after removal of deck

Project Name	Placement of Deck and Barrier (in.)			Removal of Barrier and Deck (in.)			Ratio = Removal/Placement	
	Prior to Placement of Deck (a)	After Placement of Deck (b)	After Placement of Barrier (c)	Prior to Removal of Barrier (d)	After Removal of Barrier (e)	After Removal of Deck and Locked in Forces (f)	f/a	e/b
S11	6.47	3.53	3.59	0.93	1.67	4.99	0.77	0.47
S10-2	4.93	3.42	3.17	2.30	2.62	4.56	0.92	0.77
M5	3.69	2.21	1.15	-1.31	-0.37	1.75	0.47	-0.17
TSO	2.47	1.60	1.45	0.75	0.95	2.08	0.84	0.59
S05	5.74	1.99	1.03	-1.58	-0.69	3.35	0.58	-0.35
M20*	11.68	2.07	0.00 ⁺	-3.86	-2.97	11.68	1.00	-1.44
*Steel project; ⁺ Fabricated camber is arranged such a way that after barrier load is applied, net camber is zero.								

7.3 Influence of Deck Replacement Time

The influence of the time when the old deck is replaced on the magnitude of rebound, net camber after deck removal, and net camber before new deck placement was investigated using Iteration No. 6 by considering various deck replacement times (40-60 years in increments of five years). This exercise was conducted for the S-11 project. As can be seen, from Table 7.3 deck replacement time had no influence on the magnitude of beam rebound and net camber after deck removal provided that the deck is replaced at least after 40 years. Again, this is due to the fact that the modulus of the beam has reached a stable value after 40 years. This is evident from all full

beam displacement history curves shown in previous figures. Deck replacement time had a minor influence on the net camber before new deck placement with greater deck replacement times resulting in slightly lower net cambers before new deck placement. However, as shown in Table 7.3 this influence is minimal. This minimal reduction in net camber before new deck placement as the deck replacement time increases is due to the fact that concrete creeps less when the load is applied or removed at a later time rather than at an earlier time.

Table 7.3. Influence of deck replacement time on beam rebound, net camber after deck removal, and net camber before new deck placement based on Iteration No. 6 (S-11 project)

Time when old deck is replaced (years)	Elastic change (rebound) in camber* (in.)	Net camber after deck removal ⁺ (in.)	Net camber before new deck placement ⁺ (in.)
40	4.44	4.74	5.11
45	4.44	4.74	5.11
50	4.44	4.74	5.10
55	4.44	4.74	5.10
60	4.44	4.74	5.09

*Old deck is assumed to be removed at 50 years.
⁺Elapsed time between after deck removal and before new deck placement is assumed to be 10 days.

7.4 Summary and Conclusions

The influence of solution method (Iteration No. 5 vs. Iteration No. 6) on beam rebound, net camber after deck removal, and net camber before new deck placement was investigated. It was determined that Iteration No. 6 leads to smaller rebounds compared to Iteration No. 5. Additionally, predictions based on Iteration No. 5 showed that there is no change between net camber after deck removal, and net camber before new deck placement whereas Iteration No. 6 suggests that there is a slight camber growth.

Steel beams were able to rebound to their original position once the deck was removed whereas prestressed concrete beams rebounded to 47-92% of their original position depending on whether differential shrinkage or prestressing induced creep dominated the behavior of the composite system.

When Iteration No. 6 was used, deck replacement time had no influence on the magnitude of beam rebound and net camber after deck removal provided that the deck is replaced at least after 40 years. Deck replacement time had a minor influence on the net camber before new deck placement with greater deck replacement times resulting in slightly lower net cambers before new deck placement.

Chapter 8: Evaluation of Various Prediction Methodologies for Time Dependent Flexural Deformations

Chapter 8: Evaluation of Various Prediction Methodologies for Time Dependent Flexural Deformations

8.1 Introduction

The purpose of this chapter is to:

- 1) compare the measured camber at release and pre-erection camber provided as part of the dataset with predictions based on PCI multiplier Method, MDOT multiplier method, and the proposed methodology;
- 2) compare camber predictions based on various approaches within the proposed prediction methodology to determine the impact of various assumptions.
- 3) compare predictions of prestress losses based on AASHTO LRFD Specifications (2020) and those obtained using the proposed prediction methodology

8.2 Evaluation of Predictions for Camber at Release

Measured camber at release data provided by the fabricator was compared with predicted camber at release using Iteration No. 6. The predicted camber at release was calculated once based on measured beam properties and another time based on specified properties. The measured properties in question are the concrete compressive strength at release, length of beam, concrete unit weight, and magnitude of prestressing force. In all predictions, the modulus of elasticity of concrete at release was determined using AASHTO's (2020) formula, which is a function of concrete compressive strength, unit weight, and aggregate factor. The measured camber was compared to predicted camber using Iteration No. 6. When conducting this comparison, it was assumed that camber at release was measured as soon as the strands were detensioned, thus allowing no time for the concrete to creep and shrink. Measured camber data shows that this was not always the case because the fabricator has up to seven days to report camber at release according to MDOT's Special Provisions for Structure Survey during Construction. The measured camber at release was also compared with the anticipated camber specified in the design drawings.

As stated earlier, for the prestressed concrete beams fabricated for Michigan projects information on beam storage and support conditions when camber at release was measured was not provided as part of the camber data set. However, in several cases bridge drawings specified where such supports should be placed. Therefore, predictions were based on the assumption that such specifications were followed during beam fabrication and considered the placement of beam

supports after fabrication. When camber at release was measured for the beams fabricated by PSI Windsor, the beams had been removed from the prestressing bed and stored on wooden blocks positioned 3 feet away from the ends of the beam. This support condition was taken into consideration when estimating displacements due to self-weight for this project.

Summary of camber at release predictions

The comparison between measured, predicted (based on proposed methodology), and design (specified in drawings) camber at prestress release was conducted on a beam-by-beam basis. The results of this comparison are provided in Fig. 8.1 and Table 8.1. Fig. 8.1 provides a graphical comparison between measured and predicted camber at release for each beam using measured and specified properties. Design camber values specified in drawings are also included. Table 8.1 provides a summary of statistical indicators for the beam-by-beam evaluation. The average ratio of measured over predicted camber when the proposed method was used is 1.06 and 0.98 when measured and specified properties were employed with 23% and 24% COVs, respectively. The ratio of measured over predicted camber using the current MDOT method (i.e. design camber) is 1.13 and the COV is 42%. This suggests that the current MDOT method is less accurate and less consistent than the proposed methodology regardless of whether specified or measured properties are used. The range of measured over predicted camber when the proposed methodology is used is 0.42-1.57 when measured properties are employed, and 0.41-1.50 when specified properties are utilized. When MDOT's method is used the range of measured over predicted camber is 0.48-3.36. These statistics suggest that the proposed methodology contains the error in prediction much better than the current MDOT method.

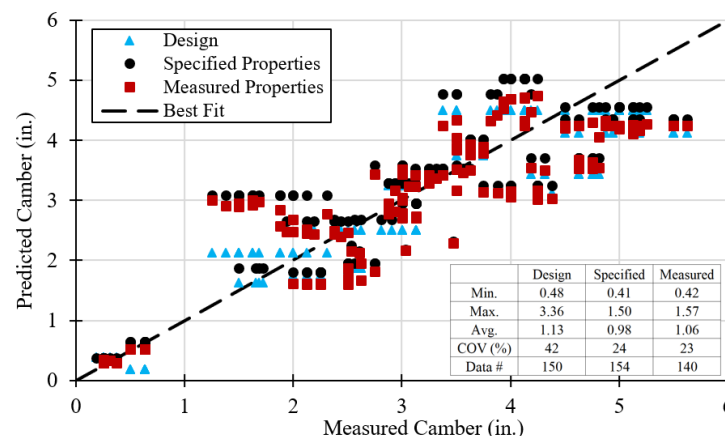


Fig. 8.1. Comparison of measured, predicted, and design camber at prestress release

Table 8.1. Summary of camber at prestress release predictions

Statistical Indicators	Camber at Release Ratio		
	Δ_m/Δ_d	$\Delta_m/\Delta_{p,m}$	$\Delta_m/\Delta_{p,s}$
Min.	0.48	0.42	0.41
Max.	3.36	1.57	1.50
Avg.	1.13	1.06	0.98
St. Dev.	0.47	0.24	0.23
COV (%)	42	23	24
# of beams	150	140	154

Δ_m = measured camber (in.); Δ_d = design camber (in.); $\Delta_{p,m}$ = predicted camber based on measured properties (in.); $\Delta_{p,s}$ = predicted camber based on specified properties (in.)

8.3 Evaluation of Predictions for Pre-erection Camber

Measured pre-erection camber was compared with predicted pre-erection camber using the proposed methodology, the PCI multiplier method, and the MDOT multiplier method to demonstrate the higher accuracy of the proposed methodology. When the PCI and MDOT multiplier methods were used, camber at release was based on predictions obtained using the Iteration No. 6 to contain the source of error solely to that introduced by the multiplier as opposed to compounding the errors identified in camber at prestress release predictions. Predictions based on the proposed methodology were once based on the specified properties and another time on the measured properties. Creep coefficients, shrinkage strains, and modulus of elasticity were based on the models provided in AASHTO LRFD Specifications (2020). Variation of modulus of elasticity with time was based on ACI 209R-92 model and the coefficients α and β were back calculated using the modulus of elasticity at prestress release and 28 days as anchor points.

Summary of pre-erection camber predictions

Fig. 8.2 and Table 8.2 provide a summary of the pre-erection camber predictions. The average ratio of measured over predicted camber when measured and specified properties are used is 1.06 and 0.98 and the corresponding COVs are 19% and 19%, respectively. The average ratio of measured over predicted camber when the PCI multiplier method is used based on measured and specified properties is used is 0.82 and 0.78, respectively, and the corresponding COVs are 21% and 20%, respectively. The average ratio of measured over predicted camber when the MDOT multiplier method is used based on measured and specified properties is used is 0.67 and 0.62, respectively, and the corresponding COVs are 23% and 20%, respectively. These statistics suggest

that the proposed prediction methodology results in more accurate and consistent predictions of pre-erection camber compared to the PCI multiplier method and MDOT multiplier method regardless of whether measured or specified properties are used.

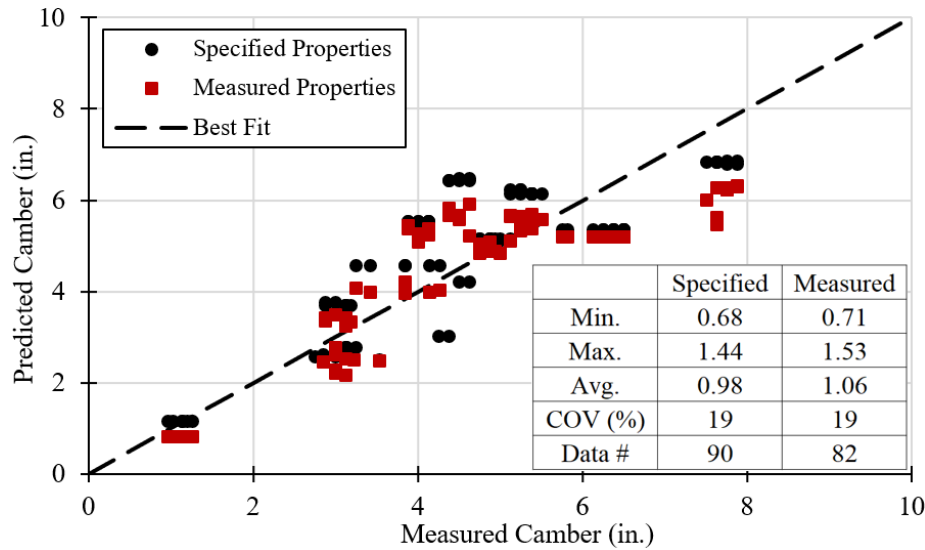


Fig. 8.2. Comparison of measured and predicted pre-erection camber

Table 8.2. Summary of pre-erection camber predictions on a beam-by-beam basis

Statistical Indicators	Pre-erection Camber Ratio					
	Δ_m / Δ_{p_m}	Δ_m / Δ_{p_s}	$\Delta_m / \Delta_{PCI_m}$	$\Delta_m / \Delta_{PCI_s}$	$\Delta_m / \Delta_{MDOT_m}$	$\Delta_m / \Delta_{MDOT_s}$
Min.	0.71	0.68	0.56	0.52	0.47	0.46
Max.	1.53	1.44	1.36	1.13	1.30	1.00
Avg.	1.06	0.98	0.82	0.78	0.73	0.68
St. Dev.	0.21	0.19	0.17	0.16	0.17	0.14
COV (%)	19	19	21	20	23	20
# of beams	82	90	82	90	82	90

Δ_m = measured camber (in.); Δ_{p_m} = predicted camber based on measured properties (in.); Δ_{p_s} = predicted camber based on specified properties (in.); Δ_{PCI_m} = predicted camber using PCI multipliers and measured properties (in.); Δ_{PCI_s} = predicted camber using PCI multipliers and specified properties (in.); Δ_{MDOT_m} = predicted camber using MDOT multipliers and measured properties (in.); Δ_{MDOT_s} = predicted camber using MDOT multipliers and specified properties (in.)

8.4 Evaluation of Predicted Camber Growth Curve

Camber growth curves were developed for the beams that were fabricated by PSI Windsor as part of the Tiffin Street Overpass project since multiple camber readings were taken for these beams during the time that these beams were stored in the precast facility. Fig. 8.3 shows the variation of measured and predicted camber with time for all four beams for which camber data

was recorded. The predicted camber growth curves were obtained based on various creep and shrinkage models. In Fig. 8.3a the measured camber data is compared with predicted camber based on creep coefficients and shrinkage strains obtained from all considered models. As can be seen, the B3 total creep model and the GL2000 model significantly overestimate beam camber. Therefore, these two models are excluded in Fig. 8.3b so that the difference between the other models can be assessed more clearly. AASHTO LRFD Specifications (2020) provide two sets of equations to account for the effect of volume-to-surface ratio (V/S). The first set of equations is provided in the body of AASHTO (2020) and the second in the commentary. The maximum V/S ratio considered in the development of the equations provided in the commentary was 6 in. Fig. 8.3b suggests that for one out of four beams, the AASHTO LRFD (2020) body model leads to more accurate predictions when compared to other models. For two out of four beams, the CEB MC90-99 model results in a better match with the measured camber data, and for one out of four beams, the fib MC 2010 model provides the best prediction.

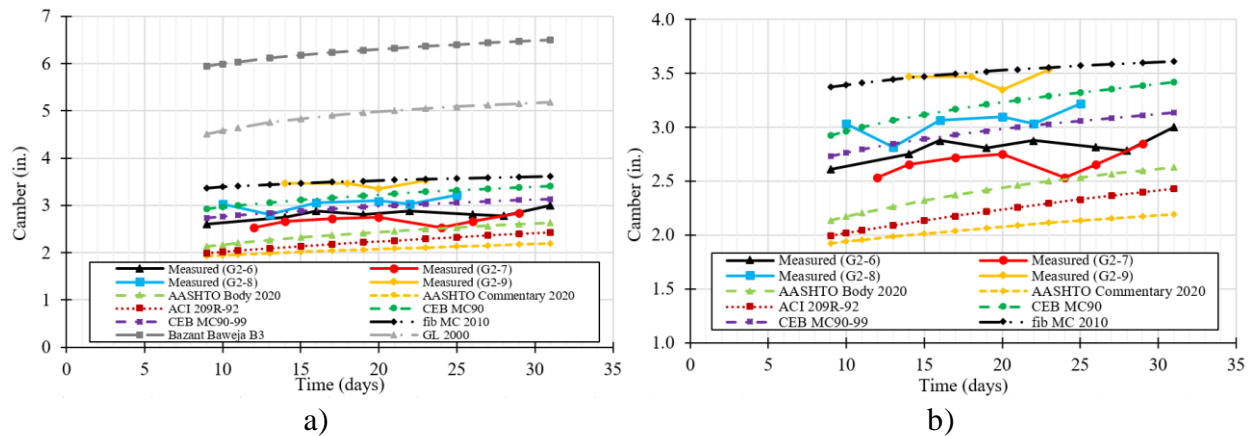


Fig. 8.3. Variation of measured and predicted camber for the prestressed concrete beams fabricated in PSI Windsor for the Tiffin Street Overpass Project: a) full scale, b) reduced scale

Fig. 8.4 shows the contribution of creep and shrinkage to the predicted long-term camber based on the AASHTO LRFD (2020) model. The difference in downward deflections caused by beam shrinkage based on the two sets of equations for V/S ratio is negligible, whereas the difference in camber caused by creep is noticeable. Additionally, the difference between predictions based on the provisions for V/S ratio provided in the body of AASHTO (2020) and those provided in the commentary are also noticeable. Since the provisions in the body of AASHTO LRFD (2020) Specifications for creep and shrinkage led to more accurate camber predictions compared to the other models for the beams in question, this model was used to

evaluate the rest of the camber and displacement data. It should be noted, however, that this conclusion is based solely on four beams. Menkulasi et al. (2018) arrived at a similar conclusion for three sets of prestressed concrete beams fabricated in Virginia. In addition, the AASHTO (2020) creep model provided the best match for the creep coefficient obtained based on measured creep data collected as part of this research project for one Michigan prestressed concrete beam mix. While the reasons stated above should provide a level of comfort in using the benchmark model set used in this research (i.e. AASHTO (2020) model for creep, shrinkage, and modulus at prestress release and 28 days, and ACI 209R-92 model for the variation of modulus of elasticity with time) it should be noted that other combinations of models could also result in accurate pre-erection camber predictions. ACI Committee 209 is perhaps in the best position to recommend a model for predicting creep and shrinkage. However, as stated earlier, the committee has refrained from doing so due to a lack of consensus regarding the data set and statistical indicators that should be used to arrive at such conclusion.

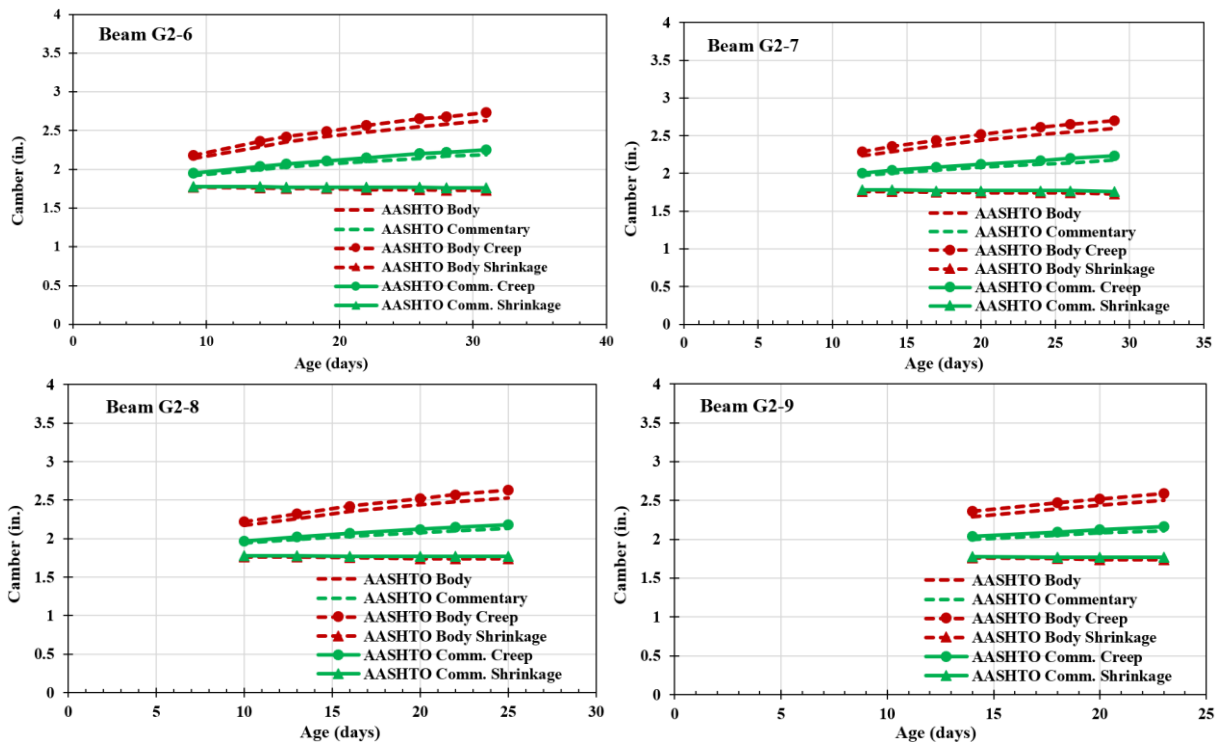


Fig. 8.4. Influence of beam creep coefficient and beam shrinkage strain on beam camber considering the beams used in the Tiffin Street Overpass project

8.5 Comparison of Incremental Time Step Method (Nilson 1987) and Proposed Prediction Methodology

The incremental time step method (ITSM) (Nilson 1987) described in Chapter 2 was used to compare pre-erection camber predictions with those obtained using the proposed prediction methodology. As noted in Chapter 2, the ITSM (Nilson 1987) relies on updating the prestressing force for various time steps to capture the variation of this force with time so that the influence of this variation on beam camber and displacements can be quantified. The ITSM does not capture the direct effect that phenomena such as differential shrinkage between the deck and the girder can have on beam camber and displacement in cases where there is no prestress (such as a steel bridge). Therefore, this comparison was limited to pre-erection camber predictions in which the effect of differential shrinkage is limited compared to the condition after the deck is cast. Because, the ITSM relies primarily on an accurate estimation of prestress losses to determine the variation of the prestress force with time and consequently the variation of camber and displacements, a comparison between prestress losses computed using the AASHTO LRFD Specifications (2020) and those computed using the proposed methodology is conducted.

8.5.1 Variation of Prestress and Prestress Losses with Time

Variation of Total Prestressing Force with Time

The variation of prestressing force and prestress losses with time was investigated to show the effect that certain construction activities such as deck placement or replacement have on the magnitude of the prestressing force and consequently on the magnitude of camber and displacements. This investigation was done using Iteration No. 6 of the proposed prediction methodology. Fig. 8.5 shows the variation of prestress with time in S1 1 project. The variation of the prestress is shown at mid-span. The variation of the total prestressing force over time is characterized by an initial gradual reduction due to time dependent prestress losses caused by creep and shrinkage of beam concrete and relaxation of prestressing steel. When the deck is placed, there is a sudden increase in the prestressing force (prestress gain) due to the weight of the deck. Between deck placement and installation of superimposed dead loads (barrier + overlay) there is a minor gradual decrease due to time dependent losses. The installation of barrier and overlay causes another increase in the prestressing force due to the induced tension. Then, there is a gradual decrease in the prestressing force due to the combined effects of creep of beam concrete, creep of

deck concrete, differential shrinkage between beam and deck concrete, and differential shrinkage induced creep. When the deck is replaced (for example after 50 years), there is a sudden decrease in the prestressing force due to the rebound of the beam and the compression caused at the centroid of tendons because of this rebound. The sudden decrease in prestress (prestress loss) is recovered when the new deck is placed. These observations are intuitive and are a confirmation that the proposed prediction methodology has the ability to quantify the variation of prestressing force with time and lead to logical results.

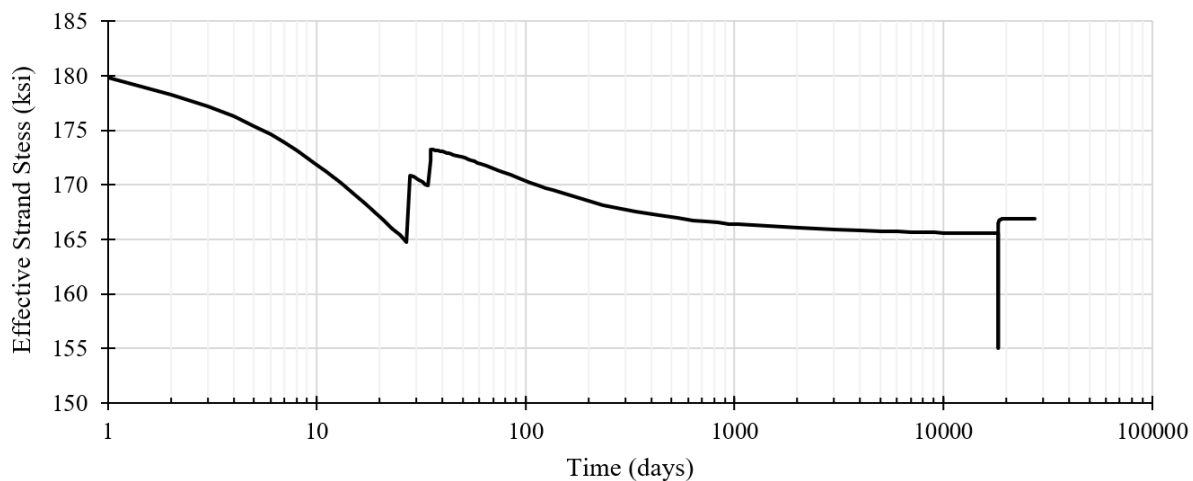


Fig. 8.5. Variation of prestress as a function of time in a composite bridge system at mid-span (S-11 project)

Variation of Prestress Loss with Time

There are various factors that affect the magnitude of the prestressing force over time. To illustrate the effect of these factors on the prestressing force, the prestress loss was plotted as function of time in Fig. 8.6. A prestress loss is designated as positive, and a prestress gain is designated as negative. Fig. 8.6 shows the variation of prestress loss or gain due creep and shrinkage of concrete and relaxation of steel as a function of time. The solid lines represent net effect that creep, shrinkage, and relaxation of steel have on prestress losses. The dashed lines represent the separate effects of girder and deck creep and girder and deck shrinkage. It should be noted that in reality these losses are interdependent (i.e. the loss due to shrinkage affects the loss due to creep, etc.). However, in this exercise, the variation of each loss with time was considered separately (i.e. when creep loss is calculated, the other losses are set equal to zero). As can be seen, concrete creep is the main contributor to prestress loss, followed by concrete shrinkage, and

relaxation of steel. Girder creep causes the majority of prestress loss a portion of which is counterbalanced by deck creep, which helps increase positive curvature when the deck is placed. Girder shrinkage is the second largest source of prestress loss, a portion of which is counterbalanced by deck shrinkage, which causes positive curvature in the composite system thus causing a prestress gain. Finally, the relaxation of prestressing strands is also partly responsible for prestress losses although it has a lower influence compared to girder creep and shrinkage.

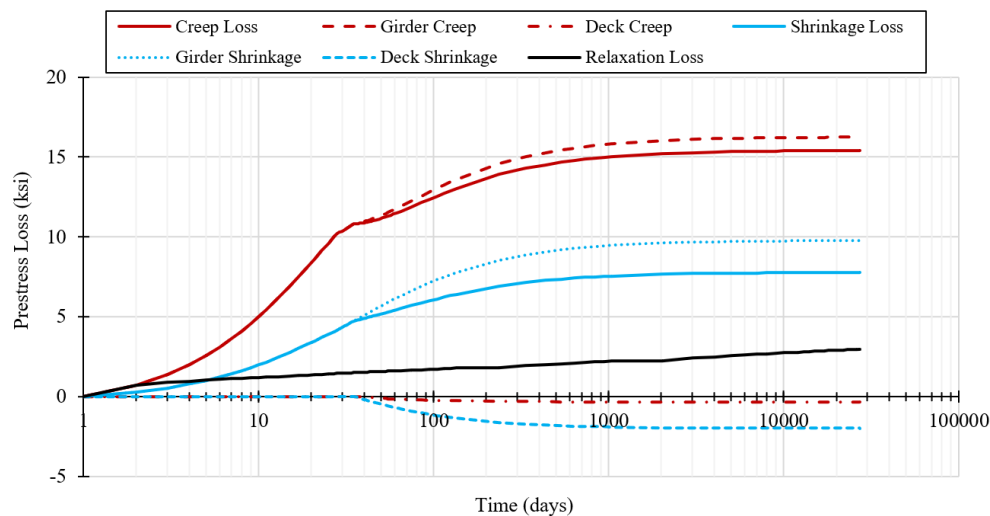


Fig. 8.6. Variation of prestress losses with time in a composite bridge system at midspan (S-11 project)

Comparison of Prestress Losses

An accurate prediction of prestress losses is important when estimating camber and displacements. The research team believes that the proposed approach is accurate not only in terms of predicting time dependent camber and displacements but also in terms of predicting long terms losses. Recognizing that various states or consulting companies may use the incremental time step method (Nilson 1987) to predict time dependent camber and displacement, the long-term losses computed based on the proposed method were compared with those obtained using AASHTO's provisions (2020). An accurate prediction of prestress losses is also important when checking stresses at service.

AASHTO LRFD Specifications (2020) provide a refined method for estimating losses by considering two main time steps. The first covers the period from release of prestress to deck placement, and the second from deck placement to final time. Results obtained from AASHTO's

(2020) refined method for calculating prestress losses were compared with those obtained from the proposed prediction methodology and are illustrated in Fig. 8.7 and Table 8.3. When using the proposed prediction methodology total losses were once computed by ignoring the interdependence of losses and another time by considering this interdependence. The former approach was used to be able to compare prestress loss components caused by each phenomenon and the latter was used for a more realistic assessment. It should be noted that the proposed prediction methodology provides losses due to creep and shrinkage as a single numerical value since these phenomena are considered simultaneously. To separate these losses, the analysis was once run by setting the creep coefficient equal to zero to obtain the shrinkage loss, and another time by setting the shrinkage strain equal to zero to obtain the creep loss.

In general, predictions based on AASHTO's (2020) provisions were consistent with those obtained from the proposed prediction methodology. The largest difference was exhibited by the creep loss. The difference in creep loss prediction was smaller between transfer and deck placement and became larger from deck placement to final time. This is expected because once the deck is placed creep loss is affected by girder and deck concrete creep, and the AASHTO (2020) model captures only the influence of girder concrete creep. Predictions for shrinkage loss were rather consistent throughout the lifetime of the bridge. AASHTO LRFD Specifications (2020) have provisions that capture prestress gains due to deck shrinkage after the deck is placed and for the S-11 project these provisions seem to be working well. Relaxation loss predictions were also consistent. A time dependent function was used to predict losses due to relaxation of prestressing steel in the proposed prediction methodology as opposed to the step-wise function recommended in AASHTO (2020). Total time dependent losses from release of prestress to deck placement based on the proposed prediction methodology were equal to 7.8% and 7.5% of the jacking stress when loss interdependence was ignored and considered, respectively, whereas those obtained from AASHTO Specifications (2020) were equal to 8.1%. Similarly, losses from deck placement to final time based on the proposed prediction methodology were equal to 5.3% and 4.4% whereas those based on AASHTO specifications (2020) were equal to 3.8%. When elastic shortening losses are considered total losses based on the proposed prediction methodology are equal to 24.0% and 22.8% and those based on AASHTO (2020) provisions are equal to 22.9% (Table 8.3). Overall, predictions based on AASHTO LRFD Specifications (2020) were rather accurate. The % difference for creep and shrinkage is no greater than 11%. Relaxation loss

prediction differences are up to 68% although this is due to the small benchmark relaxation loss value. The maximum difference for total loss when interdependence is ignored does not exceed 33%. When interdependence is considered, the % difference for total loss between proposed prediction methodology and AASHTO LRFD (2020) body provision does not exceed 34%.

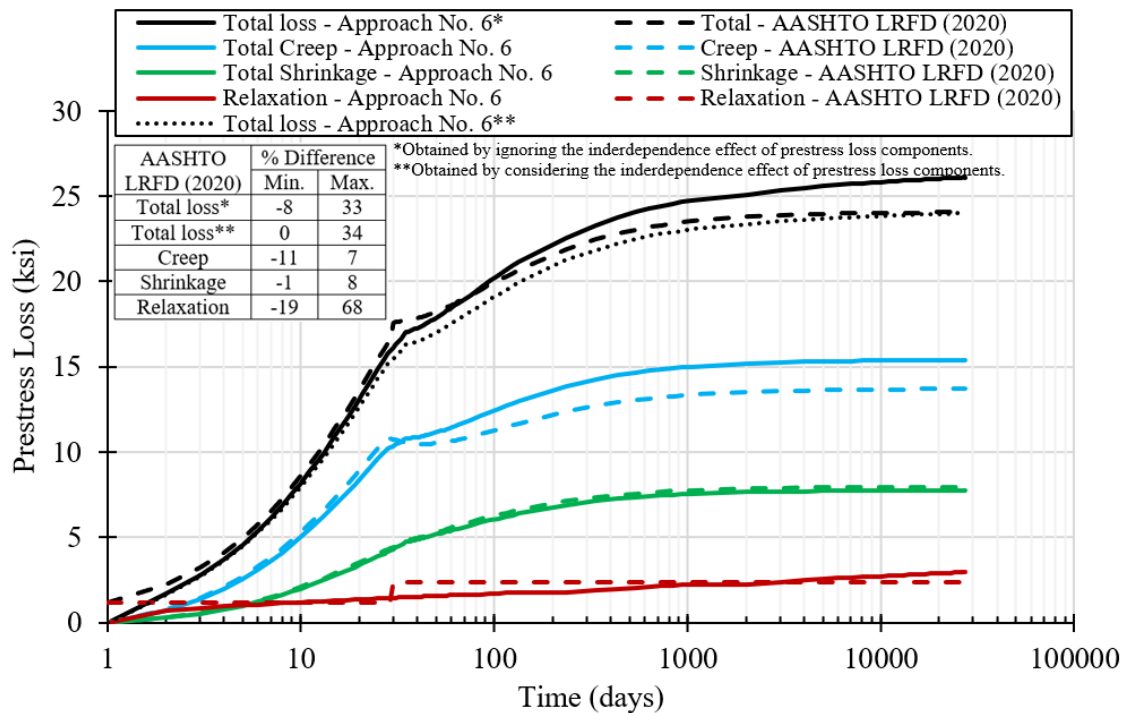


Fig. 8.7. Comparison of calculated separate and total prestress losses for S-11 project using proposed prediction methodology and AASHTO (2020) Body provisions

Table 8.3. Comparison of separate and total prestress losses computed using the proposed prediction methodology and AASHTO LRFD Specifications (2020) for the S-11 project

Losses	From initial to deck placement		From deck to final		Total from initial to final	
	Approach No. 6	AASHTO LRFD [‡] (2020)	Approach No. 6	AASHTO LRFD [‡] (2020)	Approach No. 6	AASHTO LRFD [‡] (2020)
Elastic shortening* (%)	10.9	11.0	NA ⁺	NA ⁺		
Relaxation (%)	0.7 (0.5 ⁺)	0.6	0.8 (0.3 ⁺)	0.6		
Creep (%)						
Due to girder	5.0	5.4	3.0	1.4		
Due to deck	NA ⁺	NA ⁺	-0.2	NA ⁺	24.0	22.9
Shrinkage (%)						
Due to girder	2.0	2.1	2.8	2.2		
Due to deck	NA ⁺	NA ⁺	-1.0	-0.3		
Total time-dependent losses** (%)	7.8 (7.5 ⁺)	8.1	5.3 (4.4 ⁺)	3.8		

* Although it is shown in the table as a loss occurring between from initial to deck placement, it is an instantaneous loss, not time dependent; ** Combined time-dependent loss - elastic shortening is not included; ⁺Not applicable; [‡]Body provision; [†]Predicted by considering interdependence of losses.

Comparison of Camber Prediction

The prestress losses computed using the AASHTO LRFD Bridge Design Specifications (2020) were used to update the prestressing force for several time steps with the purpose of computing pre-erection camber using the Incremental Time Step Method (Nilson 1987) described in Chapter 2. A total of 20 logarithmic like time steps were considered for the S10-2, S-11, and S12-1 projects and 37 time steps were used for the M-5 project when using the Incremental Time Step Method (Nilson 1987) as well as the proposed method. This means that the number of steps considered at the beginning of the considered time interval (i.e. between prestress transfer and pre-erection) was higher than that towards the end of the time interval to mimic the logarithmic like variation in creep and shrinkage of concrete. The results of this comparison are shown in Fig. 8.8. In general, pre-erection camber predictions based on the proposed prediction methodology and Incremental Time Step Method (Nilson 1987) were similar with the proposed methodology providing better predictions for three out of four projects. For general use, the proposed prediction methodology is recommended since it considers phenomena not accounted for by the Incremental Time Step Method (Nilson 1982) such as the influence of differential shrinkage between concrete and strands.

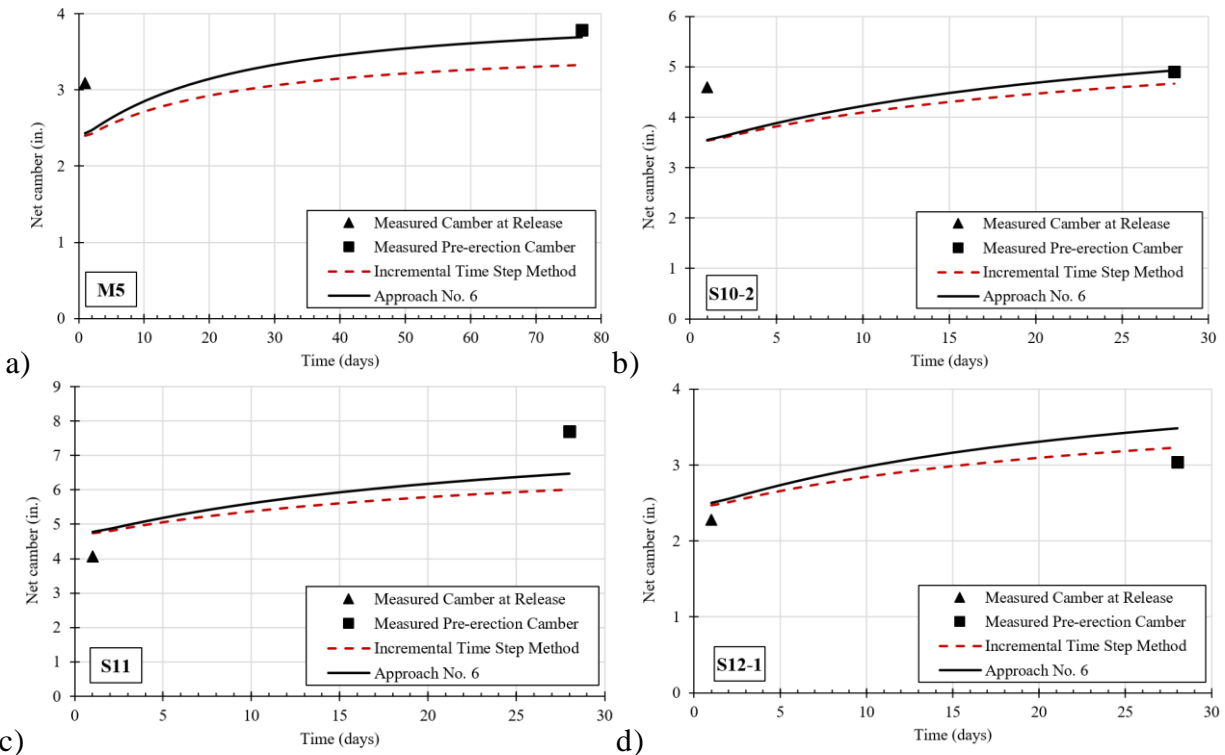


Fig. 8.8. Comparison of proposed method with the Incremental Time Step Method (Nilson 1987) for the: a) M5 project; b) S10-2 project; c) S11 project and d) S12-1 project

8.6 Comparison of Various Approaches within the Proposed Prediction Methodology

Since the latest version of the proposed prediction methodology was based on several iterations each of which introduced a level of theoretically enhanced accuracy, it is natural to ask what the impact of the improvements introduced in each layer is on predictions of camber and displacements over time. This section provides a comparison of predictions conducted using each iteration and contains three subsections. The first includes a comparison of all iterations for the displacement history of the beam up to pre-erection. The second includes the full-service life of the beam but excludes deck replacement. The third addresses the full displacement history including deck replacement.

8.6.1 Comparison of Iterations No. 1 through No. 6 for Pre-erection Camber

Camber growth up to pre-erection was predicted using all iterations for the prestressed concrete beams used in S10-2 and S-11 project. The results are shown in Fig. 8.10. Iterations No. 1 and No. 2 can provide predictions at discrete points and are shown by the green dots, which represent camber at release of prestress and pre-erection camber. Iterations No. 3 through No. 6 can provide the full displacement history. Predictions based on Iterations No. 1-6 are virtually identical with % differences being smaller than 4%. Iterations No. 1 and No. 2 despite their relative simplicity lead to similar predictions of pre-erection camber with Iteration No. 6, which is believed to be the most accurate. On the other hand, ITSM (Nilson 1987) predicts lower camber than all other iterations for S10-2 and S11 project. Although % difference for Iteration No. 1-5 does not exceed 5%, it reaches almost 10% for ITSM. It should be noted that differences between the different iterations may vary for other projects. For the S10-2 and S-11 projects, differences in pre-erection camber were no more than 10% despite fundamental differences in each prediction methodology.

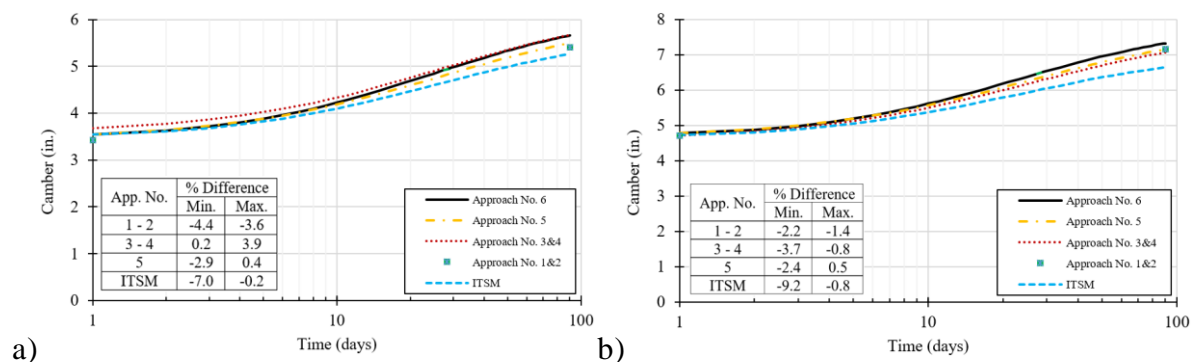


Fig. 8.9. Comparison of various iterations for pre-erection camber for: a) S10-2 project, b) S-11 project

8.6.2 Comparison of Iterations No. 2 to No. 6 for Service camber without Deck Replacement

Camber and displacements were predicted using Iterations No. 2 – 6 up to 75 years for the prestressed concrete beams used in the S10-2, S-11, and M-20 projects. The results are shown in Fig. 8.10. In this comparison, Iteration No. 1 is not included because its scope was to provide predictions up to pre-erection and not beyond. All iterations result in rather similar predictions up to pre-erection for both prestressed concrete beam bridge projects (S10-2 and S-11) with differences being less than 5%. For S10-2 project, while Iteration No. 5 provides the highest service camber at 75 years, Iteration No. 2 predicts the lowest one. In addition, Iterations No. 2, No. 3, No. 4 and No. 6 results in similar service camber results at 75 years. The difference in service camber with respect to Iteration No. 6 remains less than 22 % for Iteration No.2; 6% for Iterations No. 3 and 4; and 12% for Iteration No. 5. For S11 project, Iteration No. 6 provides the lowest prediction all iterations provide similar service camber predictions. The difference between Iteration No. 5 and 6 is at most 101%. The difference between Iterations No. 3 and 4 and Iteration No. 6 is around 8%. The difference between Iteration No. 2 and No. 6 is approximately 80%. For the steel beam bridge project (M-20) the difference between Iteration No. 3, 4 and 5 and Iteration No. 6 is less than 9%, whereas the difference between Iteration No. 2 and Iteration No. 6 is approximately 0.6%. It should be noted that in Iteration No. 2 the placement of the deck and superimposed dead loads (barrier +overlay) is assumed to take place simultaneously whereas in Iterations No. 3 and above a period of seven days is assumed between the placement of the deck and placement of superimposed dead loads. As can be seen from Fig. 8.10 the fundamental theoretical differences in each prediction methodology start to produce notable differences in camber and displacements at service in some cases.

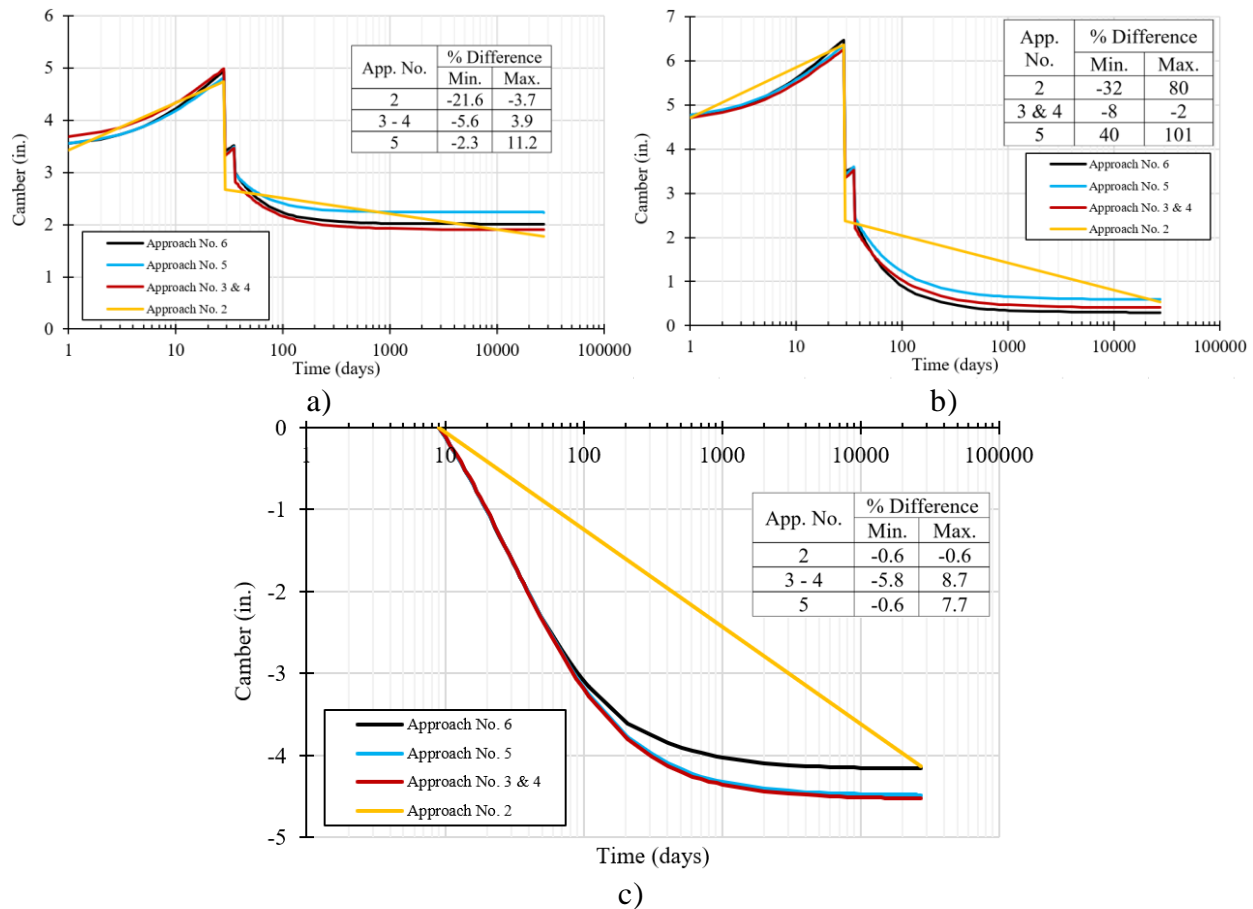


Fig. 8.10. Comparison of various approaches for service camber without deck replacement for: a) S10-2 project, b) S-11 Project, c) M-20 project

8.6.3 Comparison of Iterations No. 4 to No. 6 for Service Camber with Deck Replacement.

The full displacement history of the prestressed concrete beams used in the S-10-2 and S-11 projects was predicted using Iterations No. 4, 5, and 6. A similar comparison was conducted for the steel beams in the M-20 project. This comparison includes an assumed deck replacement activity after 50 years of service. Iterations No. 1, 2, and 3 were not included in this comparison because their scope was limited either to the prediction of pre-erection camber (Iteration No. 1) or the prediction of service camber without a deck replacement activity. The results are shown in Fig. 8.11 in terms of the full displacement history. Fig. 8.11a and Fig. 8.11b suggest that there are notable differences in predictions for camber and displacements at service based on Iteration No. 4 and Iterations No. 5 and 6. Additionally, Fig. 8.11a and Fig. 8.11b suggest that the difference in camber and displacements for the S10-2 and S-11 projects (prestressed concrete beam projects) between Iteration No. 4 and 6 can be up to 589%, whereas the differences between Iteration No. 5

and 6 can be up to 1795%. For the M-20 project which featured steel beams the difference between camber and displacements did not exceed 11% and all iterations resulted in rather similar predictions. The results presented so far suggest that the difference in predictions based on various iterations is more pronounced in prestressed concrete beam bridge projects compared to steel beam bridge projects. This is due to the fact that any uncertainties related to the creep and shrinkage of the beam are removed when the beam is a steel beam since a steel beam does not creep or shrink. The fundamental differences between the various iterations are related for how to best predict the structural effects of creep in a prestressed concrete beam, which is subject to a varying stress history.

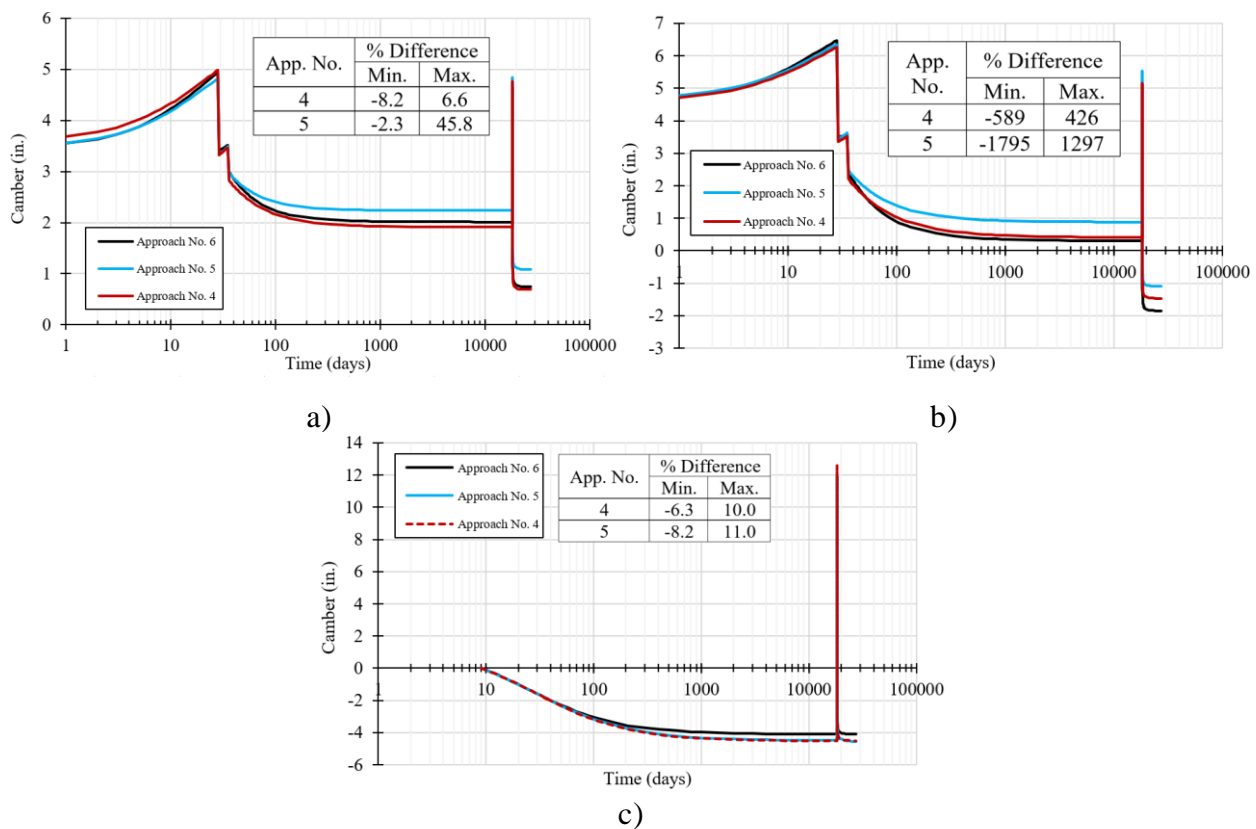


Fig. 8.11 Comparison of predicted displacement history based on Iterations No. 4, 5, and 6 including a deck replacement activity after 50 years of service for: a) S10-2 project, b) S11 project, c) M-20 project

8.6.4 Impact of Method to Generate Time Steps within Iteration No. 6

As described in Chapter 3, Iteration No. 6 produces time steps using a stepwise function in which more time steps are used at the beginning of an event and fewer at later times. Another approach is that proposed by Gilbert and Ranzi (2012) who suggest the use of a geometric series for the

generation of the number of time steps. The impact of the method for generating the number of time steps used for a given loading event was evaluated by running Iteration No. 6 one time using the stepwise function described in Chapter 3 and another time using the geometric series proposed by Gilbert and Ranzi (2012) using 1, 5, and 10 time substeps for every major time step. The results are shown in Fig. 8.12 for S-10-2 and S-11 projects. The figures shown on the right-hand side show the % differences between using a logarithmic time substep generation approach or using a geometric series based on a certain number of time substeps. Predictions based on the step wise function and the geometric series differ no more than 21% and 100% for S10-2 and S11 projects, respectively. The proposed prediction methodology allows the user to select either method for the generation of time steps for a given event.

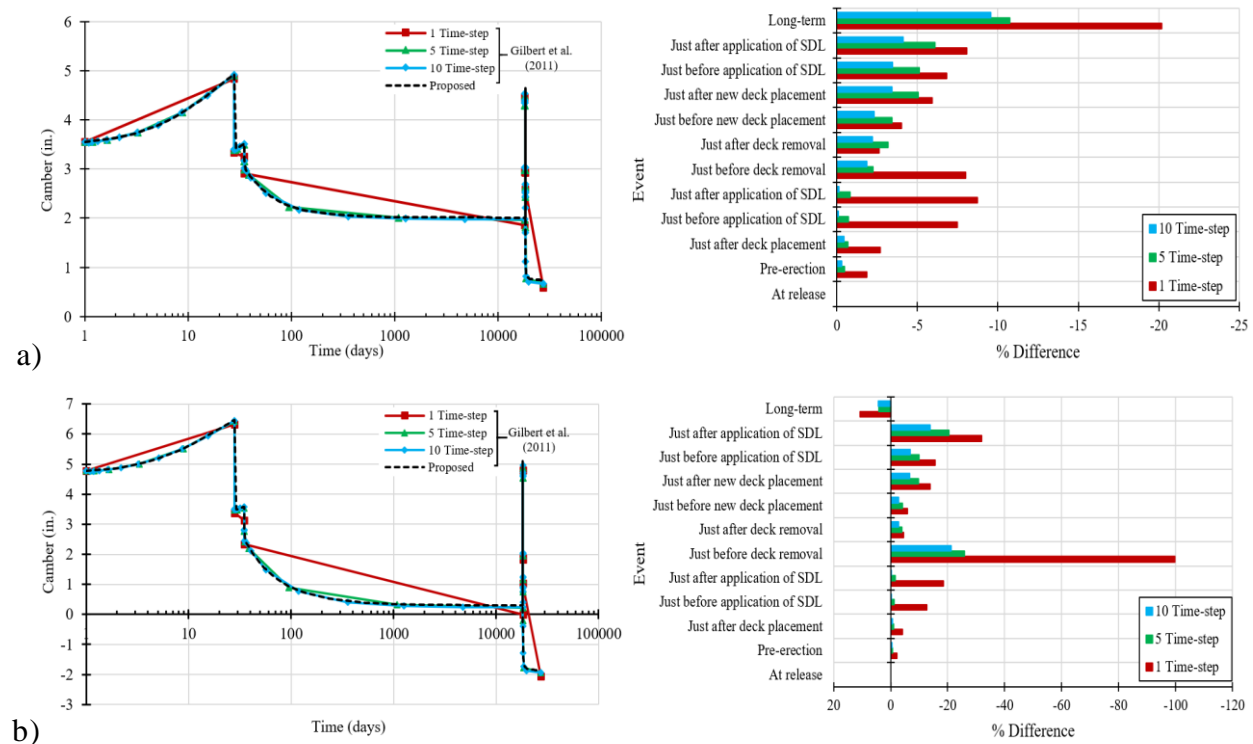


Fig. 8.12. Impact of method to generate the number of time steps on full camber and displacement history for: a) S10-2 project, b) S-11 project

8.6.5 Influence of Number of Beam Sections Specified in Iteration No. 6

When using the Matlab based algorithm (Iteration No. 6) the user needs to specify the number of beam sections. This decision influences the prediction of camber, which is obtained by numerically integrating the curvature diagram along the beam span based on the selected number of sections. It also influences the smoothness of the deflected shape of the beam for a given time

step. To obtain a realistic deflected shape, the user needs to specify enough sections so that the algorithm can produce a smooth deflected shape.

The sensitivity of camber predictions based on the approach used in Iteration No. 6 to the number of beam sections selected was evaluated by varying the number of odd sections from three to 99 and the number of even sections from two to 100. The benchmark for conducting this evaluation is the camber predicted using 100 beam sections. The results of this evaluation are shown in Fig. 8.13 for camber at release and pre-erection at midspan for the beams used in S-11 project. Fig. 8.13a suggest that the estimation of camber is not sensitive to the number of beam sections selected when this number is odd. For example, the difference in camber predictions between three and 100 beam sections is less than 0.5%. This shows the efficiency of the selected numerical integration technique when an odd number of beam sections are selected. Conversely, when the selected number of beam sections is even, camber predictions become notably sensitive to the selected number of beam sections. For example, Fig. 8.13b shows that the difference in camber prediction between two and 100 beam sections is greater than 35%. This difference reduces rapidly as the number of beam sections increases and becomes negligible when the number of sections exceeds 50. Therefore, it is recommended that at least 51 sections are selected when conducting a time dependent analysis using the Matlab based software developed based on Iteration No. 6.

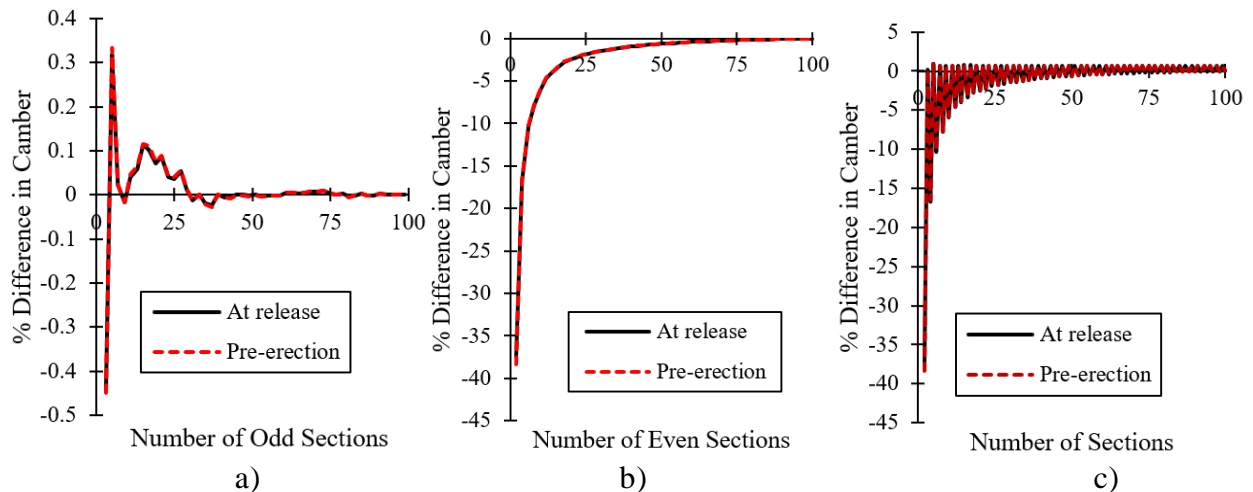


Fig. 8.13. Sensitivity of camber predictions at midspan for the beams used in S-11 project to the number of sections considered: a) number of odd sections, b) number of even sections, c) number of sections (odd or even)

8.7 Derivation of Time Dependent Multiplier Method

Camber predictions obtained using the proposed prediction methodology were compared with those obtained using the time dependent multiplier method. As explained in Chapter 3, time dependent multiplier curves were developed for the each project based on results obtained from the proposed prediction methodology. This was done by computing the ratio between long term camber and camber at release (i.e. the multiplier) at various points in time up to 90 days for all prestressed concrete beams used in the projects considered as part of this research project. These curves are shown in Fig. 8.14. Then a logarithmic curve fit was conducted to develop a function that expresses the multiplier as a function of time (Eq. 8.1).

$$\begin{array}{ll} \text{If } t < 3 \text{ days} & \lambda = 1 \\ \text{otherwise} & \lambda = 0.17 \ln(t) + 0.85 \text{ } (\lambda: \text{multiplier, and } t: \text{time in days}) \end{array} \quad (8.1)$$

It should be noted that the time dependent multiplier is valid only for predicting pre-erection camber and cannot be used after the deck is cast. Such time dependent multipliers may be useful and convenient during the preliminary design stage. This convenience should be used with caution as the proposed time depend multiplier values are empirically derived and may or may not be valid for all types of beams.

8.8 Comparison of Proposed Prediction Methodology and Time Dependent Multiplier Method

Measured pre-erection camber was compared with predicted pre-erection camber based on the proposed prediction methodology (Iteration No. 6), the proposed time dependent multiplier method, MDOT's fixed multiplier method, and PCI's fixed multiplier method. The comparison was done on a beam by beam basis using both specified and measured properties (Table 8.4). This comparison was conducted by calculating ratios of measured over predicted camber using each prediction methodology. Table 8.4 suggests that the proposed prediction methodology and the time dependent multiplier method offer significantly better predictions than those obtained using PCI and MDOT multipliers. While the use of measured properties resulted overall in more accurate predictions, the COV of was higher than when specified properties were used. Average ratios of measured over predicted camber when specified properties were used for the proposed prediction methodology and time dependent multiplier method were 0.98 and 0.96, respectively; whereas

those for the PCI and MDOT multiplier approach were 0.78 and 0.68, respectively. When measured properties were used the average ratio of measured over predicted camber for the proposed prediction methodology and time dependent multiplier method were 1.06 and 1.02, respectively; whereas those for the PCI and MDOT multiplier approach were 0.82 and 0.73, respectively.

The time dependent multiplier method was also evaluated by calculating the ratio of measured over predicted camber using initial camber predictions based on the proposed methodology as well as measured initial camber. The initial camber predictions were based on specified and measured properties. This evaluation was done with the purpose of determining the benefit of using measured camber data when available to improve pre-erection camber predictions.

Table 8.6 suggests that when measured initial camber is used, the time dependent multiplier method results in comparable predictions with those based on calculated initial camber using measured properties, however, the COV is larger indicating a lower degree of consistency in predictions.

Finally, the time dependent multiplier method was evaluated by comparing measured camber for four beams used in the Tiffin Street Overpass project at various points in time when they were in the precast facility. The results are shown in Table 8.7 and Fig. 8.15. Since the beams are theoretically identical predictions are also identical. However, as can be seen there are some differences in measured camber despite the fact the beams are identical. These differences are attributed to inherent variability and unintended variation from specifications. The time dependent multiplier method predicted camber growth rather well in beam G2-7, however, the accuracy in prediction reduced for the other beams. As stated earlier, one of the reasons for the variation of measured camber could be the influence of temperature gradients, which can be evaluated using the developed algorithm in Matlab.

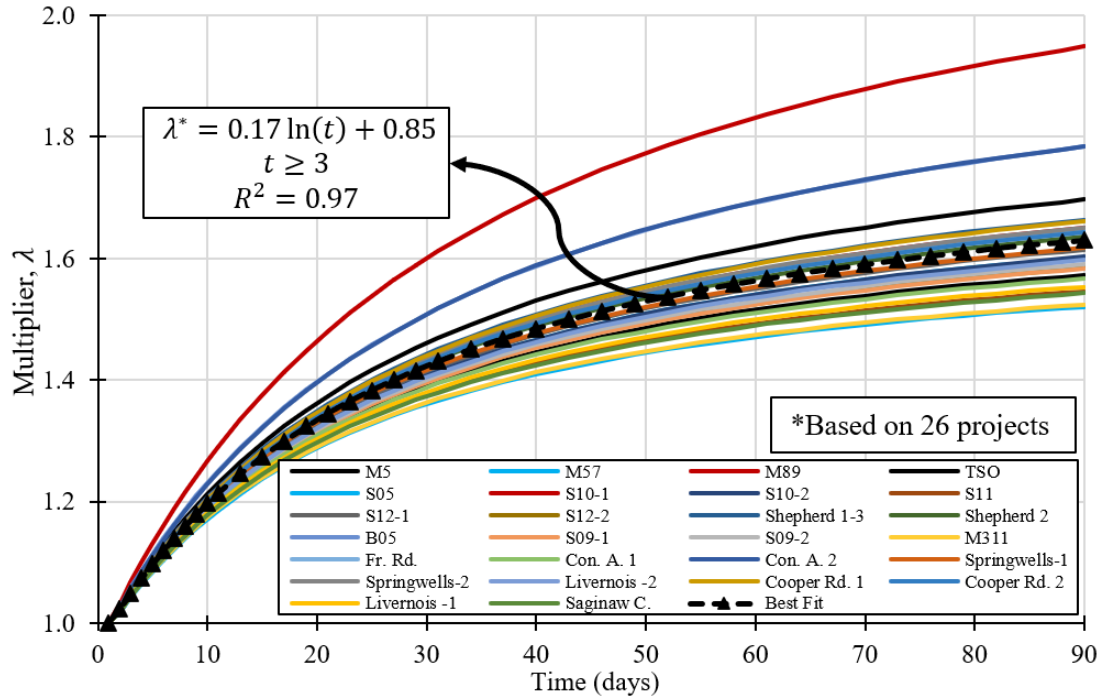


Fig. 8.14. Variation of multipliers as a function of time (prediction curves for each project are based on specified properties)

Table 8.4. Beam based comparison of several approaches for pre-erection camber

Pre-erection Camber								
Ratio	Δ_m/Δ_{pmp_m}	Δ_m/Δ_{pmp_s}	Δ_m/Δ_{p_m}	Δ_m/Δ_{p_s}	Δ_m/Δ_{PCI_m}	Δ_m/Δ_{PCI_s}	Δ_m/Δ_{MDOT_m}	Δ_m/Δ_{MDOT_s}
Min.	0.70	0.65	0.71	0.68	0.56	0.52	0.47	0.46
Max.	1.59	1.41	1.53	1.44	1.36	1.13	1.30	1.00
Avg.	1.02	0.96	1.06	0.98	0.82	0.78	0.73	0.68
St. Dev.	0.21	0.19	0.21	0.19	0.17	0.16	0.17	0.14
COV (%)	21	20	19	19	21	20	23	20
# of beams	82	90	82	90	82	90	82	90

Δ_m : measured camber; Δ_{pmp_s} : predicted camber based on proposed multipliers and specified properties; Δ_{pmp_m} : predicted camber based on proposed multipliers and measured properties; Δ_{p_s} : predicted camber based on analysis and specified properties; Δ_{p_m} : predicted camber based on analysis and measured properties; Δ_{MDOT_s} : predicted camber based on MDOT multipliers and specified properties; Δ_{MDOT_m} : predicted camber based on MDOT multipliers and measured properties; Δ_{PCI_s} : predicted camber based on PCI multipliers and specified properties; Δ_{PCI_m} : predicted camber based on PCI multipliers and measured properties;

Table 8.5. Comparison of proposed multiplier with different initial camber values

Statistical Indicators	Pre-erection Camber		
	Δ_m/Δ_{pmp_m}	Δ_m/Δ_{pmp_s}	Δ_m/Δ_{pmp_mm}
Min.	0.65	0.65	0.66
Max.	1.57	1.41	1.58
Avg.	0.92	0.96	0.92
St. Dev.	0.21	0.19	0.22
COV (%)	23	20	25
# of beams	80	90	72

Δ_m : measured camber; Δ_{pmp_s} : predicted camber based on proposed multipliers and specified properties; Δ_{pmp_m} : predicted camber based on proposed multipliers and measured properties; Δ_{pmp_mm} : predicted camber based on proposed multipliers and measured initial camber.

Table 8.6. Camber growth prediction for Tiffin Street Overpass Project using proposed time-dependent multiplier

Girder Name	Time at measurement (days)	Measured camber (in.)	Proposed Multiplier*	Estimated camber at release† (in.)	Estimated camber at measurement date (in.)	Measured camber / estimated camber
G2-6	9	2.61	1.22	1.79	2.19	1.19
G2-6	14	2.75	1.30		2.32	1.18
G2-6	16	2.88	1.32		2.37	1.22
G2-6	19	2.81	1.35		2.42	1.16
G2-6	22	2.88	1.38		2.46	1.17
G2-6	26	2.81	1.40		2.51	1.12
G2-6	28	2.78	1.42		2.54	1.10
G2-6	31	3.00	1.43		2.57	1.17
G2-7	12	2.53	1.27	1.79	2.28	1.11
G2-7	14	2.66	1.30		2.32	1.14
G2-7	17	2.72	1.33		2.38	1.14
G2-7	20	2.75	1.36		2.43	1.13
G2-7	24	2.53	1.39		2.49	1.02
G2-7	26	2.66	1.40		2.51	1.06
G2-7	29	2.84	1.42		2.55	1.12
G2-8	10	3.03	1.24	1.79	2.22	1.36
G2-8	13	2.81	1.29		2.30	1.22
G2-8	16	3.06	1.32		2.37	1.29
G2-8	20	3.09	1.36		2.43	1.27
G2-8	22	3.03	1.38		2.46	1.23
G2-8	25	3.22	1.40		2.50	1.29
G2-9	14	3.47	1.30	1.79	2.32	1.49
G2-9	18	3.47	1.34		2.40	1.45
G2-9	20	3.34	1.36		2.43	1.37
G2-9	23	3.53	1.38		2.48	1.43
*calculated by using proposed equation: $y = 0.17 \ln(t) + 0.85$. †obtained from Approach No. 6 using specified properties.					Min.	1.02
					Max.	1.49
					Ave.	1.21
					St. Dev.	0.12
					COV (%)	10

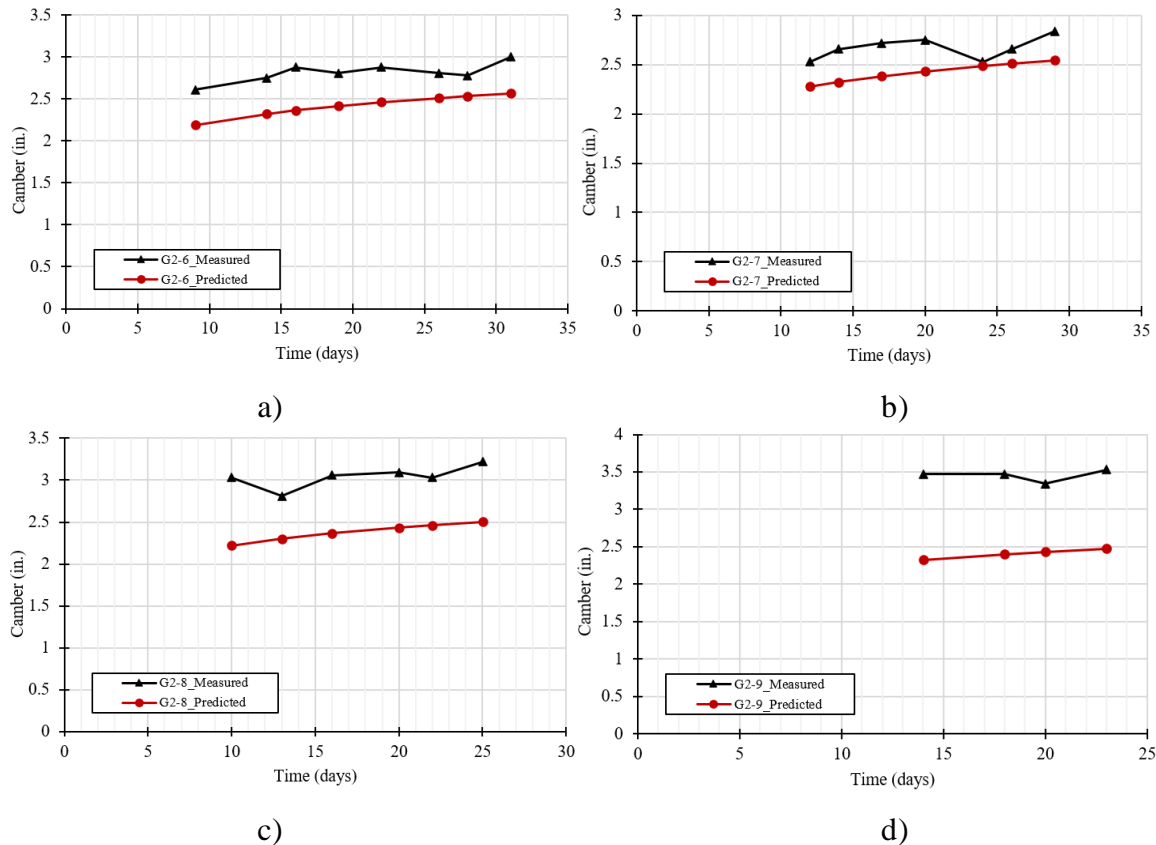


Fig. 8.15. Camber growth prediction for Tiffin Street Overpass Project using proposed time-dependent multiplier for: a) G2-6 beam; b) G2-7 beam; c) G2-8 beam; and d) G2-9 beam

8.9 Summary and Conclusions

- 1) With respect to predictions for camber at release, the proposed prediction methodology resulted in more accurate and consistent predictions than the current MDOT method regardless of whether measured or specified properties are used.
- 2) With respect to predictions for pre-erection camber the proposed prediction methodology resulted in more accurate and consistent predictions compared to the PCI multiplier method and MDOT multiplier method regardless of whether measured or specified properties are used. Additionally, predictions based on the Time Dependent Multiplier Method and Incremental Time Step method (Nilson 1987) were also more accurate compared to the PCI Multiplier Method and the MDOT multiplier method.
- 3) A time dependent multiplier method was derived for predicting pre-erection camber. This method should be used for preliminary design purposes and the proposed prediction methodology (Iteration No. 6) should be used for final design. The proposed time

dependent multiplier method led to more accurate predictions of pre-erection camber compared to the PCI multiplier method and MDOT multiplier method.

- 4) Most pre-erection camber and full displacement history predictions were based on creep and shrinkage models provided in the body of AASHTO LFRD Specifications (2020), the AASHTO LRFD (2020) equation for predicting modulus at prestress release and 28 days, and ACI 209R-92 model for predicting the variation of modulus with time. When compared to measured pre-erection camber values, this set of prediction models, inserted in the proposed prediction methodology, resulted in reasonably accurate pre-erection camber predictions. The proposed methodology allows the user to select various models for creep and shrinkage of beam and deck concrete, prediction of modulus at prestress release and 28 days, and its variation with time. The user is encouraged to evaluate the use of different models to obtain a sense for the anticipated variation of predicted camber and displacements.
- 5) Prestress losses predicted based on Iteration No. 6 and those predicted using AASHTO LFRD Specifications (2020) were similar. The Incremental Time Step Method (Nilson 1987) and Iteration No. 6 led to rather similar predictions of pre-erection camber.
- 6) Differences between predicted pre-erection camber based on Iterations No. 1-5 and Iteration No. 6 did not exceed 4%. Differences between predicted service camber without deck replacement based on Iterations No. 2-5 and Iteration No. 6 did not exceed 101%. Differences between predicted service camber with deck replacement based on Iterations No. 3-5 and Iteration No. 6 did not exceed 1795%.
- 7) The proposed prediction methodology (Iteration No. 6) requires that the user specifies the number of beam sections to be used in the time dependent analysis. It is recommended that this number is at least 51 to obtain accurate results.

Chapter 9: Summary and Conclusions

Chapter 9: Summary and Conclusions

A methodology for predicting camber and displacements in prestressed concrete and steel girder bridges was presented. For prestressed concrete beams the prediction methodology can be used to predict camber and displacements at any point in time during the life of the beam. For steel beams, the prediction methodology can be used to predict camber and displacements in the composite bridge system. The proposed methodology was based on six iterations each of which represents a theoretical improvement in prediction accuracy compared to the previous iteration. The last iteration (i.e. Iteration No. 6) is presented as an algorithm written in Matlab that features a graphical user interface. In addition to the proposed prediction methodology, two alternative methods for predicting pre-erection camber were evaluated. These include the Incremental Time Step method (Nilson 1987) and the Time Dependent Multiplier Method. The Time Dependent Multiplier Method was derived from the proposed prediction methodology using curve-fitting techniques. The following conclusions are drawn:

9.1 Chapter 3 - General:

- 1) The proposed prediction methodology can be used to predict camber and displacements at any point in time during the life of the bridge including cases in which the deck is replaced. The proposed methodology may be used for prestressed concrete and steel girder bridges.
- 2) The proposed prediction methodology considers the effects of concrete creep, shrinkage, and aging, as well as steel relaxation. The effects of differential shrinkage and differential creep as well as shrinkage induced creep are also considered. The proposed prediction methodology considers the effects of temperature gradients thus providing bracketed predictions for camber and displacements at any point in time.
- 3) Camber and displacement predictions obtained from the proposed prediction methodology are blind predictions, in the sense that no calibration is conducted to match measured camber values based on Michigan specific conditions, and all predictions are based on principles of engineering mechanics when internal force redistribution is considered. Empirical models are used to predict modulus of elasticity, creep and shrinkage of concrete, relaxation of prestressing strands, and expected concrete compressive strength.

9.2 Chapter 5 - Factors that Affect Prestressed Concrete Beam Camber

- 4) While it is determined that the unit weight of concrete, w , the magnitude of the prestressing force at jacking, $P_{jacking}$, and beam length, L , all have a significant influence on camber at release and pre-erection beam camber, it is determined that these parameters do not vary significantly from specified values and therefore do not represent a significant source of uncertainty.
- 5) Modulus of elasticity at release, E_{ci} , had a proportional influence on camber at release and pre-erection beam camber.
- 6) Similarly, beam compressive strength at release, f'_{ci} , also had a close to proportional influence on camber at release and pre-erection camber, although this influence was quantified through the use of compressive strength dependent equation for modulus of elasticity.
- 7) Transfer length, $L_{transfer}$, debonded length, $L_{debonded}$, support conditions during storage, $L_{overhang}$, and location of harping point, $L_{harping}$, influence camber at release and pre-erection camber at a degree that in some cases is worth considering.
- 8) The selection of the creep and shrinkage model has a marked influence on the prediction of pre-erection camber development.
- 9) The time when initial camber is measured appears to be an important parameter since marked differences were found between predicted camber at release and predicted camber during the first 10 days. The proposed prediction methodology (Iteration No. 6) provides the user the flexibility of accounting for the influence of all the abovementioned factors.

9.3 Chapter 6 - Factors that Affect Camber and Displacements in the Composite System

- 10) Factors that led to a single digit average % change in net camber and displacement due to the induced 10% change include: beam overhang length at precast facility (i.e. storage conditions), transfer length, debonded length, deck modulus, and beam overhang length at the bridge site.
- 11) Factors that led to a double digit average % change in net camber and displacement due to the induced 10% change include: beam concrete compressive strength at release and 28 days, beam concrete unit weight, beam concrete modulus of elasticity at release and 28

days, location of harping point, beam spacing, compressive strength of deck at 28 days, and unit weight of deck.

- 12) Factors that led to a triple digit average % change in net camber and displacement due to the induced 10% change include: beam length, and prestressing force.
- 13) The influence of the selected creep and shrinkage model on the full displacement history of a prestressed concrete beam bridge was investigated and it was concluded that this selection has a marked influence on the beam displacement history. Some models result in rather similar displacements after 75 years despite initial differences in pre-erection camber and net displacements after deck placement.
- 14) Influence of deck placement time on the full beam displacement history was investigated and it was concluded that while pre-erection camber is highly influenced by it, camber and displacements after 75 years were rather similar.
- 15) The influence of temperature gradients was rather uniform throughout the displacement history of the beam with positive temperature gradients having a higher influence on camber and displacements compared to negative temperature gradients.

9.4 Chapter 7 - Factors that Affect Beam Rebound and Behavior after Deck Replacement

- 16) Deck replacement time had no influence on the magnitude of beam rebound and net camber after deck removal provided that the deck is replaced at least after 40 years. Deck replacement time had a minor influence on the net camber before new deck placement with greater deck replacement times resulting in slightly lower net cambers before new deck placement.
- 17) The influence of solution method (Iteration No. 5 vs. Iteration No. 6) on beam rebound, net camber after deck removal, and net camber before new deck placement was investigated. It was determined that Iteration No. 6 leads to smaller rebounds compared to Iteration No. 5. Additionally, predictions based on Iteration No. 5 showed that there is no change between net camber after deck removal, and net camber before new deck placement whereas Iteration No. 6 suggests that there is a slight camber growth.

9.5 Chapter 8 - Evaluation of Various Design Procedures

- 18) With respect to predictions for camber at release, the proposed prediction methodology resulted in more accurate and consistent predictions than the current MDOT method regardless of whether measured or specified properties are used.
- 19) With respect to predictions for pre-erection camber the proposed prediction methodology resulted in more accurate and consistent predictions compared to the PCI multiplier method and MDOT multiplier method regardless of whether measured or specified properties are used. Additionally, predictions based on the Time Dependent Multiplier Method and Incremental Time Step method (Nilson 1987) were also more accurate compared to the PCI Multiplier Method and the MDOT multiplier method.
- 20) A time dependent multiplier method was derived for predicting pre-erection camber. This method should be used for preliminary design purposes and the proposed prediction methodology (Iteration No. 6) should be used for final design. The proposed time dependent multiplier method led to more accurate predictions of pre-erection camber compared to the PCI multiplier method and MDOT multiplier method.
- 21) Most pre-erection camber and full displacement history predictions were based on creep and shrinkage models provided in the body of AASHTO LFRD Specifications (2020), the AASHTO LRFD (2020) equation for predicting modulus at prestress release and 28 days, and ACI 209R-92 model for predicting the variation of modulus with time. When compared to measured pre-erection camber values, this set of prediction models, inserted in the proposed prediction methodology, resulted in reasonably accurate pre-erection camber predictions. The proposed methodology allows the user to select various models for creep and shrinkage of beam and deck concrete, prediction of modulus at prestress release and 28 days, and its variation with time. The user is encouraged to evaluate the use of different models to obtain a sense for the anticipated variation of predicted camber and displacements.
- 22) Prestress losses predicted based on Iteration No. 6 and those predicted using AASHTO LFRD Specifications (2020) were similar. The Incremental Time Step Method (Nilson 1987) and Iteration No. 6 led to rather similar predictions of pre-erection camber.
- 23) Differences between predicted pre-erection camber based on Iterations 1-5 and Iteration No. 6 did not exceed 4%. Differences between predicted service camber without deck

replacement based on Iterations No. 2-5 and Iteration No. 6 did not exceed 101%. Differences between predicted service camber with deck replacement based on Iterations No. 4-5 and Iteration No. 6 did not exceed 1795%.

- 24) The proposed prediction methodology (Iteration No. 6) requires that the user specifies the number of beam sections to be used in the time dependent analysis. It is recommended that this number is at least 51 to obtain accurate results.

References

- AASHTO LRFD Bridge Design Specifications. (2020). 9th ed., Washington, DC.
- ACI Committee 209.1. (2005). Factors Affecting Shrinkage and Creep of Hardened Concrete (ACI 209.1R). Farmington Hills, MI: American Concrete Institute.
- ACI Committee 209.2. (2008). Guide for Modeling and Calculating Shrinkage and Creep of Concrete (ACI 209.2R-08). Farmington Hills, MI: American Concrete Institute.
- ACI Committee 435. (2003). Control of Deflection in Concrete Structures (ACI 435R), Farmington Hills, MI: American Concrete Institute.
- ACI Committee 435/Subcommittee 5. 1963. Deflections of Prestressed Concrete Members. *Journal of the American Concrete Institute* 60 (12): 1697-1728.
- ASTM C512. 2002. Standard Test Method for Creep of Concrete in Compression. ASTM International. West Conshohocken, PA.
- Baldwin Jr, J. W., Guell, D. L. (1975). Permanent Deflections and Loss of Camber in Steel Bridge Beams. NCHRP Summary of Progress.
- Barr, P.J., and F. Angomas. 2010. Differences between Calculated and Measured Long-Term Deflections in a Prestressed Concrete Girder Bridge. *ASCE J. Perform. Constr. Facil.*, 24 (6), 603-609.
- Barr, P. & Stanton, John & Eberhard, M. (2005). Effects of Temperature Variations on Precast, Prestressed Concrete Bridge Girders. *Journal of Bridge Engineering - J BRIDGE ENG.* 10. 10.1061/(ASCE)1084-0702(2005)10:2(186).
- Bazant, Z. P. (1972). Prediction of concrete creep effects using age-adjusted effective. *Journal of the American Concrete Institute*, 69(4), 212-217.
- Bazant, Z. P., and Baweja, S., 1995, "Creep and Shrinkage Prediction Model for Analysis and Design of Concrete Structures—Model B3," *Materials and Structures*, V. 28, pp. 357-365, 415-430, 488-495.
- Bazant, Zdenek & Asce, Hon & Yu, Qiang & Li, Guang-Hua. (2012). Excessive Long-Time Deflections of Prestressed Box Girders. I: Record-Span Bridge in Palau and Other Paradigms. *Journal of Structural Engineering*. 138. 10.1061/(ASCE)ST.1943-541X.0000487.

- Branson, D. E., and Christianson, M. L. (1971). "Time Dependent Concrete Properties Related to Design—Strength and Elastic Properties, Creep and Shrinkage," Creep, Shrinkage and Temperature Effects, SP-27, American Concrete Institute, Farmington Hills, MI, pp. 257-277.
- Branson, D.E., Ozell, A.M. (1961). Camber in Prestressed Concrete Beams. Journal of the American Concrete Institute 57 (12): 1549-1574.
- Brown, K.M. 1998. Camber Growth Prediction in Precast Prestressed Concrete Bridge Girders. PhD Dissertation, University of Idaho.
- Buettner, D.R., Libby, J.R. (1979). "Camber" Requirements for Pretensioned Members." Concrete International, February 1979: 66-72.
- Cook, R.A., and D. Bloomquist. 2005. Field Verification of Camber Estimates for Prestressed Concrete Bridge Girders. Final Project Report, University of Florida, Tallahassee, FL: Florida Department of Transportation.
- Davison, B. 2014. Prediction of Time-Dependent Stresses and Deflections in Prestressed Concrete Girders: From Start of Fabrication to End of Service Life. MS Thesis, Seattle Washington: University of Washington.
- Dilger, W., Neville, A. M. (1971). Method of creep analysis of structural members. Special Publication, 27, 349-372.
- French, C.E., and C. O'Neill. 2012. Validation of Prestressed Concrete I-Beam Deflection and Camber Estimates. Final Report, University of Minnesota, St. Paul, MN: Minnesota Department of Transportation.
- Gardner, N. J., and Lockman, M. J. (2001). "Design Provisions for Drying Shrinkage and Creep of Normal Strength Concrete," ACI Materials Journal, V. 98, No. 2, Mar.-Apr., pp. 159-167.
- Gilbert, R. I., & Ranzi, G. (2010). *Time-dependent behaviour of concrete structures*. CRC Press.
- Granata, M., Margiotta, P., Arici, M. (2013). Simplified Procedure for Evaluating the Effects of Creep and Shrinkage on Prestressed Concrete Girder Bridges and the Application of European and North American Prediction Models. Journal of Bridge Engineering. 18. 1281-1297. 10.1061/(ASCE)BE.1943-5592.0000483.

- He, W. 2013. Creep and Shrinkage of High-Performance Concrete and Prediction of the Long-term Camber of Prestressed Bridge Girders. MS Thesis, Ames, Iowa: Iowa State University.
- Hinkle, S.D. 2006. Investigation of Time-Dependent Deflection in Long Span, High Strength, Prestressed Concrete Bridge Beams. MS Thesis, Blacksburg, VA: Virginia Polytechnic Institute and State University.
- Hofrichter, A. 2014. Compressive Strength and Modulus of Elasticity Relationships for Alabama Prestressed Concrete Bridge Girders. MS Thesis, Auburn, AL: Auburn University.
- Honarvar, E., Nervig, J., He, W., Rouse, J. M., Sritharan, S. (2015). Improving the Accuracy of Camber Predictions for Precast Pretensioned Concrete Beams.
- Huo, X.S. & Al-Omaishi, N. & Tadros, Maher. (2001). Creep, shrinkage, and modulus of elasticity of high-performance concrete. ACI Materials Journal. 98. 440-449.
- Imbsen, R.A., D.E. Vandershaf, R.A. Schamber, and R.V. Nutt (1985). Thermal Effects in Concrete Bridge Superstructures (NCHRP Report 276). Washington, DC: Transportation Research Board.
- Isbiliroglu, L. 2014. Predicting Time-Dependent Deformations in Prestressed Concrete Girders. MS Thesis, Auburn, AL: Auburn University.
- Jayaseelan, H., and B.W. Russell. 2007. Prestress Losses and the Estimation of Long-Term Deflections and Camber for Prestressed Concrete Bridges. Final Report, Stillwater, OK: Oklahoma State University.
- Jáuregui, David & White, Kenneth & Woodward, Clinton & Leitch, Kenneth. (2003). Noncontact Photogrammetric Measurement of Vertical Bridge Deflection. Journal of Bridge Engineering - J BRIDGE ENG. 8. 10.1061/(ASCE)1084-0702(2003)8:4(212).
- Johnson, Brandon Ray. Time-Dependent Deformation in Precast, Prestressed Bridge Girders. MS Thesis, Auburn, AL: Auburn University, 2012.
- Kelly, D.J., T.E. Bradberry, and J.E. Breen. 1987. Time Dependent Deflections of Pretensioned Beams (Research Report 381-1). The University of Texas at Austin, Austin, TX: Center for Transportation Research.
- Keraga, C. S. (2016). Development of Camber Multipliers for Precast Prestressed Box Girders, Master Thesis, University of Colorado Denver.

- Keske, S.D. 2014. Use of Self-Consolidating Concrete in Precast, Prestressed Girders. PhD Dissertation, Auburn, AL: Auburn University.
- Lee, J.H. 2010. Experimental and Analytical Investigations of the Thermal Behavior of Prestressed Concrete Bridge Girders Including Imperfections. PhD Dissertation, Atlanta, GA: Georgia Institute of Technology.
- Le Roy, R., De Larrad, F., Pons, G. (1996). The AFREM Code Type Model for Creep and Shrinkage of High-Performance Concrete. Utilization of high strength/high performance concrete. International symposium on the utilization of high strength high performance concrete. 2. 387-396.
- Lopez, Mauricio & Kahn, Lawrence & Kurtis, Kimberly. (2004). Creep and shrinkage of high-performance lightweight concrete. ACI Materials Journal. 101. 391-399.
- Mahmood, O.I. 2013. Camber Control in Simply Supported Prestressed Concrete Bridge Girders. MS Thesis, Lexington, KY: University of Kentucky.
- Mante, D. M. (2016). Improving Camber Predictions for Precast, Prestressed Concrete Bridge Girders (Doctoral dissertation), Auburn University, Auburn, Alabama.
- Mante, David & Barnes, Robert & Isbilioğlu, Levent & Hofrichter, Andric & Schindler, Anton. (2019). Effective Strategies for Improving Camber Predictions in Precast, Prestressed Concrete Bridge Girders. Transportation Research Record: Journal of the Transportation Research Board. 2673. 036119811983396. 10.1177/0361198119833965.
- Martin, L. D. 1977. "A Rational Method for Estimating Camber and Deflection of Precast Prestressed Members." PCI Journal 22 (1): 100–108.
- Michigan Department of Transportation (MDOT) (2018). "Special Provision for Structure Survey During Construction", Lansing, MI.
- Menkulasi, F., Patel, A., Baghi, H. (2018). "An investigation of AASHTO's requirements for providing continuity in simple span bridges made continuous" - Engineering Structures Journal, Volume 158, 2018, Pages 175-198.
- Menkulasi, F., Nelson, D., Wollmann, C.L.R., Cousins, T. (2015). "Reducing Deck Cracking in Composite Bridges by Controlling Shrinkage and Creep Properties", ACI Special Publication, SP-304 Sustainable Performance of Concrete Bridges and Elements Subjected to Aggressive Environments: Monitoring, Evaluation and Rehabilitation, pp. 21 -42.

- Menkulasi, F., Wollmann, C.L.R., Cousins, T. (2013). “Investigation of Time Dependent Effects on Composite Bridges with Precast Inverted T-Beams”, Proceedings of the PCI 2013 Convention and National Bridge Conference, September 21 -24.
- Menkulasi, F., Wollmann, C.L.R., Cousins, T. (2014a). “Investigation of Composite Action in Bridges Built with Adjacent Precast Inverted T-Beams and Cast-in-place Topping”, PCI 2014 Convention and National Bridge Conference, September 6-9.
- Menkulasi, F., Wollmann, C.L.R., Cousins, T. (2014b). “Investigation of Stresses in the End Zones of Precast Inverted T-Beams with Tapered Webs” PCI 2014 Convention and National Bridge Conference, September 6-9.
- Morcous, G., and M. K. Tadros. (2009). “Applications of Ultra-High Performance Concrete in Bridge Girders”, Nebraska Department of Roads (NDOR) report P310. Lincoln, NE: NDOR.
- Muller, H. S., and Hilsdorf, H. K., 1990, “General Task Group 9,” CEB Comité Euro-International du Béton, Paris, France, 201 pp.
- Nervig, J. 2014. Improving Predictions of Instantaneous Camber for Prestressed Concrete Bridge Girders (Paper 13817). MS Thesis. Iowa State University.
- Nguyen, H. T. N. (2014). Improving Predictions for Camber in Precast, Prestressed Concrete Bridge Girders. Master’s Thesis. University of Washington.
- Nilson, A. H. (1987). Design of prestressed concrete. Second Edition. John Wiley and Sons, 1987, New York, New York.
- Omar, W., T. Pui Lai, L. Poh Huat, and R. Omar. 2008. Improved Prediction of Pre - Camber of Post-Tensioned Prestressed I-Beam. Journal of the Institution of Engineers 69 (1):32-37.
- Partov, D., Kantchev, V. (2009). Time-Dependent Analysis of Composite Steel-Concrete Beams Using Integral Equation of Volterra, According EUROCODE-4. Engineering Mechanics. 16.
- Pauw, A. “Static Modulus of Elasticity as Affected by Density.” ACI Journal, 57(6): 679-683.
- PCI. 2010. PCI Design Handbook. 7th ed. Chicago, IL: PCI.
- PCI. 2011. PCI Bridge Design Manual. 3rd ed. Chicago, IL: PCI.
- PCI Committee on Bridges. 2012. Camber FAST Team. Chicago, IL: PCI.
- Raphael, J. (1985) “Tensile Strength of Concrete.” ACI Journal, 81 (2):158-165.

- Rosa, M.A., J. F. Stanton, and M.O. Eberhard. 2007. Improving Predictions for Camber In Precast, Prestressed Concrete Bridge Girders. Research Report, University of Washington, Seattle, WA: Washington State Transportation Center (TRAC).
- Schrantz, C.E. 2012. Development of a User-Guided Program for Predicting Time-Dependent Deformations in Prestressed Bridge Girders. MS Thesis, Auburn, AL: Auburn University.
- Shams, M. and Kahn, L.F. (2000). "Time-Dependent Behavior of High-Performance Concrete." Georgia Tech Structural Engineering, Mechanics and Materials Research Report No. 00-5, Georgia Department of Transportation Research Project No. 9510, April 2000, 395 pp.
- Stallings, J.M., and S. Eskildsen. 2001. Camber and Prestress Losses in High Performance *Concrete Bridge Girders*. Final Research Report: Project 930-373, Auburn, AL: Auburn University Highway Research Center.
- Stallings, J.M., R.W Barnes, and S. Eskildsen. 2003. Camber and Prestress Losses in Alabama HPC Bridge Girders. *PCI Journal* 48 (5): 2-16.
- Storm, T.K., S.H. Rizkalla, and P.Z. Zia. 2013. Effects of Production Practices on Camber of Prestressed Concrete Bridge Girders. *PCI Journal* 58 (1): 96-111.
- Tadros, M. K., Fawzy, F. F., Hanna, K. E. (2011). "Precast, prestressed girder camber variability", *PCI journal*, 56(1).
- Tadros, M.K., A. Ghali, and A.W. Meyer. 1985. Prestressed Loss and Deflection of Precast Concrete Members. *PCI Journal* 30 (1): 114-141.
- Tadros, M.K, N. Al-Omaishi, S.J Seguirant, and J.G. Gallt. 2003. Prestress Losses in Pretensioned High-Strength Concrete Bridge Girders (NCHRP Report 496), Washington, DC: National Cooperative Highway Research Program, Project 18-07.
- Trost, H. (1967). Auswirkungen des Superpositionsprinzips auf Kriech und Spannbeton, Beton und Stahlbetonbau, 62(10), 230-238, No. 11, 261-269.
- Waldron, Christopher J., "Investigation of long-term prestress losses in prestensioned high performance concrete girders," Ph.D. Dissertation, Department of Civil Engineering, Virginia Polytechnic Institute and State University, Blacksburg, A (November 16,2004) p.220.
- Wyffels, T.A., C.E. French, and C.K. Shield. 2000. *Effects of Pre-Release Cracks in High-Strength Prestressed Concrete*. Final Project Report, University of Minnesota, St. Paul, MN: Mn DOT Office of Research Administration.

- Yazdani, Nur & Mtenga, Primus & Richardson, N.. (1999). Camber Variations in Precast Bridge Girders. American Concrete Institute Concrete International. 21. 45-49.
- Zia, P., H. K. Preston, N. L. Scott, and E. B. Workman. (1979). "Estimating Prestress Losses." Concrete International 1 (6): 32-38.

APPENDIX A: PREVIOUS STUDIES

A.1 Buettner and Libby (1979)

Buettner and Libby (1979) explored several serviceability issues caused by inaccurate predictions of camber in prestressed concrete girders. The study documented the variation in the predicted and measured camber for 37 short span (less than 50 feet) bridge girders produced in Fairfax County, VA. The study concluded that there was consistent variability in the measured camber and the computational method used resulted in over predictions of camber. The errors in prediction were attributed to (1) inaccurate assumptions for the concrete compressive strength and modulus of elasticity, (2) using uncracked concrete properties when the section may have actually cracked, (3) inaccuracies in the assumed magnitude of the prestressing force, (4) shipping and erection times being inconsistent and/or inaccurate, and (5) a lack of consideration of the influence of temperature gradients. It was concluded that: (1) camber at release should be accurately recorded for all projects, (2) predicted camber should be noted in the shop drawings, and (3) the difference between the predicted and measured camber shall not exceed $L/1200$. It is not clear how many states are implementing the last requirements and what the ramifications for not meeting it are if it is implemented. However, in cases when it is implemented as a project requirement, any deviation from it can either result in the rejection of the beams or accommodations for the difference can be made. This research was the first to document the growing issues of inaccurate camber prediction and correctly hypothesized many probable causes for such inaccuracies.

A.2 Tadros et al. (1985)

Tadros et al. (1985) investigated methods for how to more accurately predict long-term camber by considering the influence of time dependent effects in prestressed concrete members. The goal of this study was to improve the predictions based on the PCI multiplier method proposed by Martin (1977) by considering the effects of higher strength concrete, relative humidity on creep and shrinkage, presence of non-prestressed steel, and concrete cracking. The developed method was a more elaborate multiplier method, which produced similar results in typical bridge girders under average environmental conditions with those obtained based on Martin's method. Despite this revision to the original multiplier method, the multipliers used in the PCI Bridge Design Manual (Precast/Prestressed Concrete Institute 2011) are unchanged and are still based on the work of Martin (1977).

A.3 Kelly et al. (1987)

Kelly, Bradberry, and Breen (1987) investigated camber growth in eight (8) – 127 ft long AASHTO Type IV high strength concrete bridge girders with low-relaxation steel tendons. The girders were monitored over a period of time, starting at the time of girder production and ending a year after entering service. The measurements during this period of time included concrete surface strains, prestressing strand strains, and deflections at quarter and mid-span. Internal beam temperature was also monitored and recorded. This set of data was used in evaluating various time-dependent methods used to calculate deflections. The study concluded that the rate at which concrete strength varies with time, concrete creep, relative humidity, age and strength of concrete at release, construction schedule, support conditions during storage are all factors, which influence time-dependent camber. The study also concluded that the introduction of regional practices into the PCI multiplier method increased the accuracy of predicting time-dependent camber.

A.4 Brown (1998)

Brown (1998) examined the methods for predicting camber growth used by the Idaho Department of Transportation (IDOT) for prestressed concrete girders at that time. Camber measurements were collected from four different prestressed concrete girder manufacturers and compared to camber predictions computed by then-current IDOT design procedures. It was found that the prediction method tended to underestimate camber at the time of prestress release. Primary conclusions from the study included the following: (1) the primary contributor to prestress losses at release is elastic shortening, while losses due to steel relaxation are minimal and can be neglected, (2) the incremental time-steps method (Nilson 1987) provided an accurate prediction of camber after calibration of creep and shrinkage coefficients, (3) a modified PCI multiplier method was developed to include local concrete material properties and a regionally appropriate construction timeline, and (4) relative humidity was not observed to significantly affect camber growth. It was stressed that the recommended camber prediction methods are based on estimates of the modulus of elasticity, ultimate creep coefficient, and ultimate shrinkage strain and should be validated by a future material testing program. Various methods to control camber growth in girders were also explored.

A.5 Yazdani et al. (1999)

Yazdani et al. (1999) monitored the camber growth in several AASHTO girders as part of a study for the Florida Department of Transportation (FDOT) to identify some of the reasons for the problems encountered during construction as a result of inaccurate camber predictions. It was determined that microcracks and vibrations affect girder stiffness and consequently camber predictions. Measured camber was always greater than predicted camber. It was also determined that the rate of camber growth was higher during the first month of storage and that camber in shorter girders was found to increase quicker than camber in longer girders. The average variation between predicted and measured camber ranged from 3-11% with maximum variations as high as 20%.

A.6 Wyffels et al. (2000)

Wyffels et al. (2000) investigated the influence of pre-release cracking due to formwork removal on prestressed concrete beam behavior for the Minnesota Department of Transportation (MnDOT) and concluded that: (1) compressive strength at the bottom of a section may be reduced as a result of cracks closing if the majority of pre-release cracking occurs above the neutral axis of the girder, and (2) bridge girders that have widespread pre-release cracking exhibit a reduced camber effect. It was noted that experimental testing is needed to validate these conclusions because despite evidence from the analytical models, some researchers still argue that pre-release cracking in precast, prestressed concrete bridge girders produces negligible effects due to the closing of the cracks upon prestress release and the corresponding autogenous healing which may occur thereafter.

A.7 Jáuregui et al. (2002)

Jáuregui et al. (2002) explored the use of digital close-range terrestrial photogrammetry (DCRTP) to estimate deflections in bridges. Two bridge structures were analyzed using DCRTP; a new bridge constructed with prestressed concrete, and a 64-year-old non-composite steel girder bridge. DCRTP measurements taken from the new bridge were compared with field-measurements during pre-erection, deck casting, and at service. The DCRTP measurements were found to compare well to field measured data. Also, live load deflections in the steel bridge were estimated using DCRTP and were found to be precise enough to capture the very small deflections produced

due to live loads. It was recommended that DC RTP could be used to accurately examine deflections and structural behavior in lieu of specialized instrumentation.

A.8 Stallings, Barnes, and Eskildsen (2003)

Stallings, Barnes and Eskildsen (2003) conducted a study for the Alabama Department of Transportation (ALDOT), which focused on evaluating various camber and prestress loss prediction methods for bridge girders constructed with high-performance concrete (HPC). Five BT-54 girders were instrumented and monitored. Mid-span camber, concrete strain, and internal temperature were measured and recorded throughout the duration of the project. Creep, shrinkage and modulus testing was conducted using HPC samples from the girders to determine such properties. The study concluded that: (1) By using actual material properties of the girder, both incremental and approximate time-step methods can produce accurate predictions of camber, (2) The PCI multiplier method significantly overestimated camber when compared to measured pre-erection camber, (3) strains in the concrete at the prestressing strand level was within 20 percent of predicted values for times up to 300 days, (4) accurate predictions of time-dependent prestress loss can be obtained using the HPC material parameters.

A.9 Waldron (2004)

Waldron investigated long-term prestress losses in pretensioned high performance concrete girders and monitored changes in strains and prestresses losses for nine high performance concrete (HPC) girders. It was concluded that Shams and Kahn (2010) model resulted in the best predictions of strain. For the normal weight HPC girders, the considered creep and shrinkage models underestimated the measured strains at early ages and over-estimated the measured strains at later ages, and the B3 model was the best-predictor of the measured strains. The PCI-BDM model was the most consistent model across all of the instrumented girders (Waldron 2004). Several methods for estimating prestress losses were also investigated and the PCI-BDM and NCHRP 496 methods predicted the total losses more accurately than the methods provided in the AASHTO Specifications at that time. The newer methods over-predicted the total losses of the HPLWC girders by no more than 8 ksi, and although they under-predicted the total losses of the normal weight HPC girders, they did so by less than 5 ksi (Waldron 2004).

A.10 Cook and Bloomquist (2005)

Cook and Bloomquist (2005) compared camber measurements of prestressed girders to numerical predictions. Funded by the Florida Department of Transportation (FDOT), part of the study monitored time-dependent deformations and surface temperatures of 13 precast prestressed concrete bridge girders. Data collected from the 13 girders was compared to predicted camber using the software package *PSBEAM*. To account for the effects of temperature gradients on field-measured camber, a curvature-based model was used, which provided consistent comparisons between measurements regardless of ambient conditions. The research concluded that: (1) the observed camber increase with time for the field-monitored girders was significantly less than predicted by design software, (2) future work is needed to experimentally determine the creep and shrinkage properties of typical FDOT concretes, (3) the influence of thermal gradients on camber must be accounted for in field measurements, (4) storage conditions (namely, the height between the bottom of the girder and the ground) seem to affect the development of time-dependent concrete properties and, therefore, can affect the time-dependent development of camber, and (5) consistent differences were documented between camber measurements taken at prestress release and measurements taken shortly thereafter when girders were relocated to storage. Also, FDOT sponsored a follow-up study performed by Tia, Liu, and Brown (2005) to examine modulus of elasticity, creep, and shrinkage behavior for various FDOT concrete mixes.

A.11 Barr et al. (2005)

Barr et al. (2005) examined five precast, prestressed concrete girders throughout fabrication and service to determine the influence of elevated curing temperatures on prestress losses. The study was funded by the Washington Department of Transportation (WSDOT) and the data collected was also used to produce and validate a temperature correction procedure based on curvature. The study concluded that: (1) based on the observed thermal behavior of the girders, a curvature-based approach was developed and proved to accurately predict deformations and stresses due to thermal response, and (2) mid-span camber decreases significantly from elevated curing temperatures observed in precast, prestressed concrete due to significant loss in prestressing force.

A.12 Hinkle (2006)

Hinkle (2006) used data collected from twenty-seven high-strength prestressed bridge girders to determine the most accurate method to predict time-dependent camber. The study, conducted in South Carolina, used 79 in. Bulb Tee beams with a design compressive strength of 9,000 psi. The girders were periodically measured to determine camber growth over time. An incremental time-step method (Nilson 1987) was employed using changes in beam curvature to predict camber and compare it with measured values. The study considered the effect of season of casting as well as the effects of solar radiation on camber growth. It was concluded that: (1) camber in girders could vary up to 0.5 inches during the day due to solar exposure, (2) the PCI multiplier method tended to overestimate camber by 48 percent at an age of 60 days, (3) the revised PCI multiplier method (proposed by Tadros et al. 1985) tended to overestimate camber by 21 percent at an age of 60 days, and (4) for all 27 beams studied, the incremental time-step method (Nilson 1987) using the estimated creep, and shrinkage, as well as modulus of elasticity calculated based on the model developed by Shams and Kahn (2000), resulted in camber predictions that best matched the measured camber values.

A.13 Rosa et al. (2007)

Rosa et al. (2007) collected short term camber data for 146 girders and long term camber data for 91 girders as part of a study funded by WSDOT. Camber was measured at various girder ages. Data on compressive strength, modulus, creep and shrinkage behavior of girders were also recorded. These data were then used to calibrate constitutive models for use in a prediction framework. The calibrated material models were used in an incremental time-step method (Nilson 1987) and resulted in improved camber predictions. Recommendations regarding concrete strength, stiffness, and creep and shrinkage behavior were presented. Additionally, it was concluded that the effect of lifting and re-seating a girder tended to increase the measured camber by 0.15 in., and that girders stored on oak blocks tended to behave as if they were approximately 50 percent stiffer than those seated on elastomeric bearings (attributed to the partial restraint provided by oak blocks).

A.14 Jayaseelan and Russell (2007)

Jayaseelan and Russell (2007) studied prestress losses and camber in an AASHTO Type IV girder detailed to typical Oklahoma Department of Transportation (OKDOT) specifications and arrived at the following conclusions: (1) expected camber was reduced by 35% by adding two top prestressing strands and 70% by adding four strands, (2) long-term camber decreased by approximately 17% due to the addition of five No. 9 mild steel bars in the longitudinal direction, although this did not significantly affect long-term losses, (3) decreasing the creep coefficient by 20% yields a 6.8% decrease in long-term camber, and (4) reducing the modulus of elasticity by 20% yields 6% increase in long-term prestress loss and a 12% increase in long-term camber.

A.15 Omar et al. (2008)

Omar et al. (2008) conducted a study on camber prediction for prestressed concrete girders in Malaysia where “camber” is referred to as “pre-camber”. Similar to other researchers, Omar recommended the use of actual material properties in terms of concrete compressive strength and stiffness for computation of pre-camber. It was determined that the time-dependent change in pre-camber after girder fabrication could be modeled by a proposed equation similar to the PCI multiplier method. The proposed equation takes into account creep effects and assumes an average prestressing force. Through the proposed method, it was found that the accuracy of pre-camber predictions could be improved significantly for time periods up to 15 days from girder fabrication.

A.16 Barr and Angomas (2010)

Barr and Angomas (2010) revisited a previous study conducted by Barr et al. (2005) and offered a revised analytical procedure. The new procedure provided a better match between predicted and observed behavior in the field in the precast, prestressed concrete girders used in the study. It was found that: (1) computed reduction in camber due to high curing temperatures was 33% rather than 40% as previously calculated, (2) a reduction in strand stress and non-uniform temperature gradients at estimated time of bonding are produced from elevated curing temperatures, which cause a change in camber, (3) by employing an incremental time-step method (Nilson 1987) and using material properties as suggested by Tadros et al. (2003) in NCHRP Report 496, camber was predicted to within 10% of measured long-term camber, and (4) camber was observed to be 22% lower than that obtained using the PCI multiplier method (Martin 1977), and

27% higher than that obtained using the modified multiplier method developed by Tadros et al. (1985).

A.17 Lee (2010)

Lee (2010) investigated thermal effects in prestressed concrete girders both experimentally and analytically. Using a segment of a BT-63 prestressed concrete girder, Lee measured environmental conditions and created finite element models to calculate vertical and lateral displacements. Both a two-dimensional heat-transfer model and a three-dimensional solid model were used in the analysis. After validating the analytical model with experimental data, four PCI girder shapes were selected, and maximum vertical and lateral deflections due to thermal effects were predicted with the model. It was found that the deeper and wider sections of Type-V and BT-63 girders exhibited the largest vertical and transverse temperature differentials. The research suggested that more experimental and analytical investigations be performed on prestressed concrete girders from the construction stages until service load conditions.

A.18 Tadros et al. (2011)

Tadros et al. (2011) reviewed the most-current camber prediction methods for precast, prestressed concrete girders and also discussed the variability in camber and best practices for accommodating this variability in design. The following were concluded: (1) when detailing bridges, designers should consider camber variations of up to 50% from the predicted design values, (2) all bridges should be designed with a minimum girder haunch of 2.5 in., (3) shear reinforcement should be detailed to accommodate camber variability by keeping protruding bars vertical prior to erection and bending on-site to final elevations, (4) girder seats should be finalized near the time of girder installation to accommodate variable elevations, (5) contractor pay items based on concrete volume should be avoided and instead, the contractor should account for girder variability in their initial bid, and (6) designers should accommodate local material properties and storage and construction practices during design, if practical.

A.19 French and O'Neill (2012)

French and O'Neill (2012) used data recorded from 1,067 bridge I-girders as part of a study sponsored by the Minnesota Department of Transportation (MNDOT) and determined that camber

at release was over-predicted by 74% and camber at erection was over-predicted by 86%. The over-predictions resulted primarily from variations in the concrete compressive strength and consequently modulus of elasticity used in the calculations. Field testing was performed on a limited number of concrete samples to determine strength and stiffness. In addition, 14 various sized girders were monitored for time-dependent deflections from time of fabrication through shipment. Time-dependent effects on long-term camber were evaluated using an analytical model which was used to validate a multiplier based prediction model for use by MNDOT. It was concluded that their multipliers greatly improved pre-erection camber predictions. The study also gave recommendations on fabrication methods to reduce the variability of girders produced. By using the combined multipliers and guidelines for fabrication it was suggested that variability in camber could be reduced to less than $\pm 15\%$.

A.20 Schrantz (2012)

Schrantz (2012) developed a Visual Basic based computer program to predict long-term camber in prestressed concrete beams. The computer program takes into account creep, and shrinkage effects in addition to modulus of elasticity and was validated using measured strain and camber data from Boehm (2008), Levy (2007), and Stallings et al. (2003). The computer program was used to evaluate various prediction models in terms of their capability to accurately predict camber. The work of Schrantz (2012), was later refined by Johnson (2012), and also used by Mante (2016) to develop a prediction method based on an incremental time-step approach (Nilson 1987).

A.21 Johnson (2012)

Johnson (2012) collected camber data on 28 bulb-tee girders constructed with self-consolidating concrete supplied for an Alabama Department of Transportation (ALDOT) bridge project. Predictions of time-dependent camber were compared to actual measurements taken over the course of the project. Material testing was conducted to determine time-dependent properties. The following conclusions were drawn: (1) when considering the bottom-flange of girders, time-dependent strain predictions were reasonably accurate for all creep and shrinkage models used, (2) concrete strains were over-estimated at later girder ages, (3) the effective prestressing force was overpredicted in the first months after prestress transfer and underpredicted at later ages, (4) measured mid-span camber was usually less than predicted for ages up to 200 days, and (5) none

of the time-dependent models used predicted camber growth well. The study demonstrated that improved methods for predicting time-dependent camber growth needed to be developed for ALDOT, which was later addressed by Mante (2016).

A.22 Precast/Prestressed Concrete Institute Committee on Bridges (2012)

The PCI Committee on Bridges (2012) conducted a study to evaluate the construction tolerances for camber in prestressed concrete bridge girders specified by then current PCI standards. Camber values were collected for 1,835 bridge girders from eight different states for analysis. Using the measured and predicted camber values of these girders, changes to the allowable camber tolerances at release were recommended. The Committee recommended increasing the tolerance limits to match historical data. The percent of predictions that were within the new tolerance limits increased to 90% compared to the 66%, which was based on the old tolerance limits.

A.23 Bažant et al. (2012)

Bažant et al. (2012) investigated long-term deflections in a segmental prestressed concrete box girder bridge located in Palau, . The span of the bridge was 791 ft; the bridge was erected in 1977 and collapsed in 1996 after failed attempts to repair it. At the age of 18 years, the bridge was found to have a measured mid-span camber 5.3 ft greater than the design camber. Results from finite element models were compared to time-step predictions using creep and shrinkage models from then-current provisions of American Concrete Institute, Japan Society of Civil Engineers, Comité Euro-International du Béton, and Gardner and Lockman (2000) recommendations. These prediction models were found to provide inaccurate estimates of the effects of long-term creep and shrinkage. For 18-year deflection estimates, the models were 50–77% lower than measured deflections and yielded unrealistic shapes of the deflection history. They also predicted the 18-year prestress loss to be 46–56% less than measured. The analysis done by Bažant et al. (2012) emphasized the importance of accurate calculations for time-dependent properties and prestress losses. Future work was recommended to develop newer, more accurate prediction models.

A.24 Storm et al. (2013)

Storm, Rizkalla, and Zia (2013) performed a study on various factors affecting prediction of camber, with a focus on the factors related to girder fabrication. A field study was conducted using 382 pretensioned concrete girders from nine different states. Camber measurements from the 382 girders were collected and analyzed from four different stages: (1) immediately after prestress transfer, (2) at the beginning of storage, (3) prior to shipping, and (4) after erection. A laboratory study was also conducted to obtain compressive strength, modulus, and unit weight of concrete at various ages. It was concluded that: (1) Camber predictions should account for the typically higher compressive strength at prestress transfer and service compared with specified values, (2) camber predictions should consider debonding and transfer length, especially for girders with long debonding lengths, (3) curing method can significantly affect camber at time of prestress, (4) Measured camber can vary significantly among girders that are identical in their design even for girders cast at the same time on the same casting bed, this is due in part to multiple batches of concrete being used for a single casting and (5) A refined method (time-step method) provides the most accurate camber predictions for most girder types and curing methods, while the approximate method (PCI multiplier) generally overestimates camber at erection, but can still be useful for preliminary estimates.

A.25 Mahmood (2013)

Many of the studies discussed so far were concerned with the topic of how to accurately predict camber. Another topic of interest is how to control camber in cases when camber is initially higher than predicted and consequently grows to higher than predicted values. Mahmood (2013) explored the feasibility of controlling camber in simply-supported prestressed concrete bridge girders by using post-tensioned strands. This theoretical study also considered the reduction in load capacity of the girder. The research demonstrated that using the post-tensioned strands to control camber was proved to be a feasible option and that the method resulted in minimal reduction to load-carrying capacity. For instance, an AASHTO Type IV girder experienced a load-carrying capacity reduction of 2.9 % per 100 kips of jacking force. Recommendations for future studies include: (1) using other girder types to further investigate the effects of such a camber control method; and (2) conduct a study on the practicality of the proposed method.

A.26 He (2013)

He (2013) conducted a study for the Iowa Department of transportation on improving prediction of long-term camber in prestressed concrete girders. Seven concrete mixes with regional properties were tested for modulus of elasticity, creep and shrinkage. The recorded properties were used to compare several prediction techniques to the camber measured in 26 prestressed high-performance concrete girders. Conclusions from the work include: (1) the prediction method in current use over predicts camber by 30% in long-span bridges, (2) modulus of elasticity in concrete varied by 205 between the AASHTO (2012) predicted values and measured values, (3) sealed concrete specimens tended to represent the creep and shrinkage behavior of the full scale prestressed girder better than unsealed specimens, (4) when calculated by gross section properties instead of transformed section properties, girder camber was on average 13 percent higher, (5) the time-steps method implemented in this study predicted camber within 25 percent accuracy, and (6) about 50% of ultimate camber growth had occurred one year after girder production.

A.27 Nervig (2014)

Nervig (2014) performed a study funded by the Iowa Department of Transportation (IDOT), focusing on improving camber at release estimates for concrete bridge girders. The camber at release of 105 prestressed concrete beams was measured and compared to predicted values. Inconsistent field measurement methods and inaccurate estimates of material properties were found to be the main cause for discrepancies in camber at release estimates. To increase the accuracy of camber at release estimates, Nervig (2014) recommended that: (1) AASHTO LRFD (2010) equation for transfer length should be used in calculations, (2) using AASHTO LRFD (2010) modulus of elasticity equation with an accurate release strength and unit weight will improve camber predictions, (3) designers should increase the design release strength by 40% and 10% for beams with designed release strength of 4500-5500 psi and 6000-8500 psi, respectively, (4) actual prestressing force should be used for calculations, as well as accurate prestressing losses, and (5) sacrificial prestress strands should be accounted for as they can affect camber by as much as 6.46%.

A.28 Hofrichter (2014)

Provided that many previous studies emphasized the use of measured material properties to obtain more accurate estimates of camber, Hofrichter (2014) conducted a study to establish a relationship between specified and measured properties so that this information can be used during the design phase. Compressive strength data from more than 1,900 prestressed concrete beams was collected. The beams were fabricated in Alabama and consequently the collected data was regionally exclusive to Alabama. The collected data was used to refine methods for predicting average concrete compressive strength at prestress transfer and at 28 days. It was found that release strengths and 28-day strengths are often much higher than the specified strengths, more so for the 28 day strengths. An strength prediction equation was proposed which incorporated an assumed aggregate factor. The proposed equation resulted in better prediction of compressive strength and modulus of elasticity.

A.29 Isbilibiroglu (2014)

Isbilibiroglu (2014) expanded on the work of Schrantz (2012) and Johnson (2012) to finalize a camber prediction software that incorporated an incremental time-step method (Nilson 1987). Experimental research produced by Johnson (2012), Schrantz (2012), Boehm (2008), Stallings et al. (2003), and Levy (2007), were used in validation of the program. Isbilibiroglu (2014) worked to improve the camber prediction software by: (1) Allowing the user to import and export files, creating an easier-to-use interface, (2) refining material prediction models and utilizing newer design code parameters; and (3) including recommendations made by Hofrichter (2014) and Keske (2014).

A.30 Nguyen (2014)

Nguyen (2014) explored methods to predict camber in precast, prestressed concrete girders, with a focus on the effects of temperature on camber during curing and in while in service. Historical data from Rosa et al. (2007) was used, as well as new data acquired from the fabrication of nine girders for the Alaska Way Viaduct project in Tacoma, WA. Research focused on using both fabrication camber and field-measured camber to calibrate models predicting camber. The effect of daily temperature variations on girder camber was also studied using recorded temperature histories at release and service. Two models were developed to predict daily camber

changes under solar radiation, which correlated well with the ambient temperature data collected during the research. Some notable conclusions from the study include: (1) using actual, rather than design compressive strength will improve camber predictions, especially for long-term camber, (2) camber estimates using the elastic modulus from the AASHTO 2006 and ACI 363 recommendations tended to overestimate the measured camber, (3) the NCHRP 496 method of calculating the elastic modulus led to better predictions of camber, (4) girder camber is significantly affected by daily variations in the girder temperature distribution and the effects should be considered in estimating the camber, and (5) thermal effects are potentially major causes of the discrepancies between measured and predicted release camber.

A.31 Honarvar et al. (2015)

Honarvar et al. (2015) conducted a study funded by the Iowa Department of Transportation (IDOT) to address discrepancies between the design and measured camber in precast pretensioned concrete beams. IDOT's current practice at the time of study was to perform elastic analysis and apply Martin's multipliers (1977) to estimate the camber at release and erection. This method was observed by IDOT to frequently overpredict camber. The study included material testing for creep and shrinkage of both normal and high-performance concrete specimens, as well as identified other variables affecting camber. Long-term camber was evaluated using finite element analysis and time-step methods. The study resulted in new multipliers for camber that, when used with accurate camber at release measurements greatly increase the accuracy of predicted camber.

A.32 Keraga (2016)

Keraga (2016) compared predicted and measured camber for a variety of prestressed concrete box girder bridges and recommended a set of multipliers including lower and upper bounds. The recommended multipliers are lower than those recommended by PCI and Martin (1977) and are 1.65 for the prestress camber and 1.70 for the self-weight deflection.

A.33 Menkulasi et al. (2018)

Menkulasi et al. (2018) performed a study on the restraint moments developed in simple span bridges made continuous for live loads. Long-term beam camber was also examined by comparing predicted and measured values as camber growth affects the magnitude of restraint

moments after continuity has been established. It was concluded that camber predictions based on the AASHTO (2020) and CEB MC90-99 models matched rather well with measured values, while the ACI 209R-92 model resulted in slightly higher camber values, and the GL2000 and B3 models overestimated beam camber significantly.

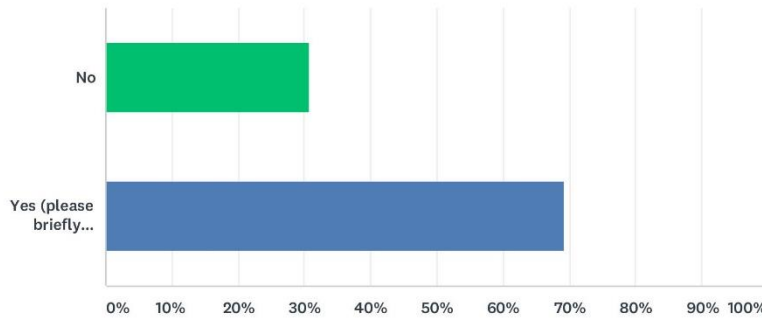
A.34 Mante et al. (2019)

Mante et al. (2019) conducted a comprehensive camber prediction study sponsored by the Alabama Department of Transportation (ALDOT). The research objective was to provide practical recommendations to improve camber predictions for precast, prestressed concrete bridge girders. The study incorporated concrete materials data from nearly 2000 girder production cycles among four regional producers, the data was used to develop regional calibration factors for properties essential in predicting camber growth, including compressive strength, modulus, creep, and shrinkage. A standard incremental time-step analysis software (ALCAMBER V1.0) was developed and utilized for conducting a parametric study. Using the developed regional calibration factors resulted in the elimination of approximately 80% of the prediction error associated with current camber prediction practices within the region. Current design practices resulted in a mean over prediction in camber of 68% whereas regionally calibrated prediction models had a mean over prediction of approximately 10%. Using expected vs. specified compressive strength values, aggregate correction factors for modulus of elasticity, and incremental time-step method (Nilson 1987), was shown to have the most effective improvement in predictions.

APPENDIX B: CAMBER SURVEY

Q1 Have you ever experienced any camber related problems with prestressed concrete bridge beams that are often beyond normal construction tolerances?

Answered: 39 Skipped: 4



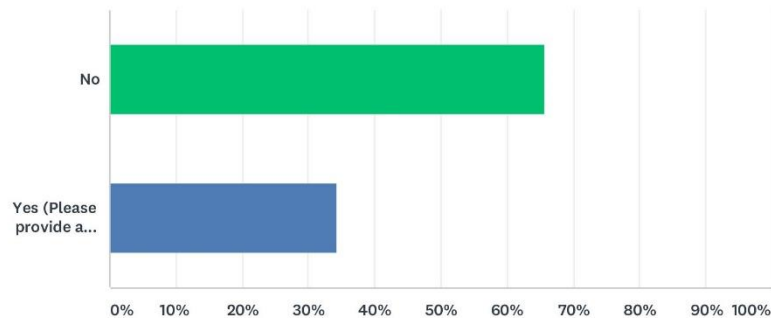
ANSWER CHOICES	RESPONSES	
No	30.77%	12
Yes (please briefly describe)	69.23%	27
TOTAL		39

#	YES (PLEASE BRIEFLY DESCRIBE)	DATE
1	We have had instances where cambers greatly exceeded the normally expected values. In rare cases, these girders had to be re-cast because they could not be made to fit into the bridge elevation profiles using normal mitigation measures. Other more common cases involve girders fabricated at the same time but with large variations in storage duration due to project phasing. The second phase girders usually arrive with higher cambers than the 1st phase girders but no adjustment of the bridge grades can be made to accommodate the 2nd phase girders	9/12/2019 4:44 AM
2	Occasionally, actual camber exceeds the provided camber strip thickness between the top of girder and bottom of deck. When this occurs, an adjustment to the finished grade profile is required to maintain minimum deck thickness.	8/26/2019 10:55 AM
3	Camber that is over tolerance as well as the opposite, situations where the cast deck results in beams having negative camber.	8/21/2019 7:12 AM
4	Note that all answers herein assume your questions are regarding pretensioned beam members (p/t members are not addressed). In the early 2000s, it was observed that cambers were typically much lower than predicted.	8/12/2019 11:40 AM
5	The actual camber was less than the predicted camber. Thus, the erected beams once the deck was placed resulted in zero to negative camber. We are monitoring a few bridges built to this situation.	8/12/2019 6:42 AM
6	There has been camber variation greater than the maximum 1 inch tolerance per MNL-116 Appendix B, B-10 I-Beam (Girder) or Bulb Tee-Girder.	8/9/2019 9:09 AM
7	Trey Carroll, thcarroll1@ncdot.gov, 919-707-6465, submitting for North Carolina DOT. Before NCDOT's camber research project was implemented camber predictions (particularly for cored slabs and box beams) were not reliable.	8/7/2019 7:45 AM
8	Sometimes camber between adjacent beams is not similar and camber calculated by AASHTO equations is not the same as the camber in the fabricator's shop.	8/7/2019 3:27 AM

9	The primary issue appears to be with prestressed beams that sit at the fabricator unloaded for extended (6 mo +) period prior to deck placement. This is especially problematic for project built in phases when the beams are all cast at once. The camber growth between phases is critical.	8/6/2019 9:15 AM
10	The camber of the beams is sometimes inconsistent between abutting beams and the value calculated by AASHTO equations is lower than what is seen at the precast plant.	8/6/2019 6:22 AM
11	Most bridges are ok, but at times there is variance between girders.	8/6/2019 5:01 AM
12	For the most part, projects seem to be within tolerance, but can occasionally have variance between girders.	8/6/2019 4:55 AM
13	Problems with prestressed concrete bridge members are typically experienced where members are cast more than three months prior to planned erection. Contractors are assumed to schedule this early fabrication typically to ensure members are available for their planned erection schedule and, for multi-stage projects, to achieve potential cost savings or ease of fabrication. In the case of multi-stage projects, the period between staged erection could be 6 months or in excess of one year. Problems with prestressed concrete bridge members are also typically experienced where a member depth is selected in the lower range of applicability and a larger number of strands and higher concrete strength are used accordingly.	8/5/2019 12:10 PM
14	It has been difficult sometimes to get the predicted camber	8/2/2019 9:04 AM
15	Our primary issue is the discrepancy between the estimated time and actual time of girder placement after strand are released. Girders that are estimated to camber up may actually sag when construction is accelerated.	8/2/2019 8:13 AM
16	We have had over cambering occur due to beams not being put in service soon enough such construction delays	8/2/2019 7:48 AM
17	Camber growth that compromises the deck thickness.	8/2/2019 4:58 AM
18	In long-span (greater than 120-feet) bulb-tee girders (such as the SCDOT Modified 72" Bulb Tee), we have had multiple cases where the camber did not grow as much as the PCI equations predict. In these examples the concrete strength was 10ksi (min.).	8/1/2019 3:27 PM
19	We had a beam with zero camber that we rejected due to concerns over loss of prestress. The beam was rejected.	8/1/2019 12:47 PM
20	Beams that have excessive camber and beams have less than designed for camber.	8/1/2019 3:46 AM
21	Most of the time, large cambers were observed where debonded strands design was utilized. Other occasions camber growth was an issue. Long term issues were related to girders designed with no tension allowed at final condition	7/31/2019 1:05 PM
22	In the past, we have had issues with cambers not matching the values that were calculated using the AASHTO equations. In response, we developed our own equations that are included in our bridge design manual.	7/31/2019 12:44 PM
23	Many factors affect cambers, such as concrete mix/strength/quality/curing, rest time (from fabrication to installation), prestressing force, section properties, formulas for calculating camber and so forth. We added Camber Management Plan in the specifications to mitigate this issue. We also adjusted the tolerances.	7/31/2019 12:20 PM
24	Most issues are from beam camber growth from sitting in the fabricator's yard too long.	7/31/2019 11:42 AM
25	Have camber issues fairly often, especially when the beams are made far in advance.	7/31/2019 11:36 AM
26	A couple of bridges over the last 5 years have less camber than estimated. The constructed bridges essentially have zero or negative camber. We are monitoring (elevation survey) these couple of bridges to determine if we are continuing to lose camber. To date these bridges are functioning adequately.	7/31/2019 11:35 AM
27	Increased amount of camber that caused fit up issues with adjacent beams on a high skewed bridge	7/31/2019 11:22 AM

Q2 Have you conducted or sponsored any research related to prestress losses, camber, and deflections?

Answered: 38 Skipped: 5



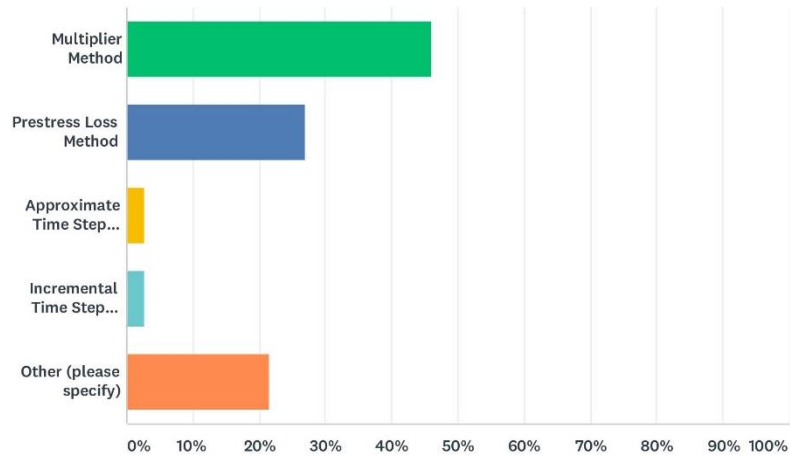
ANSWER CHOICES	RESPONSES	
No	65.79%	25
Yes (Please provide a reference to your report and indicate whether the results of the research have been implemented into your state's practices)	34.21%	13
TOTAL		38

#	YES (PLEASE PROVIDE A REFERENCE TO YOUR REPORT AND INDICATE WHETHER THE RESULTS OF THE RESEARCH HAVE BEEN IMPLEMENTED INTO YOUR STATE'S PRACTICES)	DATE
1	Sinno, Raouf. The Time-Dependent Deflections of Prestressed Concrete Bridge Beams, Ph.D. Dissertation, Texas A&M University, College Station, Texas, January 1968. Kelly, D. J., Bradberry, T. E., and Breen, J. E. "Time-Dependant Deflections of Pretensioned Beams," Research Report 381-1, Research Project 3-5-84-381, Center for Transportation Research, Bureau of Engineering Research, The University of Texas at Austin, Austin, TX (August 1987) 211 pp. URL: https://library.ctr.utexas.edu/digitized/texasarchive/phase2/381-1-CTR.pdf We used this research to design beams, until we adopted PGSuper for prestressed concrete girder design. We now use the same method used by the program.	9/12/2019 4:44 AM
2	Report No. UT-09.10: UDOT Calibration of AASHTO's New Prestress Loss Design Equations Link: https://www.udot.utah.gov/main/uconowner.gf?n=7904804259161866	8/26/2019 10:55 AM
3	A small internal study resulted in changing camber multipliers from the PCI values to a value of 1.5. We also sponsored a camber study to confirm/change the camber multiplier. The result was implementation of a slightly modified approach using a multiplier of 1.4. Report is "Validation of Prestressed Concrete I-Beam Deflections and Camber Estimates", which can be found at: https://www.lrrb.org/media/reports/201216.pdf	8/12/2019 11:40 AM
4	Keraga, Cody. Development of Camber Multipliers for Precast Prestressed Box Girders. 2016, digital.auraria.edu/content/AA/00/00/51/37/00001/Keraga_ucdenver_0765N_10686.pdf . This has been implemented into the state's practice by allowing a camber tolerance for precast girders. This tolerance is used in the design.	8/9/2019 9:09 AM
5	NCDOT sponsored research titled "Predicting Camber, Deflection, and Prestress Losses in Prestressed Members" and results from this report have been successfully implemented. https://connect.ncdot.gov/resources/Structures/Pages/Structure-Resources.aspx	8/7/2019 7:45 AM
6	We looked at girder camber values of 800 girders and compared those values to the theoretical value at release. From this, we require a multiplier of 1.4.	8/6/2019 5:01 AM

7	We looked at the camber of about 800 girders in Wisconsin and compared values to the design values. From this study, we implemented a camber multiplier of 1.4 to be applied to the theoretical camber at release.	8/6/2019 4:55 AM
8	Cousins, T.E., and Gomez, J.P. Investigation of Long-term Prestress Losses in Pretensioned High Performance Concrete Girders, VTRC Report 05-CR20. Virginia Transportation Research Council, Charlottesville, 2005 Cousins, T.E., and Nassar, A.J. Investigation of Transfer Length, Development Length, Flexural Strength, and Prestress Losses in Lightweight Prestressed Concrete Girders, VTRC Report 03-CR20. VTRC Report 05-CR20. Virginia Transportation Research Council, Charlottesville, 2003 In-formal research was conducted in support of specification updates related to camber, but a report was not developed.	8/5/2019 12:10 PM
9	We have monitored lots of girder production to compare with predicted. NDOT ended up using k factor of 0.9 instead of 1.0 in calculating the section modulus	8/2/2019 9:04 AM
10	http://www.virginiadot.org/vtrc/main/online_reports/pdf/05-cr20.pdf	7/31/2019 12:20 PM
11	https://fdotwww.blob.core.windows.net/sitefinity/docs/default-source/content/structures/structuresresearchcenter/final-reports/bd545_07.pdf?sfvrsn=d665c214_0	7/31/2019 12:00 PM
12	Improving the Accuracy of Camber Predictions for Precast Pretensioned Concrete Beams, IHRB Project TR-625, Sri Sritharan, July 2015. Implemented to a limited degree. Additional implementation likely with future beam standards update.	7/31/2019 11:42 AM
13	Research project to measure prestress loss of decked bulb-T girders has recently begun by Dr. Il-Sang Ahn at the University of Alaska Fairbanks.	7/31/2019 11:38 AM

Q3 What method do you use to predict prestressed concrete beam camber?

Answered: 37 Skipped: 6

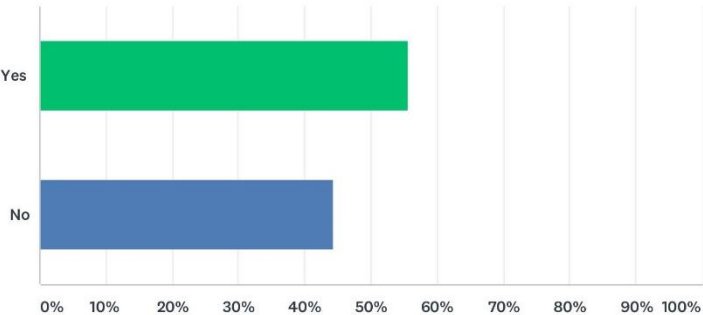


ANSWER CHOICES	RESPONSES	
Multiplier Method	45.95%	17
Prestress Loss Method	27.03%	10
Approximate Time Step Method	2.70%	1
Incremental Time Step Method	2.70%	1
Other (please specify)	21.62%	8
TOTAL		37

#	OTHER (PLEASE SPECIFY)	DATE
1	WSDOTs method as programmed in PGSuper.	9/12/2019 4:44 AM
2	The use of FDOT research that quantifies elastic shortening and shrinkage-related losses.	8/21/2019 7:13 AM
3	NCDOT Refined Method for Camber (uses a modified approximate time step method) See page 70 of the research report.	8/7/2019 7:46 AM
4	Please refer to ODOT BDM Section 302.5.2.3 at the following link: http://www.dot.state.oh.us/Divisions/Engineering/Structures/standard/Bridges/BDM/2019_BDM_07-19-19.pdf	8/6/2019 9:17 AM
5	Multiplier method with all factors set to 1.0	8/2/2019 4:59 AM
6	State specific equations	7/31/2019 12:44 PM
7	University of Florida Method. or the PCI multiplier method.	7/31/2019 12:02 PM
8	None of the above	7/31/2019 11:37 AM

Q4 Does this method explicitly consider the effects of creep and shrinkage?

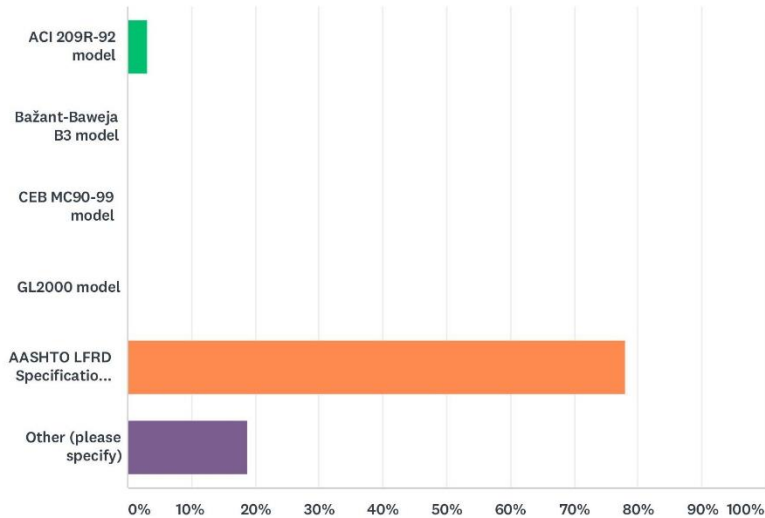
Answered: 9 Skipped: 34



ANSWER CHOICES		RESPONSES	
Yes		55.56%	5
No		44.44%	4
TOTAL			9

Q5 What model do you use to account for creep and shrinkage effects?

Answered: 32 Skipped: 11



ANSWER CHOICES	RESPONSES	
ACI 209R-92 model	3.13%	1
Bažant-Baweja B3 model	0.00%	0
CEB MC90-99 model	0.00%	0
GL2000 model	0.00%	0
AASHTO LFRD Specifications model	78.13%	25
Other (please specify)	18.75%	6
TOTAL		32

#	OTHER (PLEASE SPECIFY)	DATE
1	?	9/19/2019 5:16 AM
2	In PGSuper - Modulus of elasticity at transfer is computed using a modified form of AASHTO LFRD Equation 5.4.2.4-1 using f_{ci} . This equation is modified with the factors K1 and K2 as defined in NCHRP Report 496. Creep and shrinkage are computed with modified versions of AASHTO LFRD Equations 5.4.2.3.2-1 and 5.4.2.3.3-1. These equations are modified with K1 and K2 factors as defined in NCHRP Report 496. For girders having temporary top strand to control stability during transportation, the elastic shortening losses and K_{id} and K_{df} transformed section coefficients are modified to compute the shortening, creep, and shrinkage losses in the permanent strands. Modifications account for the fact that the temporary strands raise the CG of the prestressing force while the majority of the creep and shrinkage losses are taking place.	9/12/2019 4:45 AM
3	Creep and shrinkage are accounted for by way of calculation in the FDOT Prestressed Beam Program.	8/21/2019 7:14 AM
4	For camber, creep and shrinkage are not explicitly calculated. Instead, they are lumped into the multiplier.	8/12/2019 11:42 AM
5	Just Creep	8/12/2019 6:42 AM
6	Do not explicitly consider.	8/5/2019 12:12 PM

Q6 Do you have a procedure or a tool that you use to predict camber and displacement at a given time after the erection of the deck and after the opening of the bridge to traffic?

Answered: 30 Skipped: 13

#	RESPONSES	DATE
1	No	9/12/2019 4:46 AM
2	Multipliers in UDOT Structures Design and Detailing Manual 14.6.4.	8/26/2019 11:30 AM
3	N/A.	8/21/2019 7:16 AM
4	No.	8/12/2019 11:48 AM
5	No	8/12/2019 6:44 AM
6	Multipliers in Bentley LEAP Concrete Bridge. There is not a specific tool used to predict time dependent camber and displacements.	8/9/2019 9:19 AM
7	Final Camber Prediction = Girder Alone - Superimposed Dead Load	8/7/2019 7:46 AM
8	No.	8/7/2019 3:32 AM
9	Please see ODOT C&MS Section 511.07 for construction procedure and ODOT C&MS Table 515.16-5 for tolerances at the following link: http://www.dot.state.oh.us/Divisions/ConstructionMgt/OnlineDocs/Specifications/2019CMS/2019_CMS_07192019_for_web_letter_size.pdf	8/6/2019 9:25 AM
10	No.	8/6/2019 6:36 AM
11	No	8/6/2019 5:13 AM
12	No.	8/5/2019 12:15 PM
13	We would use the same equations that we use to predict final camber after deck placement (90 days).	8/2/2019 9:09 AM
14	No. We use AASHTO time dependent method	8/2/2019 9:08 AM
15	No	8/2/2019 8:16 AM
16	No.	8/2/2019 4:48 AM
17	No	8/1/2019 3:30 PM
18	No	8/1/2019 6:48 AM
19	NO	8/1/2019 3:59 AM
20	No	8/1/2019 2:27 AM
21	Leap Conspan	7/31/2019 1:48 PM
22	Take measurements at various stages including pre installation of the risers	7/31/2019 1:46 PM
23	No	7/31/2019 1:09 PM
24	No.	7/31/2019 12:48 PM
25	No.	7/31/2019 12:23 PM
26	Long term camber (after composite) is not checked.	7/31/2019 12:06 PM
27	No	7/31/2019 11:51 AM
28	We use the deflection multiplier method. We have multipliers for short-term and long-term predictions but these are only used as a check of fabricator predicted values. Girder fabricators working for the Alaska DOT&PF have the capability to sag the forms to compensate for predicted camber.	7/31/2019 11:43 AM
29	We have an inhouse program, PSLRFD	7/31/2019 11:42 AM
30	No	7/31/2019 11:39 AM

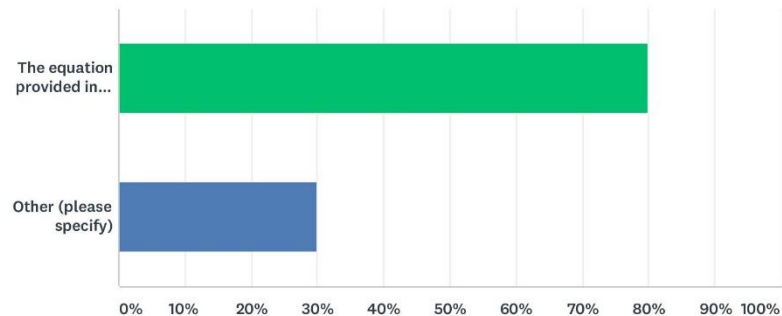
Q7 What is the range of 28-day compressive strength and compressive strength at release that you typically specify for prestressed concrete beams?

Answered: 31 Skipped: 12

#	RESPONSES	DATE
1	f_{ci} – 4 ksi to 6 ksi f'_c – 5 ksi to 8.5 ksi	9/12/2019 4:46 AM
2	28-day compressive strength = 5.0 to 8.5 ksi Compressive strength at release = 5.0 to 7.5 ksi	8/26/2019 11:30 AM
3	Ranges of compressive strength are typically 8.5 ksi, but may be occasionally higher even to 10 ksi.	8/21/2019 7:16 AM
4	f_{ci} range is from 4.5 ksi to 7.5 ksi f'_c range is from 5.0 ksi to 9.0 ksi	8/12/2019 11:48 AM
5	Varies based on design. Typically, we see 6.8 ksi before stress transfer and see 8 ksi for 28-day design compressive strengths.	8/12/2019 6:44 AM
6	f_{ci} =6,500psi f'_c =8,500psi	8/9/2019 9:19 AM
7	28-Day = 5ksi-10ksi Release = 4ksi-8ksi	8/7/2019 7:46 AM
8	The release strength typically dictates the 28 day compressive strength. We specify the minimum release strength to satisfy the top of the end of the beams stresses. Release is approximately 80% of final so if we need 4800 psi at release we specify 6000 for final. Anything that needs 4800+ to 6400 psi at release will be specified as 8000 psi for final/	8/7/2019 3:32 AM
9	f_{ci} = 5 ksi f'_c = 7 ksi These are ODOT minimums as specified in the ODOT Standard Bridge Drawings PSBD-2-07 and PSID-1-13. Designers may increase these with prior written approval of our fabricators. Standards may be found at the following link: http://www.dot.state.oh.us/Divisions/Engineering/Structures/standard/Bridges/Pages/StandardBridgeDrawings.aspx	8/6/2019 9:25 AM
10	We typically will specify the strength that we need for release to avoid cracking at the top ends of the girders. The final strength is determined so that the release is 80% of that. So if we needed 4800 at release we would specify 6000. if we needed a release strength between 4800 and 6400 we would specify 8000.	8/6/2019 6:36 AM
11	f_{ci} = 6400 to 6800 psi for girders with f'_c = 8000 is typical.	8/6/2019 5:13 AM
12	0.8 f'_c (e.g., release typically minimum of 6.4 ksi for 8 ksi concrete)	8/5/2019 12:15 PM
13	6.5 ksi (release) 8.0 ksi (final)	8/2/2019 9:09 AM
14	8 ksi- 12 ksi	8/2/2019 9:08 AM
15	no range - specify strength at release and strength 28-day	8/2/2019 8:16 AM
16	min	8/2/2019 7:49 AM
17	Usually it's 6,000 psi, but we have gone up to 8,000 psi.	8/2/2019 4:48 AM
18	6ksi - 10 ksi	8/1/2019 3:30 PM
19	10 ksi	8/1/2019 6:48 AM
20	Range for 28 days varies between 5 Ksi to 8 Ksi Range at release varies between 4 Ksi and 7 Ksi. 1 to 1.5 Ksi difference between release and 28 days.	8/1/2019 3:59 AM
21	Compressive strength at release is approximately 90% of 28-day strength.	8/1/2019 2:27 AM
22	8,000 psi/6,000 psi	7/31/2019 1:48 PM
23	4500 RELEASE 6000 -28 DAYS FOR PILES ONLY 6000 PSI TO 6500 PSI RELEASE 8500 PSI - 28 DAYS RELEASE 7500 PSI AND 10000 PSI -28 DAYS	7/31/2019 1:46 PM
24	28 day 6000 at release 5000	7/31/2019 1:09 PM
25	6-8ksi for 28-day strength, 80% for release	7/31/2019 12:48 PM
26	5,000psi to 10,000psi	7/31/2019 12:23 PM
27	Release 6-6.8 ksi. 28 day strength 8.5 ksi	7/31/2019 12:06 PM
28	Release 4.5 ksi to 8 ksi Final 5 ksi to 9 ksi	7/31/2019 11:51 AM
29	28 day f'_c ~ 7500 psi to 8500 psi with test results typically between 9000 psi and 12000 psi 16-hour f_{ci} ~ 6000 psi to 7500 psi with test results typically between 7000 psi and 9000 psi	7/31/2019 11:43 AM
30	8 ksi 6.8 ksi	7/31/2019 11:42 AM
31	28 day 6-8 ksi At release 4-7 ksi	7/31/2019 11:39 AM

Q8 How do you determine modulus of elasticity when conducting camber calculations? (choose all that apply)

Answered: 30 Skipped: 13



ANSWER CHOICES	RESPONSES	
The equation provided in AASHTO LRFD Bridge Design Specifications	80.00%	24
Other (please specify)	30.00%	9
Total Respondents: 30		

#	OTHER (PLEASE SPECIFY)	DATE
1	TxDOT policy is to set all concrete moduli to 5000 ksi for both stress and deflection calculations and to indicate on the plans that the deflections shown are calculated assuming an E'c of 5000 ksi.	9/12/2019 4:46 AM
2	We use the ACI 363 equation: $E_c = 1265 \times (f'_c)^{0.5} + 1000$ where f'_c and E_c are in ksi.	8/12/2019 11:48 AM
3	modulus of elasticity of beam concrete at transfer	8/12/2019 6:44 AM
4	AASHTO LRFD Bridge Design Specification equation (7th Edition) $K_1=0.85$	8/7/2019 7:46 AM
5	$(5500 \times \text{SQRT}(f'_c)) / (\text{SQRT}(6))$ This is based on historical data.	8/6/2019 5:13 AM
6	We use the AASHTO LRFD equation that was removed around 2015. $E_c = 33000K_1(w_c 1.5)(f'_c 0.5)$	8/2/2019 9:09 AM
7	we use K of 0.9 instead of 1.0 because of Nebraska aggregate	8/2/2019 9:08 AM
8	Provided by the contractor	7/31/2019 1:46 PM
9	$K=1.0$	7/31/2019 12:06 PM

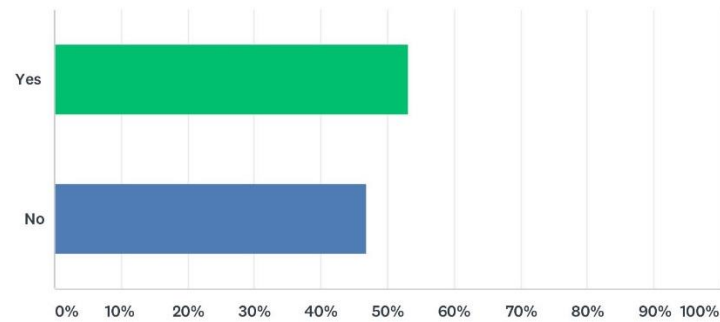
Q9 If the equation provided in AASHTO LRFD Bridge Design Specifications is used to determine the modulus of elasticity, do you use the specified compressive strength at release and the 28-day compressive strength from the plans or some other value?

Answered: 29 Skipped: 14

#	RESPONSES	DATE
1	N/A	9/12/2019 4:46 AM
2	Use specified compressive strength at release and the 28-day compressive strength from the plans	8/26/2019 11:30 AM
3	Compressive strength at release and 28-day as stated in the Plans.	8/21/2019 7:16 AM
4	We use the compressive strengths given in the bridge plan for calculating E_c in the equation above.	8/12/2019 11:48 AM
5	$f_c = f_{ci}$	8/12/2019 6:44 AM
6	Usually the specified compressive strengths are used. The designer has the option of using actual average values of $f_{ci}=8.5\text{ksi}$ and $f_c=12.5\text{ksi}$	8/9/2019 9:19 AM
7	Specified release strength is increased by 25% and the specified 28-day strength is increased by 45%	8/7/2019 7:46 AM
8	We use the 28 day compressive strength.	8/7/2019 3:32 AM
9	Plans	8/6/2019 9:25 AM
10	We use the final design strength. This is usually lower than what is being provided by the precaster. The precaster tries to turn their beds every 24 hours so they will use a higher strength mix to get the design release strength earlier.	8/6/2019 6:36 AM
11	NA	8/6/2019 5:13 AM
12	Plans	8/5/2019 12:15 PM
13	Plan Values	8/2/2019 9:09 AM
14	from the plans	8/2/2019 9:08 AM
15	From plans	8/2/2019 8:16 AM
16	We use the specified compressive strength at release and the 28-day compressive strength from the plans.	8/2/2019 4:48 AM
17	Specified compressive strength at release and the 28-day compressive strength.	8/1/2019 3:30 PM
18	Yes	8/1/2019 6:48 AM
19	We use specified compressive strength at release and 28-day compressive strength from the plans.	8/1/2019 3:59 AM
20	Use 28 day compressive strength	8/1/2019 2:27 AM
21	Values from the plans.	7/31/2019 1:48 PM
22	we use release and 28 day.	7/31/2019 1:09 PM
23	Yes.	7/31/2019 12:48 PM
24	From the plans.	7/31/2019 12:23 PM
25	Specified 28-day strength in the plans.	7/31/2019 12:06 PM
26	At release, although we have adopted a procedure to adjust based on expected strengths since they are typically higher.	7/31/2019 11:51 AM
27	Yes, we use the specified (not expected) f_{ci} and assume that the variability is included in the deflection multipliers. We use the E_{ci} modulus as the basis for deflection.	7/31/2019 11:43 AM
28	From the plans	7/31/2019 11:42 AM
29	release and the 28-day	7/31/2019 11:39 AM

Q10 Do you require a specific curing technique for prestressed concrete beams?

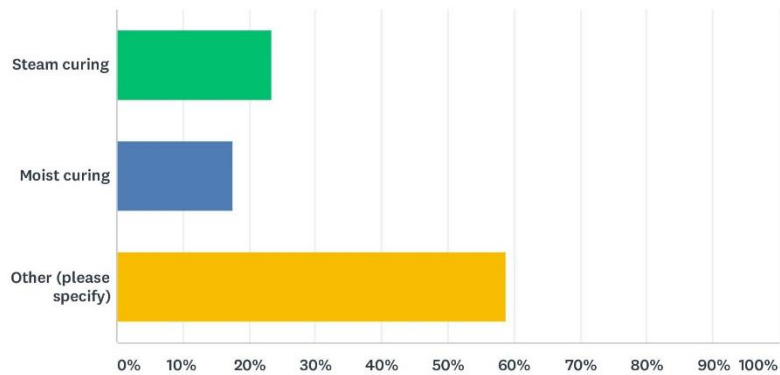
Answered: 32 Skipped: 11



ANSWER CHOICES	RESPONSES	
Yes	53.13%	17
No	46.88%	15
TOTAL		32

Q11 Which curing technique do you specify?

Answered: 17 Skipped: 26



ANSWER CHOICES	RESPONSES
Steam curing	23.53% 4
Moist curing	17.65% 3
Other (please specify)	58.82% 10
TOTAL	17

#	OTHER (PLEASE SPECIFY)	DATE
1	any curing technique is acceptable provided all exposed surfaces remain wet until release strength is achieved. Curing compound is not allowed on the top surface girders. Standard Specifications for Construction and Maintenance of Highways, Streets and Bridges, Item 424 - ftp://ftp.dot.state.tx.us/pub/txdot-info/des/spec-book-1114.pdf - This specification allows steam, moist, barrier, and wet mat. Wet mat is the most commonly used.	9/12/2019 4:47 AM
2	Steam or radiant heat. (Typically, radiant heat is used.)	8/26/2019 11:33 AM
3	All of the following methods are allowed by our specs: 1) covering with wet burlap or canvas 2) continuous water mist 3) airtight seal using plastic curing blankets 4) steam curing	8/12/2019 11:49 AM
4	Steam Curing, Water Curing, and Radiant Heat Curing are all options given to the precasters.	8/7/2019 7:47 AM
5	Please refer to ODOT C&MS 515.15 for specific curing requirements at the following link: http://www.dot.state.oh.us/Divisions/ConstructionMgt/OnlineDocs/Specifications/2019CMS/2019_CMS_07192019_for_web_letter_size.pdf	8/6/2019 9:27 AM
6	Steam cure "or cure by other methods identified by the contractor's fabrication quality control plan". Curing compound is not allowed.	8/6/2019 5:16 AM
7	Moist curing is specified with Contractor option of steam curing with adherence to requirements.	8/5/2019 12:15 PM
8	steam cure in the winter and moist cure in the summer	8/1/2019 1:09 PM
9	Steam and Moist curing are allowed	8/1/2019 4:09 AM
10	steam or wet method with thermocouples "match cure"	7/31/2019 1:55 PM

Q12 Which curing technique is more prevalent in your state?

Answered: 27 Skipped: 16

#	RESPONSES	DATE
1	Moist or water curing (wet mat or soaker hoses)	9/12/2019 4:47 AM
2	Radiant heat	8/26/2019 11:34 AM
3	Moist curing with curing compound and burlap sheeting on the top flange.	8/21/2019 7:19 AM
4	Steam curing	8/12/2019 11:50 AM
5	Fabricators have the option of steam or saturated cover curing. Pub 408, Section 1107.03(d)5.g provides PennDOT's requirements on initial and intermediate curing phases. Each phase has temperature requirements. Typically, PennDOT utilizes the saturated covering in conjunction with a steam cure.	8/12/2019 6:44 AM
6	Steam Cure	8/9/2019 9:22 AM
7	Steam Curing	8/7/2019 7:47 AM
8	Steam curing	8/7/2019 3:33 AM
9	Steam curing.	8/6/2019 6:37 AM
10	Moist curing	8/6/2019 5:16 AM
11	Moist curing	8/5/2019 12:16 PM
12	Steam Curing	8/2/2019 9:29 AM
13	steam accelerated method	8/2/2019 9:09 AM
14	moist curing	8/2/2019 7:50 AM
15	Moist curing.	8/2/2019 4:50 AM
16	moist curing method	8/1/2019 3:34 PM
17	moist curing	8/1/2019 1:10 PM
18	radiant heat curing/electric	8/1/2019 6:49 AM
19	Moist (Wet) Curing and accelerated curing using low pressure steam or radiant heat curing.	8/1/2019 4:10 AM
20	Saturated cover curing.	7/31/2019 1:54 PM
21	Steam cured.	7/31/2019 1:10 PM
22	Steam	7/31/2019 12:48 PM
23	Moist curing.	7/31/2019 12:25 PM
24	Unsure	7/31/2019 11:54 AM
25	Steam methods are used by the Alaska fabricators Heated forms are used by the Washington fabricator	7/31/2019 11:44 AM
26	Steam	7/31/2019 11:42 AM
27	Wet cure	7/31/2019 11:40 AM

Q13 What method do you use to measure camber?

Answered: 25 Skipped: 18

#	RESPONSES	DATE
1	No prescribed method. Camber is only measured when there is a problem.	9/12/2019 4:49 AM
2	Deviation from stringline	8/26/2019 11:42 AM
3	At fabricator yard before shipping, measurements may be done using stringline or survey instruments. After beam erection, measurement is done using survey instruments.	8/12/2019 12:13 PM
4	a. Beams less than 70' – string line b. Longer than 70' – Surveyor's Transit	8/12/2019 6:45 AM
5	Survey, note it is up to the fabricator's inspector to submit camber measurements.	8/9/2019 9:36 AM
6	Inspectors manually measure the camber at the precast plant.	8/7/2019 7:48 AM
7	It is specified for the fabricator to manage camber if they think that the actual camber will be higher than the calculated camber. Typically the fabricator will take shots on the top of the beam at the ends and midspan and record the information.	8/7/2019 3:59 AM
8	Taut stringline with beams sitting on proper donnage.	8/6/2019 9:37 AM
9	Tape measure at midspan	8/6/2019 5:21 AM
10	None specifically prescribed in Specifications. Typically string line or shooting elevations.	8/5/2019 12:18 PM
11	survey	8/2/2019 9:14 AM
12	string line method	8/2/2019 7:53 AM
13	Tension line with measured offsets at the tenth points.	8/2/2019 5:05 AM
14	Survey shots at tenth points along the beam top flange.	8/1/2019 3:50 PM
15	Laser beam	8/1/2019 6:52 AM
16	Survey	8/1/2019 4:40 AM
17	None unless there is a concern. If needed, would use tape measure.	8/1/2019 2:30 AM
18	Survey or string line method.	7/31/2019 2:00 PM
19	Shots on top of beam after beam is set on substructures.	7/31/2019 1:13 PM
20	Not specified	7/31/2019 12:49 PM
21	Not specified.	7/31/2019 12:29 PM
22	Camber measured by fabricator	7/31/2019 12:13 PM
23	Camber measurement procedure listed in IM 570 at https://iowadot.gov/erl/current/IM/content/570.htm Measure elevations at beam ends and center after lifting and resetting beams within 3 hours of detensioning.	7/31/2019 12:02 PM
24	As I understand, chord offset is measured using a laser level. Girder lift off distance at mid-span (distance between bottom pan and concrete girder after release) is also measured for each girder	7/31/2019 11:53 AM
25	Survey	7/31/2019 11:42 AM

Q14 What tools do you use to measure camber?

Answered: 26 Skipped: 17

#	RESPONSES	DATE
1	Steel wire line	9/12/2019 4:49 AM
2	Stringline and tape measure	8/26/2019 11:42 AM
3	Stringline and survey.	8/21/2019 7:22 AM
4	See answer to previous question.	8/12/2019 12:13 PM
5	a. String lines b. Steel tape measure c. Surveyor's transit	8/12/2019 6:45 AM
6	Total Station	8/9/2019 9:36 AM
7	String Line and tape measure	8/7/2019 7:48 AM
8	See above	8/7/2019 3:59 AM
9	String, tape measure, 3 individuals.	8/6/2019 9:37 AM
10	Tape measure	8/6/2019 5:21 AM
11	None specifically prescribed in Specifications.	8/5/2019 12:18 PM
12	level	8/2/2019 9:14 AM
13	tape measure and string line	8/2/2019 7:53 AM
14	See 12.	8/2/2019 5:05 AM
15	Survey shots at tenth points along the beam top flange.	8/1/2019 3:50 PM
16	laser	8/1/2019 6:52 AM
17	Laser Level	8/1/2019 4:40 AM
18	tape measure	8/1/2019 2:30 AM
19	Survey equipment or string line and tape measure.	7/31/2019 2:00 PM
20	Survey Level.	7/31/2019 1:13 PM
21	Not specified	7/31/2019 12:49 PM
22	Not specified.	7/31/2019 12:29 PM
23	survey equipment (distance from tensioned strings are not used anymore)	7/31/2019 12:13 PM
24	Typically surveyed.	7/31/2019 12:02 PM
25	Laser level for chord-offset method Tape measure for girder lift-off	7/31/2019 11:53 AM
26	Depends on contractor - Level	7/31/2019 11:42 AM

Q15 How frequently do you measure camber?

Answered: 27 Skipped: 16

#	RESPONSES	DATE
1	Rarely. Only when there is a problem.	9/12/2019 4:49 AM
2	Once a week	8/26/2019 11:42 AM
3	Monthly measurement is required per our Specification.	8/21/2019 7:22 AM
4	Initial camber is measured before removal from the casting bed. During storage, camber is measured at frequencies < 60 days and within 7 to 21 days of shipment. It is also measured after beam erection when setting grades for the deck pour.	8/12/2019 12:13 PM
5	a. Camber is measured after cutting the strands (form release) or at beginning of beam storage b. According to Publication 408, Section 1107, camber verification is required within 2 weeks of shipping	8/12/2019 6:45 AM
6	At release and prior to shipment	8/9/2019 9:36 AM
7	Camber is measured when member is removed from the casting bed and at the time of final inspection.	8/7/2019 7:48 AM
8	It is specified at regular intervals and in the fabricator's camber control procedure. Some fabricators will check it every three days to control camber growth.	8/7/2019 3:59 AM
9	Post pour after release, prior to storage and prior to shipment. The contractor can request a measurement at any time.	8/6/2019 9:37 AM
10	Once	8/6/2019 5:21 AM
11	Once members have been placed on temporary supports for storage at release, camber measurements are taken and at 2 week intervals thereafter up to 120 days after detensioning.	8/5/2019 12:18 PM
12	we require camber measure on every project before shipping	8/2/2019 9:14 AM
13	once unless delayed construction	8/2/2019 7:53 AM
14	Only at the plant (acceptance) before shipment.	8/2/2019 5:05 AM
15	First within 72 hours of release. Additional times if it is out of tolerance. Then again when the beams are erected / before deck stay-in-place formwork is installed.	8/1/2019 3:50 PM
16	As needed	8/1/2019 6:52 AM
17	During construction	8/1/2019 4:40 AM
18	Only when there are problems	8/1/2019 2:30 AM
19	During every hands-on bridge safety inspection (every six years).	7/31/2019 2:00 PM
20	3 times, initial , 28 days and 21 days prior to installation	7/31/2019 1:57 PM
21	Only when beams are set.	7/31/2019 1:13 PM
22	Not specified	7/31/2019 12:49 PM
23	Every 2 weeks.	7/31/2019 12:29 PM
24	weekly	7/31/2019 12:13 PM
25	Once	7/31/2019 12:02 PM
26	Usually twice - immediately after release of prestress force and prior to transport	7/31/2019 11:53 AM
27	Contractor measures before deck placement.	7/31/2019 11:42 AM

Q16 At what time of the day do you measure camber?

Answered: 25 Skipped: 18

#	RESPONSES	DATE
1	Any day light hours.	9/12/2019 4:49 AM
2	No specific time	8/26/2019 11:42 AM
3	Not specified in our Specs.	8/21/2019 7:22 AM
4	Our spec says to measure at a time when camber and alignment of beam is not influenced by temporary differences in surface temperature.	8/12/2019 12:13 PM
5	Varies, while PennDOT does not have a specification limit on this, camber is typically checked in the early morning to avoid direct sunlight	8/12/2019 6:45 AM
6	No specified time.	8/9/2019 9:36 AM
7	Various	8/7/2019 7:48 AM
8	It is in the fabricator's camber control procedure. Some fabricators check it in the morning.	8/7/2019 3:59 AM
9	Not specified.	8/6/2019 9:37 AM
10	Unknown	8/6/2019 5:21 AM
11	These measurements are recorded in the morning to reduce the effects of solar radiation for each unit and entries include the date, time, weather conditions and measurements taken.	8/5/2019 12:18 PM
12	no requirements	8/2/2019 7:53 AM
13	There is no particular time of the day that we insist the camber be measured.	8/2/2019 5:05 AM
14	Various.	8/1/2019 3:50 PM
15	Mid day	8/1/2019 6:52 AM
16	Day time	8/1/2019 4:40 AM
17	N/A	8/1/2019 2:30 AM
18	Normally during midday.	7/31/2019 2:00 PM
19	Any time.	7/31/2019 1:13 PM
20	Not specified	7/31/2019 12:49 PM
21	Not specified.	7/31/2019 12:29 PM
22	Early in the morning	7/31/2019 12:13 PM
23	Not specified.	7/31/2019 12:02 PM
24	16-hours and about within about 1 or 2 days after setting on temporary bunking points	7/31/2019 11:53 AM
25	At discretion of contractor	7/31/2019 11:42 AM

Q17 What procedure or approach (such as pre-loading) do you use to minimize or control camber overgrowth?

Answered: 27 Skipped: 16

#	RESPONSES	DATE
1	No prescribed method.	9/12/2019 4:49 AM
2	Static weight (pre-loading) or change dunnage position	8/26/2019 11:42 AM
3	Pre-loading or ballasting.	8/21/2019 7:22 AM
4	Our spec assumes we can reasonably predict the camber for beams that will be erected and have the deck formed between 30 and 180 days of prestress release. For beams between 30 and 180 days old, fabricator must report if cambers become greater than 1 inch plus or minus beyond the erection camber given in the bridge plan. Limits are specified on beam end overhang during storage. For beams expected to be > 180 days old at erection, contractor is required to submit a plan to prevent/accommodate excess camber.	8/12/2019 12:13 PM
5	a. Only done on occasions. Pre-loading is accomplished by loading with precast roadway barrier or similar. In general, camber is not an issue.	8/12/2019 6:45 AM
6	Precast barrier has been used to pre-load, but results have not been successful.	8/9/2019 9:36 AM
7	Pre-loading is occasionally used on shorter beams.	8/7/2019 7:48 AM
8	Preloading is used by the fabricator to control camber growth.	8/7/2019 3:59 AM
9	Not permitted.	8/6/2019 9:37 AM
10	Pre-loading very rarely done, except if long term storage.	8/6/2019 5:21 AM
11	The Contractor is required to submit a camber management plan prior to fabrication indicating the method for controlling camber. Pre-loading is the primary method utilized. The Contractor is required to implement the plan if specific thresholds are exceeded. Contractors are required to implement the camber management plan for any members that will be erected 120 days or more after detensioning. Where a change in construction schedule occurs which will result in erection 120 days or more after detensioning, the Contractor is required to implement the camber management plan. The Contractor may submit a request to delay the implementation of the camber management plan to the next scheduled camber measurement if documentation is submitted showing the camber growth is following an established camber development path that will not exceed the camber tolerance at erection under the current construction schedule.	8/5/2019 12:18 PM
12	We don't do this	8/2/2019 9:14 AM
13	have had to preload in construction in a few cases	8/2/2019 7:53 AM
14	We have used pre-loading on occasion.	8/2/2019 5:05 AM
15	none	8/1/2019 3:50 PM
16	Preloading	8/1/2019 6:52 AM
17	None	8/1/2019 4:40 AM
18	none	8/1/2019 2:30 AM
19	None.	7/31/2019 2:00 PM
20	nonea	7/31/2019 1:57 PM
21	We have used pre-load or temporary prestressing.	7/31/2019 1:13 PM
22	Pre-loading	7/31/2019 12:49 PM
23	Up to the contractor/fabricator.	7/31/2019 12:29 PM
24	Over growth has not been a concern. Specifications allow fabricator to move the supports in the storage to increase camber, if needed.	7/31/2019 12:13 PM
25	Fabricator may adjust supports in yard to control camber growth.	7/31/2019 12:02 PM
26	Fabricators can sag (parabolic vertical depression) for Alaska style decked bulb-T girders (most commonly used in out state)	7/31/2019 11:53 AM
27	Pre-loading has occasionally been used in our state.	7/31/2019 11:42 AM

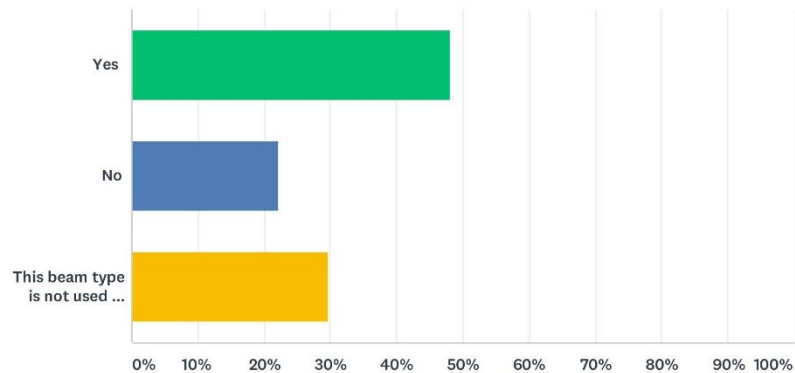
Q18 How do you typically deal with inaccurate predictions of camber?

Answered: 27 Skipped: 16

#	RESPONSES	DATE
1	Fabricator - TxDOT specifications state, "Variations greater than those specified in Table 3 (there is no camber tolerance) are subject to review. However, these tolerances do not relieve the Contractor from the responsibility of furnishing a completed structure that is in reasonably close conformity with the lines, grades, cross-sections, dimensions, and details specified. Correct members not meeting these tolerances at no additional expense to the Department, to achieve a satisfactory completed structure. This also includes costs for correction due to variations in vertical beam camber. Correction may require replacement of the member. In the Field - For girder with significantly less than predicted camber tend to be rejected. For girders with higher than predicted camber, we will try to adjust the roadway grade. If we cannot, then in rare cases, these are rejected.	9/12/2019 4:49 AM
2	Adjustment to deck finished grade profile when necessary	8/26/2019 11:42 AM
3	Accommodate the product into the bridge by pedestal adjustments, build-up adjustments.	8/21/2019 7:22 AM
4	For cambers that are low, additional stool/haunch above the beams is built in to get the deck to proper grade. For cambers that are high, deck grades are adjusted (raised) in the field to accommodate cambers and avoid negative stools/haunches.	8/12/2019 12:13 PM
5	Case by case, limited cases. Measure deflections at erection, deck placement and barrier placement. The deflections are assessed to ensure water does not pond on the bridge.	8/12/2019 6:45 AM
6	Increase haunch thickness to allow camber variability. Place shims to adjust bearing seat elevations.	8/9/2019 9:36 AM
7	The bridge deck buildup (haunch) accommodates minor inaccuracies in camber predictions.	8/7/2019 7:48 AM
8	If camber is predicted inaccurately it is sometimes necessary to adjust the deck overpour to account for it.	8/7/2019 3:59 AM
9	ODOT C&MS 511.07 at the following link: http://www.dot.state.oh.us/Divisions/ConstructionMgt/OnlineDocs/Specifications/2019CMS/2019_CMS_07192019_for_web_letter_size.pdf	8/6/2019 9:37 AM
10	May have to add "hat" bars (supplemental bars to ensure stirrups project 3" min. into the deck).	8/6/2019 5:21 AM
11	Preloading and Contractor adjustments to seat elevations or grade if approved by the Department. Use of top strands has been proposed to alleviate continued inaccuracies and reduce camber growth.	8/5/2019 12:18 PM
12	we use 1.5 in of fillet on our NU girder and we add hat bars in the field	8/2/2019 9:14 AM
13	make up for it in the haunch	8/2/2019 7:53 AM
14	As with steel beams, the camber for prestress concrete beams is about twice that anticipated at installation. Over time, with creep and with the camber deflections decreasing, there are usually other more significant issues which will warrant bridge rehabilitation or replacement.	8/2/2019 5:05 AM
15	We add a 1" camber tolerance into the required haunch thickness for all spans greater than 80'. This avoids camber issues in most cases. In long-span bulb tee girders we deal with issues such as accepting net negative camber in the final condition in approximately 25% of those bridges (spans > 120-feet).	8/1/2019 3:50 PM
16	Slab Haunch - "A" Dimension	8/1/2019 6:52 AM
17	Adjust screeds,	8/1/2019 4:40 AM
18	A minimum coping thickness is applied on top of the beam that provides room for errors in predicted camber.	8/1/2019 2:30 AM
19	Asphalt overlay.	7/31/2019 2:00 PM
20	modify haunch depth if necessary	7/31/2019 1:57 PM
21	Adjust the riser or change the profile on the deck.	7/31/2019 1:13 PM
22	Case-by-case	7/31/2019 12:49 PM
23	Adjust bridge seats, bolster/haunch and grade.	7/31/2019 12:29 PM
24	The contractor is required to construct the bearing seat elevation based on actual measured camber.	7/31/2019 12:13 PM
25	Built-in tolerance in stirrups, then modify road profile, then stirrup height modification.	7/31/2019 12:02 PM
26	If differential camber exceeds contract tolerances (i.e., 0.25" at ends and 0.5" at midspan) then forces devices cast in the girders are used to level up girders	7/31/2019 11:53 AM
27	Contractor has to adjust deck at his expense.	7/31/2019 11:42 AM

Q19 Are box beams prone to inaccurate camber predictions?

Answered: 27 Skipped: 16



ANSWER CHOICES	RESPONSES	
Yes	48.15%	13
No	22.22%	6
This beam type is not used in my state	29.63%	8
TOTAL		27

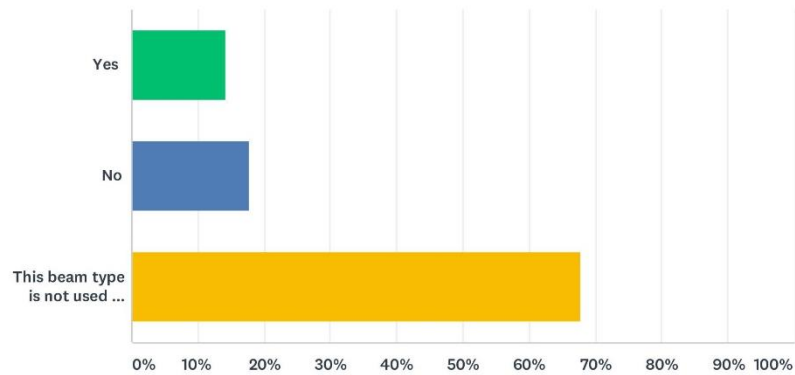
Q20 Is there a specific size(s) of the member that is more prone?

Answered: 14 Skipped: 29

#	RESPONSES	DATE
1	no	9/12/2019 4:49 AM
2	48 inch	8/12/2019 6:45 AM
3	No, based on internal research camber variation is the same over different span/depth ratios. Note, girders with larger cambers will have larger variation, but the over/under camber percentage is the same.	8/9/2019 9:41 AM
4	Box Beam camber predictions have significantly improved since the implementation of NCDOT's camber research.	8/7/2019 7:49 AM
5	No.	8/7/2019 3:59 AM
6	No	8/6/2019 9:37 AM
7	Box beams designed for concrete strength in upper range of allowable with larger number of strands are more prone, but can typically be dealt with by Contractor field adjustments.	8/5/2019 12:18 PM
8	We have not investigated this issue.	8/2/2019 5:06 AM
9	no	8/1/2019 1:22 PM
10	No.	7/31/2019 2:00 PM
11	No	7/31/2019 1:13 PM
12	No	7/31/2019 12:49 PM
13	No.	7/31/2019 12:30 PM
14	Not sure	7/31/2019 11:43 AM

Q21 Are cored slabs prone to inaccurate camber predictions?

Answered: 28 Skipped: 15



ANSWER CHOICES	RESPONSES	
Yes	14.29%	4
No	17.86%	5
This beam type is not used in my state	67.86%	19
TOTAL		28

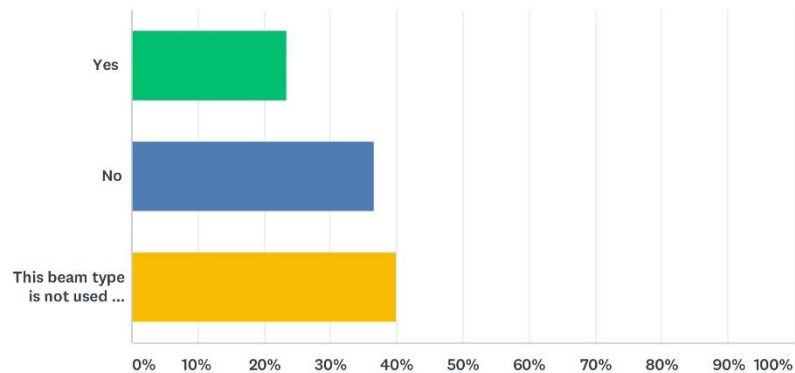
Q22 Are there specific cored slab size(s) of the member that is more prone?

Answered: 4 Skipped: 39

#	RESPONSES	DATE
1	Cored Slab camber predictions have significantly improved since the implementation of NCDOT's camber research.	8/7/2019 7:50 AM
2	No.	8/7/2019 3:59 AM
3	Voided slabs designed for concrete strength in upper range of allowable with larger number of strands are more prone, but can typically be dealt with by Contractor field adjustments (assume voided slabs are similar to cored slabs in response here and in Question 20).	8/5/2019 12:19 PM
4	No	7/31/2019 12:50 PM

Q23 Are AASHTO I-beams prone to inaccurate camber predictions?

Answered: 30 Skipped: 13



ANSWER CHOICES	RESPONSES	
Yes	23.33%	7
No	36.67%	11
This beam type is not used in my state	40.00%	12
TOTAL		30

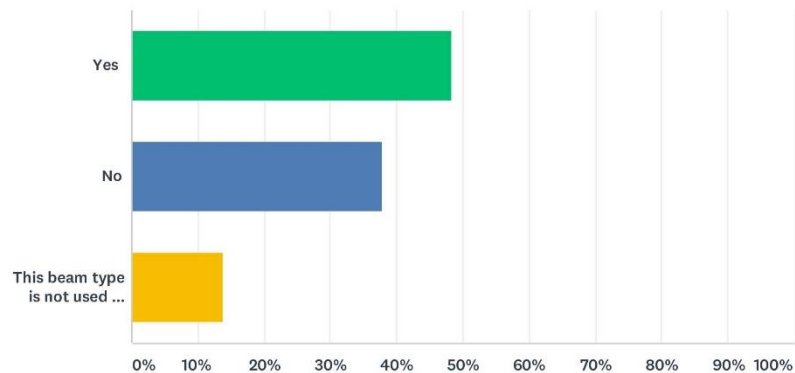
Q24 Are there specific I-beam size(s) of the member that is more prone?

Answered: 7 Skipped: 36

#	RESPONSES	DATE
1	Larger sizes that approach maximum span lengths for that size	8/26/2019 2:18 PM
2	No	8/6/2019 9:38 AM
3	These beam types are only used on in-kind widening and rarely utilized. Historically, VDOT previously designed using 5 ksi concrete and cracking overload so less strain differential. Type 6 are more prone where span lengths are near maximum range for section or where shallower section than existing is utilized due to existing vertical clearances and exterior widening.	8/5/2019 12:20 PM
4	We do not know.	8/2/2019 5:07 AM
5	All	8/1/2019 4:40 AM
6	no	7/31/2019 1:14 PM
7	Not sure	7/31/2019 11:43 AM

Q25 Are bulb T beams prone to inaccurate camber predictions?

Answered: 29 Skipped: 14



ANSWER CHOICES	RESPONSES	
Yes	48.28%	14
No	37.93%	11
This beam type is not used in my state	13.79%	4
TOTAL		29

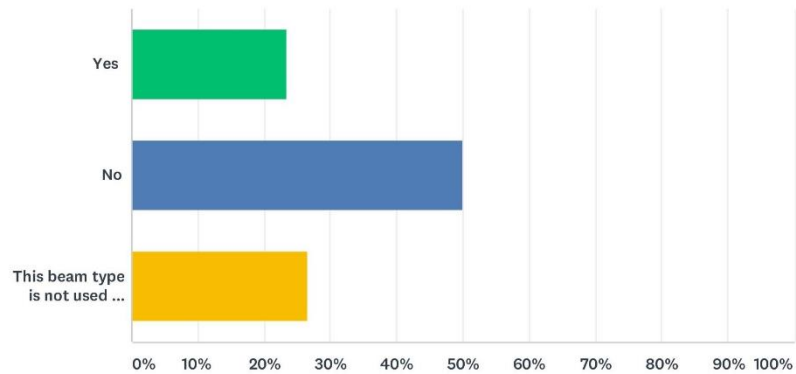
Q26 Are there specific bulb T beams size(s) of the member that is more prone?

Answered: 14 Skipped: 29

#	RESPONSES	DATE
1	no	9/12/2019 4:49 AM
2	Larger sizes that approach maximum span lengths for that size	8/26/2019 2:20 PM
3	No, see previous response.	8/9/2019 9:43 AM
4	No.	8/7/2019 4:00 AM
5	No, 36" to 72". To clarify #21, we haven't had some camber problems, but not significant lately.	8/6/2019 5:23 AM
6	Whether 29" bulb-T sections (smallest size used by VDOT) are more prone where designed for concrete strength in upper range of allowable with larger number of strands are more prone to experience inaccurate camber predictions is debatable but appears to depend on whether design-bid-build or design-build procurement process is used. 85" bulb-T and primarily 93" bulb-T sections are more prone where designed for concrete strength in upper range of allowable with larger number of strands where span lengths are near maximum range for section. Stability during fabrication, transportation and erection are also issues with these sections.	8/5/2019 12:20 PM
7	We do not know.	8/2/2019 5:08 AM
8	Generally any bulb tee with span lengths greater than 125-feet.	8/1/2019 3:52 PM
9	All	8/1/2019 4:40 AM
10	No	7/31/2019 12:50 PM
11	No.	7/31/2019 12:30 PM
12	The cambers typically have been lower than predicted. The longer beams would tend to be more troublesome since the cambers are larger.	7/31/2019 12:04 PM
13	Although no systematic evaluation has been undertaken by the Department, it seems that deeper, longer girders are more prone to camber variability	7/31/2019 11:55 AM
14	Not Sure	7/31/2019 11:44 AM

Q27 Are other beam types prone to inaccurate camber predictions?

Answered: 30 Skipped: 13



ANSWER CHOICES	RESPONSES	
Yes	23.33%	7
No	50.00%	15
This beam type is not used in my state	26.67%	8
TOTAL		30

Q28 Are there specific other beams size(s) of the member that is more prone?

Answered: 6 Skipped: 37

#	RESPONSES	DATE
1	All beam types can be subject to inaccurate camber issues. We use bulb T beams, box beams, solid slab beams, and U beams. Rarely we see the longer beams with higher amounts of strand have more inaccurate camber issues. Typically, inaccurate camber issues arise in the different materials and practices the various precast fabricators use.	9/12/2019 4:50 AM
2	We use an Inverted T section 300mm to 800mm It seems they are more prone	8/2/2019 9:17 AM
3	We do not know.	8/2/2019 5:08 AM
4	no	7/31/2019 1:14 PM
5	Not sure	7/31/2019 11:44 AM
6	no	7/31/2019 11:25 AM

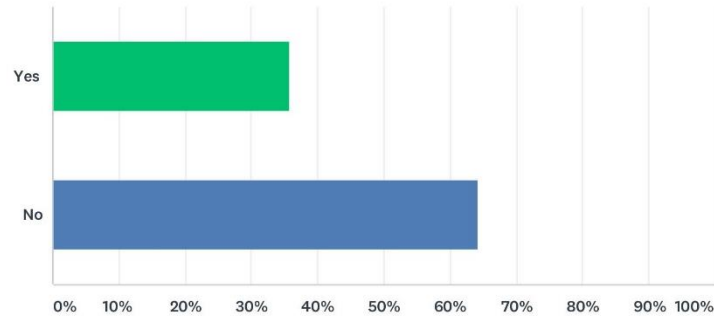
Q29 On past deck replacement projects MDOT has observed that existing prestressed and steel beams/girders do not rebound to the original camber when the deck weight is removed. Do you have a procedure or tool that you use to predict beam rebound in deck replacement projects?

Answered: 28 Skipped: 15

#	RESPONSES	DATE
1	no	9/12/2019 4:50 AM
2	No.	8/26/2019 2:23 PM
3	N/A	8/21/2019 7:23 AM
4	No	8/12/2019 12:14 PM
5	No	8/12/2019 6:46 AM
6	No.	8/9/2019 9:44 AM
7	No procedure or tool, but beam rebound should be considered in deck replacement projects.	8/7/2019 7:50 AM
8	No.	8/7/2019 4:00 AM
9	Please see BDM Section 403.5 at the following link: http://www.dot.state.oh.us/Divisions/Engineering/Structures/standard/Bridges/BDM/2019_BDM_07-19-19.pdf	8/6/2019 9:42 AM
10	At times we've measured girder location before and after deck removal, but seem to have gotten away from that practice.	8/6/2019 5:24 AM
11	No.	8/5/2019 12:21 PM
12	We had similar situation on few AASHTO type girders. We don't have a tool to predict beam rebound if any	8/2/2019 9:18 AM
13	make it up in the haunch	8/2/2019 7:55 AM
14	No. We do, however, believe that although camber predictions may be inaccurate, they are at least consistently off and conservative. We measure camber before placing the new deck -- the camber is still well within the predicted limits.	8/2/2019 5:14 AM
15	No. SCDOT has performed less than five total deck replacements.	8/1/2019 3:53 PM
16	No	8/1/2019 1:24 PM
17	No	8/1/2019 6:53 AM
18	No	8/1/2019 4:42 AM
19	No	8/1/2019 2:31 AM
20	no.	7/31/2019 2:02 PM
21	No	7/31/2019 1:58 PM
22	No	7/31/2019 1:15 PM
23	No	7/31/2019 12:50 PM
24	No.	7/31/2019 12:31 PM
25	We do not.	7/31/2019 12:14 PM
26	No. I don't know that we've done very many deck replacements on prestressed beams.	7/31/2019 12:05 PM
27	No	7/31/2019 11:56 AM
28	No	7/31/2019 11:45 AM

Q30 Have you measured the rebound of existing beams/girders after the deck weight is removed and deflection of the beams/girders after the new deck has been constructed on deck replacement projects?

Answered: 28 Skipped: 15



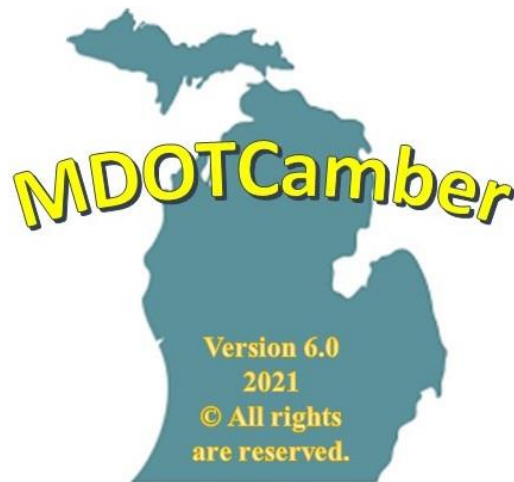
ANSWER CHOICES	RESPONSES	
Yes	35.71%	10
No	64.29%	18
TOTAL		28

Q31 Have you found a correlation between the rebound and the deflection?

Answered: 10 Skipped: 33

#	RESPONSES	DATE
1	No	8/12/2019 6:46 AM
2	Yes	8/6/2019 9:42 AM
3	Some	8/6/2019 5:25 AM
4	Yes but inconclusive because of the creep and strength gain effect	8/2/2019 9:20 AM
5	No	8/2/2019 7:55 AM
6	As you stated previously in this questionnaire, most states do not see a significant rebound. The same is true of our state.	8/2/2019 5:17 AM
7	No	8/1/2019 4:43 AM
8	No.	7/31/2019 2:02 PM
9	No	7/31/2019 12:51 PM
10	Yes.	7/31/2019 12:31 PM

APPENDIX C: COMPUTATIONAL INFRASTRUCTURE FRAMEWORK AND IMPLEMENTATION



Research Team

Wayne State University:

Fatmir Menkulasi

Christopher Eamon

Furkan Cakmak

Anthony Victor

Benesch Company:

Ihab Darwish



March 2021

Acknowledgments

Funding of this project was provided by Michigan Department of Transportation (MDOT). The research team would like to express their gratitude to MDOT for providing the opportunity to work on this project. The methods and procedures included in the proposed algorithm for predicting time dependent camber and displacements reflect authors' recommendations and do not necessarily reflect the official procedures or methods of MDOT.

Disclaimer

Though every effort has been devoted toward its accuracy, the software should not be used as a replacement for local standards of practice, design requirements, and engineering judgment. In no event shall the software developers or anyone distributing the software be liable for any damages or other liability arising from use of the software.

Software Limitations

The presented software is a tool to predict camber and displacements in fully prestressed concrete and steel beams when such beams are used in a simply supported configuration. The software considers non-composite fully prestressed concrete beams, and fully prestressed concrete and steel beams made composite with a cast in place concrete deck. The software considers one beam at a time. Continuous bridges superstructures are not addressed. For additional information refer to this manual as well as the final MDOT report titled "Evaluation of Camber and Deflections for Bridge Girders"

Table of Contents

C.1 Tab 1: Introduction	208
C.2 Tab 2: Girder Properties.....	210
C.3 Tab 3: Girder Concrete Properties	214
C.4 Tab 4: Deck Properties.....	217
C.5 Tab 5: Prestressing Steel Properties	219
C.6 Tab 6: Creep and Shrinkage Model Selection.....	221
C.7 Tab 7: Time, Environment and Measured Camber Properties	222
C.8 Tab 8: Results.....	225

List of Figures

Fig. C.1. Introduction tab.....	209
Fig. C.2. Selection of Beam Type and Analysis Type	210
Fig. C.3. Steel girder properties	211
Fig. C.4. Selection of girder type	212
Fig. C.5. Girder properties for prestressed concrete girder	213
Fig. C.6. Custom girder properties for bulb tee 49” top flange width – 54” height.....	213
Fig. C.7. Model selection for development of concrete strength and modulus of elasticity.....	215
Fig. C.8. Inputs for concrete compressive strength and overstrength factors	215
Fig. C.9. Model for modulus of elasticity at release and 28 days	216
Fig. C.10. Inputs for the decks	218
Fig. C.11. Inputs for computation of slab and screed elevations	218
Fig. C.12. Inputs for prestressing steel properties	220
Fig. C.13. Available creep and shrinkage models.....	221
Fig. C.14. Input to specify the timeline of certain construction activities and information regarding relative humidity and curing time; method to generate time matrix; and measured camber properties.....	223
Fig. C.15. Drop-down list for measured camber input.....	224
Fig. C.16. Results of time dependent analysis.....	227
Fig. C.17. Detailed analysis results: a) time dependent analysis, b) location dependent analysis for a specified time	228
Fig. C.18. Time dependent stress analysis results: a) girder, b) deck.....	229
Fig. C.19. Location based stress analysis results for a specified time: a) girder, b) deck, and c) along the depth of the composite cross-section.....	230
Fig. C.20. Slab Screed Information	231




C.1 Tab 1: Introduction

In this page, it is required to provide general project information such as project name, job number, name of the person who conducts the analysis, name of the person who checks the analysis, and date of the analysis. In addition, previously saved input files can be loaded using the “Load Project Data” button. General information about how the program works is presented and the sign convention employed throughout the analysis is shown. In this program, upward deflection (camber), negative curvature and moment (tension in the top and compression in the bottom), and compression forces are shown as negative, whereas downward deflection, positive curvature and moment (compression in the top and tension in the bottom), and tension forces are shown as positive. It is important to consider this sign convention when providing a user defined input for the program such as pre-fabricated camber values for steel beams, or measured prestressed concrete beam camber values at specific time.

MDOTCamber v6.0

Introduction
Girder Properties
Girder Concrete Properties
Deck Properties
Prestressing Steel I

Predicting Camber and Deflections in Composite Bridge Superstructures

Name of the Project:
I 75 - S11

Date:
Mar 04, 2021

Job Number:
201437


Project Data:
Load Project Data


Conducted By:
Furkan Cakmak

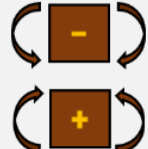
About:

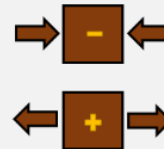
Checked By:
Fatmir Menkulasi

Sign Convention

(-) Upward Deflection

(+) Downward Deflection

(-) Negative Curvature

(+) Positive Curvature

(-) Negative Moment

(+) Positive Moment

(-) Compression

(+) Tension

Copyright © 2021 MDOTCamber. All rights reserved.

Fig. C.1. Introduction tab

C.2 Tab 2: Girder Properties

In this page, firstly, the beam type, either steel or prestressed concrete, and time dependent analysis type should be selected as shown in Fig. C.2. If the user selects to predict camber at service, then the boxes for camber at release and pre-erection camber are automatically selected. The user has the option to conduct the time dependent analysis with or without including the effects of temperature gradients. Since the inclusion of temperature gradients effects involves many numerical integrations, the analysis may take up to 120 seconds in Dell Laptop Computer with Intel Core i7 2.8 GHz and 16 GB of RAM. If the inclusion of temperature gradient effects is omitted the analysis should be completed in less than 15 seconds in a similar computer. After selecting the beam type and analysis type, the button shown inside the red box in Fig. C.2 must be clicked so that the selections are locked. Without locking the selections, the user cannot proceed with the analysis. If steel girder is selected as a beam type, the necessary input must be provided to before proceeding to the next step. Fig. C.3 shows what these necessary inputs would be if a steel beam is selected.

The screenshot displays a software interface for selecting beam type and analysis type. It is divided into two main sections: 'Select the Beam Type' and 'Analysis Type'. In the 'Select the Beam Type' section, there are two radio buttons: 'Steel Beam' (unselected) and 'Prestressed Concrete Beam' (selected). Below these is a button labeled 'Lock the selections made above', which is highlighted with a red rectangular border. The 'Analysis Type' section contains several options: 'Temperature Gradient Analysis' (checked), 'Camber at Release' (checked), 'Pre-erection Camber' (checked), and 'Service Camber' (checked). There is also a dropdown menu labeled 'Zone III' with a downward arrow.

Fig. C.2. Selection of Beam Type and Analysis Type

If a prestressed concrete beam type is selected, a drop-down menu appears as shown in Fig. C.4. This menu includes several standard girder cross-sections used by MDOT such as ASSHTO Type I-IV, MI 1800, Bulb Tees, and Box Beams. The menu includes three types of girder cross-section: I-shaped, Rectangular, and Box. If the girder to be used in the analysis matches with one of the standardized cross-sections, cross-sectional properties are automatically calculated. To see the automatically calculated values the button with the exclamation mark shown in Fig. C.5 must be clicked. If the girder in question has a I-shape, rectangular shape, or box shape but does not match with one the standardized cross-sections, then the user has the option to enter custom cross-sectional properties.

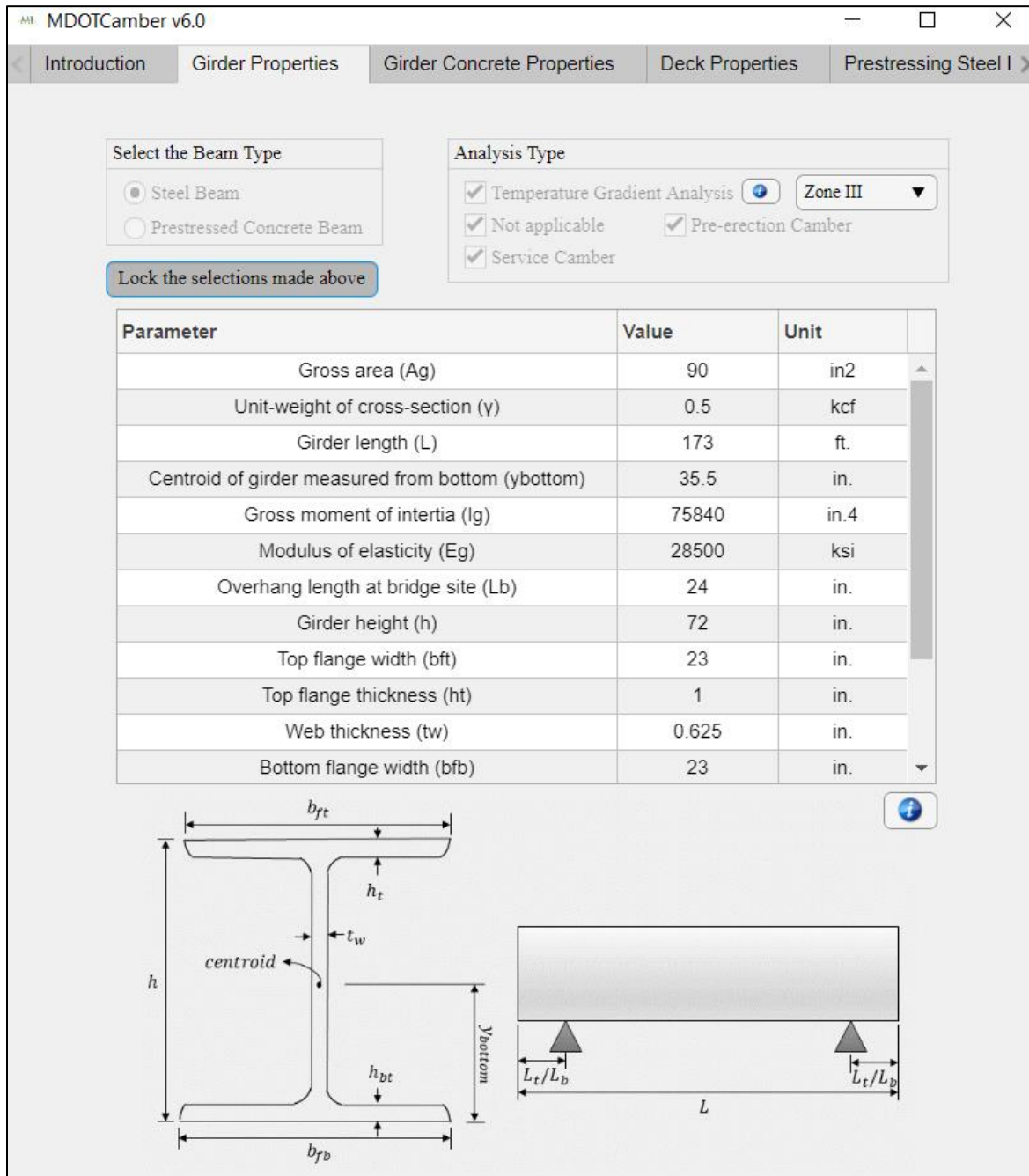


Fig. C.3. Steel girder properties

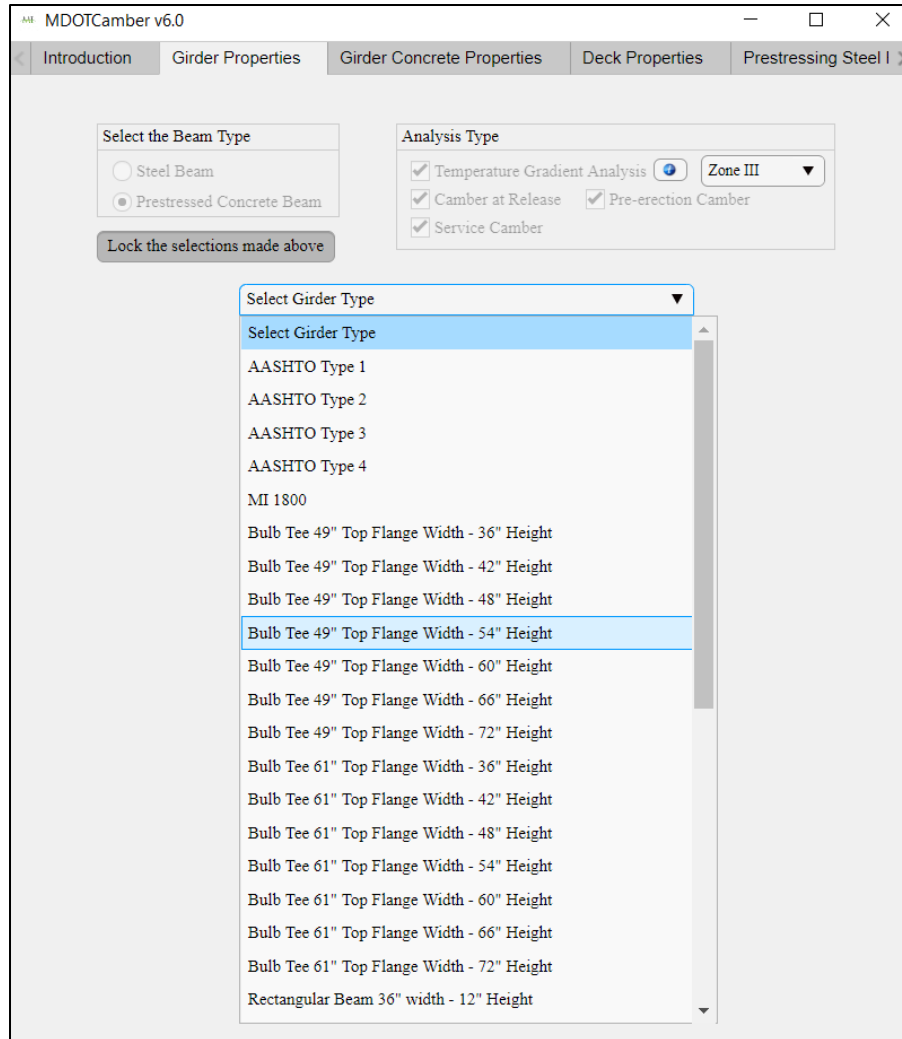


Fig. C.4. Selection of girder type

MDOTCamber v6.0

Introduction Girder Properties Girder Concrete Properties Deck Properties Prestressing Steel I >

Select the Beam Type

☐ Steel Beam

☒ Prestressed Concrete Beam

Lock the selections made above

Analysis Type

☒ Temperature Gradient Analysis ☒ Zone III

☒ Camber at Release ☒ Pre-erection Camber

☒ Service Camber

Bulb Tee 49" Top Flange Width - 54" Height

Parameter	Value	Unit
Unit-weight of cross-section* (γ)	0.15	kcf
Girder length (L)	136.9	ft.
Overhang length at precast facility (L_t)	21.5	in.
Overhang length at bridge site (L_b)	5.5	in.
Girder tributary width** (s)	8.41	ft.
Thermal expansion coefficient (α)	6.7e-06	1/F

Diagram illustrating the cross-section and geometry of a Bulb Tee girder. The cross-section shows dimensions: b_f (top flange width), h_f (top flange thickness), h_t (height of top inclined surface), t_w (web thickness), h (total height), and y_{bottom} (centroid measured from bottom). The diagram also shows the girder length L and overhang lengths L_t/L_b at the precast facility and bridge site.

Fig. C.5. Girder properties for prestressed concrete girder

MDOTCamber

Parameter for Bulb Tee 49" Top Flange Width - 5...	Value	Unit
Gross area (A_g)	1022.3	in.2
Centroid of girder measured from bottom (y_{bottom})	27	in.
Gross moment of inertia (I_g)	412056	in.4
Girder height (h)	54	in.
Perimeter of cross-section (S_g)	251.4	in.
Top flange width (b_f)	49	in.
Top flange thickness (h_f)	5	in.
Web thickness (t_w)	8	in.
Height of top inclined surface (h_t)	3.51	in.

Fig. C.6. Custom girder properties for bulb tee 49" top flange width – 54" height

C.3 Tab 3: Girder Concrete Properties

This page applies only to prestressed concrete girders and consists of three parts. The first involves the selection of a model to determine the variation of modulus of elasticity with time (Fig. C.7). The user has two options: 1) ACI 209R-92, and 2) fib MC 2010. ACI 209R-92 is recommended solely because the camber data provided in the final report was evaluated based on the selection of this model as well as other applicable American models for predicting modulus of elasticity at prestress release and at 28 days, as well as creep and shrinkage models. While the use of these combination of models resulted in reasonable estimations of pre-erection camber when compared to measured data, the user is encouraged to evaluate other models with the purpose of obtaining a range of camber and displacements estimations and be prepared to accommodate this range of variation.

The second part requires the specification of compressive strength at prestress release and 28 days (Fig. C.8 and Fig. C.9). Here the user has the option of providing specified values and no overstrength factors or adjusting the specified values with overstrength factors. Various options are provided for specifying overstrength factors including Michigan overstrength factors that were derived based on compressive strength data analyzed as part of this research. The specification of compressive strength at release and 28 days is required to determine the modulus of elasticity at release and 28 days, which is the focus of the third part (Fig. C.10 and Fig. C.12). The modulus at 28 days serves as an anchor point to obtain the development of modulus with time, which is obtained based on the model selected in the first part (Fig. C.7). The user has the option of either entering measured values of modulus at release and 28 days, which is uncommon, but possible in special cases, or the option of selecting a model that relates compressive strength at release and 28 days to modulus at these two times. The models available for relating compressive strength to modulus are AASHTO LRFD 2020, fib MC 2010, ACI 318-19, and ACI 363R-92. It is recommended that the AASHTO LRFD 2020 model is selected and since this model together with other applicable models was evaluated as part of this research effort and resulted in reasonable predictions of pre-erection camber and displacements when compared to measured values. Although, as indicated above the user is encouraged to explore the use of other models to get an idea about the range of variation in results. The evaluations of other models and their combinations was outside the scope of this research. Even if such a comparison is made, no definitive conclusion can be drawn as the results are a function of the dataset considered. Once a model is selected the

user has the option to either select certain parameters to determine the variation of modulus with time based on the model selected in part 1, or, to back calculate these parameters using the modulus at release and 28 days as anchor points. The latter option is recommended.

A. Variation of Modulus of Elasticity with Time

ACI 209R-92 (Recommended) ▼

Select a Model
ACI 209R-92 (Recommended)
fib MC 2010

☐ Click to provide actual concrete

8 Days

Fig. C.7. Model selection for development of concrete strength and modulus of elasticity

B. Concrete Compressive Strength at Release and at 28 Days

☐ Click to provide actual concrete compressive strength values.

Specified Concrete Compressive Strength

Symbol	Definition	Value (ksi)
f _{ci}	Specified concrete compressive strength at release	7
f _c	Specified concrete compressive strength at 28 day	10

Overstrength Factors for Concrete Strength

Michigan Factors (Recommended) ▼

Symbol	Definition	Factor
OS _i	Overstrength factor for concrete at release	1.2
OS ₂₈	Overstrength factor for concrete at 28 day	1.2

Fig. C.8. Inputs for concrete compressive strength and overstrength factors


C. Modulus of Elasticity at Release and at 28 Days

☒ Click to provide actual modulus of elasticity values.

Actual Modulus of Elasticity


Symbol	Definition	Value (ksi)
Eci	Actual modulus of elasticity at release	5000
Ec	Actual modulus of elasticity at 28 day	6000

Required Parameters for modulus of elasticity


☒ Back-calculate parameters. 


C. Modulus of Elasticity at Release and at 28 Days

☐ Click to provide actual modulus of elasticity values.

Model for estimating elastic modulus: AASHTO LRFD 2020 (Recommended) ▼ 

Required Parameters for modulus of elasticity

☒ Back-calculate parameters. 

Unit-weight of plain concrete (wc): 0.15 kcf 

Aggregate factor (K1): 1

Fig. C.9. Model for modulus of elasticity at release and 28 days

C.4 Tab 4: Deck Properties

If the user wishes to predict camber and displacements at service then this page can be used to enter parameters related to deck properties. If the scope of the analysis is limited to pre-erection camber then no deck parameters need to be specified. The program has the capability to consider the effect of existing deck removal and new deck placement on prestressed concrete beam camber and displacements. If project in question does not involve deck replacement, only the properties for the existing deck need to be entered. If the project includes deck replacement, then the user must specify the properties of the new deck to predict net camber and displacements after the placement of the new deck. Additionally, it should be noted that unlike in the girder concrete properties tab, only the concrete compressive strength at 28 days is required for the deck. It is assumed that deck concrete compressive strength at the end of curing period is assumed to be 80 % of its 28 day value, and the AASHTO LRFD 2020 model is selected to estimate the deck concrete modulus of elasticity at 28 days. Also, the development of deck concrete modulus with time is based on the ACI 209R-92 model assuming Type 1 cement and moist curing. Since deck concrete compressive strength and modulus are not as influential as girder concrete compressive strength and modulus on camber and displacements, it was decided to use only the models specified above.

To facilitate the determination of slab and screed elevations, the user must specify information related to the weight of deck formwork, reinforcement weight, and diaphragm weight and number. This information is used to compute the deflected beam shape at various stages of loading. The required information is shown in Fig. C.11.

Has the deck been replaced?

☒ Yes
☐ No

Parameter for the First Deck	Value	Unit
Specified concrete compressive strength at 28 day (f_{cd})	4	ksi
Unit-weight of deck and haunch* (with mild steel) (γ)	0.15	kcf
Average deck thickness** (td)	9	in.
Aggregate factor^ (K1)	1	-
Unit weight of plain concrete^ (wc)	0.145	kcf
Average haunch thickness (th)	0	in.
Overlay thickness (to)	2	in.
Unit-weight of overlay (γ_o)	0.14	kcf
Barrier load^^ (wb)	0.04	klf

Parameter for the Second Deck	Value	Unit
Specified concrete compressive strength at 28 day (f_{cd})	4	ksi
Unit-weight of deck and haunch* (with mild steel) (γ)	0.15	kcf
Average deck thickness** (td)	9	in.
Aggregate factor^ (K1)	1	-
Unit weight of plain concrete^ (wc)	0.145	kcf
Average haunch thickness (th)	0	in.
Overlay thickness (to)	2	in.
Unit-weight of overlay (γ_o)	0.14	kcf
Barrier load^^ (wb)	0.04	klf

Fig. C.10. Inputs for the decks

Parameter	Value	Unit
Slab formwork load (wsf)	10	psf
Surface load due to rebars (wsr)	4	psf
Diaphragm load (Pd)	5	kips
Number of interior diaphragms* (Ndp)	1	-

Fig. C.11. Inputs for computation of slab and screed elevations

C.5 Tab 5: Prestressing Steel Properties

In this page, the user specifies the properties and configuration of prestressing strands. This information is provided in three tables. The first table includes information about cross-sectional and mechanical properties. The second and third table include information regarding the configuration of strands. For example, in the second layer the user has the option to specify bonded as well as debonded strands including the length of debonding. The third table provides the opportunity to specify the configuration of any harped strands including harping point and eccentricities at the end and midspan. The following additional explanation can be found by clicking the button with the exclamation mark.

- a. Layer: It is a set of strands positioned at the same elevation.
- b. Layer Group: It is a subset of strands within a Layer with identical harping or debonding configurations.
 - Fully Bonded, Straight Strands (Table 2)
 - Debonded, Straight Strands (Table 2)
 - Harped Strands (Table 3)
- c. Layer Group Detail Length = debonded length
- d. Hold-down location from girder end = harping point
- e. Distance from bottom of girder represents the distance from the bottom of girder to centroid of a layer group.
- f. To add or remove a Layer Group, the +/- buttons next to the tables shall be used.
- g. Nominal diameter, d_{ps} , for strands must be provided as a decimal value, and shall be selected from the available options:

- | | |
|------------------------|-----------------------|
| ▪ $d_{ps} = 0.375$ in. | $d_{ps} = 0.4375$ in. |
| ▪ $d_{ps} = 0.5$ in. | $d_{ps} = 0.5625$ in. |
| ▪ $d_{ps} = 0.60$ in. | $d_{ps} = 0.62$ in. |
| | $d_{ps} = 0.70$ in. |

- h. For the strand type, the input value must be either 1 or 2 for low-relaxation and stress-relieved strand types, respectively.
- i. To perform the analysis, at least one layer group must be fully bonded. It can be either fully bonded straight or harped. In other words, analysis with only debonded strands cannot be conducted.

☒ Check if there is any harped strand.

f

Parameter	Value	Unit
Modulus of elasticity (Eps)	28500	ksi
Nominal diameter (dps)	0.6	in.
Ultimate tensile strength (fpu)	270	ksi
Jacking stress (fpj)	202.5	ksi
Yield stress (fpy)	243	ksi
Strand Type	1	1:Low-r...

Layer Group	Group Type	Number of Strands in Layer Group	Distance from Bottom of Girder (in.)	Debonded Length (ft.)
1	Fully Bonded, Straight	14	2	0
2	Fully Bonded, Straight	16	4	0
3	Fully Bonded, Straight	12	6	0
4	Fully Bonded, Straight	8	8	0
5	Fully Bonded, Straight	2	10	0
6	Debonded, Straight	1	2	4
7	Debonded, Straight	2	2	12

Layer Group	Group Type	Number of Strands in Layer Group	Distance from Bottom of Girder at Midspan (in.)	Distance from Bottom of Girder at End (in.)	Harping Point (ft.)
1	Harped	12	7	46	44.77

Fig. C.12. Inputs for prestressing steel properties

C.6 Tab 6: Creep and Shrinkage Model Selection

In this page, the user can select one of out of eight creep and shrinkage models (Fig. C.13), which would be used for beam and deck concrete. The AASHTO Body 2020 model is recommended as this is the model that was evaluated as part of this research and together with the other selected models resulted in reasonable estimations of pre-erection camber when compared to measured values. As noted earlier, the user is encouraged to evaluate all models to get a sense for the anticipated variability in camber and displacement predictions. The model labeled as AASHTO Body 2020 is based on creep the shrinkage models provided in AASHTO LRFD Specifications using equations presented in the body of AASHTO. AASHTO Commentary means that the creep and shrinkage models are based on alternative parameters provided in the commentary of AASHTO. Depending on the selected model type, additional parameters about properties of concrete mixture such as water content, air content, and cement content may be required. The default parameters were taken from MDOT project (I75-S11 Job No. 201437). The user should specify the applicable values for the project in question (if they are known). Additional information can be obtained by clicking the “i” (information) buttons or by consulting the final MDOT report titled “Evaluation of Camber and Deflections for Bridge Girders”.

Note: After the model is selected, the parameters corresponding to the selected model should be provided. If they are not known, default values (shown below if appropriate) will be assigned to them.

Creep and Shrinkage Model: AASHTO Body 2020 (Recommended) ▼ i

Parameter
Tensile creep magnif
Flexural creep magni

Parameters needed to be defined:

AASHTO Body 2020
For this model, no parameter is required.

Select a Model

AASHTO Body 2020 (Recommended)

AASHTO Commentary 2020

ACI 209R-92

Bazant-Baweja B3

CEB MC90

CEB MC90-99

GL 2000

fib MC 2010

i

Fig. C.13. Available creep and shrinkage models

C.7 Tab 7: Time, Environment and Measured Camber Properties

In this page, the user has the option to specify the timeline of certain construction activities and information regarding relative humidity and curing time (Fig. C.14). The user has also the option to select the method for generating the time matrix. Two options are available: Proposed, and Gilbert and Ranzi (2010). For additional information regarding these two methods please consult the final MDOT report titled “Evaluation of Camber and Deflections for Bridge Girders” or click the “i” button for a brief explanation. In addition, the user has the option of entering any measured camber data that may be available at a certain time (Fig. C.14). If such data is entered, then the algorithm conducts camber and displacements predictions for any point in time after the time when such measurements were taken. It should be noted that the measured camber values should be entered based on the sign convention stated in page 1. Additionally, the user should specify the number of beam sections to be considered in analysis. This number affects accuracy as well as the deflected shape of the beam. To obtain a smooth curve for the deflected shape at least 51 sections are recommended. Since analysis time highly depends on this input, values higher than 200 are not recommended as they are not necessary.

MDOTCamber v6.0

Creep and Shrinkage Model Selection

Time, Environment and Measured Camber Properties

Results

Number of sections to be investigated:

A. Time and Environment Properties

Parameter	Value	Unit
Relative humidity* (H)	70	%
Age of girder when prestressing strands are released (t1)	1	days
Age of girder at deck placement (t2)	28	days
Age of girder when barrier load is applied on first super-structure (t3)	35	days
Age of girder when overlay load is applied on first super-structure (t4)	35	days
Age of girder at deck removal (t5)	18250	days
Age of girder at new deck placement (t6)	18260	days
Age of girder when barrier load is applied on second super-structur...	18267	days
Age of girder when overlay load is applied on second super-structur...	18267	days

Time Matrix Generation

Proposed (Recommended)

Gilbert et al. (2010)

A logarithmic timescale will be assigned for conducting time-dependent calculations. Please consult user's manual for detailed information.

B. Measured Camber Properties

☒ Check if there is any measured camber value.

Provide measured camber input for a particular time

Fig. C.14. Input to specify the timeline of certain construction activities and information regarding relative humidity and curing time; method to generate time matrix; and measured camber properties

Provide measured camber input for a particular time
Measured camber at release (Δ_{im})
Measured camber at pre-erection state (Δ_{pm})
Measured camber just after deck placement (Δ_{adp})
Measured camber just before application of barrier load (Δ_{babl})
Measured camber just after application of barrier load (Δ_{aab1})
Measured camber just before application of overlay load (Δ_{baol})
Measured camber just after application of overlay load (Δ_{aaol})
Measured camber just before deck removal (Δ_{bdr})
Measured camber just after deck removal (Δ_{adr})
Measured camber just before new deck placement (Δ_{bndp})
Measured camber just after new deck placement (Δ_{andp})
Measured camber just before application of barrier load (Δ_{babl2})
Measured camber just after application of barrier load (Δ_{aab12})
Measured camber just before application of overlay load (Δ_{baol2})
Measured camber just after application of overlay load (Δ_{aaol2})
Provide measured camber input for a particular time ▼

Fig. C.15. Drop-down list for measured camber input

C.8 Tab 8: Results

In this page the user can click on the “calculate” button to conduct the time dependent analysis. Once the analysis is completed, the results will be presented as shown in Fig. C.16. The first table shows the net camber with and without the effects of positive and negative temperature gradients at several discrete times. This data can be downloaded as an excel file using the “Download Data” button. The figure shows the full camber and displacement history from the inception of prestressed concrete girders to the end of the service life of the bridge. The second table provides the data for the full camber and displacement history in a tabular format. This data can also be downloaded as an excel file using the “Download Data” button. The user has also the option of calculating camber at a specific time by entering the desired time in days and by clicking the “Get Camber” button. The user can save the project data by clicking on the “Save Project Data” button. This greatly facilitates the re-running of the analysis if one of the parameters is decided to be changed at a later time. The results shown in this tab can be saved as an image file and later printed by clicking on the “Print Results” file.

In addition to this information, the user can obtain additional results by clicking on the “Detailed Analysis” button next to the “Calculate” button. This prompts the generation of a new window with two tabs: “Time Based Analysis” and “Location Based Analysis”. Clicking on the “Time Based Analysis” tab the user will prompt the generation of three figures (Fig. C.17a). The first shows the full 3D camber and displacement history along the span of the beam starting from support to midspan. The second shows the variation of curvature with time at midspan, and the third shows the variation of prestress with time at midspan.

Clicking on the “Location Based Analysis” tab will prompt the user to enter the time at which analysis is to be conducted (for example 1000 days). Providing this information and clicking on the “Calculate” button will prompt the generation of three figures and one table Fig. C.17b. The first shows the variation of curvature along the span at the specified time, the second shows the variation of camber along the span at the specified time (i.e. deflected shape), and the third shows the variation of prestress along the span at the specified time. The table provides the data that is used to plot the deflected shape of the beam for half of the span and can be downloaded by clicking the “Download Data” button.

To conduct a time dependent stress analysis, the user must click on the “Stress Analysis” button. This option provides information how the stresses in the beam and deck vary as a function of time along the span. After clicking on the stress analysis button, a new window appears, which features three tabs: a) “Stress Analysis for Girder”; b) “Stress Analysis for Deck”, and c) “Location Based Analysis”. Under the “Stress Analysis for Girder” tab, the user can see two 3D graphs which shows the stress history for girder top and bottom fibers, and one 2D graph which shows the variation in stresses at the top and bottom fibers for girder at midspan (Fig. C.18a). The same results can also be obtained for the deck, or decks if there is deck replacement activity by selecting the “Stress Analysis for Deck” tab (Fig. C.18.b). Under “Location Based Analysis” tab, the user can select a time to obtain the girder and deck stresses at the top and bottom fibers along the span (Fig. C.19.a and Fig. C.19.b). In addition, the cross-sectional stress distribution for a given time can be obtained as shown in Fig. C.19c.

Finally, by clicking on “Slab and Screed Guidance” button the user may obtain information to plot the deflected shape of the beam at different stages (Fig. C.20).

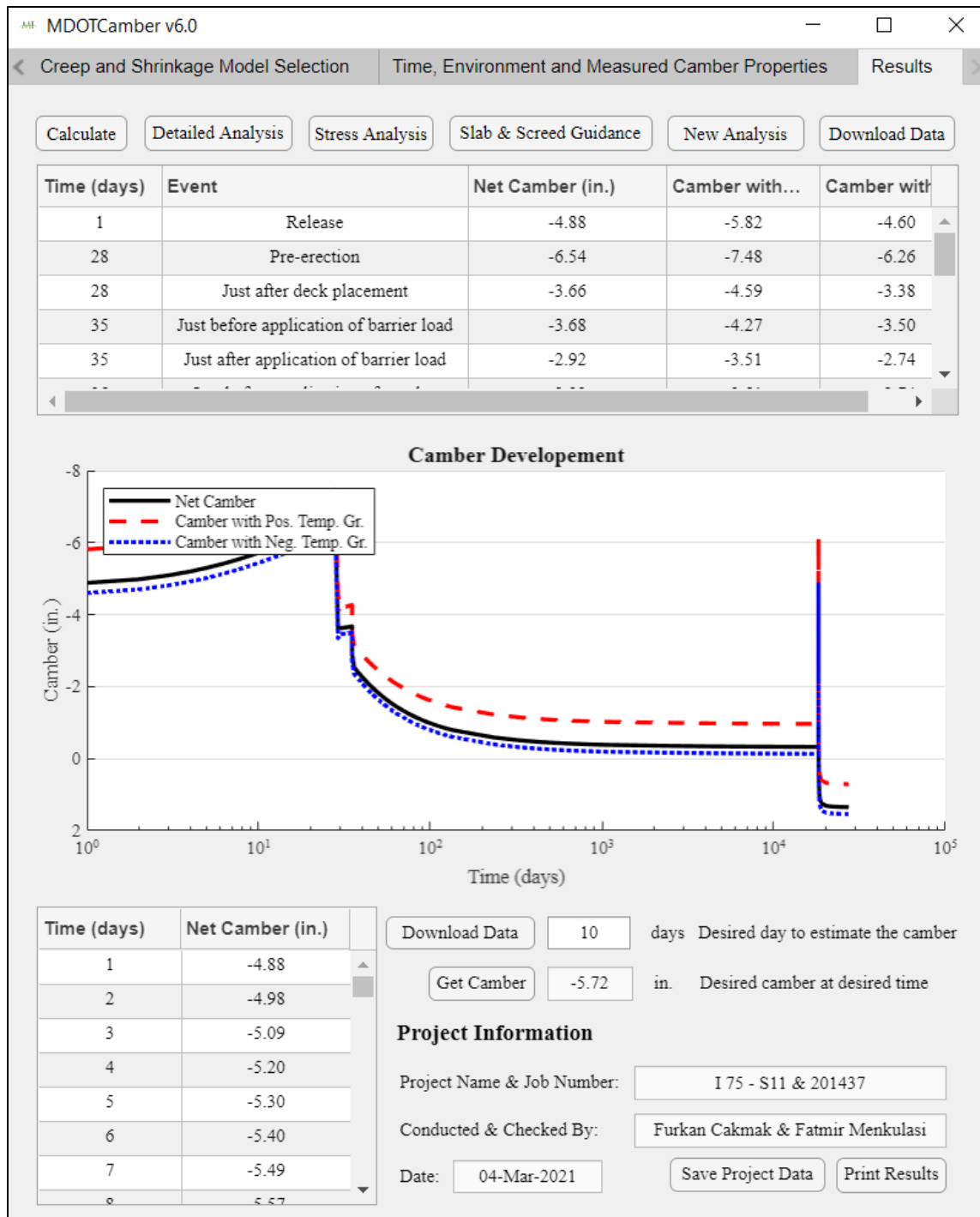
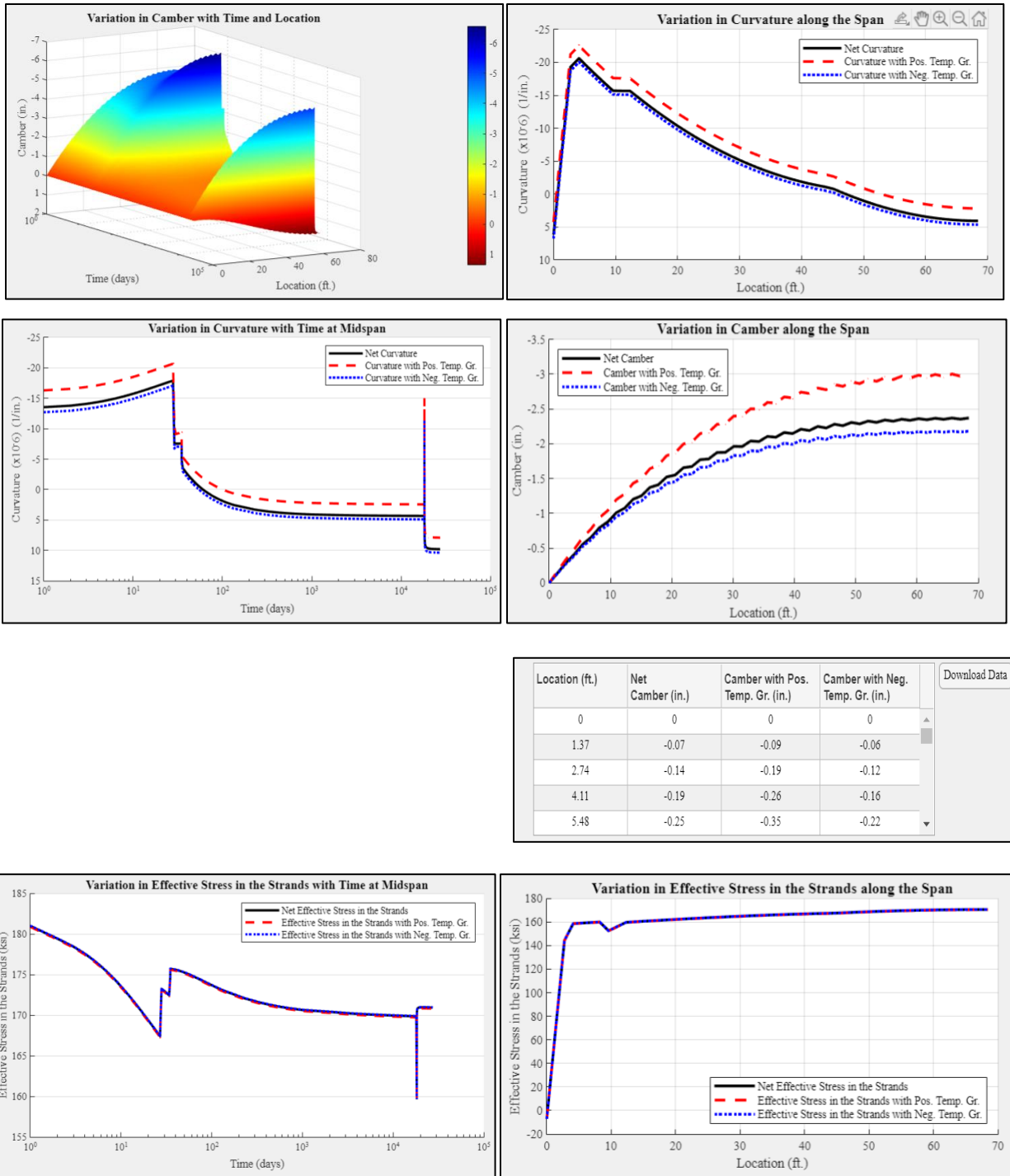


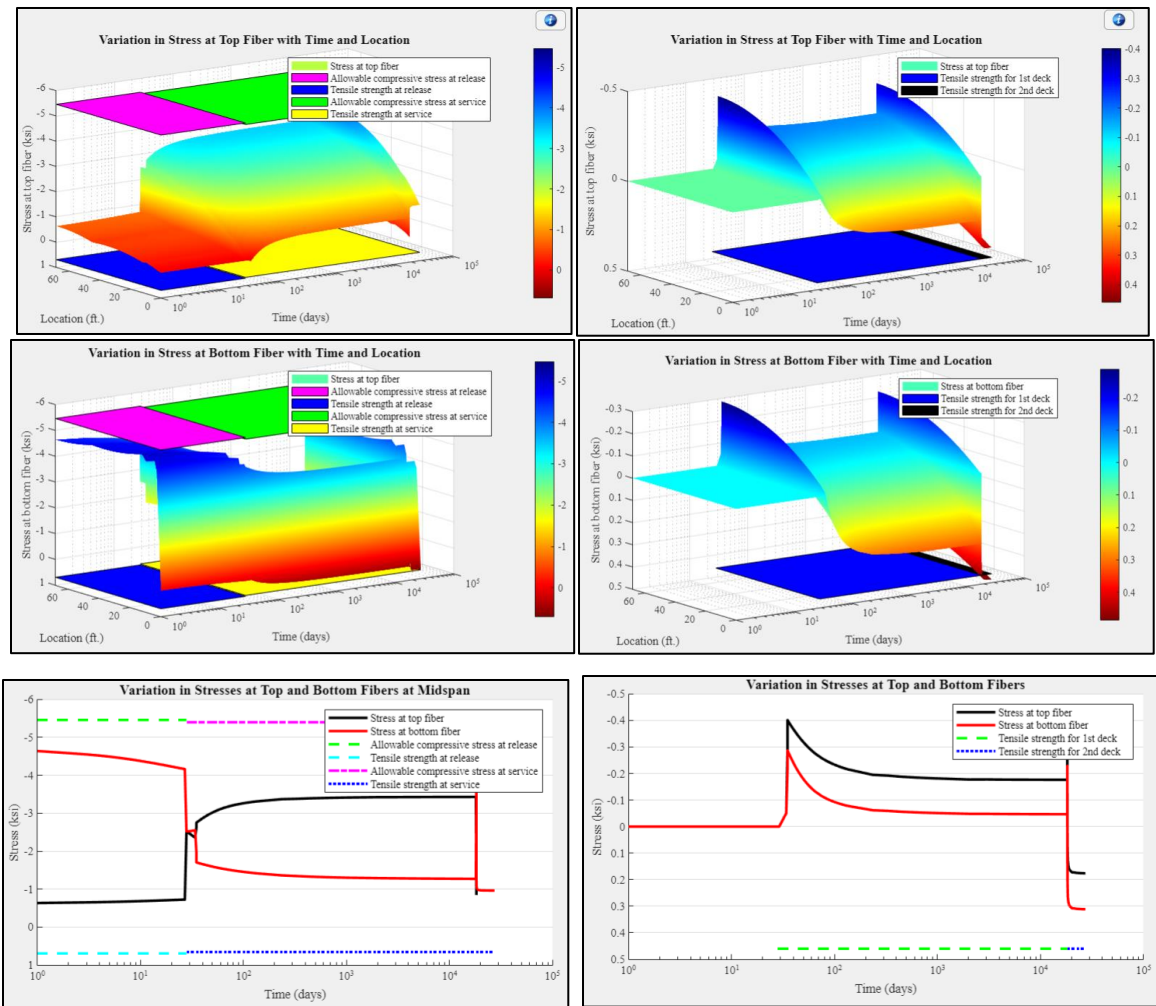
Fig. C.16. Results of time dependent analysis



a)

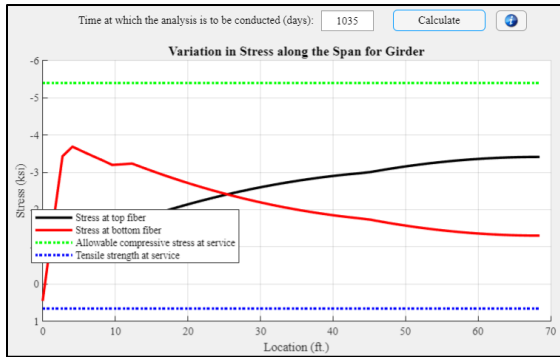
b)

Fig. C.17. Detailed analysis results: a) time dependent analysis, b) location dependent analysis for a specified time

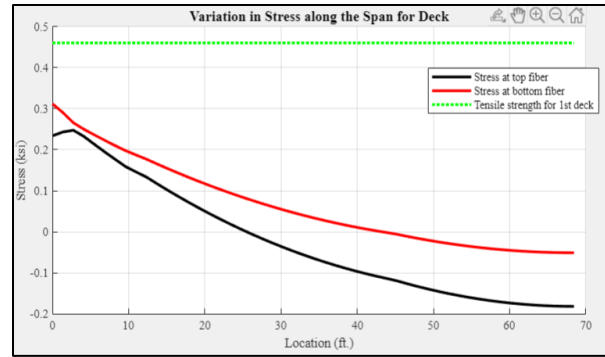


a) b)

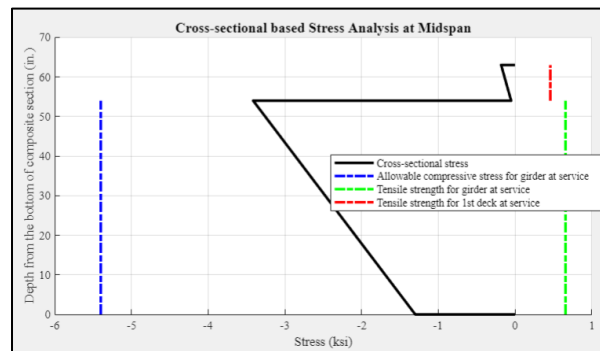
Fig. C.18. Time dependent stress analysis results: a) girder, b) deck



a)



b)



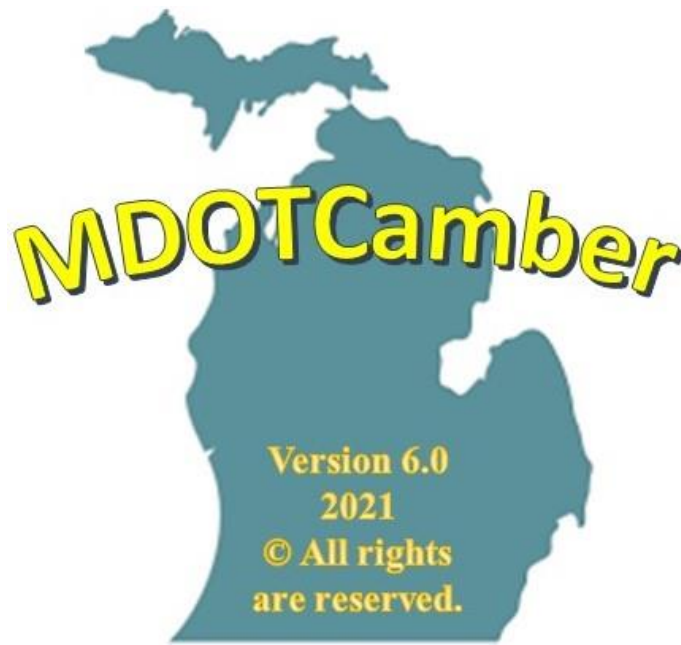
c)

Fig. C.19. Location based stress analysis results for a specified time: a) girder, b) deck, and c) along the depth of the composite cross-section

For the first super-structure					Download Data
Location (ft.)	Net Camber just after girder erection (in.)	Net Camber just after app. of formwork and deck rein. (in.)	Net Camber just after app. of diaphragm load (in.)	Net Camber just after app. of deck load (in.)	
0	0	0	0	0	▲
1.37	-0.30	-0.30	-0.30	-0.21	
2.74	-0.60	-0.59	-0.59	-0.42	
4.11	-0.88	-0.87	-0.87	-0.62	
5.48	-1.18	-1.17	-1.16	-0.83	
6.84	-1.43	-1.42	-1.42	-1.00	
8.21	-1.73	-1.71	-1.71	-1.30	▼
For the second super-structure					Download Data
Location (ft.)	Net Camber of girder alone on bridge site (in.)	Net Camber just after app. of formwork and deck rein. (in.)	Net Camber just after app. of diaphragm load (in.)	Net Camber j after app. of deck load (in	
0	0	0	0	0	▲
1.37	-0.30	-0.30	-0.29	-0.21	
2.74	-0.60	-0.59	-0.59	-0.42	
4.11	-0.87	-0.86	-0.86	-0.61	
5.48	-1.17	-1.16	-1.15	-0.82	
6.84	-1.42	-1.40	-1.40	-0.98	
8.21	-1.71	-1.60	-1.60	-1.10	▼

Fig. C.20. Slab Screed Information

APPENDIX D: PRESTRESSED CONCRETE BEAM EXAMPLE



Research Team

Wayne State University:

Fatmir Menkulasi

Christopher Eamon

Furkan Cakmak

Anthony Victor

Alfred Benesch & Company:

Ihab Darwish



March 2021

Table of Contents

D.1 Definition of the Problem.....	240
D.2 Definition of Parameters	244
D.3 Camber at Release	273
D.4 Pre-erection Camber	278
D.5 Camber just after Placement of 1 st Deck.....	284
D.6 Camber just before Application of Barrier and Overlay Loads on 1 st Superstructure.....	286
D.7 Camber just after Application of Barrier and Overlay Loads on 1 st Superstructure	291
D.8 Camber just before Deck Removal Process.....	292
D.9 Camber just after Deck Removal Process	295
D.10 Camber just before 2 nd Deck Placement.....	299
D.11 Camber just after 2 nd Deck Placement.....	300
D.12 Camber just before Application of Barrier and Overlay Loads on 2 nd Super-structure.	301
D.13 Camber just after Application of Barrier and Overlay Loads on 2 nd Super-structure ...	303
D.14 Camber at Final Time	305
D.15 Nomenclature	309

List of Figures

Fig. D.1. PCBT 54 girder dimension and strand pattern at; a) end and b) midspan	240
Fig. D.2. Notations used for bridge super-structure.....	242
Fig. D.3. Sign convention	244

List of Tables

Table D.1. Debonded strand information	241
Table D.2. Detailed strand location information	241
Table D.3. Prestressing strand properties	241
Table D.4. Parameters for PCBT 54" girder and project specific information.....	242
Table D.5. Parameters related to first and second decks.....	243
Table D.6. Time arrangement for major activities.....	243
Table D.7. Section array.....	245
Table D.8. Creep function for girder.....	251
Table D.9. Shrinkage array for girder.....	252
Table D.10. Creep function for 1 st deck.....	253
Table D.11. Shrinkage array for 1 st deck.....	254
Table D.12. Creep function for 2 nd deck.....	254
Table D.13. Shrinkage array for 2 nd deck	255
Table D.14. Elastic modulus development for girder with time.....	256
Table D.15. Elastic modulus development for 1 st and 2 nd deck with time.....	257
Table D.16. Modular ratio and transformed area for prestressing strands.....	258
Table D.17. Modular ratio and transformed area for the 1 st and 2 nd deck	258
Table D.18. Net transformed area for the non-composite structure.....	259
Table D.19. Net transformed area for the 1 st and 2 nd composite structures	259
Table D.20. Location of prestressing strands with respect to bottom of girder	260
Table D.21. Eccentricity of prestressing strand in transformed non-composite structure	260
Table D.22. Centroid of transformed non-composite structure with respect to bottom of girder	260
Table D.23. Moment of inertia of transformed non-composite structure	261
Table D.24. Centroid of transformed composite structure with respect to bottom of girder.....	262
Table D.25. Eccentricity of prestressing strand in transformed composite structure	262
Table D.26. Transformed moment of inertia for the 1 st and 2 nd deck.....	262
Table D.27. Moment of inertia of transformed composite structure with 1 st and 2 nd deck.....	263
Table D.28. Moment applied on non-composite structure due to girder self-weight	274
Table D.29. Axial force and moment on non-composite structure due to straight strands	275

Table D.30. Axial force and moment on non-composite structure due to debonded strands....	275
Table D.31. Axial force and moment on non-composite structure due to harped strands	276
Table D.32. Axial force and moment on non-composite structure due to prestressing	277
Table D.33. Net axial force and moment on non-composite structure due to prestressing and girder self-weight effect.....	277
Table D.34. Net curvature due to combined effects at camber at release.....	277
Table D.35. Application of Simpson's rule and camber at release	278
Table D.36. Forces on girder alone due to girder self-weight	279
Table D.37. Forces on girder alone due to prestressing.....	279
Table D.38. Net axial force and moment on girder due to combined effect at release.....	280
Table D.39. Coefficient K_i as a function of location.....	280
Table D.40. Stress on the strands along the span prior to transfer.....	280
Table D.41. Force history array on girder as a function of time and location.....	280
Table D.42. Change in curvature between time t_1 and t_2	284
Table D.43. Net curvature at pre-erection.....	284
Table D.44. Pre-erection camber	284
Table D.45. Moment applied on non-composite structure due to girder self-weight on bridge site	284
Table D.46. Change in curvature due to change in support conditions.....	285
Table D.47. Moment applied on non-composite structure due to 1 st deck self-weight.....	285
Table D.48. Change in curvature due to 1 st deck self-weight.....	285
Table D.49. Net curvature just after 1 st deck is placed	286
Table D.50. Camber just after placement of 1 st deck.....	286
Table D.51. Change in forces on girder due to time-dependent effects between t_1 and t_2	286
Table D.52. Change in forces on girder due to change in support conditions	286
Table D.53. Change in forces on girder due to 1 st deck self-weight	287
Table D.54. Net force history array just after 1 st deck is placed.....	287
Table D.55. Change in curvature between time t_2 and t_3	290
Table D.56. Net curvature just before application of barrier and overlay loads	290
Table D.57. Camber just before application of barrier and overlay loads on 1 st superstructure	290
Table D.58. Moment applied on composite structure due to barrier and overlay loads	291

Table D.59. Change in curvature due to barrier and overlay load	291
Table D.60. Net curvature just after application of barrier and overlay loads	292
Table D.61. Camber just after application of barrier and overlay loads.....	292
Table D.62. Change in forces on girder and deck due to time-dependent effects between t_2 and t_3	292
Table D.63. Change in forces on girder and deck due to barrier load.....	293
Table D.64. Change in forces on girder and deck due to overlay load.....	293
Table D.65. Net force history array just after application of barrier and overlay loads.....	294
Table D.66. Change in forces on girder and deck due to time-dependent effects between t_4 and t_5	295
Table D.67. Change in curvature between time t_4 and t_5	295
Table D.68. Camber just before deck removal process.....	295
Table D.69. Change in forces on girder and deck due to removal of barrier and overlay loads	296
Table D.70. Change in curvature due to removal of barrier and overlay loads.....	296
Table D.71. Net forces on the deck just before it is removed.....	297
Table D.72. Change in forces on non-composite structure and girder due to removal of locked forces inside the deck.....	297
Table D.73. Change in curvature due to removal of locked forces inside the deck	297
Table D.74. Change in forces on girder due to deck removal	298
Table D.75. Net curvature just after deck removal.....	298
Table D.76. Camber just after deck removal	299
Table D.77. Net force history array just after 1 st deck is removed.....	299
Table D.78. Change in curvature between t_5 and t_6	299
Table D.79. Net curvature just before new deck placement.....	300
Table D.80. Camber just before new deck placement	300
Table D.81. Moment applied on non-composite structure due to 2 nd deck self-weight.....	300
Table D.82. Change in curvature due to 2 nd deck self-weight.....	301
Table D.83. Net curvature just after 2 nd deck is placed.....	301
Table D.84. Camber just after placement of 2 nd deck.....	301
Table D.85. Change in forces on girder due to time-dependent effects between t_5 and t_6	301
Table D.86. Change in forces on girder due to 2 nd deck self-weight	302

Table D.87. Net force history array just after 2 nd deck is placed	302
Table D.88. Change in curvature between time t_6 and t_7	302
Table D.89. Net curvature just before application of barrier and overlay loads	303
Table D.90. Camber just before application of barrier and overlay loads on 2 nd superstructure	303
Table D.91. Moment applied on 2 nd composite structure due to barrier and overlay loads	304
Table D.92. Change in curvature on 2 nd super-structure due to barrier and overlay load.....	304
Table D.93. Net curvature just after application of barrier and overlay loads on 2 nd super- structure	304
Table D.94. Camber just after application of barrier and overlay loads on 2 nd super-structure	305
Table D.95. Change in forces on girder and deck due to time-dependent effects between t_6 and t_7	305
Table D.96. Change in forces on girder and deck due to barrier load.....	306
Table D.97. Change in forces on girder and deck due to overlay load.....	306
Table D.98. Net force history array just after application of barrier and overlay loads.....	307
Table D.99. Change in forces on girder and deck due to time-dependent effects between t_8 and t_9	308
Table D.100. Change in curvature between time t_8 and t_9	308
Table D.101. Net curvature at final considered time	308
Table D.102. Camber at final considered time.....	308

D.1 Definition of the Problem

Using the proposed prediction methodology, Approach No. 6, explained in this thesis, camber and displacement along the span is going to be estimated at:

1. detensioning of the strands (t_1);
2. time at which the deck is placed (t_2);
3. time at placement of barriers and the opening of bridge to traffic (t_3);
4. time at placement of overlay (t_4);
5. time at deck removal for projects that features a deck replacement (t_5);
6. time at new deck placement (t_6);
7. time at placement of barrier and reopening of bridge to traffic (t_7);
8. time at placement of overlay (t_8);
9. time at the end of service life (t_9);

for the following prestressed concrete beam used in S11 project:

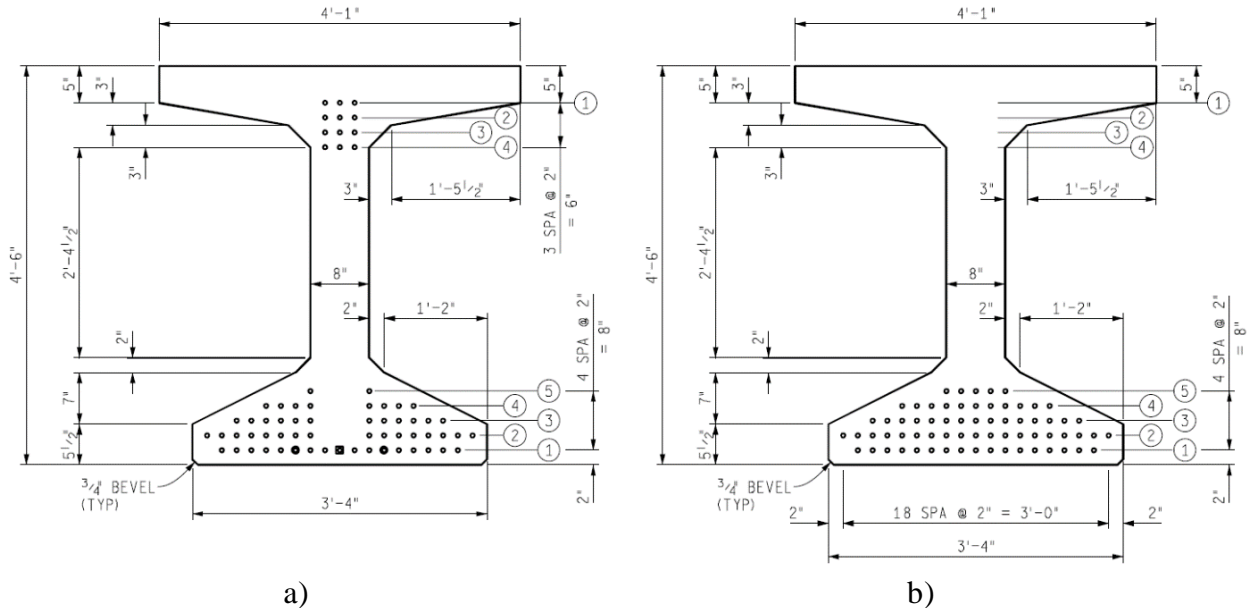


Fig. D.1. PCBT 54 girder dimension and strand pattern at; a) end and b) midspan

The strand patterns at ends and midspan are shown in Figure D.1. The strands indicated inside the circles and squares represent debonded strands whose information is provided in Table D.1.

Table D.1. Debonded strand information

STRAND LEGEND & DEBONDING TABLE		
LEGEND	NUMBER	LENGTH
■	1	4'-0"
●	2	12'-0"

Additionally, the detailed strand location as well as debonded strand information is provided in Table D.2. All the harped strands are harped at $0.33L_G$ with respect to end of the girder.

Table D.2. Detailed strand location information

Strand Location Table																		
Location	End (a)									Midspan (b)								
	Bottom					Top				Bottom					Top			
Layer #	<u>1</u>	<u>2</u>	<u>3</u>	<u>4</u>	<u>5</u>	<u>1</u>	<u>2</u>	<u>3</u>	<u>4</u>	<u>1</u>	<u>2</u>	<u>3</u>	<u>4</u>	<u>5</u>	<u>1</u>	<u>2</u>	<u>3</u>	<u>4</u>
Strand #	17	16	12	8	2	3	3	3	3	17	19	15	11	5	0	0	0	0

Furthermore, the strand properties are provided in Table D.3.

Table D.3. Prestressing strand properties

Parameter	Value
Modulus of elasticity (E_{ps}) (ksi)	28500
Nominal diameter (d_{ps}) (in.)	0.6
Ultimate tensile strength (f_{pu}) (ksi)	270
Jacking stress (f_{pj}) (ksi)	202.5
Yield stress (f_{py}) (ksi)	243
Strand type	Low-relaxation

The girder used in this project is a type of bulb tee girder with 49" top flange width and 54" height, as shown in Figure D.1. Girder properties and other relevant information are given in Table D.4. In addition to this, Figure D.2 indicates the notation used in this example problem.

Table D.4. Parameters for PCBT 54" girder and project specific information

Parameter	Value
Gross Area (A_G) ($in.^2$)	1022.3
Centroid of girder measured from bottom ($y_{Gbottom}$) ($in.$)	27
Gross moment of inertia (I_G) ($in.^4$)	412056
Girder height (h) ($in.$)	54
Perimeter of the cross-section (S_G) ($in.$)	251.4
Top flange width (b_f) ($in.$)	49
Top flange thickness (h_f) ($in.$)	5
Web thickness (t_w) ($in.$)	8
Height of top inclined surface (h_t) ($in.$)	3.51
Unit-weight of cross-section* (γ_G) (kcf)	0.155
Girder length (L_G) ($ft.$)	136.9
Girder overhang length at precast facility (L_t) ($in.$)	21.5
Girder overhang length at bridge site (L_b) ($in.$)	5.5
Average spacing of girder from center to center [†] (s_d) ($ft.$)	8.41
Thermal expansion coefficient (α) ($1/^\circ F$)	6.7E-06
*Calculated based on AASHTO LRFD (2020) Bridge Design Specifications Table 3.5.1.1 by Reinforcement weight is considered as 5 pcf.	
[†] For the fascia beams, spacing should be adjusted accordingly.	

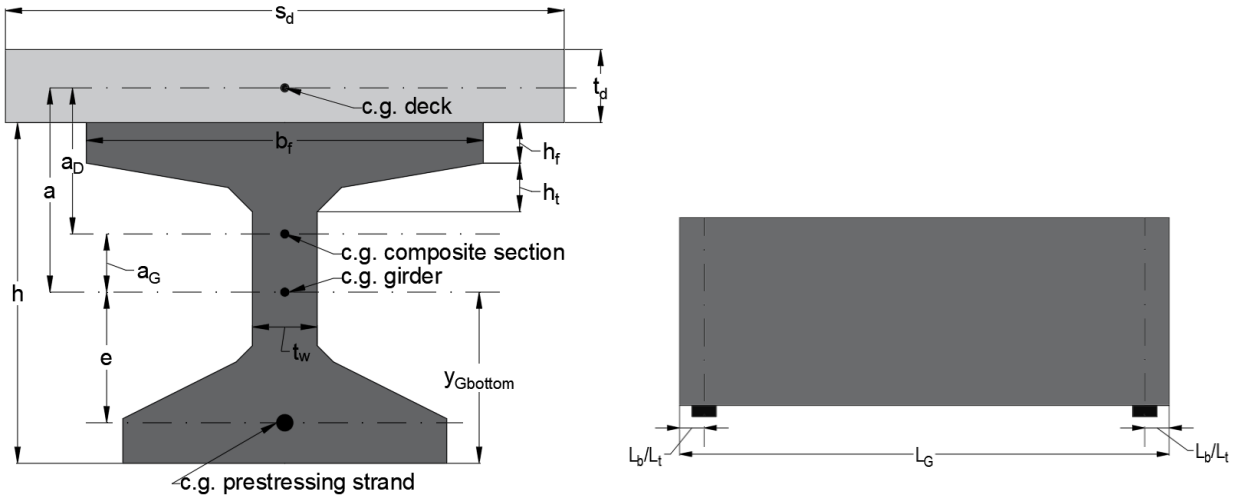


Fig. D.2. Notations used for bridge super-structure

The initial and 28-days specified concrete compressive strength for the girder are $f'_{ci} = 7$ ksi and $f'_c = 10$ ksi, respectively. Moreover, the deck concrete compressive strength at 28-days is given $f'_{cd} = 4$ ksi. The unit weight of concrete is 0.145 kcf. It is assumed that the deck is replaced

after the bridge has been in service for 50 years. The properties related to first and second decks are given in Table D.5.

Table D.5. Parameters related to first and second decks

Parameter for the First Deck	Value
Unit-weight of deck and haunch* (γ_{d1}) (pcf)	0.150
Deck thickness (t_{d1}) (in.)	9
Average haunch thickness (t_{h1}) (in.)	0
Overlay thickness (t_{o1}) (in.)	2
Unit-weight of overlay (γ_{o1}) (pcf)	0.140
Barrier load (w_{h1}) (klf)	0.475
Parameter for the Second Deck	Value
Unit-weight of deck and haunch* (γ_{d2}) (pcf)	0.150
Deck thickness (t_{d2}) (in.)	9
Average haunch thickness (t_{h2}) (in.)	0
Overlay thickness (t_{o2}) (in.)	2
Unit-weight of overlay (γ_{o2}) (pcf)	0.140
Barrier load (w_{h2}) (klf)	0.475
*Reinforcement weight is considered as 5 pcf.	

In this example, the following time arrangement is going to be utilized. It should be noted that the barrier and overlay load is applied to super-structure simultaneously so that there is no additional time-dependent activity taking place between these two events.

Table D.6. Time arrangement for major activities

Event	time index (t)	t(t) (days)
Detensioning of strands	<u>1</u>	1
Time at which the deck is placed	<u>2</u>	28
Time at placement of barriers and the opening of bridge to traffic	<u>3</u>	35
Time at placement of overlay	<u>4</u>	35
Time at deck removal for projects that features a deck replacement	<u>5</u>	18250
Time at new deck placement	<u>6</u>	18260
Time at placement of barrier and reopening of bridge to traffic	<u>7</u>	18267
Time at placement of overlay	<u>8</u>	18267
Time at the end of service life	<u>9</u>	27375

For this analysis, ACI 209R-92 model is going to be used with back-calculated parameters for the development of modulus of elasticity with time. In addition, AASHTO LRFD (2020) equation is going to be used for the estimation of modulus of elasticity at release and 28-days. Throughout the analysis, specified concrete compressive strength values are going to be utilized with no overstrength factor. Moreover, for conducting time-dependent analysis, AASHTO LRFD (2020) Body creep and shrinkage models are going to be used assuming that flexural and tensile creep are equal to compression creep. In addition to this, three sections are going to be considered along the half-span to minimize the computation effort. To estimate the deflection from curvature diagram, Simpson's rule is employed for numerical integration. It is assumed that the ambient relative humidity is 70 % for Michigan based on the map provided in AASHTO LRFD (2020) 9th Edition Figure 5.4.2.3.3-1. Moreover, it is assumed that both decks (first and second) are cured 7-days using moist curing, and the girder is cured 1-day using steam curing. While generating the time matrix for the analysis, only 1 time-step is going to be taken between the major activities stated above. Finally, the sign convention adopted in this example problem is given in the Figure D.3.

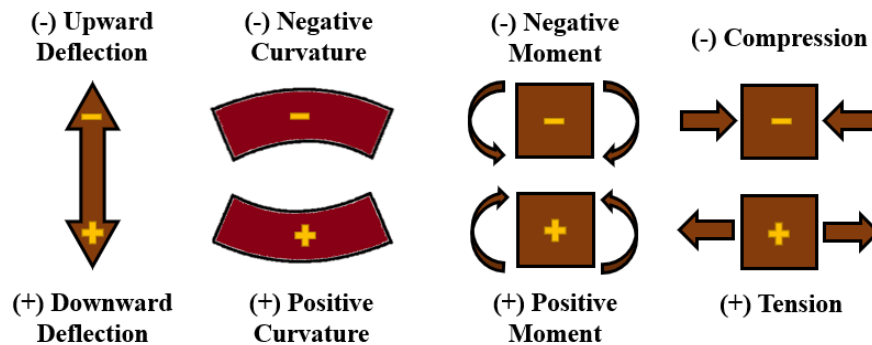


Fig. D.3. Sign convention

D.2 Definition of Parameters

- *Generate the time and section matrix*

Since only 1 time step is going to be considered in this example, the time matrix generated for this specific example would be same as in Table D.7. In addition to this, since three sections are going to be considered along the half-span, the section matrix can be assigned as follows:

Table D.7. Section array

<i>section index (x)</i>	<i>loc(x) (in.)</i>
<u>1</u>	0
<u>2</u>	410.7
<u>3</u>	821.4

It should be noted that when creating time and section dependent arrays, index number is going to be used for simplicity throughout the analysis. For example, say a parameter $A(t, x)$ is both time and section-dependent. $A(6, 3)$ refers to the value of A at time $t(t) = t(6) = 18260$ days and $loc(x) = loc(3) = 821.4$ in. from girder end.

- *Determine the prestressing related parameters such as eccentricity, strand area, debonding length, transfer length along the span and jacking force*

- Transfer length:

As specified in AASHTO LRFD (2020) 9th Edition section 5.9.4.3.1, the transfer length is assumed to be 60 times strand diameter. Between the points where bonding commences and transfer length finishes, the stress in the strands is assumed to be varying linearly.

$$L_{tr} = 60 \cdot d_{ps} \quad \text{D-1}$$

$$L_{tr} = 60 \cdot (0.6) = 36 \text{ in.}$$

- Average debonding length, total debonded strand area and eccentricity of debonded strands:

Using Table D.1, the average debonding length, total debonded strand area and eccentricity of debonded strands can be calculated as follows:

$$L_{dbavg} = \frac{\sum L_{dbi} \cdot N_i}{N_{db}} \quad \text{D-2}$$

$$A_{psdb} = A_{psi} \cdot N_{db} \quad \text{D-3}$$

$$e_{db} = y_{Gbottom} - \frac{\sum y_{dbi} \cdot N_i}{N_{db}} \quad \text{D-4}$$

Nominal area for Ø0.6 in. strand:

$$A_{psi} = 0.217 \text{ in.}^2$$

$$L_{dbavg} = \frac{(4 \cdot 12) \cdot 1 + (12 \cdot 12) \cdot 2}{1 + 2} = 112 \text{ in.}$$

$$A_{psdb} = (0.217) \cdot (2 + 1) = 0.651 \text{ in.}^2$$

$$e_{db} = 27 - \frac{(2) \cdot 2 + (2) \cdot 1}{1 + 2} = 25 \text{ in.}$$

- Average harping length, total harped strand area and eccentricity of harped strands:

Similarly, using Figure D.1 and Table D.2, the average harping length, total harped strand area and eccentricity of harped strands along the half-span can be calculated as follows:

$$L_{hpavg} = \frac{\sum L_{hpi} \cdot N_i}{N_{hp}} \quad \text{D-5}$$

$$A_{pshp} = A_{psi} \cdot N_{hp} \quad \text{D-6}$$

$$e_{hp,end} = y_{Gbottom} - \frac{\sum y_{hpi,end} \cdot N_i}{N_{hp}} \quad \text{D-7}$$

$$e_{hp,mid} = y_{Gbottom} - \frac{\sum y_{hpi,mid} \cdot N_i}{N_{hp}} \quad \text{D-8}$$

Since they change along the span, eccentricity of harped strands should be determined for each section shown in Table D.7. For this, a linear equation is going to be generated such that the eccentricity of harped strand along the span can be determined as follows:

$$\text{if } x \leq L_{hpavg} \quad e_{hp}(x) = e_{hp,end} - \frac{x \cdot (e_{hp,end} - e_{hp,mid})}{L_{hpavg}} \quad \text{D-9}$$

$$\text{if } x > L_{hpavg} \quad e_{hp}(x) = e_{hp,mid} \quad \text{D-10}$$

Since all the harped strands are harped at $0.33L_G$ from end of girder, average harping length equals to $0.33L_G$.

$$L_{hpavg} = 0.33 \cdot L_G = (0.33) \cdot (136.9 \cdot 12) = 542.1 \text{ in.}$$

$$A_{pshp} = (0.217) \cdot (3 + 3 + 3 + 3) = 2.604 \text{ in.}^2$$

$$e_{hp,end} = 27 - \frac{(3 \cdot 43 + 3 \cdot 45 + 3 \cdot 47 + 3 \cdot 51)}{(3 + 3 + 3 + 3)} = -19.5 \text{ in.}$$

$$e_{hp,mid} = 27 - \frac{(3 \cdot 4 + 3 \cdot 6 + 3 \cdot 8 + 3 \cdot 10)}{(3 + 3 + 3 + 3)} = 20 \text{ in.}$$

$$\text{if } x \leq 542.1 \text{ in.} \quad e_{hp}(x) = -19.5 - \frac{x \cdot (-19.5 - 20)}{542.1} = x \cdot (0.0729) - 19.5$$

$$\text{if } x > 542.1 \text{ in.} \quad e_{hp}(x) = 20$$

The eccentricities of harped strands at sections given in Table D.7 are provided in Table D.8.

Table D.8. Eccentricity of harped strands along the half-span

$e_{hp}(x) \text{ (in.)}$		
$e_{hp}(1)$	$e_{hp}(2)$	$e_{hp}(3)$
-19.5	10.44	20.00

- Total area and eccentricity of fully bonded, straight strands:

Using Figure D.1 and Table D.2, the total area of the remaining fully bonded, straight strand and their eccentricity can be calculated as follows:

$$A_{psst} = A_{psi} \cdot N_{st} \quad \text{D-11}$$

$$e_{st} = y_{Gbottom} - \frac{\sum y_{sti} \cdot N_i}{N_{st}} \quad \text{D-12}$$

$$A_{psst} = (67 - 3 - 12) \cdot 0.217 = 11.284 \text{ in.}^2$$

$$e_{st} = 27 - \frac{14 \cdot 2 + 16 \cdot 4 + 12 \cdot 6 + 8 \cdot 8 + 2 \cdot 10}{14 + 16 + 12 + 8 + 2} = 22.23 \text{ in.}$$

- Total effective strand area and net eccentricity along the half-span:

Using the calculation above and Table D.2, the effective strand area and net eccentricity along the half-span can be calculated as follows:

- *Net eccentricity at end, midspan and end of debonding length*

$$e_e = \frac{e_{st} \cdot N_{st} + e_{hp,end} \cdot N_{hp}}{N_{st} + N_{hp}} \quad D-13$$

$$e_{atdb} = \frac{e_{st} \cdot N_{st} + e_{db} \cdot N_{db} + \left[e_{hp,end} - (e_{hp,end} - e_{hp,mid}) \cdot \frac{L_{dbavg}}{L_{hpavg}} \right] \cdot N_{hp}}{N_{st} + N_{hp} + N_{db}} \quad D-14$$

$$e_m = \frac{e_{st} \cdot N_{st} + e_{hp,mid} \cdot N_{hp} + e_{db} \cdot N_{db}}{N_{st} + N_{hp} + N_{db}} \quad D-15$$

$$e_e = \frac{22.23 \cdot 52 - 19.5 \cdot 12}{52 + 12} = 14.64 \text{ in.}$$

$$e_{atdb} = \frac{22.23 \cdot 52 + 25 \cdot 3 + \left[-19.5 - (-19.5 - 20) \cdot \frac{112}{542.1} \right] \cdot 12}{52 + 12 + 3} = 16.34 \text{ in.}$$

$$e_m = \frac{22.23 \cdot 52 + 20 \cdot 12 + 25 \cdot 3}{52 + 12 + 3} = 21.95 \text{ in.}$$

- *Net eccentricity along the half-span*

✓ if $x \leq L_{dbavg} = 112 \text{ in.}$ & $x \leq L_{hpavg} = 542.1 \text{ in.}$

$$e(x) = e_e + \frac{x \cdot (e_{atdb} - e_e)}{L_{dbavg}} \quad D-16$$

$$e(x) = 14.64 + \frac{x \cdot (16.34 - 14.64)}{112} = 14.64 + 0.0152 \cdot x$$

✓ if $L_{dbavg} = 112 \text{ in.} < x \leq L_{hpavg} = 542.1 \text{ in.}$

$$e(x) = e_{atdb} + \frac{(e_m - e_{atdb}) \cdot (x - L_{dbavg})}{(L_{hpavg} - L_{dbavg})} \quad D-17$$

$$e(x) = 16.34 + \frac{(21.95 - 16.34) \cdot (x - 112)}{(542.1 - 112)} = 16.34 + 0.0130 \cdot (x - 112)$$

$$\checkmark \text{ if } L_{hpavg} = 542.1 \text{ in.} < x$$

$$e(x) = e_m$$

D-18

$$e(x) = 21.95$$

Table D.9. Net eccentricity along the half-span

$e(x) \text{ (in.)}$		
$e(1)$	$e(2)$	$e(3)$
14.64	20.22	21.95

- *Effective prestressing area along the half-span*

$$\checkmark \text{ if } x \leq L_{dbavg} = 112 \text{ in.}$$

$$A_{ps}(x) = A_{psst} + A_{pshp}$$

D-19

$$A_{ps}(x) = 11.284 + 2.604 = 13.388 \text{ in.}^2$$

$$\checkmark \text{ if } x > L_{dbavg} = 112 \text{ in.}$$

$$A_{ps}(x) = A_{psst} + A_{psdb} + A_{pshp}$$

D-20

$$A_{ps}(x) = 11.284 + 0.651 + 2.604 = 14.539 \text{ in.}^2$$

Table D.10. Effective strand area along the half-span

$A_{ps}(x) \text{ (in.}^2\text{)}$		
$A_{ps}(1)$	$A_{ps}(2)$	$A_{ps}(3)$
13.388	14.539	14.539

- *Generate creep and shrinkage arrays*

- Creep function based on AASHTO LRFD (2020) 9th edition

$$\psi(t, t_i) = 1.9 \cdot k_s \cdot k_{hc} \cdot k_f \cdot k_{td} \cdot t_i^{-0.118} \quad \text{D-21}$$

$$k_s = 1.45 - 0.13 \cdot \left(\frac{V}{S}\right) \geq 1.0 \quad \text{D-22}$$

$$k_{hc} = 1.56 - 0.008 \cdot H_r \quad \text{D-23}$$

$$k_f = \frac{5}{1 + f'_{ci}} \quad \text{D-24}$$

$$k_{td}(t) = \frac{t}{12 \cdot \left(\frac{100 - 4 \cdot f'_{ci}}{f'_{ci} + 20}\right) + t} \quad \text{D-25}$$

- Shrinkage function based on AASHTO LRFD (2020) 9th edition

$$\varepsilon_{sh}(t) = k_s \cdot k_{hs} \cdot k_f \cdot k_{td} \cdot 0.00048 \quad \text{D-26}$$

$$k_{hs} = 2.00 - 0.014 \cdot H_r \quad \text{D-27}$$

Here, the volume-to-surface ratio can also be expressed as surface-to-perimeter ratio. Moreover, according to AASHTO LRFD (2020) Bridge Design Specification section 5.4.2.3.3, shrinkage as determined in Eqn. D-26 should be increased by 20 % if the concrete is exposed to drying before 5 days of curing have elapsed.

- *Creep and shrinkage calculation for girder*

$$k_s = 1.45 - 0.13 \cdot \left(\frac{1022.3}{251.4}\right) = 0.921 < 1.0 \rightarrow k_s = 1.0$$

$$k_{hc} = 1.56 - 0.008 \cdot (70) = 1.00$$

$$k_{hs} = 2.00 - 0.014 \cdot (70) = 1.02$$

$$k_f = \frac{5}{1 + 7} = 0.625$$

$$k_{tdc}(t) = \frac{t - t_i}{12 \cdot \left(\frac{100 - 4 \cdot (7)}{7 + 20} \right) + (t - t_i)} = \frac{t - t_i}{32 + (t - t_i)}$$

$$k_{tds}(t) = \frac{t - 1}{12 \cdot \left(\frac{100 - 4 \cdot (7)}{7 + 20} \right) + (t - 1)} = \frac{t - 1}{31 + t}$$

Using Eqns. D-21 and D-26, creep and shrinkage strain values at desired time can be calculated. To exemplify, $\psi(t_9, t_4) = \psi(27375, 36)$ and $\varepsilon_{sh}(t_9) = \varepsilon_{sh}(27375)$ can be calculated as shown below. In addition to this, creep and shrinkage arrays are provided in Table D.11 and Table D.12.

$$\psi(27375, 36) = 1.9 \cdot 1.0 \cdot 1.0 \cdot 0.625 \cdot \frac{27375 - 36}{32 + (27375 - 36)} \cdot 36^{-0.118} = 0.78$$

$$\varepsilon_{sh}(27375) = 1.2 \cdot 1.0 \cdot 1.02 \cdot 0.625 \cdot \frac{27375 - 1}{31 + 27375} \cdot 0.00048 = 367 \mu\varepsilon$$

Table D.8. Creep function for girder

$\psi_G(t, t_i)$		t (days)						
		<u>1</u>	<u>29</u>	<u>36</u>	<u>18250</u>	<u>18260</u>	<u>18627</u>	<u>27375</u>
t_i (days)	<u>1</u>	0.00	0.54	0.61	1.19	1.19	1.19	1.19
	<u>29</u>	-	0.00	0.14	0.80	0.80	0.80	0.80
	<u>36</u>	-	-	0.00	0.78	0.78	0.78	0.78
	<u>18250</u>	-	-	-	0.00	0.09	0.13	0.37
	<u>18260</u>	-	-	-	-	0.00	0.07	0.37
	<u>18627</u>	-	-	-	-	-	0.00	0.37
	<u>27375</u>	-	-	-	-	-	-	0.00
t_i = loading time, t = desired time								

Table D.9. Shrinkage array for girder

Event	<i>time index (t)</i>	$\epsilon_{shG}(t) (\mu\epsilon)$
Detensioning of strands	<u>1</u>	0.00
Time at which the deck is placed	<u>2</u>	168
Time at placement of barriers and the opening of bridge to traffic	<u>3</u>	189
Time at placement of overlay	<u>4</u>	189
Time at deck removal for projects that features a deck replacement	<u>5</u>	367
Time at new deck placement	<u>6</u>	367
Time at placement of barrier and reopening of bridge to traffic	<u>7</u>	367
Time at placement of overlay	<u>8</u>	367
Time at the end of service life	<u>9</u>	367

▪ *Creep and shrinkage calculation for 1st deck*

Since initial concrete compressive strength for the deck is generally unknown, it is assumed:

$$f'_{cdi} = 0.80 \cdot f'_{cd} \quad \text{D-28}$$

$$f'_{cdi} = 0.80 \cdot 4 = 3.2 \text{ ksi}$$

It should be noted that since the deck is 7-days moist-cured, there will be no shrinkage that takes places within the 7-days period after it is cast. Similarly, before deck is cast, there will be no creep in the deck.

$$A_{d1} = s_d \cdot t_{d1} + t_{h1} \cdot b_f \quad \text{D-29}$$

$$S_{d1} = 2 \cdot s_d - b_f + t_{h1} \quad \text{D-30}$$

$$\frac{V_{d1}}{A_{d1}} = \frac{A_{d1}}{S_{d1}} \quad \text{D-31}$$

$$A_{d1} = (8.41 \cdot 12) \cdot 9 = 908.28 \text{ in.}^2$$

$$S_{d1} = 2 \cdot (8.41 \cdot 12) - 49 + 0 = 152.84 \text{ in.}$$

$$k_s = 1.45 - 0.13 \cdot \left(\frac{908.28}{152.84} \right) = 0.677 < 1.0 \rightarrow k_s = 1.0$$

$$k_{hc} = 1.56 - 0.008 \cdot (70) = 1.00$$

$$k_{hs} = 2.00 - 0.014 \cdot (70) = 1.02$$

$$k_f = \frac{5}{1 + 3.2} = 1.190$$

$$k_{tdc}(t) = \frac{t - t_i}{12 \cdot \left(\frac{100 - 4 \cdot (3.2)}{3.2 + 20} \right) + (t - t_i)} = \frac{t - t_i}{45.1 + (t - t_i)}$$

$$k_{tds}(t) = \frac{t - 29 - 7}{12 \cdot \left(\frac{100 - 4 \cdot (3.2)}{3.2 + 20} \right) + (t - 29 - 7)} = \frac{t - 36}{9.10 + t}$$

Using Eqns. D-21 and D-26, the creep and shrinkage array for the 1st deck can be obtained as follows:

Table D.10. Creep function for 1st deck

$\psi_{D1}(t, t_i)$		t (days)					
		<u>29</u>	<u>36</u>	<u>18250</u>	<u>18260</u>	<u>18627</u>	<u>27375</u>
t_i (days)	<u>29</u>	0.00	0.00	0.00	0.00	0.00	0.00
	<u>36</u>	-	0.00	1.79	1.79	1.79	1.79
	<u>18250</u>	-	-	0.00	0.13	0.20	0.71
	<u>18260</u>	-	-	-	0.00	0.10	0.71
	<u>18267</u>	-	-	-	-	0.00	0.71
	<u>27375</u>	-	-	-	-	-	0.00
t_i = loading time, t = desired time							

Table D.11. Shrinkage array for 1st deck

Event	<i>time index (t)</i>	$\epsilon_{shD1}(t) (\mu\epsilon)$
Detensioning of strands	<u>1</u>	0
Time at which the deck is placed	<u>2</u>	0
Time at placement of barriers and the opening of bridge to traffic	<u>3</u>	0
Time at placement of overlay	<u>4</u>	0
Time at deck removal for projects that features a deck replacement	<u>5</u>	581
Time at new deck placement	<u>6</u>	581
Time at placement of barrier and reopening of bridge to traffic	<u>7</u>	581
Time at placement of overlay	<u>8</u>	581
Time at the end of service life	<u>9</u>	582

▪ *Creep and shrinkage calculation for 2nd deck*

Similar to the 1st deck, the creep and shrinkage arrays for the 2nd deck can also be determined. For simplicity, it is assumed that the 2nd deck has exactly the same features with 1st deck. The only formulation that is different for the 2nd deck is as follows:

$$k_{tds}(t) = \frac{t - 18260 - 7}{12 \cdot \left(\frac{100 - 4 \cdot (3.2)}{3.2 + 20} \right) + (t - 18260 - 7)} = \frac{t - 18267}{t - 18221.9}$$

Table D.12. Creep function for 2nd deck

$\psi_{D2}(t, t_i)$		<i>t (days)</i>		
		<u>18260</u>	<u>18627</u>	<u>27375</u>
<i>t_i (days)</i>	<u>18260</u>	0.00	0.00	0.00
	<u>18267</u>	-	0.00	1.79
	<u>27375</u>	-	-	0.00
<i>t_i</i> = loading time, <i>t</i> = desired time				

Table D.13. Shrinkage array for 2nd deck

Event	<i>time index (t)</i>	<i>ε_{shD2} (t) (μ</i>
Detensioning of strands	<u>1</u>	0
Time at which the deck is placed	<u>2</u>	0
Time at placement of barriers and the opening of bridge to traffic	<u>3</u>	0
Time at placement of overlay	<u>4</u>	0
Time at deck removal for projects that features a deck replacement	<u>5</u>	0
Time at new deck placement	<u>6</u>	0
Time at reopening of bridge to traffic	<u>7</u>	0
Time at placement of overlay	<u>8</u>	0
Time at the end of service life	<u>9</u>	580

- *Generate time and section dependent arrays for material and section properties*
- Modulus of elasticity based on AASHTO LRFD (2020) 9th edition with ACI 209R-92 development function

$$E_c(t) = \left(\frac{t}{\alpha + \beta t} \right)^{0.5} E_{c28} \quad \text{D-32}$$

$$E_{ci} = 120,000 K_1 w^2 (f'_{ci})^{1/3} \quad \text{D-33}$$

$$E_{c28} = 120,000 K_1 w^2 (f'_c)^{1/3} \quad \text{D-34}$$

- *For girder*

For girder, development model parameters, α and β , are back-calculated using the equations below:

$$\beta = \frac{E_{c28}^2 \cdot t_1 - 28 E_{ci}^2}{E_{ci}^2 \cdot (t_1 - 28)} \quad \text{D-35}$$

$$\alpha = 28(1 - \beta) \quad \text{D-36}$$

According to AASHTO LRFD (2020) Bridge Design Specifications Table 3.5.1.1, the unit weight of concrete, w , may be estimated in terms of kcf using the equations below:

$$\text{If } f'_c > 4 \text{ ksi} \quad w = 0.140 + 0.001 \cdot (f'_c) \quad \text{D-37}$$

$$\text{If } f'_c \leq 4 \text{ ksi} \quad w = 0.145 \text{ kcf} \quad \text{D-38}$$

$$w = 0.140 + 0.001 \cdot (10) = 0.150 \text{ kcf}$$

$$E'_{ci} = 120,000 \cdot (1.0) \cdot (0.150)^2 \cdot (7)^{1/3} = 5165 \text{ ksi}$$

$$E'_{c28} = 120,000 \cdot (1.0) \cdot (0.150)^2 \cdot (10)^{1/3} = 5817 \text{ ksi}$$

$$\beta = \frac{(5817)^2 \cdot (1) - 28 \cdot (5165)^2}{(5165)^2 \cdot (1 - 28)} = 0.990$$

$$\alpha = 28 \cdot (1 - 0.990) = 0.278$$

$$E_{cG}(t) = \left(\frac{t}{0.278 + (0.990) \cdot t} \right)^{0.5} \cdot 5817$$

Table D.14. Elastic modulus development for girder with time

Event	time index (t)	$E_{cG}(t)$ (ksi)
Detensioning of strands	<u>1</u>	5165
Time at which the deck is placed	<u>2</u>	5817
Time at placement of barriers and the opening of bridge to traffic	<u>3</u>	5823
Time at placement of overlay	<u>4</u>	5823
Time at deck removal for projects that features a deck replacement	<u>5</u>	5846
Time at new deck placement	<u>6</u>	5846
Time at placement of barrier and reopening of bridge to traffic	<u>7</u>	5846
Time at placement of overlay	<u>8</u>	5846
Time at the end of service life	<u>9</u>	5846

- For 1st and 2nd deck

Unlike in girder concrete, in deck concrete, same development model with coefficients corresponding to Type I – Moist-cured concrete is going to be utilized.

$$\alpha = 4 \text{ \& } \beta = 0.85 \text{ \& } w = 0.145 \text{ kcf}$$

$$E'_{c28} = 120,000 \cdot (1.0) \cdot (0.145)^2 \cdot (4)^{1/3} = 3644.1 \text{ ksi}$$

$$E_{cD1}(t) = \left(\frac{t - 28}{4 + (0.85) \cdot (t - 28)} \right)^{0.5} \cdot 3644.1$$

$$E_{cD2}(t) = \left(\frac{t - 18260}{4 + (0.85) \cdot (t - 18260)} \right)^{0.5} \cdot 3644.1$$

Table D.15. Elastic modulus development for 1st and 2nd deck with time

Event	<i>time index (t)</i>	$E_{cD1}(t)$ (ksi)	$E_{cD2}(t)$ (ksi)
Detensioning of strands	<u>1</u>	-	-
Time at which the deck is placed	<u>2</u>	-	-
Time at placement of barriers and the opening of bridge to traffic	<u>3</u>	3447	-
Time at placement of overlay	<u>4</u>	3447	-
Time at deck removal for projects that features a deck replacement	<u>5</u>	4343	-
Time at new deck placement	<u>6</u>	4343	-
Time at placement of barrier and reopening of bridge to traffic	<u>7</u>	4343	3359
Time at placement of overlay	<u>8</u>	4343	3359
Time at the end of service life	<u>9</u>	4344	4343

- Modular ratio and transformed area

Since transformed section properties are utilized in Approach No. 6, all the materials apart from girder are transformed to girder by using the equation below. Since girder modulus of elasticity varies with time, the modular ratio for the elements will also vary with respect to time.

$$\eta(t) = \frac{E_{tr}}{E_{cG}(t)} \quad \text{D-39}$$

$$A_{tr} = A \cdot \eta(t) \quad \text{D-40}$$

- *For prestressing strands*

$$\eta_{ps}(t) = \frac{E_{ps}}{E_{cG}(t)} = \frac{28500}{E_{cG}(t)}$$

$$A_{pstr}(t, x) = A_{ps}(x) \cdot (\eta_{ps}(t) - 1)$$

Table D.16. Modular ratio and transformed area for prestressing strands

$A_{pstr}(t, x) (in.^2)$		$\eta_{ps}(t)$	<i>section index (x)</i>		
<i>time index (t)</i>			<u>1</u>	<u>2</u>	<u>3</u>
	<u>1</u>	5.52	62.7	65.7	65.7
	<u>2</u>	4.90	54.2	56.7	56.7
	<u>3</u>	4.89	54.1	56.7	56.7
	<u>4</u>	4.89	54.1	56.7	56.7
	<u>5</u>	4.88	53.8	56.3	56.3
	<u>6</u>	4.88	53.8	56.3	56.3
	<u>7</u>	4.88	53.8	56.3	56.3
	<u>8</u>	4.88	53.8	56.3	56.3
	<u>9</u>	4.88	53.8	56.3	56.3

- For 1st and 2nd deck

$$\eta_D(t) = \frac{E_{cD}(t)}{E_{cG}(t)}$$

$$A_{dtr}(t) = A_d \cdot \eta_d(t)$$

Table D.17. Modular ratio and transformed area for the 1st and 2nd deck

<i>time index (t)</i>	Modular ratio		Transformed deck area (in. ²)	
	$\eta_{d1}(t)$	$\eta_{d2}(t)$	$A_{d1tr}(t)$	$A_{d2tr}(t)$
<u>3</u>	0.61	-	555.6	-
<u>4</u>	0.61	-	555.6	-
<u>5</u>	0.72	-	656.8	-
<u>6</u>	0.72	-	656.8	-
<u>7</u>	0.72	0.61	656.8	553.4
<u>8</u>	0.72	0.61	656.8	553.4
<u>9</u>	0.72	0.72	656.8	656.8

- Transformed area for composite and non-composite structures

$$A_{nctr}(t, x) = A_G + A_{pstr}(t, x)$$

$$A_{ctr}(t, x) = A_G + A_{pstr}(t, x) + A_{dtr}(t)$$

Table D.18. Net transformed area for the non-composite structure

$A_{nctr}(t, x) (in.^2)$		<i>section index (x)</i>		
		<u>1</u>	<u>2</u>	<u>3</u>
<i>time index (t)</i>	<u>1</u>	1085	1088	1088
	<u>2</u>	1076	1079	1079
	<u>3</u>	1076	1079	1079
	<u>4</u>	1076	1079	1079
	<u>5</u>	1076	1079	1079
	<u>6</u>	1076	1079	1079
	<u>7</u>	1076	1079	1079
	<u>8</u>	1076	1079	1079
	<u>9</u>	1076	1079	1079

Table D.19. Net transformed area for the 1st and 2nd composite structures

$A_{ctr}(t, x) (in.^2)$		$A_{c1tr}(t, x)$			$A_{c2tr}(t, x)$		
		<i>section index (x)</i>			<i>section index (x)</i>		
		<u>1</u>	<u>2</u>	<u>3</u>	<u>1</u>	<u>2</u>	<u>3</u>
<i>time index (t)</i>	<u>3</u>	1632	1635	1635	-	-	-
	<u>4</u>	1733	1736	1736	-	-	-
	<u>5</u>	1733	1736	1736	-	-	-
	<u>6</u>	1733	1736	1736	-	-	-
	<u>7</u>	1733	1736	1736	1630	1632	1632
	<u>8</u>	1733	1736	1736	1733	1735	1735
	<u>9</u>	1733	1736	1736	1733	1735	1735

- *Transformed moment of inertia for non-composite structure*

$$y_{psbottom}(x) = y_{Gbottom} - e(x) \quad D-41$$

$$y_t(t, x) = \frac{A_G \cdot y_{Gbottom} + A_{pstr}(t, x) \cdot y_{psbottom}(x)}{A_{nctr}(t, x)} \quad D-42$$

$$e_{ts}(t, x) = y_t(t, x) - y_{psbottom}(x) \quad D-43$$

$$I_{ts}(t, x) = I_G + A_G \cdot (y_{Gbottom} - y_t(t, x))^2 + A_{pstr}(t, x) \cdot (y_t(t, x) - y_{psbottom}(x))^2 \quad D-44$$

Table D.20. Location of prestressing strands with respect to bottom of girder

$y_{psbottom}(x)$ (in.)		
$y_{psbottom}(1)$	$y_{psbottom}(2)$	$y_{psbottom}(3)$
12.5	6.7	5.0

Table D.21. Eccentricity of prestressing strand in transformed non-composite structure

$e_{ts}(t, x)$ (in.)		<i>section index</i> (x)		
		<u>1</u>	<u>2</u>	<u>3</u>
<i>time index</i> (t)	<u>1</u>	13.7	19.1	20.6
	<u>2</u>	13.8	19.2	20.8
	<u>3</u>	13.8	19.2	20.8
	<u>4</u>	13.8	19.2	20.8
	<u>5</u>	13.8	19.3	20.8
	<u>6</u>	13.8	19.3	20.8
	<u>7</u>	13.8	19.3	20.8
	<u>8</u>	13.8	19.3	20.8
	<u>9</u>	13.8	19.3	20.8

Table D.22. Centroid of transformed non-composite structure with respect to bottom of girder

$y_t(t, x)$ (in.)		<i>section index</i> (x)		
		<u>1</u>	<u>2</u>	<u>3</u>
<i>time index</i> (t)	<u>1</u>	26.2	25.8	25.7
	<u>2</u>	26.3	25.9	25.8
	<u>3</u>	26.3	25.9	25.9
	<u>4</u>	26.3	25.9	25.9
	<u>5</u>	26.3	25.9	25.9
	<u>6</u>	26.3	25.9	25.9
	<u>7</u>	26.3	25.9	25.9
	<u>8</u>	26.3	25.9	25.9
	<u>9</u>	26.3	25.9	25.9

Table D.23. Moment of inertia of transformed non-composite structure

$I_{ts}(t, x) (in.^4)$		<i>section index</i> (x)		
		<u>1</u>	<u>2</u>	<u>3</u>
<i>time index</i> (t)	<u>1</u>	424490	437520	441810
	<u>2</u>	422870	434210	437950
	<u>3</u>	422860	434190	437920
	<u>4</u>	422860	434190	437920
	<u>5</u>	422810	434080	437800
	<u>6</u>	422810	434080	437800
	<u>7</u>	422810	434080	437800
	<u>8</u>	422810	434080	437800
	<u>9</u>	422810	434080	437790

- *Transformed moment of inertia for composite structure*

$$y_{dc} = \frac{s_d \cdot t_d \cdot (0.5 \cdot t_d + t_h) + 0.5 \cdot b_f \cdot t_h^2}{A_d} \quad D-45$$

$$y_{dbottom} = h + y_{dc} \quad D-46$$

$$y_c(t, x) = \frac{A_G \cdot y_{Gbottom} + A_{pstr}(t, x) \cdot y_{psbottom}(x) + A_{dtr} \cdot y_{dbottom}}{A_{ctr}(t, x)} \quad D-47$$

$$e_c(t, x) = y_c(t, x) - y_{psbottom}(x) \quad D-48$$

$$I_d = \frac{s_d \cdot t_d^3 + b_f \cdot t_h^3}{12} + s_d \cdot t_d \cdot (y_{dc} - 0.5 \cdot t_d - t_h)^2 + b_f \cdot t_h \cdot (y_{dc} - 0.5 \cdot t_h)^2 \quad D-49$$

$$I_{dtr} = I_d \cdot \eta_{d1}(t) \quad D-50$$

$$I_c(t, x) = I_G + A_G \cdot (y_c(t, x) - y_{Gbottom})^2 + A_{pstr}(t, x) \cdot (y_c(t, x) - y_{psbottom}(x))^2 + I_{dtr}(t) + A_{dtr}(t) \cdot (y_c(t, x) - y_{dbottom})^2 \quad D-51$$

Table D.24. Centroid of transformed composite structure with respect to bottom of girder

$y_c(t, x)$ (in.)		$y_{c1}(t, x)$			$y_{c2}(t, x)$		
		<i>section index (x)</i>			<i>section index (x)</i>		
		<u>1</u>	<u>2</u>	<u>3</u>	<u>1</u>	<u>2</u>	<u>3</u>
<i>time index (t)</i>	<u>3</u>	37.2	37.0	36.9	-	-	-
	<u>4</u>	38.5	37.0	36.9	-	-	-
	<u>5</u>	38.5	37.0	38.2	-	-	-
	<u>6</u>	38.5	38.3	38.2	-	-	-
	<u>7</u>	38.5	38.3	38.2	37.2	37.0	36.9
	<u>8</u>	38.5	38.3	38.2	37.2	37.0	36.9
	<u>9</u>	38.5	38.3	38.2	38.5	38.3	38.2

Table D.25. Eccentricity of prestressing strand in transformed composite structure

$e_c(t, x)$ (in.)		$e_{c1}(t, x)$			$e_{c2}(t, x)$		
		<i>section index (x)</i>			<i>section index (x)</i>		
		<u>1</u>	<u>2</u>	<u>3</u>	<u>1</u>	<u>2</u>	<u>3</u>
<i>time index (t)</i>	<u>3</u>	24.7	30.3	31.9	-	-	-
	<u>4</u>	24.7	30.3	31.9	-	-	-
	<u>5</u>	26.0	31.6	33.2	-	-	-
	<u>6</u>	26.0	31.6	33.2	-	-	-
	<u>7</u>	26.0	31.6	33.2	24.7	30.3	31.9
	<u>8</u>	26.0	31.6	33.2	24.7	30.3	31.9
	<u>9</u>	26.0	31.6	33.2	26.0	31.6	33.2

Table D.26. Transformed moment of inertia for the 1st and 2nd deck

<i>time index (t)</i>	Transformed moment of inertia ($in.^4$)	
	I_{d1tr}	I_{d2tr}
<u>3</u>	3751	-
<u>4</u>	3751	-
<u>5</u>	4434	-
<u>6</u>	4434	-
<u>7</u>	4434	3736
<u>8</u>	4434	3736
<u>9</u>	4434	4433

Table D.27. Moment of inertia of transformed composite structure with 1st and 2nd deck

$I_c(t, x) (in.^4)$		$I_{c1}(t, x)$			$I_{c2}(t, x)$		
		section index (x)			section index (x)		
		<u>1</u>	<u>2</u>	<u>3</u>	<u>1</u>	<u>2</u>	<u>3</u>
time index (t)	<u>3</u>	807250	826900	832690	-	-	-
	<u>4</u>	807250	826900	832690	-	-	-
	<u>5</u>	850800	871330	877330	-	-	-
	<u>6</u>	850800	871330	877330	-	-	-
	<u>7</u>	850800	871330	877330	806060	825600	831360
	<u>8</u>	850800	871330	877330	806060	825600	831360
	<u>9</u>	850810	871340	877340	850780	871310	877310

- Simpson's 1/3rd rule for numerical integration

A general idea behind the Simpson's 1/3rd rule is explained briefly below.

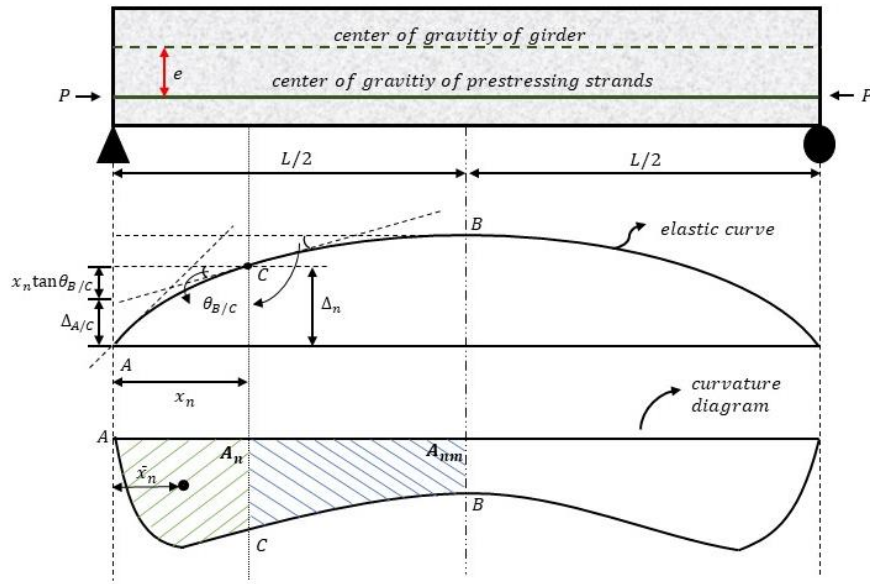


Fig. D.1. Elastic curve and curvature diagram for typical prestressed concrete beam at release

$$\Delta_n = \Delta_{A/C} + x_n \tan \theta_{B/C} \quad \text{D-52}$$

$$\theta_{B/C} = A_{nm} \quad \text{D-53}$$

$$\Delta_{A/C} = A_n \bar{x}_n \quad \text{D-54}$$

$$\bar{x}_n = \frac{Q_n}{A_n} \quad \text{D-55}$$

$$Q_n = \frac{\Delta x}{3} (\phi_1 x_1 + 4\phi_2 x_2 + 2\phi_3 x_3 + 4\phi_4 x_4 + 2\phi_5 x_5 + \cdots + 4\phi_{n-1} x_{n-1} + \phi_n x_n) \quad \text{D-56}$$

$$A_n = \frac{\Delta x}{3} (\phi_1 + 4\phi_2 + 2\phi_3 + 4\phi_4 + 2\phi_5 + \cdots + 4\phi_{n-1} + \phi_n) \quad \text{D-57}$$

$$A_{nm} = \frac{\Delta x}{3} (\phi_n + 4\phi_{n+1} + 2\phi_{n+2} + \cdots + 4\phi_{m-1} + \phi_m) \quad \text{D-58}$$

$$\Delta x = \frac{L_G/2}{\text{number of sections} - 1} \quad \text{D-59}$$

- Time-dependent deflection calculations

Note: For both instantaneous and time-dependent deflection calculations, all matrices such as location, load effects, material properties and creep and shrinkage functions will be recalled using index number.

$$K_i(t, x) = \frac{1}{1 + \frac{E_{ps} \cdot A_{ps}(x)}{E_{cG}(1) \cdot A_G} \cdot \left(1 + \frac{A_G \cdot e(x)^2}{I_G}\right) \cdot [1 + \psi_G(t, t_1)]} \quad \text{D-60}$$

$$f_{psj}(x) = -\frac{(N_{psdb} + N_{pshp} + N_{psst})}{A_{ps}(x)} \quad \text{D-61}$$

$$z = \text{rownumber}(N_G(t, x)) \quad \text{D-62}$$

$$q = \text{rownumber}(N_D(t, x)) \quad \text{D-63}$$

$$m = \text{rownumber}(\text{loc}(x)) \quad \text{D-64}$$

$$\phi_p = \phi_0 \quad \text{D-65}$$

$$N_{tloss}(1, \text{loc}(x)) = N_{tloss_0} \quad \text{D-66}$$

$$\Delta f_{pR}(1, loc(x)) = \Delta f_{pR_0} \quad D-67$$

$$\Delta \phi_t(1, loc(x)) = 0 \quad D-68$$

- For non-composite structure

$$i = index(t_i) \quad D-69$$

$$p = index(t_{i+1}) \quad D-70$$

$$r = i \quad D-71$$

$$k = [r; (r + 1); (r + 2); \dots (p - 2); (p - 1)] \quad D-72$$

- For each value in "k" array:

$$Co_{NG}(1, loc(x)) = 0 \ \& \ Co_{MG}(1, loc(x)) = 0 \quad D-73$$

$$\varepsilon_{shG} = -(\varepsilon_G(k + 1) - \varepsilon_G(k)) \quad D-74$$

$$u = [1; 2; \dots (z - 1); z] \quad D-75$$

- For each value in "u" array:

$$\psi_{crG} = \psi_G(t(k + 1), t(u)) - \psi_G(t(k), t(u)) \quad D-76$$

$$\psi_{crG, flex} = \psi_{crG} \cdot \beta_{flex} \quad D-77$$

$$E_G = E_{cG}(u) \quad D-78$$

$$h = [1; 2; \dots (m - 1); m] \quad D-79$$

- For each value in "h" array:

$$if \ N_G(u, h) > 0 \quad \psi_{crG, ax} = \psi_{crG} \cdot \beta_{ax} \quad D-80$$

$$\text{if } N_G(u, h) \leq 0 \quad \psi_{crG,ax} = \psi_{crG} \quad \text{D-81}$$

$$Co_{NG}(h) = \frac{N_G(u, h) \cdot \psi_{crG,ax}}{E_G \cdot A_G} + Co_{NG} \quad \text{D-82}$$

$$Co_{MG}(h) = \frac{M_G(u, h) \cdot \psi_{crG,flex}}{E_G \cdot I_G} + Co_{MG} \quad \text{D-83}$$

- End of "h" array.
- End of "u" array.

$$\psi_{crG,ax} = \psi_{crG} \quad \text{D-84}$$

$$stopper = 1 \quad \text{D-85}$$

$$j = [1; 2; \dots (m - 1); m] \quad \text{D-86}$$

➤ For each value in "j" array:

$$M_{co} = \begin{bmatrix} 1 & 1 & 0 & 0 & 0 & 0 \\ 0 & e(j) & 1 & 0 & 0 & 0 \\ 0 & 0 & -\frac{1 + \psi_{crG,flex}}{E_G \cdot I_G} & 0 & 0 & 1 \\ 0 & -\frac{1}{E_{ps} \cdot A_{ps}(j)} & 0 & 0 & 1 & 0 \\ -\frac{1 + \psi_{crG,ax}}{E_G \cdot A_G} & 0 & 0 & 1 & 0 & 0 \\ 0 & 0 & 0 & -1 & 1 & -e(j) \end{bmatrix} \quad \text{D-87}$$

$$M_c = \begin{bmatrix} 0 \\ 0 \\ Co_{MG}(j) \\ 0 \\ Co_{NG}(j) + \varepsilon_{shG} \\ 0 \end{bmatrix} \quad \text{D-88}$$

$$M_s = [M_{co}^{-1}] \cdot [M_c] \quad \text{D-89}$$

$$\begin{aligned}
& \text{if } M_s(1) > 0 \\
& \quad \text{stopper} = 0 \\
& \quad \psi_{crG,ax} = \psi_{crG} \cdot \beta_{ax} \\
& \text{if stopper} = 1 \\
& \quad \text{continue}
\end{aligned} \tag{D-90}$$

$$f_{pR}(k, j) = \Delta f_{pR}(k, j) \tag{D-91}$$

$$\begin{aligned}
& \Delta f_{pR}(k+1, j) = - \left[\frac{(f_{psj}(j) + \Delta f_{pES}(j)) \cdot \log(24 \cdot t(k) + 1)}{K'_L \cdot \log(24 \cdot t_1 + 1)} \right. \\
& \text{if } f_{psj}(j) \\
& \geq 0.55 \cdot f_{py} \\
& \quad \cdot \left(\frac{f_{psj}(j) + \Delta f_{pES}(j)}{f_{py}} - 0.55 \right) \left. \right] \left[1 \right. \\
& \quad \left. + \frac{3 \cdot (N_{tloss}(k, j) + M_s(2))}{(f_{psj}(j) + \Delta f_{pES}(j)) \cdot A_{ps}(j)} \right] \cdot K_i(k+1, j) \cdot A_{ps}(j)
\end{aligned} \tag{D-92}$$

$$\begin{aligned}
& \text{if } f_{psj}(j) \\
& < 0.55 \cdot f_{py} - \Delta f_{pES}(j) \\
& \quad \Delta f_{pR}(k+1, j) = 0
\end{aligned} \tag{D-93}$$

$$\begin{aligned}
& \text{if } \Delta f_{pR}(k+1, j) \\
& > \Delta f_{pR}(k, j) \\
& \quad \Delta f_{pR}(k+1, j) = \Delta f_{pR}(k, j)
\end{aligned} \tag{D-94}$$

$$f_{pR}(k+1, j) = \Delta f_{pR}(k+1, j) - f_{pR}(k, j) \tag{D-95}$$

$$M_{pR}(k+1, j) = f_{pR}(k+1, j) \cdot [e(j) - (y_{Gbottom} - y_t(k, x))] \tag{D-96}$$

$$N_{tloss}(k+1, j) = M_s(2) + N_{tloss}(k, j) \tag{D-97}$$

$$\begin{aligned}
& N_G(k+1, j) = M_s(1) - f_{pR}(k+1, j) \cdot \frac{A_G}{A_{nctr}(k, j)} \\
& \quad - \frac{M_{pR}(k+1, j) \cdot A_G \cdot (y_t(k, x) - y_{Gbottom})}{I_{ts}(k, x)}
\end{aligned} \tag{D-98}$$

$$M_G(k+1, j) = M_s(3) - M_{pR}(k+1, j) \cdot \frac{I_G}{I_{ts}(k, j)} \quad \text{D-99}$$

$$\Delta\phi_t(k+1, j) = M_s(6) + \Delta\phi_t(k, j) - \frac{M_{pR}(k+1, j)}{E_G \cdot I_{ts}(k, j)} \quad \text{D-100}$$

$$stopper = 1 \quad \text{D-101}$$

$$\psi_{crG,ax} = \psi_{crG} \quad \text{D-102}$$

➤ End of "j" array.

$$\phi_t(k+1, loc(x)) = \phi_p + \Delta\phi_t(k+1, loc(x)) \quad \text{D-103}$$

➤ End of "k" array.

▪ For composite structure

$$y_{dG} = y_{dbottom} - y_{Gbottom} \quad \text{D-104}$$

$$i = index(t_i) \quad \text{D-105}$$

$$p = index(t_{i+1}) \quad \text{D-106}$$

$$r = i \quad \text{D-107}$$

$$g = index(t_2) \quad \text{D-108}$$

$$k = [r; (r+1); (r+2); \dots (p-2); (p-1)] \quad \text{D-109}$$

• For each value in "k" array:

$$Co_{NG}(1, loc(x)) = 0 \ \& \ Co_{MG}(1, loc(x)) = 0 \quad \text{D-110}$$

$$Co_{ND}(1, loc(x)) = 0 \ \& \ Co_{MD}(1, loc(x)) = 0$$

$$\varepsilon_{shG} = -(\varepsilon_G(k+1) - \varepsilon_G(k)) \quad \text{D-111}$$

$$\varepsilon_{shD} = -(\varepsilon_{d1}(k+1) - \varepsilon_{d1}(k))$$

$$u = [1; 2; \dots (z-1); z] \quad \text{D-112}$$

- For each value in "u" array:

$$\psi_{crG} = \psi_G(t(k+1), t(u)) - \psi_G(t(k), t(u)) \quad \text{D-113}$$

$$\psi_{crG,flex} = \psi_{crG} \cdot \beta_{flex} \quad \text{D-114}$$

$$E_G = E_{cG}(u) \quad \text{D-115}$$

$$h = [1; 2; \dots (m-1); m] \quad \text{D-116}$$

- For each value in "h" array:

$$\text{if } N_G(u, h) > 0 \quad \psi_{crG,ax} = \psi_{crG} \cdot \beta_{ax} \quad \text{D-117}$$

$$\text{if } N_G(u, h) \leq 0 \quad \psi_{crG,ax} = \psi_{crG} \quad \text{D-118}$$

$$Co_{NG}(h) = \frac{N_G(u, h) \cdot \psi_{crG,ax}}{E_G \cdot A_G} + Co_{NG} \quad \text{D-119}$$

$$Co_{MG}(h) = \frac{M_G(u, h) \cdot \psi_{crG,flex}}{E_G \cdot I_G} + Co_{MG} \quad \text{D-120}$$

- End of "h" array.
- End of "u" array.

$$z = [g; g+1; \dots (q-1); q] \quad \text{D-121}$$

- For each value in "z" array.

$$\psi_{crD} = \psi_D(t(k+1), t(z)) - \psi_D(t(k), t(z)) \quad \text{D-122}$$

$$\psi_{crD,flex} = \psi_{crD} \cdot \beta_{flex} \quad \text{D-123}$$

$$E_D = E_{cD}(z) \quad \text{D-124}$$

$$h = [1; 2; \dots (m-1); m] \quad \text{D-125}$$

- For each value in "h" array:

$$\text{if } N_D(z, h) > 0 \quad \psi_{crD,ax} = \psi_{crD} \cdot \beta_{ax} \quad \text{D-126}$$

$$\text{if } N_D(z, h) \leq 0 \quad \psi_{crD,ax} = \psi_{crD} \quad \text{D-127}$$

$$Co_{ND}(h) = \frac{N_D(z, h) \cdot \psi_{crD,ax}}{E_D \cdot A_D} + Co_{ND} \quad \text{D-128}$$

$$Co_{MD}(h) = \frac{M_D(z, h) \cdot \psi_{crD,flex}}{E_D \cdot I_D} + Co_{MD} \quad \text{D-129}$$

- End of "h" array.
- End of "z" array.

$$\psi_{crG,ax} = \psi_{crG} \quad \text{D-130}$$

$$\psi_{crD,ax} = \psi_{crD} \quad \text{D-131}$$

$$stopper = 1 \quad \text{D-132}$$

$$j = [1; 2; \dots (m-1); m] \quad \text{D-133}$$

- For each value in "j" array: D-134

$$\begin{aligned}
& M_{co} \\
& = \begin{bmatrix} 1 & 1 & 1 & 0 & 0 & 0 & 0 & 0 & 0 \\ -y_{dG} & 0 & e(j) & 1 & 1 & 0 & 0 & 0 & 0 \\ -\frac{1+\psi_{crD,ax}}{E_D \cdot A_D} & 0 & 0 & 0 & 0 & 1 & 0 & 0 & 0 \\ 0 & -\frac{1+\psi_{crG,ax}}{E_G \cdot A_G} & 0 & 0 & 0 & 0 & 1 & 0 & 0 \\ 0 & 0 & 0 & -\frac{1+\psi_{crD,flex}}{E_D \cdot I_D} & 0 & 0 & 0 & 0 & 1 \\ 0 & 0 & 0 & 0 & -\frac{1+\psi_{crG,flex}}{E_G \cdot I_G} & 0 & 0 & 0 & 1 \\ 0 & 0 & -\frac{1}{E_{ps} \cdot A_{ps}(j)} & 0 & 0 & 0 & 0 & 1 & 0 \\ 0 & 0 & 0 & 0 & 0 & 1 & -1 & 0 & y_{dG} \\ 0 & 0 & 0 & 0 & 0 & 0 & -1 & 1 & -e(j) \end{bmatrix} \\
& M_c = \begin{bmatrix} 0 \\ 0 \\ Co_{ND}(j) + \varepsilon_{shD} \\ Co_{NG}(j) + \varepsilon_{shG} \\ Co_{MD}(j) \\ Co_{MG}(j) \\ 0 \\ 0 \\ 0 \end{bmatrix}
\end{aligned} \tag{D-135}$$

$$M_s = [M_{co}^{-1}] \cdot [M_c] \tag{D-136}$$

$$\begin{aligned}
& stopper = 0 \\
& if [M_s(1) \text{ or } M_s(2)] > 0 \quad if M_s(2) > 0; \psi_{crG,ax} = \psi_{crG} \cdot \beta_{ax} \\
& if stopper = 1 \quad if M_s(1) > 0; \psi_{crD,ax} = \psi_{crD} \cdot \beta_{ax} \\
& continue
\end{aligned} \tag{D-137}$$

$$f_{pR}(k, j) = \Delta f_{pR}(k, j) \tag{D-138}$$

$$\begin{aligned}
& \Delta f_{pR}(k+1, j) = - \left[\frac{(f_{psj}(j) + \Delta f_{pES}(j)) \cdot \log(24 \cdot t(k) + 1)}{K'_L \cdot \log(24 \cdot t_1 + 1)} \right. \\
& \text{if } f_{psj}(j) \\
& \geq 0.55 \cdot f_{py} \quad \cdot \left(\frac{f_{psj}(j) + \Delta f_{pES}(j)}{f_{py}} - 0.55 \right) \Bigg] \Bigg| 1 \\
& - \Delta f_{pES}(j) \\
& + \frac{3 \cdot (N_{tloss}(k, j) + M_s(3))}{(f_{psj}(j) + \Delta f_{pES}(j)) \cdot A_{ps}(j)} \Bigg] \cdot K_i(k+1, j) \cdot A_{ps}(j)
\end{aligned} \tag{D-139}$$

$$\begin{aligned}
& \text{if } f_{psj}(j) \\
& < 0.55 \cdot f_{py} - \Delta f_{pES}(j) \\
& \Delta f_{pR}(k+1, j) = 0
\end{aligned} \tag{D-140}$$

$$\begin{aligned}
& \text{if } \Delta f_{pR}(k+1, j) \\
& > \Delta f_{pR}(k, j) \\
& \Delta f_{pR}(k+1, j) = \Delta f_{pR}(k, j)
\end{aligned} \tag{D-141}$$

$$f_{pR}(k+1, j) = \Delta f_{pR}(k+1, j) + f_{pR}(k, j) \tag{D-142}$$

$$M_{pR}(k+1, j) = f_{pR}(k+1, j) \cdot e_c(j) \tag{D-143}$$

$$N_{tloss}(k+1, j) = M_s(3) + N_{tloss}(k, j) \tag{D-144}$$

$$\begin{aligned}
& \delta N_{GpR}(k+1, j) \\
& = f_{pR}(k+1, j) \cdot \frac{A_G}{A_{ctr}(k, t)} \\
& + \frac{M_{pR}(k+1, j) \cdot A_G \cdot (y_c(k, x) - y_{Gbottom})}{I_c(k, x)}
\end{aligned} \tag{D-145}$$

$$\begin{aligned}
& \delta N_{DpR}(k+1, j) \\
& = f_{pR}(k+1, j) \frac{A_{dtr}(k)}{A_{ctr}(k, j)} \\
& + \frac{M_{pR}(k+1, j) \cdot A_{dtr}(k) \cdot (y_c(k, x) - y_{dbottom})}{I_c(k, x)}
\end{aligned} \tag{D-146}$$

$$\delta M_{GpR}(k+1, j) = \frac{M_{pR}(k+1, j) \cdot I_G}{I_c(k, x)} \quad \text{D-147}$$

$$\delta M_{DpR}(k+1, j) = \frac{M_{pR}(k+1, j) \cdot I_{dtr}(k)}{I_c(k, x)} \quad \text{D-148}$$

$$N_G(k+1, j) = M_s(2) - \delta N_{GpR}(k+1) \quad \text{D-149}$$

$$M_G(k+1, j) = M_s(5) - \delta M_{GpR}(k+1) \quad \text{D-150}$$

$$N_D(k+1, j) = M_s(1) - \delta N_{DpR}(k+1) \quad \text{D-151}$$

$$M_D(k+1, j) = M_s(4) - \delta M_{DpR}(k+1) \quad \text{D-152}$$

$$\Delta \phi_t(k+1, j) = M_s(9) + \Delta \phi_t(k, j) - \frac{M_{pR}(k+1, j)}{E_G \cdot I_c(k, j)} \quad \text{D-153}$$

$$stopper = 1 \quad \text{D-154}$$

$$\psi_{crG,ax} = \psi_{crG} \quad \text{D-155}$$

$$\psi_{crD,ax} = \psi_{crD} \quad \text{D-156}$$

➤ End of "j" array.

$$\phi_t(k+1, loc(x)) = \phi_p + \Delta \phi_t(k+1, loc(x)) \quad \text{D-157}$$

➤ End of "k" array.

D.3 Camber at Release

➤ Girder Self-weight Effect

$$w_G = \gamma_G \cdot A_G \quad \text{D-158}$$

$$\text{if } x \leq L_t \quad M_{Gsw}(x) = -\frac{w_G \cdot x^2}{2} \quad \text{D-159}$$

$$\text{if } L_t < x \quad M_{Gsw}(x) = \frac{w_G \cdot L_G \cdot (x - L_t)}{2} - \frac{w_G \cdot x^2}{2} \quad \text{D-160}$$

$$w_G = \frac{0.155 \cdot 1022.3}{12^3} = 0.0917 \text{ kips/in.}$$

$$\text{if } x \leq 21.5 \text{ in.} \quad M_{Gsw}(x) = -\frac{0.0917 \cdot x^2}{2} = -0.046 \cdot x^2$$

$$\text{if } 21.5 < x \quad M_{Gsw}(x) = \frac{0.092 \cdot 136.9 \cdot 12 \cdot (x - 21.5)}{2} - \frac{0.092 \cdot x^2}{2}$$

Table D.28. Moment applied on non-composite structure due to girder self-weight

$M_{Gsw}(x) \text{ (kips} \cdot \text{in.)}$		
$M_{Gsw}(1)$	$M_{Gsw}(2)$	$M_{Gsw}(3)$
0	21582	29315

➤ Prestressing Effect

- Straight, fully bonded strands

$$P_{psst} = A_{psst} \cdot f_{pj} \quad \text{D-161}$$

$$\text{if } x \leq L_{tr} \quad N_{psst}(x) = -\frac{P_{psst} \cdot x}{L_{tr}} \quad \text{D-162}$$

$$\text{if } L_{tr} < x \quad N_{psst}(x) = -P_{psst} \quad \text{D-163}$$

$$M_{psst}(x) = N_{psst}(x) \cdot [e_{st} - (y_{Gbottom} - y_t(1, x))] \quad \text{D-164}$$

$$P_{psst} = 11.284 \cdot 202.5 = 2285.01 \text{ kips}$$

$$\text{if } x \leq 36 \quad N_{psst}(x) = -\frac{2285.01 \cdot x}{36} = -63.47 \cdot x$$

$$M_{psst}(x) = -63.47 \cdot x \cdot [22.23 - (27 - y_t(1, x))]$$

$$\text{if } 36 < x \quad N_{psst}(x) = -P_{psst} = -2285.01 \text{ kips}$$

$$M_{psst}(x) = -2285.01 \cdot [22.23 - (27 - y_t(1, x))]$$

Table D.29. Axial force and moment on non-composite structure due to straight strands

$N_{psst}(x) \text{ (kips)}$			$M_{psst}(x) \text{ (kips-in.)}$		
$N_{psst}(1)$	$N_{psst}(2)$	$N_{psst}(3)$	$M_{psst}(1)$	$M_{psst}(2)$	$M_{psst}(3)$
0	-2285	-2285	0	-47996	-47769

- Debonded strands

$$P_{psdb} = A_{psdb} \cdot f_{pj} \quad \text{D-165}$$

$$\text{if } x \leq L_{dbavg} \quad N_{psdb}(x) = 0 \quad \text{D-166}$$

$$\text{if } L_{dbavg} < x \leq (L_{dbavg} + L_{tr}) \quad N_{psdb}(x) = -\frac{P_{psdb} \cdot (x - L_{dbavg})}{L_{tr}} \quad \text{D-167}$$

$$\text{if } (L_{dbavg} + L_{tr}) < x \quad N_{psdb}(x) = -P_{psdb} \quad \text{D-168}$$

$$M_{psdb}(x) = N_{psdb}(x) \cdot [e_{db} - (y_{Gbottom} - y_t(1, x))] \quad \text{D-169}$$

$$P_{psdb} = 0.651 \cdot 202.5 = 131.83 \text{ kips}$$

$$\text{if } x \leq 112 \quad N_{psdb}(x) = 0$$

$$M_{psdb}(x) = 0$$

$$\text{if } 112 < x \quad N_{psdb}(x) = -\frac{131.83 \cdot (x - 112)}{36} = -3.66 \cdot (x - 112)$$

$$\leq (112 + 36) \quad M_{psdb}(x) = -3.66 \cdot (x - 112) \cdot [25 - (27 - y_t(1, x))]$$

$$\text{if } (112 + 36) < x \quad N_{psdb}(x) = -131.83 \text{ kips}$$

$$M_{psdb}(x) = -131.83 \cdot [25 - (27 - y_t(1, x))]$$

Table D.30. Axial force and moment on non-composite structure due to debonded strands

$N_{psdb}(x) \text{ (kips)}$			$M_{psdb}(x) \text{ (kips-in.)}$		
$N_{psdb}(1)$	$N_{psdb}(2)$	$N_{psdb}(3)$	$M_{psdb}(1)$	$M_{psdb}(2)$	$M_{psdb}(3)$
0	-1312	-132	0	-3134	-3121

- Harped strands

$$P_{pshp} = A_{pshp} \cdot f_{pj} \quad \text{D-170}$$

$$\text{if } x \leq L_{tr} \quad N_{pshp}(x) = -\frac{P_{pshp} \cdot x}{L_{tr}} \quad \text{D-171}$$

$$\text{if } L_{tr} < x \leq L_{hpavg} \quad N_{pshp}(x) = -P_{pshp} \quad \text{D-172}$$

$$\text{if } L_{hpavg} < x \quad N_{pshp}(x) = -P_{pshp} \quad \text{D-173}$$

$$M_{pshp}(x) = N_{pshp}(x) \cdot [e_{hp}(x) - (y_{Gbottom} - y_t(1, x))] \quad \text{D-174}$$

$$P_{pshp} = 2.604 \cdot 202.5 = 527.31 \text{ kips}$$

$$\text{if } x \leq 36 \quad N_{pshp}(x) = -\frac{527.31 \cdot x}{36} = -14.65 \cdot x$$

$$M_{pshp}(x) = (-14.65 \cdot x) \cdot [x \cdot (0.0729) - 19.5 - (27 - y_t(1, x))]$$

$$\text{if } 36 < x \leq 542.1 \quad N_{pshp}(x) = -527.31$$

$$M_{pshp}(x) = -527.31 \cdot [x \cdot (0.0729) - (27 - y_t(1, x))]$$

$$\text{if } 542.1 < x \quad N_{pshp}(x) = -527.31$$

$$M_{pshp}(x) = -527.31 \cdot [20 - (27 - y_t(1, x))]$$

Table D.31. Axial force and moment on non-composite structure due to harped strands

$N_{pshp}(x) \text{ (kips)}$			$M_{pshp}(x) \text{ (kips-in.)}$		
$N_{pshp}(1)$	$N_{pshp}(2)$	$N_{pshp}(3)$	$M_{pshp}(1)$	$M_{pshp}(2)$	$M_{pshp}(3)$
0	-527	-527	0	-5056	-9847

➤ Net prestressing effect

$$M_{ps}(x) = M_{psst}(x) + M_{psdb}(x) + M_{pshp}(x) \quad \text{D-175}$$

$$N_{ps}(x) = N_{psst}(x) + N_{psdb}(x) + N_{pshp}(x) \quad \text{D-176}$$

Table D.32. Axial force and moment on non-composite structure due to prestressing

$N_{ps}(x) \text{ (kips)}$			$M_{ps}(x) \text{ (kips} - \text{in.)}$		
$N_{ps}(1)$	$N_{ps}(2)$	$N_{ps}(3)$	$M_{ps}(1)$	$M_{ps}(2)$	$M_{ps}(3)$
0	-2944	-2944	0	-56186	-60737

➤ Calculation of camber at release

$$M_{Gi}(x) = M_{Gsw}(x) + M_{ps}(x) \quad \text{D-177}$$

$$N_{Gi}(x) = N_{ps}(x) \quad \text{D-178}$$

$$\phi_t(1, x) = \frac{M_{Gi}(x)}{E_{cG}(1) \cdot I_{ts}(1, x)} \quad \text{D-179}$$

Table D.33. Net axial force and moment on non-composite structure due to prestressing and girder self-weight effect

$N_{Gi}(x) \text{ (kips)}$			$M_{Gi}(x) \text{ (kips} - \text{in.)}$		
$N_{Gi}(1)$	$N_{Gi}(2)$	$N_{Gi}(3)$	$M_{Gi}(1)$	$M_{Gi}(2)$	$M_{Gi}(3)$
0	-2944	-2944	0	-34604	-31422

Table D.34. Net curvature due to combined effects at camber at release

$\phi_t(t, x) \text{ (1/in.)}$		
$\phi_t(1,1)$	$\phi_t(1,2)$	$\phi_t(1,3)$
0	-1.53E-05	-1.38E-05

Using the Eqns. between D-52 and D-59, camber at considered sections can be calculated as follows:

$$\Delta x = \frac{\frac{136.9 \cdot 12}{2}}{3 - 1} = 410.70 \text{ in.}$$

$$A_{nm}(1) = \frac{410.70}{3} \cdot [0 + 4 \cdot (-1.53 \cdot 10^{-5}) + (-1.38 \cdot 10^{-5})] = -10.27 \cdot 10^{-3} \text{ in.}^2$$

$$A_{nm}(2) = \frac{410.70}{3} \cdot [(-1.53 \cdot 10^{-5}) + (-1.38 \cdot 10^{-5})] = -3.98 \cdot 10^{-3} \text{ in.}^2$$

$$A_{nm}(3) = 0$$

$$A_n(1) = 0$$

$$A_n(2) = \frac{410.70}{3} \cdot [0 + (-1.53 \cdot 10^{-5})] = -2.09 \cdot 10^{-3} \text{ in.}^2$$

$$A_n(3) = \frac{410.70}{3} \cdot [0 + 4 \cdot (-1.53 \cdot 10^{-5}) + (-1.38 \cdot 10^{-5})] - 10.27 \cdot 10^{-3} \text{ in.}^2$$

$$Q_n(1) = 0$$

$$Q_n(2) = \frac{410.70}{3} \cdot [0 + (-1.53 \cdot 10^{-5}) \cdot 410.70] = -0.86 \text{ in.}^3$$

$$Q_n(3) = \frac{410.70}{3} \cdot [0 + 4 \cdot (-1.53 \cdot 10^{-5}) \cdot 410.70 + (-1.38 \cdot 10^{-5}) \cdot 820.40] = -4.99 \text{ in.}^3$$

Table D.35. Application of Simpson's rule and camber at release

Parameters	Section index (x)		
	<u>1</u>	<u>2</u>	<u>3</u>
$Q_n(x) \text{ (in.}^3\text{)}$	0	-0.86	-4.99
$A_n(x) \text{ (in.}^2\text{)}$	0	-2.09E-03	-10.27E-03
$\bar{x}_n(x) \text{ (in.)}$	0	411.48	485.88
$\Delta_{A/C}(x) \text{ (in.)}$	0	-0.86	-4.99
$\theta_{B/C}(x) \text{ (rad.)}$	-10.27E-03	-3.98E-03	0
$x_n(x) \text{ (in.)}$	0	410.70	820.40
$\Delta_{ni}(x) \text{ (in.)}$	0	-2.50	-4.99

D.4 Pre-erection Camber

- Elastic shortening loss

A section-dependent elastic shortening loss is calculated based on AASHTO LRFD (2020) 9th Edition section C5.9.3.2.3a-1.

$$\Delta f_{pES}(x) = - \frac{-N_{ps}(x) \cdot [I_G + e(x)^2 \cdot A_G] - e(x) \cdot M_{Gsw}(x) \cdot A_G}{A_{ps}(x) \cdot [I_G + e(x)^2 \cdot A_G] + A_G \cdot I_G \cdot \frac{E_{cG}(1)}{E_{ps}}} \quad D-180$$

Table D.38. Elastic shortening loss along the half-span

$\Delta f_{pES}(x) \text{ (ksi)}$			$\Delta P_{pES}(x) \text{ (kips)}$		
$\Delta f_{pES}(1)$	$\Delta f_{pES}(2)$	$\Delta f_{pES}(3)$	$\Delta P_{pES}(1)$	$\Delta P_{pES}(2)$	$\Delta P_{pES}(3)$
0	-23	-22	0	-330	-326

- Effect of self-weight on girder only

$$M_{Gsi}(x) = \frac{M_{Gsw}(x) \cdot I_G}{I_{ts}(1, x)} \quad D-181$$

$$N_{Gsi}(x) = \frac{M_{Gsw}(x) \cdot A_G \cdot (y_t(1, x) - y_{Gbottom})}{I_{ts}(1, x)} \quad D-182$$

Table D.36. Forces on girder alone due to girder self-weight

$N_{Gsi}(x) \text{ (kips)}$			$M_{Gsi}(x) \text{ (kips-in.)}$		
$N_{Gsi}(1)$	$N_{Gsi}(2)$	$N_{Gsi}(3)$	$M_{Gsi}(1)$	$M_{Gsi}(2)$	$M_{Gsi}(3)$
0	-62	-90	0	20326	27341

- Effect of prestressing on girder only

$$M_{Gps}(x) = \frac{M_{ps}(x) \cdot I_G}{I_{ts}(1, x)} \quad D-183$$

$$N_{Gps}(x) = \frac{N_{ps}(x) \cdot A_G}{A_{nctr}(1, x)} + \frac{M_{ps}(x) \cdot A_G \cdot (y_t(1, x) - y_{Gbottom})}{I_{ts}(1, x)} \quad D-184$$

Table D.37. Forces on girder alone due to prestressing

$N_{Gps}(x) \text{ (kips)}$			$M_{Gps}(x) \text{ (kips-in.)}$		
$N_{Gps}(1)$	$N_{Gps}(2)$	$N_{Gps}(3)$	$M_{Gps}(1)$	$M_{Gps}(2)$	$M_{Gps}(3)$
0	-2615	-2593	0	-52916	-56647

- Net forces on girder due to combined effects

$$M_{Gp}(x) = M_{Gsi}(x) + M_{Gps}(x) \quad \text{D-185}$$

$$N_{Gp}(x) = N_{Gsi}(x) + N_{Gps}(x) \quad \text{D-186}$$

Table D.38. Net axial force and moment on girder due to combined effect at release

$N_{Gp}(x)$ (kips)			$M_{Gp}(x)$ (kips – in.)		
$N_{Gp}(1)$	$N_{Gp}(2)$	$N_{Gp}(3)$	$M_{Gp}(1)$	$M_{Gp}(2)$	$M_{Gp}(3)$
0	-2677	-2683	0	-32590	-29306

- Calculation of pre-erection camber

$$E_{cG}(1) = 5165 \text{ ksi}$$

$$\psi_G(t_2, t_1) - \psi_G(t_1, t_1) = \psi_G(29, 1) - \psi_G(1, 1) = 0.54$$

$$K_i(2, x) = \frac{1}{1 + \frac{28500 \cdot A_{ps}(x)}{5165 \cdot 1022.3} \cdot \left(1 + \frac{1022.3 \cdot e(x)^2}{412056}\right) \cdot [1 + 0.54]}$$

Table D.39. Coefficient K_i as a function of location

$K_i(t, x)$		
$K_i(2, 1)$	$K_i(2, 2)$	$K_i(2, 3)$
0.887	0.887	0.887

Table D.40. Stress on the strands along the span prior to transfer

$f_{psj}(x)$ (ksi)		
$f_{psj}(1)$	$f_{psj}(2)$	$f_{psj}(3)$
0.00	202.50	202.50

Table D.41. Force history array on girder as a function of time and location

index	$N_G(t, x)$ (kips)			$M_G(t, x)$ (kips – in.)		
	<u>1</u>	<u>2</u>	<u>3</u>	<u>1</u>	<u>2</u>	<u>3</u>
<u>1</u>	0	-2677	-2683	0	-32590	-29306

Using Eqns. between D-60 and D-103, the time-dependent calculation can be performed between time t_1 and t_2 .

$$z = 1 \ \& \ m = 3$$

$$N_{tloss_0} = 0 \ \& \ \Delta f_{pR_0} = 0$$

$$\emptyset_0 = \phi_t(1, x)$$

$$i = 1 \ \& \ p = 2 \ \& \ r = 1$$

$$k = [1]$$

$$-[\varepsilon_G(t_2) - \varepsilon_G(t_1)] = -168 \cdot 10^{-6}$$

$$u = [1]$$

$$\psi_G(t_2, t_1) - \psi_G(t_1, t_1) = 0.54$$

$$\psi_{crG} = \psi_{crG, flex} = \psi_{crG, ax} = 0.54$$

$$E_G = 5165$$

$$Co_{NG} = [0, -2.75 \cdot 10^{-4}, -2.76 \cdot 10^{-4}]$$

$$Co_{MG} = [0, -8.32 \cdot 10^{-6}, -7.48 \cdot 10^{-6}]$$

$$j = [1, 2, 3]$$

➤ For $j = 1$

$$M_{co} = \begin{bmatrix} 1 & 1 & 0 & 0 & 0 & 0 \\ 0 & 14.5 & 1 & 0 & 0 & 0 \\ 0 & 0 & -7.25 \cdot 10^{-10} & 0 & 0 & 1 \\ 0 & -2.53 \cdot 10^{-6} & 0 & 0 & 1 & 0 \\ -2.92 \cdot 10^{-7} & 0 & 0 & 1 & 0 & 0 \\ 0 & 0 & 0 & -1 & 1 & -14.5 \end{bmatrix}$$

$$M_c = \begin{bmatrix} 0 \\ 0 \\ 0 \\ 0 \\ -1.68 \cdot 10^{-4} \\ 0 \end{bmatrix} \ \& \ M_s = \begin{bmatrix} 56.56 \\ -56.56 \\ 820.05 \\ -1.51 \cdot 10^{-4} \\ -1.42 \cdot 10^{-4} \\ 5.95 \cdot 10^{-7} \end{bmatrix}$$

$$\Delta f_{pR}(2,1) = 0$$

$$f_{pR}(2,1) = 0$$

$$M_{pR}(2,1) = 0$$

$$N_{tloss}(2,1) = -56.56$$

$$N_G(2,1) = 56.56$$

$$M_G(2,1) = 820.05$$

$$\Delta\phi_t(2,1) = 5.95 \cdot 10^{-7}$$

➤ For $j = 2$

$$M_{co} = \begin{bmatrix} 1 & 1 & 0 & 0 & 0 & 0 \\ 0 & 20.31 & 1 & 0 & 0 & 0 \\ 0 & 0 & -7.25 \cdot 10^{-10} & 0 & 0 & 1 \\ 0 & -2.41 \cdot 10^{-6} & 0 & 0 & 1 & 0 \\ -2.92 \cdot 10^{-7} & 0 & 0 & 1 & 0 & 0 \\ 0 & 0 & 0 & -1 & 1 & -20.31 \end{bmatrix}$$

$$M_c = \begin{bmatrix} 0 \\ 0 \\ -8.32 \cdot 10^{-6} \\ 0 \\ -4.43 \cdot 10^{-4} \\ 0 \end{bmatrix} \& M_s = \begin{bmatrix} 203.85 \\ -203.85 \\ 4140.2 \\ -3.84 \cdot 10^{-4} \\ -4.91 \cdot 10^{-4} \\ -5.32 \cdot 10^{-6} \end{bmatrix}$$

$$\Delta f_{pR}(2,2) = - \left[\frac{(202.5 - 23) \cdot \log(24 \cdot 29 + 1)}{45 \cdot \log(24 \cdot 1 + 1)} \cdot \left(\frac{202.5 - 23}{243} - 0.55 \right) \right] \left[1 \right. \\ \left. + \frac{3 \cdot (0 - 203.85)}{((202.5 - 23) \cdot 14.54)} \right] \cdot 0.887 \cdot 14.54 = -7.50$$

$$f_{pR}(2,2) = -7.50$$

$$M_{pR}(2,2) = -7.50 \cdot [20.22 - (27 - 25.7)] = -143.15$$

$$N_{tloss}(2,2) = -203.85$$

$$N_G(2,2) = 203.85 + 7.50 \cdot \frac{1022.30}{1088} + \frac{143.2 \cdot 1022.3 \cdot (25.7 - 27)}{437520} = 210.62$$

$$M_G(2,2) = 4140.2 + 143.2 \cdot \frac{412056}{437520} = 4275$$

$$\Delta\phi_t(2,2) = -5.32 \cdot 10^{-6} + \frac{143.15}{5165 \cdot 437520} = -5.26 \cdot 10^{-6}$$

➤ For $j = 3$

$$M_{co} = \begin{bmatrix} 1 & 1 & 0 & 0 & 0 & 0 \\ 0 & 21.96 & 1 & 0 & 0 & 0 \\ 0 & 0 & -7.25 \cdot 10^{-10} & 0 & 0 & 1 \\ 0 & -2.41 \cdot 10^{-6} & 0 & 0 & 1 & 0 \\ -2.92 \cdot 10^{-7} & 0 & 0 & 1 & 0 & 0 \\ 0 & 0 & 0 & -1 & 1 & -21.96 \end{bmatrix}$$

$$M_c = \begin{bmatrix} 0 \\ 0 \\ -7.48 \cdot 10^{-6} \\ 0 \\ -4.44 \cdot 10^{-4} \\ 0 \end{bmatrix} \& M_s = \begin{bmatrix} 199.14 \\ -199.14 \\ 4372.2 \\ -3.86 \cdot 10^{-4} \\ -4.80 \cdot 10^{-4} \\ -4.31 \cdot 10^{-6} \end{bmatrix}$$

$$\Delta f_{pR}(2,3) = - \left[\frac{(202.5 - 22) \cdot \log(24 \cdot 29 + 1)}{45 \cdot \log(24 \cdot 1 + 1)} \cdot \left(\frac{202.5 - 222}{243} - 0.55 \right) \right] \left[1 \right. \\ \left. + \frac{3 \cdot (0 - 199.14)}{(202.5 - 22) \cdot 14.54} \right] \cdot 0.887 \cdot 14.54 = -7.61$$

$$f_{pR}(2,3) = -7.61$$

$$M_{pR}(2,3) = -7.61 \cdot [21.95 - (27 - 25.7)] = -157$$

$$N_{tloss}(2,3) = -199.14$$

$$N_G(2,3) = 199.14 + 7.61 \cdot \frac{1022.30}{1088} + \frac{157 \cdot 1022.3 \cdot (25.7 - 27)}{441810} = 206$$

$$M_G(2,3) = 4372.2 + 157 \cdot \frac{412056.0}{441810} = 4518.6$$

$$\Delta\phi_t(2,3) = -4.31 \cdot 10^{-6} + \frac{157}{5165 \cdot 441810} = -4.24 \cdot 10^{-6}$$

Table D.42. Change in curvature between time t_1 and t_2

$\Delta\phi_t$ (1/in.)		
$\Delta\phi_t$	$\Delta\phi_t$	$\Delta\phi_t$
5.95E-07	-5.26E-06	-4.24E-06

Table D.43. Net curvature at pre-erection

$\phi_t(t, x)$ (1/in.)		
$\phi_t(2,1)$	$\phi_t(2,2)$	$\phi_t(2,3)$
5.95E-07	-2.06E-05	-1.80E-05

Using net curvature values provided in Table D.46 and Eqns. between D-52 and D-59, the pre-erection camber can be calculated, as shown in Table D.47.

Table D.44. Pre-erection camber

Camber (in.)	section index (x)		
	<u>1</u>	<u>2</u>	<u>3</u>
$\Delta_{np}(x)$	0	-3.33	-6.65

D.5 Camber just after Placement of 1st Deck

- Effect due to change in support condition

$$\text{if } x \leq 5.5 \quad M_{Gsp}(x) = -\frac{0.092 \cdot x^2}{2} = -0.046 \cdot x^2 \quad \text{D-187}$$

$$\text{if } 5.5 < x \quad M_{Gsp}(x) = \frac{0.092 \cdot 136.9 \cdot 12 \cdot (x - 5.5)}{2} - \frac{0.092 \cdot x^2}{2} \quad \text{D-188}$$

Table D.45. Moment applied on non-composite structure due to girder self-weight on bridge site

$M_{Gsp}(x)$ (kips · in.)		
$M_{Gsp}(1)$	$M_{Gsp}(2)$	$M_{Gsp}(3)$
0	22787	30520

$$\Delta\phi_{sc}(x) = \frac{M_{Gsp}(x) - M_{Gsw}(x)}{E_{cG}(2) \cdot I_{ts}(2, x)} \quad \text{D-189}$$

Table D.46. Change in curvature due to change in support conditions

$\Delta\phi_{sc}(x) \text{ (1/in.)}$		
$\Delta\phi_{sc}(1)$	$\Delta\phi_{sc}(2)$	$\Delta\phi_{sc}(3)$
0	4.77E-07	4.73E-07

- Deck self-weight effect

$$w_{d1} = A_{d1} \cdot \gamma_{d1} = \frac{908.28 \cdot 0.150}{12^3} = 0.0788 \text{ kips/in.}$$

$$\text{if } x \leq 5.5 \quad M_{d1sw}(x) = -0.0394 \cdot x^2 \quad \text{D-190}$$

$$\text{if } 5.5 < x \quad M_{d1sw}(x) = 64.33 \cdot x - 0.0394 \cdot (x - 5.5)^2 - 352.60 \quad \text{D-191}$$

Table D.47. Moment applied on non-composite structure due to 1st deck self-weight

$M_{d1sw}(x) \text{ (kips} \cdot \text{in.)}$		
$M_{d1sw}(1)$	$M_{d1sw}(2)$	$M_{d1sw}(3)$
0	19592	26242

$$\Delta\phi_{d1sw}(x) = \frac{M_{d1sw}(x)}{E_{cG}(2) \cdot I_{ts}(2, x)} \quad \text{D-192}$$

Table D.48. Change in curvature due to 1st deck self-weight

$\Delta\phi_{d1sw}(x) \text{ (1/in.)}$		
$\Delta\phi_{d1sw}(1)$	$\Delta\phi_{d1sw}(2)$	$\Delta\phi_{d1sw}(3)$
0	7.76E-06	1.03E-05

To obtain the net curvature just after 1st deck is placed, the net curvature values from previous time-step Table D.46 should be summed up with the change in curvature values given in Table D.49 and Table D.51.

Table D.49. Net curvature just after 1st deck is placed

$\phi_{ad1p}(x) (1/in.)$		
$\phi_{ad1p}(1)$	$\phi_{ad1p}(2)$	$\phi_{ad1p}(3)$
5.95E-07	-1.23E-05	-7.24E-06

- Calculation of camber just after placement of 1st deck

Using eqns. between D-52 and D-59 with the net curvature values given in Table D.51, the camber just after 1st deck is placed can be estimated.

Table D.50. Camber just after placement of 1st deck

Camber (in.)	<i>section index (x)</i>		
	<u>1</u>	<u>2</u>	<u>3</u>
$\Delta_{nad1p}(x)$	0	-1.79	-3.59

D.6 Camber just before Application of Barrier and Overlay Loads on 1st Superstructure

In this part, a time-dependent analysis for composite structure is conducted. To do so, the force history array for girder should be updated by considering the change in forces on the girder due to previous time-dependent effects between t_1 and t_2 , change in support conditions and deck self-weight.

Table D.51. Change in forces on girder due to time-dependent effects between t_1 and t_2

$\Delta N_{Gt_1t_2}(x) (kips)$			$\Delta M_{Gt_1t_2}(x) (kips - in.)$		
$\Delta N_{Gt_1t_2}(1)$	$\Delta N_{Gt_1t_2}(2)$	$\Delta N_{Gt_1t_2}(3)$	$\Delta M_{Gt_1t_2}(1)$	$\Delta M_{Gt_1t_2}(2)$	$\Delta M_{Gt_1t_2}(3)$
56	211	206	820	4275	4519

$$\Delta N_{Gsc}(x) = \frac{[M_{Gsp}(x) - M_{Gsw}(x)] \cdot A_G \cdot [y_t(2, x) - y_{Gbottom}]}{I_{ts}(2, x)} \quad D-193$$

$$\Delta M_{Gsc}(x) = \frac{[M_{Gsp}(x) - M_{Gsw}(x)] \cdot I_G}{I_{ts}(2, x)} \quad D-194$$

Table D.52. Change in forces on girder due to change in support conditions

$\Delta N_{Gsc}(kips)$			$\Delta M_{Gsc}(kips - in.)$		
$\Delta N_{Gsc}(1)$	$\Delta N_{Gsc}(2)$	$\Delta N_{Gsc}(3)$	$\Delta M_{Gsc}(1)$	$\Delta M_{Gsc}(2)$	$\Delta M_{Gsc}(3)$
0	-3	-3	0	1144	1134

$$\Delta N_{Gd1sw}(x) = \frac{M_{d1sw}(x) \cdot A_G \cdot [y_t(2, x) - y_{Gbottom}]}{I_{ts}(2, x)} \quad D-195$$

$$\Delta M_{Gd1sw}(x) = \frac{M_{d1sw}(x) \cdot I_G}{I_{ts}(2, x)} \quad D-196$$

Table D.53. Change in forces on girder due to 1st deck self-weight

$\Delta N_{Gd1sw}(kips)$			$\Delta M_{Gd1sw}(kips - in.)$		
$\Delta N_{Gd1sw}(1)$	$\Delta N_{Gd1sw}(2)$	$\Delta N_{Gd1sw}(3)$	$\Delta M_{Gd1sw}(1)$	$\Delta M_{Gd1sw}(2)$	$\Delta M_{Gd1sw}(3)$
0	-49	-71	0	18592	24690

The second row in Table D.57 can be obtained by simply summing the values up in the tables Table D.54, Table D.55 and Table D.56.

Table D.54. Net force history array just after 1st deck is placed

<i>index</i>	$N_G(t, x)(kips)$			$M_G(x)(kips - in.)$		
	<u>1</u>	<u>2</u>	<u>3</u>	<u>1</u>	<u>2</u>	<u>3</u>
<u>1</u>	0	-2677	-2683	0	-32590	-29306
<u>2</u>	57	158	132	820	24011	30343

Using Eqns. between D-60 and D-68, and D-104 and D-157, the time-dependent calculation can be performed time t_2 and t_3 .

$$z = 2 \text{ \& } m = 3 \text{ \& } q = 1$$

$$\Delta f_{pR_0} = \begin{bmatrix} 0 & 0 & 0 \\ 0 & -7.5 & -7.6 \end{bmatrix}$$

$$N_{tloss_0} = \begin{bmatrix} 0 & 0 & 0 \\ -56.6 & -204 & -199 \end{bmatrix}$$

$$\emptyset_0 = [5.95 \cdot 10^{-7} \quad -1.23 \cdot 10^{-5} \quad -7.24 \cdot 10^{-6}]$$

$$y_{dG} = 31.5 \text{ in.}$$

$$i = 2 \text{ \& } p = 3 \text{ \& } r = 2$$

$$g = [2] \text{ \& } k = [2]$$

- For $k = 2$

$$Co_{NG}(1, loc(x)) = 0 \ \& \ Co_{MG}(1, loc(x)) = 0$$

$$Co_{ND}(1, loc(x)) = 0 \ \& \ Co_{MD}(1, loc(x)) = 0$$

$$\varepsilon_{shG} = -(\varepsilon_G(3) - \varepsilon_G(2)) \cdot 10^{-6} = -21.12 \cdot 10^{-6}$$

$$\varepsilon_{shD} = -(\varepsilon_{d1}(3) - \varepsilon_{d1}(2)) = 0$$

$$u = [1; 2]$$

$$\psi_G(t(3), t(1)) - \psi_G(t(2), t(1)) = 0.6203 - 0.5542 = 0.06$$

$$\psi_G(t(3), t(2)) - \psi_G(t(2), t(2)) = 0.1433 - 0 = 0.14$$

$$E_G = [5165; 5817]$$

$$Co_{NG} = [1.37 \cdot 10^{-6}; -3.08 \cdot 10^{-5}; -3.15 \cdot 10^{-5}]$$

$$Co_{MG} = [4.92 \cdot 10^{-8}; 3.94 \cdot 10^{-7}; 8.80 \cdot 10^{-7}]$$

$$z = [2]$$

- For $z = 2$

$$\psi_{crD} = \psi_D(t(3), t(2)) - \psi_D(t(2), t(2)) = 0$$

$$\psi_{crD, flex} = \psi_{crD} \cdot \beta_{flex}$$

$$E_D = 0$$

$$h = [1; 2; 3]$$

$$Co_{ND} = [0; 0; 0]$$

$$Co_{MD} = [0; 0; 0]$$

- End of "z" array.

$$j = [1; 2; 3]$$

- For $j = 1$

$$M_{co} = \begin{bmatrix} 1 & 1 & 1 & 0 & 0 & 0 & 0 & 0 & 0 \\ -31.5 & 0 & 14.5 & 1 & 1 & 0 & 0 & 0 & 0 \\ -10^{20} & 0 & 0 & 0 & 0 & 1 & 0 & 0 & 0 \\ 0 & -1.9 \cdot 10^{-7} & 0 & 0 & 0 & 0 & 1 & 0 & 0 \\ 0 & 0 & 0 & -10^{20} & 0 & 0 & 0 & 0 & 1 \\ 0 & 0 & 0 & 0 & -4.8 \cdot 10^{-10} & 0 & 0 & 0 & 1 \\ 0 & 0 & -2.5 \cdot 10^{-6} & 0 & 0 & 0 & 0 & 1 & 0 \\ 0 & 0 & 0 & 0 & 0 & 1 & -1 & 0 & 31.5 \\ 0 & 0 & 0 & 0 & 0 & 0 & -1 & 1 & -14.5 \end{bmatrix}$$

$$M_c = \begin{bmatrix} 0 \\ 0 \\ 0 \\ -1.98 \cdot 10^{-5} \\ 0 \\ 4.92 \cdot 10^{-8} \\ 0 \\ 0 \\ 0 \end{bmatrix}$$

$$M_s = [M_{co}^{-1}] \cdot [M_c]$$

$$f_{pR}(2,1) = 0$$

$$\Delta f_{pR}(3,1) = 0$$

$$f_{pR}(3,1) = 0$$

$$M_{pR}(3,1) = 0$$

$$N_{tloss}(3,1) = -6.8 - 56.6 = -63.3$$

$$\delta N_{GpR}(3,1) = 0$$

$$\delta N_{DpR}(3,1) = 0$$

$$\delta M_{GpR}(3,1) = 0$$

$$\delta M_{DpR}(3,1) = 0$$

$$\delta N_{GpR}(3,1) = 0$$

$$N_G(3,1) = 6.8$$

$$M_G(3,1) = 97.9$$

$$N_D(3,1) = 0$$

$$M_D(3,1) = 0$$

$$\Delta\phi_t(3,1) = 9.6 \cdot 10^{-8}$$

Repeat the same procedure for other sections: $j = 2$ and $j = 3$

➤ End of "j" array.

$$\phi_t(3, loc(x)) = \phi_p + \Delta\phi_t(k + 1, loc(x))$$

$$\phi_t(3, loc(x)) = [6.9 \cdot 10^{-7} \quad -1.2 \cdot 10^{-5} \quad -6.2 \cdot 10^{-6}]$$

➤ End of "k" array.

Table D.55. Change in curvature between time t_2 and t_3

$\Delta\phi_t(x) (1/in.)$		
$\Delta\phi_t(1)$	$\Delta\phi_t(2)$	$\Delta\phi_t(3)$
9.6E-08	6.0E-07	1.1E-06

Using the previous net curvature values given in Table D.52 and change in curvature values in Table D.58, net curvature values just before the application of barrier and overlay loads can be obtained as follows:

Table D.56. Net curvature just before application of barrier and overlay loads

$\phi_t(3, x) (1/in.)$		
$\phi_t(3,1)$	$\phi_t(3,2)$	$\phi_t(3,3)$
6.9E-07	-1.2E-05	-6.2E-06

Using net curvature values provided in Table D.59 and Eqns. between D-52 and D-59, camber just before application of barrier and overlay loads can be calculated as shown in Table D.60.

Table D.57. Camber just before application of barrier and overlay loads on 1st superstructure

Camber (in.)	<i>section index</i> (x)		
	<u>1</u>	<u>2</u>	<u>3</u>
$\Delta_{nbas1}(x)$	0	-1.67	-3.33

D.7 Camber just after Application of Barrier and Overlay Loads on 1st Superstructure

As it is indicated above, it is assumed that barrier and overlay loads are applied simultaneously on the 1st composite structure. In this part, only instantaneous changes in camber due to application of superimposes deadloads that is barrier and overlay are calculated. In other words, no time-dependent calculation is performed.

- Barrier load effect

$$w_{b1} = 0.04 \text{ kips/in.}$$

$$\text{if } x \leq 5.5 \quad M_{b1sw}(x) = -0.02 \cdot x^2 \quad \text{D-197}$$

$$\text{if } 5.5 < x \quad M_{b1sw}(x) = 32.636 \cdot x - 0.02 \cdot (x - 5.5)^2 - 180.103 \quad \text{D-198}$$

$$\Delta\phi_{b1sw}(x) = \frac{M_{b1sw}(x)}{E_{cG}(3) \cdot I_{c1}(3, x)} \quad \text{D-199}$$

- Overlay load effect

$$w_{o1} = t_{o1} \cdot s_d \cdot \gamma_{o1} = \frac{2 \cdot 100.92 \cdot 0.140}{12^3} = 0.0164 \text{ kips/in.}$$

$$\text{if } x \leq 5.5 \quad M_{o1sw}(x) = -8.18 \cdot 10^{-3} \cdot x^2 \quad \text{D-200}$$

$$\text{if } 5.5 < x \quad M_{o1sw}(x) = 13.34 \cdot x - 8.18 \cdot 10^{-3} \cdot (x - 5.5)^2 - 73.43 \quad \text{D-201}$$

$$\Delta\phi_{o1sw}(x) = \frac{M_{o1sw}(x)}{E_{cG}(4) \cdot I_{c1}(4, x)} \quad \text{D-202}$$

Table D.58. Moment applied on composite structure due to barrier and overlay loads

$M_{b1sw}(x) \text{ (kips} \cdot \text{in.)}$			$M_{o1sw}(x) \text{ (kips} \cdot \text{in.)}$		
$M_{b1sw}(1)$	$M_{b1sw}(2)$	$M_{b1sw}(3)$	$M_{o1sw}(1)$	$M_{o1sw}(2)$	$M_{o1sw}(3)$
0	9940	13313	0	4064	5443

Table D.59. Change in curvature due to barrier and overlay load

$\Delta\phi_{b1sw}(x) \text{ (1/in.)}$			$\Delta\phi_{o1sw}(x) \text{ (1/in.)}$		
$\Delta\phi_{b1sw}(1)$	$\Delta\phi_{b1sw}(2)$	$\Delta\phi_{b1sw}(3)$	$\Delta\phi_{o1sw}(1)$	$\Delta\phi_{o1sw}(2)$	$\Delta\phi_{o1sw}(3)$
0	2.06E-06	2.75E-06	0	8.44E-07	1.12E-06

- Calculation of camber just after application of barrier and overlay loads

By summing the net curvature values from previous part, Table D.59, with the change in curvature values due to barrier and overlay loads, Table D.62, the net curvature can be obtained as shown in Table D.63. Then, using Eqns. between D-52 and D-59, the camber just after application of barrier and overlay loads can be estimated as shown in Table D.64.

Table D.60. Net curvature just after application of barrier and overlay loads

$\phi_{naas1}(x) \text{ (1/in.)}$		
$\phi_{naas1}(1)$	$\phi_{naabo1}(2)$	$\phi_{naabo1}(3)$
6.90E-07	-8.82E-06	-2.31E-06

Table D.61. Camber just after application of barrier and overlay loads

Camber (in.)	section index (x)		
	<u>1</u>	<u>2</u>	<u>3</u>
$\Delta_{naas1}(x) \text{ (in.)}$	0	-1.28	-2.56

D.8 Camber just before Deck Removal Process

In this part, a time-dependent analysis for composite structure is conducted. To do so, the force history array for both girder and deck should be updated by considering the change in forces on the girder due to previous time-dependent effects between t_2 and t_3 , barrier and overlay self-weight.

- Time-dependent effect between t_2 and t_3

Table D.62. Change in forces on girder and deck due to time-dependent effects between t_2 and t_3

$\Delta N_{Gt_2t_3} \text{ (kips)}$			$\Delta M_{Gt_2t_3} \text{ (kips - in.)}$		
$\Delta N_{Gt_2t_3}(1)$	$\Delta N_{Gt_2t_3}(2)$	$\Delta N_{Gt_2t_3}(3)$	$\Delta M_{Gt_2t_3}(1)$	$\Delta M_{Gt_2t_3}(2)$	$\Delta M_{Gt_2t_3}(3)$
6.8	22.2	18.4	97.9	450.4	403.5
$\Delta N_{Dt_2t_3} \text{ (kips)}$			$\Delta M_{Dt_2t_3} \text{ (kips - in.)}$		
$\Delta N_{Dt_2t_3}(1)$	$\Delta N_{Dt_2t_3}(2)$	$\Delta N_{Dt_2t_3}(3)$	$\Delta M_{Dt_2t_3}(1)$	$\Delta M_{Dt_2t_3}(2)$	$\Delta M_{Dt_2t_3}(3)$
0	0	0	0	0	0

- Barrier load effect

$$\Delta N_{Gb1sw}(x) = \frac{M_{b1sw}(x) \cdot A_G \cdot [y_{c1}(3, x) - y_{Gbottom}]}{I_{c1}(3, x)} \quad D-203$$

$$\Delta M_{Gb1sw}(x) = \frac{M_{b1sw}(x) \cdot I_G}{I_{c1}(3, x)} \quad D-204$$

$$\Delta N_{d1b1sw}(x) = \frac{M_{b1sw}(x) \cdot A_{d1tr}(3, x) \cdot [y_{c1}(3, x) - y_{d1bottom}]}{I_{c1}(3, x)} \quad D-205$$

$$\Delta M_{d1b1sw}(x) = \frac{M_{b1sw}(x) \cdot I_{d1tr}(3, x)}{I_{c1}(3, x)} \quad D-206$$

Table D.63. Change in forces on girder and deck due to barrier load

$\Delta N_{Gb1sw}(kips)$			$\Delta M_{Gb1sw}(kips - in.)$		
$\Delta N_{Gd1sw}(1)$	$\Delta N_{Gd1sw}(2)$	$\Delta N_{Gd1sw}(3)$	$\Delta M_{Gd1sw}(1)$	$\Delta M_{Gd1sw}(2)$	$\Delta M_{Gd1sw}(3)$
0	123	163	0	4953	6588
$\Delta N_{d1b1sw}(kips)$			$\Delta M_{d1b1sw}(kips - in.)$		
$\Delta N_{d1b1sw}(1)$	$\Delta N_{d1b1sw}(2)$	$\Delta N_{d1b1sw}(3)$	$\Delta M_{d1b1sw}(1)$	$\Delta M_{d1b1sw}(2)$	$\Delta M_{d1b1sw}(3)$
0	-144	-191	0	45	60

- Overlay load effect

$$\Delta N_{Go1sw}(x) = \frac{M_{o1sw}(x) \cdot A_G \cdot [y_{c1}(4, x) - y_{Gbottom}]}{I_{c1}(4, x)} \quad D-207$$

$$\Delta M_{Go1sw}(x) = \frac{M_{o1sw}(x) \cdot I_G}{I_{c1}(4, x)} \quad D-208$$

$$\Delta N_{d1o1sw}(x) = \frac{M_{o1sw}(x) \cdot A_{d1tr}(4, x) \cdot [y_{c1}(4, x) - y_{d1bottom}]}{I_{c1}(4, x)} \quad D-209$$

$$\Delta M_{d1o1sw}(x) = \frac{M_{o1sw}(x) \cdot I_{d1tr}(4, x)}{I_{c1}(4, x)} \quad D-210$$

Table D.64. Change in forces on girder and deck due to overlay load

$\Delta N_{Go1sw}(kips)$			$\Delta M_{Go1sw}(kips - in.)$		
$\Delta N_{Go1sw}(1)$	$\Delta N_{Go1sw}(2)$	$\Delta N_{Go1sw}(3)$	$\Delta M_{Go1sw}(1)$	$\Delta M_{Go1sw}(2)$	$\Delta M_{Go1sw}(3)$
0	50	66	0	2025	2693

$\Delta N_{d1b1sw}(kips)$			$\Delta M_{d1b1sw}(kips - in.)$		
$\Delta N_{d1o1sw}(1)$	$\Delta N_{d1o1sw}(2)$	$\Delta N_{d1o1sw}(3)$	$\Delta M_{d1o1sw}(1)$	$\Delta M_{d1o1sw}(2)$	$\Delta M_{d1o1sw}(3)$
0	-59	-78	0	18	25

By summing up the change in forces for deck and girder separately due to abovementioned effects, the force history array for them can be updated as shown in Table D.68.

Table D.65. Net force history array just after application of barrier and overlay loads

<i>index</i>	$N_G(t, x) (kips)$			$M_G(t, x) (kips - in.)$		
	<u>1</u>	<u>2</u>	<u>3</u>	<u>1</u>	<u>2</u>	<u>3</u>
<u>1</u>	0	-2677	-2683	0	-32590	-29306
<u>2</u>	57	158	132	820	24011	30343
<u>3</u>	7	145	181	98	5404	6992
<u>4</u>	0	50	66	0	2025	2693
<i>index</i>	$N_D(t, x) (kips)$			$M_D(t, x) (kips - in.)$		
	<u>1</u>	<u>2</u>	<u>3</u>	<u>1</u>	<u>2</u>	<u>3</u>
<u>1</u>	0	0	0	0	0	0
<u>2</u>	0	0	0	0	0	0
<u>3</u>	0	-144	-191	0	45	60
<u>4</u>	0	-59	-78	0	18	25

It should be noted that although there is no time-dependent change in forces between t_3 and t_4 , an additional row is added for this in Table D.68. This is done on purpose so that the time indexes match with the MDOTCamber program where the effects of barrier and overlay loads are considered separately.

After obtaining the force history array for deck and girder, using Eqns. between D-60 and D-68, and D-104 and D-157, time-dependent calculation can be performed between time t_4 and t_5 . Since it is done explicitly in section D.6, it is not repeated here.

After conducting time-dependent calculation, the following change in force and curvature values can be obtained.

Table D.66. Change in forces on girder and deck due to time-dependent effects between t_4 and t_5

$\Delta N_{Gt_4t_5} (kips)$			$\Delta M_{Gt_4t_5} (kips - in.)$		
$\Delta N_{Gt_4t_5}(1)$	$\Delta N_{Gt_4t_5}(2)$	$\Delta N_{Gt_4t_5}(3)$	$\Delta M_{Gt_4t_5}(1)$	$\Delta M_{Gt_4t_5}(2)$	$\Delta M_{Gt_4t_5}(3)$
-159	6	14	7398	6649	5214
$\Delta N_{Dt_4t_5} (kips)$			$\Delta M_{Dt_4t_5} (kips - in.)$		
$\Delta N_{Dt_4t_5}(1)$	$\Delta N_{Dt_4t_5}(2)$	$\Delta N_{Dt_4t_5}(3)$	$\Delta M_{Dt_4t_5}(1)$	$\Delta M_{Dt_4t_5}(2)$	$\Delta M_{Dt_4t_5}(3)$
212	126	92	45	-1	4

Table D.67. Change in curvature between time t_4 and t_5

$\Delta \phi_t(x) (1/in.)$		
$\Delta \phi_t(1)$	$\Delta \phi_t(2)$	$\Delta \phi_t(3)$
5.74E-06	5.13E-06	7.42E-06

Using the previous net curvature values given in Table D.63 and change in curvature values in Table D.70 net curvature values just before the deck removal process can be obtained as follows:

Table D.71. Net curvature just before deck removal process

$\phi_t(5, x) (1/in.)$		
$\phi_t(5,1)$	$\phi_t(5,2)$	$\phi_t(5,3)$
6.43E-06	-3.69E-06	5.11E-06

Using net curvature values provided in Table D.71 and Eqns. between D-52 and D-59, camber just before the deck removal process can be calculated as shown in Table D.72.

Table D.68. Camber just before deck removal process

Camber (in.)	<i>section index</i> (x)		
	<i>1</i>	<i>2</i>	<i>3</i>
$\Delta_{nbd1r}(x)$	0	-0.13	-0.26

D.9 Camber just after Deck Removal Process

Instantaneous change in camber just after deck is removed is composed of two parts: one is due to removal of self-weight loads of deck, overlay and barrier; other is due to effect of locked forces inside the deck on girder.

- Removal of barrier and overlay loads

$$\Delta N_{Gob1r}(x) = - \frac{[M_{b1sw}(x) + M_{o1sw}(x)] \cdot A_G \cdot [y_{c1}(5, x) - y_{Gbottom}]}{I_{c1}(5, x)} \quad D-211$$

$$\Delta M_{Gob1r}(x) = - \frac{[M_{b1sw}(x) + M_{o1sw}(x)] \cdot I_G}{I_{c1}(5, x)} \quad D-212$$

$$\Delta N_{d1ob1r}(x) = - \frac{[M_{b1sw}(x) + M_{o1sw}(x)] \cdot A_{d1tr}(5, x) \cdot [y_{c1}(5, x) - y_{d1bottom}]}{I_{c1}(5, x)} \quad D-213$$

$$\Delta M_{d1ob1r}(x) = - \frac{[M_{b1sw}(x) + M_{o1sw}(x)] \cdot I_{d1tr}(5, x)}{I_{c1}(5, x)} \quad D-214$$

$$\Delta \phi_{ob1r}(x) = - \frac{[M_{b1sw}(x) + M_{o1sw}(x)]}{E_{cG}(5) \cdot I_{c1}(5, x)} \quad D-215$$

Table D.69. Change in forces on girder and deck due to removal of barrier and overlay loads

$\Delta N_{Gob1r}(x)$ (kips)			$\Delta M_{Gob1r}(x)$ (kips – in.)		
$\Delta N_{Gob1r}(1)$	$\Delta N_{Gob1r}(2)$	$\Delta N_{Gob1r}(3)$	$\Delta M_{Gob1r}(1)$	$\Delta M_{Gob1r}(2)$	$\Delta M_{Gob1r}(3)$
0	-185	-244	0	-6622	-8809
$\Delta N_{d1ob1r}(x)$ (kips)			$\Delta M_{d1ob1r}(x)$ (kips – in.)		
$\Delta N_{d1ob1r}(1)$	$\Delta N_{d1ob1r}(2)$	$\Delta N_{d1ob1r}(3)$	$\Delta M_{d1ob1r}(1)$	$\Delta M_{d1ob1r}(2)$	$\Delta M_{d1ob1r}(3)$
0	214	285	0	-71	-95

Table D.70. Change in curvature due to removal of barrier and overlay loads

$\Delta \phi_{ob1r}(x)$ (1/in.)		
$\Delta \phi_{ob1r}(1)$	$\Delta \phi_{ob1r}(2)$	$\Delta \phi_{ob1r}(3)$
0	-2.75E-06	-3.66E-06

- Removal of locked forces in the deck before it is removed

Using Table D.68, Table D.69 and Table D.73, the total net forces on the deck can be calculated as shown in Table D.75.

Table D.71. Net forces on the deck just before it is removed

$N_{d1br}(kips)$			$M_{d1br}(kips - in.)$		
$N_{d1br}(1)$	$N_{d1br}(2)$	$N_{d1br}(3)$	$M_{d1br}(1)$	$M_{d1br}(2)$	$M_{d1br}(3)$
212	137	107	44	-8	-7

After determined the net forces on the deck, their effects on non-composite section is considered when estimating the camber using the equations below:

$$\Delta N_{tsd1r}(x) = N_{d1br}(x) \quad D-216$$

$$\Delta M_{tsd1r}(x) = M_{d1br}(x) + N_{d1br}(x) \cdot [y_{ts}(5, x) - y_{d1bottom}] \quad D-217$$

$$\Delta N_{Gtsd1r}(x) = \frac{\Delta N_{tsd1r}(x) \cdot A_G}{A_{nctr}(5, x)} + \frac{\Delta M_{tsd1r}(x) \cdot A_G \cdot [y_t(5, x) - y_{Gbottom}]}{I_{ts}(5, x)} \quad D-218$$

$$\Delta M_{Gtsd1r}(x) = \frac{\Delta M_{tsd1r}(x) \cdot I_G}{I_{ts}(5, x)} \quad D-219$$

$$\Delta \phi_{d1r}(x) = \frac{\Delta M_{tsd1r}(x)}{E_{cG}(5) \cdot I_{c1}(5, x)} \quad D-220$$

Table D.72. Change in forces on non-composite structure and girder due to removal of locked forces inside the deck

$\Delta N_{tsd1r}(x) (kips)$			$\Delta M_{tsd1r}(x) (kips - in.)$		
$\Delta N_{tsd1r}(1)$	$\Delta N_{tsd1r}(2)$	$\Delta N_{tsd1r}(3)$	$\Delta M_{tsd1r}(1)$	$\Delta M_{tsd1r}(2)$	$\Delta M_{tsd1r}(3)$
212	137	107	-6782	-4475	-3506
$\Delta N_{Gtsd1r}(x) (kips)$			$\Delta M_{Gtsd1r}(x) (kips - in.)$		
$\Delta N_{Gtsd1r}(1)$	$\Delta N_{Gtsd1r}(2)$	$\Delta N_{Gtsd1r}(3)$	$\Delta M_{Gtsd1r}(1)$	$\Delta M_{Gtsd1r}(2)$	$\Delta M_{Gtsd1r}(3)$
213	142	111	-6608	-4248	-3300

Table D.73. Change in curvature due to removal of locked forces inside the deck

$\Delta \phi_{d1r}(x) (1/in.)$		
$\Delta \phi_{d1r}(1)$	$\Delta \phi_{d1r}(2)$	$\Delta \phi_{d1r}(3)$
-2.74E-06	-1.76E-06	-1.37E-06

- Removal of deck load

$$\Delta N_{Gd1swr}(x) = - \frac{M_{d1sw}(x) \cdot A_G \cdot [y_t(5, x) - y_{Gbottom}]}{I_{ts}(5, x)} \quad \text{D-221}$$

$$\Delta M_{Gd1swr}(x) = - \frac{M_{d1sw}(x) \cdot I_G}{I_{ts}(5, x)} \quad \text{D-222}$$

$$\Delta \phi_{d1swr}(x) = - \frac{M_{d1sw}(x)}{E_{cG}(5) \cdot I_{ts}(5, x)} \quad \text{D-223}$$

Table D.74. Change in forces on girder due to deck removal

$\Delta N_{Gd1swr}(x)$ (kips)			$\Delta M_{Gd1swr}(x)$ (kips – in.)		
$\Delta N_{Gd1swr}(1)$	$\Delta N_{Gd1swr}(2)$	$\Delta N_{Gd1swr}(3)$	$\Delta M_{Gd1swr}(1)$	$\Delta M_{Gd1swr}(2)$	$\Delta M_{Gd1swr}(3)$
0	49	70	0	-18598	-24699

Table D.79. Change in curvature due to deck removal

$\Delta \phi_{d1swr}(x)$ (1/in.)		
$\Delta \phi_{d1swr}(1)$	$\Delta \phi_{d1swr}(2)$	$\Delta \phi_{d1swr}(3)$
0	-7.72E-06	-1.02E-05

After considered all effects, curvature changes given in Table D.74, Table D.77 and Table D.79 need to be summed together with the previous net curvature values provided in Table D.71 so that the net curvature just after deck removal can be obtained as shown in Table D.80.

Table D.75. Net curvature just after deck removal

$\phi_{ad1r}(x)$ (1/in.)		
$\phi_{ad1r}(1)$	$\phi_{ad1r}(2)$	$\phi_{ad1r}(3)$
3.69E-06	-1.59E-05	-1.02E-05

Using net curvature values provided in Table D.80 and Eqns. between D-52 and D-59, camber just after the deck is removed can be calculated as shown in Table D.81.

Table D.76. Camber just after deck removal

Camber (in.)	<i>section index (x)</i>		
	<u>1</u>	<u>2</u>	<u>3</u>
$\Delta_{nad1r}(x)$	0	-2.37	-4.73

D.10 Camber just before 2nd Deck Placement

In this part, a time-dependent analysis for non-composite structure is performed to estimate the camber just before the new deck is placed. Before starting this, force history array for girder needs to be updated by using Table D.68, Table D.69, Table D.73, Table D.76 and Table D.78.

Table D.77. Net force history array just after 1st deck is removed

<i>index</i>	$N_G(t, x)$ (kips)			$M_G(t, x)$ (kips – in.)		
	<u>1</u>	<u>2</u>	<u>3</u>	<u>1</u>	<u>2</u>	<u>3</u>
<u>1</u>	0	-2677	-2683	0	-32590	-29306
<u>2</u>	57	158	132	820	24011	30343
<u>3</u>	7	145	181	98	5404	6992
<u>4</u>	0	50	66	0	2025	2693
<u>5</u>	55	12	-50	790	-22820	-31594

Using Eqns. between D-60 and D-103, time-dependent calculation can be performed. From analysis results, change in curvature values can be obtained as follows:

Table D.78. Change in curvature between t_5 and t_6

$\Delta\phi_t(x)$ (1/in.)		
$\Delta\phi_t(1)$	$\Delta\phi_t(2)$	$\Delta\phi_t(3)$
2.63E-08	-7.29E-07	-1.00E-07

To be able to obtain the net curvature values just before the new deck is placed, the time-dependent change in curvature values given in Table D.83 is summed up with the net curvature values from previous part presented in Table D.80. By doing this, the net curvature values just before the new deck is placed are obtained as follows:

Table D.79. Net curvature just before new deck placement

$\phi_t(6, x) \text{ (1/in.)}$		
$\phi_t(3,1)$	$\phi_t(3,2)$	$\phi_t(3,3)$
3.72E-06	-1.67E-05	-1.12E-05

Using net curvature values provided in Table D.84 and Eqns. between D-52 and D-59, camber just before new deck placed can be calculated as shown in Table D.85.

Table D.80. Camber just before new deck placement

Camber (in.)	<i>section index</i> (x)		
	<u>1</u>	<u>2</u>	<u>3</u>
$\Delta_{nbndp}(x)$	0	-2.50	-5.00

D.11 Camber just after 2nd Deck Placement

A similar process that is explained in section F.4 is followed in this part to estimate the camber. Since it is assumed that 1st and 2nd decks are identical, equations used for 1st deck are valid for 2nd deck, however, parameters that are time-dependent should be updated accordingly.

- Deck self-weight effect

$$w_{d2} = A_{d2} \cdot \gamma_{d2} = \frac{908.28 \cdot 0.150}{12^3} = 0.0788 \text{ kips/in.}$$

$$\text{if } x \leq 5.5 \quad M_{d2sw}(x) = -0.0394 \cdot x^2 \quad \text{D-224}$$

$$\text{if } 5.5 < x \quad M_{d2sw}(x) = 64.33 \cdot x - 0.0394 \cdot (x - 5.5)^2 - 352.60 \quad \text{D-225}$$

Table D.81. Moment applied on non-composite structure due to 2nd deck self-weight

$M_{d2sw}(x) \text{ (kips} \cdot \text{in.)}$		
$M_{d2sw}(1)$	$M_{d2sw}(2)$	$M_{d2sw}(3)$
0	19592	26242

$$\Delta\phi_{d2sw}(x) = \frac{M_{d2sw}(x)}{E_{cG}(2) \cdot I_{ts}(6, x)} \quad \text{D-226}$$

Table D.82. Change in curvature due to 2nd deck self-weight

$\Delta\phi_{d2sw}(x) \text{ (1/in.)}$		
$\Delta\phi_{d2sw}(1)$	$\Delta\phi_{d2sw}(2)$	$\Delta\phi_{d2sw}(3)$
0	7.72E-06	1.03E-05

- Calculation of camber just after placement of 2nd deck

Table D.83. Net curvature just after 2nd deck is placed

$\phi_{ad2p}(x) \text{ (1/in.)}$		
$\phi_{ad2p}(1)$	$\phi_{ad2p}(2)$	$\phi_{ad2p}(3)$
3.72E-06	-8.93E-06	-9.16E-07

Using net curvature values given in Table D.88, and Eqns. between D-52 and D-59, the camber just after 2nd deck is placed can be estimated.

Table D.84. Camber just after placement of 2nd deck

Camber (in.)	<i>section index (x)</i>		
	<i>1</i>	<i>2</i>	<i>3</i>
$\Delta_{nad2p}(x)$	0	-1.06	-2.11

D.12 Camber just before Application of Barrier and Overlay Loads on 2nd Super-structure

In this part, a time-dependent analysis for composite structure is conducted similar to section F.5. To do so, the force history array for girder should be updated by considering the change in forces on the girder due to previous time-dependent effects between t_5 and t_6 and deck self-weight.

Table D.85. Change in forces on girder due to time-dependent effects between t_5 and t_6

$\Delta N_{Gt_5t_6}(x) \text{ (kips)}$			$\Delta M_{Gt_5t_6}(x) \text{ (kips - in.)}$		
$\Delta N_{Gt_5t_6}(1)$	$\Delta N_{Gt_5t_6}(2)$	$\Delta N_{Gt_5t_6}(3)$	$\Delta M_{Gt_5t_6}(1)$	$\Delta M_{Gt_5t_6}(2)$	$\Delta M_{Gt_5t_6}(3)$
0	13	18	-6	261	377

$$\Delta N_{Gd2sw}(x) = \frac{M_{d2sw}(x) \cdot A_G \cdot [y_t(6, x) - y_{Gbottom}]}{I_{ts}(6, x)} \quad \text{D-227}$$

$$\Delta M_{Gd2sw}(x) = \frac{M_{d2sw}(x) \cdot I_G}{I_{ts}(6, x)} \quad \text{D-228}$$

Table D.86. Change in forces on girder due to 2nd deck self-weight

$\Delta N_{Gd2sw}(kips)$			$\Delta M_{Gd2sw}(kips - in.)$		
$\Delta N_{Gd2sw}(1)$	$\Delta N_{Gd2sw}(2)$	$\Delta N_{Gd2sw}(3)$	$\Delta M_{Gd2sw}(1)$	$\Delta M_{Gd2sw}(2)$	$\Delta M_{Gd2sw}(3)$
0	-49	-70	0	18598	24699

The sixth row in Table D.92 can be obtained by simply summing the values up in the Table D.90 and Table D.91.

Table D.87. Net force history array just after 2nd deck is placed

<i>index</i>	$N_G(t, x)(kips)$			$M_G(t, x)(kips - in.)$		
	<u>1</u>	<u>2</u>	<u>3</u>	<u>1</u>	<u>2</u>	<u>3</u>
<u>1</u>	0	-2677	-2683	0	-32590	-29306
<u>2</u>	57	158	132	820	24011	30343
<u>3</u>	7	145	181	98	5404	6992
<u>4</u>	0	50	66	0	2025	2693
<u>5</u>	55	12	-50	790	-22820	-31594
<u>6</u>	0	-36	-52	-6	18859	25076

Using Eqns. between D-60 and D-68, and D-104 and D-157, time-dependent calculation for 2nd composite structure between time t_6 and t_7 can be performed. Hence, the change in curvatures can be obtained as follows:

Table D.88. Change in curvature between time t_6 and t_7

$\Delta \phi_t(x) (1/in.)$		
$\Delta \phi_t(1)$	$\Delta \phi_t(2)$	$\Delta \phi_t(3)$
1.19E-08	1.32E-07	1.55E-07

Summing the change in curvature values in Table D.93 with the previous net curvature values in Table D.88, the net curvature values just before application of barrier and overlay loads on 2nd super-structure can be obtained as follows:

Table D.89. Net curvature just before application of barrier and overlay loads

$\phi_t(7,x) (1/in.)$		
$\phi_t(7,1)$	$\phi_t(7,2)$	$\phi_t(7,3)$
3.73E-06	-8.80E-06	-7.60E-07

Using net curvature values provided in Table D.94 and Eqns. between D-52 and D-59, camber just before application of barrier and overlay loads on 2nd super-structure can be calculated as follows:

Table D.90. Camber just before application of barrier and overlay loads on 2nd superstructure

Camber (in.)	<i>section array</i> (<i>x</i>)		
	<u>1</u>	<u>2</u>	<u>3</u>
$\Delta_{nbas2}(x)$	0	-1.03	-2.07

D.13 Camber just after Application of Barrier and Overlay Loads on 2nd Super-structure

Similarly, the process provided in section D.7, is followed in this part to estimate the camber just after application of barrier and overlay loads on 2nd super-structure. Since it is assumed that same barrier and overlay loads are applied on it, equations used previously for the effect of barrier and overlay loads on 1st super-structure are valid for 2nd super-structure, however, parameters that are time-dependent should be updated accordingly. Similarly, it is assumed that overlay load is simultaneously applied with the barrier load for simplicity.

- Barrier load effect

$$w_{b2} = 0.04 \text{ kips/in.}$$

$$\text{if } x \leq 5.5 \quad M_{b2sw}(x) = -0.02 \cdot x^2 \quad \text{D-229}$$

$$\text{if } 5.5 < x \quad M_{b2sw}(x) = 32.636 \cdot x - 0.02 \cdot (x - 5.5)^2 - 180.103 \quad \text{D-230}$$

$$\Delta\phi_{b2sw}(x) = \frac{M_{b2sw}(x)}{E_{cG}(7) \cdot I_{c2}(7,x)} \quad \text{D-231}$$

- Overlay load effect

$$w_{o2} = t_{o2} \cdot s_d \cdot \gamma_{o2} = \frac{2 \cdot 100.92 \cdot 0.140}{12^3} = 0.0164 \text{ kips/in.}$$

$$\text{if } x \leq 5.5 \quad M_{o2sw}(x) = -8.18 \cdot 10^{-3} \cdot x^2 \quad \text{D-232}$$

$$\text{if } 5.5 < x \quad M_{o2sw}(x) = 13.34 \cdot x - 8.18 \cdot 10^{-3} \cdot (x - 5.5)^2 - 73.43 \quad \text{D-233}$$

$$\Delta\phi_{o2sw}(x) = \frac{M_{o2sw}(x)}{E_{cG}(8) \cdot I_{c2}(8, x)} \quad \text{D-234}$$

Table D.91. Moment applied on 2nd composite structure due to barrier and overlay loads

$M_{b2sw}(x) \text{ (kips} \cdot \text{in.)}$			$M_{o2sw}(x) \text{ (kips} \cdot \text{in.)}$		
$M_{b2sw}(1)$	$M_{b2sw}(2)$	$M_{b2sw}(3)$	$M_{o2sw}(1)$	$M_{o2sw}(2)$	$M_{o2sw}(3)$
0	9940	13313	0	4064	5443

Table D.92. Change in curvature on 2nd super-structure due to barrier and overlay load

$\Delta\phi_{b2sw}(x) \text{ (1/in.)}$			$\Delta\phi_{o2sw}(x) \text{ (1/in.)}$		
$\Delta\phi_{b2sw}(1)$	$\Delta\phi_{b2sw}(2)$	$\Delta\phi_{b2sw}(3)$	$\Delta\phi_{o2sw}(1)$	$\Delta\phi_{o2sw}(2)$	$\Delta\phi_{o2sw}(3)$
0	2.06E-06	2.74E-06	0	8.42E-07	1.12E-06

- Calculation of camber just after application of barrier and overlay loads on 2nd super-structure

By summing up the curvature changes given in Table D.92 and previous net curvature values in Table D.94, the net curvature values just after application of barrier and overlay loads on 2nd super-structure can be obtained as follows:

Table D.93. Net curvature just after application of barrier and overlay loads on 2nd super-structure

$\phi_{naas2}(x) \text{ (1/in.)}$		
$\phi_{naas2}(1)$	$\phi_{naas2}(2)$	$\phi_{naas2}(3)$
3.73E-06	-5.90E-06	3.10E-06

After obtaining the net curvature values along the half-span, camber just after application of barrier and overlay loads on 2nd super-structure can be estimated using Eqns. between D-52 and D-59.

Table D.94. Camber just after application of barrier and overlay loads on 2nd super-structure

Camber (in.)	<i>section index (x)</i>		
	<u>1</u>	<u>2</u>	<u>3</u>
$\Delta_{naas2}(x)$	0	-0.49	-0.98

D.14 Camber at Final Time

The effect of barrier and overlay loads on girder and deck should be determined and force histories for both deck and girder should be updated before conducting time-dependent analysis. To do so, a similar approach stated in Part 8 is followed. Equations used in section D.8 are valid in this part, however, parameters that are time-dependent should be updated accordingly.

- Time-dependent effect between t_6 and t_7

Table D.95. Change in forces on girder and deck due to time-dependent effects between t_6 and t_7

$\Delta N_{Gt_6t_7}(x)(kips)$			$\Delta M_{Gt_6t_7}(x)(kips - in.)$		
$\Delta N_{Gt_6t_7}(1)$	$\Delta N_{Gt_6t_7}(2)$	$\Delta N_{Gt_6t_7}(3)$	$\Delta M_{Gt_6t_7}(1)$	$\Delta M_{Gt_6t_7}(2)$	$\Delta M_{Gt_6t_7}(3)$
0	-1	-1	-3	-18	-20
$\Delta N_{Dt_6t_7}(x)(kips)$			$\Delta M_{Dt_6t_7}(x)(kips - in.)$		
$\Delta N_{Dt_6t_7}(1)$	$\Delta N_{Dt_6t_7}(2)$	$\Delta N_{Dt_6t_7}(3)$	$\Delta M_{Dt_6t_7}(1)$	$\Delta M_{Dt_6t_7}(2)$	$\Delta M_{Dt_6t_7}(3)$
0	0	0	0	0	0

- Barrier load effect

$$\Delta N_{Gb2sw}(x) = \frac{M_{b2sw}(x) \cdot A_G \cdot [y_{c2}(7, x) - y_{Gbottom}]}{I_{c2}(7, x)} \quad D-235$$

$$\Delta M_{Gb2sw}(x) = \frac{M_{b2sw}(x) \cdot I_G}{I_{c2}(7, x)} \quad D-236$$

$$\Delta N_{d2b2sw}(x) = \frac{M_{b2sw}(x) \cdot A_{d2tr}(7, x) \cdot [y_{c2}(7, x) - y_{d2bottom}]}{I_{c2}(7, x)} \quad D-237$$

$$\Delta M_{d2b2sw}(x) = \frac{M_{b2sw}(x) \cdot I_{d2tr}(7, x)}{I_{c2}(7, x)} \quad D-238$$

Table D.96. Change in forces on girder and deck due to barrier load

$\Delta N_{Gb2sw}(x)$ (<i>kips</i>)			$\Delta M_{Gb2sw}(x)$ (<i>kips – in.</i>)		
$\Delta N_{Gb2sw}(1)$	$\Delta N_{Gb2sw}(2)$	$\Delta N_{Gb2sw}(3)$	$\Delta M_{Gb2sw}(1)$	$\Delta M_{Gb2sw}(2)$	$\Delta M_{Gb2sw}(3)$
0	123	162	0	4961	6599
$\Delta N_{d2b2sw}(x)$ (<i>kips</i>)			$\Delta M_{d2b2sw}(x)$ (<i>kips – in.</i>)		
$\Delta N_{d2b2sw}(1)$	$\Delta N_{d2b2sw}(2)$	$\Delta N_{d2b2sw}(3)$	$\Delta M_{d2b2sw}(1)$	$\Delta M_{d2b2sw}(2)$	$\Delta M_{d2b2sw}(3)$
0	-143	-191	0	45	60

- Overlay load effect

$$\Delta N_{Go2sw}(x) = \frac{M_{o2sw}(x) \cdot A_G \cdot [y_{c2}(8,x) - y_{Gbottom}]}{I_{c2}(8,x)} \quad \text{D-239}$$

$$\Delta M_{Go2sw}(x) = \frac{M_{b2sw}(x) \cdot I_G}{I_{c2}(8,x)} \quad \text{D-240}$$

$$\Delta N_{d2o2sw}(x) = \frac{M_{o2sw}(x) \cdot A_{d2tr}(8,x) \cdot [y_{c2}(8,x) - y_{d2bottom}]}{I_{c2}(4,x)} \quad \text{D-241}$$

$$\Delta M_{d2o2sw}(x) = \frac{M_{o2sw}(x) \cdot I_{d2tr}(8,x)}{I_{c2}(8,x)} \quad \text{D-242}$$

Table D.97. Change in forces on girder and deck due to overlay load

$\Delta N_{Go2sw}(x)$ (<i>kips</i>)			$\Delta M_{Go2sw}(x)$ (<i>kips – in.</i>)		
$\Delta N_{Go2sw}(1)$	$\Delta N_{Go2sw}(2)$	$\Delta N_{Go2sw}(3)$	$\Delta M_{Go2sw}(1)$	$\Delta M_{Go2sw}(2)$	$\Delta M_{Go2sw}(3)$
0	50	66	0	2028	2698
$\Delta N_{d2o2sw}(x)$ (<i>kips</i>)			$\Delta M_{d2o2sw}(x)$ (<i>kips – in.</i>)		
$\Delta N_{d2o2sw}(1)$	$\Delta N_{d2o2sw}(2)$	$\Delta N_{d2o2sw}(3)$	$\Delta M_{d2o2sw}(1)$	$\Delta M_{d2o2sw}(2)$	$\Delta M_{d2o2sw}(3)$
0	-59	-78	0	18	24

By summing up the change in forces for deck and girder separately due to abovementioned effects, the force history array for them can be updated as shown in Table D.103.

Table D.98. Net force history array just after application of barrier and overlay loads

<i>index</i>	$N_G(t, x)(kips)$			$M_G(t, x)(kips - in.)$		
	<u>1</u>	<u>2</u>	<u>3</u>	<u>1</u>	<u>2</u>	<u>3</u>
<u>1</u>	0	-2677	-2683	0	-32590	-29306
<u>2</u>	57	158	132	820	24011	30343
<u>3</u>	7	145	181	98	5404	6992
<u>4</u>	0	50	66	0	2025	2693
<u>5</u>	55	12	-50	790	-22820	-31594
<u>6</u>	0	-36	-52	-6	18859	25076
<u>7</u>	0	122	162	-3	4943	6578
<u>8</u>	0	50	66	0	2028	2698
<i>index</i>	$N_D(t, x)(kips)$			$M_D(t, x)(kips - in.)$		
	<u>1</u>	<u>2</u>	<u>3</u>	<u>1</u>	<u>2</u>	<u>3</u>
<u>1</u>	0	0	0	0	0	0
<u>2</u>	0	0	0	0	0	0
<u>3</u>	0	0	0	0	0	0
<u>4</u>	0	0	0	0	0	0
<u>5</u>	0	0	0	0	0	0
<u>6</u>	0	0	0	0	0	0
<u>7</u>	0	-143	-191	0	45	60
<u>8</u>	0	-59	-78	0	18	13

It should be noted that although there is no time-dependent change in forces between t_7 and t_8 , an additional row is added for this in Table D.103. This is done on purpose so that the time indices match with the MDOTCamber program where the effects of barrier and overlay loads are considered separately. After obtaining the force history array for deck and girder, using Eqns. between D-60 and D-68, and D-104 and D-157, time-dependent calculation can be performed between time t_8 and t_9 . Since it is done explicitly in section D.8, it is not repeated here. After conducting time-dependent calculation, the following change in force and curvature values can be obtained.

Table D.99. Change in forces on girder and deck due to time-dependent effects between t_8 and t_9

$\Delta N_{Gt_8t_9}(x)$ (kips)			$\Delta M_{Gt_8t_9}(x)$ (kips – in.)		
$\Delta N_{Gt_8t_9}(1)$	$\Delta N_{Gt_8t_9}(2)$	$\Delta N_{Gt_8t_9}(3)$	$\Delta M_{Gt_8t_9}(1)$	$\Delta M_{Gt_8t_9}(2)$	$\Delta M_{Gt_8t_9}(3)$
-355	-432	-458	10921	12096	12489
$\Delta N_{Dt_8t_9}(x)$ (kips)			$\Delta M_{Dt_8t_9}(x)$ (kips – in.)		
$\Delta N_{Dt_8t_9}(1)$	$\Delta N_{Dt_8t_9}(2)$	$\Delta N_{Dt_8t_9}(3)$	$\Delta M_{Dt_8t_9}(1)$	$\Delta M_{Dt_8t_9}(2)$	$\Delta M_{Dt_8t_9}(3)$
350	403	422	49	22	13

Table D.100. Change in curvature between time t_8 and t_9

$\Delta \phi_t(x)$ (1/in.)		
$\Delta \phi_t(1)$	$\Delta \phi_t(2)$	$\Delta \phi_t(3)$
6.30E-06	8.05E-06	8.53E-06

Using the previous net curvature values given in Table D.98 and change in curvature values provided in Table D.105, the net curvature at final time can be calculated as follows:

Table D.101. Net curvature at final considered time

$\phi_t(9, x)$ (1/in.)		
$\phi_t(9,1)$	$\phi_t(9,2)$	$\phi_t(9,3)$
1.00E-05	2.15E-06	1.16E-05

Using the net curvature values in Table D.106, and Eqns. between D-52 and D-59, the net camber at considered final time which is 75 years in this example can be estimated as follows:

Table D.102. Camber at final considered time

Camber (in.)	section index (x)		
	<u>1</u>	<u>2</u>	<u>3</u>
$\Delta_{ns2}(x)$	0	0.90	1.79

D.15 Nomenclature

A_G = girder area, (in.²),
 A_{nm} = area under curvature diagram between nth section and midspan, (in.²)
 A_n = area under curvature diagram between nth section and closest girder end, (in.²)
 A_{psi} = nominal area for a strand, (in.²),
 A_{ps} = effective area of strands as a function of location, (in.²),
 A_{psdb} = total debonded strand area, (in.²),
 A_{pshp} = total harped strand area as a function of location, (in.²),
 A_{psst} = total straight strand area, (in.²),
 A_{d1} = area of the first deck, (in.²),
 A_{nctr} = transformed area of non-composite structure, (in.²),
 A_{ctr} = transformed area of composite structure, (in.²),
 A_{c1tr} = transformed area of 1st composite structure, (in.²),
 A_{c2tr} = transformed area of 2nd composite structure, (in.²),
 A = net area of the element that is going to be transformed, (in.²),
 A_d = area of the deck, (in.²),
 A_{pstr} = transformed area of the prestressing strand, (in.²),
 A_{dtr} = transformed area for the deck, (in.²),
 A_{d1tr} = transformed area for the 1st deck, (in.²),
 A_{d2tr} = transformed area for the 2nd deck, (in.²),
 b_f = girder top flange width, (in.),
 C_{oNG} = coefficient related to axial force on the girder,
 C_{oMG} = coefficient related to moment on the girder,
 C_{oNG} = coefficient related to axial force on the deck,
 C_{oMG} = coefficient related to moment on the deck,
 d_{ps} = nominal strand diameter, (in.),
 e_{db} = eccentricity of debonded strands, (in.²),

$e_{hp,end}$ = eccentricity of harped strands at girder end, (in.),
 $e_{hp,mid}$ = eccentricity of harped strands at girder midspan, (in.),
 e_{hp} = eccentricity of harped strand as a function of location, (in.),
 e_{st} = eccentricity of straight strands, (in.),
 e_e = net end eccentricity, (in.),
 e_{atdb} = net eccentricity at the end of debonding length, (in.),
 e_m = net midspan eccentricity, (in.),
 e_{ts} = eccentricity of prestressing strand in transformed non-composite structure, (in.),
 e_c = eccentricity of prestressing strand in transformed composite structure, (in.),
 e_{c1} = eccentricity of prestressing strand in transformed composite structure with 1st deck, (in.),
 e_{c2} = eccentricity of prestressing strand in transformed composite structure with 2nd deck, (in.),
 E_c = modulus of elasticity as a function of time, (ksi),
 E_{cG} = modulus of elasticity function for girder as a function of time, (ksi),
 E_{cD} = the modulus of elasticity function for deck as a function of time, (ksi),
 E_{cD1} = the modulus of elasticity function for the first deck as a function of time, (ksi),
 E_{cD2} = the modulus of elasticity function for the second deck as a function of time, (ksi),
 E'_{c28} = 28-day modulus of elasticity of concrete, (ksi),
 E'_{ci} = modulus of elasticity value when strands are released, (ksi),
 E_G = modulus of elasticity of girder concrete at a specific time, (ksi),
 E_D = modulus of elasticity of deck concrete at a specific time, (ksi),
 E_{tr} = modulus of elasticity of the transformed material, (ksi),
 f_{py} = yield stress of the prestressing strands, (ksi),

f_{psj} = stress on the strands along the span prior to transfer, (ksi),
 f_{pR} = remaining relaxation loss array as a function of time and location, (kips),
 f'_{cdi} = initial concrete compressive strength for deck, (ksi),
 f'_{cd} = 28-day concrete compressive strength for deck, (ksi),
 f'_{ci} and f'_c are initial concrete compressive strength, (ksi),
 f'_c = 28-day concrete compressive strength, (ksi),
 f_{pj} = jacking stress of the prestressing strands, (ksi),
 g = a time index for the initiation of composite action,
 h = section index array,
 H_r = the average annual ambient relative humidity (%),
 i = index for initial reference time,
 I_{ts} = moment of inertia of the transformed non-composite structure, (in.⁴),
 I_{dtr} = transformed moment of inertia of the deck, (in.⁴),
 I_{d1tr} = transformed moment of inertia of the 1st deck, (in.⁴),
 I_{d2tr} = transformed moment of inertia of the 2nd deck, (in.⁴),
 I_c = transformed moment of inertia of composite structure, (in.⁴),
 I_{c1} = transformed moment of inertia of composite structure with 1st deck, (in.⁴),
 I_{c2} = transformed moment of inertia of composite structure with 2nd deck, (in.⁴),
 j = section index array,
 k = time index array,
 k_s = factor for the effect of the volume-to-surface ratio of the component
 k_{hc} = humidity factor for creep,
 k_f = factor for the effect of concrete strength,
 k_{tdc} = time development factor for creep,
 k_{tds} = time development factor for shrinkage,
 k_{hs} = humidity factor for shrinkage,
 K_L = factor accounting for type of prestressing strand, equal to 45 for low

relaxation strands (AASHTO LRFD 9th Edition section 5.9.3.4.2c)
 K_i = accounts for time-dependent interaction between concrete and bonded steel in the section being considered (AASHTO LRFD 8th Edition section 5.9.3.4.2a-2),
 K_1 = coefficient depending on aggregate type: for normal weight concrete $K_1 = 1.0$,
 L_{tr} = transfer length (in.),
 L_{dbavg} = average debonding length, (in.),
 L_{hpavg} = average harping length, (in.),
 L_{hpi} = harping length for i^{th} harped strand group, (in.),
 L_{dbi} = debonding length for i^{th} debonded strand group, (in.),
 L_t = girder overhang length at precast facility, (in.),
 m = number of sections to be investigated,
 M_{ps} = moment on the non-composite structure due to prestressing effect, (kips – in.),
 M_{Gi} = net moment on the non-composite structure due to prestressing and girder self-weight effect, (kips – in.),
 M_{Gsw} = moment on the non-composite structure due to girder self-weight at precast facility, (kips – in.),
 M_{Gsi} = moment on girder alone due to girder self-weight at precast facility, (kips – in.),
 M_{psst} = moment on the non-composite structure due to straight prestressing strand, (kips – in.),
 M_{psdb} = moment on the non-composite structure due to debonded prestressing strand, (kips – in.),
 M_{pshp} = moment on the non-composite structure due to harped prestressing strand, (kips – in.),
 M_{Gps} = moment on girder only caused by prestressing effect as a function of location, (kips – in.),
 M_{Gp} = net moment on girder only due to combined effect at release, (kips – in.),
 M_{co} = matrix composed of coefficients for time-dependent calculations,

M_c = matrix of constants for time-dependent calculations,

M_s = solution matrix for time-dependent calculations,

M_G = array of moment on the girder a function of time and location, (*kips – in.*),

N_D = array of axial force on the deck a function of time and location, (*kips*),

M_D = array of moment on the deck a function of time and location, (*kips – in.*),

M_{d1sw} = moment caused by 1st deck load as a function of location, (*kips – in.*),

M_{d2sw} = moment caused by 2nd deck load as a function of location, (*kips – in.*),

M_{b1sw} = moment caused by 1st barrier load as a function of location, (*kips – in.*),

M_{b2sw} = moment caused by 2nd barrier load as a function of location, (*kips – in.*),

M_{o1sw} = moment caused by 1st overlay load as a function of location, (*kips – in.*),

M_{o2sw} = moment caused by 2nd overlay load as a function of location, (*kips – in.*),

M_{Gsp} = moment due to girder self-weight on non-composite structure on bridge site, (*kips – in.*),

M_{d1br} = net moment on the 1st deck before it is removed, (*kips – in.*),

M_{pR} = array of moment on non-composite structure caused by remaining relaxation loss as a function of time and location, (*kips – in.*),

N_{st} = total number of straight strand, (*in.*²),

N_{db} = total number of debonded strand, (*in.*²),

N_{hp} = total area of harped strand, (*in.*²),

N_i = number of strands debonded in *i*th strand group,

N_{ps} = axial force on the non-composite structure due to prestressing effect, (*kips*),

N_{Gi} = net axial force on the non-composite structure due to prestressing and girder self-weight effect, (*kips*),

N_{Gsi} = axial force on girder alone due to girder self-weight at precast facility, (*kips*),

N_{psst} = axial force on the non-composite structure due to straight prestressing strand, (*kips*),

N_{psdb} = axial force on the non-composite structure due to debonded prestressing strand, (*kips*),

N_{pshp} = axial force on the non-composite structure due to harped prestressing strand, (*kips*),

N_{Gps} = axial force on girder only caused by prestressing effect as a function of location, (*kips*),

N_{Gp} = net axial force on girder only due to combined effect at release, (*kips*),

N_G = array of axial force on the girder a function of time and location, (*kips*),

N_{d1br} = net axial force on the 1st deck before it is removed, (*kips*),

N_{tloss} = total time-dependent loss with respect to time along the half-span, (*kips*),

N_{tloss_0} = initial time-dependent loss with respect to time along the half-span, (*kips*),

P_{psst} = axial force on the straight prestressing strand, (*kips*),

P_{psdb} = axial force on the debonded prestressing strand, (*kips*),

P_{pshp} = axial force on the harped prestressing strand, (*kips*),

p = index for final reference time,

Q_n = first moment of the area under curvature diagram between *n*th section and closest girder end, (*in.*³),

r = helper symbol that is related to time reference for time-dependent calculations,

s_d = average center-to-center spacing of the girders, (*in.*),

s_{d1} = perimeter of the first deck, (*in.*),

t_1 = time when strands are released, (*days*),

t_i = age of concrete at the time of load application (*days*),

t = maturity of concrete, defined as age of concrete between time of loading for creep calculations, or end of curing for shrinkage calculations, and time being considered for

analysis of creep or shrinkage effects, (days),
 t_d = average deck thickness, (in.),
 t_h = average haunch thickness, (in.),
 t_{o1} = 1st overlay thickness, (in.),
 t_{o2} = 2nd overlay thickness, (in.),
 u = time index array,
 V_{d1} = volume of the first deck, (in.³),
 V/S = volume-to-surface ratio (in.),
 w = unit weight of concrete, (kcf),
 w_G = load due to girder self-weight, kips/in.,
 w_{d1} = load due to 1st deck, (kips/in.),
 w_{d2} = load due to 2nd deck, (kips/in.),
 w_{b1} = load due to 1st barrier load, (kips/in.),
 w_{b2} = load due to 2nd barrier load, (kips/in.),
 w_{o1} = load due to 1st overlay load, (kips/in.),
 w_{o2} = load due to 2nd overlay load, (kips/in.),
 x_n = location of nth section measured from closest girder end, (in.),
 X_n = curvature at nth section, (1/in.),
 x_m = location of midspan measured from girder end, (in.),
 X_m = curvature at midspan, (1/in.),
 \bar{x}_n = centroid of the area under curvature diagram between nth section and closest girder end, (in.),
 y_{dG} = a parameter indicating the distance between centroids of girder and deck, (in.),
 $y_{hpi,end}$ = distance from centroid of ith harped strand group to the bottom of the girder at end, (in.),
 $y_{hpi,mid}$ = distance from centroid of ith harped strand group to the bottom of the girder at midspan, (in.),
 $y_{Gbottom}$ = centroid of prestressed concrete beam with respect to bottom of girder, (in.),
 y_{dbi} = distance from centroid of ith debonded strand group to the bottom of the girder, (in.),
 y_{sti} = distance from centroid of ith straight strand group to the bottom of the girder, (in.),

$y_{psbottom}$ = distance of centroid of prestressing strands to the bottom of girder, (in.),
 y_t = distance of centroid of transformed non-composite structure to the bottom of girder, (in.),
 y_{dc} = centroid of the deck & haunch couple with respect to the bottom of the haunch, (in.),
 $y_{dbottom}$ = distance between centroid of deck & haunch couple with respect to bottom of the girder, (in.),
 y_c = distance of centroid of transformed composite structure to the bottom of girder, (in.),
 y_{c1} = distance of centroid of transformed composite structure to the bottom of girder with 1st deck, (in.),
 y_{c2} = distance of centroid of transformed composite structure to the bottom of girder with 2nd deck, (in.),
 z = time index array,
 z_d = row number of the axial force history array,
 loc = array for location, (in.),
 $stopper$ = helper word for time-dependent calculations,
 $continue$ = loop term that restarts the current iteration,
 α = parameters for ACI209R-92 development model depending on curing type,
 β = parameters for ACI209R-92 development model depending on cement type,
 $\theta_{B/C}$ = relative slope at point B relative to point C, (rad.),
 γ_G = unit-weight of girder including reinforcement weight, (kcf),
 γ_{o1} = unit-weight of 1st overlay, (pcf),
 γ_{o2} = unit-weight of 2nd overlay, (pcf),
 ε_{shG} = remaining girder shrinkage at a given time, (in./in.),
 ε_{shD} = remaining deck shrinkage at a given time, (in./in.),
 β_{ax} = magnification factor tension creep,

β_{flex} = magnification factor flexural creep,
 ψ_{crG} = remaining girder creep at a given time,
 $\psi_{crG,flex}$ = remaining girder flexural creep at a given time,
 ψ_{crD} = remaining deck creep at a given time,
 $\psi_{crD,flex}$ = remaining deck flexural creep at a given time,
 $\psi_{crG,ax}$ = remaining girder tension creep at a given time,
 $\psi_{crD,ax}$ = remaining deck tension creep at a given time,
 $\psi(t, t_i)$ = the creep coefficient at concrete at t due to load applied at t_i ,
 \emptyset_0 = initial curvature array as a function of time and location, (1/in.),
 \emptyset_p = initial curvature array as a function of time and location, (1/in.),
 $\Delta\emptyset_t$ = change in curvature due to time-dependent effects as a function of time and location, (1/in.),
 \emptyset_{ad1p} = net curvature just after 1st deck is placed, (1/in.),
 \emptyset_{ad2p} = net curvature just after 2nd deck is placed, (1/in.),
 \emptyset_{naas1} = net curvature just after application of barrier and overlay loads on 1st superstructure, (1/in.),
 \emptyset_{naas2} = net curvature just after application of barrier and overlay loads on 2nd superstructure, (1/in.),
 \emptyset_{ad1r} = net curvature just after deck removal, (1/in.),
 η = modular ratio,
 η_{ps} = modular ratio for prestressing strands,
 η_D = modular ratio for the deck
 η_{D1} = modular ratio for the 1st deck,
 η_{D2} = modular ratio for the 2nd deck,
 Δ_{ni} = camber at release (in.),
 Δ_{np} = pre-erection camber (in.),
 Δ_{nad1p} = camber just after placement of 1st deck, (in.),
 Δ_{nbas1} = camber just before application of barrier and overlay loads on 1st superstructure, (in.),

Δ_{nbas2} = camber just before application of barrier and overlay loads on 2nd superstructure, (in.),
 Δ_{naas1} = camber just after application of barrier and overlay loads on 1st superstructure, (in.),
 Δ_{naas2} = camber just after application of barrier and overlay loads on 2nd superstructure, (in.),
 Δ_{nbd1r} = camber just before deck removal process, (in.),
 Δ_{nad1r} = camber just after deck removal process, (in.),
 Δ_{nbdnp} = camber just before new deck placement, (in.),
 Δ_{nad2p} = camber just after placement of 2nd deck, (in.),
 Δ_{ns2} = camber at final considered time, (in.),
 Δ_n = net deflection at n^{th} section according to end of the girder, (in.),
 $\Delta_{A/C}$ = relative displacement at point C according to point A, (in.),
 Δx = length of a section, (in.),
 δN_{GpR} = axial effect of relaxation loss on girder as a function of time and location, (kips),
 δN_{DpR} = axial effect of relaxation loss on deck as a function of time and location, (kips),
 δM_{GpR} = moment effect of relaxation loss on girder as a function of time and location, (kips – in.),
 δM_{DpR} = moment effect of relaxation loss on deck as a function of time and location, (kips – in.),
 Δf_{pR} = relaxation loss array as a function of time and location, (kips),
 Δf_{pR_0} = initial relaxation loss array as a function of time and location, (kips),
 Δf_{pES} = elastic shortening loss array as a function of time and location, (ksi),
 ΔM_{Gob1r} = change in moment on the girder due to removal of barrier and overlay loads, (kips – in.),

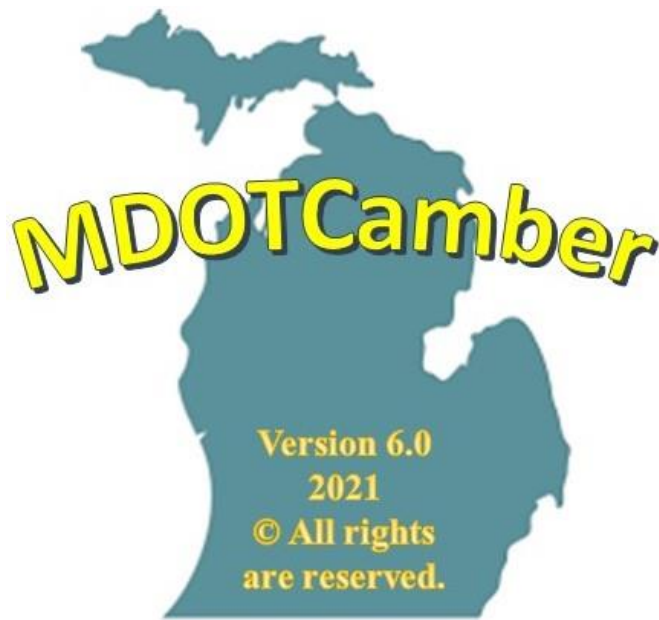
ΔM_{d1ob1r} = change in moment on the 1st deck due to removal of barrier and overlay loads, (*kips – in.*),
 ΔM_{Gd1swr} = change in moment on girder due to deck self-weight removal, (*kips – in.*),
 ΔM_{tsd1r} = change in moment on non-composite structure due to removal of locked forces inside the 1st deck, (*kips – in.*),
 ΔM_{Gtsd1r} = change in moment on girder due to removal of locked forces inside the 1st deck, (*kips – in.*),
 ΔM_{Gsc} = change in moment on the girder due to change in support condition, (*kips – in.*),
 ΔM_{Gd1sw} = change in moment on the girder due to 1st deck load, (*kips – in.*),
 ΔM_{Gd2sw} = change in moment on the girder due to 2nd deck load, (*kips – in.*),
 ΔM_{Gb1sw} = change in moment on the girder due to 1st barrier load, (*kips – in.*),
 ΔM_{d1b1sw} = change in moment on the 1st deck due to 1st barrier load, (*kips – in.*),
 ΔM_{Gb2sw} = change in moment on the girder due to 2nd barrier load, (*kips – in.*),
 ΔM_{d2b2sw} = change in moment on the 2nd deck due to 2nd barrier load, (*kips – in.*),
 ΔM_{Go1sw} = change in moment on the girder due to 1st overlay load, (*kips – in.*),
 ΔM_{d1o1sw} = change in moment on the 1st deck due to 1st overlay load, (*kips – in.*),
 ΔM_{Go2sw} = change in moment on the girder due to 2nd overlay load, (*kips – in.*),
 ΔM_{d2o2sw} = change in moment on the 2nd deck due to 2nd overlay load, (*kips – in.*),
 $\Delta M_{Gt_1t_2}$ = change in moment on girder due to time-dependent effects between t_1 and t_2 , (*kips – in.*),
 $\Delta M_{Gt_2t_3}$ = change in moment on girder due to time-dependent effects between t_2 and t_3 , (*kips – in.*),
 $\Delta M_{Dt_2t_3}$ = change in moment on deck due to time-dependent effects between t_2 and t_3 , (*kips – in.*),

$\Delta M_{Gt_4t_5}$ = change in moment on girder due to time-dependent effects between t_4 and t_5 , (*kips – in.*),
 $\Delta M_{Dt_4t_5}$ = change in moment on deck due to time-dependent effects between t_4 and t_5 , (*kips – in.*),
 $\Delta M_{Gt_5t_6}$ = change in moment on girder due to time-dependent effects between t_5 and t_6 , (*kips – in.*),
 $\Delta M_{Gt_6t_7}$ = change in moment on girder due to time-dependent effects between t_6 and t_7 , (*kips – in.*),
 $\Delta M_{Dt_6t_7}$ = change in moment on deck due to time-dependent effects between t_6 and t_7 , (*kips – in.*),
 $\Delta M_{Gt_8t_9}$ = change in moment on girder due to time-dependent effects between t_8 and t_9 , (*kips – in.*),
 $\Delta M_{Dt_8t_9}$ = change in moment on deck due to time-dependent effects between t_8 and t_9 , (*kips – in.*),
 ΔN_{Gob1r} = change in axial force on the girder due to removal of barrier and overlay loads, (*kips*),
 ΔN_{d1ob1r} = change in axial force on the 1st deck due to removal of barrier and overlay loads, (*kips*),
 ΔN_{Gd1swr} = change in axial force on girder due to deck self-weight removal, (*kips*),
 ΔN_{tsd1r} = change in axial force on non-composite structure due to removal of locked forces inside the 1st deck, (*kips*),
 ΔN_{Gtsd1r} = change in axial force on girder due to removal of locked forces inside the 1st deck, (*kips*),
 ΔN_{Gsc} = change in axial force on the girder due to change in support condition, (*kips*),
 ΔN_{Gd1sw} = change in axial force on the girder due to 1st deck load, (*kips*),
 ΔN_{Gd2sw} = change in axial force on the girder due to 2nd deck load, (*kips*),
 ΔN_{Gb1sw} = change in axial force on the girder due to 1st barrier load, (*kips*),
 ΔN_{d1b1sw} = change in axial force on the 1st deck due to 1st barrier load, (*kips*),

ΔN_{Gb2sw} = change in axial force on the girder due to 2nd barrier load, (*kips*),
 ΔN_{d2b2sw} = change in axial force on the 2nd deck due to 2nd barrier load, (*kips*),
 ΔN_{Go1sw} = change in axial force on the girder due to 1st overlay load, (*kips*),
 ΔN_{d1o1sw} = change in axial force on the 1st deck due to 1st overlay load, (*kips*),
 ΔN_{Go2sw} = change in axial force on the girder due to 2nd overlay load, (*kips*),
 ΔN_{d2o2sw} = change in axial force on the 2nd deck due to 2nd overlay load, (*kips*),
 $\Delta N_{Gt_1t_2}$ = change in axial force on girder due to time-dependent effects between t_1 and t_2 , (*kips*),
 $\Delta N_{Gt_2t_3}$ = change in axial force on girder due to time-dependent effects between t_2 and t_3 , (*kips*),
 $\Delta N_{Dt_2t_3}$ = change in axial force on deck due to time-dependent effects between t_2 and t_3 , (*kips*),
 $\Delta N_{Gt_4t_5}$ = change in axial force on girder due to time-dependent effects between t_4 and t_5 , (*kips*),
 $\Delta N_{Dt_4t_5}$ = change in axial force on deck due to time-dependent effects between t_4 and t_5 , (*kips*),
 $\Delta N_{Gt_5t_6}$ = change in axial force on girder due to time-dependent effects between t_5 and t_6 , (*kips*),
 $\Delta N_{Gt_6t_7}$ = change in axial force on girder due to time-dependent effects between t_6 and t_7 , (*kips*),
 $\Delta N_{Dt_6t_7}$ = change in axial force on deck due to time-dependent effects between t_6 and t_7 , (*kips*),
 $\Delta N_{Gt_8t_9}$ = change in axial force on girder due to time-dependent effects between t_8 and t_9 , (*kips*),
 $\Delta N_{Dt_8t_9}$ = change in axial force on deck due to time-dependent effects between t_8 and t_9 , (*kips*),
 $\Delta \emptyset_{sc}$ = change in curvature due to change in support conditions, (*1/in.*),

$\Delta \emptyset_{d1sw}$ = change in curvature due to 1st deck self-weight, (*1/in.*),
 $\Delta \emptyset_{d2sw}$ = change in curvature due to 2nd deck self-weight, (*1/in.*),
 $\Delta \emptyset_{b1sw}$ = change in curvature due to 1st barrier self-weight, (*1/in.*),
 $\Delta \emptyset_{b2sw}$ = change in curvature due to 2nd barrier self-weight, (*1/in.*),
 $\Delta \emptyset_{o1sw}$ = change in curvature due to 1st barrier self-weight, (*1/in.*),
 $\Delta \emptyset_{o2sw}$ = change in curvature due to 2nd barrier self-weight, (*1/in.*),
 $\Delta \emptyset_{ob1r}$ = change in curvature due to removal of barrier and overlay loads, (*1/in.*),
 $\Delta \emptyset_{d1r}$ = change in curvature due to removal of locked forces inside the deck, (*1/in.*),
 $\Delta \emptyset_{d1swr}$ = change in curvature due to deck self-weight removal, (*1/in.*)

APPENDIX E: STEEL BEAM EXAMPLE



Research Team

Wayne State University:

Fatmir Menkulasi

Christopher Eamon

Furkan Cakmak

Anthony Victor

Alfred Benesch & Company:

Ihab Darwish



March 2021

Table of Contents

E.1 Definition of the Problem.....	322
E.2 Definition of Parameters.....	325
E.3 Pre-erection Camber	338
E.4 Camber just after Placement of 1 st Deck.....	340
E.5 Camber just before Application of Barrier and Overlay Loads on 1 st Superstructure	341
E.6 Camber just after Application of Barrier and Overlay Loads on 1 st Superstructure.....	344
E.7 Camber just before Deck Removal Process	346
E.8 Camber just after Deck Removal Process.....	348
E.9 Camber just before 2 nd Deck Placement.....	351
E.10 Camber just after 2 nd Deck Placement.....	351
E.11 Camber just before Application of Barrier and Overlay Loads on 2 nd Superstructure ..	352
E.12 Camber just after Application of Barrier and Overlay Loads on 2 nd Superstructure	353
E.13 Camber at Final Time.....	355
E.14 Nomenclature	358

List of Figures

Fig. E.1. Notation used for steel girder.....	322
Fig. E.2. Sign convention	325
Fig. E.3. Elastic curve and curvature diagram for typical prestressed concrete beam at release.....	334

List of Tables

Table E.1. Girder and project specific properties.....	323
Table E.2. Parameters related to first and second decks.....	324
Table E.3. Time arrangement for major activities.....	324
Table E.4. Section array.....	326
Table E.5. Creep function for 1 st deck.....	328
Table E.6. Shrinkage array for 1 st deck.....	328
Table E.7. Creep function for 2 nd deck.....	329
Table E.8. Shrinkage array for 2 nd deck.....	329
Table E.9. Elastic modulus development for 1 st and 2 nd deck with time.....	330
Table E.10. Modular ratio and transformed area for the 1 st and 2 nd deck.....	331
Table E.11. Net transformed area for the 1 st and 2 nd composite structures.....	332
Table E.12. Centroid of transformed composite structure with respect to bottom of girder.....	332
Table E.13. Transformed moment of inertia for the 1 st and 2 nd deck.....	333
Table E.14. Moment of inertia of transformed composite structure with 1 st and 2 nd deck.....	333
Table E.15. Fabricated camber and curvature along the span.....	338
Table E.16. Moment and change in curvature due to girder self-weight along the span.....	339
Table E.17. Net curvature after girder erection.....	339
Table E.18. Application of Simpson's rule and pre-erection camber.....	340
Table E.19. Moment and change in curvature due to 1 st deck self-weight.....	341
Table E.20. Net curvature just after 1 st deck is placed.....	341
Table E.21. Camber just after placement of 1 st deck.....	341
Table E.22. Camber just before application of barrier and overlay loads on 1 st superstructure.....	344
Table E.23. Moment applied on composite structure due to barrier and overlay loads.....	345
Table E.24. Change in curvature due to barrier and overlay load.....	345
Table E.25. Net curvature just after application of barrier and overlay loads.....	345
Table E.26. Camber just after application of barrier and overlay loads.....	345
Table E.27. Change in forces on deck due to barrier load.....	346
Table E.28. Change in forces on deck due to overlay load.....	347
Table E.29. Net force history array just after application of barrier and overlay loads.....	347
Table E.30. Change in forces on deck due to time-dependent effects between t_3 and t_4	348

Table E.31. Change in curvature between time t_3 and t_4	348
Table E.32. Net curvature just before deck removal process	348
Table E.33. Camber just before deck removal process.....	348
Table E.34. Change in forces on deck due to removal of barrier and overlay loads	349
Table E.35. Change in curvature due to removal of barrier and overlay loads.....	349
Table E.36. Net forces on the deck just before it is removed.....	349
Table E.37. Change in moment due to removal of locked forces inside the deck	350
Table E.38. Change in curvature due to removal of locked forces inside the deck.....	350
Table E.39. Change in curvature due to deck removal.....	350
Table E.40. Net curvature just after deck removal.....	350
Table E.41. Camber just after deck removal.....	351
Table E.42. Net curvature just before new deck placement.....	351
Table E.43. Camber just before new deck placement.....	351
Table E.44. Moment and change in curvature due to 2 nd deck self-weight.....	352
Table E.45. Net curvature just after 2 nd deck is placed.....	352
Table E.46. Camber just after placement of 2 nd deck.....	352
Table E.47. Net curvature just before application of barrier and overlay loads.....	353
Table E.48. Camber just before application of barrier and overlay loads on 2 nd superstructure.....	353
Table E.49. Moment applied on composite structure due to barrier and overlay loads.....	354
Table E.50. Change in curvature due to barrier and overlay load	354
Table E.51. Net curvature just after application of barrier and overlay loads on 2 nd super- structure.....	354
Table E.52. Camber just after application of barrier and overlay loads on 2 nd super-structure.....	355
Table E.53. Change in forces on deck due to barrier load	355
Table E.54. Change in forces on deck due to overlay load	356
Table E.55. Net force history array just after application of barrier and overlay loads.....	356
Table E.56. Change in forces on deck due to time-dependent effects between t_7 and t_8	356
Table E.57. Change in curvature between time t_7 and t_8	357
Table E.58. Net curvature at final considered time	357
Table E.59. Camber at final considered time.....	357

E.1 Definition of the Problem

Using the proposed prediction methodology, Approach No. 6, explained in this thesis, camber and displacement along the span is going to be estimated at:

1. time at which the deck is placed (t_1);
2. time at placement of barriers and the opening of bridge to traffic (t_2);
3. time at placement of overlay (t_3);
4. time at deck removal for projects that features a deck replacement (t_4);
5. time at new deck placement (t_5);
6. time at reopening of bridge to traffic (t_6);
7. time at placement of overlay (t_7);
8. time at the end of service life (t_8);

for the following steel beam used in M20 project:

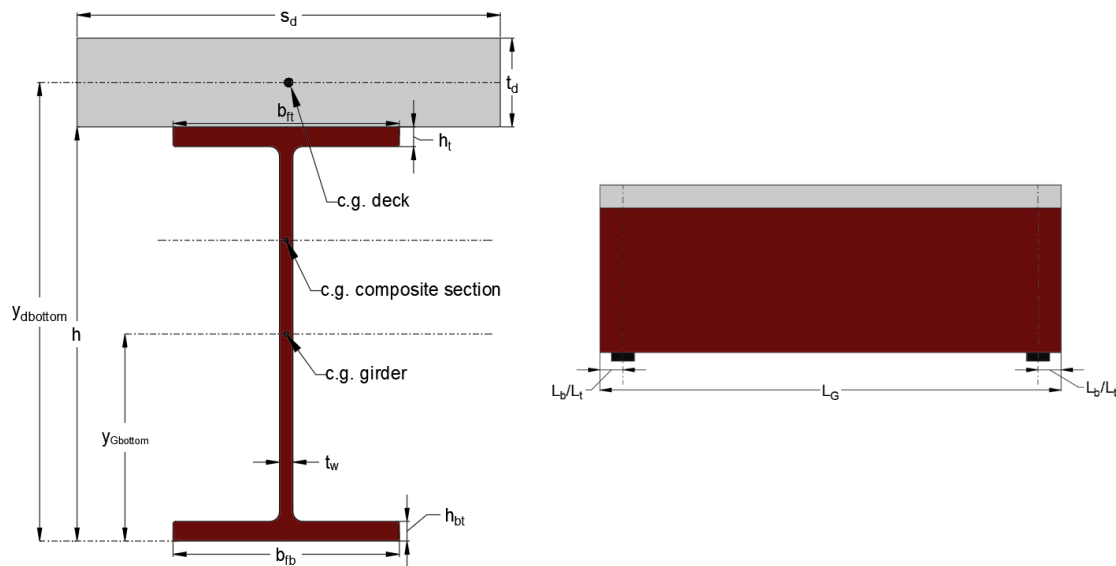


Fig. E.1. Notation used for steel girder

Parameters related to girder and project specific properties are provided in Table E.1.

Table E.1. Girder and project specific properties

Parameter	Value
Gross Area (A_G) ($in.^2$)	90
Unit-weight of cross-section (γ_G) (kcf)	0.490
Girder length (L_G) ($ft.$)	173
Centroid of girder measured from bottom ($y_{Gbottom}$) ($in.$)	35.5
Gross moment of inertia (I_G) ($in.^4$)	75840
Modulus of elasticity (E_G) (ksi)	28500
Girder overhang length at bridge site (L_b) ($in.$)	24
Girder height (h) ($in.$)	72
Top flange width (b_{ft}) ($in.$)	23
Top flange thickness (h_t) ($in.$)	1
Web thickness (t_w) ($in.$)	0.625
Bottom flange width (b_{fb}) ($in.$)	23
Bottom flange thickness (h_{bt}) ($in.$)	1
Girder tributary width* (s_d) ($ft.$)	9.17
Thermal expansion coefficient (α) ($1/^\circ F$)	6.7E-06
Fabricated camber** (Δ_{G0}) ($in.$)	-14.64
*For the fascia beams, spacing should be adjusted accordingly.	
**Fabricated camber does not include the deflection caused by girder self-weight.	

Moreover, parameters related of 1st and 2nd super-structures are provided in Table E.2.

Table E.2. Parameters related to first and second decks

Parameter for the First Deck	Value
Specified concrete compressive strength (f'_{cd1}) (ksi)	4
Unit-weight of deck and haunch* (γ_{d1}) (pcf)	0.150
Average deck thickness** (t_{d1}) (in.)	9
Average haunch thickness (t_{h1}) (in.)	0
Overlay thickness (t_{o1}) (in.)	2
Unit-weight of overlay (γ_{o1}) (pcf)	0.140
Barrier load (w_{b1}) (klf)	0.475
Aggregate factor [†] (K_1)	1
Unit-weight of plain concrete [†] (w_{c1}) (pcf)	0.145
Parameter for the Second Deck	Value
Specified concrete compressive strength (f'_{cd2}) (ksi)	4
Unit-weight of deck and haunch* (γ_{d2}) (pcf)	0.150
Average deck thickness** (t_{d2}) (in.)	9
Average haunch thickness (t_{h2}) (in.)	0
Overlay thickness (t_{o2}) (in.)	2
Unit-weight of overlay (γ_{o2}) (pcf)	0.140
Barrier load (w_{b2}) (klf)	0.475
Aggregate factor [†] (K_1)	1
Unit-weight of plain concrete [†] (w_{c2}) (pcf)	0.145
[*] Reinforcement weight is considered as 5 pcf. ^{**} For fascia beam analysis, deck thickness should be adjusted accordingly. [†] These are used for AAHSTO LRFD (2020) 9 th Edition elastic modulus calculations.	

In this example, the following time arrangement is going to be utilized. It should be noted that the barrier and overlay load is applied to super-structure simultaneously so that there is no additional time-dependent activity taking place between these two events.

Table E.3. Time arrangement for major activities

Event	time index (t)	t(t) (days)
Time at which the deck is placed	<u>1</u>	2
Time at placement of barriers and the opening of bridge to traffic	<u>2</u>	9
Time at placement of overlay	<u>3</u>	9
Time at deck removal for projects that features a deck replacement	<u>4</u>	18250
Time at new deck placement	<u>5</u>	18260
Time at reopening of bridge to traffic	<u>6</u>	18267
Time at placement of overlay	<u>7</u>	18267
Time at the end of service life	<u>8</u>	27375

For the analysis, it is assumed that both decks (first and second) subject to 7 days of moist curing, and Type I cement is used in concrete composition. In addition, it is assumed that deck concrete reaches 80% of its 28-day strength at the end of curing period. ACI 209R-92 model is used with corresponding parameters for the development of modulus of elasticity with time. In addition, AASHTO LRFD (2020) equation is utilized for the estimation of modulus of elasticity. For conducting time-dependent analysis, AASHTO LRFD (2020) Body creep and shrinkage models are employed by assuming the flexural and tensile creep are equal to compression creep. In addition to this, three sections are considered along the half-span to minimize the computation effort. To estimate the deflection from curvature diagram, Simpson's rule is employed for numerical integration. It is assumed that the ambient relative humidity is 70% for Michigan based on the map provided in AASHTO LRFD (2020) 9th Edition Figure 5.4.2.3.3-1. While generating the time matrix for the analysis, only one time-step is going to be taken between the major activities as stated above. Finally, the sign convention adopted in this example problem is given in the Fig. E.2.

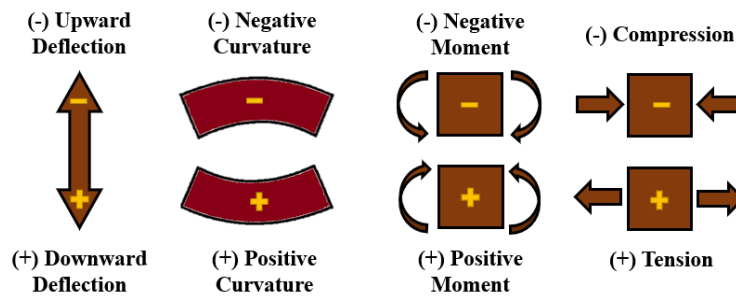


Fig. E.2. Sign convention

E.2 Definition of Parameters

- *Generate the time and section matrix*

Since only one time step is going to be considered in this example, the time matrix generated for this specific example would be same as in Table E.3. In addition to this, since three sections are going to be considered along the half-span, the section matrix can be assigned as follows (Table E.4):

Table E.4. Section array

<i>section index (x)</i>	<i>loc(x) (in.)</i>
<u>1</u>	0
<u>2</u>	519
<u>3</u>	1038

It should be noted that when creating time and section dependent arrays, index number is going to be used for simplicity throughout the analysis. For example, say a parameter $A(t, x)$ is both time and section-dependent. $A(6, 3)$ refers to the value of A at time $t(t) = t(6) = 18267$ days and at location $loc(x) = loc(3) = 1038$ in. from girder end.

- *Generate creep and shrinkage arrays*

- Creep function based on AASHTO LRFD (2020) 9th edition

$$\psi(t, t_i) = 1.9 \cdot k_s \cdot k_{hc} \cdot k_f \cdot k_{td} \cdot t_i^{-0.118} \quad \text{E-1}$$

$$k_s = 1.45 - 0.13 \cdot \left(\frac{V}{S}\right) \geq 1.0 \quad \text{E-2}$$

$$k_{hc} = 1.56 - 0.008 \cdot H_r \quad \text{E-3}$$

$$k_f = \frac{5}{1 + f'_{cdi}} \quad \text{E-4}$$

$$k_{td}(t) = \frac{t}{12 \cdot \left(\frac{100 - 4 \cdot f'_{cdi}}{f'_{cdi} + 20}\right) + t} \quad \text{E-5}$$

- Shrinkage function based on AASHTO LRFD (2020) 9th edition

$$\varepsilon_{sh}(t) = k_s \cdot k_{hs} \cdot k_f \cdot k_{td} \cdot 0.00048 \quad \text{E-6}$$

$$k_{hs} = 2.00 - 0.014 \cdot H_r \quad \text{E-7}$$

Here, the volume-to-surface ratio can also be expressed as surface-to-perimeter ratio. Moreover, according to AASHTO LRFD (2020) Bridge Design Specification section 5.4.2.3.3, shrinkage as determined in Eqn. E-6 should be increased by 20 % if the concrete is exposed to drying before 5 days of curing have elapsed.

- *Creep and shrinkage calculation for 1st deck*

Since initial concrete compressive strength for the deck is generally unknown, it is assumed:

$$f'_{cdi} = 0.80 \cdot f'_{cd} \quad \text{E-8}$$

$$f'_{cdi} = 0.80 \cdot 4 = 3.2 \text{ ksi}$$

It should be noted that since the deck is 7-days moist-cured, there will be no shrinkage that takes places within the 7-days period after it is cast.

$$A_{d1} = s_d \cdot t_{d1} + t_{h1} \cdot b_f \quad \text{E-9}$$

$$S_{d1} = 2 \cdot s_d - b_f + t_{h1} \quad \text{E-10}$$

$$\frac{V_{d1}}{A_{d1}} = \frac{A_{d1}}{S_{d1}} \quad \text{E-11}$$

$$A_{d1} = (9.17 \cdot 12) \cdot 9 = 990.4 \text{ in.}^2$$

$$S_{d1} = 2 \cdot (9.17 \cdot 12) - 23 + 0 = 197.1 \text{ in.}$$

$$k_s = 1.45 - 0.13 \cdot \left(\frac{990.4}{197.1} \right) = 0.797 < 1.0 \rightarrow k_s = 1.0$$

$$k_{hc} = 1.56 - 0.008 \cdot (70) = 1.00$$

$$k_{hs} = 2.00 - 0.014 \cdot (70) = 1.02$$

$$k_f = \frac{5}{1 + 3.2} = 1.190$$

$$k_{tdc}(t, t_i) = \frac{t - t_i}{12 \cdot \left(\frac{100 - 4 \cdot (3.2)}{3.2 + 20} \right) + (t - t_i)} = \frac{t - t_i}{45.1 + (t - t_i)}$$

$$k_{tds}(t, t_i) = \frac{t - 2 - 7}{12 \cdot \left(\frac{100 - 4 \cdot (3.2)}{3.2 + 20} \right) + (t - 2 - 7)} = \frac{t - 9}{36.1 + t}$$

Using Eqns. E-1 and E-6, the creep and shrinkage array for the 1st deck can be obtained as provided in Table E.5 and Table E.6. To exemplify, $\psi_{D1}(t_8, t_3) = \psi_{D1}(27375, 9)$ and $\varepsilon_{shD1}(t_8) = \varepsilon_{shD1}(27375)$ can be calculated as shown below.

$$\psi_{D1}(27375, 9) = 1.9 \cdot 1.0 \cdot 1.0 \cdot 1.19 \cdot \frac{27375 - 9}{45.1 + (27375 - 9)} \cdot (9 - 2)^{-0.118} = 1.79$$

$$\varepsilon_{shD1}(27375) = 1.0 \cdot 1.02 \cdot 1.19 \cdot \frac{27375 - 9}{36.1 + 27375} \cdot 0.00048 = 581.67 \mu\varepsilon$$

Table E.5. Creep function for 1st deck

$\psi_{D1}(t, t_i)$		t (days)					
		<u>2</u>	<u>9</u>	<u>18250</u>	<u>18260</u>	<u>18627</u>	<u>27375</u>
t_i (days)	<u>2</u>	0.00	0.00	0.00	0.00	0.00	0.00
	<u>9</u>	-	0.00	1.79	1.79	1.79	1.79
	<u>18250</u>	-	-	0.00	0.13	0.19	0.71
	<u>18260</u>	-	-	-	0.00	0.01	0.71
	<u>18267</u>	-	-	-	-	0.00	0.71
	<u>27375</u>	-	-	-	-	-	0.00
t_i = loading time, t = desired time							

Table E.6. Shrinkage array for 1st deck

Event	$time\ index\ (t)$	$\varepsilon_{shD1}(t)$ ($\mu\varepsilon$)
Time at which the deck is placed	<u>1</u>	0
Time at placement of barriers and the opening of bridge to traffic	<u>2</u>	0
Time at placement of overlay	<u>3</u>	0
Time at deck removal for projects that features a deck replacement	<u>4</u>	581
Time at new deck placement	<u>5</u>	581
Time at reopening of bridge to traffic	<u>6</u>	581
Time at placement of overlay	<u>7</u>	581
Time at the end of service life	<u>8</u>	581

- *Creep and shrinkage calculation for 2nd deck*

Similar to the 1st deck, the creep and shrinkage arrays for the 2nd deck can also be determined. For simplicity, it is assumed that the 2nd deck has exactly the same features with 1st deck. The only formulation that is different for the 2nd deck is as follows:

$$k_{tds}(t) = \frac{t - 18260 - 7}{12 \cdot \left(\frac{100 - 4 \cdot (3.2)}{3.2 + 20} \right) + (t - 18260 - 7)} = \frac{t - 18267}{t - 18221.9}$$

Table E.7. Creep function for 2nd deck

$\psi_{D2}(t, t_i)$		t (days)		
		<u>18260</u>	<u>18627</u>	<u>27375</u>
t_i (days)	<u>18260</u>	0.00	0.00	0.00
	<u>18267</u>	-	0.00	1.79
	<u>27375</u>	-	-	0.00
t_i = loading time, t = desired time				

Table E.8. Shrinkage array for 2nd deck

Event	<i>time index</i> (t)	$\epsilon_{shD2}(t)$ ($\mu\epsilon$)
Time at which the deck is placed	<u>1</u>	0
Time at placement of barriers and the opening of bridge to traffic	<u>2</u>	0
Time at placement of overlay	<u>3</u>	0
Time at deck removal for projects that features a deck replacement	<u>4</u>	0
Time at new deck placement	<u>5</u>	0
Time at reopening of bridge to traffic	<u>6</u>	0
Time at placement of overlay	<u>7</u>	0
Time at the end of service life	<u>8</u>	580

- *Generate time and section dependent arrays for material and section properties*
- Modulus of elasticity based on AASHTO LRFD (2020) 9th edition with ACI 209R-92 development function

$$E_c(t) = \left(\frac{t}{\alpha + \beta t} \right)^{0.5} E_{c28} \quad \text{E-12}$$

$$E_{ci} = 120,000 K_1 w^{2.0} (f'_{ci})^{1/3} \quad \text{E-13}$$

$$E_{c28} = 120,000 K_1 w^{2.0} (f'_c)^{1/3} \quad \text{E-14}$$

- For 1st and 2nd deck

ACI 209R-92 development model with coefficients corresponding to Type I – Moist-cured concrete is going to be utilized.

$$\alpha = 4 \text{ \& } \beta = 0.85$$

$$E'_{c28} = 120,000 \cdot (1.0) \cdot (0.145)^2 (4)^{1/3} = 4005 \text{ ksi}$$

$$E_{cD1}(t) = \left(\frac{t - 2}{4 + (0.85) \cdot (t - 2)} \right)^{0.5} \cdot 4005$$

$$E_{cD2}(t) = \left(\frac{t - 18260}{4 + (0.85) \cdot (t - 18260)} \right)^{0.5} \cdot 4005$$

Table E.9. Elastic modulus development for 1st and 2nd deck with time

Event	<i>time index (t)</i>	<i>E_{cD1}(t) (ksi)</i>	<i>E_{cD2}(t) (ksi)</i>
Time at which the deck is placed	<u>1</u>	-	-
Time at placement of barriers and the opening of bridge to traffic	<u>2</u>	3359	-
Time at placement of overlay	<u>3</u>	3359	-
Time at deck removal for projects that features a deck replacement	<u>4</u>	4344	-
Time at new deck placement	<u>5</u>	4344	-
Time at reopening of bridge to traffic	<u>6</u>	4344	3359
Time at placement of overlay	<u>7</u>	4344	3359
Time at the end of service life	<u>8</u>	4344	4344

- Modular ratio and transformed area

Since transformed section properties are utilized in Approach No. 6, the deck is transformed to girder by using the equation below. Since deck modulus of elasticity varies with time, the modular ratio will also vary with respect to time.

$$\eta(t) = \frac{E_{tr}(t)}{E_G} \quad \text{E-15}$$

$$A_{dtr} = A \cdot \eta(t) \quad \text{E-16}$$

- *For 1st and 2nd deck*

$$\eta_D(t) = \frac{E_{cD}(t)}{E_G}$$

$$A_{dtr}(t) = A_d \cdot \eta_d(t)$$

Table E.10. Modular ratio and transformed area for the 1st and 2nd deck

<i>time index (t)</i>	Modular ratio		Transformed deck area (in.²)	
	$\eta_{d1}(t)$	$\eta_{d2}(t)$	$A_{d1tr}(t)$	$A_{d2tr}(t)$
<u>1</u>	-	-	-	-
<u>2</u>	0.12	-	117	-
<u>3</u>	0.12	-	117	-
<u>4</u>	0.15	-	151	-
<u>5</u>	0.15	-	151	-
<u>6</u>	0.15	0.12	151	117
<u>7</u>	0.15	0.12	151	117
<u>8</u>	0.15	0.15	151	151

- *Transformed area for composite structures*

$$A_{ctr}(t) = A_G + A_{dtr}(t) \quad \text{E-17}$$

Table E.11. Net transformed area for the 1st and 2nd composite structures

$A_{ctr}(t, x) (in.^2)$	$A_{c1tr}(t)$	$A_{c2tr}(t)$
time index (t)	<u>1</u>	90
	<u>2</u>	207
	<u>3</u>	207
	<u>4</u>	241
	<u>5</u>	241
	<u>6</u>	241
	<u>7</u>	241
	<u>8</u>	241

- *Transformed moment of inertia for composite structure*

$$y_{dc} = \frac{s_d \cdot t_d \cdot (0.5 \cdot t_d + t_h) + 0.5 \cdot b_f \cdot t_h^2}{A_d} \quad E-18$$

$$y_{dbottom} = h + y_{dc} \quad E-19$$

$$y_c(t) = \frac{A_G \cdot y_{Gbottom} + A_{dtr}(t) \cdot y_{dbottom}}{A_{ctr}(t)} \quad E-20$$

$$I_d = \frac{s_d \cdot t_d^3 + b_f \cdot t_h^3}{12} + s_d \cdot t_d \cdot (y_{dc} - 0.5 \cdot t_d - t_h)^2 + b_f \cdot t_h \cdot (y_{dc} - 0.5 \cdot t_h)^2 \quad E-21$$

$$I_{dtr} = I_d \cdot \eta_{d1}(t) \quad E-22$$

$$I_c(t) = I_G + A_G \cdot (y_c(t) - y_{Gbottom})^2 + I_{dtr}(t) + A_{dtr}(t) \cdot (y_c(t) - y_{dbottom})^2 \quad E-23$$

Table E.12. Centroid of transformed composite structure with respect to bottom of girder

$y_c(t) (in.)$	$y_{c1}(t)$	$y_{c2}(t)$
time index (t)	<u>1</u>	35.5
	<u>2</u>	58.7
	<u>3</u>	58.7
	<u>4</u>	61.2
	<u>5</u>	61.2
	<u>6</u>	61.2
	<u>7</u>	61.2
	<u>8</u>	61.2

Table E.13. Transformed moment of inertia for the 1st and 2nd deck

<i>time index (t)</i>	Transformed moment of inertia (<i>in.</i> ⁴)	
	<i>I_{d1tr}</i>	<i>I_{d2tr}</i>
<u>1</u>	-	-
<u>2</u>	788	-
<u>3</u>	788	-
<u>4</u>	1019	-
<u>5</u>	1019	-
<u>6</u>	1019	788
<u>7</u>	1019	788
<u>8</u>	1019	1019

Table E.14. Moment of inertia of transformed composite structure with 1st and 2nd deck

<i>I_c(t) (in.</i> ⁴)		<i>I_{c1}(t)</i>	<i>I_{c2}(t)</i>
<i>time index (t)</i>	<u>1</u>	75840	-
	<u>2</u>	162050	-
	<u>3</u>	162050	-
	<u>4</u>	171630	-
	<u>5</u>	171630	75840
	<u>6</u>	171630	162050
	<u>7</u>	171630	162050
	<u>8</u>	171640	171630

- Simpson's 1/3rd rule for numerical integration

A general idea behind the Simpson's 1/3rd rule is explained briefly below.

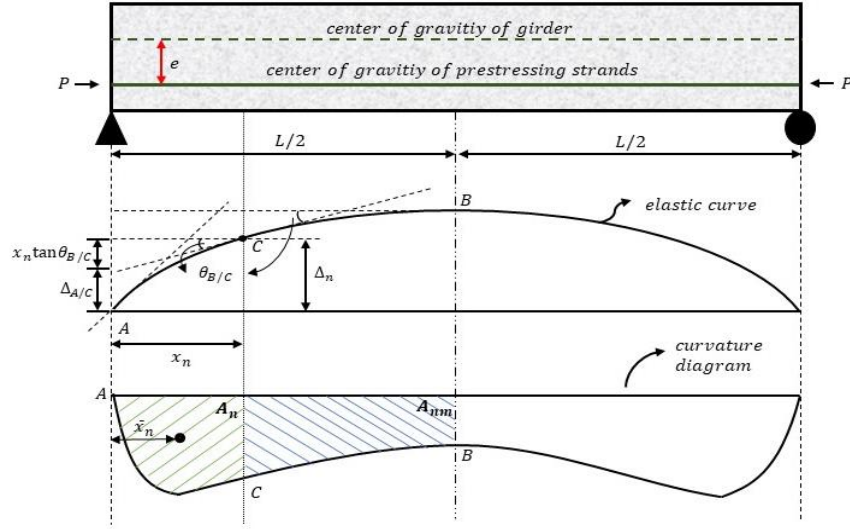


Fig. E.3. Elastic curve and curvature diagram for typical prestressed concrete beam at release

$$\Delta_n = \Delta_{A/C} + x_n \tan \theta_{B/C} \quad \text{E-24}$$

$$\theta_{B/C} = A_{nm} \quad \text{E-25}$$

$$\Delta_{A/C} = A_n \bar{x}_n \quad \text{E-26}$$

$$\bar{x}_n = \frac{Q_n}{A_n} \quad \text{E-27}$$

$$Q_n = \frac{\Delta x}{3} (\phi_1 x_1 + 4\phi_2 x_2 + 2\phi_3 x_3 + 4\phi_4 x_4 + 2\phi_5 x_5 + \cdots + 4\phi_{n-1} x_{n-1} + \phi_n x_n) \quad \text{E-28}$$

$$A_n = \frac{\Delta x}{3} (\phi_1 + 4\phi_2 + 2\phi_3 + 4\phi_4 + 2\phi_5 + \cdots + 4\phi_{n-1} + \phi_n) \quad \text{E-29}$$

$$A_{nm} = \frac{\Delta x}{3} (\phi_n + 4\phi_{n+1} + 2\phi_{n+2} + \cdots + 4\phi_{m-1} + \phi_m) \quad \text{E-30}$$

$$\Delta x = \frac{L_G/2}{\text{number of sections} - 1} \quad \text{E-31}$$

- Time-dependent deflection calculations

Note: For both instantaneous and time-dependent deflection calculations, all matrices such as location, load effects, material properties and creep and shrinkage functions will be recalled using index number. In addition, steel girder itself does not creep or shrinkage, there is no time-dependent effect on camber and deflection.

- *For composite structure*

$$q = \text{rownumber}(N_D(t, x)) \quad \text{E-32}$$

$$m = \text{rownumber}(loc(x)) \quad \text{E-33}$$

$$\phi_p = \phi_0 \quad \text{E-34}$$

$$\Delta\phi_t(1, loc(x)) = 0 \quad \text{E-35}$$

$$y_{dG} = y_{dbottom} - y_{Gbottom} \quad \text{E-36}$$

$$i = \text{index}(t_i) \quad \text{E-37}$$

$$p = \text{index}(t_{i+1}) \quad \text{E-38}$$

$$r = i \quad \text{E-39}$$

$$k = [r; (r + 1); (r + 2); \dots (p - 2); (p - 1)] \quad \text{E-40}$$

- For each value in "k" array:

$$Co_{ND}(1, loc(x)) = 0 \ \& \ Co_{MD}(1, loc(x)) = 0 \quad \text{E-41}$$

$$\varepsilon_{shD} = -(\varepsilon_{d1}(k + 1) - \varepsilon_{d1}(k)) \quad \text{E-42}$$

$$z = [1; 2; \dots (q - 1); q] \quad \text{E-43}$$

- For each value in "z" array:

$$\psi_{crD} = \psi_D(t(k+1), t(z)) - \psi_D(t(k), t(z)) \quad \text{E-44}$$

$$\psi_{crD,flex} = \psi_{crD} \cdot \beta_{flex} \quad \text{E-45}$$

$$E_D = E_{cD}(z) \quad \text{E-46}$$

$$h = [1; 2; \dots (m-1); m] \quad \text{E-47}$$

- For each value in "h" array:

$$\text{if } N_D(z, h) > 0 \quad \psi_{crD,ax} = \psi_{crD} \cdot \beta_{ax} \quad \text{E-48}$$

$$\text{if } N_D(z, h) \leq 0 \quad \psi_{crD,ax} = \psi_{crD} \quad \text{E-49}$$

$$Co_{ND}(h) = \frac{N_D(z, h) \cdot \psi_{crD,ax}}{E_D \cdot A_D} + Co_{ND}(h) \quad \text{E-50}$$

$$Co_{MD}(h) = \frac{M_D(z, h) \cdot \psi_{crD,flex}}{E_D \cdot I_D} + Co_{MD}(h) \quad \text{E-51}$$

- End of "h" array.
- End of "z" array.

$$\psi_{crD,ax} = \psi_{crD} \quad \text{E-52}$$

$$stopper = 1 \quad \text{E-53}$$

$$j = [1; 2; \dots (m-1); m] \quad \text{E-54}$$

- For each value in "j" array:

$$M_{co} = \begin{bmatrix} 1 & 1 & 0 & 0 & 0 & 0 & 0 \\ -y_{dG} & 0 & 1 & 1 & 0 & 0 & 0 \\ -\frac{1 + \psi_{crD,ax}}{E_D \cdot A_D} & 0 & 0 & 0 & 1 & 0 & 0 \\ 0 & -\frac{1}{E_G \cdot A_G} & 0 & 0 & 0 & 1 & 0 \\ 0 & 0 & -\frac{1 + \psi_{crD,flex}}{E_D \cdot I_D} & 0 & 0 & 0 & 1 \\ 0 & 0 & 0 & -\frac{1}{E_G \cdot A_G} & 0 & 0 & 1 \\ 0 & 0 & 0 & 0 & 1 & -1 & y_{dG} \end{bmatrix} \quad \text{E-55}$$

$$M_c = \begin{bmatrix} 0 \\ 0 \\ Co_{ND}(j) + \varepsilon_{shD} \\ 0 \\ Co_{MD}(j) \\ 0 \\ 0 \end{bmatrix} \quad \text{E-56}$$

$$M_s = [M_{co}^{-1}] \cdot [M_c] \quad \text{E-57}$$

$$\begin{aligned} & \text{if } M_s(1) > 0 \\ & \quad \psi_{crD,ax} = \psi_{crD} \cdot \beta_{ax} \\ & \quad \text{stopper} = 0 \\ & \quad \text{continue} \end{aligned} \quad \text{E-58}$$

$$N_D(k+1, j) = M_s(1) \quad \text{E-59}$$

$$M_D(k+1, j) = M_s(3) \quad \text{E-60}$$

$$\Delta\phi_t(k+1, j) = M_s(7) + \Delta\phi_t(k, j) \quad \text{E-61}$$

$$\text{stopper} = 1 \quad \text{E-62}$$

$$\psi_{crd,ax} = \psi_{crD} \quad \text{E-63}$$

➤ End of "j" array.

$$\phi_t(k + 1, loc(x)) = \phi_p + \Delta\phi_t(k + 1, loc(x)) \quad E-64$$

➤ End of "k" array.

E.3 Pre-erection Camber

As it is stated in the problem definition, fabricated camber does not include the deflection caused by girder self-weight. Therefore, to be able to determine pre-erection camber, the girder self-weight effect needs to be calculated. Before, to be able to perform sectional analysis through the span, initial curvatures as well as camber at locations apart from midspan need to be calculated.

$$\alpha_2 = \frac{192 \cdot \Delta_{G0}}{5 \cdot L_G^4} \quad E-65$$

$$X_{G0f}(x) = \alpha_2 \cdot (x) \cdot (L_G - x) \quad E-66$$

Using fabricated curvature along the span with Eqns. between E-24 and E-31, fabricated camber can be determined. It should be noted that although the fabricated camber along the span could be calculated exactly without using numerical integration, it is preferred to be calculated via this approach to get a consistent results. If sufficiently enough section is considered, this would not yield significant error in the calculations.

Table E.15. Fabricated camber and curvature along the span

$\Delta_{G0f}(x)$ (in.)			$X_{G0f}(x)$ (1/in.)		
$\Delta_{G0f}(1)$	$\Delta_{G0f}(2)$	$\Delta_{G0f}(3)$	$X_{G0f}(1)$	$X_{G0f}(2)$	$X_{G0f}(3)$
0.00	-7.32	-14.64	0.00	-2.45E-05	-3.26E-05

➤ Girder Self-weight Effect

$$w_G = \gamma_G \cdot A_G \quad E-67$$

$$\text{if } x \leq L_b \quad M_{Gsw}(x) = -\frac{w_G \cdot x^2}{2} \quad \text{E-68}$$

$$\text{if } x > L_b \quad M_{Gsw}(x) = \frac{w_G \cdot L_G \cdot (x - L_b)}{2} - \frac{w_G \cdot x^2}{2} \quad \text{E-69}$$

$$\Delta\phi_{Gsw}(x) = \frac{M_{Gsw}(x)}{E_G \cdot I_G} \quad \text{E-70}$$

$$w_G = \frac{0.490 \cdot 90}{12^3} = 0.026 \text{ kips/in.}$$

Using Eqns. E-67, E-68 and E-69, moment and change in curvature due to girder self-weight along the span can be calculated as shown in Table E.16.

Table E.16. Moment and change in curvature due to girder self-weight along the span

$M_{Gsw}(x)$ (kips – in.)			$\Delta\phi_{Gsw}(x)$ (1/in.)		
$M_{Gsw}(1)$	$M_{Gsw}(2)$	$M_{Gsw}(3)$	$\Delta\phi_{Gsw}(1)$	$\Delta\phi_{Gsw}(2)$	$\Delta\phi_{Gsw}(3)$
0	9677	13113	0	4.48E-06	6.07E-06

Net curvature after girder erection can be calculated by simply summing the curvature values in Table E.15 and Table E.16, as provided in Table E.17.

Table E.17. Net curvature after girder erection

$\phi_{pre}(x)$ (1/in.)		
$\phi_{pre}(1)$	$\phi_{pre}(2)$	$\phi_{pre}(3)$
0	-2.00E-05	-2.65E-05

Using the Eqns. between E-24 and E-31, camber at considered sections can be calculated as follows:

$$\Delta x = \frac{\frac{173 \cdot 12}{2}}{3 - 1} = 519 \text{ in.}$$

$$A_{nm}(1) = \frac{519}{3} \cdot [0 + 4 \cdot (-2.00 \cdot 10^{-5}) + (-2.65 \cdot 10^{-5})] = -18.42 \cdot 10^{-3} \text{ in.}^2$$

$$A_{nm}(2) = \frac{519}{3} \cdot [(-2.00 \cdot 10^{-5}) + (-2.65 \cdot 10^{-5})] = -8.04 \cdot 10^{-3} \text{ in.}^2$$

$$A_{nm}(3) = 0$$

$$A_n(1) = 0$$

$$A_n(2) = \frac{519}{3} \cdot [0 + (-2.00 \cdot 10^{-5})] = -3.46 \cdot 10^{-3} \text{ in.}^2$$

$$A_n(3) = \frac{519}{3} \cdot [0 + 4 \cdot (-2.00 \cdot 10^{-5}) + (-2.65 \cdot 10^{-5})] = -18.42 \cdot 10^{-3} \text{ in.}^2$$

$$Q_n(1) = 0$$

$$Q_n(2) = \frac{519}{3} \cdot [0 + (-2.00 \cdot 10^{-5}) \cdot 519] = -1.80 \text{ in.}^3$$

$$Q_n(3) = \frac{519}{3} \cdot [0 + 4 \cdot (-2.00 \cdot 10^{-5}) \cdot 519 + (-2.65 \cdot 10^{-5}) \cdot 1038] = -11.94 \text{ in.}^3$$

Table E.18. Application of Simpson's rule and pre-erection camber

Parameters	Section index (x)		
	<u>1</u>	<u>2</u>	<u>3</u>
$Q_n(x) \text{ (in.}^3\text{)}$	0	-1.80	-11.94
$A_n(x) \text{ (in.}^2\text{)}$	0	-3.46E-03	-1.84E-02
$\bar{x}_n(x) \text{ (in.)}$	0	520.23	648.91
$\Delta_{A/C}(x) \text{ (in.)}$	0	-1.80	-11.94
$\theta_{B/C}(x) \text{ (rad.)}$	-1.84E-02	-8.04E-03	0
$x_n(x) \text{ (in.)}$	0	519.00	1038.00
$\Delta_{pre}(x) \text{ (in.)}$	0	-5.97	-11.94

E.4 Camber just after Placement of 1st Deck

- Deck self-weight effect

$$w_{d1} = A_{d1} \cdot \gamma_{d1} = \frac{990.36 \cdot 0.150}{12^3} = 0.086 \text{ kips/in.}$$

$$\text{if } x \leq 24 \quad M_{d1sw}(x) = -0.043 \cdot x^2 \quad \text{E-71}$$

$$\text{if } 24 < x \quad M_{d1sw}(x) = 87.2 \cdot x - 0.043 \cdot (x - 24)^2 - 2117.5 \quad \text{E-72}$$

$$\Delta\phi_{d1sw}(x) = \frac{M_{d1sw}(x)}{E_G \cdot I_G} \quad \text{E-73}$$

Table E.19. Moment and change in curvature due to 1st deck self-weight

$M_{d1sw}(x) \text{ (kips} \cdot \text{in.)}$			$\Delta\phi_{d1sw}(x) \text{ (1/in.)}$		
$M_{d1sw}(1)$	$M_{d1sw}(2)$	$M_{d1sw}(3)$	$\Delta\phi_{d1sw}(1)$	$\Delta\phi_{d1sw}(2)$	$\Delta\phi_{d1sw}(3)$
0	32593	44172	0	1.51E-05	2.04E-05

To obtain the net curvature just after 1st deck is placed, the net curvature values from previous calculation, Table E.17, should be summed up with the change in curvature values given in Table E.19.

Table E.20. Net curvature just after 1st deck is placed

$\phi_{ad1p}(x) \text{ (1/in.)}$		
$\phi_{ad1p}(1)$	$\phi_{ad1p}(2)$	$\phi_{ad1p}(3)$
0	-4.90E-06	-6.11E-06

- Calculation of camber just after placement of 1st deck

Using eqns. between E-24 and E-31 with the net curvature values given in Table E.20, the camber just after 1st deck is placed can be estimated.

Table E.21. Camber just after placement of 1st deck

Camber (in.)	$section \text{ index } (x)$		
	<u>1</u>	<u>2</u>	<u>3</u>
$\Delta_{nad1p}(x)$	0	-1.43	-2.86

E.5 Camber just before Application of Barrier and Overlay Loads on 1st Superstructure

In this part, a time-dependent analysis for composite structure is conducted. Since steel girder does not creep or shrink, only the force history of deck is considered. In this step, there is no force on the deck.

Using Eqns. between E-24 and E-64, the time-dependent calculation can be performed time t_1 and t_2 .

$$m = 3 \text{ \& } q = 1$$

$$\emptyset_p(x) = [0 \quad -5.01 \cdot 10^{-6} \quad -6.25 \cdot 10^{-6}]$$

$$\Delta \emptyset_t(x) = [0; 0; 0]$$

$$y_{dG} = 41 \text{ in.}$$

$$i = 1 \ \& \ p = 2 \ \& \ r = 1$$

$$k = [1]$$

- For $k = 1$

$$Co_{ND}(1,loc(x)) = 0 \ \& \ Co_{MD}(1,loc(x)) = 0$$

$$\varepsilon_{shD} = -(\varepsilon_{d1}(2) - \varepsilon_{d1}(1)) = 0$$

$$z = [1]$$

- For $z = 1$

$$\psi_{crD} = \psi_D(t(2),t(1)) - \psi_D(t(1),t(1)) = 0$$

$$\psi_{crD,flex} = \psi_{crD}$$

$$E_D = 0$$

$$h = [1; 2; 3]$$

$$Co_{ND} = [0; 0; 0]$$

$$Co_{MD} = [0; 0; 0]$$

- End of "z" array.

$$j = [1; 2; 3]$$

- For $j = 1$

$$M_{co} = \begin{bmatrix} 1 & 1 & 0 & 0 & 0 & 0 & 0 \\ -41 & 0 & 1 & 1 & 0 & 0 & 0 \\ -10^{20} & 0 & 0 & 0 & 1 & 0 & 0 \\ 0 & -3.90 \cdot 10^{-7} & 0 & 0 & 0 & 1 & 0 \\ 0 & 0 & -10^{20} & 0 & 0 & 0 & 1 \\ 0 & 0 & 0 & -4.63 \cdot 10^{-10} & 0 & 0 & 1 \\ 0 & 0 & 0 & 0 & 1 & -1 & 41 \end{bmatrix}$$

$$M_c = \begin{bmatrix} 0 \\ 0 \\ 0 \\ 0 \\ 0 \\ 0 \\ 0 \\ 0 \\ 0 \end{bmatrix}$$

$$M_s = [M_{co}^{-1}] \cdot [M_c]$$

$$N_D(2,1) = 0$$

$$M_D(2,1) = 0$$

$$\Delta\phi_t(2,1) = 0$$

Repeat the same procedure for other sections: $j = 2$ and $j = 3$. Basically, since both creep coefficient and shrinkage strain values are 0 in this step, there will be no change in curvature thus in camber.

➤ End of "j" array.

$$\phi_t(2, loc(x)) = \phi_p + \Delta\phi_t(2, loc(x))$$

$$\phi_t(2, loc(x)) = \phi_p = [0 \quad -4.90 \cdot 10^{-6} \quad -6.11 \cdot 10^{-6}]$$

➤ End of "k" array.

Since there is no change in curvature in this time step, previous camber remains as it is.

Table E.22. Camber just before application of barrier and overlay loads on 1st superstructure

Camber (in.)	<i>section index (x)</i>		
	<u>1</u>	<u>2</u>	<u>3</u>
$\Delta_{nbas1}(x)$	0	-1.43	-2.86

E.6 Camber just after Application of Barrier and Overlay Loads on 1st Superstructure

As it is indicated above, it is assumed that barrier and overlay loads are applied simultaneously on the 1st composite structure. In this part, only instantaneous changes in camber due to application of superimposed dead loads that are barrier and overlay loads are calculated. In other words, no time-dependent calculation is going to be performed.

- Barrier load effect

$$w_{b1} = 0.04 \text{ kips/in.}$$

$$\text{if } x \leq 24 \quad M_{b1sw}(x) = -0.02 \cdot x^2 \quad \text{E-74}$$

$$\text{if } 24 < x \quad M_{b1sw}(x) = 40.56 \cdot x - 0.02 \cdot (x - 24)^2 - 984.96 \quad \text{E-75}$$

$$\Delta\phi_{b1sw}(x) = \frac{M_{b1sw}(x)}{E_G \cdot I_{c1}(2)} \quad \text{E-76}$$

- Overlay load effect

$$w_{o1} = t_{o1} \cdot s_d \cdot \gamma_{o1} = \frac{2 \cdot 110.04 \cdot 0.140}{12^3} = 0.0178 \text{ kips/in.}$$

$$\text{if } x \leq 24 \quad M_{o1sw}(x) = -8.92 \cdot 10^{-3} \cdot x^2 \quad \text{E-77}$$

$$\text{if } 24 < x \quad M_{o1sw}(x) = 18.08 \cdot x - 8.92 \cdot 10^{-3} \cdot (x - 24)^2 - 439.06 \quad \text{E-78}$$

$$\Delta\phi_{o1sw}(x) = \frac{M_{o1sw}(x)}{E_G \cdot I_{c1}(3)} \quad \text{E-79}$$

Table E.23. Moment applied on composite structure due to barrier and overlay loads

$M_{b1sw}(x) \text{ (kips} \cdot \text{in.)}$			$M_{o1sw}(x) \text{ (kips} \cdot \text{in.)}$		
$M_{b1sw}(1)$	$M_{b1sw}(2)$	$M_{b1sw}(3)$	$M_{o1sw}(1)$	$M_{o1sw}(2)$	$M_{o1sw}(3)$
0	15165	20552	0	6760	9162

Table E.24. Change in curvature due to barrier and overlay load

$\Delta\phi_{b1sw}(x) \text{ (1/in.)}$			$\Delta\phi_{o1sw}(x) \text{ (1/in.)}$		
$\Delta\phi_{b1sw}(1)$	$\Delta\phi_{b1sw}(2)$	$\Delta\phi_{b1sw}(3)$	$\Delta\phi_{o1sw}(1)$	$\Delta\phi_{o1sw}(2)$	$\Delta\phi_{o1sw}(3)$
0	3.28E-06	4.45E-06	0	1.46E-06	1.98E-06

- Calculation of camber just after application of barrier and overlay loads

By summing the net curvature values from previous part, Table E.20, with the change in curvature values due to barrier and overlay loads, Table E.24, the net curvature can be obtained as shown in Table E.25. Then, using eqns. between E-24 and E-31, the camber just after application of barrier and overlay loads can be estimated as shown in Table E.26. Actually, zero curvature values mean that the girder is flat that is there is no camber and deflection in the girder just after application of barrier and overlay load.

Table E.25. Net curvature just after application of barrier and overlay loads

$\phi_{naas1}(x) \text{ (1/in.)}$		
$\phi_{naas1}(1)$	$\phi_{naas1}(2)$	$\phi_{naas1}(3)$
0	0	0

Table E.26. Camber just after application of barrier and overlay loads

Camber (in.)	<i>section index (x)</i>		
	<u>1</u>	<u>2</u>	<u>3</u>
$\Delta_{naas1}(x) \text{ (in.)}$	0	0	0

Please note that there no camber or deflection on the girder just after application of barrier and overlay loads. This was done on purpose such that the fabricated camber value was adjusted accordingly.

E.7 Camber just before Deck Removal Process

In this part, a time-dependent analysis for composite structure is conducted. To do so, the force history array for deck should be updated by considering the change in forces on the deck due to previous time-dependent effects between t_1 and t_2 (which is zero in this case), barrier and overlay self-weight

- Time-dependent effect between t_1 and t_2

In this case, since only one time step is considered between t_1 and t_2 , there is no force generated on the deck.

- Barrier load effect

$$\Delta N_{Gb1sw}(x) = \frac{M_{b1sw}(x) \cdot A_G \cdot [y_{c1}(2) - y_{Gbottom}]}{I_{c1}(2)} \quad E-80$$

$$\Delta M_{Gb1sw}(x) = \frac{M_{b1sw}(x) \cdot I_G}{I_{c1}(2)} \quad E-81$$

$$\Delta N_{d1b1sw}(x) = \frac{M_{b1sw}(x) \cdot A_{d1tr}(2) \cdot [y_{c1}(2) - y_{d1bottom}]}{I_{c1}(2)} \quad E-82$$

$$\Delta M_{d1b1sw}(x) = \frac{M_{b1sw}(x) \cdot I_{d1tr}(2)}{I_{c1}(2)} \quad E-83$$

Table E.27. Change in forces on deck due to barrier load

$\Delta N_{d1b1sw}(kips)$			$\Delta M_{d1b1sw}(kips - in.)$		
$\Delta N_{d1b1sw}(1)$	$\Delta N_{d1b1sw}(2)$	$\Delta N_{d1b1sw}(3)$	$\Delta M_{d1b1sw}(1)$	$\Delta M_{d1b1sw}(2)$	$\Delta M_{d1b1sw}(3)$
0	-195	-264	0	73	100

- Overlay load effect

$$\Delta N_{Go1sw}(x) = \frac{M_{o1sw}(x) \cdot A_G \cdot [y_{c1}(3) - y_{Gbottom}]}{I_{c1}(3)} \quad E-84$$

$$\Delta M_{Go1sw}(x) = \frac{M_{b1sw}(x) \cdot I_G}{I_{c1}(3)} \quad \text{E-85}$$

$$\Delta N_{d1o1sw}(x) = \frac{M_{o1sw}(x) \cdot A_{d1tr}(3) \cdot [y_{c1}(3) - y_{d1bottom}]}{I_{c1}(3)} \quad \text{E-86}$$

$$\Delta M_{d1o1sw}(x) = \frac{M_{o1sw}(x) \cdot I_{d1tr}(3)}{I_{c1}(3)} \quad \text{E-87}$$

Table E.28. Change in forces on deck due to overlay load

$\Delta N_{d1o1sw}(kips)$			$\Delta M_{d1o1sw}(kips - in.)$		
$\Delta N_{d1o1sw}(1)$	$\Delta N_{d1o1sw}(2)$	$\Delta N_{d1o1sw}(3)$	$\Delta M_{d1o1sw}(1)$	$\Delta M_{d1o1sw}(2)$	$\Delta M_{d1o1sw}(3)$
0	-87	-118	0	33	45

By summing up the change in forces for deck due to abovementioned effects, the force history array for deck can be generated as shown in Table E.29.

Table E.29. Net force history array just after application of barrier and overlay loads

<i>index</i>	$N_D(t, x) (kips)$			$M_D(t, x) (kips - in.)$		
	<u>1</u>	<u>2</u>	<u>3</u>	<u>1</u>	<u>2</u>	<u>3</u>
<u>1</u>	0	0	0	0	0	0
<u>2</u>	0	-195	-264	0	73	100
<u>3</u>	0	-87	-118	0	33	45

It should be noted that although there is no time-dependent change in forces between t_2 and t_3 , an additional row is added for this in Table E.29. This is done on purpose so that the time indexes match with the MDOTCamber program where the effects of barrier and overlay loads are considered separately.

After obtaining the force history array for the deck, using Eqns. between E-24 and E-31, time-dependent calculation can be performed between time t_3 and t_4 . Since it is done explicitly in section E.5, it is not repeated here.

After conducting time-dependent calculation, the following change in force and curvature values can be obtained.

Table E.30. Change in forces on deck due to time-dependent effects between t_3 and t_4

$\Delta N_{Dt_3t_4} (kips)$			$\Delta M_{Dt_3t_4} (kips - in.)$		
$\Delta N_{Dt_3t_4} (1)$	$\Delta N_{Dt_3t_4} (2)$	$\Delta N_{Dt_3t_4} (3)$	$\Delta M_{Dt_3t_4} (1)$	$\Delta M_{Dt_3t_4} (2)$	$\Delta M_{Dt_3t_4} (3)$
290	365	392	44	-13	-33

Table E.31. Change in curvature between time t_3 and t_4

$\Delta \phi_t(x) (1/in.)$		
$\Delta \phi_t(1)$	$\Delta \phi_t(2)$	$\Delta \phi_t(3)$
5.48E-06	6.93E-06	7.45E-06

Using the previous net curvature values given in Table E.25, and change in curvature values in Table E.31, net curvature values just before the deck removal process can be obtained as follows:

Table E.32. Net curvature just before deck removal process

$\phi_t(4, x) (1/in.)$		
$\phi_t(4,1)$	$\phi_t(4,2)$	$\phi_t(4,3)$
5.48E-06	6.78E-06	7.78E-06

Using net curvature values provided in Table E.32 and Eqns. between E-24 and E-31, camber just before the deck removal process can be calculated as shown in Table E.33.

Table E.33. Camber just before deck removal process

Camber (in.)	<i>section index</i> (x)		
	<u>1</u>	<u>2</u>	<u>3</u>
$\Delta_{nbd1r}(x)$	0	1.92	3.83

E.8 Camber just after Deck Removal Process

Instantaneous change in camber just after deck is removed is composed of two parts: one is due to removal of self-weight loads of deck, overlay and barrier; other is due to effect of locked forces inside the deck on girder.

- Removal of barrier and overlay loads

$$\Delta N_{d1ob1r}(x) = - \frac{[M_{b1sw}(x) + M_{o1sw}(x)] \cdot A_{d1tr}(4) \cdot [y_{c1}(4) - y_{d1bottom}]}{I_{c1}(4)} \quad E-88$$

$$\Delta M_{d1ob1r}(x) = - \frac{[M_{b1sw}(x) + M_{o1sw}(x)] \cdot I_{d1tr}(4)}{I_{c1}(4)} \quad \text{E-89}$$

$$\Delta \phi_{ob1r}(x) = - \frac{[M_{b1sw}(x) + M_{o1sw}(x)]}{E_G \cdot I_{c1}(4)} \quad \text{E-90}$$

Table E.34. Change in forces on deck due to removal of barrier and overlay loads

$\Delta N_{d1ob1r}(x) \text{ (kips)}$			$\Delta M_{d1ob1r}(x) \text{ (kips} - \text{in.)}$		
$\Delta N_{d1ob1r}(1)$	$\Delta N_{d1ob1r}(2)$	$\Delta N_{d1ob1r}(3)$	$\Delta M_{d1ob1r}(1)$	$\Delta M_{d1ob1r}(2)$	$\Delta M_{d1ob1r}(3)$
0	295	400	0	-130	-176

Table E.35. Change in curvature due to removal of barrier and overlay loads

$\Delta \phi_{ob1r}(x) \text{ (1/in.)}$		
$\Delta \phi_{ob1r}(1)$	$\Delta \phi_{ob1r}(2)$	$\Delta \phi_{ob1r}(3)$
0	-4.48E-06	-6.07E-06

- Removal of locked forces in the deck before it is removed

Using Table E.29, Table E.30 and Table E.34, the total net forces on the deck can be calculated as shown in Table E.36.

Table E.36. Net forces on the deck just before it is removed

$N_{d1br} \text{ (kips)}$			$M_{d1br} \text{ (kips} - \text{in.)}$		
$N_{d1br}(1)$	$N_{d1br}(2)$	$N_{d1br}(3)$	$M_{d1br}(1)$	$M_{d1br}(2)$	$M_{d1br}(3)$
290	379	410	44	-36	-65

After determined the net forces on the deck, their effects on steel girder is considered when estimating the camber using the equations below. It should be noted that only change in moment would be sufficient to calculate change in curvature due to removal of locked forces inside the deck.

$$\Delta M_{Gd1r}(x) = M_{d1br}(x) + N_{d1br}(x) \cdot [y_{Gbottom} - y_{d1bottom}] \quad \text{E-91}$$

$$\Delta \phi_{d1r}(x) = \frac{\Delta M_{Gd1r}(x)}{E_G \cdot I_G} \quad \text{E-92}$$

Table E.37. Change in moment due to removal of locked forces inside the deck

$\Delta M_{Gd1r}(x) \text{ (kips} - \text{in.)}$		
$\Delta M_{Gd1r}(1)$	$\Delta M_{Gd1r}(2)$	$\Delta M_{Gd1r}(3)$
-11849	-15561	-16879

Table E.38. Change in curvature due to removal of locked forces inside the deck

$\Delta \phi_{d1r}(x) \text{ (1/in.)}$		
$\Delta \phi_{d1r}(1)$	$\Delta \phi_{d1r}(2)$	$\Delta \phi_{d1r}(3)$
-5.48E-06	-7.19E-06	-7.81E-06

- Removal of deck load

$$\Delta M_{Gd1swr}(x) = -M_{d1sw}(x) \quad \text{E-93}$$

$$\Delta \phi_{d1swr}(x) = \frac{\Delta M_{Gd1swr}(x)}{E_G \cdot I_G} \quad \text{E-94}$$

Table E.39. Change in curvature due to deck removal

$\Delta \phi_{d1swr}(x) \text{ (1/in.)}$		
$\Delta \phi_{d1swr}(1)$	$\Delta \phi_{d1swr}(2)$	$\Delta \phi_{d1swr}(3)$
0	-1.51E-05	-2.04E-05

After considered all effects, curvature changes given in Table E.35, Table E.38 and Table E.39 need to be summed together with the previous net curvature values provided in Table E.32 so that the net curvature just after deck removal can be obtained as shown in Table E.40.

Table E.40. Net curvature just after deck removal

$\phi_{ad1r}(x) \text{ (1/in.)}$		
$\phi_{ad1r}(1)$	$\phi_{ad1r}(2)$	$\phi_{ad1r}(3)$
0	-2.00E-05	-2.65E-05

Using net curvature values provided in Table E.40 and Eqns. between E-24 and E-31, camber just after the deck is removed can be calculated as shown in Table E.41.

Table E.41. Camber just after deck removal

Camber (in.)	<i>section index (x)</i>		
	<u>1</u>	<u>2</u>	<u>3</u>
$\Delta_{nad1r}(x)$	0	-5.97	-11.94

It should be noted here that the net curvature and camber values given in Table E.40 and Table E.41, respectively, are same with the curvature and camber values just after girder is erected, Table E.17 and Table E.18. Basically, it means that after the deck is removed, girder turns back to its original position, and this is expected because steel girder itself does not creep or shrink.

E.9 Camber just before 2nd Deck Placement

In this part, since steel girder does not creep or shrinkage, no time-dependent analysis is conducted, and the net curvature and camber values provided in Table E.40 and Table E.41 remains as they are, respectively.

Table E.42. Net curvature just before new deck placement

$\phi_{nbndp}(x)$ (1/in.)		
$\phi_{nbndp}(1)$	$\phi_{nbndp}(2)$	$\phi_{nbndp}(3)$
0	-2.00E-05	-2.65E-05

Table E.43. Camber just before new deck placement

Camber (in.)	<i>section index (x)</i>		
	<u>1</u>	<u>2</u>	<u>3</u>
$\Delta_{nbndp}(x)$	0	-5.97	-11.94

E.10 Camber just after 2nd Deck Placement

A similar process that is explained in section E.4 is followed in this part to estimate the camber. Since it is assumed that 1st and 2nd decks are identical, equations used for 1st deck are valid for 2nd deck.

- Deck self-weight effect

$$w_{d2} = A_{d2} \cdot \gamma_{d2} = \frac{990.36 \cdot 0.150}{12^3} = 0.086 \text{ kips/in..}$$

$$\text{if } x \leq 24 \quad M_{d2sw}(x) = -0.043 \cdot x^2 \quad \text{E-95}$$

$$\text{if } 24 < x \quad M_{d2sw}(x) = 87.2 \cdot x - 0.043 \cdot (x - 24)^2 - 2117.5 \quad \text{E-96}$$

$$\Delta\phi_{d2sw}(x) = \frac{M_{d2sw}(x)}{E_G \cdot I_G} \quad \text{E-97}$$

Table E.44. Moment and change in curvature due to 2nd deck self-weight

$M_{d2sw}(x)$ (kips – in.)			$\Delta\phi_{d2sw}(x)$ (1/in.)		
$M_{d2sw}(1)$	$M_{d2sw}(2)$	$M_{d2sw}(3)$	$\Delta\phi_{d2sw}(1)$	$\Delta\phi_{d2sw}(2)$	$\Delta\phi_{d2sw}(3)$
0	32593	44172	0.00	1.51E-05	2.04E-05

To obtain the net curvature just after 2nd deck is placed, the net curvature values from previous step, Table E.42, should be summed up with the change in curvature values given in Table E.44.

Table E.45. Net curvature just after 2nd deck is placed

$\phi_{ad2p}(x)$ (1/in.)		
$\phi_{ad2p}(1)$	$\phi_{ad2p}(2)$	$\phi_{ad2p}(3)$
0	-4.90E-06	-6.11E-06

- Calculation of camber just after placement of 2nd deck

Using Eqns. between E-24 and E-31 with the net curvature values given in Table E.45, the camber just after 1st deck is placed can be estimated.

Table E.46. Camber just after placement of 2nd deck

Camber (in.)	$\text{section index } (x)$		
	<u>1</u>	<u>2</u>	<u>3</u>
$\Delta_{nad2p}(x)$	0	-1.43	-2.86

E.11 Camber just before Application of Barrier and Overlay Loads on 2nd Superstructure

In this part, a time-dependent analysis for composite structure is conducted similar to section E.5. Since steel girder does not creep or shrink, only the force history of deck is considered. In this step, since the deck is placed recently, there is no force on the deck.

Using Eqns. between E-32 and E-64, the time-dependent calculation for 2nd composite structure between time t_5 and t_6 can be performed. As it is done in section E.5, it will not be repeated here, but in any way, since creep coefficient and shrinkage strain values for 2nd deck are zero in this time step, there will be no time-dependent change in curvature, thus in camber, at the end of time step. Therefore, net curvature and camber values in Table E.45 and Table E.46 remains as they are, respectively.

Table E.47. Net curvature just before application of barrier and overlay loads

$\phi_t(6, x) (1/in.)$		
$\phi_t(6,1)$	$\phi_t(6,2)$	$\phi_t(6,3)$
0	-4.90E-06	-6.11E-06

Table E.48. Camber just before application of barrier and overlay loads on 2nd superstructure

Camber (in.)	<i>section array</i> (x)		
	<u>1</u>	<u>2</u>	<u>3</u>
$\Delta_{nbas2}(x)$	0	-1.43	-2.86

E.12 Camber just after Application of Barrier and Overlay Loads on 2nd Superstructure

Similarly, the process provided in section E.6, is followed in this part to estimate the camber just after application of barrier and overlay loads on 2nd super-structure. Since it is assumed that same barrier and overlay loads are applied on it, equations used previously for the effect of barrier and overlay loads on 1st super-structure are valid for 2nd super-structure, however, parameters that are time-dependent should be updated accordingly. Similarly, it is assumed that overlay load is simultaneously applied with the barrier load for simplicity, hence no time-dependent calculation is going to be performed between application of barrier and overlay loads.

- Barrier load effect

$$w_{b2} = 0.04 \text{ kips/in.}$$

$$\text{if } x \leq 24 \quad M_{b2sw}(x) = -0.02 \cdot x^2 \quad \text{E-98}$$

$$\text{if } 24 < x \quad M_{b2sw}(x) = 40.56 \cdot x - 0.02 \cdot (x - 24)^2 - 984.96 \quad \text{E-99}$$

$$\Delta\phi_{b2sw}(x) = \frac{M_{b2sw}(x)}{E_G \cdot I_{c2}(6)} \quad \text{E-100}$$

- Overlay load effect

$$w_{o2} = t_{o2} \cdot s_d \cdot \gamma_{o2} = \frac{2 \cdot 110.04 \cdot 0.140}{12^3} = 0.0178 \text{ kips/in.}$$

$$\text{if } x \leq 24 \quad M_{o2sw}(x) = -8.92 \cdot 10^{-3} \cdot x^2 \quad \text{E-101}$$

$$\text{if } 24 < x \quad M_{o2sw}(x) = 18.08 \cdot x - 8.92 \cdot 10^{-3} \cdot (x - 24)^2 - 439.06 \quad \text{E-102}$$

$$\Delta\phi_{o2sw}(x) = \frac{M_{o2sw}(x)}{E_G \cdot I_{c2}(7)} \quad \text{E-103}$$

Table E.49. Moment applied on composite structure due to barrier and overlay loads

$M_{b2sw}(x) \text{ (kips} \cdot \text{in.)}$			$M_{o2sw}(x) \text{ (kips} \cdot \text{in.)}$		
$M_{b2sw}(1)$	$M_{b2sw}(2)$	$M_{b2sw}(3)$	$M_{o2sw}(1)$	$M_{o2sw}(2)$	$M_{o2sw}(3)$
0	15165	20552	0	6760	9162

Table E.50. Change in curvature due to barrier and overlay load

$\Delta\phi_{b2sw}(x) \text{ (1/in.)}$			$\Delta\phi_{o2sw}(x) \text{ (1/in.)}$		
$\Delta\phi_{b2sw}(1)$	$\Delta\phi_{b2sw}(2)$	$\Delta\phi_{b2sw}(3)$	$\Delta\phi_{o2sw}(1)$	$\Delta\phi_{o2sw}(2)$	$\Delta\phi_{o2sw}(3)$
0	3.28E-06	4.45E-06	0	1.46E-07	1.98E-06

- Calculation of camber just after application of barrier and overlay loads

By summing the net curvature values from previous part, Table E.47, with the change in curvature values due to barrier and overlay loads, Table E.50, the net curvature can be obtained as shown in Table E.51. Then, using Eqns. between E-24 and E-31, the camber just after application of barrier and overlay loads on 2nd super-structure can be estimated as shown in Table E.52.

Table E.51. Net curvature just after application of barrier and overlay loads on 2nd super-structure

$\phi_{naas2}(x) \text{ (1/in.)}$		
$\phi_{naas1}(1)$	$\phi_{naabho1}(2)$	$\phi_{naabho1}(3)$
0	0	0

Table E.52. Camber just after application of barrier and overlay loads on 2nd super-structure

Camber (in.)	<i>section index (x)</i>		
	<u>1</u>	<u>2</u>	<u>3</u>
$\Delta_{naas2}(x)$ (in.)	0	0	0

E.13 Camber at Final Time

In this part, a time-dependent analysis for composite structure is conducted. To do so, the force history array for deck should be generated by considering the change in forces on the deck due to previous time-dependent effects between t_5 and t_6 (which is zero in this case), barrier and overlay self-weight. A similar approach stated in section E.7 is followed. Equations used in section E.7 are valid in this part, however, parameters that are time-dependent should be updated accordingly.

- Time-dependent effect between t_5 and t_6

In this case, since only one time step is considered between t_5 and t_6 , there is no force generated on the deck.

- Barrier load effect

$$\Delta N_{d2b2sw}(x) = \frac{M_{b2sw}(x) \cdot A_{d2tr}(6) \cdot [y_{c2}(6) - y_{d2bottom}]}{I_{c2}(6)} \quad \text{E-104}$$

$$\Delta M_{d2b2sw}(x) = \frac{M_{b2sw}(x) \cdot I_{d2tr}(6)}{I_{c2}(6)} \quad \text{E-105}$$

Table E.53. Change in forces on deck due to barrier load

$\Delta N_{d2b2sw}(kips)$			$\Delta M_{d2b2sw}(kips - in.)$		
$\Delta N_{d2b2sw}(1)$	$\Delta N_{d2b2sw}(2)$	$\Delta N_{d2b2sw}(3)$	$\Delta M_{d2b2sw}(1)$	$\Delta M_{d2b2sw}(2)$	$\Delta M_{d2b2sw}(3)$
0	-195	-264	0	74	100

- Overlay load effect

$$\Delta N_{d2o2sw}(x) = \frac{M_{o2sw}(x) \cdot A_{d2tr}(7) \cdot [y_{c2}(7) - y_{d2bottom}]}{I_{c2}(3)} \quad \text{E-106}$$

$$\Delta M_{d2o2sw}(x) = \frac{M_{o2sw}(x) \cdot I_{d2tr}(7)}{I_{c2}(7)} \quad \text{E-107}$$

Table E.54. Change in forces on deck due to overlay load

$\Delta N_{d2o2sw}(kips)$			$\Delta M_{d2o2sw}(kips - in.)$		
$\Delta N_{d2o2sw}(1)$	$\Delta N_{d2o2sw}(2)$	$\Delta N_{d2o2sw}(3)$	$\Delta M_{d2o2sw}(1)$	$\Delta M_{d2o2sw}(2)$	$\Delta M_{d2o2sw}(3)$
0	-87	-118	0	33	45

By summing up the change in forces for deck due to abovementioned effects, the force history array for deck can be generated as shown in Table E.55. Please note that the values in force history array for the 2nd deck for the indices from 1 to 5 are taken as 0 because the 2nd is casted after time index 5.

Table E.55. Net force history array just after application of barrier and overlay loads

<i>index</i>	$N_p(t, x) (kips)$			$M_p(t, x) (kips - in.)$		
	<u>1</u>	<u>2</u>	<u>3</u>	<u>1</u>	<u>2</u>	<u>3</u>
<u>5</u>	0	0	0	0	0	0
<u>6</u>	0	-195	-264	0	74	100
<u>7</u>	0	-87	-118	0	33	45

It should be noted that although there is no time-dependent change in forces between t_6 and t_7 , an additional row is added for this in Table E.55. This is done on purpose so that the time indices match with the MDOTCamber program where the effects of barrier and overlay loads are considered separately.

After obtaining the force history array for the 2nd deck, using Eqns. between E-24 and E-64, time-dependent calculation can be performed between time t_7 and t_8 . Since it is done explicitly in section E.7, it is not repeated here.

After conducting time-dependent calculation, the following change in force and curvature values can be obtained.

Table E.56. Change in forces on deck due to time-dependent effects between t_7 and t_8

$\Delta N_{Dt_7t_8} (kips)$			$\Delta M_{Dt_7t_8} (kips - in.)$		
$\Delta N_{Dt_7t_8} (1)$	$\Delta N_{Dt_7t_8} (2)$	$\Delta N_{Dt_7t_8} (3)$	$\Delta M_{Dt_7t_8} (1)$	$\Delta M_{Dt_7t_8} (2)$	$\Delta M_{Dt_7t_8} (3)$
290	365	391	44	-13	-33

Table E.57. Change in curvature between time t_7 and t_8

$\Delta \phi_t(x) (1/in.)$		
$\Delta \phi_t(1)$	$\Delta \phi_t(2)$	$\Delta \phi_t(3)$
5.47E-06	6.92E-06	7.44E-06

Using the previous net curvature values given in Table E.51, and change in curvature values in Table E.57, respectively, the net curvature at final time can be calculated as follows:

Table E.58. Net curvature at final considered time

$\phi_t(8,x) (1/in.)$		
$\phi_t(4,1)$	$\phi_t(4,2)$	$\phi_t(4,3)$
5.4E-06	6.77E-06	7.76E-06

Using net curvature values provided in Table E.58 and Eqns. between E-24 and E-31, the net camber at considered final time which is 75 years in this example can be estimated as follows:

Table E.59. Camber at final considered time

Camber (in.)	<i>section index</i> (x)		
	<u>1</u>	<u>2</u>	<u>3</u>
$\Delta_{ns2}(x)$	0	1.91	3.82

E.14 Nomenclature

A_G = girder area, (in.²),
 A_{nm} = area under curvature diagram between nth section and midspan, (in.²)
 A_n = area under curvature diagram between nth section and closest girder end, (in.²)
 A_{ctr} = transformed area of composite structure, (in.²),
 A_{c1tr} = transformed area of 1st composite structure, (in.²),
 A_{c2tr} = transformed area of 2nd composite structure, (in.²),
 A = net area of the element that is going to be transformed, (in.²),
 A_d = area of the deck, (in.²),
 A_{dtr} = transformed area for the deck, (in.²),
 A_{d1tr} = transformed area for the 1st deck, (in.²),
 A_{d2tr} = transformed area for the 2nd deck, (in.²),
 CO_{NG} = coefficient related to axial force on the deck,
 CO_{MG} = coefficient related to moment on the deck,
 E_{CD} = the modulus of elasticity function for deck as a function of time, (ksi),
 E_{CD1} = the modulus of elasticity function for the first deck as a function of time, (ksi),
 E_{CD2} = the modulus of elasticity function for the second deck as a function of time, (ksi),
 E'_{c28} = 28-day modulus of elasticity of concrete, (ksi),
 E_G = modulus of elasticity of girder concrete, (ksi),
 E_D = modulus of elasticity of deck concrete at a specific time, (ksi),
 E_{tr} = modulus of elasticity of the transformed material, (ksi),
 f'_{cdi} = initial concrete compressive strength for deck, (ksi),
 f'_{cd} = 28-day concrete compressive strength for deck, (ksi),
 h = section index array,
 H_r = the average annual ambient relative humidity (%),

i = index for initial reference time,
 I_{dtr} = transformed moment of inertia of the deck, (in.⁴),
 I_{d1tr} = transformed moment of inertia of the 1st deck, (in.⁴),
 I_{d2tr} = transformed moment of inertia of the 2nd deck, (in.⁴),
 I_c = transformed moment of inertia of composite structure, (in.⁴),
 I_{c1} = transformed moment of inertia of composite structure with 1st deck, (in.⁴),
 I_{c2} = transformed moment of inertia of composite structure with 2nd deck, (in.⁴),
 j = section index array,
 k = time index array,
 k_s = factor for the effect of the volume-to-surface ratio of the component
 k_{hc} = humidity factor for creep,
 k_f = factor for the effect of concrete strength,
 k_{tdc} = time development factor for creep,
 k_{tds} = time development factor for shrinkage,
 k_{hs} = humidity factor for shrinkage,
 K_1 = coefficient depending on aggregate type: for normal weight concrete $K_1 = 1.0$,
 m = number of sections to be investigated,
 M_{Gsw} = moment due to girder self-weight, (kips – in.),
 M_{co} = matrix composed of coefficients for time-dependent calculations,
 M_c = matrix of constants for time-dependent calculations,
 M_s = solution matrix for time-dependent calculations,
 N_D = array of axial force on the deck a function of time and location, (kips),
 M_D = array of moment on the deck a function of time and location, (kips – in.),
 M_{d1sw} = moment caused by 1st deck load as a function of location, (kips – in.),
 M_{d2sw} = moment caused by 2nd deck load as a function of location, (kips – in.),
 M_{b1sw} = moment caused by 1st barrier load as a function of location, (kips – in.),

M_{b2sw} = moment caused by 2nd barrier load as a function of location, (*kips – in.*),
 M_{o1sw} = moment caused by 1st overlay load as a function of location, (*kips – in.*),
 M_{o2sw} = moment caused by 2nd overlay load as a function of location, (*kips – in.*),
 M_{d1br} = net moment on the 1st deck before it is removed, (*kips – in.*),
 p = index for final reference time,
 Q_n = first moment of the area under curvature diagram between nth section and closest girder end, (*in.*³),
 r = helper symbol that is related to time reference for time-dependent calculations,
 s_d = average center-to-center spacing of the girders, (*in.*),
 S_{d1} = perimeter of the first deck, (*in.*),
 t_i = age of concrete at the time of load application (*days*),
 t = maturity of concrete, defined as age of concrete between time of loading for creep calculations, or end of curing for shrinkage calculations, and time being considered for analysis of creep or shrinkage effects, (*days*),
 t_d = average deck thickness, (*in.*),
 t_h = average haunch thickness, (*in.*),
 t_{o1} = 1st overlay thickness, (*in.*),
 t_{o2} = 2nd overlay thickness, (*in.*),
 u = time index array,
 V_{d1} = volume of the first deck, (*in.*³),
 V/S = volume-to-surface ratio (*in.*),
 w = unit weight of concrete, (*kcf*),
 w_G = load due to girder self-weight, *kips/in.*,
 w_{d1} = load due to 1st deck, (*kips/in.*),
 w_{d2} = load due to 2nd deck, (*kips/in.*),
 w_{b1} = load due to 1st barrier load, (*kips/in.*),
 w_{b2} = load due to 2nd barrier load, (*kips/in.*),
 w_{o1} = load due to 1st overlay load, (*kips/in.*),
 w_{o2} = load due to 2nd overlay load, (*kips/in.*),
 x_n = location of nth section measured from closest girder end, (*in.*),

X_{Gof} = fabricated curvature along the span, (*1/in.*),
 X_n = curvature at nth section, (*1/in.*),
 x_m = location of midspan measured from girder end, (*in.*),
 X_m = curvature at midspan, (*1/in.*),
 \bar{x}_n = centroid of the area under curvature diagram between nth section and closest girder end, (*in.*),
 y_{dG} = a parameter indicating the distance between centroids of girder and deck, (*in.*),
 $y_{Gbottom}$ = centroid of girder with respect to bottom of girder, (*in.*),
 y_{dc} = centroid of the deck & haunch couple with respect to the bottom of the haunch, (*in.*),
 $y_{dbottom}$ = distance between centroid of deck & haunch couple with respect to bottom of the girder, (*in.*),
 y_c = distance of centroid of transformed composite structure to the bottom of girder, (*in.*),
 y_{c1} = distance of centroid of transformed composite structure to the bottom of girder with 1st deck, (*in.*),
 y_{c2} = distance of centroid of transformed composite structure to the bottom of girder with 2nd deck, (*in.*),
 z = time index array,
 loc = array for location, (*in.*),
 $stopper$ = helper word for time-dependent calculations,
 $continue$ = loop term that restarts the current iteration,
 α = parameters for ACI209R-92 development model depending on curing type,
 α_1 = coefficient used to determine fabricated camber along the span,
 α_2 = coefficient used to determine fabricated curvature along the span,
 β = parameters for ACI209R-92 development model depending on cement type,
 $\theta_{B/C}$ = relative slope at point B relative to point C, (*rad.*),

γ_G = unit-weight of girder, (*kcf*),
 γ_{o1} = unit-weight of 1st overlay, (*pcf*),
 γ_{o2} = unit-weight of 2nd overlay, (*pcf*),
 ε_{shD} = remaining deck shrinkage at a given time, (*in./in.*),
 β_{ax} = magnification factor tension creep,
 β_{flex} = magnification factor flexural creep,
 ψ_{crD} = remaining deck creep at a given time,
 $\psi_{crD,flex}$ = remaining deck flexural creep at a given time,
 $\psi_{crG,ax}$ = remaining girder tension creep at a given time,
 $\psi_{crD,ax}$ = remaining deck tension creep at a given time,
 $\psi(t, t_i)$ = the creep coefficient at concrete at t due to load applied at t_i ,
 ϕ_{pre} = net curvature after girder erection, (*1/in.*),
 ϕ_0 = initial curvature array as a function of time and location, (*1/in.*),
 ϕ_p = initial curvature array as a function of time and location, (*1/in.*),
 $\Delta\phi_t$ = change in curvature due to time-dependent effects as a function of time and location, (*1/in.*),
 ϕ_{ad1p} = net curvature just after 1st deck is placed, (*1/in.*),
 ϕ_{ad2p} = net curvature just after 2nd deck is placed, (*1/in.*),
 ϕ_{naas1} = net curvature just after application of barrier and overlay loads on 1st superstructure, (*1/in.*),
 ϕ_{nbndp} = net curvature before new deck placement, (*1/in.*),
 ϕ_{naas2} = net curvature just after application of barrier and overlay loads on 2nd superstructure, (*1/in.*),
 ϕ_{ad1r} = net curvature just after deck removal, (*1/in.*),
 η = modular ratio,
 η_D = modular ratio for the deck
 η_{D1} = modular ratio for the 1st deck,
 η_{D2} = modular ratio for the 2nd deck,
 Δ_{Gof} = fabricated camber along the span, (*in.*),

Δ_{pre} = pre-erection camber along the span, (*in.*),
 Δ_{nad1p} = camber just after placement of 1st deck, (*in.*),
 Δ_{nbas1} = camber just before application of barrier and overlay loads on 1st superstructure, (*in.*),
 Δ_{nbas2} = camber just before application of barrier and overlay loads on 2nd superstructure, (*in.*),
 Δ_{naas1} = camber just after application of barrier and overlay loads on 1st superstructure, (*in.*),
 Δ_{naas2} = camber just after application of barrier and overlay loads on 2nd superstructure, (*in.*),
 Δ_{nbd1r} = camber just before deck removal process, (*in.*),
 Δ_{nad1r} = camber just after deck removal process, (*in.*),
 Δ_{nbndp} = camber just before new deck placement, (*in.*),
 Δ_{nad2p} = camber just after placement of 2nd deck, (*in.*),
 Δ_{ns2} = camber at final considered time, (*in.*),
 Δ_n = net deflection at n^{th} section according to end of the girder, (*in.*),
 $\Delta_{A/C}$ = relative displacement at point C according to point A, (*in.*),
 Δx = length of a section, (*in.*),
 ΔM_{d1ob1r} = change in moment on the 1st deck due to removal of barrier and overlay loads, (*kips – in.*),
 ΔM_{Gd1swr} = change in moment on girder due to deck self-weight removal, (*kips – in.*),
 ΔM_{d1b1sw} = change in moment on the 1st deck due to 1st barrier load, (*kips – in.*),
 ΔM_{Gb2sw} = change in moment on the girder due to 2nd barrier load, (*kips – in.*),
 ΔM_{d2b2sw} = change in moment on the 2nd deck due to 2nd barrier load, (*kips – in.*),
 ΔM_{d1o1sw} = change in moment on the 1st deck due to 1st overlay load, (*kips – in.*),

ΔM_{d2o2sw} = change in moment on the 2nd deck due to 2nd overlay load, (*kips – in.*),
 $\Delta M_{Dt_3t_4}$ = change in moment on deck due to time-dependent effects between t_3 and t_4 , (*kips – in.*),
 $\Delta M_{Dt_7t_8}$ = change in moment on deck due to time-dependent effects between t_7 and t_8 , (*kips – in.*),
 ΔN_{d1ob1r} = change in axial force on the 1st deck due to removal of barrier and overlay loads, (*kips*),
 ΔN_{d1b1sw} = change in axial force on the 1st deck due to 1st barrier load, (*kips*),
 ΔN_{d2b2sw} = change in axial force on the 2nd deck due to 2nd barrier load, (*kips*),
 ΔN_{d1o1sw} = change in axial force on the 1st deck due to 1st overlay load, (*kips*),
 ΔN_{d2o2sw} = change in axial force on the 2nd deck due to 2nd overlay load, (*kips*),
 $\Delta N_{Dt_3t_4}$ = change in axial force on deck due to time-dependent effects between t_3 and t_4 , (*kips – in.*),
 $\Delta N_{Dt_7t_8}$ = change in axial force on deck due to time-dependent effects between t_7 and t_8 , (*kips – in.*),
 $\Delta \phi_{sc}$ = change in curvature due to change in support conditions, (*1/in.*),
 $\Delta \phi_{Gsw}$ = change in curvature due to girder self-weight, (*1/in.*),
 $\Delta \phi_{d1sw}$ = change in curvature due to 1st deck self-weight, (*1/in.*),
 $\Delta \phi_{d2sw}$ = change in curvature due to 2nd deck self-weight, (*1/in.*),
 $\Delta \phi_{b1sw}$ = change in curvature due to 1st barrier self-weight, (*1/in.*),
 $\Delta \phi_{b2sw}$ = change in curvature due to 2nd barrier self-weight, (*1/in.*),
 $\Delta \phi_{o1sw}$ = change in curvature due to 1st barrier self-weight, (*1/in.*),
 $\Delta \phi_{o2sw}$ = change in curvature due to 2nd barrier self-weight, (*1/in.*),
 $\Delta \phi_{ob1r}$ = change in curvature due to removal of barrier and overlay loads, (*1/in.*),

$\Delta \phi_{d1r}$ = change in curvature due to removal of locked forces inside the deck, (*1/in.*),
 $\Delta \phi_{d1swr}$ = change in curvature due to deck self-weight removal, (*1/in.*)

APPENDIX F: RECOMMENDED REVISIONS, UPDATES AND GUIDELINES

Appendix F: Recommended Revision, Updates, and Guidelines

It is recommended that the computational tool developed as part of this research project titled MDOT Camber together with the user's manual provided in Appendix C be used as guidelines to compute the complete camber history of fully prestressed concrete beams used in simply supported configurations. Additionally, MDOT Camber may be used to predict the camber and displacement history of steel beams made composite with a concrete deck and used in a simply supported configurations. The following MDOT documents were reviewed:

- Slab and Screed Guidance
- Michigan Design Manual - Bridge Design – Chapter 7: LRFD – Section 7.02.22 – Screeding
- Special Provision for Structure Survey During Construction
- Standard Specifications for Construction – Section 708. Prestressed Concrete

A new slab and screed guidance document is provided as part of this report. This new guidance includes step by step examples for how to determine camber and deflections in prestressed concrete and steel beams during the placement of the deck with the purpose of ascertaining slab screed and bottom of slab elevations. The information provided in the original guide, which explains what slab screed and bottom of slab elevations are, together with other clarifications, remains essentially unchanged and includes only editorial changes. However, the old appendix, which showed how beam camber and deflections were calculated was rewritten to include step by step examples for prestressed concrete and steel beams.

Section 7.02.22-Screeding of the Michigan Design Manual includes comments that indicate that the current fixed multiplier based method should be replaced with the MDOT Camber program.

The document titled “Special Provision for Structure Survey During Construction” includes some recommendations.

No revisions are proposed for the document titled “Standard Specification for Construction – Section 708. Prestressed Concrete”.

Appendix F.1 - Sample Camber and Deflection Calculations – Prestressed Concrete Beam

Problem Statement: Determine camber and deflections for a precast bulb tee beam used in the I-75 S-11 project due to: 1) prestress and self weight, 2) weight of forms and rebar, 3) weight of concrete deck, and 4) weight of sidewalk or barrier. This information can be used to determine slab screed and bottom of slab elevations according to MDOT’s “Slab and Screed Guidance” document. For example, the beam camber profile together with the specified minimum haunch and beam bearing elevations can be used to determine slab and screed elevations. The biggest unknown in the process is the deflected shape of the beam at different stages. This deflected shape can be obtained from the MDOT Camber program as shown below.

Solution:

Step 1): Start the MDOTCamber Program and fill in the information required in the introduction tab.

The screenshot displays the MDOTCamber v6.0 software window. The 'Introduction' tab is active, showing project information and a sign convention diagram.

Predicting Camber and Deflections in Composite Bridge Superstructures

Logos for MDOT (Michigan Department of Transportation), Wayne State College of Engineering, and benesch are displayed.

Project Information:

- Name of the Project: I 75 - S11
- Date: Mar 04, 2021
- Job Number: 201437
- Project Data: Load Project Data
- Conducted By: Furkan Cakmak
- About: [Facebook icon]
- Checked By: Fatmir Menkulasi

Sign Convention

(-) Upward Deflection	(-) Negative Curvature	(-) Negative Moment	(-) Compression
(+) Downward Deflection	(+) Positive Curvature	(+) Positive Moment	(+) Tension

Step 2): Click on the “Girder Properties” tab and select the type of the beam. In this case, it is a prestressed concrete beam. Check the box next to “Service Camber”. Check the box next to “Temperature Gradient Analysis” and select the appropriate zone to obtain a sense for the influence of positive and negative temperature gradients on beam camber and deflections. Click on “Lock the selections made above”. Select the appropriate beam type from the dropdown menu. In this case it is a Bulb Tee 49” Top Flange Width – 54” Height. Then enter information about unit weight of girder concrete, girder length, girder overhang length at precast facility, girder overhang length at bridge site, girder tributary width (to determine the portion of the deck supported by the girder), and coefficient of thermal expansion (this is needed to conduct temperature gradient analysis).

MDOTCamber v6.0

Introduction Girder Properties Girder Concrete Properties Deck Properties Prestressing Steel I >

Select the Beam Type

☐ Steel Beam

☒ Prestressed Concrete Beam

Lock the selections made above

Analysis Type

☒ Temperature Gradient Analysis ☒ Zone III

☒ Camber at Release ☒ Pre-erection Camber

☒ Service Camber

Bulb Tee 49" Top Flange Width - 54" Height

Parameter	Value	Unit
Unit-weight of cross-section* (γ)	0.15	kcf
Girder length (L)	136.9	ft.
Overhang length at precast facility (L_t)	21.5	in.
Overhang length at bridge site (L_b)	5.5	in.
Girder tributary width** (s)	8.41	ft.
Thermal expansion coefficient (α)	6.7e-06	1/F

Diagram illustrating the cross-section and dimensions of a Bulb Tee girder. The cross-section shows the top flange width b_f , flange thickness h_f , web thickness t_w , and total height h . The centroid is marked, and the distance from the bottom of the web to the centroid is y_{bottom} . The diagram also shows the girder length L and the overhang lengths L_t/L_b at the precast facility and bridge site, respectively.

Step 3: Click on “Girder Concrete Properties” tab. Select a model to predict the variation of concrete modulus of elasticity with time. The ACI 209R-92 model is recommended since the selection of this model together with other model which will be discussed later in this example led to accurate predictions for pre-erection camber. The user may also run the program another time by selecting the fib MC 2010 model to get a sense for the variability in results. Then the user has the option to either enter actual concrete compressive strengths at prestress release and 28 days or enter the specified values with or without overstrength factors. If measured concrete compressive strength values are not available it is recommended that the specified properties with Michigan overstrength factors be used. Then the user has to select a model for predicting the modulus of elasticity at prestress release and 28 days. It is recommended that the AASHTO LRFD 2020 model is selected although the program can be run several times to investigate the influence of other model selections on beam camber and displacements. After selecting the AASHTO LRFD 2020 model, the parameters needed to predict the modulus need to be entered.

MDOTCamber v6.0

Introduction Girder Properties **Girder Concrete Properties** Deck Properties Prestressing Steel I

A. Variation of Modulus of Elasticity with Time

ACI 209R-92 (Recommended) ⓘ

B. Concrete Compressive Strength at Release and at 28 Days

☐ Click to provide actual concrete compressive strength values.

Specified Concrete Compressive Strength

Symbol	Definition	Value (ksi)
f_{ci}	Specified concrete compressive strength at release	7
f_c	Specified concrete compressive strength at 28 day	10

Overstrength Factors for Concrete Strength

Michigan Factors (Recommended) ⓘ

Symbol	Definition	Factor
OSi	Overstrength factor for concrete at release	1.2
OS28	Overstrength factor for concrete at 28 day	1.2

C. Modulus of Elasticity at Release and at 28 Days

☐ Click to provide actual modulus of elasticity values.

Model for estimating elastic modulus: AASHTO LRFD 2020 (Recommended) ⓘ

Required Parameters for modulus of elasticity

☒ Back-calculate parameters. ⓘ

Unit-weight of plain concrete (wc): 0.145 kcf ⓘ

Aggregate factor (K1): 1

Step 4: Click on the “Deck Properties” tab. Enter surface loads pertaining to deck formwork and rebar weight, as well as concentrated loads for diaphragms. In this case only one interior diaphragm at midspan is selected. Then determine whether the deck will be replaced. In this example it is assumed that the deck will not be replaced. Enter parameters related to the first deck, any potential overlay, and barrier.

Parameter	Value	Unit
Slab formwork load (wsf)	10	psf
Surface load due to rebars (wsr)	4	psf
Diaphragm load (Pd)	5	kips
Number of interior diaphragms* (Ndp)	1	-

Has the deck been replaced?

☐ Yes

☒ No

Parameter for the First Deck	Value	Unit
Specified concrete compressive strength at 28 day (fcd)	4	ksi
Unit-weight of deck and haunch* (with mild steel) (γ)	0.15	kcf
Average deck thickness** (td)	9	in.
Aggregate factor^ (K1)	1	-
Unit weight of plain concrete^ (wc)	0.145	kcf
Average haunch thickness (th)	0	in.
Overlay thickness (to)	2	in.
Unit-weight of overlay (γo)	0.14	kcf
Barrier load^^ (wb)	0.04	klf

Step 5: Click on “Prestressing Steel Properties” tab and enter information related to prestressing steel material properties and strand configuration. This includes information related to modulus of elasticity, nominal diameter, ultimate tensile strength, jacking stress, yield stress, and strand type. In terms of prestressing strand geometry and layout the user has the opportunity to enter whether the strands are straight, harped, or debonded. The number of debonded strands and the length of debonding may be entered. The location of harping point may also be entered. Finally, the location of the strands in the cross-section with respect to the bottom of the beam may be entered.

MDOTCamber v6.0

☒ Check if there is any harped strand.

Parameter	Value	Unit
Modulus of elasticity (Eps)	28500	ksi
Nominal diameter (dps)	0.6	in.
Ultimate tensile strength (fpu)	270	ksi
Jacking stress (fpj)	202.5	ksi
Yield stress (fpy)	243	ksi
Strand Type	1	1:Low-r...

Layer Group	Group Type	Number of Strands in Layer Group	Distance from Bottom of Girder (in.)	Debonded Length (ft.)
1	Fully Bonded, Straight	14	2	0
2	Fully Bonded, Straight	16	4	0
3	Fully Bonded, Straight	12	6	0
4	Fully Bonded, Straight	8	8	0
5	Fully Bonded, Straight	2	10	0
6	Debonded, Straight	1	2	4
7	Debonded, Straight	2	2	12

Layer Group	Group Type	Number of Strands in Layer Group	Distance from Bottom of Girder at Midspan (in.)	Distance from Bottom of Girder at End (in.)	Harping Point (ft.)
1	Harped	12	7	46	44.77

Step 6: Click on “Creep and Shrinkage Model Selection” tab and select the AASHTO Body (2020) model. Other models may be investigated to get a sense about the impact of this selection on beam camber and displacements. Additional information on this topic may be found on MDOT Final Report “Evaluation of Camber and Deflections for Bridge Girders”. The user also the opportunity to enter magnification factors for tensile creep and flexural creep. However, since there is no consensus in the engineering community as to what these magnification factors should be, and since most prediction methodologies (ACI 435R-95) assume that compressive creep is equal to tensile creep and flexural creep, it is recommended that these factors be specified as 1.0.

MDOTCamber v6.0

Deck Properties | Prestressing Steel Properties | Creep and Shrinkage Model Selection | Time, Enviror

Note: After the model is selected, the parameters corresponding to the selected model should be provided. If they are not known, default values (shown below if appropriate) will be assigned to them.

Creep and Shrinkage Model: AASHTO Body 2020 (Recommended) ⓘ

Parameter	Magnification Factor	ⓘ
Tensile creep magnification factor	1	
Flexural creep magnification factor	1	

Parameters needed to be defined:

AASHTO Body 2020

For this model, no parameter is required.


Step 7: Click on “Time, Environment and Measured Camber Properties” tab. Select the number of beam sections along the span for which a time dependent cross-sectional analysis should be conducted. It is recommended that this number be at least 51 to obtain a smooth curve for the deflected shape of the beam, which is important in terms of setting slab screed and bottom of slab elevations. Indicate parameters related to time and environment such as relative humidity, age of girder when strands are detensioned, age of girder when the deck is placed, and number of curing days for the girder. In this example it is assumed that the relative humidity is 70%, the strands are detensioned one days after the girder concrete is cast, the deck is cast 29 days after the girder concrete is cast, and that the girder concrete is steam cured for one day. Then select method to generate the number of time steps that need to be considered in the type dependent analysis. It is recommended that the proposed method is selected although as explained in MDOT Final report “Evaluation of Camber and Deflections for Bridge Girders” the use of the Gilbert et al. (2010) method also leads to similar predictions. If measured camber at prestress release is available, then the user has the opportunity to enter this information so that pre-erection camber predictions can be informed accordingly. In this example, it is assumed that this information is not available.


MDOTCamber v6.0

Creep and Shrinkage Model Selection

Time, Environment and Measured Camber Properties

Results

Number of sections to be investigated:



A. Time and Environment Properties


Parameter	Value	Unit
Relative humidity* (H)	70	%
Age of girder when prestressing strands are released (t1)	1	days
Age of girder at deck placement (t2)	28	days
Age of girder when barrier load is applied on first super-structure (t3)	35	days
Age of girder when overlay load is applied on first super-structure (t4)	35	days
Time being considered at final (t5)	27375	days
Number of curing day for girder (tcur_g)	1	days
Number of curing day for first deck (tcur_d1)	7	days


Time Matrix Generation

Proposed (Recommended)

Gilbert et al. (2010)

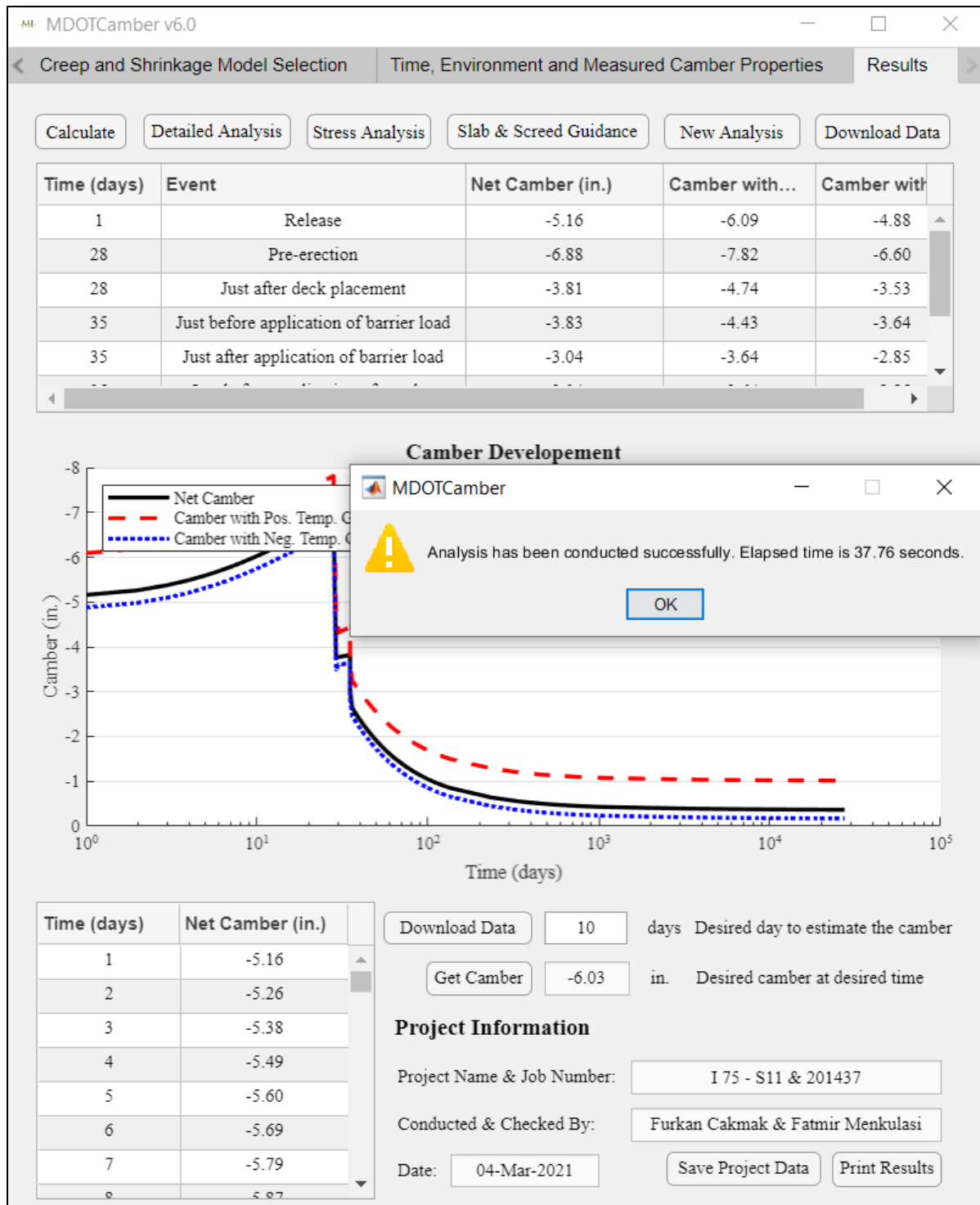


A logarithmic timescale will be assigned for conducting time-dependent calculations. Please consult user's manual for detailed information.

B. Measured Camber Properties


☐ Check if there is any measured camber value.

Step 8: Click on the “Results” tab and click on “Calculate”. The following should appear when the analysis is complete. In this example, it took 37.76 seconds to complete the analysis. The first table presents camber at prestress release, pre-erection, just after deck placement, just before application of barrier load, just after application of barrier load, just before application of overlay, just after application of overlay, and camber or displacement at final time with and without the influence of temperature gradients. The first figure shows how camber grows and reduces at various stages with and without the influence of temperature gradients. The third table provides net camber values without the influence of temperature gradients (i.e. the data used to construct the black line in the figure). The user has the opportunity to obtain camber at a specific time by clicking on the “Get Camber” button. The user has the opportunity to save the project data and print the results shown in this tab by clicking the “Print Results” button. This takes a screenshot of the results shown on this tab and allows the use to save this screenshot and print it if necessary.



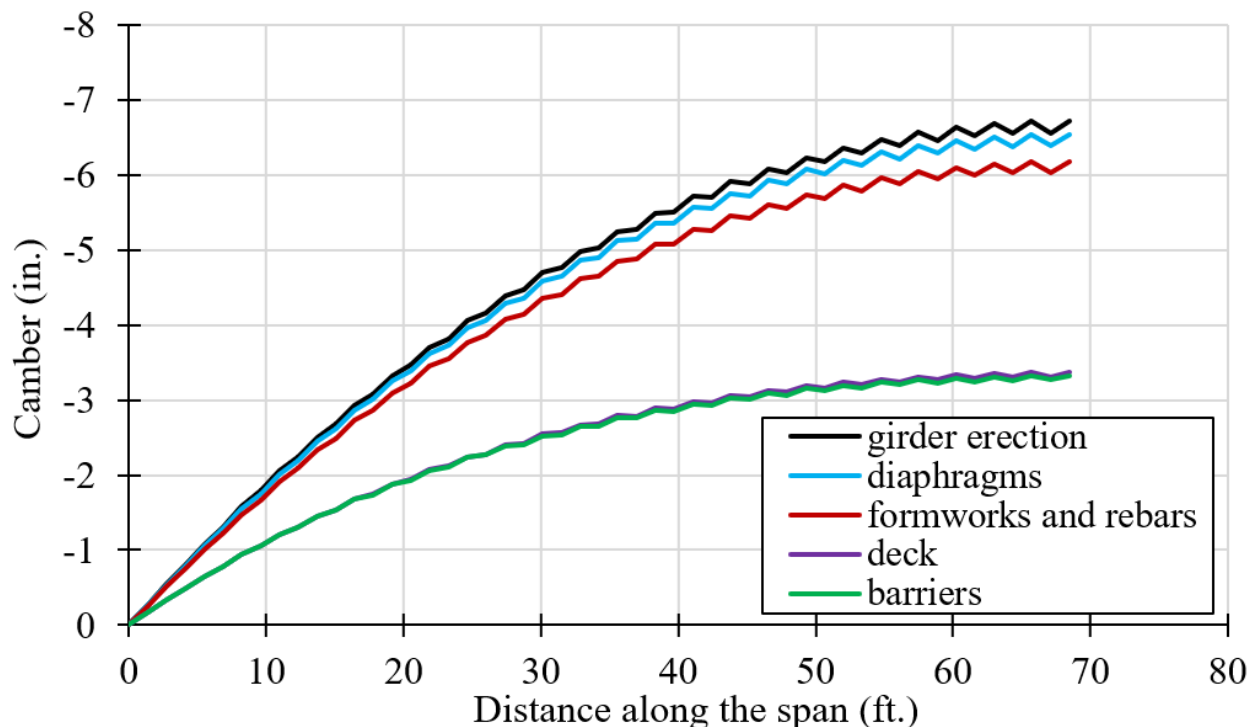
To obtain information for setting screed and bottom of slab elevations click on “Slab and Screed Guidance” button. This produces the table below, which provides camber and displacement estimates at various points along the span of the beam: 1) just after girder erection, 2) just after installation of diaphragms, 3) just after installation of formwork and deck reinforcement, 4) just after application of deck load, 5) just after application of barrier load; and 6) effect of positive and

negative temperature gradients. This information can be downloaded and be used to plot the deflected shape of the beam for the various stages of deflection described in MDOT's "Slab and Screenshot Guidance Document". This is illustrated by the graph below. The black line represents the deflected shape of the girder after it has been erected on the bridge site; the blue line represents the deflected shape of the girder after the diaphragms have been erected; the dark red line represents the deflected shape of the girder after the deck formwork and reinforcement have been erected; the purple line represents the deflected shape of the girder after the deck concrete has been placed; and finally the green line represents the deflected shape of the girder after the barriers have been installed.

MDOTCamber v6.0

For the first super-structure [Download Data](#)

Location (ft.)	Net Camber just after girder erection (in.)	Net Camber just after app. of diaphragm load (in.)	Net Camber just after app. of formwork and deck rein. (in.)	Net Camber just after app. of deck load (in.)
0	0	0	0	0
1.37	-0.27	-0.27	-0.26	-0.17
2.74	-0.55	-0.54	-0.51	-0.33
4.11	-0.80	-0.78	-0.75	-0.48
5.48	-1.07	-1.05	-1.00	-0.65
6.84	-1.31	-1.28	-1.22	-0.78
8.21	-1.57	-1.54	-1.47	-0.94



Appendix F.2 - Sample Camber and Deflection Calculations – Steel Beam

Problem Statement: Determine camber and deflections for a steel beam used in the M-20 project (J.N. 119069A) due to: 1) beam self-weight, 2) weight of deck forms and deck reinforcement, 3) weight of concrete deck, and 4) weight of sidewalk or barrier. This information can be used to determine slab screed and bottom of slab elevations according to MDOT’s “Slab and Screed Guidance” document. For example, the beam camber profile together with the specified minimum haunch and beam bearing elevations can be used to determine slab and screed elevations. The biggest unknown in the process is the deflected shape of the beam at different stages. This deflected shape can be obtained from the MDOT Camber program as shown below.

Solution:

Step 1): Start the MDOT Camber Program and fill in the information required in the introduction tab.

The screenshot shows the MDOTCamber v6.0 software window. The 'Introduction' tab is selected, displaying project information and a sign convention diagram.

Predicting Camber and Deflections in Composite Bridge Superstructures

Logos for MDOT (Michigan Department of Transportation), Wayne State College of Engineering, and benesch are displayed.

Project Information:

- Name of the Project: M20
- Job Number: 119069A
- Conducted By: Furkan Cakmak
- Checked By: Fatmir Menkulasi
- Date: Mar 05, 2021
- Project Data: Load Project Data
- About: [Globe icon]

Sign Convention

(-) Upward Deflection	(-) Negative Curvature	(-) Negative Moment	(-) Compression
(+) Downward Deflection	(+) Positive Curvature	(+) Positive Moment	(+) Tension

Step 2): Click on the “Girder Properties” tab and select the type of the beam. In this case, it is a steel beam. Check the box next to “Service Camber”. Check the box next to “Temperature Gradient Analysis” and select the appropriate zone to obtain a sense for the influence of positive and negative temperature gradients on beam camber and deflections. Click on “Lock the selections made above”. Then enter girder properties including fabricated camber (use the scroll down bar to see this). Fabricated camber represents the intentionally induced camber, which excludes self-weight.

MDOTCamber v6.0

Introduction Girder Properties Girder Concrete Properties Deck Properties Prestressing Steel I

Select the Beam Type

☒ Steel Beam

☐ Prestressed Concrete Beam

Lock the selections made above

Analysis Type

☒ Temperature Gradient Analysis Zone III

☒ Not applicable ☒ Pre-erection Camber

☒ Service Camber

Parameter	Value	Unit
Gross area (A_g)	90	in ²
Unit-weight of cross-section (γ)	0.490	kcf
Girder length (L)	173	ft.
Centroid of girder measured from bottom (y_{bottom})	35.5	in.
Gross moment of inertia (I_g)	75840	in. ⁴
Modulus of elasticity (E_g)	28500	ksi
Overhang length at bridge site (L_b)	24	in.
Girder height (h)	72	in.
Top flange width (b_{ft})	23	in.
Top flange thickness (h_t)	1	in.
Web thickness (t_w)	0.625	in.
Bottom flange width (b_{fb})	23	in.

Step 3: Skip on “Girder Concrete Properties” tab since this tab does not apply to steel girders.

Step 4: Click on the “Deck Properties” tab. Enter surface loads pertaining to deck formwork and rebar weight, as well as concentrated loads for diaphragms. In this case three interior diaphragms are selected; one at midspan and two at quarter points. Then determine whether the deck will be replaced. In this example it is assumed that the deck will not be replaced. Enter parameters related to the first deck, any potential overlay, and barrier.

Parameter	Value	Unit
Slab formwork load (wsf)	10	psf
Surface load due to rebars (wsr)	4	psf
Diaphragm load (Pd)	5	kips
Number of interior diaphragms* (Ndp)	3	-

Has the deck been replaced?

☐ Yes

☒ No

Parameter for the First Deck	Value	Unit
Specified concrete compressive strength at 28 day (f_{cd})	4	ksi
Unit-weight of deck and haunch* (with mild steel) (γ)	0.15	kcf
Average deck thickness** (td)	9	in.
Aggregate factor^ (K1)	1	-
Unit weight of plain concrete^ (w_c)	0.145	kcf
Average haunch thickness (th)	0	in.
Overlay thickness (to)	2	in.
Unit-weight of overlay (γ_o)	0.14	kcf
Barrier load^^ (wb)	0.04	klf

Step 5: Skip on “Prestressing Steel Properties” tab since this tab does not apply to steel beams.

Step 6: Click on “Creep and Shrinkage Model Selection” tab and select the AASHTO Body (2020) model. Other models may be investigated to get a sense about the impact of this selection on beam camber and displacements. Additional information on this topic may be found on MDOT Final Report “Evaluation of Camber and Deflections for Bridge Girders”. The user also has the opportunity to enter magnification factors for tensile creep and flexural creep. However, since there is no consensus in the engineering community as to what these magnification factors should be, and

since most prediction methodologies (ACI 435R-95) assume that compressive creep is equal to tensile creep and flexural creep, it is recommended that these factors be specified as 1.0.

Note: After the model is selected, the parameters corresponding to the selected model should be provided. If they are not known, default values (shown below if appropriate) will be assigned to them.

Creep and Shrinkage Model: AASHTO Body 2020 (Recommended)

Parameter	Magnification Factor
Tensile creep magnification factor	1
Flexural creep magnification factor	1

Parameters needed to be defined:

AASHTO Body 2020

For this model, no parameter is required.

Step 7: Click on “Time, Environment and Measured Camber Properties” tab. Select the number of beam sections along the span for which a time dependent cross-sectional analysis should be conducted. It is recommended that this number be at least 51 to obtain a smooth curve for the deflected shape of the beam, which is important in terms of setting slab screed and bottom of slab elevations. Indicate parameters related to time and environment such as relative humidity, age of girder when the deck is placed, etc. In this example it is assumed that the relative humidity is 70%, the deck is cast 2 days after the girder is fabricated. Then select method to generate the number of time steps that need to be considered in the type dependent analysis. It is recommended that the proposed method is selected although as explained in MDOT Final report “Evaluation of Camber and Deflections for Bridge Girders” the use of the Gilbert et al. (2010) method also leads to similar predictions. Then the user has the opportunity to enter pre-erection camber so that this information can be used to predict the rest of the camber history. This is typically useful for prestressed concrete girder in which pre-erection camber varies with time. In this example, it is assumed that such information is not available and it will be computed by the MDOT Camber program.

MDOTCamber v6.0

Time, Environment and Measured Camber Properties
Results

Number of sections to be investigated:
51

A. Time and Environment Properties

Note: All time properties must be based on the assumption that deck is placed after 2 days of girder erection.

Parameter	Value	Unit
Relative humidity* (H)	70	%
Age of girder at deck placement (reference) (t1)	2	days
Age of girder when barrier load is applied on first super-structure (t2)	9	days
Age of girder when overlay load is applied on first super-structure (t3)	9	days
Time being considered at final (t4)	27375	days
Number of curing day for first deck (tcur_d1)	7	days

Time Matrix Generation

Proposed (Recommended)
Gilbert et al. (2010)

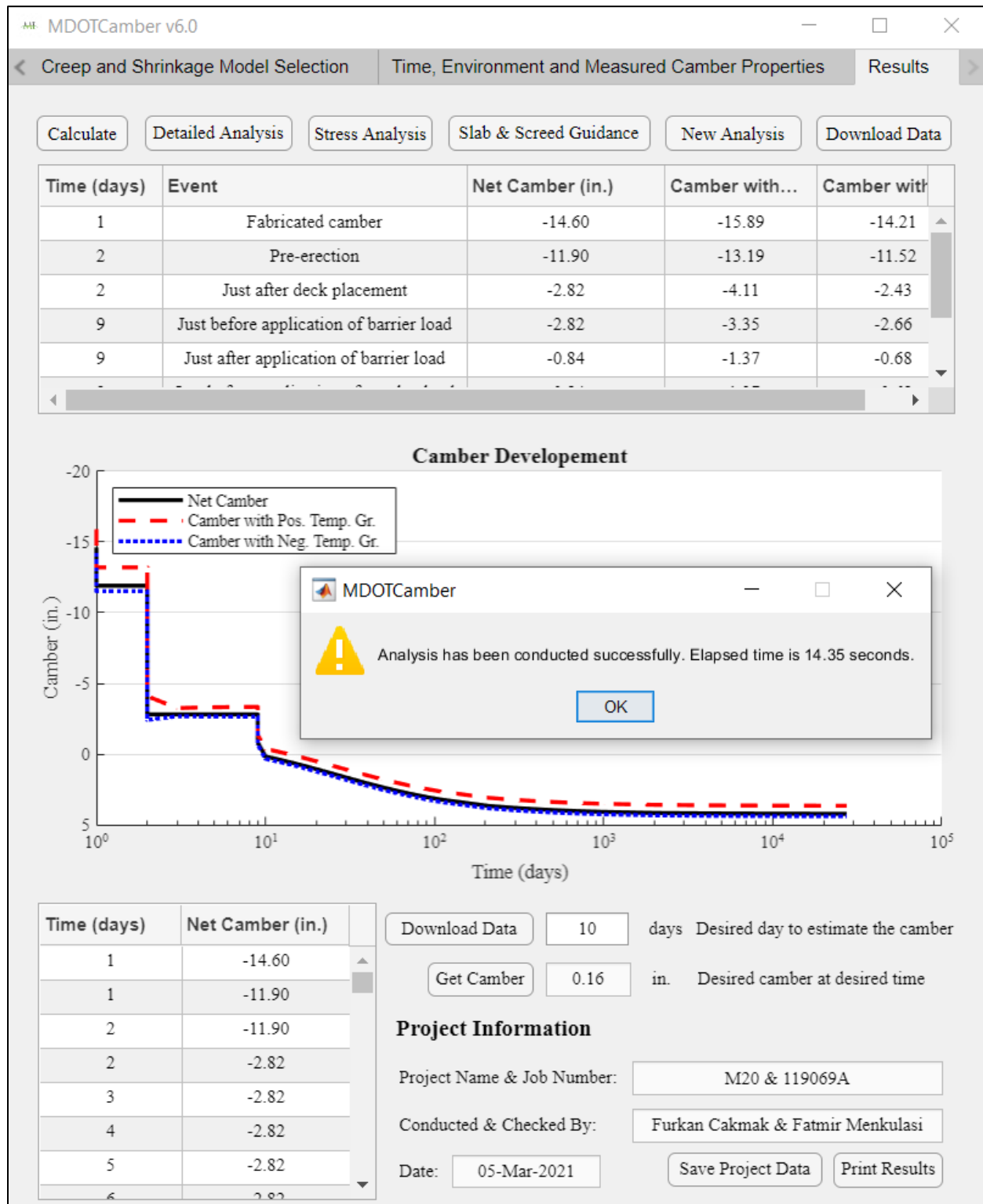
A logarithmic timescale will be assigned for conducting time-dependent calculations. Please consult user's manual for detailed information.

B. Measured Camber Properties

☐ Check if there is any measured camber value.

Step 8: Click on the “Results” tab and click on “Calculate”. The following should appear when the analysis is complete. In this example, it took 13.69 seconds to complete the analysis. The first table presents fabricated camber (provided as an input), pre-erection camber (fabricated camber minus deflection due to self weight), camber just after deck placement, just before application of barrier load, just after application of barrier load, just before application of overlay, just after application of overlay, and camber or displacement at final time with and without the influence of temperature gradients. The first figure shows how camber grows and reduces at various stages with and without the influence of temperature gradients. The third table provides net camber values without the influence of temperature gradients (i.e. the data used to construct the black line in the

figure). The user has the opportunity to obtain camber at a specific time by clicking on the “Get Camber” button. The user has the opportunity to save the project data and print the results shown in this tab by clicking the “Print Results” button. This takes a screenshot of the results shown on this tab and allows the use to save this screenshot and print it if necessary.

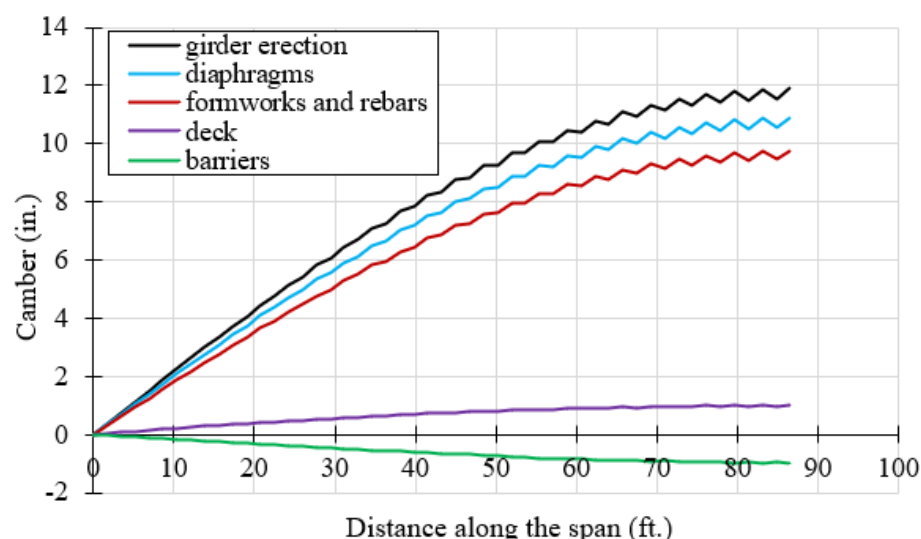


To obtain information for setting screed and bottom of slab elevations click on “Slab and Screed Guidance” button. This produces the table below, which provides camber and displacement estimates at various points along the span of the beam: 1) just after girder erection, 2) just after installation of diaphragms, 3) just after installation of formwork and deck reinforcement, 4) just after application of deck load, 5) just after application of barrier load; and 6) effect of positive and negative temperature gradients. This information can be downloaded and be used to plot the deflected shape of the beam for the various stages of deflection described in MDOT’s “Slab and Screed Guidance Document”. This is illustrated by the graph below. The black line represents the deflected shape of the girder after it has been erected on the bridge site; the blue line represents the deflected shape of the girder after the diaphragms have been erected; the dark red line represents the deflected shape of the girder after the deck formwork and reinforcement have been erected; the purple line represents the deflected shape of the girder after the deck concrete has been placed; and finally the green line represents the deflected shape of the girder after the barriers have been installed.

MDOTCamber v6.0

For the first super-structure [Download Data](#)

Location (ft.)	Net Camber just after girder erection (in.)	Net Camber just after app. of diaphragm load (in.)	Net Camber just after app. of formwork and deck rein. (in.)	Net Camber just after app. of deck load (in.)
0	0	0	0	0
1.73	-0.38	-0.35	-0.31	-0.04
3.46	-0.76	-0.70	-0.63	-0.08
5.19	-1.14	-1.05	-0.94	-0.11
6.92	-1.52	-1.40	-1.26	-0.15
8.65	-1.89	-1.74	-1.56	-0.18
10.38	-2.27	-2.09	-1.97	-0.22



Appendix F.3 - MDOT Camber Multipliers

MICHIGAN DESIGN MANUAL BRIDGE DESIGN – CHAPTER 7:LRFD

Screeding

A. Transfer Screeding

Transverse screeding shall be used for finishing all bridge decks.

When the skew angle is greater than or equal to 45°, the strike equipment is placed parallel to the reference lines.

B. Screed Elevations

In computing screed elevations, the specified camber should be used.

The following dead loads should be used in computing beam deflection for screed elevations:

10 LBS/SFT for formwork

10 LBS/SFT for reinforcing steel

145 LBS/SFT for plain concrete

150 LBS/SFT for reinforced concrete

Screed elevations for suspended spans are to be figured for the case of no deck concrete having been poured in any span.

Screed elevations for prestressed concrete beams are to account for long term effects by modifying the beam deflection using the following factors:

Factor applied to prestressing force at release
 $= 1.9 + 0.6(I_{\text{Girder}} / I_{\text{Composite}})$

Factor applied to beam self-weight at release
 $= 2.1 + 0.7(I_{\text{Girder}} / I_{\text{Composite}})$

Factor applied to slab when poured (including SIP forms, diaphragms and utility loads) $= 1.0 + 1.1(I_{\text{Girder}} / I_{\text{Composite}})$

Factor applied to barrier and sidewalk when poured $= 2.3$

I_{Girder} = moment of inertia of girder

$I_{\text{Composite}}$ = moment of inertia of composite section

7.02.23

Stay-In-Place Forms

A. Use (9-2-2003)

Because of the design accommodations, any need for stay-in-place forms should be anticipated in the Contract Plans and Specifications.

The criteria for the use of metal stay-in-place forms are safety and economy in construction. Where practical, they should be included as a contractor option.

The use of concrete stay-in-place forms is not allowed.

B. Design (5-6-99) (9-21-2015)

The design of metal stay-in-place forms is the responsibility of the contractor. If the beams on a deck replacement project can't accommodate an increased dead load of 15 LBS/SFT (7.01.04 I) then note 8.07.01 R shall be used on the plans. Because of the load and deflection limits of the forms, it may be necessary to reduce the beam spacing resulting in the use of one or more additional rows of beams. This additional cost should be justified by the improved safety and/or in the cost reduction of maintaining traffic on the roadway below.

When the use of stay-in-place forms cannot be economically justified the designer shall prohibit their use by including note 8.07.01 S. on the plans. (9-2-2003)

Detail steel beam tension zones on plans. Welding or mechanically fastening permanent metal deck forms or accessories to structural steel is prohibited. (6-16-2014) (3-26-2018)

It is recommended that the highlighted text is replaced with:

“Screed elevations for prestressed concrete beams shall be obtained from the MDOTCamber computer program in accordance with the Slab and Screed Guidance document”.

It is recommended that the units for these two items be changed to pounds per cubic feet to indicate the unit weight of plain and reinforced concrete. For a 9 in. slab the load in terms of pounds per square foot for plain and reinforced concrete will be 109 psf and 113 psf, respectively. For a more accurate estimation of plain concrete unit weight refer to AASHTO LRFD (2020) Table 3.5.1-1. To estimate reinforced concrete unit weight 5 pcf may be added to the unreinforced concrete unit weight.

Appendix F.4 - MDOT Camber Multipliers
MICHIGAN DEPARTMENT OF TRANSPORTATION
SPECIAL PROVISION
FOR
STRUCTURE SURVEY DURING CONSTRUCTION

BRG:KCK

1 of 3

APPR:KB:JAB:06-08-18

FHWA:APPR:06-11-18

a. Description. This work consists of providing all the necessary labor, materials, and equipment to obtain elevation observations along existing and proposed beams or girders at the stages of construction set forth in this special provision. Complete all work in accordance with section 824 of the Standard Specifications for Construction, except as modified herein.

Submit the qualifications of the survey crew chief used to complete this work for review and approval by the Engineer in accordance with subsection 824.01 of the Standard Specifications for Construction.

b. Materials. None specified.

c. Construction. Witness horizontal control points in accordance with subsection 824.03.A of the Standard Specifications for Construction and verify plan benchmarks and establish new benchmarks in accordance with subsection 824.03.B of the Standard Specifications for Construction prior to starting work.

Provide the Engineer with elevation observations at the same points along the existing and proposed beams or girders as the bottom of slab and screed point locations included on the plans and at the stages of construction listed below. Measure the elevations requested to an accuracy of 0.01 feet. Provide the information using the Bridge Elevation Table spreadsheet included in the Reference Information Documents (RID).

1. Deck Replacement Projects.

A. Elevation observations along the bottom of the bottom flange of the existing beams or girders prior to the removal of any of the existing superstructure and without any live load or materials or equipment stored on top of the existing superstructure.

B. Elevation observations along the bottom of the bottom flange of the existing beams or girders after the existing bridge deck has been removed and prior to installing forms or reinforcement. Include information regarding any false decking in place.

C. Elevation observations along the bottom of the bottom flange of the existing beams or girders after installing the forms and reinforcement and prior to placing the superstructure concrete. Include formwork information.

D. Elevation observations along the bottom of the bottom flange of the existing beams or girders after the proposed superstructure is complete and without any live load or materials or equipment stored on top of the proposed superstructure. Provide these elevations no more than 7 calendar days after the bridge has been opened to traffic.

2. Projects with a New Prestressed Concrete Superstructure.

A. Provide to the Engineer the release date of the prestressing force and the observed camber at midspan for each beam no more than 7 calendar days after releasing the prestressing force. **The date and time when the measurements are taken shall be noted as camber may vary markedly during the first 7 days.**

B. Elevation observations relative to a local datum, with an elevation of 100.00 feet at one end of the proposed prestressed concrete beam, along the top of the proposed beams while they are still at the Precaster's facility and prior to setting the beam seat elevations at the abutments and piers. Measure the height of the beam at the point of each elevation observation and provide this information to the Engineer. Complete this work and submit the elevations to the Engineer between 14 and 21 calendar days prior to setting the beam seat elevations at the abutments and piers. Indicate the distance from the end of each beam to the support location at the time elevations are surveyed. **Report the date and time when measurements are taken.**

C. Elevation observations along the top of the proposed prestressed concrete beams after they have been erected on the abutments and piers and prior to installing forms or reinforcement. Include information regarding any false decking in place.

D. Elevation observations along the bottom of the bottom flange of the proposed prestressed concrete beams after installing forms and reinforcement and prior to placing the superstructure concrete. Include formwork information.

E. Elevation observations along the bottom of the bottom flange of the proposed prestressed concrete beams after the proposed superstructure is complete and without any live load or materials or equipment stored on top of the proposed superstructure. Provide these elevations no more than 7 calendar days after the bridge has been opened to traffic.

3. Projects with a New Steel Superstructure.

A. Elevation observations along the top and bottom of the proposed steel beams or girders after they have been erected on the abutments and piers and prior to installing forms or reinforcement. Include information regarding any false decking in place.

B. Elevation observations along the bottom of the bottom flange of the proposed beams or girders after installing the forms and reinforcement and prior to placing the superstructure concrete. Include formwork information.

C. Elevation observations along the bottom of the bottom flange of the proposed beams or girders after the proposed superstructure is complete and without any live load or materials or equipment stored on top of the proposed superstructure. Provide these elevations no more than 7 calendar days after the bridge has been opened to traffic.

4. Superstructure Widening Projects. Provide the information specified above for deck replacement projects for the existing beams or girders that will remain in place. Provide the information specified above for projects with a new prestressed concrete superstructure or for projects with a new steel superstructure for the proposed beams or girders.

5. The following information must be submitted with the elevation observations for all projects:

A. False Decking.

- (1) Material type(s).
- (2) Material dimension(s).
- (3) False decking layout.

B. Formwork.

- (1) Material type(s).
- (2) Material dimension(s).
- (3) Formwork layout.

Work on a subsequent stage must not begin until the Engineer has reviewed and approved the required information. The Engineer may elect to adjust the proposed bottom of slab and screed elevations following a review of the documentation.

d. Measurement and Payment. The completed work, as described, will not be paid for separately, but will be included in other bid items.

Appendix F – Slab and Screed Guidance

The existing slab and screed guidance was reviewed. The old appendix was replaced with two new appendices F.1 and F.2 that show step by step how beam camber and deflections can be calculated for prestressed concrete and steel beams in simply supported configurations. The text provided in the existing guidance is shown in black. In cases where existing text is recommended to be removed, red color with strikethrough is used. New text is shown in green.

Slab and Screed Guidance

The purpose of this guidance is to further define the determination of slab and screed elevations and haunch thicknesses for bridge decks in simply supported bridge superstructures, and to establish standard interaction between design and field offices during construction. ~~Example calculations done during the design phase will be presented in the appendix, along with emphasis on the specified material properties, and their impact on beam camber and various stages of deflection.~~

Examples for how prestressed concrete and steel beam camber and deflections can be determined for various stages of deflections are presented in the Appendix F.1 and F.2.

This guidance also serves to present a new process for verification of camber and deflection values to ensure comprehensive determination of slab and screed grades on bridge decks for optimal ride quality.

Screed Elevations:

Screed elevations are shown at the toe of barrier, or toe of sidewalk, as the contractor will typically place the screed rail for the self-propelled transverse finishing machine on the fascia beams, or as close as possible to limit the extent of hand finishing of the bridge deck. Elevations will also be shown at bulkheads and at the crown point to facilitate setting up the finishing machine properly prior to dry runs. ~~Screed elevations are calculated by taking the beam self weight and forms and rebar deflection values, and adding that value to the top deck surface elevation based on the theoretical roadway alignment.~~ Screed elevations are based on the condition that no deck concrete has been cast, and beams have already deflected under self-weight, and forms and rebar weight (See Stages of Deflection section).

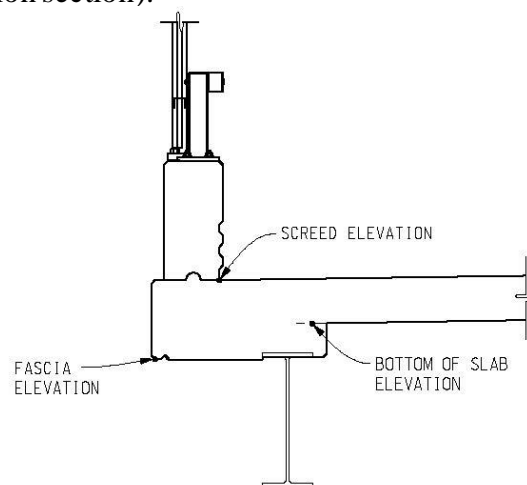


Figure 1. Screed elevation location at toe of barrier

Screed elevations are set higher than the finished deck surface elevations in an amount equal to the calculated deflections due to the deck concrete, and any sidewalk or barrier to ensure once the deck, sidewalk and barrier are cast; the deck surface matches the final roadway geometry. On rare occasions such as long spans, or horizontally curved girders, the self-weight of the transverse finishing machine resting on the screed rails may induce beam deflections. The deflections from the machine are insignificant when compared to the deflections caused by the plastic concrete; however, deflection of the screed rail and finishing machine itself may need to be accounted for.

Standard specifications subsection 706.03.A.2 requires the actual screed rail grades to be within 1/16 inch of the screed grades shown on the plans. The contractor is responsible to adjust the rail grades at their supports or to install tighter support spacing to ensure deflection of the rails (between supports) due to the weight of the self-propelled transverse screed machine does not exceed 1/16 inch.

Bottom of Slab Elevations:

Bottom of slab elevations are typically provided on the slab and screed sheet, and are calculated based on the proposed roadway vertical alignment (and horizontal alignment if on a curve or transition) and cross section. Elevations are provided at the right and left edge of each beam line. ~~and represent the final elevation of the deck surface, plus deflections due to dead load, then minus the 9-inch deck thickness.~~

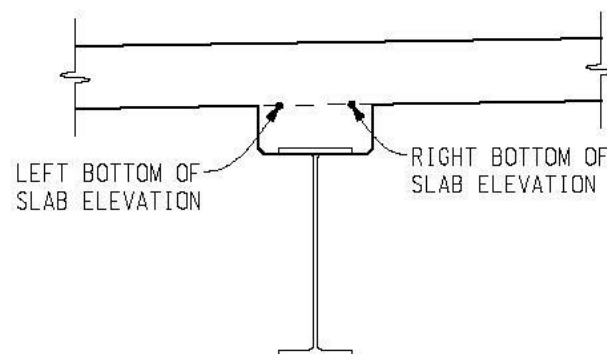


Figure 2. Bottom of Slab elevation points

The bottom of slab elevations take into account the fact that the beams and diaphragms are erected, and allowances are made for vertical alignment, and deflections due to forms and rebar weight, and bridge deck concrete weight. Bottom of slab elevations shown on the plans are set higher than the actual finished bottom of slab elevations in an amount equal to all the calculated dead load deflections (except for beam self-weight) to ensure once the deck, sidewalk and barrier are cast; the bottom of slab elevations equal the deck surface elevations minus deck thickness (typically 9 inches).

~~As a check, on the slab and screed details sheet, the screed elevation minus the bottom of slab elevation at the same point will result in approximately the 9 inch deck thickness. Due to the A-crown of the deck and the fact that bottom of slab elevations take into account weight of forms and rebar and the top of slab elevation do not, small variations of 9" will exist. Also, most fascia~~

~~beams are poured with a negative haunch, therefore top and bottom elevation difference will exceed 9".~~

Bottom of slab elevations are important, as the contractors typically tack welds the stay-in-place metal deck form angles to the appropriate haunch height based on these elevations, except in tension zones, where straps are used. If the actual beam camber, or deflections deviate from the calculated values too much, this impacts the bottom of slab elevation, and could result in excessive or negative haunches.

Bulkhead Elevations:

Bulkhead elevations are deck surface elevations transverse to beam lines at each abutment, and when crossing expansion or construction joints. The intent is to provide the contractor with an elevation to place expansion joint rails, or metal bulkheads for construction joints when following the deck pour sequence as shown on the plans. Similar to bottom of slab elevations, bulkhead elevations take into account vertical alignment, and deflections (there is no deflection at the abutments or piers) due to beam self-weight, forms and rebar, and bridge deck concrete weight. Bulkheads may be eliminated when combining deck pours. Changes to the pour sequence or the combining of deck pours must be approved by the design engineer.

Haunches:

Haunches are determined based on the fact that the final deflected shape of the beam will not exactly match the proposed roadway vertical alignment. Designers calculate haunch thicknesses based on the difference between the bottom of slab elevation, and the top of beam elevations. On new structures or superstructure replacements, designers will assume a minimum haunch thickness to afford flexibility in the field if bottom of slab elevations require adjustment. On deck replacements, designers are at the mercy of existing beam conditions and must calculate haunches on known conditions and calculated deflections. The beam elevations are determined based on the elevations of points of support, and the in-span deflections. Haunch thicknesses are variable along the length of the beam to accommodate the difference between roadway geometry, and structural deflections of the beams. The goal being satisfactory ride quality transitioning from road to bridge.

For structures on sag vertical curves with ideal beam camber, the haunch will typically be maximum at the ends of the span, and minimum at midspan. For structures on crest vertical curves, the haunch may be minimum at the ends of the span, and maximum at midspan. Designers try to coordinate the beam camber to match the crested roadway when possible to offer consistent haunch grades. The Michigan Bridge Design Manual, section 7.02.19C directs designers to use a uniform 1" thick haunch for steel beams, and a minimum 2" thick haunch for prestressed concrete beams.

Haunch thicknesses are also variable across the cross section, given the crown, or superelevation of the roadway surface, or the skew of the bridge.

Beam Camber:

Beams are positively or negatively cambered to compensate for dead load and live load deflections to match the proposed roadway vertical alignment. There are several stages of dead load deflection that are taken into account as described in the Stages of Deflection section, and the camber ordinates are determined based on the magnitude of these deflections. There are differences in

control of camber and deflections between steel beams and prestressed concrete beams as described below.

Steel Beams:

Camber ordinates on steel beams are developed based on the vertical alignment going across the bridge, haunches, and the calculated dead load and superimposed dead load. As a minimum, typically, a 1.0 in. haunch is targeted for deck replacement, and a 2.0 in. haunch is targeted for new superstructures. All of the stages of dead load deflection, plus the live load deflection are summated to determine the maximum required midspan camber ordinate value. Additional camber may also be required for geometry.

MDOT Bridge Design Manual section 7.02.06 requires a compensating camber to be designed into the beams where dead load deflection or vertical curve offset are greater than $\frac{1}{4}$ ". This may include a negative camber for portions of beams on continuous spans to ensure uniform haunch depths, and bottom of slab elevations such that the sum of all dead load deflections results in the deck top surface matching the proposed roadway vertical alignment as close as practicable.

During fabrication, camber is easier to control for steel beams than for prestressed concrete beams. For built up steel plate girder, fabricators have two options to fabricate beams to the specified camber:

- The web plate can be cut in a parabolic shape to match the camber ordinates shown on the contract plans, and the top and bottom flange plates are then welded to the shaped web plate.
- The web plate can be cut straight, the top and bottom flanges welded on, and the entire beam heated as to allow manipulation to the desired camber. The beam is then allowed to cool while being restrained to the required position as to lock in the cambered shape.

For rolled wide flange shapes, fabricators heat the beams in the same fashion as the second option for built up plate girders to achieve the required camber. As a result, the maximum camber for steel beams is a function of fabricated geometry and greater control of camber can be achieved.

For deck replacement projects on steel beam superstructures, the slab and screed elevations in the plans will be based on the beams rebounding to their original elevation prior to weight of the concrete deck. This does not always occur **due to beam deterioration, change in support conditions (i.e. pin supports not acting as pin supports), and influence of end and intermediate diaphragms.** ~~and permanent camber loss can result due to years of dead and live load deflection during service.~~ It is always important to survey the tops of the beams at the same intervals as shown on the slab and screed sheets, and provide this information to the designer for review, and to make adjustments to grades if necessary.

Prestressed Concrete Beams:

Similar to steel beams, camber is also required for prestressed concrete beams; however, the amount of upward deflection is a function of the prestress force, the eccentricity of the prestressing strands to the neutral axis of the beam, the beam shape, **short term and long term** properties of the concrete mix, **beam concrete age at prestress release, erection, placement of deck, and placement of superimposed dead loads.** For a complete discussion on the factors that affects beam camber and displacements please refer to MDOT Final Report "Evaluation of Camber and Deflections for

Bridge Girders”. Examples for how prestressed concrete and steel beam camber and deflections can be determined for various stages of deflections are presented in the Appendix.

Designers specify a minimum compressive strength required at prestress strand release based on acceptable levels of stress in the beams, and this value is used in the deflection calculations when calculating the modulus of elasticity. Fabricators often add accelerators and water reducers to increase the short-term strength gain in the concrete mix, to ensure the prestressing beds can be turned around in a specified time needed for production. Although fabricators are required to meet camber tolerances per Table 708-1 of the standard specifications, the result is the actual prestress beam deflections diverging from the theoretical deflection calculated during design due to the higher compressive strength. The MDOT Camber program allows the user to account for expected material properties thus leading to more accurate camber and deflection predictions.

Stages of Deflection:

The slab and screed, and bulkhead elevations on the project plans are calculated to ensure the final deck position closely matches the design roadway alignment taking into account camber, and all stages of superstructure deflection. To accomplish this, the calculations assume that a beam lying on its side is fully cambered, as shown in Figure 3.

The camber ordinates shown in Figure 3 will be shown on the project plans for steel girders to direct the fabricator what camber is required. These camber ordinates exclude beam self-weight for steel beams.

Maximum midspan camber taking into account beam dead load deflection will be shown on the plans for prestressed concrete beams.

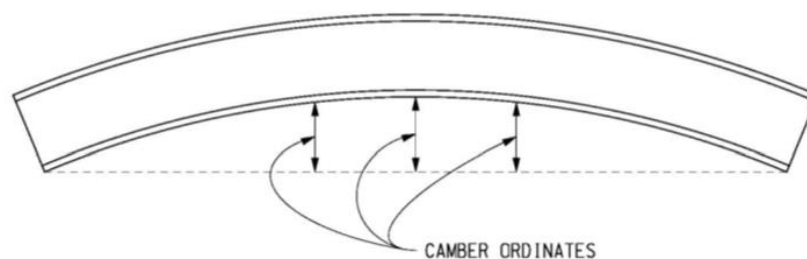


Figure 3. Steel beam lying on its side

The first step in determining the slab and screed grades is calculating the reduction in camber due to the girder self-weight. When a girder is supported at points of bearing, either on a pier or abutment, the girder will deflect under its own self-weight. At support points there will be no deflection. For simply supported spans, maximum deflection will occur at midspan, and for continuous girders, maximum downward deflection will occur at some point prior to midspan, and upward deflection in adjacent spans is considered in the bridge deck pour sequence. Figure 4 shows a span supported at bearing points deflecting under the girder self-weight load, which is designated as Δ_1 .

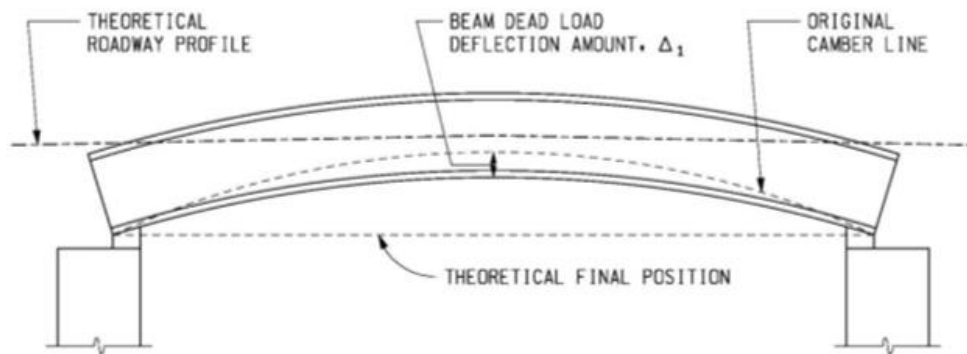


Figure 4. Deflection of the beam due to self-weight (applies to steel beams; prestressed concrete beams already include beam self-weight deflection)

Note that the theoretical roadway profile is actually below the top flange line during this stage, as the beam has not fully deflected into its final position. The theoretical final position of the bottom flange of the girder is the position required to ensure the top surface of the bridge deck matches the roadway vertical alignment as closely as practicable.

Another stage of deflection to consider is that produced by the weight of the forms and rebar. The MDOT Bridge Design Manual section 7.02.22.B instructs designers to assume 10lbs/sft each for the weight of forms and rebar in computing the screed elevations. Figure 5 shows the additional deflection, Δ_2 , due to the weight of forms and rebar that is taken into account by designers in computing slab and screed grades. This results in a relatively small deflection when compared to self-weight, or deck dead load deflection, however, it needs to be taken into account, and field offices should communicate with the designers if the actual deflections significantly vary from the design assumptions.

At this stage during construction, if Contractor Staking is included in the contract, the Contractor may take shots along the top flange of the girder, at the same interval as shown on the slab and screed detail sheet in the project plans, and provide this survey information to the engineer and designer. If Contractor Staking is not included in the contract, the project office may have their surveyor perform this function. If there is cause for concern, or significant anomalies in deflection are identified, this information should be submitted to the designer to compare these elevations to the theoretical elevations based on the camber and self-weight deflection calculations. This allows the designer to make any necessary grade adjustments to the haunch or deck thicknesses to ensure proper corroboration of the deck surface with the final roadway vertical alignment, and provide the new grade information to the field. Because the deflections due to forms and rebar is relatively small, most deflection issues may be identified after beam erection and evaluation of beam self-weight effects.

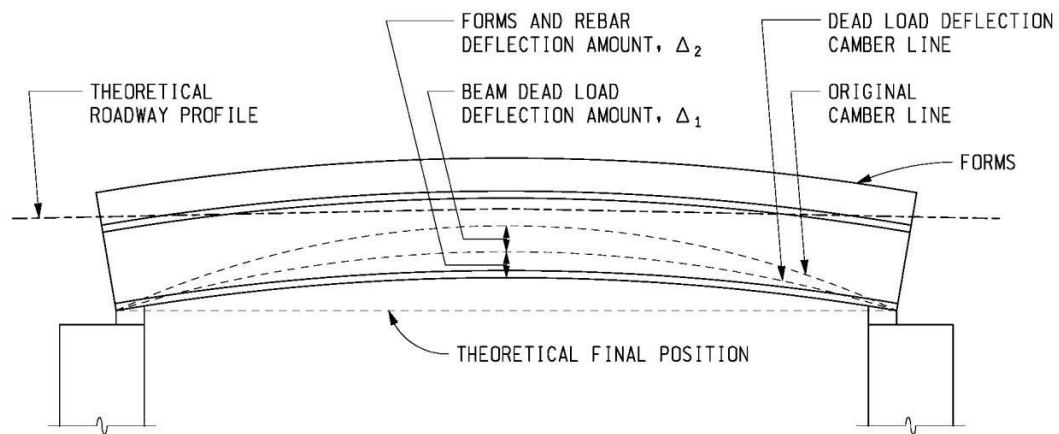


Figure 5. Deflection of the beam due to the weight of forms and rebar

Once the forms and rebar are set, the screed rails for the self-propelled transverse finishing machine should be set on the fascia beams to either the elevations shown on the plans, or adjusted elevations based on changes between the theoretical and actual camber and beam self-weight deflections. At this stage, a dry run is to be conducted by the contractor to ensure proper deck thickness measurements from the bottom of finishing machine to the top of the deck forms.

The most significant deflections of the beams occur under the wet load of concrete, prior to concrete cure, and attainment of composite action. Figure 6 shows the deflection, Δ_3 due to the weight of the deck concrete. At this stage the beams should be very near their theoretical final position.

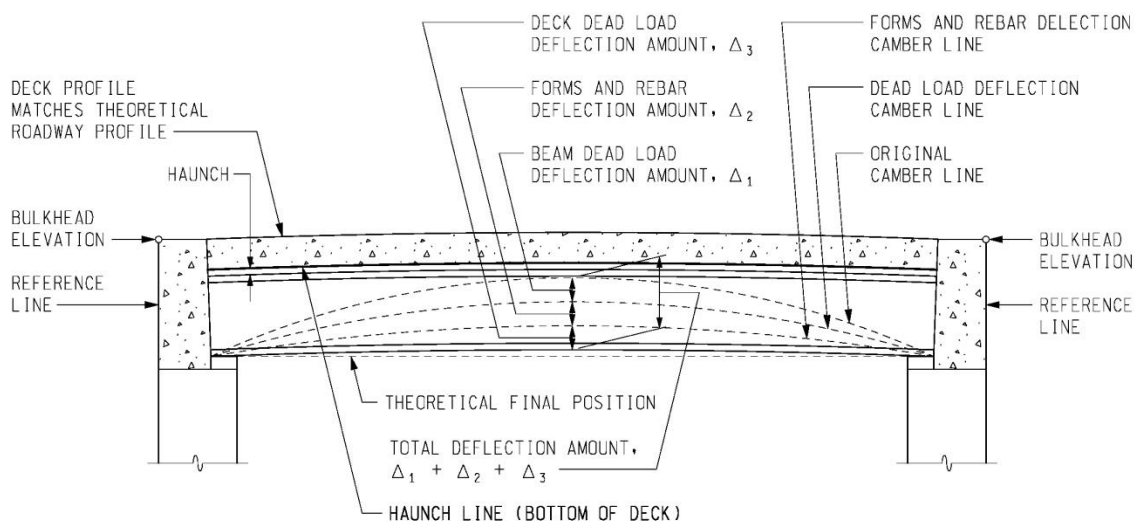


Figure 6. Deflection of the beam due to the weight of deck concrete

Once the bridge deck has been continuously wet cured for seven days per Standard Specifications subsection 706.03.N, succeeding portions of the structure, such as sidewalk and

bridge barrier railing may be cast on the deck. Figure 7 shows the deflection, Δ_4 due to the weight of sidewalk and barrier.

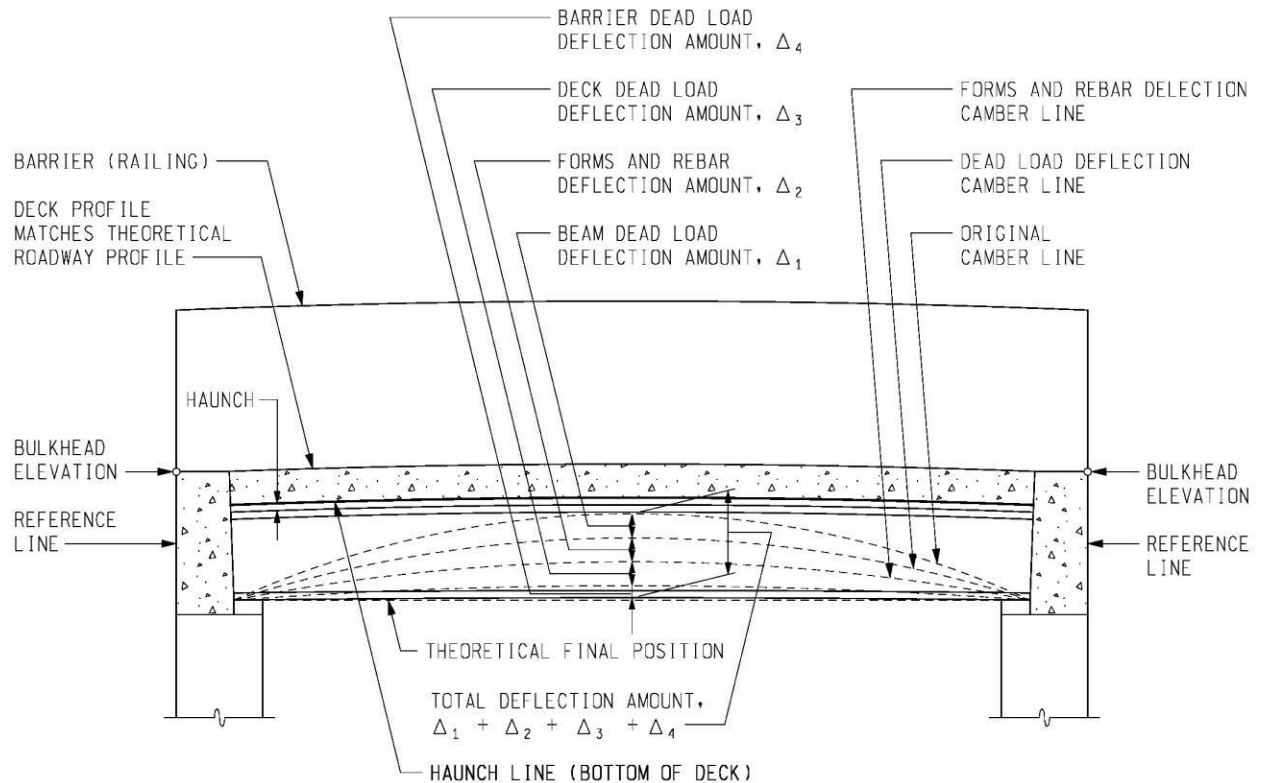


Figure 7. Deflection of the beam due to the weight of sidewalk or barrier

The value of Δ_4 will be relatively small, as the moment of inertia used in the deflection calculation is now that of the composite section of beam and concrete deck.

The slab and screed grades shown on the plans take into account the beam camber minus the sum of all stages of construction deflection ($\Delta_1 + \Delta_2 + \Delta_3 + \Delta_4$) to obtain grades that result in the bridge deck surface closely matching the theoretical roadway alignment upon completion of the sidewalk and barrier concrete pours.

At this stage, any bumps in the bridge deck, or surface tolerances exceeding 1/8 inch over 10 feet must be removed via grinding. This results in the removal of the densified floated finish portion of the bridge deck, and can introduce micro-cracks into the deck structure, both of which are undesirable. Ensuring the finished deck surface matches the final vertical roadway geometry as close as possible will help prevent grinding on the finished bridge deck. This requires careful attention to detail on the actual beam camber and deflections compared to what is shown on the plans and communication with the designer when values do not correspond.

Staged Construction:

Staged construction on bridge projects presents a challenge for geometry control on the finished deck surface.

On curved steel girder bridges constructed part width, there is a potential for the bridge deck not matching at the stage line due to differential deflections from the difference in beam stiffness (due to length and curvature) from beam to beam. This can be compensated by taking survey measurements on the tops of the Stage 2 beams, and the Stage 1 bridge deck, and providing these elevations to the designer for review.

On prestressed side-by-side box beam bridges constructed part width, all the box beams may be fabricated at the same time. The Stage 1 beams will be erected and experience full dead load deflection, while the Stage 2 beams may experience camber growth due to the prestressing force eccentricity. This causes issues during Stage 2 construction such as transverse post tensioning ducts not lining up, or potential change in deck thickness at the stage line. If all the beams for a staged construction project are cast together, the Stage 2 beams should be monitored for camber growth. The most significant camber growth is a result of curing concrete and strength gain and occurs within the first 28 days after beam casting. Any growth in camber should be communicated to the designer and adjustments made to the haunch grades if necessary. Preloading the beams after erection may be necessary to align post tensioning ducts. Contact the designer for assistance with prestressed side-by-side box beam bridge projects that are done part width.